POLITECNICO
MILANO 1863

Department of Civil and Environmental Engineering

Ph. D. in Structural Seismic and Geotechnical Engineering

Seismic Response and Strengthening of Flat Slab Buildings

Doctoral dissertation of:
Teresa Netti

Supervisor:
Prof. Dario Coronelli

Co - Supervisors:
Prof. Patrick Bamonte
Ing. Marco Lamperti Tornaghi

Tutor:
Prof. Maurizio Lualdi

The Chair of the Doctoral Program
Prof. Umberto Perego

XXXIII Cycle - MAY 2021

Summary

Flat slabs represent one of the most common structural solutions for reinforced concrete building floors. Several experimental studies have been carried out with the aim to clarify flat slab seismic design rules. The state of the art concerns numerous isolated slab column connections, fewer single flat slab floors, and even fewer multi-storey flat slab frames. All of these tests – but one – were carried out on specimens to scale. No experimental campaign was carried out for building structure with primary walls and secondary frames. The main reason for this lack of tests on a real scale building structure lies is the limitation imposed by the dimensions; in fact, it is frequently impossible to build and to test such a system inside a laboratory. The related costs are another important factor, limiting this type of research.

The SlabSTRESS project was developed to satisfy this need, and was proposed by four European universities (Polimi, Milano, EPFL Lausanne, UNOVA Lisbon and UTCB Bucharest) and carried out in collaboration with the European Commission's Joint Research Centre (JRC) in Ispra (VA, Italy). The SlabSTRESS experimental campaign was performed at the ELSA (European Laboratory for Structural Assessment), Reaction Wall at the JRC in Ispra. The project was part of the transnational access activities of the SERA project.

Forming a part of an extensive research project, this thesis proposes and applies a methodology for the analysis of measurement data to characterise and put into relation the global and local structural response. Moreover, the state of the art is analysed, and compared to the SlabSTRESS results, therefore to understand what part of the existing knowledge is confirmed and illustrate the innovative findings.

The real-scale mock-up consisted of a reinforced concrete building with two ordinary thick slabs, supported by twelve columns on each floor, one of which was provided with transverse reinforcement. Two different longitudinal reinforcement layouts were used.

The building was designed to consider the flat slabs as secondary members, with seismic resistant walls as primary ductile elements. The structure was designed to bear gravity loads and capable of reaching a lateral relative inter-storey drift compatible with moderate-high seismic lateral action. This design procedure was inspired by the method used in the North American codes for the seismic design of flat slabs. The primary seismic walls were not actually built in the structure but were virtual elements, simulated by the sub-structuring allowed by the pseudo-dynamic method used in the host lab.

A specific design was made for the RC columns, with a structural steel stub at

the centre of these members. The latter were required for measuring internal forces and bending moment in each slab-column connection.

The first phase of the test programme simulated two levels of seismic activity: the service limit state (SLS) and the ultimate limit state (ULS). Seismic loading was applied using the pseudo-dynamic technique with linear sub-structuring. The seismic response of large-size specimens can be obtained by the combination of the experimental restoring forces with the analytical inertia and seismic-equivalent forces.

Successively, during the second phase two cyclic tests were carried out to test the floors for a combination of gravity and lateral cyclic loading of increasing amplitude, up to near-failure conditions. Prior to the second cyclic test some of the damaged connections were strengthened and then were tested again.

Both the global and the local measurements were acquired. Each column on both floors was provided with an *ad hoc* system designed to allow the internal forces and bending moment to be measured. A large number of sensors were used in this experimental campaign: 80 inclinometers, 48 extensometers and 192 strain-gauges, which permitted a series of data to be collected. All the sensors had been previously calibrated to ensure the precision of the measurement system. A new controller and data acquisition system, called ElsaREC, was developed by the ELSA laboratory team and used here for the first time, permitting a systematic calibration procedure for all the sensors adopted in the experiment at ELSA.

Using the main statics and kinematics parameters, two schemes were chosen to represent the structure from both a global and a local point of view. Two kinematics parameters, one displacement for each floor and two static parameters, one force for each floor, described the global system. These parameters were acquired by the load cells applied to the actuators, while displacement transducers applied on two reference frames near the structure recorded the corresponding displacements.

The local system to capture the behaviour of each slab-column connection was more complex. The slab and the column rotations represented the local kinematic parameters that were recorded by the inclinometers, and the slab cracks opening was recorded by the displacement transducers. Local kinematic measurements were acquired in the surrounding area of the slab on eight out of the twelve columns. The three connection (internal, edge and corner) were analysed with four, three and two instrumented sides respectively. Each side of the slab-column connection was equipped with an inclinometer to measure slab rotation along the East-West direction and a set of displacement transducers to measure crack opening through an increase of the slab thickness. Using the acquired slab rotation data and the column of each slab-column connection, it was possible to derive the relative rotation of the slab with respect to the column. Bending moment and shear were acquired from load cells located at the centre of each column on each floor, specially designed for this experimental campaign. The unbalanced moment for each

connection was then calculated.

The recorded signals were processed in order to characterise both the global behaviour and the local behaviour of slab-column connections. All the global analyses were performed using the inter-storey drift ratio as main coordinates to represent the behaviour of the structure. At local level the inter-storey drift ratio was correlated to local measurements, columns and slabs rotations. Lastly described, the procedure followed to obtain conversion factors that allow the inter-storey drift ratio to be converted to the column-slab rotation as a function of the slab-column connections typology is described.

The global and local response are analysed using force deformation relations, stiffness deteriorations diagrams, energy dissipation and ductility analysis. The local response is further investigated using the measurements of slab thickness variations, related to cracking; together with the crack patterns, these were used to study the different failure modes.

The results obtained were then compared to the state of the art. Some results confirm findings obtained from individual connection and scaled frame tests. Other aspects are innovative.

The tests showed global deformation capacity of the structure up to 2.5% global drift ratio with the 1st floor without shear reinforcement and 6% with some strengthening. This confirms global tests of scaled floor and frame specimens reaching deformation capacities in the range 3-6%. The connection response confirms the deformation capacity results of the data bases collected in the literature, for specimens without and with shear reinforcement. failure modes similar to those shown in the literature were observed.

The innovative results are several. The response of a building structure with a flat slab frame and primary seismic resistant walls was verified experimentally for the design SLS and ULS seismic action. very limited damage was inflicted to the flat slab frame, because of the limited drift ratio allowed by the primary seismic system.

A full-scale flat slab frame was tested for the first time up to global near failure conditions (i.e. 16% lateral load bearing resistance loss). This showed that the structure could bear the gravity loads at the conclusion of the test without progressive collapse, and highlighted the efficiency of single integrity reinforcement details.

The local response in a multi-storey frame was measured with an innovative measurement system, the connection response is thus studied under the real boundary conditions and the internal force redistribution in the whole structure.

The response was measured for different types of connections, i.e. interior, edge and corner, the data on the latter two not being very numerous in the literature.

The efficiency of a strengthening system for flat slab connections in a floor was shown, with redistribution of internal forces and moments.

The information collected in this study represents the basis for further understanding of flat slab response to combined gravity and lateral loading, the calibration of a

model can take advantage of the measurements carried out on a complete full scale structure. This experimental work and its developments path the way to new and more advantage design rules, in particular for the European Codes.

Keywords: reinforced concrete, flat slab building, full-scale testing, seismic behaviour, cyclic and pseudo-dynamic lateral loading, connection response, strengthening, measurement systems.

Index

Images Index

Tables Index

1 Introduction

1.1 Flat slab structural response and design

Nowadays, many buildings such as commercial, office, industrial, residential buildings and car parks are constructed with reinforced concrete flat slabs supported on columns.
The extensive use of choosing flat slabs is mainly due to the several advantages this system offers compared to other construction systems, and lies mainly in the simplicity of its use in construction.[1]

Figure 1.1 Example of flat-slab building in Milan [1].

These buildings are characterised by a simple form and reinforcement layout, their construction without beams and with flat ceilings allows for freedom in the

[1] Flat slab is the European term that corresponds to the American flat plate. Park and Gamble, 2000 [1] have used flat plate to indicate frames constructed with slab without beams. The European term of flat plate indicates frame with slab and with beams.

architectural design of the building and their construction does not entail intensive labour for the formworks. The heating, ventilation, air-conditioning, lighting and water systems can be easily installed and maintenance is also facilitated. The lack of beams allows the installation of partition walls, without incurring in the problem of having visible beams in the ceiling.
Among other advantages, flat slabs also allow for a reduction of overall height compared to that of traditional buildings with conventional beams, even when the free height between the floor and the ceiling is the same. This represents an added advantage during seismic loading.
A reduction of time and costs of construction compared with those of a traditional slab of the same dimensions represent other significant advantages.
Flat slab buildings are also widely constructed in regions of high seismicity. In fact, many European countries with a high seismic hazard level, choose this solution for their buildings. Fardis (2009) [4] reported that of all the earthquakes which inflicted heavy damage to urban centres in Greece in the 1980s and 1990s (Kalamata 1986, Aegio 1995, Athens 1999), buildings with “flat slab frames” performed well, despite their lacking proper design and detailing for earthquake resistance.
A flat slab panel is a structure of extreme simplicity, consisting of a horizontal element, a slab of uniform thickness directly supported by vertical elements, the columns, and absence of beams (Figure 1.2).

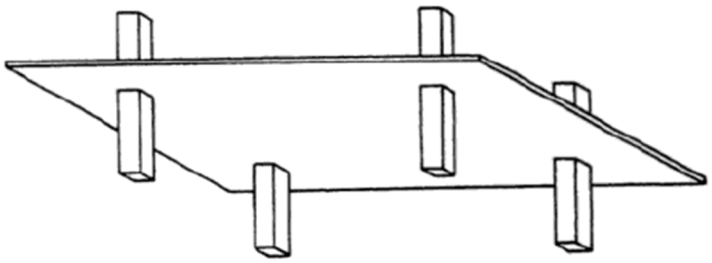

Figure 1.2 Flat slab [2].

This is the basic of the structure that can be modified according to requirements.
It is possible to add capitals to the top of the column or drop panels or thickened areas of the slab surrounding each column (Figure 1.3).

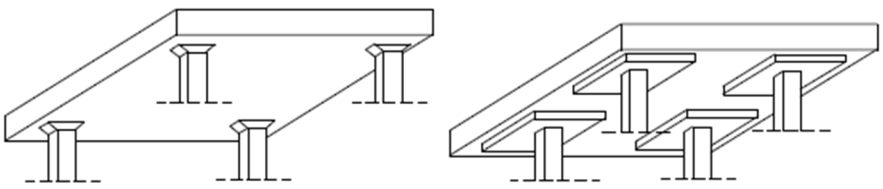

Figure 1.3 Flat Slab with a) capitals and b) with drop panel [3]**.**

Slabs can be supported by walls or by beams on two sides or four sides, the two-way slab is a particular category in which slabs are supported on beams on all sides of the

panel.

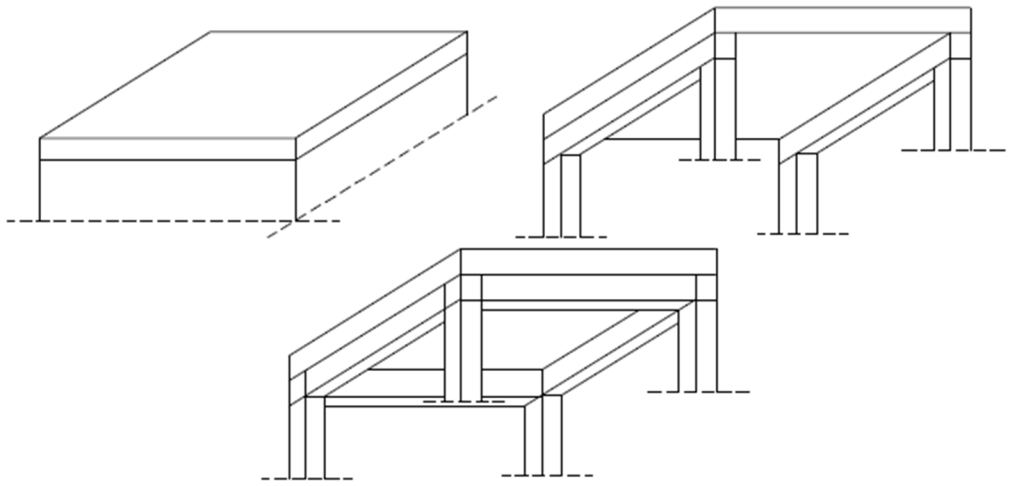

Figure 1.4 Flat Slab a) on walls, b) on two beams, c) on four beams [3].

A variant of the solid slab is the waffle slab, having a set of crossing joists, set closely spaced in relation to the span, which support a thin top slab.

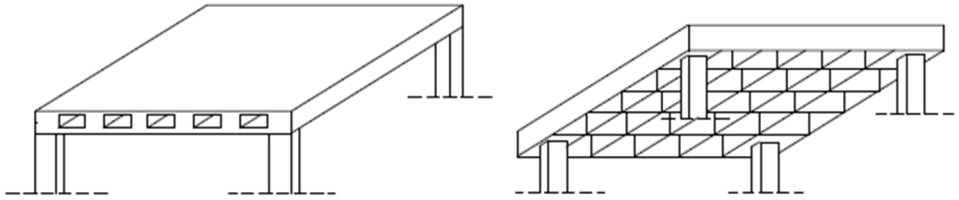

Figure 1.5 a) Voided slab and b) waffle slab [3].

1.2 Motivation of the research and specific aims

As demonstrated, flat slabs offer many advantages but they also have their drawbacks, among which, the punching shear failure and the development of large 2nd order (P-Δ) effects (Zaharia et al. [5]), due to the great flexibility of the flat slab towards horizontal actions.

During a seismic event, all the deformation demand is satisfied by the vertical elements (columns and walls) whereas the contribution of the horizontal elements to the resistance is generally considered to be very low and this is due to the great flexibility of these structures. The punching shear failure constitutes the main disadvantage and is due to the conformation of flat slab structures in which high shear forces concentrated around columns develop brittle shear failures. When a flat slab is subjected to a combination of gravity loads and unbalanced moments arising from the lateral deformation of the building, punching shear failure occurs. This can cause very great damage, ranging from local rupture to the global collapse. A punched connection in a slab with insufficient support, can cause it to fall on the slab on a lower level with consequences that involve the entire structure.

Flat slab structures have aroused interest in the scientific community. Although it is possible to find many studies on a single slab-column connection under seismic-type loading since the 1970s, there have been fewer studies on single flat-slab floors and fewer still on entire flat slab buildings. The greater part of the scientific contribution having been that of North American researchers, while recently the interest on the subject has spread to Europe.
In Europe, the seismic design is regulated by the Eurocode 8 [6] however, flat slabs are not considered in the code either as primary seismic members or as a secondary seismic member. Information is lacking on how to regulate the seismic design of this building typology. If the flat slab is considered as a secondary seismic member in collaboration with a primary earthquake resistant element, in this case the flat slab and its connections would necessarily be designed and detailed to carry the gravity loading when subjected to the displacements of the primary seismic element.
The need to increase the safety of existing buildings, making them compatible with the most modern standards, even when there are limited financial means and possibly avoiding the relocation of the activities carried on in the structure, has also driven research towards innovative strengthening solutions. Moreover, the recovery of the structural efficiency of an existing building, not conforming to current standards or damaged by an earthquake, is desirable in terms of environmental sustainability, rather than recourse to the demolition and reconstruction of the entire building.
Even though flat slab structures are without a specific design and detailing regulation, nowadays many buildings use this construction typology. It is possible to find flat slabs in commercial, office, industrial, residential buildings and carparks. In the increasingly instable global conditions it is fundamental to be able to restore existing buildings. Depending on the damage entity, the damage location and the financial means available, there exist different solutions for structural strengthening, ranging from the more invasive to the least, maybe without even the need to evacuate the structure.
In order to clarify flat slab design rules and to establish a specific design code, several experimental studies have been carried out and a specific section of this dissertation examines the state of the art for these tests. Many tests regard the isolated slab column connections, fewer the single flat slab floor and even fewer that of a complete building. The main reason for this lack of tests on actual scale building is due to the limitations imposed by its dimensions, in fact it is frequently impossible to build and to test a whole building inside a laboratory. The related costs are another important factor, limiting this type of research.
The SlabSTRESS project was developed to satisfy this need. The contribution of this dissertation covers several aspects of the project with the final aim of studying the behaviour of a real scale flat-slab building. Due to the huge number of sensors installed (200 channels) the first contribution of this dissertation consisted in the design and in the execution of the calibration of the measuring instruments. This

procedure has demonstrated its importance in reducing errors in measurements and allowed to achieve recorded data of good quality. Successively, it was necessary to design and develop a methodology that allowed the elaboration of this mass of data. All the recorded data was organized in a database. Finally, an assessment procedure was developed to correlate global and local measurements. The local measurements were compared with each other in order to study the effects of the different features characterising the mock-up: different layouts of longitudinal reinforcement (smeared and concentrated), presence or absence of punching reinforcement, effects of local strengthening. All the reported analyses were critically described and the outcomes of this process compared with the results available in literature.

1.3 Research needs and Objectives

SlabSTRESS is an experimental program carried out on an actual scale, two storeys, flat slab structure having seismic resistant walls, under combined gravity and lateral loads. The testing of the building complements the knowledge of experiments on isolated slab-column connections, extending this knowledge to the entire structural system, while gaining information about the stiffness and deformation capacity.

The main objectives of this works are:

- Due to the lack of studies on tests on real-scale buildings, a real scale flat- slab building was tested considering both gravity and lateral load. The aim is to understand the seismic response of a flat slab building, investigating both the overall behaviour and single connection response of the building, under real boundary conditions;
- Experimental results on flat-slab single floor or entire building with a seismic-resistant primary system do not exist. In the SlabSTRESS seismic tests the presence of numerical walls as primary seismic elements was introduced to experimentally explore for the first time (albeit only in hybrid mode) the interaction between flat slabs and a primary seismic system;
- Tests on single slab-column connection lead to internal forces in the slab near to the column which can differ from those in a real building configuration. By carrying out a test on a complete building this allows to consider the realistic boundary conditions of the critical zones in the slab close to the column, to consider the membrane effect of the slab and also the size effect on a specimen of realistic dimensions;
- Flat slab frames are characterized by a concentration of bending moments and shear forces near the column and by a complex structural behaviour under lateral loading. When testing a single slab-column connection it is not possible to have a global vision of what consequences the local response will have on the behaviour of the single floor and of the entire building. Tests on

a real-scale, flat-slab building allow to understand the behaviour of the connections; which connection typology fails first, how the system redistributes internal forces and damage and whether the flat slab floor collapse occurs;

- Few studies have considered the influence of the longitudinal reinforcement arrangement so in SlabSTRESS two different longitudinal reinforcement layouts (smeared and concentrated) were collocated;
- No tests exist on slab-column connections to real scale flat slab frames that had been strengthened after the seismic damage and were tested again. In SlabSTRESS this was done to study the effect of reinforcement on the response of the flat-slab buildings when submitted to cyclic loads, in terms of stiffness and deformation capacity assessment;
- Providing a benchmark study for the development of models;
- The current European seismic design code Eurocode 8 [6] offers general guidance and regulations for secondary seismic members, but it does not regard flat slabs as part of the primary load resisting system. On the contrary, the draft of the new Eurocode 8 contains provisions to verify flat slabs as primary seismic elements but does not provide any indication to verify flat slabs when considered as secondary elements. This project was developed following a design approach for flat slab frames considered as secondary elements with primary ductile walls. The testing carried out in the program up to near-failure conditions provides indications on the ultimate drift capacity as well as giving some insight into the response of flat slabs as seismic resistant elements;
- From the obtained results, experimental evidence was provided by the response of this building typology with the purpose of developing the European seismic code for this typology of structures and to verify whether the design method could be considered to be correct.

1.4 Procedure

All the objectives previously described (1.3), were achieved by following the steps that are described in this work.
The SlabSTRESS experimental campaign was performed at the ELSA Reaction Wall of the European Commission's Joint Research Centre (JRC) in Ispra (VA) in accordance with the transnational access activities of the SERA project.
The design of a real scale, two storeys, flat slab building was produced. The structure comprised a traditional reinforced concrete building with two flat slab floors supported on twelve columns on each floor. One of the two floors was provided with shear reinforcement.

Due to the lack of regulations for the seismic design of flat slab structures, the SlabSTRESS building was designed, considering the flat slabs as secondary seismic members with seismic resistant walls as primary ductile elements. The two elements having different stiffnesses, and as prescribed in the EC8 [6] the total contribution to the lateral stiffness of the secondary seismic members should not to exceed 15% of that of the primary seismic members.
The structural design was that of a structure bearing gravity loads and able to reach a given lateral inter-storey drift with moderate-high seismic lateral actions in presence of seismic resistant walls. This design procedure was inspired by the design method used in the North American codes for the seismic design of "non-participating" i.e. secondary flat slabs.
The primary seismic walls were not actually built in this structure but were virtual elements, simulated by a pseudo-dynamic procedure, carried out using the reaction wall facility at the ELSA laboratory.
A specific design was made for the columns, with RC column portions above and below the slab, and a structural steel stub in the middle of the column, for measuring internal forces and bending moment.
After the design and construction, the structure was submitted to a testing program. The experimental campaign was divided into two different phases each of them was characterised by a different typology of test and with a different aim.
During the first phase seismic loading was applied, using the pseudo-dynamic technique with non-linear substructuring for two levels of seismic activity, the service limit state (SLS) and the ultimate limit state (ULS).
The pseudodynamic (PsD) testing method is a hybrid technique based on an equation of motion formulated for a discrete number of degrees of freedoms (DoFs), integrated in time, using appropriate numerical schemes [9]. The seismic response of large-size specimens can be obtained from the combination of the experimental restoring forces with the analytical inertia and seismic-equivalent forces. The method is based on a formulation that combines a numerical model for the inertial and external forces with an experimental model for the restoring forces.
Successively, during the second phase two cyclic tests were carried out to test the floors for gravity and lateral cyclic loading of increasing amplitude, up to near-failure conditions. Prior to the second cyclic test some of the damaged connections were strengthened and were tested again.
The recorded signals were then processed in order to characterise both the global behaviour and the local behaviour of slab-column connections.

1.5 Work organisation

The dissertation is presented in ten chapters.

The first chapter, in which the flat slabs are presented with the advantages and disadvantages of the application, in the current legislative scenario. The chapter

follows with the description of the main objectives of the work and with a description of the procedure followed to reach these ends.

The second chapter contains the State of the Art of flat slab experimental studies. Three different levels of the structure in a flat slab system are identified, from the simplest to the most complex. The first one is the isolated slab column connection; then there is the single flat-slab floor and finally the complete building, comprising a minimum two storeys. For each of these level, the experimental works available in the literature are analysed critically, using tables and graphs to collect and summarise the data. A final section presents relevant models for the resistance and rotation at failure of the connections.

The third chapter provides a thorough description of the SlabSTRESS project presenting the conceptual design of the specimens, the description of their geometry and materials. Details of the reinforcement and the repair procedures are also given.

The fourth chapter presents the experimental campaign, the facility that hosted the tests, the utilized instrumentation, the test programme and the test setup. An in depth description of the calibration procedure of the utilised instrumentation is presented, with a description of the procedure followed, the analysed quantities and the obtained results.
The chapter concludes with the description of each test in the experimental campaign, the two seismic and the two cyclic, with a special section dedicated to the pseudo-dynamic procedure.

Chapter five illustrates the methodology applied to the SlabSTRESS results for a detailed analysis of the obtained results. The inter-storey drift ratio is used as main kinematic parameter to describe the global behaviour, while columns and slabs rotation are used on site. Moreover, the force at each floor and the parameters acquired using the load cells steel member systems, located at the centre of each column are the static parameters, used to analyse the global and the local response respectively. Composite indicators, that combine static and kinematic parameters have also been used.
After a broad description of the analysis that allowed to consider the rotation as a valid parameter, the conversion factors, to convert the inter-storey drift ratio to the column-slab rotation, have been derived in function of the slab-column connections typology. The final aim of the developed methodology is to compare SlabSTRESS results with the experimental results obtained in the past, mainly on single slab-column connections, together with the simplifications of those numerical analyses, in which the inter-storey drift is known but the corresponding rotation is unknown.

The sixth, the seventh and the eight chapters contain a detailed analysis of the experimental results, following the sequence of the tests in the experimental campaign. Both the results of the seismic tests Seis-SLS and Seis-ULS are described in the fifth chapter, whereas for the two cyclic tests Cyc-1 and Cyc-2, a single chapter

for each is dedicated.

The ninth chapter provides a comparison between the experimental results and the literature results. The SlabSTRESS results are compared, evidencing their innovative aspects.

The tenth chapter draws the conclusions and provides indications for future works.

The dissertation has three appendices. The first appendix contains details regarding the slab gravity design. In the second one the column design is reported. The description of the additional load for the tests is given in the last appendix.

1.6 Concluding remarks

Testing a sole building of limited number spans and floors does not allow to cover all the aspects and design parameters of a flat slab building. These structures are employed for floors with many bays e.g. In commercial centres; multi-storey office or residential buildings; high-rise buildings. In relation to the span, different slab thicknesses, column sizes and column-thickness ratios, etc. are employed. One sufficiently simple structural typology was chosen for the SlabSTRESS tests, compatible with laboratory real-scale testing. Some attention was given to common design choice of several countries of Europe – although different choices may be made.

Figure 1.6 Example of flat-slab building in Milan [1]

The study provides extensive data describing the response to gravity, seismic and lateral cyclic loading, parting from the initial response to near failure conditions; this

can be used to calibrate models and provide ways in which to study other typologies. The comparison with scaled specimens and individual connections taken from the literature, is essential to validate or extend the knowledge gained from these types of tests, in order to develop essential new design rules and standards.

References

[1] https://www.peri.it/progetti/grattacieli-torri/porta-nuova-varesine-milano.html

[2] R., Park and W. L., Gamble. Reinforced Concrete Slab. John Wiley & Sons, inc. (2000)

[3] P. G. gambarova, D. Coronelli, P. Bamonte, “Linee guida per la Progettazione della Piastre in C.A.” PERI, Patron Editore, Bologna, 2007, 118 pp.

[4] M. N., Fardis. Seismic design, assessment and retrofitting of concrete buildings based on Eurocode 8. Springer.

[5] R. Zaharia, F. Taucer, A. Pinto, J. Molina, V. Vidal, E. Coelho, P. Candeias. Pseudodynamic Earthquake Tests on a Full-Scale RC Flat-Slab Building Structure. 2006.

[6] CEN (European Committee for Standardization). 2004. Design of structures for earthquake resistance, general rules, seismic actions and rules for buildings part 1. Eurocode 8, Brussels, Belgium: CEN

[7] CEN (European Committee for Standardization). 2004. Design of concrete structures, general rules and rules for buildings part 1.1. Eurocode 2, Brussels, Belgium: CEN.

[8] NTC2008 - Norme tecniche per le costruzioni 2008 (NTC 2008) - D.M. 14 Gennaio 2008 (D.M. 14/1/08) – in Italian.

[9] F. J. Molina, G. Magonette, P. Pegon, B. Zapico (2011). “Monitoring damping in psudo-dynamic tests.” Journal of Earthquake Engineering, 15:6, 877-900.

2 Flat slab frame tests, State of the Art

2.1 Introduction

Many studies on flat slab and flat slab RC buildings have been carried out in North America, whereas European research is lagging behind (Fardis, 2009 [1]; Coronelli, 2010 [2]). The European Code EN1998.1 [3], prescribes in 5.1.1(2): "Concrete buildings with flat slab frames used as primary seismic elements in accordance with 4.2.2 are not fully covered by the EC8 [3] section on concrete structures". This statement stems from a lack of knowledge about the stiffness of the slab-column connections and the potential brittleness of the punching failure under seismic actions, showing the need for further research on the resistance under cyclic and dynamic horizontal loading.

Flat slab construction for low-rise buildings is common in many European countries with a high seismic risk. Fardis (2009) [1] shows the importance of developing studies so that "the cost-effectiveness and seismic performance of earthquake resistant concrete buildings will benefit from the rational use of flat slab frames as part of the lateral-load-resisting system". Fardis (2009) [1] proposes the use of flat slabs as secondary seismic elements designed according to Eurocode 2 [4], in order to bear the gravity loads in correspondence of the lateral drift imposed by the primary seismic system (e.g. shear walls), without contributing to the lateral load-resisting system. Other scholars have also advocated the introduction, within the European seismic regulations, of the possibility to adopt slab floors also in seismic areas. Pinto et al., 2007 [5] indicate flat slab design as one of the topics deserving pre-normative research for EC8 [3], on the base of experimental research conducted at JRC ELSA (Zaharia et al., 2006) [6].

The North American research and codes provide extensive scientific literature, code regulations and design rules (ACI-ASCE committee 421, 2010; 2015 [7]). ACI 318 [8] stipulates that these systems can be used as seismic-resistant systems ("intermediate moment frames") with appropriate construction details in areas of moderate seismicity. In areas of higher seismicity, however, slab-column frames without beams are not generally permitted as part of seismic-force-resisting systems, (i.e. secondary systems bearing the gravity loads, using the EC8 [3] definitions). Strength assessments are combined with deformability assessments.

Experimental results show that, even in the absence of punching reinforcement, the slab-column connection can potentially achieve significant deformation capacities, inversely proportional to the shear force of the connection due to gravity load alone, and much controlled by the size of the supported area of the slab and the amount of

flexural reinforcement at the connection. That deformation capacity increases significantly in the presence of shear-punching shear reinforcement. Based on a large database analysis, the standard ACI 318 [8] defines the ultimate deformation capacity of slabs without transverse reinforcement as a function of the ratio between the shear demand of the connections due to the gravitational load, too, and the punching shear capacity the Gravity Shear Ratio (GSR).
The widespread and growing use of RC flat slabs in many European seismic countries with relevant seismic action, and the lack of specific provisions in the Eurocode 8 [1] require detailed and deeper study about this building typology.
The State of the Art of flat slab experimental studies is reported here. Three different levels tests could be identified, from the simplest to the most complex. The first one is the isolated slab column connection; then there is the single flat-slab floor and finally the complete building, comprising a minimum of two storeys. The experimental works available in the literature are analysed critically at each of these levels. This provided a basis for the comparison with the SlabSTRESS results at the end of this dissertation.
A final section presents relevant models for the resistance and rotation at failure of the connections. these will then be applied in Chapter 0 to provide some interpretation of the results.

2.2 Experimental works

The experimental research on the slab system can be sorted into three different levels of the structure, from the simplest to the most complex. The first level is the isolated slab column connection; followed by the single flat-slab floors; and finally the complete building at least two stories high.
The choice of the size of the test specimens is determined by the laboratory dimensions, because it is frequently impossible to test a whole building. This is the main reason why much work has been done on the behaviour of isolated slab-column connections, but less on a complete scale size floor that would require a laboratory of a certain size. Hwang and Moehle, 1993 [10], Hwang and Moehle, 2000 [11], Rha et al., 2014 [12] and only three tests on the whole structural system (a full-scale test: Fick et al., 2017 [13]; two scaled frames: Moehle and Diebold, 1984 [14]; and two under seismic loads using a shaking table: Kang and Wallace, 2004 [15], Moehle and Diebold, 1984 [14]), but there are not many laboratories with such large dimensions.

2.2.1 TESTS ON ISOLATED SLAB-COLUMN CONNECTIONS

The behaviour of isolated slab-column connections under combined gravity and lateral loading is a topic that has raised much interest in the scientific community. Due to its conformation, the flat-slab structure is subject to brittle punching shear failure in the connection between the slab and the column, so many studies in the literature investigate their behaviour and design (Hawkins and Mitchell, 1979 [17], Pan and Mohele, 1987 [18], Robertson et al., 2002 [19], Dovich and Wight, 2005 [20],

Kang and Wallace, 2006 [21], Hueste et al., 2007 [22], Drakatos et al., 2016[23], Almeida et al., 2019 [24], Almeida et al., 2020 [25], Gouveia et al., 2019 [26], Isufi et al., 2019 [27], amongst many others). Works available in the literature mainly regard the internal connections; few results are also available for edge and corner connections [30], [31], [32].
These studies show the different failure modes that may occur in a slab-column connection subjected to gravity and lateral loads, flexural, punching and mixed flexural-punching [22] and define the gravity shear ratio between the acting vertical shear force and the punching shear resistance (ACI 318-14 [8]).
Hueste et al., 2007 [22] reported the relation between the ultimate drift capacity and the gravity shear ratio. From those tests, it is possible to note that larger gravity shear ratios imply lower deformation capability (horizontal drift) and that larger horizontal drift ratios are achievable when shear reinforcement is used.
These test typologies on isolated connections (internal, edge or corner) have the drawback that the boundary conditions may not accurately represent actual moment distribution and redistribution in multi bay slab column frames (Einpaul et al., 2015 [28], Einpaul et al., 2016 [29]).

2.2.2 TESTS ON SINGLE FLAT-SLAB FLOORS

A flat-slab floor includes several internal, corner and edge connections. Some reported works analysed scaled specimens; Hwang and Mohele [10] [11] tested a slab specimen constructed at 40% of a full-scale floor, whereas Rha et al. [12] investigated samples at about half-scale of the prototype structure.
The specimens tested in these two works have rectangular panels with similar spans, column size and slab thickness.

HWANG AND MOHELE, 1993

Hwang and Mohele [10], [11] tested four different column geometries (reported in Figure 2.1) to collect data related to effects of column regularity, and the reinforcement layout was varied in the slab-column connections.

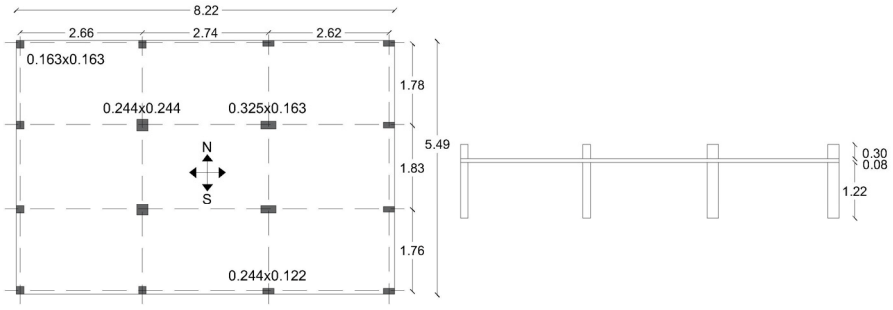

Figure 2.1 Specimen geometry - Single flat-slab floor (m) [10], [11]

Design

The RC flat-plate frame was designed as secondary system in accordance with ACI 318-83 to carry combined gravity and lateral load. The gravity load effects were analysed using the Direct Design method moments (ACI 318-83). The lateral load effects were analysed using a frame model considering only the column strip, increasing steel reinforcement by 50% with respect to that required by gravity loads. In half of the slab, moment redistribution was considered, reducing the top layer steel at supports by up to one third. The columns were designed in conformity with the seismic design in a zone of moderate seismic risk.
As reported by the authors, all the connections have a gravity shear ratio (GSR) of 0.3.

Test setup

Amongst tests on flat slab floors, this is the only one with biaxial lateral loading.

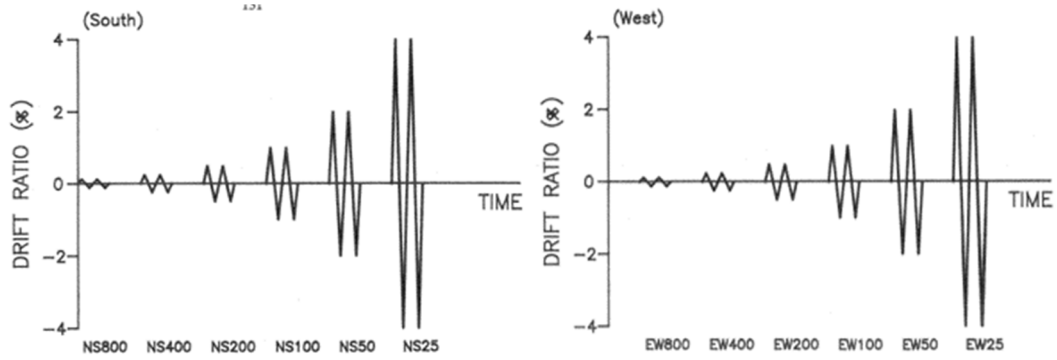

Figure 2.2 Lateral displacement histories [10], [11].

The lateral load was transferred to the slab by a perimeter steel frame, with compression forces on alternate sides in each orthogonal direction. The column portions beneath the slab developed shear and moment. A biaxial cyclic displacement history of increasing amplitude was imposed, with lateral drifts from 0.25% to 4%. The gravity loads consisted of the slab weight and additional lead blocks distributed on the upper surface.
All columns were pinned at their base to collect data on the three force components of the bearing forces. In this way, moment-drift relations for the joints could be determined in addition to the global response. The occurrence of punching was determined by observations of cracking during the test and post-processing joint moment-rotation diagrams.

Measuring device for local actions

Sixteen reaction transducers, one for each column, measured the vertical axial load and horizontal shears loads in three orthogonal directions. Each reaction transducer is a tripod consisting of a spherical bearing connector supported by three inclined steel legs. Therefore, this set-up did not require any measurement of bending moment.

Results

Figure 2.3 shows the entire response history up to failure for the test. The global response followed a first relatively stiff branch up to a drift of 0.5%. After the drift of 1%, the test slab displayed a relatively plastic response up to a drift of 4%. It reached the maximum load in the first N-S cycle at 4%, while the following first cycle at 4% in E-W showed a drop in lateral load with respect to the previous 2%.

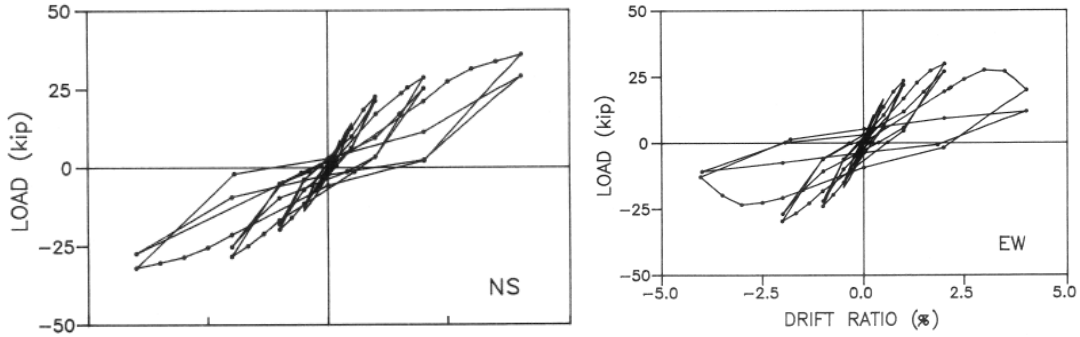

Figure 2.3 Load-Deflection response to failure [10], [11].

From the moment-drift relation of each connection, a progressive yielding in the response was deduced, this being typical of flat slab connection response [18].
The test setup allowed the measurement of the moment-drift relation for each connection. The response showed a progressive yielding in the response, as is typical of flat slab connection response [18]. The authors highlight a plastic branch in the cycle envelope curves approximately between 1% and 4% drift.

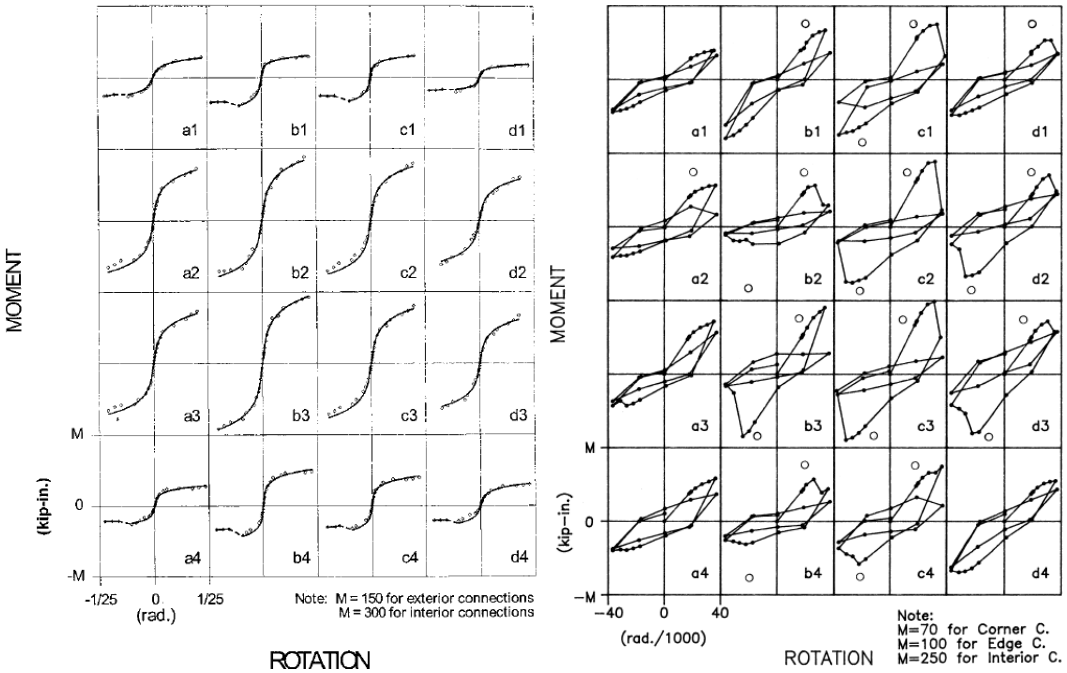

Figure 2.4 Moment- rotation curves [10], [11].

The authors make a distinction between joint resistance and punching failure. The

first one is defined as the reaching of the maximum unbalanced load, the latter as the failure that occurred at higher drift values and lower unbalanced moment identified by visual observation of the formation of the punching cracks.

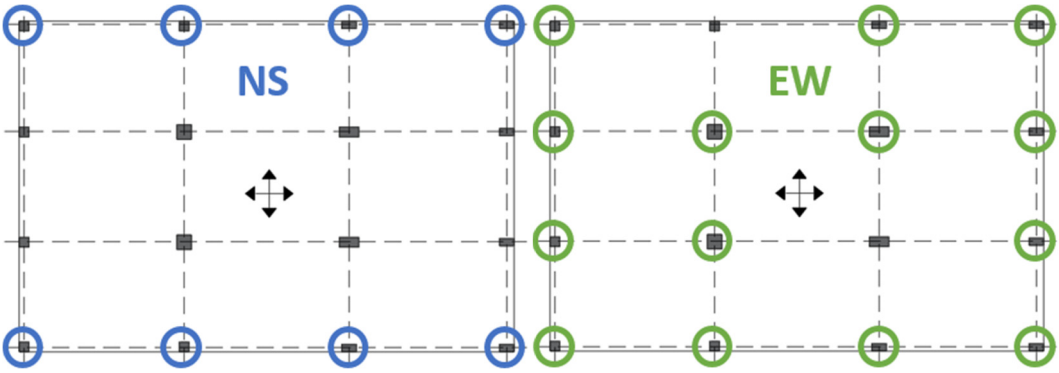

Figure 2.5 Maximum unbalanced moment in the connections ±2%.

The resistance of the connections (Figure 2.5) was reached first on the edges and corners in the +/-2% drift cycles in the N-S direction. The same occurred in the lateral and corner connections during the following +/-2% E-W cycles, with three out of four of the internal connections reaching their resistance as well.

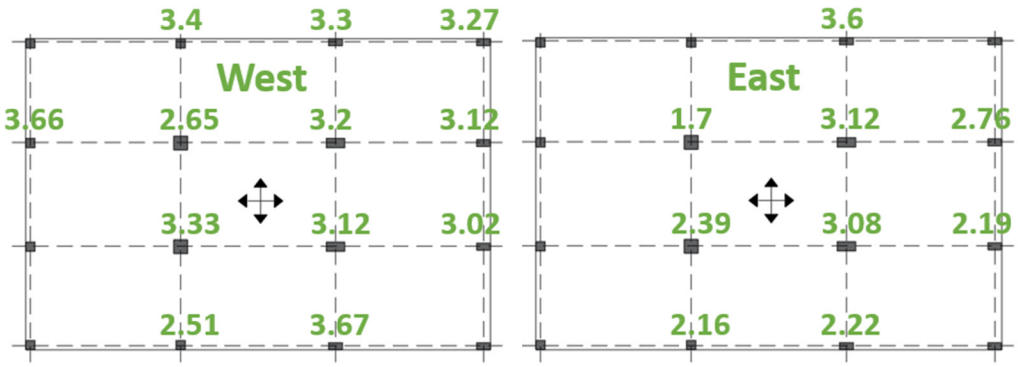

Figure 2.6 Punching in the connections, numbers indicate drift ratio (%) at punching.

The punching of several connections (Figure 2.6) occurred in the +/-4% E-W cycles, at drifts between 3.1% and 3.7%. Both internal and edge connections punched, but only one in a corner. A progressive cracking of the different connections was observed during the experiments; the lateral and internal punched connections showed the typical failure surface on the extrados around the column. Lateral connections showed wide torsion cracks on the sides of the slab at the connection with the column. Once most of the connections failed, the slab was still capable of supporting the gravity loads and the values of the shear forces were close enough to the initial values.

RHA ET AL., 2014

Rha et al. [12] present an experimental work on thin two-way continuous flat plate

systems, all the columns having the same dimensions with three different gravity shear ratio depending on the column position; corner columns, 0.21, lateral columns, 0.28, internal columns 0.44.

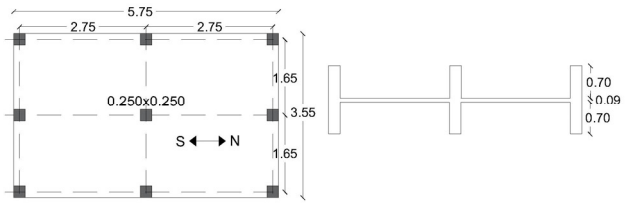

Figure 2.7 Specimen geometry - Single flat-slab floor [12] (m).

Design

The slab reinforcement for the scaled specimen was of three different typologies called S1, S2 and S3. The S1 configuration of slab reinforcement is a typical representation of a slab-column moment frame according to the direct design method (ACI 318-11, section 13.6). The S2 and S3 configuration have a larger top reinforcement ratio with S3 that has additional continuous bottom bars at each connection. The first reinforcement configuration was used for testing with gravity loading only, the second for tests with gravity loading, lateral monotonic (LM) and lateral cyclic (LC) loading and the last for testing with lateral monotonic loading only.

Test setup

The gravity loading for lateral loading tests was imposed by concrete blocks piled on the slab top surface.

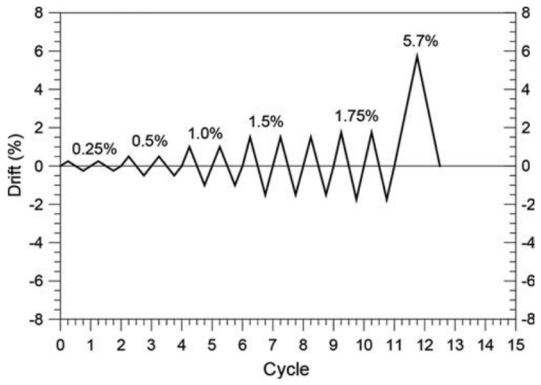

Figure 2.8 Loading cycles for LC-S2 [4].

The slab with half-column members above and below; the load was transferred by a steel frame linking the column tops to an actuator (supported independently in order not to impose its weight on the columns).

Measuring device for local action

The lateral forces were measured at the top of each column, while the vertical

reactions at the base, using horizontal and vertical load cells. Lateral force-drift diagrams are given for each column, and the vertical force readings at the column bases for gravity loading and at failure were provided.

Results

The three different test typologies reached all the global maximum lateral loads for drifts between 4% and 6 % (Figure 2.9).

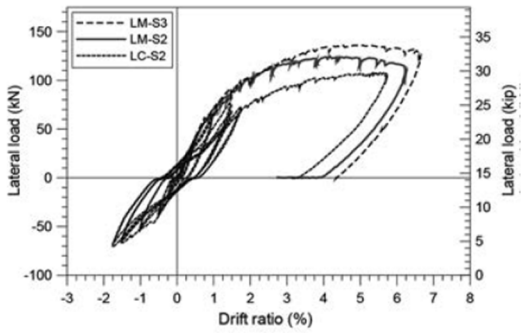

Figure 2.9 Load versus drift ratio comparison for the three tests [4].

Two identical specimens were tested, one for lateral monotonic load (LM-S2) and one for cyclic lateral load (LC-S2) up to the first punching failure followed by monotonic lateral loads.

The ultimate drift of the structure was close to 6% in both tests, the cyclic test (LC) reaching a lower maximum load. With cyclic loading (LC), the internal joint (C5) was the first to punch at 1.5% drift (Figure 2.10 b), while the failure in this location with monotonic loading (LM) occurred at 5.5% drift (Figure 2.10 a).

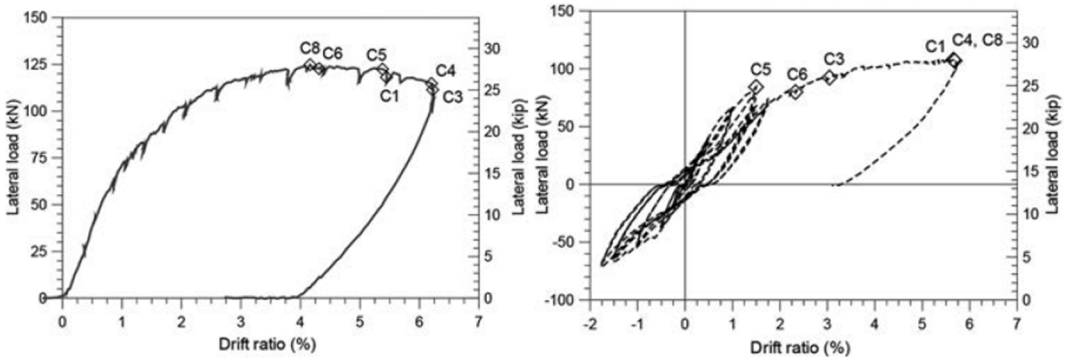

Figure 2.10 Load-Drift ratio relations with the connections punching failure, a) LM and b) LC [4].

In addition, some of the lateral joints (C6) failed in the cyclic test at drifts lower than in the monotonic test. This can be explained by damage accumulation.

In all tests, the response up to the drift capacity showed a progressive sequence of joint failures at different drift levels, with one or groups of two or three joints failing together distanced by drift increases of 1-2%.

The reported damage shows radial cracking around internal and lateral columns, and

torsional cracking on the sides of the slab at corner columns.

2.2.3 TESTS ON FLAT-SLAB MULTI-STOREY FRAMES

Three different works are analysed.

FICK ET AL., 2017

Fick et al. [13] studied a full-scale three-story, two-bay reinforced concrete flat-plate frame designed to resist gravity loading. The overall slab dimensions were 9.1mx15.2m with a thickness of 180mm. The six columns all had the same geometry and dimensions: squares of 460mm spaced 6.1m apart in both directions, and 1.5m overhangs enclosed the perimeters. Each storey had a height of 3.0m for a total measurement of the tested structure of 9.1m above the footings.

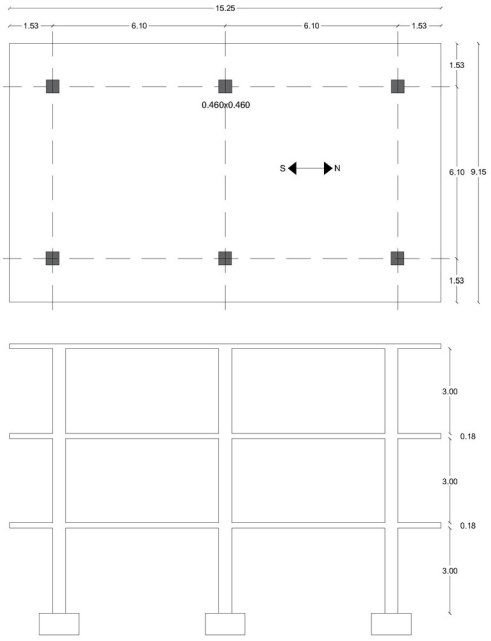

Figure 2.11 Specimen geometry – Flat-slab multi-storey frame [13] (m).

The authors reported only one value for the gravity shear ratio of 0.21 but edge and corner columns have different tributary areas so it should be appropriate to make a distinction. These different values are calculated and are compared with the authors' values in the table.

Design

The design was made with the aim to study the performance of existing structures using the direct method according to ACI 318 (2002). The authors did not consider the seismic zone.

Test setup

The structure was tested to failure under cycles of increasing quasi-static lateral displacement imposed on the top floor, with forces acting on the other floors controlled to vary linearly with height. The gravity load was applied from a tank filled with water. The lateral load was transferred by steel framing connected to the sides of the slab floors at the centreline.

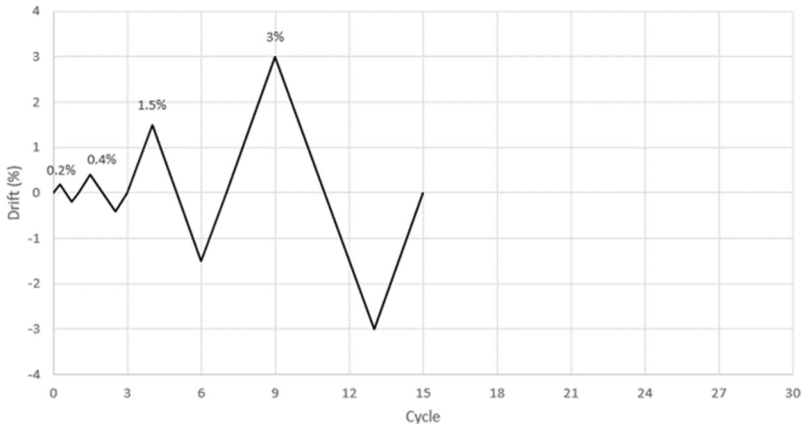

Figure 2.12 Drift pattern used in the test [13].

The lateral force-drift relations were measured for each of the three storeys. The authors also submitted photographs, with drawings of the cracks in the connections and in the columns.

Measuring device for local action

No local measurements were recorded.

Results

A linear response was observed during the first cycle to a mean drift ratio of 0.2%. Flexural cracks appeared in both first- and second-storey columns during the second cycle of loading to a roof-drift ratio of 0.4%. In the successive load cycles, the imposed drift increased and the nonlinear response also increased, with both slab and column cracking. During the tests, the structure suffered very limited damage up to a mean drift ratio of 1.5% whereas at a mean drift ratio of 3.3% north, one of the internal slab-column connections reached failure due to punching. The test was not continued beyond the occurrence of the first punching failure. This was characterised by a wide punching crack perimeter on the outer surface extending from 2d to 5d around the column, with a separation of the crack surfaces ranging from 5-20mm (Figure 2.13).

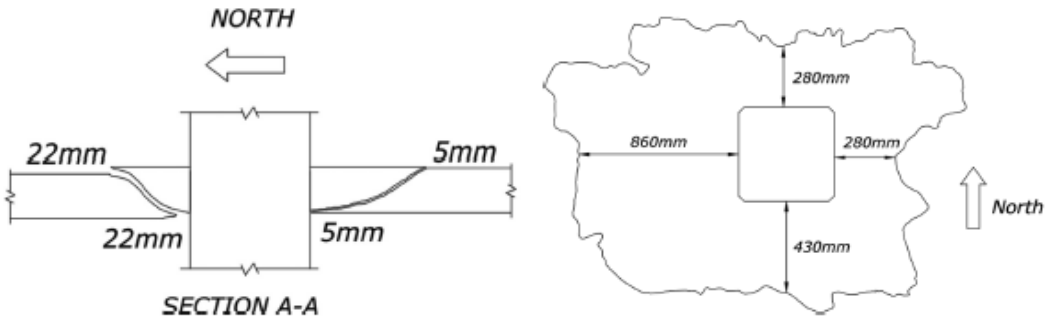

Figure 2.13 a) Vertical section after failure in punching shear and b) Dimensions defining boundaries of shear failure [5].

MOHELE AND DIEBOLD, 1984

Mohele and Diebold [14] studied a two-storey reinforced concrete flat-plate system built to three-tenths of the dimensions of a typical structure. The slab presented a different contour around the perimeter: a shallow beam with a depth of 107mm and width of 137mm on the two edges perpendicular to the test direction and overhanging on the other two sides. Authors do not report the gravity shear ratio.

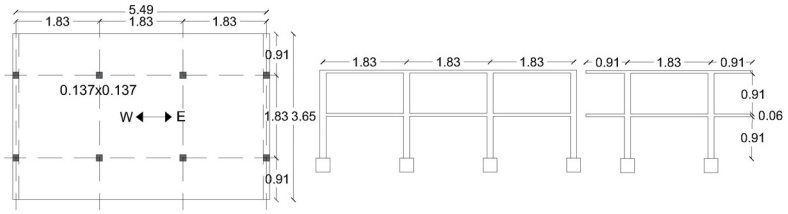

Figure 2.14 Specimen geometry – Flat-slab multi-storey frame [14] (m).

Design

The structure was a primary slab frame located in seismic zone 2, according to UBC 1982 and designed to support combined gravity and seismic loads with ACI 318-83. The moments due to gravity loads were determined used the direct design method, whereas the lateral load effects were analysed using a frame model considering only the column strip. Load combinations showed that the design of the slab was controlled by the gravity loads, though the seismic combination produced comparable internal forces and moments.

Test setup

Some lead blocks were added to the slab surface to define the gravity loading and to reproduce the correct magnitude of slab moments and shears. The acceleration histories recorded during the 1940 Imperial Valley earthquake were used for the test. The structure was tested with eleven base motions of successively increasing intensity from 0.012g to 0.83g. The action was both lateral and vertical in four runs. The dynamic response of each floor was measured recording acceleration and

displacements.
Transducers located at the base of each column measured shear and moment in the foundations. The damage was reported photographically and by visual observation (manual reporting on paper for the crack pattern in the slab and columns).

Measuring device for local action

Eight shear and moment measuring transducers supported the footings, connecting the structure to a steel foundation frame which was fastened to the shaking table during the experiment. Transducers were made with a rectangular hollow steel section, welded in the centre of end plates, and with two vertical plates welded close to the edges of end plates along the main axis of the experiment. Two strain gages were applied on vertical plates to measure flexure, while two other measured shear on the hollow core stub. The transducer was not designed to acquire axial load, authors report the base shear only and no bending moment measurements. A detailed evaluation of the stiffness variation introduced by transducers was performed.

Results

The structure did not develop significant non-linearity in the overall load displacement relationship until drifts reached approximately equal to 1.5% of structure height, after which the structure displayed a relatively plastic response to lateral drifts exceeding 5% of structure height, without reaching collapse.
Regarding the connection response, cracking of the slab surface around the columns spread with the increasing intensity of the runs. After the last run, a column penetration of 1-2 mm was observed at the internal connection, indicating a possible incipient failure. The exterior slab-column-spandrel showed spalling of concrete of the beam at a lateral drift of 5.5% of specimen height. The exterior connections continued to support load at increasing drifts. The second-floor slab damage was less severe than first-floor damage, apparently because the slab was stronger than the columns on the second-floor level, which suffered from evident cracking.

KANG AND WALLACE, 2004

The last analysed test conducted on a shaking table is by Kang and Wallace [15]. They studied two different reinforcement typologies: a conventional reinforced-concrete (RC) two storey flat plate frame, and a post-tensioned (PT) slab-column frame incorporating shear reinforcement. Shear reinforcement for the RC and PT specimens consisted of stud-rails satisfying the requirements of ACI3 18-02 and ACI 421.1R-99. Due to the dimensional limitations of the shaking table, a scale factor of approximately one third of typical buildings was used for both specimens (RC and PT), resulting in a relatively thin slab (89mm and 73mm respectively).

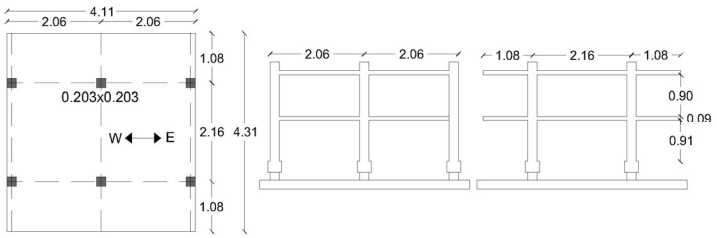

Figure 2.15 Specimen geometry – Flat-slab multi-story frame [15] (m).

The authors reported only the gravity shear ratio for the RC specimen, that is 0.25 for the internal columns and 0.20 for the edge ones.

Design

The structure was designed according to ACI 318-02 and was located in a zone with high seismicity (zone 4). The aim of the project was to strengthen the longitudinal reinforcement that yielded before punching. Stud shear reinforcement was placed in cross layout ACI 421.1R (1999) spaced at 0.5d = 35 mm, extending 4d from the column face to prevent failure outside the shear reinforced zone.

Test setup

Weights were added to the slab surface with the aim of controlling the gravity shear ratio that has to correspond to the design. The ground motion of the September 21, 1999, earthquake in Taiwan was selected. The signal was scaled to obtain this in five subsequent runs with maximum lateral accelerations from 0.11g to 1.25g. The action was lateral along one direction.

Measuring device for local action

Reactions at the column bases were recorded using triaxial load cells. Story shear and moment, floor displacement and accelerations were used to study the global response. Regarding the local joint response, slab and column reinforcement strains were used to obtain moments and curvatures in these members and to study punching failure.

Results

Storey shear versus inter-storey displacements relations indicate that the inter-storey drift capacities at punching range between 2.5% and 3.4% for the RC specimen, and 2.8% to 4.3% for the PT specimen.
Damage was more significant and more widely distributed in the joints of the RC structure than in the PT specimen.
Despite the fact that the use of slab shear reinforcement reduced the extent of damage, punching failures occurred at significantly lower drift ratios than was expected. The authors also observed that the reduced drift capacity might be due to loss of shear capacity at the column-slab interface (deterioration of the zone between the concrete and the first shear reinforcement unit), a phenomenon which was not

observed in the quasi-static tests in the literature.

2.3 Comparison between flat slab building tests for gravity and lateral loading

The comparison between all the previous analysed tests is made here focusing on both the configuration and scale of the specimens, the reinforcement layout, the type of loading and response results.

2.3.1 GEOMETRY AND DESIGN

The analysed tests present buildings with several differences: in the span dimensions, in the panel shapes, the presence or not of overhangs, in column size, single o multi-storey frame. In Table 2.1 the tests are grouped based on the same characteristics of test typology, prototype scale and the number of storeys.
All specimens but one are scaled to 30-50% of the prototype, panels are either square or rectangular, one test considers edge beams orthogonal to the loading direction, three tests include overhangs on two or four sides of the slab which determine a particular configuration with connections that can be considered as internal if the portion of the slab surrounding the column is sufficiently large (Park and Gamble, 2000 [16]).

Table 2.1 Tests description.

Author	Test typology	Scale	Nr. of Floors
Hwang and Moehle	Cyclic quasi-static (biaxial)	40%	1
Rha et al.	Cyclic/Monotonic quasi-static	50%	1
Fick et al	Cyclic quasi-static	100%	3
Moehle and Diebold	Shake table (biaxial)	30%	2
Kang and Wallace	Shake table	30%	2

Comparing the geometry of the different tests in Table 1, the scaled specimens can be grouped in similar pairs: the two quasi-static campaigns by Hwang and Moehle, 1993 [10] and Rha et al. 2014 [12]; the two shaking table tests by Moehle and Diebold, 1984 [14] and Kang and Wallace, 2004 [15].
Table 2.2 reports a summary of the geometrical characteristics of all the previous analysed tests.
Span to depth ratios presented in the range 30-35 with the exception of one test with a ratio equal to 24 (Kang and Wallace 2004 [15]). The size of the columns relative to

the span ranges from 1/10 to 1/13. Most tests had square columns, one test varied the proportions of the column sizes and had different internal, lateral and corner columns (Hwang and Moehle, 1993 [10]).

Table 2.2 Test specimen geometry.

Author	Span L (m)	Span L' (m)	Span (#)	Overhang (m)	Slab thickness t (mm)	$\frac{L}{t}$	$\frac{L'}{t}$	Internal column c	Lateral, corner column c' (m)	$\frac{L}{c}$
Hwang and Moehle	2.7	1.8	3 x 3	-	81	33	23	0.24	0.16	11.3
Rha et al.	2.75	1.65	2 x 2	-	90	31	18	0.25	0.25	11
Fick et al	6.1	6.1	2 x 1	1.5 , 1.5	180	34	34	0.46	0.46	13.3
Moehle and Diebold	1.83	1.83	3 x 1	0.9	61	30	30	0.14	0.14	13.1
Kang and Wallace	2.06	2.06	2 x 1	0.9	89	23	23	0.2	0.2	10.3

From the previous comparison, it is possible to group the tests bearing the same characteristics of test typology, prototype scale and number of floors (Table 2.1).
All specimens but one are scaled to from 30% to 50% of the prototype and they can be grouped in two pairs: the quasi-static tests by Hwang and Moehle [10] and Rha et al. [12] and the shaking table tests by Moehle and Diebold [14] and Kang and Wallace [15].
Regarding the design (Table 2.3), all the specimens are based on the North American codes, whereas the punching shear verifications are carried out using the ACI 318 models (1983-2002). A primary element is defined as providing seismic resistance in a structure, whereas secondary elements are not considered part of the seismic action resisting system, rather they are designed to maintain support of gravity load when subjected to the imposed deformations related to the lateral actions.

Table 2.3 Design comparison.

Author	Design	Type of frame	Design notes
Hwang and Moehle	ACI 318-83, Prototype Structure high rise-building with secondary slabs, wind and seismic load effects calculated	Secondary	Different column sections
Rha et al.	Not specified	-	Different reinforcement arrangements (3 specimens)
Fick et al	Gravity Design – Direct Method ACI 318 (2002)	Gravity load design, without lateral load resisting elements	-
Moehle and Diebold	Prototype Structure Primary slab frame for Zone 2 UBC 1982 and ACI 318-03	Primary	Spandrel beams transverse to lateral actions. Load combinations results show that gravity shears and moments dominate. Strong columns relative to slab.
Kang and Wallace	Secondary slab frames for buildings with primary walls or frames, ACI 318-02, Zone 4 (high) seismic region	Non-participating for high seismic risk regions / intermediate frames in moderate seismic regions	Longitudinal reinforcement yield before punch. Strong columns relative to slab. Shear failure within shear reinforced zone.

The comparison showed a better performance of the specimen designed for seismic actions.

The global response in all the analysed tests reaches a drift level in a range between 3% and 5% which can be considered rather high. Each of these results is influenced by all the characteristics previously described (specimen dimensions, panel shapes, loading typology, single o multi-storey frame). The values reached in some tests are due to column deformation and damage.

Hwang and Moehle [10], the only test available in literature with biaxial loading, showed that this has a different effect in the two directions of the load application. In the first direction, the maximum load was reached for a drift of 4%, whereas the maximum drift reached was 2% in the orthogonal direction. This difference is due to the fact that the load was applied firstly in the North-South direction and then in the East-West one. The results show noticeable damage accumulation caused by the biaxial loading. During the first loading application, the North-South one reached the 4% of the global drift ratio without any loss but with some damage in the edge of the

slab. During the second East-West loading application, the structure reached the peak for a global drift ratio around 2%.
Comparing the tests with seismic actions, that of Moehle and Diebold [14] is the only one including a vertical component. From the comparison with the Kang and Wallace [15] work, no effects seem to arise from the biaxial load but more research would be needed in this field.
The shear reinforcement has shown to have a positive effect on damage limitation. The only test on slab-column connections with shear reinforcement (Kang and Wallace, 2004 [15]) reported different results but the ratio between span and slab thickness of the specimen was lower than all the other ones.
In all the specimens designed for seismic actions, the gravity loads could be carried after local punching of the slab-column connections. This could also be due to the relatively low GSRs chosen for all tests (Table 2.4).

2.3.2 GRAVITY SHEAR RATIO

The tests results were compared using the gravity shear ratio (Table 2.4). Studies on interior slab-column connections have shown that the increase of the shear force on the connection produces a diminished deformation capacity of this connection typology, therefore the gravity shear ratio is an important parameter when studying the capacity of flat slabs to resist cyclic lateral drift (Pan and Moehle, 1987 [18], Robertson and Johnson, 2006 [33], Pan and Moehle, 1992 [34]).
The gravity shear ratio is usually defined as the ratio between the acting vertical shear force (V_g) and the nominal punching shear strength (V_0) according to ACI 318-14 [8].
The acting vertical shear force (V_g) is defined as the product from the total load, the relevant surface and the correction coefficient function of the column position (internal, corner, lateral).
The nominal punching shear strength (V_0) is defined as the product of the nominal shear strength $v_c = \left(1/3 * \sqrt{f_c{}'}\right)$, the length of the perimeter at a distance d/2 from the column, and the average effective depth, d.
The comparison between the gravity shear ratio calculated using the information gathered from the reported tests and the values given by the analysed authors, is reported in the table below.

Table 2.4 Gravity shear ratio (GSR) comparison.

Author	Connection	Tributary length 1	Tributary length 2	Added load	Self-weight	Total load	coeff. (-)	Vg (kN)	c (mm)	d (mm)	fc (MPa)	V_o (kN)	V_g Test (KN)	V_g Test/ V_g	GSR (calculated)	GSR (literature)
Hwang and Moehle	Internal	2.74	1.83	5.8	2	7.8	1.1	42	244	69	21	131	33.4	0.79	0.32	0.3
	Lateral	1.35	1.83	5.8	7.8	13.6	0.9	18	160	69	21	65	13.4	0.76	0.27	-
	Corner	1.35	0.9	5.8	7.8	13.6	0.9	8	160	69	21	41	5.79	0.69	0.2	-
Rha et al.	Internal	2.75	1.65	9	2.3	11.3	1.3	63	250	70	26	152	61.2	0.97	0.41	0.44
	Lateral	1.5	1.65	9	2.3	11.3	0.9	25	250	70	26	106	27.5	1.1	0.24	0.28
Fick et al.	Internal	6.1	4.58	0.6	4.5	5.1	1.1	157	460	152	25	623	-	-	0.25	0.21
	Lateral	4.58	4.58	0.6	4.5	5.1	0.9	99	460	152	25	623	-	-	0.16	-
Moehle and Diebold	Internal	1.83	1.83	3.4	1.5	4.9	1.1	18	137	54	28	72	-	-	0.25	-
Kang and Wallace	Internal	2.1	2.1	5.7	2.2	7.9	1.1	38	203	70	28	134	-	-	0.28	0.25
	Lateral	1.15	2.1	5.7	2.2	7.9	0.9	17	203	70	28	92	-	-	0.19	0.2

Figure 2.16 compares results obtained in the tests described in this paper with those of the isolated slab-column connections analysed by Ramos et al. (2017) [35].

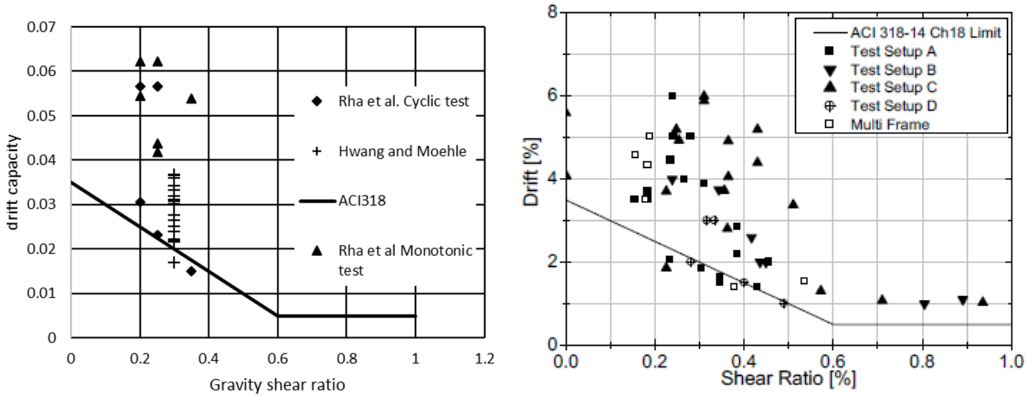

Figure 2.16 Results for floors with cyclic uniaxial (Rha et al [12]) and biaxial (Hwang and Moehle [10]) quasi-static loading (left) and for isolated slab-column connections (Ramos et al. 2017 [35]).

All the tests showed a non-linear global response reaching ultimate drifts with a lower bound of 3% and up to 6%. The gravity shear ratios were in most cases between 0.2 and 0.3 (Table 2.4). The response is characterised by a progressive spreading of damage and a sequence of failures in the different connections.
The test showing lower ultimate drift was made on the real scale multi-storey specimen designed for gravity loads only and with a low gravity shear ratio (Fick et al., 2014 [13]) but the test was interrupted after the first connection punched.
Cyclic lateral loading compared to the monotonic causes more damage and reduce ultimate drifts.
The two shaking table tests had similar proportions and gravity shear ratios (Table 2.4)., but several different features. The most relevant result is that the specimen using shear steel reinforcement reached lower ultimate drifts than the one without.

2.3.3 FAILURE

Figure 2.17 reports a summary of the geometry, the load application and the first connection to reach failure in two experiments on flat slab floors (Hwang and Moehle [10] and Rha et al. [12]) and for the multi-storey frame experiment by Fick et al [13]. As can be seen in the image above, the tests present different sequences of failure. In Hwang and Moehle [10], the connections on the edges were the first to fail, whereas in Rha et al. [12], for the specimen loaded by cyclic loading, the first failure was in the internal connections. In all the analysed tests, more than one connection did not punch.
Regarding the punching, tests on scaled specimens for cyclic and monotonic loading show an increase in the number of punched connections with the drifts rise. It is not possible to make a comparison with the real scale specimen because the test was interrupted after the first failure.

The use of monotonic or cyclic loading influences the drift at failure reached by the connections.

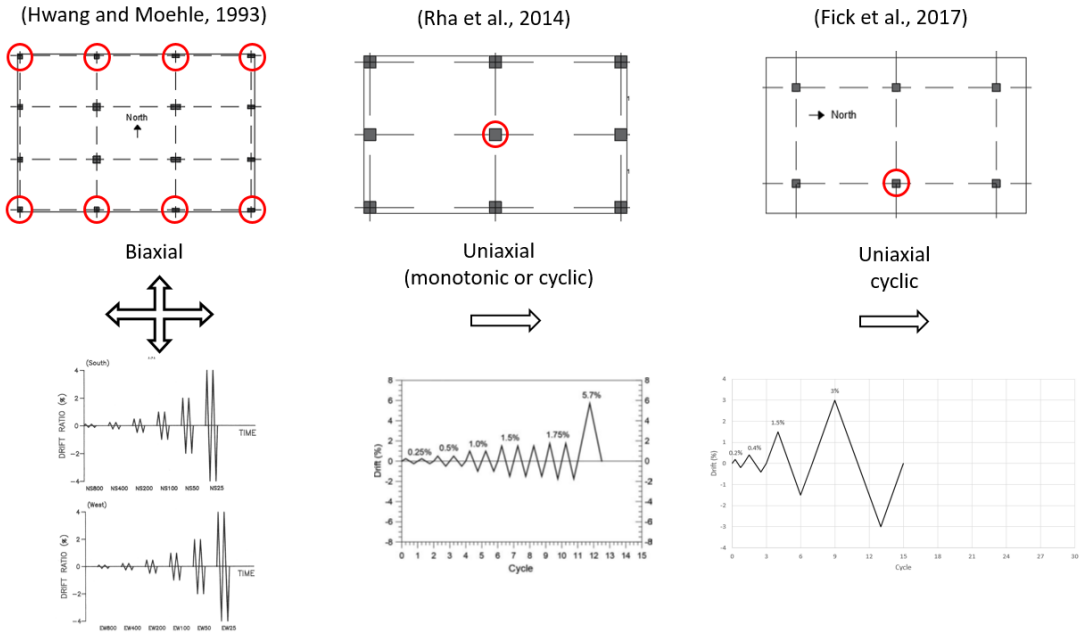

Figure 2.17 Geometry, load application and first connections failed for the flat slab floors and multi-storey frame experiments.

Finally, for the failure analysed above, the joint rotations at punching in the studies by Rha et al., 2014 [12] and Hwang and Moehle, 1993 [10] are reported in Figure 2.18. Rha et al., 2014 [12] observed punching starting from 1% drift up to 6.5% drift with GSR values ranging 0.45 to 0.2 according to the position of the connection (Figure 2.18 a), while Hwang and Moehle, 1993 [10] reported punching failures starting from 2% and in most cases between 3% and 4% with GSR 0.3 (Figure 2.18 b)

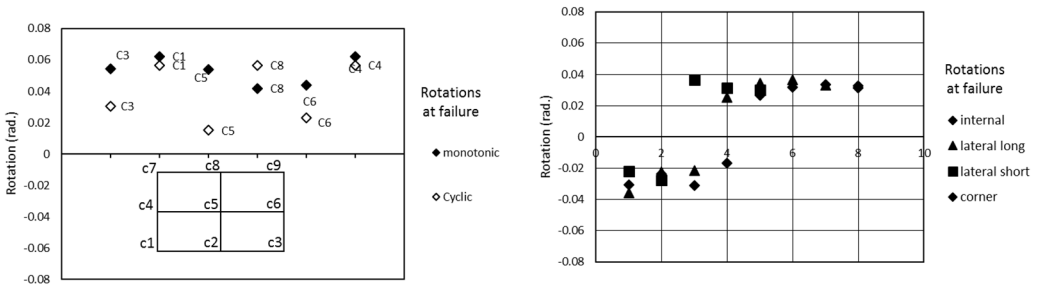

Figure 2.18 Joint rotations at punching: (a) Rha et al.(GSR internal, edge, corner 0.45, 0.25, 0.2); (b) Hwang and Moehle (GSR 0.3).

2.4 Modelling approaches

The preceding sections showed the importance of punching shear failure in flat slab frame structure under gravity and lateral loads. This last section summarises two

models for prediction of punching resistance and deformation capacity:

- The North-American ACI 318 [8] code model
- The model proposed by Setiawan et al., 2019 [44].

The former represents a well-established procedure enabling the design and verification of the resistance of internal, edge and corner connection, considering connections without or with shear reinforcement.
The latter is an analytical procedure applying the CSCT (Critical Shear Crack Theory) approach used in Model Code to the prediction of the resistance and deformation capacity of internal connections without shear reinforcement. These models are used in Chapter 9 for comparison with SlabSTRESS results.

2.4.1 ACI 318 MODEL

In the following "flat plate" will indicate slabs without beams, according to the ACI 318 [8] terminology. In the case of seismic action in one of the principal directions, the unbalanced moment of the slab-column connection is given by the moments acting at the two extremities of the columns, that are transferred to the slab, and the reaction of the column perpendicular to the slab. The effects of the shear and the moment, are analysed in a section of the slab that describe a perimeter around the column.
In the punching shear verification, ACI 318 [8] uses a portion of the unbalanced moment that is generated from the internal non uniform shear and torsion moments. The remaining portion is equilibrated by the bending moments of the slab in the loading direction.
To simplify the analysis, ACI 318 [8] considers only shear forces perpendicular to the slab plane. This simplified representation, is based on the static equivalence between the internal forces obtained with thin slab theory and the distribution of the shear force for unit length perpendicular to the mean section (Figure 2.19).

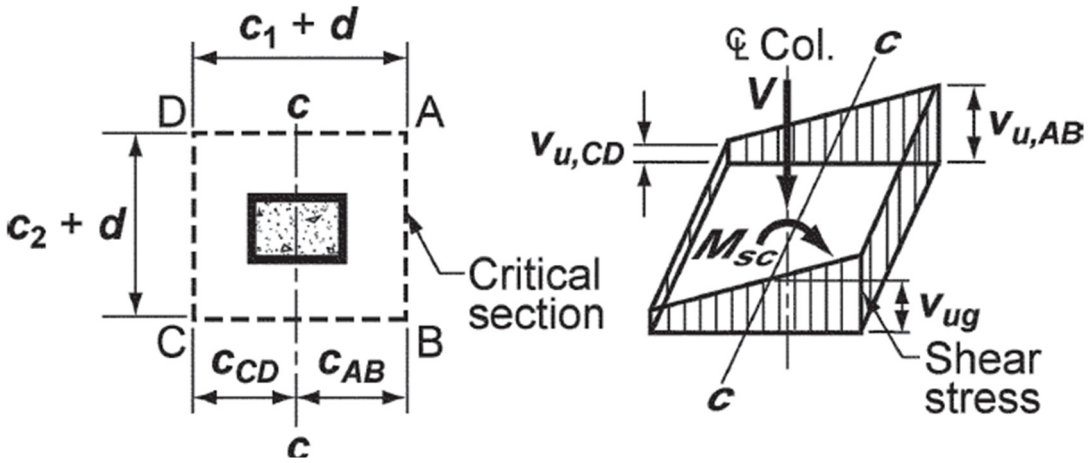

Figure 2.19 Critical section and distribution of the shear stress ACI 318 [8].

The aim of the shear punching verification is the evaluation of these forces, adding these to the effects of the column reaction and lastly, compared with the resistance defined in the code.
The ACI 318 [8] code approach is applicable for all the slab-column connection typology (internal, edge and corner) and in presence of gravitational and lateral load.
ACI 421.1R [37] reports the ACI 318 model for the verification of the punching resistance of connections with and without shear reinforcement, and recommendations for the design of shear reinforcement in slabs.
ACI 421-2R [38] focuses on the punching shear design of flat plate-column connections with or without shear reinforcement that are subject to earthquake displacement and it is supplemental to the previous ACI 421.1R [37]. A section is dedicated to the recommendations for the structural integrity reinforcement. The final aim of this guide is to give the design rules for flat-plate column-connections with sufficient ductility to accommodate the displacement of the selected lateral force resisting system without punching shear failure or loss of moment transfer capacity.
The role of the shear reinforcement is in the prevention of the formation of wide shear cracks through the interception of them. With this aim, the effective anchorage as heads, bends and hooks, is fundamental as for its positioning that should be as close as possible to the structural member's surface.
At the base of the design of critical slab sections perpendicular to the plane of a slab there is the equation

$$v_u \leq \Phi v_n \qquad Eq.2-1$$

Where:

v_u is the shear stress in the critical section caused by the transfer, between the slab and the column, of factored shearing force or factored shearing force combined with moment;

v_n is the nominal shear strength;

Φ is the strength-reduction factor.

The shear stress in the critical section, v_u, is obtained by the combination of the factored shear force, V_u, and the factored slab moment resisted by supporting column about centroidal principal axes x and y of assumed critical section, M_{sc-x} and M_{sc-y}.

$$v_u = \frac{V_u}{A_c} + \frac{\gamma_{vx} M_{sc-x}}{J_{cx}} y + \frac{\gamma_{vy} M_{sc-y}}{J_{cy}} x \qquad Eq.2-2$$

Where:

A_c is the area of concrete of assumed critical section;

γ_{vx} and γ_{vy} are the fraction of moment M_{sc} that the column transmitted by shear.

J_x and J_y are d multiplied by the second moments of the perimeter of the shear critical section about its centroidal principal axes x and y.

γ_{vx} and γ_{vy} are defined differently depending from the slab-column connections typology (interior, edge, corner).

Interior column:

$$\gamma_{vx} = 1 - \frac{1}{1 + \frac{2}{3}\sqrt{\frac{l_{py}}{l_{px}}}} \qquad Eq. 2-3a$$

$$\gamma_{vy} = 1 - \frac{1}{1 + \frac{2}{3}\sqrt{\frac{l_{px}}{l_{py}}}} \qquad Eq. 2-3b$$

Edge column:

$$\gamma_{vx} = 1 - \frac{1}{1 + \frac{2}{3}\sqrt{\frac{l_{py}}{l_{px}}}} \qquad Eq. 2-4a$$

$$\gamma_{vy} = 1 - \frac{1}{1 + \frac{2}{3}\sqrt{\frac{l_{px}}{l_{py}} - 0.2}} \left(\gamma_{vy} = 0 \; when \; \frac{l_{px}}{l_{py}} \leq 0.2\right) \qquad Eq. 2-4b$$

Corner columns

$$\gamma_{vx} = 0.4 \qquad Eq. 2-5a$$

$$\gamma_{vy} = 1 - \frac{1}{1 + \frac{2}{3}\sqrt{\frac{l_{px}}{l_{py}} - 0.2}} \left(\gamma_{vy} = 0 \; when \; \frac{l_{px}}{l_{py}} \leq 0.2\right) \qquad Eq. 2-5b$$

General expression for J_x and J_y of a shear critical section composed of straight segments are:

$$J_{cx} = \frac{d}{3}\sum\left[l_{ij}\left(y_i^2 + y_i y_j + y_j^2\right)\right] \qquad Eq. 2-6a$$

$$J_{cy} = \frac{d}{3}\sum\left[l_{ij}\left(x_i^2 + x_i x_j + x_j^2\right)\right] \qquad Eq. 2-6b$$

The nominal shear strength at critical section, v_n is obtained in a different way depending on the presence of the shear reinforcement and of its typology.

In the case without shear reinforcement, the shear strength of concrete at a critical section at d/2 from column face should be the smallest of:

$$v_n = v_c = 0.17\left(1 + \frac{2}{\beta}\right)\lambda\sqrt{f_c'} \qquad Eq.2-7a$$

$$v_n = v_c = 0.083\left(2 + \frac{\alpha_s d}{b_0}\right)\lambda\sqrt{f_c'} \qquad Eq.2-7b$$

$$v_n = v_c = 0.33\lambda\sqrt{f_c'} \qquad Eq.2-7c$$

Where:

β is the ratio of the long side to the short side of the column;

$\alpha_s = 40, 30, 20$ for interior, edge and corner connection, respectively.

λ is a reduction factor for light-weight concretes as defined in ACI 318-14, 19.2.4.2.

Slab shear reinforcement is required when the maximum shear stress at d/2 from the column face exceeds ϕv_c , where v_c, the nominal shear strength provided by concrete is given in Eq. 2-7. If Eq. 2-1 is not satisfied, it is necessary add shear reinforcement or re-design changing the column size, slab thickness or concrete strength.
In the case of shear strength with stirrups, ACI 318 requires that the maximum factored shear stress at d/2 from column face satisfy:

$$v_u \leq 0.5\sqrt{f_c'} \qquad Eq.2-8$$

The shear strength at a critical section should be calculated as

$$v_n = v_c + v_s \qquad Eq.2-9$$

Where:

$$v_c = 0.17\lambda\sqrt{f_c'} \qquad Eq.2-10a$$

$$v_s = \frac{A_v f_{yt}}{b_0 s} \qquad Eq.2-10b$$

With:

A_v the cross-sectional area of the shear reinforcement legs on one peripheral line parallel to the perimeter of the column;

s is the spacing between peripheral line of shear reinforcement.

Comparing Eq. 2-7c and 2-10a it is possible to note that in presence of shear reinforcement (Eq. 2-10a) the strength of concrete is nearly halved compared with the strength of concrete without shear reinforcement (Eq. 2-7c). Islam and Park, 1976 [46] conducted a number of tests on a series of half-scale models of reinforced concrete internal flat-plate column specimen under combined gravity and seismic

loading. Some of the specimens were without shear reinforcement and the other with various arrangement of shear reinforcement. At the end of the experimental campaign, they observed that the specimens without shear reinforcement, reported a small ductility. In these specimens, failures were done to inclined crack extending from the compression face of the slab near the column, to the tension face and to splitting of the concrete along the slab reinforcement at tension face.

If the shear reinforcement consists in headed studs with mechanical anchorage capable of developing the yield strength of the rod, the nominal shear strength provided by the concrete is:

$$v_c = 0.25\lambda\sqrt{f_c'} \qquad Eq.2-11$$

The nominal shear strength resisted by concrete and steel can be taken as high as

$$v_n \leq 0.66\sqrt{f_c'} \qquad Eq.2-12$$

In regions of high seismicity, ACI 318 [8] not permits flat plate column frames without beams and without a lateral force resisting system consisting of more rigid elements that limit the lateral displacements. Flat plates shall be able to reach the same lateral displacements as the lateral-force-resisting system and should be designed to do so without losing their capability to support gravity loads during or after an earthquake. So the lateral force resisting system structural system should have sufficient stiffness to control the story drift. Non linear deformations must be accounted in the calculation of the deformations.
In order to obtain sufficient lateral deformation capacity ACI 318 [8] prescribes specific rules for shear reinforcement. In particular, the use of minimum shear reinforcement is recommended. Connections that do not satisfy conditions of limited deformation demand and when Eq. 2-1 and 2-7 are not satisfied should have slab reinforcement that satisfy (Eq. 2-1 and 2-9) and a minimum reinforcement such that:

$$v_s = \frac{A_v f_{yt}}{b_0 s} \geq \frac{1}{4}\sqrt{f_c'} \qquad Eq.2-13$$

Where:

A_v is the area of shear reinforcement in each peripheral line parallel to the column face;

s is the spacing between peripheral lines of shear reinforcement;

b_0 is the perimeter of the critical section at d/2 from the column face;

f_{yt} is the specified yield strength of the shear reinforcement.

When $\frac{V_u}{\Phi V_c} > 0.4$ greater than those specified above, the minimum reinforcement is prescribed in these cases.

The design procedure is developed with reference to Figure 2.20, that is derived from the experimental results shown in Figure 2.16. ACI 318-14 [8] does not impose the calculation of the moment M_{sc} due to the design displacement if the point $\{V_u/(\Phi V_c), DR_u\}$ falls below the line ABC in Figure 2.20.

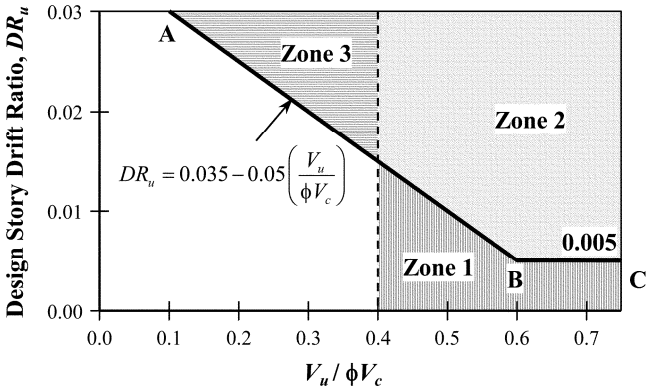

Figure 2.20 Requirement for shear reinforcement [8].

In "Zone 1" (Figure 2.20), connections are subjected to high shear due to gravitational load and low deformability demand, for this reason, the minimum shear reinforcement is recommended. "Zone 2" (Figure 2.20) requires the shear reinforcement since the connections bear high shear and high deformability. In the last one, the "Zone 3" (Figure 2.20) the shear reinforcement is required due to the low shear and the relatively high deformability demand.

Thus flat plate-column connections should have shear reinforcement equal to or exceeding the minimum amount given in Eq.2.14, except when the value of V_u is less than $0.20\Phi V_c$, and $\Phi = 0.75$ (ACI 318-14 [8], 21.2.1). This requirement ensures that the connections can sustain a design story drift ratio DR_u = 0.025.

Comparing Eq. 2-7c and 2-10a it is possible to note that in presence of shear reinforcement (Eq. 2-10a) the strength of concrete is nearly halved compared with the strength of concrete without shear reinforcement (Eq. 2-7c). Islam and Park, 1976 [46] conducted a number of tests on a series of half-scale models of reinforced concrete internal flat-plate column specimen under combined gravity and seismic loading. Some of the specimens were without shear reinforcement and the other with various arrangement of shear reinforcement. At the end of the experimental campaign, they observed that the specimens without shear reinforcement, reported a small ductility, whereas more non-linear deformation developed with shear reinforcement. Park and Gamble, 2000 [16] explained the use of a higher "two-way" shear strength concrete contribution without shear reinforcement as an effect of the confinement of the outer "elastic" slab to the material close to the column where the nonlinear deformation develops, with a limited opening of the cracks around the column. Shear reinforcement allows for wider crack opening, leading to a loss of the confinement effect and a lower shear strength contribution of concrete in combination with the shear reinforcement contribution. It must be noted that the

concrete contribution to two-way shear strength does not depend on the longitudinal reinforcement ratio. Size effect has been recently introduced in ACI 318-19 for thick slabs with a thickness over 10 in

2.4.2 SETIAWAN ET AL., 2019 [44]

A model for the verification of the resistance and deformation capacity of interior flat slab connection has been recently proposed (Setiawan et al., 2019 [44]) within the framework of the CSCT theory applied to concentric punching in Model Code 2010 [39], [40]. The CSCT and Model Code 2010 [39], [40] formulation are summarized first, followed by the model by Setiawan et al., 2019 [44].

CSCT AND MODEL CODE 2020

The Critical Shear Crack Theory (CSCT) was formulated by Muttoni and Schwartz, 1991 [42] for concentric punching and monotonic loading. It considers that the presence of a critical shear crack that propagates through the slab into the inclined compression strut transmitting the shear force to the column brings to the reduction of the shear strength. As demonstrated by Kinnunen and Nylander, 1960 [43] in their theory for the estimation of the punching strength, the punching strength is reached for a given critical rotation ψ. The punching strength decreases with increasing rotation of the slab (Figure 2.21).

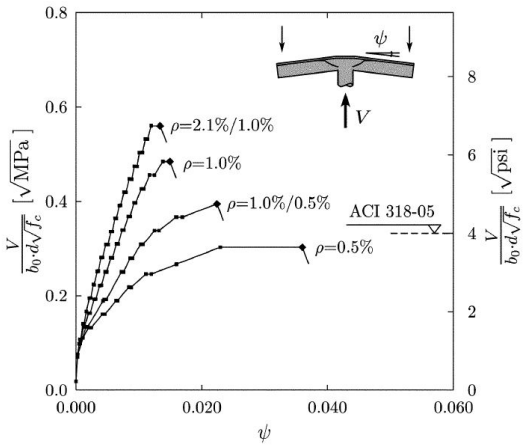

Figure 2.21 Load-rotation tests by Kinnunen and Nylander, 1960 [43].

Muttoni, 2008 [9] reported that the opening of the critical shear crack, reduces the shear strength propagating through the slab into the inclined concrete compression strut carrying shear, with the consequence of the punching shear failure.
It is possible to consider the width of the critical crack to be proportional to the product ψ times d, with ψ rotation and d thickness of the slab (Figure 2.22).

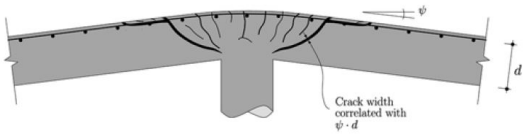

Figure 2.22 Correlation between rotation ψ and slab thickness d, Muttoni, 2008 [9].

The failure criterion takes in account the fact that the maximum aggregate size influences the roughness of the crack. The amount of shear that can be transferred across the critical cracks depend on the roughness of the crack. Consequently, the capacity of the critical crack to carry the shear force depends on the quantity ($d_{g0} + d_g$) in which d_{g0} is the maximum aggregate size and d_g is a reference size.

$$\frac{V_R}{b_0 d\sqrt{f_c}} = \frac{3/4}{1 + 15\frac{\psi d}{d_{g0} + d_g}} \qquad Eq. 2-14$$

Where:
V_R is the punching load capacity;
b_0 is the effective perimeter of the critical section ad d/2 from the column face;
ψ is the slab rotation

The punching shear resistance can be determined with three levels of approximation which differ in the complexity of the applied methods and the accuracy of the results. The Level I is the easier one and should be used for the conception or the design of a new structure, the Level II is suitable for the design of new structure or part of it. Lastly, the Level III should be used for the design of a member in a complex loading state or a more elaborate structure.
The Level II adopted by Setiawan et al., 2019 [44]will be treated.
A shear resisting control perimeter is used to calculate the punching shear resistance, ad a distance d/52 from the column face. A more detailed calculation can be carried out if the distribution of shear forces per unit width in the slab around the column is calculated, with its maximum value:

$$b_0 = \frac{V_{Ed}}{V_{perp,d,max}} \qquad Eq. 2-15$$

Where:

V_{Ed} is the design shear force;

$V_{perp,d,max}$ is the maximum value of the projection of the shear force perpendicular to the basic control perimeter.

This perimeter is reduced by the factor k_e to consider the non-uniform shear force distribution induced by the moment that is transferred between the slab and the column.

$$k_e = \frac{1}{1+\frac{e}{b}} \qquad Eq.2-16$$

Where:

$e = \left|\frac{M_d}{V_d}\right|$ is the load eccentricity;

b is the diameter of a circle with the same surface as the support region.

The punching shear resistance may be calculated as

$$V_{Rd} = V_{Rd,c} + V_{Rd,s} \qquad Eq.2-17$$

The design resistance attributed to the concrete

$$V_{Rd,c} = k_\Psi \frac{\sqrt{f_{ck}}}{\gamma_c} b_0 d_v \qquad Eq.2-18$$

Where:
f_{ck} is the characteristic value of f_c;
b_0 is the critical perimeter (Eq. 2-15);
d_v is the effective depth of the slab;
γ_c is the partial safety factor for concrete material properties;
k_Ψ is a parameter that depends on the rotations of the slab around the support region

$$k_\Psi = \frac{1}{1.5 + 0.6\psi d k_{dg}} \leq 0.6 \qquad Eq.2-19$$

The parameter ψ refers to the rotation of the slab around the support region outside the critical shear crack.
The maximum punching shear resistance is limited by crushing of concrete struts near the support region that is:

$$V_{Rd,max} = k_{sys} k_\Psi \frac{\sqrt{f_{ck}}}{\gamma_c} b_0 d_v \leq \frac{\sqrt{f_{ck}}}{\gamma_c} b_0 d_v \qquad Eq.2-20$$

k_{sys} is a coefficient that accounts for the performance of punching shear reinforcing systems. In the absence of other data, a value k_{sys}=2 can be adopted.
The slab rotation around the support region, using the Level II in slabs where significant bending moment redistributions are considered for design of the bending reinforcement is calculated as:

$$\Psi = 1.5 \frac{r_s}{d} \frac{f_{yd}}{E_s} \left(\frac{m_{Ed}}{m_{Rd}}\right)^{1.5} \qquad Eq.2-21$$

Where

m_{Ed} is the average bending moment per unit length in the support strip of the column;

m_{Rd} is the design average flexural strength per unit length in the support strip;

r_s can be approximated as $0.22\ L_x$ or $0.22\ L_y$ for regular flat slabs where the ratio of the span lengths (L_x/L_y) is between 0.5 and 2. It represents the distance of the line with zero moment from the edge of the column.

The width of the support strip for calculation of the design average flexural strength is

$$b_s = 1.5\sqrt{r_{S,x} r_{S,y}} \leq L_{min} \qquad Eq.2-22$$

Setiawan et al., 2019 [44] proposed a method for assessing punching resistance of internal flat slab-column without shear reinforcement under cyclic loading. The model is based on a proposal by Drakatos et al., 2018 [45], extending the CSCT approach to drift-induced pinching of slab-column connections.
The shear resistance provided by concrete is calculated on the basis of the failure criterion of the CSCT as Eq. 2-17:
The method formulated by Setiawan et al., 2019 [44] is an extension of Level of Approximation II of the Model Code 2010 [39], [40] and the model proposed by Drakatos et al., 2018 [45]. Both models consider the division of the slab around the column in radial sectors. The slab rotation relative to the column is calculated considering the variation of the rotation of the slab sector around the column, with a maximum and minimum value. Punching failure is initiated by the sector where the maximum rotation occurs relative to the column. The modifications proposed by Setiawan et al., 2019 [44] involve the procedure for calculation of slab rotation and an improvement of the k_e coefficient.
The maximum rotation is calculated in accordance with the Level of Approximation II in Model Code 2010 [40],

$$\Psi_{max} = 1.5 \frac{r_s}{d} \frac{f_y}{E_s} \left(\frac{m_{Edmax}}{m_{Rdhog}} \right)^{1.5} \qquad Eq.2-23$$

Where:

r_s is the position relative to the support axis where the radial bending moment is zero with $r_{s,x}$ and r_{sy} the position of the x and y axes respectively;
d is the effective height;
f_y is tension yield stress of non- prestressing reinforcement;
E_s is the modulus of elasticity of reinforcing steel;
m_{Edmax} is the maximum average moment per unit length in the support strip at the column face

$$m_{Edmax} = V_{grav}\left(\frac{1}{8} + \frac{|e_u|}{2b_s}\right) \qquad Eq.2-24$$

With:

V_{grav} is the gravity load;
e_u is the eccentricity of the resultant of shear force with respect to the centroid of the basic control perimeter
$b_s = 1.5\sqrt{r_{s,x}r_{sy}}$
m_{Rdhog} is the design average flexural strength per unit length in the support strip for hogging moment

$$m_{Rdhog} = \rho_{hog} f_y d^2\left(1 - \frac{\rho_{hog} f_y}{2f_c'}\right) \qquad Eq.2-25$$

The slab-column connection rotation is given by the equation:

$$\Psi_{SCC} = \frac{\Psi_{max} - \Psi_{min}}{2} \qquad Eq.2-26$$

The rotation Ψ_{SCC} in continuous slabs is related to the inter-storey drift Ψ_s

$$\Psi_{st} = \Psi_{SCC} + \Psi_{SO} + \Psi_{col} \qquad Eq.2-27$$

Setiawan et al., 2019 [44] proposed a calculation procedure in which Ψ_{min} depends on the sign of m_{Edmin} which determines whether hogging or sagging reinforcement is activated at the column face supporting the slab sector rotating.

For positive m_{Edmin},

$$\Psi_{\min(+)} = 1.5\frac{r_s}{d}\frac{f_y}{E_s}\left(\frac{m_{Edmin}}{m_{Rdhog}}\right)^{1.5} \qquad Eq.2-28$$

With $m_{Edmin} = V_{grav}\left(\frac{1}{8} - \frac{|e_u|}{2b_s}\right)$

For negative m_{Edmin},

$$\Psi_{\min(-)} = -1.5\frac{r_s}{d}\frac{f_y}{E_s}\left(\frac{m_{Edmin}}{m_{Rdsag}}\right)^{1.5} \qquad Eq.2-29$$

With $m_{Edmin} = V_{grav}\left(\frac{1}{8} - \frac{|e_u|}{2b_s}\right)$

m_{Rdsag} is the design average sagging flexural strength in the support strip

$$m_{Rdsag} = \rho_{sag} f_y d^2\left(1 - \frac{\rho_{sag} f_y}{2f_c'}\right) \qquad Eq.2-30$$

With $\rho_{sag} = 0.5\rho_{hog}$

In this method, the basic control perimeter is reduced by a factor k_{emod} accounting for the non-uniform shear distribution. k_{emod} is directly related to the proportion of unbalanced moment resisted by eccentric shear. The formulation is based on NLFEM analyses by the authors and the model by Drakatos et al., 2018 [45], by a systematic application of the model by Drakatos et al., 2018 [45] curve fitting expressions were derived for the influence of the column dimension relative to the slab thickness r_c/d and the slab slenderness r_s/d. In comparison with the k_e coefficient reported in the Model Code 2010 [39], [40], k_{emod} was modified as follows:

$$k_{emod} = \frac{1}{1 + \left(\frac{e_u}{b_u}\right)\left\{\left[\frac{(r_s/d)_{ref}}{r_s/d}\right]\left[0.7\left(\frac{r_c/d}{(r_c/d)_{ref}}\right) + 0.3\right]\right\}} \qquad Eq. 2-31$$

In which

b_u is the diameter of a circle with the same surface as the region inside the basic control perimeter;
r_c is the column radius.
It must be underline that both the model by Drakatos et al., 2018 [45] and the NLFEM analyses quoted above considered the effects of cyclic loading with the accumulation of plastic strains, that is thus implicitly considered in Eq. 2-31 above.

The k_e coefficient formulated in the Model Code 2010 [39], [40], does not consider the maximum shear stress that can develop in the sector with maximum rotation.

The increase of the shear stress may be limited by the yielding of the reinforcement, thus provoking redistribution of shear stress to the adjacent sectors as wider perimeter. In order to account for this, a lower limit to k_{emod} is also considered.

$$k_{emod} \geq k_{elim} = \frac{V_{grav}}{2 \cdot \pi \cdot r_s \cdot m_{rd(hogging)} \cdot \left(\frac{1}{r_q - r_c}\right)} \qquad Eq. 2-32$$

With r_q radius of the load introduction at the perimeter, approximated as r_s.

The formulations described above are used to build up a step-by-step procedure to predict the eccentricity of the shear force at punching failure and the corresponding column-slab rotation:

1. Choose a value for the ultimate eccentricity, e_u,
2. Calculate the maximum slab rotation, Ψ_{max},
3. Calculate k_{emod} and the consequent effective control perimeter length $b_{0,e} = k_{emod} b_0$,

4. Calculate V_{Rdc} from the equation $\frac{V_{Rdc}}{b_{0,e}d\sqrt{f_c'}} = \frac{0.75}{1+15\frac{\Psi d}{d_{g0}+d_g}}$
5. Repeat steps from 1 to 4 iterating the ultimate eccentricity, e_u and until $V_{Rdc} = V_{grav}$
6. Calculate Ψ_{min}
7. Calculate Ψ_{SCC}

The unbalanced moment can be calculated as the product of the shear force by the obtained eccentricity.
On the basis of NLFEM calculations, the relation between the column-slab rotation and the inter-storey drift is obtained dividing Ψ_{SCC} by 0.85, thus accounting for the slab deformation outside the portion r_s considered in the model formulation above.
The model provides the application of the CSCT to the punching shear design of flat slab interior connections, for gravity and lateral actions. The longitudinal reinforcement ratio (hogging and sagging) is taken into account. Only isotropic reinforcement is considered. The formulation includes size effect, as well as taking into account geometrical proportions such as the slab slenderness and the dimension of the column relative to slab thickness.
The formulations by Setiawan et al., 2019 [44] rely on the CSCT that is the basis of punching shear provisions in Model Code 2010 [39], [40].
These features respond to the need of new European seismic code formulations. The formulation has been developed only for interior connections without shear reinforcement, thus the extension to edge and corner connections is needed, as well as the inclusion of shear reinforcement.
Alternative formulations not reviewed here have been proposed by Broms, 2009 **Error! Reference source not found.** and more recently using a strut and tie approach Broms, 2019 [48].

2.5 Summary

This analysis of the state of the art shows that the majority of tests were carried out on isolated slab-column connections, a limited number on scaled floors or multi-storey frames, and there is only one full scale study on a multi-storey frame.

The analysis in this chapter was focused on experimental research on reinforced concrete flat slab frame tests for gravity and lateral loading. A brief review of test results on isolated slab-column connections was presented first; then a total of five studies and seven tests on single and multi-storey reinforced concrete flat slab frames were analysed.

The set of tests allowed a comparison between similar specimens, related to common and different features and parameters in the test.

Almost all tests on single and multi-storey reinforced concrete flat slab frames reported in the literature are on scaled specimens. Square and rectangular panels were investigated, with similar span-to-depth ratios and column sizes relative to slab span. The slab thickness in the scaled specimens is smaller than 100mm.

The design was carried out using mostly North American seismic regulations. The seismic designs of the prototype structures considered "non-participating" slabs with seismic resistant walls or frames, for three studies. The comparison showed better performance of the specimen designed for seismic actions.

All tests showed a non-linear global response reaching ultimate drifts with a lower bound of 2.5% and up to 6%. The gravity shear ratios were in most cases between 0.2 and 0.3. The response is characterized by a progressive spreading of damage and a sequence of failures in the different connections.

One test was carried out for a full scale multi-storey specimen designed for gravity loads only and with a low gravity shear ratio. The test was stopped after the first connection failed. Hence the occurrence of the sequence of failures has not yet been confirmed for a full-scale structure.

All specimens designed for seismic actions had integrity reinforcement. The tests showed the efficiency of the integrity reinforcement since in all cases, the gravity loads could be carried after local punching of the slab-column connections. Nevertheless, this could also be due to the relatively low GSRs chosen for all tests.

Cyclic lateral loading compared to monotonic loading causes more damage, reducing ultimate drifts. More tests on biaxial loading are needed to show these effects in flat slab frames.

The main conclusions and research developments are the following:

- Floor tests show redistribution of internal forces and the combined structural actions of internal, edge and corner connections, up to drifts equal to or higher than those observed in isolated slab-column connections;
- Only one test studied a full-scale multi-storey frame; moreover, this specimen was designed for gravity loads only. In addition, the test was stopped at the first connection failure. More tests on full scale structures with lateral loads considered in the design are needed;
- Tests on isolated slab-column connections show failures and the related drifts approximating the boundary conditions; most tests have been carried out on internal connections. Hence more tests on flat slab frames are needed with internal, edge and corner joints;

Most specimens were scaled from prototype structures designed with flat-slab frames combined with walls or beam-columns frames; the tests were conducted on the sole scaled flat-slab frame, without considering the interaction with the wall or

beam/column frame response;

A substantial amount of information was obtained from these tests, but there are some drawbacks:

- The internal forces distribution developed in multi bay slab column frames is not well represented with the considered boundary conditions;
- Tests on isolated slab column-connections do not make it possible to study the redistributions of internal forces due to cracking and yielding of reinforcement;
- It is not possible to study the effect of compressive membrane action and size-effect.

The SlabSTRESS project considers all these aspects, thus providing the means to widen knowledge on the seismic response of reinforced concrete flat-slab structures.

Finally, two relevant models for computing the resistance and the rotation capacity in the slab-column connection are reported. The ACI 318 [8] regulation complemented by ACI 421.1R [37], ACI 421-2R [38] and the model by Setiawan et al., 2019 [44] developing the European Model Code [39], [40] are presented in terms that will facilitate comparison with the experimental results obtained during the SlabSTRESS campaign.
It must be remarked that these models are mainly based on databases of isolated interior connections. Thus the comparison with a full scale test of a flat sab frame is of particular interest.
Only the ACI 318 [8] model accounts for resistance of all types (interior, edge and corner) connections, though the provision in the same approach related to deformation capacity have been formulated only for interior connections. The comparison with tests including all types of connections is thus relevant.
This chapter reviewed the state of the art for such tests, all but one carried out though on scaled specimens. The only full scale test was stopped on the first punching failure and did not include edge and corner connections. This shows the importance of the full-scale test described in this dissertation, to understand the response of a flat slab structure.

References

[1] Fardis, M., N., "Seismic Design, Assessment and Retrofitting of Concrete Buildings based on EN-Eurocode 8", Springer, 2009.

[2] Coronelli, D. (2010) "Grid Model for Flat-Slab Structures", ACI Structural Journal, 107, 6, p.645-653

[3] EN 1998-1 (2004): Eurocode 8: design of structures for earthquake resistance – Part 1: General rules, seismic actions and rules for buildings.

[4] EN 1992-1-1 (2004): Eurocode 2: design f concrete structures – Part 1-1: General rules and rules for buildings.

[5] Pinto, A., Taucer F., Dimova, S. (2007) "Pre-Normative Research Needs to Achieve Improved Design Guidelines for Seismic Protection in the EU" JRC EUR 22858 EN 2007, 34 pp.

[6] Zaharia, R. Taucer, F., Pinto, A., Molina, J., Vidal, V., Coelho, E. Candeias P. (2006) "Pseudodynamic Earthquake Tests on a Full-Scale RC Flat-Slab Building Structure" European Commission Joint Research Centre, 119 pp.

[7] ACI-ASCE 421 (2015) ACI 421.3R-15 Guide to Design of Reinforced Two-Way Slab Systems Reported by Joint ACI-ASCE Committee 421

[8] ACI 318-14. Building Code Requirements for Structural Concrete. ACI; 2014.

[9] Muttoni, A., (2008), "Punching shear strength of reinforced concrete slabs without transverse reinforcement", ACI Structural Journal, V. 105, No 4, 2008, pp. 440-450.

[10] Hwang, S.-J., Moehle, J. P. (1993) "An Experimental Study of Flat-Plate Structures under Vertical and Lateral Loads". Report N. UCB/EERC-93/03, Earthquake Engineering Research Centre, University of California, Berkeley, Feb. 1993, 278pp.

[11] Hwang, S.-J., Moehle, J. P. (2000) "Vertical and Lateral Load Tests of Nine-Panel Flat-Plate Frame". ACI Structural Journal, V. 97, No. 1, pp. 193-203.

[12] Rha, C., Kang, T. H.-K., Shin, M., Yoon, J. B. (2014). "Gravity and Lateral Load-Carrying Capacities of Reinforced Concrete Flat Plate Systems". ACI Structural Journal, V. 111, No 4, 2014, pp. 753-764.

[13] Fick, D. R., Sozen, M. A., Kreger, M. E. (2017) "Response of Full-Scale Three-Story Flat-Plate Test Structure to Cycles of Increasing Lateral Load" ACI Structural Journal, V. 114, No. 6, pp. 1507-1518.

[14] Moehle J. P., Diebold J. W. (1984) "Experimental Study of the Seismic Response of a Two-Story of a Flat-Plate Structure". University of California, Berkeley.

[15] Kang, T. H.-K., Wallace, J. W. "Shake Table Tests of Reinforced Concrete Flat

Plate Frames and Post-Tensioned Flat Plate Frames" (2004). 13th World Conference on Earthquake Engineering, Vancouver, B.C., Canada. Paper No.1119.

[16] Park R, Gamble WL. Reinforced concrete slab. 2nd ed. John Wiley & Sons, Inc., 2000.

[17] Hawkins, N. M., and Mitchell, D. (1979) "Progressive Collapse of Flat Plate Structures", ACI Journal, Proceedings, V. 76, No. 7, pp. 775-808.

[18] Pan, A., Moehle, J. P. (1987) "Lateral Displacement Ductility of Reinforced Concrete Flat Plates". ACI Structural Journal, V. 86, No. 3, pp. 250-258.

[19] Robertson, I. N., Kawai, T., Lee, J., Enemoto, B. (2002). "Cycling Testing of Slab-Column Connections with Shear Reinforcement". ACI Structural Journal, V. 99, No 5, pp. 605-613.

[20] Dovich, L. M., and Wight, J. L., (2005). "Effective Slab Width Model for Seismic Analysis of Flat Slab Frames". ACI Structural Journal, V. 102, No. 6 Nov-Dec, pp.868-875.

[21] Kang, T. H.-K., Wallace, J. W. (2006) "Dynamic Tests and Modelling of RC and PT Slab-Column Connections". Paper 0362, Proceedings of the 8th U.S. National Conference on Earthquake Engineering, San Francisco, Calif., 10 pp. (CD-ROM).

[22] Hueste, M. B. D., Browining, J., Lepage, A., Wallace, J., W. (2007) "Seismic Design Criteria for Slab-column Connections". ACI Structural Journal, V. 104, No. 4, pp. 448-458.

[23] Drakatos I.-S, Muttoni, A., Beyer, K.,(2016) "Internal slab-column connections under monotonic and cyclic imposed rotations", Engineering Structures, Volume 123, 15 September 2016, Pages 501-516, ISSN 0141-0296, (https://doi.org/10.1016/j.engstruct.2016.05.038).

[24] Almeida A., Alcobia B., Ornelas M., Marreiros R., Ramos A. P. "Behaviour of reinforced-concrete flat slabs with stirrups under reversed horizontal cyclic loading". Magazine of Concrete Research, 2019.

[25] Almeida A., Ramos A. P., Lúcio V., Marreiros R. "Behaviour of RC Flat Slabs Whit Shear Bolts Under Reversed Horizontal Cyclic Loading. Structural Concrete" Volume 21, issue 2 p. 501-516, April 2020 (https://doi.org/10.1002/suco.201900128).

[26] Gouveia, N. D., Faria D. M. V., Ramos A. P. "Assessment of SFRC flat slab punching behaviour – part II: reversed horizontal cyclic loading". Magazine of Concrete Research, Volume 71, Issue 1, p.26-42, January 2019.

[27] Isufi B, Pinho Ramos A, Lúcio V. "Reversed horizontal cyclic loading tests of flat slab specimens with studs as shear reinforcement". Structural Concrete, Volume 20, number 1, 2019, p. 330-347.

[28] Einpaul J., Fernández Ruiz M., Muttoni A., (2015) "Influence of moment redistribution and compressive membrane action on punching strength of flat slabs," Engineering Structures 86 (2015), pp. 43-57

[29] Einpaul J., Ospina C. E., Fernández Ruiz M., Muttoni A., (2016), "Punching Shear Capacity of Continuous Slabs," ACI, Structural Journal, Vol. 113 n°4, pp. 861-872.

[30] Zee, Howard L., and Jack P. Moehle. "Behaviour of interior and exterior flat plate connections subjected to inelastic load reversals". University of California, Earthquake Engineering Research Centre, 1984.

[31] El-Gendy, Mohammed, and Ehab El-Salakawy. "Effect of flexural reinforcement type and ratio on the punching behaviour of RC slab-column edge connections subjected to reversed-cyclic lateral loads." *Engineering Structures*200 (2019): 109703.

[32] Anggadjaja, Edward, and Susanto Teng. "Edge-column slab connections under gravity and lateral loading." *ACI Structural Journal* 105.5 (2008): 541.

[33] Robertson, I., and Johnson, G. (2006), "Cyclic lateral loading of nonductile slab-column connections", ACI structural Journal, vol. 103, no. 3, pp. 356-364.

[34] Pan, A., Moehle, J. P. (1992) "An experimental study of Flat Slab-Connections". ACI Structural Journal, V. 89, No. 6, pp. 626-638.

[35] Ramos A, Marreiros R, Almeida A, Isufi B, Inácio M. Chapter: Punching of flat slabs under reversed horizontal cyclic loading, pp 253-272. In: fib Bulletin 81/ACI SP-315, Punching Shear of Structural Concrete Slabs; 2017, 378 pp., (ISBN: 978-2-88394- 121-2).

[36] Lapi, M., Ramos, A. P., Orlando, M. (2019) "Flat slab strengthening techniques against punching-shear". Engineering structures 180 pp. 160-180.

[37] ACI-ACSE Committee 421.1R, "Guide for shear Reinforcement for Slabs"

[38] ACI-ACSE Committee 421.2R, "Guide to Seismic Design of Punching Shear Reinforcement in Flat Plates"

[39] Fib (2010) "CEB-FIP Model Code 2010 – Frost complete draft." Bulletin 55, Vol. 1, Federation International du Beton, Lausanne.

[40] Fib (2010) "CEB-FIP Model Code 2010 – Frost complete draft." Bulletin 55, Vol. 2, Federation International du Beton, Lausanne.

[41] Coronelli D., Martinelli L., 2017 "La progettazione sismica dei sistemi a piastra in calcestruzzo armato". Patron Editore.

[42] Muttoni, A., and Schwarts, J., "Behaviour of Beams and Punching in Slabs without Shear Reinforcement", IABSE colloquium, v. 62, Zurich, Switzerland, 1991, pp. 703-708.

[43] Kinnunen, S., and Nylander H., “Punching of Concrete Slab Without Shear Reinforcement, Transactions of the Royal Institute of Technology, No. 158, Stockholm, Sweden, 1960, 112pp.

[44] Setiawan, a., Vollum., R. L., Macorini, L., “Numerical and analytical investigation of internal slab-column connections subject to cyclic loading”. Engineering structures 184 (2019) 535-554.

[45] Drakatos I.-S, Muttoni, A., Beyer, K., “Mechanical model for drift-induced punching of slab-column connections without transverse reinforcement”, ACI Structural Journal, 2018; 115(2)

[46] Islam, S., Park, R., “Tests on Slab-Column connections with Shear and Unbalanced Flexure”, Journal of the structural division, March 1976, pp. 549-567

[47] Broms, C.E. “Design method for imposed rotations of interior slab-column connections.” ACI Struct J 2009;106(5):636–45. Farmington Hills, U.S.A.

[48] Brooms, C. E., “Structural Model for Interstory Drift Capacity of Flat Slabs without Shear Reinforcement”. ACI Structural Journal, V. 117, No. 3, May 2020. doi: 10.14359/51721363,

3 The SlabSTRESS project and design

3.1 Introduction

The chapter contains the design of the structure, the description of the geometry and the materials. Details on the reinforcement and the strengthening procedure are also given.
The research campaign is divided into two phases: the first one is the pseudodynamic test run with numerically modelled walls, the second one is the cyclic quasi-static tests.
In the SlabSTRESS project, a design approach method was defined to consider the flat slab as secondary seismic member.

3.2 Flat Slab Design as a Secondary system

The structure represents to a reinforced concrete building with two reinforced concrete flat slab floors, supported by twelve columns on each floor. The floors are ordinary reinforced concrete slabs. One of the two floors is provided with transverse reinforcement, although not requested in the design.
The structure has a reinforced concrete foundation with a slab and an orthogonal grid of stiffening beams in correspondence to the column lines.
The structural design carried out is of a structure bearing gravity loads, and able to reach a given lateral relative inter-story drift, with moderate-high seismic lateral actions, if seismic resistant walls were provided. The two walls were not constructed in reality but were considered numerically, using a linear model. They were not connected to the slab along the whole perimeter but they were linked by a geometrical constraint reaching the same lateral displacements as the slabs.
Fardis, 2009 [1], Bisch et al., 2011 [2] and Coronelli and Martinelli. 2017 [3] have shown that buildings with seismic walls in zones of moderately-high seismicity have a design inter-storey drift with a range between 0.2% and 1%.
Eurocode 8 [1] includes general definitions and concepts for the seismic design of primary and secondary elements, that are here used to develop a strategy for secondary flat slab design; according to the prescriptions the secondary members must bear the gravity loads at the deformations of the design earthquake. These are obtained by the multiplication between the displacements obtained in the structural analysis for the design earthquake and the behaviour factor, q. According to the code, even though this requirement is non-prescriptive, the secondary system must have a 15% stiffness compared to that of the primary.

The punching shear resistance in a secondary system is reduced by the moment transfer from the column to the slab (M_{Ed}), as a consequence of the imposed deformation, but also by the detrimental effect of the cyclic action as proved by Drakatos et al., (2016) [4] and Almeida et al. (2016) [5]. The calculation of internal shear forces, V_{Ed} and moments, M_{Ed} in the secondary system derives from gravity loads and lateral deformation, with cracked flexural and shear stiffness.
As a consequence, internal forces and excessively conservative moments are obtained in the secondary system making the design cumbersome. The verification of the flexural resistance of the slab is required also. The imposed deformation causes high moments in the slab that are un realistic
The North American code ACI 318-14 [11] and standard CSA A23.3-04 [12] suggest the "deformation–based" criteria for the design of flat slab-column connections under horizontal actions. The "deformation-based" criteria uses the correlation between the Gravity Shear Ratio (defined as the ratio between the acting vertical shear force and the punching shear resistance) and the ultimate drift (Hueste et al., 2007 [13], Moehle, 1996 [14], Megally and Ghali, 2000 [15], Dilger et al., 2005 [16]). These relations are based on experimental observation of slab-column connections under lateral loading as shown in Figure 3.1.

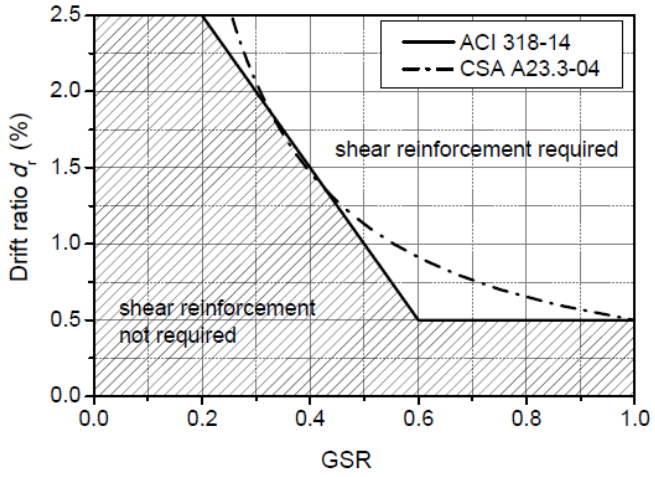

Figure 3.1 Deformation based criteria in the North American codes and standards [11], [12].

On the basis of the ultimate drift value obtained in tests with shear reinforcement, these codes use a line to identify two regions: one above the line, where shear reinforcement is required and the other below the line, where shear reinforcement is not required.

The design procedure used in this dissertations can be outlined as follow.

- The primary system typology and the design inter-storey drift level are chosen;
- The design of the flat slab frame for gravity loads is developed based on the

gravity shear ratio corresponding to the inter-storey drift level chosen in the previous point;

- The primary elements are designed for the seismic situation. The q factor and the ductility class for the chosen primary system typology are taken based on Eurocode 8;
- Successively, the primary elements deformation is calculated. the model used only considers the primary elements with cracked stiffness, after which was used and then the inter-storey drift ratios, calculated from the spectrum analysis is multiplied by the q factor to obtain the design drift. The obtained value is compared to the limit value established in the first step;
- The design drift demand should be smaller than the ultimate drift capacity of the slab frame. When this is not the case, it is possible to reduce the drift of the structure or to improve the deformation capacity. The drift of the structure can be decreased incrementing the stiffness of the primary system so changing its dimensions. The deformation capacity can be improved, by increasing the slab thickness, the column cross-section or by providing shear reinforcement.

3.3 SlabSTRESS Project Description

SlabSTRESS (Slab STructural RESponse for Seismic design) is an experimental campaign which aims to provide experimental evidence of the response of flat slab buildings under combined gravity and lateral load, with the purpose of developing a European seismic code for this structural typology.
The project was launched by a group of European universities, led by the Politecnico di Milano together with the EPFL (Ecole Polythecnique Federal Lausanne), UNOVA (Universidade NOVA de Lisboa) and UTCB (Universitatea Tehnica de Constructii Bucuresti), in collaboration with the Joint Research Centre of the European Commission in Ispra, Italy.
The research studied a real scale, flat slab structure, constructed and tested at the reaction wall facility of the ELSA laboratory of the Joint Research Centre.
The experimental campaign is part of the Transnational Access activities of the SERA (Seismology and Earthquake Engineering Research Infrastructure Alliance for Europe) project. This project has received funding from the European Union's Horizon 2020 research and innovation programme under grant agreement No.730900.
The overall objective of SERA is to give a significant contribution by improving the access to data, services and research infrastructures, and to deliver solutions based on innovative R&D in seismology and earthquake engineering, with the aim of reducing the exposure of our society to the risks posed by natural and anthropogenic earthquakes.
Among other activities, SERA will offer transnational access to the largest collection

of high-class experimental facilities for earthquake engineering testing.
The research campaign is divided into two phases: the first one is a pseudodynamic test run with numerically modelled walls. It is a seismic test to study the seismic response and damage to a flat slab frame with seismic resistant walls tested with accelerograms compatible with the serviceability limit state (SLS) and the ultimate limit state (ULS) earthquake action. This phase aims at verifying the design procedure.
The second phase of the SlabSTRESS experimental campaign is the cyclic quasi-static tests. This phase has various purposes: first of all, the study of the global response for gravity and lateral loading, with a main focus on the different connections (edge, internal and corner) and the redistribution of load effects on the floors and in the building. This phase was characterised by two cyclic tests with different gravity shear ratios and drift levels.
The first one aims to explore the non-linear response at high drift. Initially, the idea was to continue the tests up to the failure of some connections, including punching, which would later be repaired.
The second cyclic test aims to test the repaired structure and the non-linear response to punching of unrepaired slab-column connections at higher drift levels, and to explore the response of the 2nd floor up to failure.

3.4 Design of the specimen for Seismic Actions

For the choice of the design earthquake, the structure was considered to be located in the city of Gemona, in the region of Friuli-Venezia Giulia (Italy) that was struck by a 6.5 MW earthquake in 1976.
The structure was designed according to the Italian Standard NTC 2018 (DM 17.01.2018) [6]. The code provisions used are compatible with the European codes Eurocode 2 [7] and Eurocode 8 [9].
The combinations of actions considered were chosen in accordance with EN 1990 [9] (Table 3.1):

Table 3.1 Load combinations

Combination	Equation
Gravity load	$1.35G_k + 1.5Q_k$
Seismic	$G_k + 0.3Q_k + E_d$

The gravity load in the seismic design combination was 8.6 kN/m^2.
In particular, NTC2018 [6] indicates for the punching design the use of acknowledged International standards for the punching design. Eurocode 2 [7] is used for the punching verifications in this design.
The Italian code NTC2008 [17] design spectra were used (Figure 3.2 and Figure 3.3) with a peak ground acceleration PGA=0.26g. For the ULS design spectrum, a behaviour factor q = 4 was considered, for uncoupled wall systems with no more than

two long ductile walls.

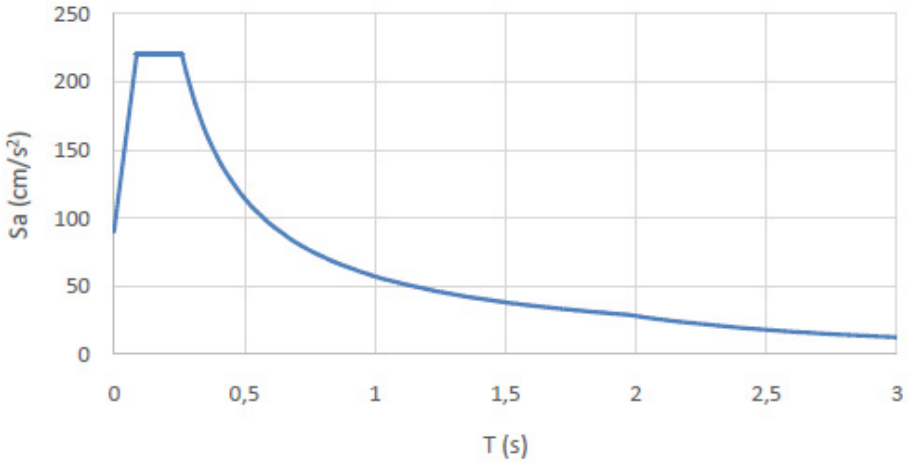

Figure 3.2 SLS horizontal acceleration design spectrum.

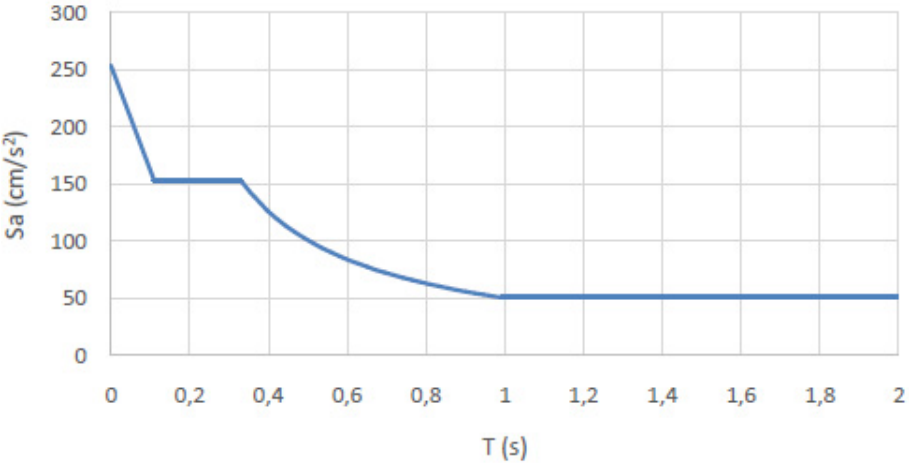

Figure 3.3 ULS horizontal acceleration design spectrum.

The seismic resistant walls were designed as primary elements for a seismic zone, based on the chosen dimensions of the plan, the number of floors and the slab thickness of the actual building.
The two walls were designed with a thickness of 0.32m and a length of 1.5m and these allowed to obtain a flat slab with a stiffness equal to 20% of the walls stiffness (Figure 3.4).

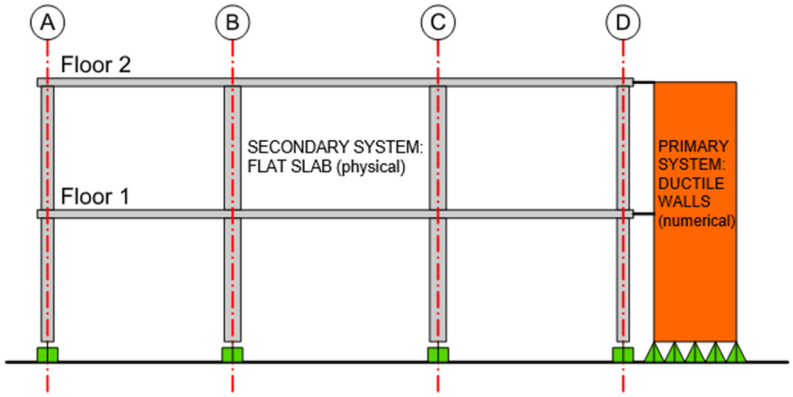

Figure 3.4 Building with virtual walls.

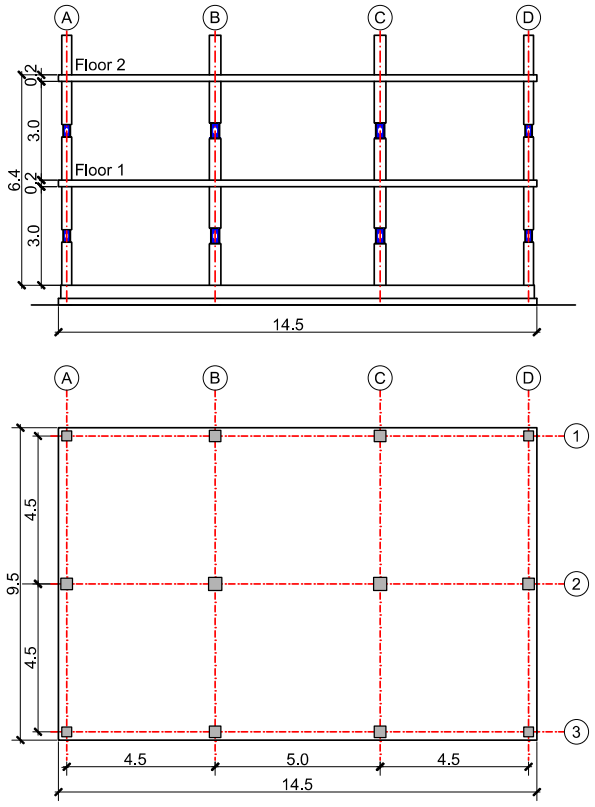

Figure 3.5 Dimensions of the physical structure for testing: a) side and b) plan view.

A modal analysis of the structure was carried out, considering the members in the cracked state with T_1 = 0.315 s as the 1st vibration period in the direction of the walls, and a_{ULS} = 153.06 cm/s^2 the corresponding ordinate of the design spectrum for the ULS. The seismic coefficient is:

$$c_s = \frac{\gamma_1 * a * S * \eta * \lambda}{g} = \frac{1 * 153.06 * 1 * 1 * 0.85}{981} = 0.132 \qquad Eq. 3-1$$

Where:
a= ordinate of the design spectrum;
S= coefficient for the subsoil category and the topographical conditions;
η= factor that modifies the elastic spectrum for conventional viscous damping coefficients different from 5%;
λ= coefficient equal to 1;
g= gravity acceleration

For SLS, the spectral ordinate is a = 182.3 cm/s^2.

The link between the walls and the flat plate system is given by the horizontal diaphragms, which are geometric constraints. These internal constraints allowed the same translation between walls and floor, at each floor height.

The design follows these steps:

- Based on the design inter-storey drift ratio in common building between 0.5% and 1% (Bisch et al., 2012 [2] and Coronelli and Martinelli, 2017 [3]) the design inter-storey drift of 0.4% was chosen;
- The flat slab frame was designed for gravity loads according to the provisions in EC2 [7];
- In the following steps, the definition of gravity shear ratio based on the North American code ACI-318 was used (Hueste et al., 2007 [13]). The gravity shear ratio for interior columns calculated using ACI318-14 [11], nominal concrete properties and a capacity reduction factor of 0.75 was 0.4, corresponding to Dru=1.5%;
- For the corner and edge connections the gravity shear ratio was approximately equal to 2/3 of that of the internal ones;
- Once chosen the dimensions of the plan, the number of floors and slab thickness, two seismic resistant walls were designed as primary elements for the seismic design loading combination. The primary elements were designed according to the Italian code NTC2018 [6], whose provisions are consistent with those of EC2 [7] and EC8 [8];
- The inter-storey drift ratio for the primary elements at the ULS was calculated. It was obtained from the response spectrum analysis using the cracked stiffness;
- The inter-storey drift ratio for the seismic design combination previously calculated was multiplied by the behaviour factor, q. In this way the design inter-storey drift ratio was obtained;

- If the deformation of the column is neglected, the design drift ratio can be compared directly to the drift ratio capacity of the flat slab frame;
- The stiffness of the flat slab frame was compared to the wall stiffness. This check led to one iteration in the design. On the basis of the resistance required for the design actions, the wall stiffness would have been smaller, leading to a higher design drift. This would have been compatible with the *GSR* and ultimate drift capacity of the slab. The wall stiffness had to be increased to make the flat slab frame stiffness to be equal to 15 % of the primary walls stiffness. A ratio of 20 % was obtained. Even though this value exceeds the limit value of 15 % recommended by EC8 [8], it was nevertheless considered acceptable since the value 15 % is a non-prescriptive provision

3.5 Design of the specimen for Gravity loading

The building is a reinforced concrete structure with two reinforced concrete flat slab floors supported on columns and shear resistant ductile walls.
The structure consists of six panels to each floor, with spans 5 m and 4.5 m in the longitudinal direction and 4.5 m in the transverse direction. Spans in the short direction were reduced in order to fit the specimens through ELSA laboratory doors. The storey height is 3.2 m. The total building dimensions are 14.5 m x 9.5 m (Figure 3.5).
The slabs are ordinary reinforced concrete without voids and have a thickness of 0.2 m.
The building foundations consist of a reinforced concrete orthogonal beams grid in correspondence to the column lines, with a bottom slab to allow the transfer of the building both to the inside and the outside of the laboratory, and to fix it to the stable floor of the ELSA laboratory.
The analysis was performed with ETABS 16. The slab is modelled with thin shell elements. The supports on the columns are modelled with one vertical displacement constraint in correspondence to the column axis. The slab bending moments are integrated to obtain strip moments.
The design for the gravity loading is carried out following the Eurocode 2 [7] specifications.
The loads considered in the design (Table 3.2) were chosen in order to be representative of those commonly adopted for a residential building:

Table 3.2 Design loads

Load typology	Load (kN/m^2)
Slab' self-weight of the slab	G_{k1}=5
Permanent load	G_{k2}=3
Live load	Q_k=2

The flat slab structure, the columns and the foundations were designed for normal-strength C30/37 concrete having a characteristic cylinder strength f_{ck}=30 MPa.
For the reinforcement, different typologies were used; in floors and foundations, B450C, in the columns, S500 Class B, for the column bases B450C and in the punching reinforcement stud
To have the maximum possible data from the experiment campaign, the top layers of the slab-column connections on the 1st floor were reinforced in two different ways "smeared" and "concentrated". The "smeared" pattern reinforcement was used in a column strip of width equal to ¼ of the span on each side of the column whereas the "concentrated" one was used in ¼ of the column strip as recommended in Eurocode 2 [7].
The connections of the west half of the slab (A and B) have smeared reinforcement, while the connections of the other one-half of the slab (C and D) have concentrated reinforcements.
Two bottom bars in each direction were placed at each connection, in accordance with Eurocode 2 [7] their role being that of integrity reinforcement.

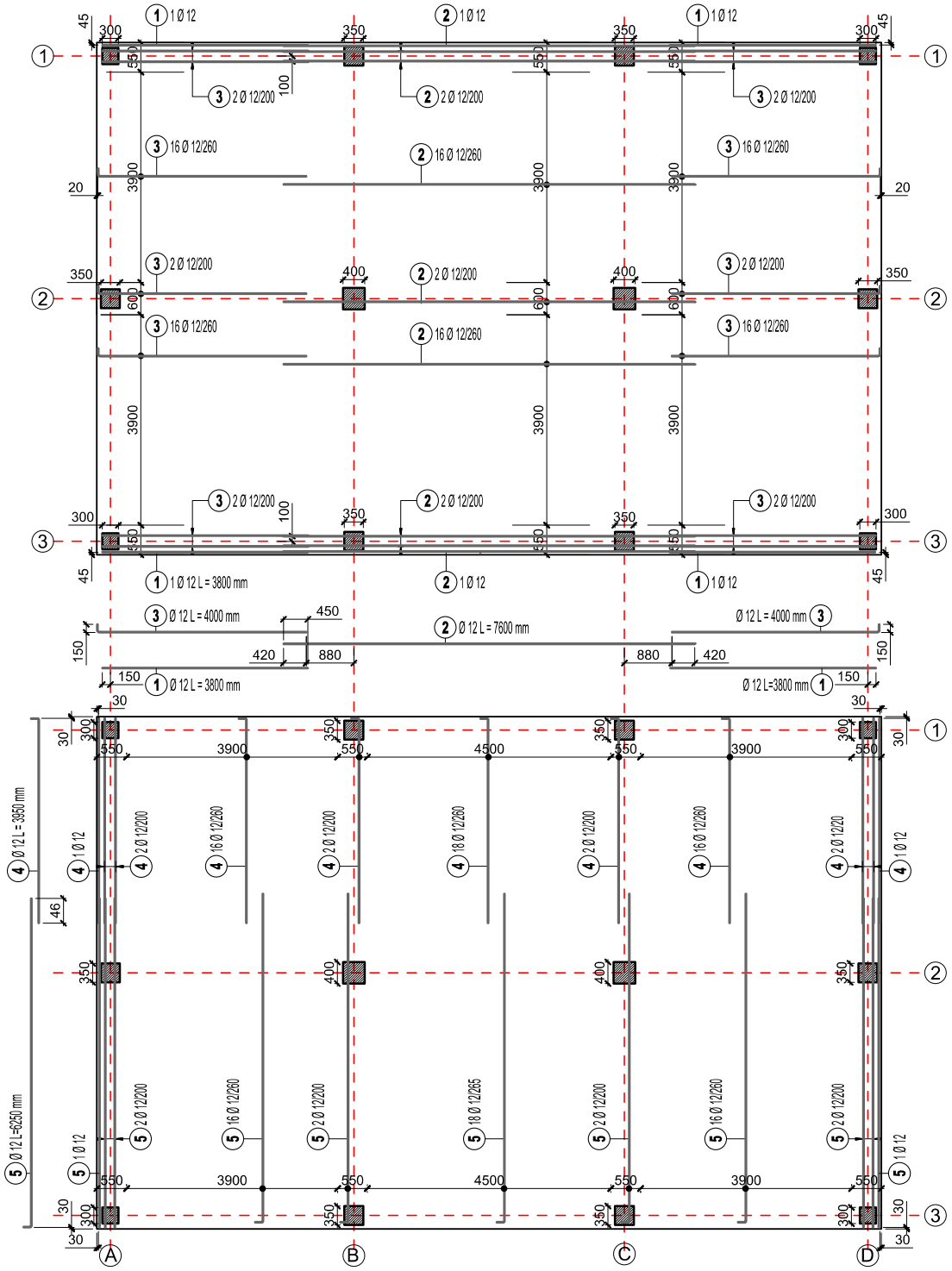

Figure 3.6 Bottom longitudinal reinforcement in the slab of the 1st and 2nd floor.

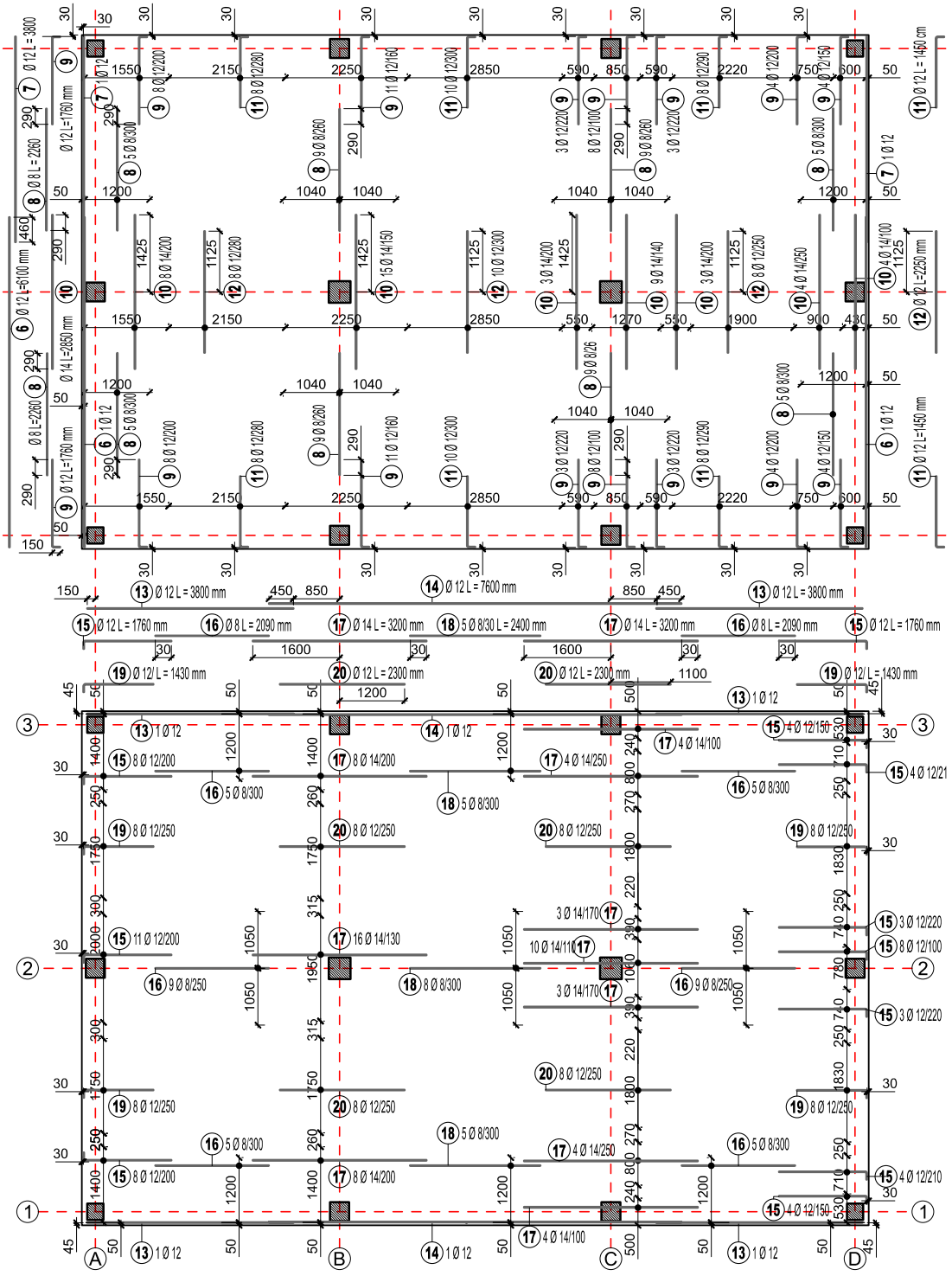

Figure 3.7 Top longitudinal reinforcement in the slab of the 1st and 2nd floor.

The anchorage at the free edge of the slab was an "L" shaped bend 40 times the length of the rebar diameter, as commonly used in the practice in European practice. Based on the gravity loading design, the slab-column connections in the 1st floors did

not require punching shear reinforcement. Therefore, the slab-column connections on the 1st floor were not reinforced against punching shear, whereas a different choice was made for the 2nd floor. On this floor, for the experimental research to be carried out in the laboratory (the economic investment in the test and the chance to test only one structure) it was chosen to test the performance with shear punching reinforcement. The 2nd floor slab was reinforced using headed studs as punching shear reinforcement (Figure 3.8). as a consequence, the study includes different slab-column connection (lateral, internal and corner) and two different flexural reinforcement layouts in a slab with realistic thickness with shear reinforcement.

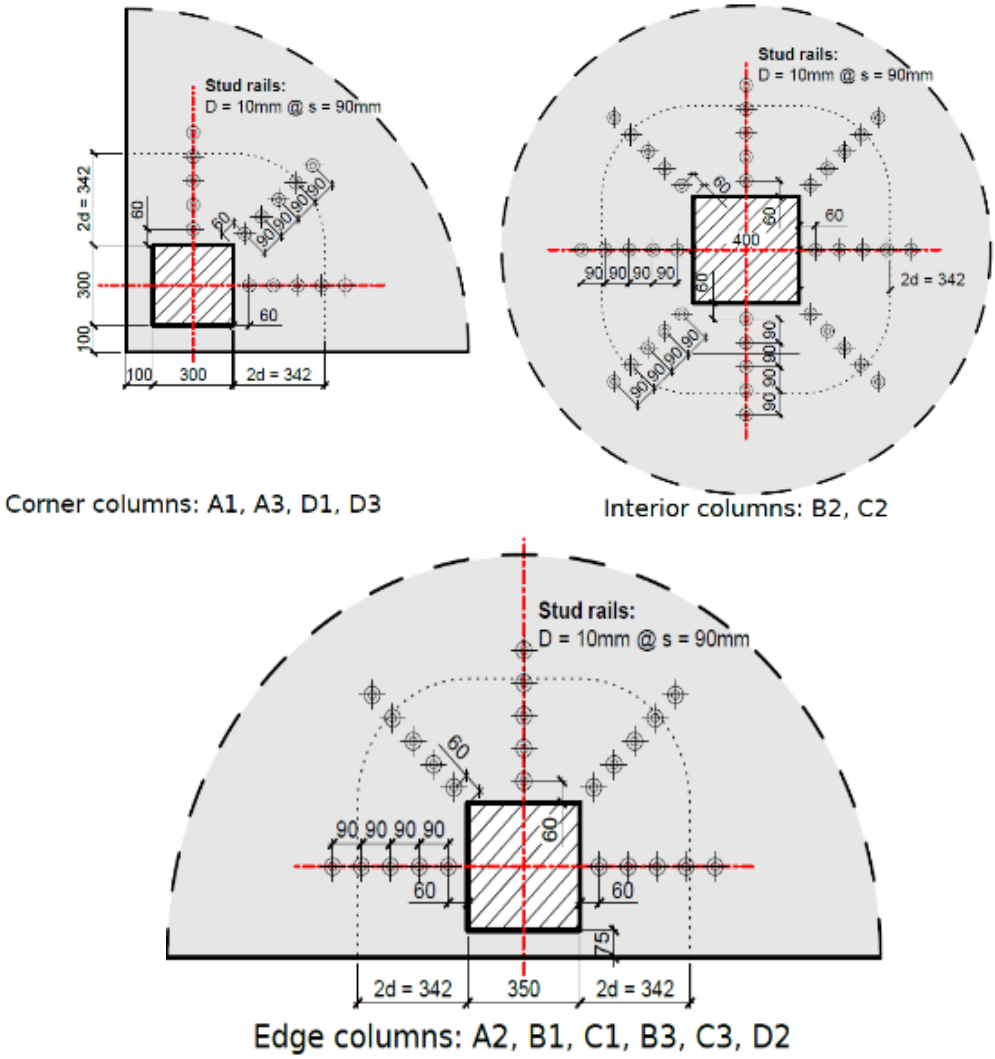

Figure 3.8 Punching reinforcement at a) corner, b) internal and c) edge slab-column connections at 2nd floor.

3.6 Column Design

The columns in the test structure are made of reinforced concrete, with a central

steel stub for internal force and moments' measurement in the columns of each floor of the structure (Figure 3.9).
The columns are 3.2 m in height between each slab, the central stub is 0.5 m long, the cross sections are square with a dimension of 0.4 m for the internal column typology, 0.35 m for the edge typology and 0.3 m for the corner typology.

Figure 3.9 Steel stub in the columns.

The choice of the cross section and dimensions of the internal stubs has been made in order to provide the same stiffness as that of the concrete cross-section.
The column design is based on the experimental research carried out, the application of large lateral forces in combination with the application of additional gravity loads during the cyclic tests bringing the structure to high lateral drift. A study has been carried out to estimate the internal forces in the columns during the laboratory test.

The design of the columns was carried out as follows:

- Calculating internal forces assuming constant stiffness along the length of the members;
- Providing the reinforcement necessary to develop plastic hinges at the base of the ground floor column during the testing with lateral loading in the laboratory that will reach high inter storey drifts (greater than 5%);
- In order to avoid damage along the length of the RC columns, heavy reinforcement is provided far from the plastic hinges. This leads to resistance of the column cross-section higher than that required for the design moments due to gravity and seismic loading previously considered.

The internal forces and moments considered in the column design were those developed in the cyclic testing phase up to failure. A conservative estimate of the maximum moment transfer from the slab was obtained using a formulation proposed by ACI421.2R-10 [10]. Finally, the bending moment distributions in the columns corresponding to maximum slab moment at the floors was calculated. On the base of these moments, the columns were designed to safety satisfy safety demands.
The design of the load cells was carried out to support the internal actions caused by the maximum moments transfer from the slab.

3.7 The Strengthening procedure

The first phase of the experimental campaign regards the execution of tests up to the achievement of a significant inter-storey drift with consequent damage to the slab-column connections. After this phase, three different connections on the 1st floor, located in the two halves of the slab with different longitudinal reinforcement, were chosen for strengthening. One lateral in the long North side, B1, one central in the eastern half, C2 and the last one lateral in the long South side, C3, were strengthened with post-installed bolts using the same layout of the pre-installed studs. The purpose of strengthening connections is to verify the effectiveness of post-installed bolts in earthquake damaged connections of a complete full-scale structure of realistic dimensions.

3.8 Summary

In this chapter the design of the structure, the description of the geometry and the materials were presented.
A design approach method was defined to consider the flat slab as secondary seismic member.
The design of the specimen was described firstly for the seismic action and then for the gravity loading. A specific section was reserved to the design of columns and to the strengthening procedure.

References

[1] M. N., Fardis. Seismic Design, Assessment and Retrofitting of Concrete Buildings: based on EN-Eurocode 8 (Geotechnical, Geological, and Earthquake Engineering). 2009.

[2] P. Bisch, E. Carvalho, H. Degee, P. Fajfar, M. Fardis, P. Franchin, M. Kreslin, A. Pecker, P. Pinto, A. Plumier, H. Somja, G. Tsionis. "Eurocode 8: Seismic Design of Buildings Worked examples". EC 8: Seismic Design of Buildings", Lisbon, 10-11 Feb. 2011.

[3] D. Coronelli, L. Martinelli, (2017) "La progettazione sismica dei sistemi a piastra in cemento armato" Pàtron Editore, 116 pp.

[4] Drakatos IS, Muttoni A, Beyer K. Mechanical model for drift-induced punching of slab-column connections without transverse reinforcement. ACI Struct J 2018; 115:463–74. doi:10.14359/51701110.

[5] Almeida A., Alcobia B., Ornelas M., Marreiros R., Ramos A. P. "Behaviour of reinforced-concrete flat slabs with stirrups under reversed horizontal cyclic loading". Magazine of Concrete Research, 2019.

[6] NTC2018 - Norme tecniche per le costruzioni 2018 (NTC 2018) - D.M. 17 Gennaio 2018 (D.M. 17/1/18) – in Italian.

[7] CEN (European Committee for Standardization). 2004. Design of concrete structures, general rules and rules for buildings part 1.1. Eurocode 2, Brussels, Belgium: CEN.

[8] CEN (European Committee for Standardization). 2004. Design of structures for earthquake resistance, general rules, seismic actions and rules for buildings part 1. Eurocode 8, Brussels, Belgium: CEN.

[9] EN 1990 (2002): Eurocode - Basis of structural design [Authority: The European Union Per Regulation305/2011, Directive 98/34/EC, Directive 2004/18/EC]

[10] ACI (American Concrete Institute). 2010. Seismic Design of Punching Shear Reinforcement in Flat Plates. ACI 421.2R-10. Farmington Hills, MI: ACI.

[11] ACI. ACI 318-14. Building Code Requirements for Structural Concrete. ACI; 2014.

[12] CSA. CSA Standard A23.3-04: Design of Concrete Structures. Ontario, Canada: 2004.

[13] Hueste MBD, Browning J, Lepage A, Wallace JW. "Seismic Design Criteria for Slab-Column Connections". ACI Struct J 2007; 104:448–58.

[14] Moehle JP. "Seismic design considerations for flat-plate construction". ACI Spec Publ 1996; 162:1–34.

[15] Megally S, Ghali A. Punching Shear Design of Earthquake-Resistant Slab-Column Connections. ACI Structural J 2000; 97:720–30.

[16] Dilger WH, Dechka DC, Brown SJ. Slab-Column Connections Under Seismic Actions. ACI Spec Publ 2005; 232:127–46.

[17] NTC2008 - Norme tecniche per le costruzioni 2008 (NTC 2008) - D.M. 14 Gennaio 2008 (D.M. 14/1/08) – in Italian.

4 Experimental programme

4.1 Introduction

The SlabSTRESS programme was conceived for the study of the global and the local response of flat-slab frames under seismic and gravity action. The experimental activities regarded the full-scale testing of a two-storey specimen with the aim to assess the seismic performance of a flat-slab building designed as secondary system with primary numerical ductile walls.
For the pseudo-dynamic tests, two seismic tests were performed, at the serviceability and ultimate limit state.
Quasi-static tests were performed with cyclic loading to study: a) the redistribution of action effects on the floors; b) the response of different types of slab-column connections (corner, edge and interior) with realistic boundary conditions, the failure modes of the different connections, and the effect of different layout and detailing of longitudinal and transverse reinforcement.
Special devices were positioned at mid-height on each column in order to analyse the internal action of columns during the experimental campaign. These devices enabled the measurement of the shear and axial forces at the bending moment.
The programme was developed to study the behaviour on existing structures also. After a first test, carried out up to the onset of punching on the first floor, some slab-column connections of different types were reinstated and a second cyclic test was performed to verify the efficiency of retrofit of slab-column connections with post-installed bolts.
The experimental campaign is presented here. After an initial description of the hosting structure (the JRC's ELSA laboratory in Ispra, Italy.), the construction phases and the transporting of the real scale specimen into the laboratory, are described.
The dissertation follows with a description of the test setup and the instrumentation used to acquire the experimental data. This section contains a full description of the calibration procedure for the measuring equipment used, with a reference to the quantities investigated and the obtained results. The positioning of sensors and loading devices are then illustrated together with a description of the loading system and the safety procedures adopted to avoid any possible accidents from unexpected events during the testing. The chapter ends with a description of each test which characterised the experimental campaign that is to say, the two seismic and the three cyclic tests, with a special section dedicated to the pseudo-dynamic procedure.
The SlabSTRESS experimental campaign was conducted at the ELSA Reaction Wall of the European Commission’s Joint Research Centre (JRC) in Ispra (Italy) associated

with the transnational access activities of the SERA project.
It is one of the larger scale experiments conducted in the ELSA laboratory; in fact, it involved the use of four ±500 kN actuators and a large number of instruments: 80 inclinometers, 48 extensometers and 192 strain-gauges used to create 72 Wheatstone bridges.
SlabSTRESS is the first setup with such a large number of channels for the acquisition of data (200 signals in total). In order to handle such a large number of signals with high quality standards, an innovative calibration procedure was used to check the entire measurement chain, divided into acquisition clusters before mounting them on the mock-up. This was achieved by introducing a new control and data acquisition system, ElsaREC, which was used for the first time on a full-scale building during the SlabSTRESS experimental campaign.

4.2 Construction and transportation

The specimen was constructed on the outside of the ELSA laboratory, on the west side and later transported inside.

Figure 4.1 Construction of the specimen outside the laboratory.

4.2.1 THE JRC-ELSA LABORATORY

ELSA is the acronym for “European Laboratory for Structural Assessment” [6]; and is part of unit E.04 "Safety and Security of Buildings", located at the Ispra site (Italy) of the European Commission's Joint Research Centre (JRC).
The aim of ELSA is to encourage research and to contribute to the European Standards harmonization in construction, and to perform vulnerability assessment of buildings and civil infrastructures to limit risk, and to develop appropriate methodologies by integrated use of experimental testing and numerical modelling in Structural Mechanics.
The core research of ELSA is developed in aid to support the standardization of construction and the EU construction industry, and to assess the physical vulnerability of critical structures
The main facility at ELSA is a Reaction Wall, unique in Europe for its size and for the

possibilities it offers, allowing the testing of full- or nearly full-scale structures, in order to experimentally assess their behaviour under earthquakes or other extreme loading. Work related to existing structures includes the development of techniques for their strengthening and/or repair that are validated by means of tests performed on representative models.
The reaction wall is one of the largest in the world. It is 21 m long, 16 m high and 4 m thick (boxed type construction), with two reaction platforms having a total surface of 760 m^2 that allow for testing real scale structural models on both sides of the wall.
It was estimated that, for the case under examination and allowing for some margin, the maximum applicable force should be limited to the order of 5000 kN.

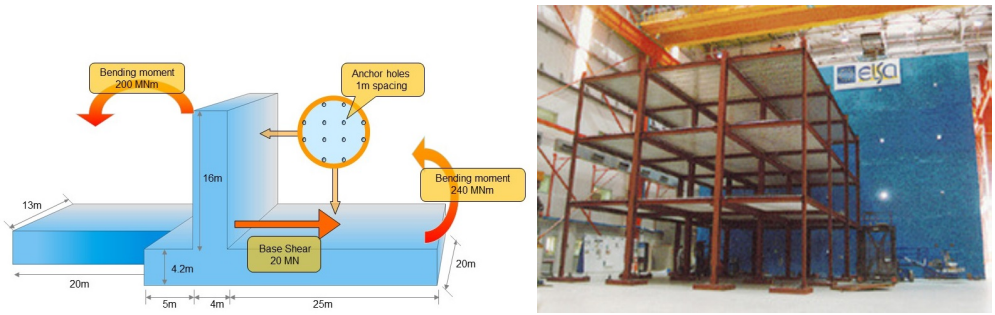

Figure 4.2 *a) Dimension of the RW b) Typical full scale mock-up [1]*

In addition to static and cyclic tests on large structures and their components, the facility is equipped for the so-called pseudo-dynamic test (PSD) technique. The PSD enables the simulation of earthquake loading on full-scale buildings. The loading capacity could be limited by the resistance of the RW in shear and/or bending.

4.2.2 CONSTRUCTION

The building of the structure was entrusted to a construction company, employing normal materials and technology.
The structure was built over plastic sheeting, to facilitate the lifting and transfer of the structure to the inside and then the outside of the laboratory.

Figure 4.3 Plastic sheet under the structure.

The work began with the preparation of the foundation slab and connecting beams between neighbouring columns, in accordance with common requirements for buildings in earthquake-prone areas. The connecting beams have also been used to accommodate the lifting systems and to provide stiff ribs during the transportation phases.
Some threaded metal bushing was inserted within the slab reinforcement of the 1st and the 2nd floors for bolting HE metal beams used to connect actuators.

Figure 4.4 Foundation slab.

Rebars with threaded couplers were inserted into the foundations as column reinforcement and, afterwards, to connect the measuring devices (load cells). Plastic (PVC) tubes were inserted to install the lifting jacks and other tubes were used to fasten the mock-up to the strong floor. The connections were placed at different heights to prevent the couplers from being all on the same plane.
The column reinforcements were installed using the positioning jigs due to the very low clearance of the load cell mounting holes.

Figure 4.5 Rebars and plastic tubes detail.

The concrete of the foundation slab was cast and vibrated, then the internal

formwork for the beams was installed.
The load cells were assembled before ground floor columns were cast. Each load cell directly connecting column rebars above and below. Therefore, reinforcement bars ranged from the lower load cell to the upper one, avoiding any lap splices. Formworks were installed successively.
The load cells were protected by a plastic film to preserve the surfaces.
A gap of 2 cm was left underneath each load cell, which was subsequently filled by non-shrinkage mortar poured into special holes in the load cell bases. In this way a perfect contact was ensured between the steel surface of the cell and the top of the concrete casting was ensured. The casting of the upper half of the column, between the top of the load cell and the floor slab of the upper floor, was carried out without any special measures.

Figure 4.6 Column details: reinforcement, load cell and formwork.

Once the concrete was setting, the column formwork was removed and the preparation work for the first slab began.

Figure 4.7 Placing of the formworks for casting the first floor.

Two different longitudinal reinforcement layouts (smeared and concentrated) were collocated on both the floors, whereas the shear reinforcement was applied only on the 2nd floor.

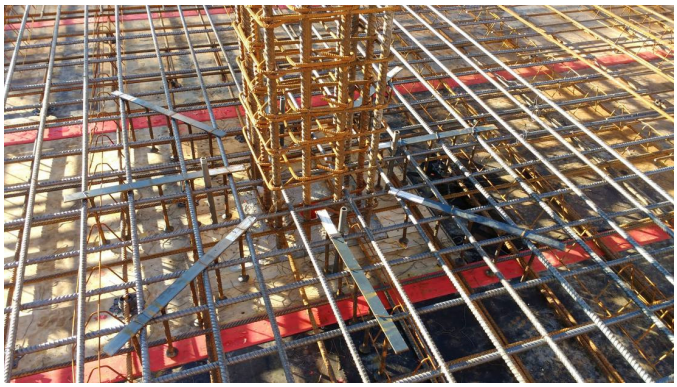

Figure 4.8 Reinforcement layout.

The second phase of the test campaign envisaged the strengthening of the 1st floor slab by the use of post-installed threaded bars bolted on both sides of the slab.
A rebar scanner correctly located existing rebars making the application effective. While this technique is valid for ordinary applications, it is less accurate and slower when performed in a laboratory environment, where interference from measuring devices must also be considered. To this purpose small pre-holes were required to ensure the positioning and verticality of drilled holes, in order to avoid any interference with the longitudinal rebar and measuring devices. Small plastic tubes (4 mm diameter) were fitted into some nails, inserted into the formwork where the pre-holes were to be made. All the nails were then removed together with the formwork.

Figure 4.9 Plastic tubes positioning in the slab-column connections that will be strengthening.

The assembly procedure of the column with the load cell at the mid-height was then repeated for the upper floor.
The formworks used for the 1st floor, were then reutilised on for the 2nd. Leaving only the props until the end of the curing time, for least 28 days.

Figure 4.10 Props and safety measure for all the structure.

After the curing time (at least 28 days) all the props were removed and safety devices were installed to allow the workers to safely operate inside the structure.

Figure 4.11 Painting of the structure.

Finally, all columns and plates were white painted to facilitate the detection of cracks during the experiments.

4.2.3 TRANSPORT OF THE SPECIMEN

After construction, the specimen was transported to the interior of the laboratory. The specimen was raised by means of 16 hydraulic jacks working at equal oil flow to prevent any rotation or misalignment of the base. A roller surface was placed underneath the specimen, which was then lowered and hauled to its final destination in front of the reaction wall, then fixed to the floor by means of DYWIDAG threaded bars. The roller was designed to work at the elastic limit in order to compensate the irregularities of the floor without transmitting significant deformation to the upper level of the structure.

Figure 4.12 Transportation of the specimen through the ELSA laboratory door.

The preparation, the transportation and positioning of the specimen was completed

in 2 days and due care was taken to ensure the integrity of the structure.
After the end of experimental campaign, the same procedure was followed in reverse when taking the specimen outside.

4.3 Test setup

The installed measuring equipment is related to the purposes of the experimental program. Both the building seismic response and the study of the connection ultimate drift capacity require the measurement of the connections response, and the recording of the damage conditions.
Given the complexity of the analysed structure, a simplifying procedure was required to break it down into sections in order to facilitate analysis. Two simplified models were chosen to represent the structure from a global and a local point of view, using the main statics and kinematics parameters. Two kinematic parameters, one displacement for each floor and two static parameters, one force for each floor describe the global system. These parameters were acquired by using load cells applied to the actuators, and displacement transducers applied on two reference frames near the structure.
The local system was more complex due to the presence of the slab-column connections. The slab and the column rotations are the local kinematic parameters that are recorded by the inclinometers, and the opening of slabs cracks recorded using the displacement transducers.
Local kinematic measurements were taken on eight out of the twelve columns and in the surrounding area of the slab. The three connections typologies (internal, edge and corner) were analysed with four, three and two instrumented sides respectively. Each side of the slab-column connection was equipped with an inclinometer to measure the rotation of the slab along the loading direction (East-West), while in the same position a set of displacement transducers was applied, to measure eventual the crack formation through the increasing thickness of the slab.
Using the acquired data concerning the rotation of the slab and the column in each slab-column connection, it was possible to evaluate the relative rotation of the slab with respect to the column.
The static parameters are three for each column: one shear, one bending moment and one axial force; so six for each column. These parameters were acquired by the load cells, steel member systems, located at the centre of each column on each floor, appositely designed for this experimental campaign. A reduction of the measure points for rotations and crack openings was permitted for by the double-symmetry of the mock-up.
The clusters of instruments for the internal columns (B2 and C2) had therefore 26 signals each, for the edge columns (A2, B1, C3 and D2) 22 signals each and finally the corner columns (A1 and D3) 18 signals each.

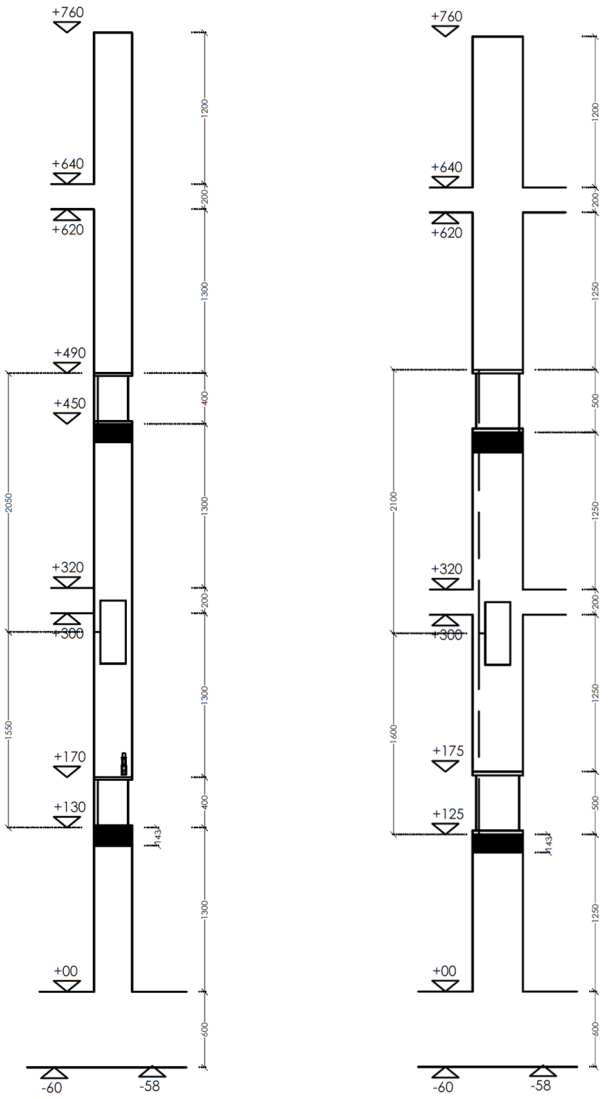

Figure 4.13 Corner and edge column.

All measurements were digitally converted and grouped and the data was sent through the local network to the data acquisition server.

A new generation of servo-hydraulic real-time digital controller/acquisition systems was developed at the ELSA laboratory and used for the first time for the SlabSTRESS experiments campaign. The hardware architecture is based on EtherCAT modules that guarantee a versatile and modular system. Other innovative features of this configuration were that all the analogue signals were digitalized in proximity to the transducers, thereby reducing noise to signal ratio, and all the different slave controllers communicated at each time sampling by way of a robust digital bus. The simplified software architecture developed, in addition to the increasing computer performances, guarantees a substantial improvement in control quality in terms of speed, safety and accuracy, compared with conventional/commercial systems.

Each kinematic measuring device was calibrated on a measuring bench before it was placed on the specimen.
An identification code was created for each sensor. This code contains:

- Acronym of the sensor:

  SR= slab rotation, (inclinometer in the slab);
  CR= column rotation, (inclinometer in the column);
  SC=slab crack opening displacement (crack opening displacement transducer);
  M= column bending moment (load cell);
  V= column shear force (load cell);
  N= column normal force (load cell);

- Floor in which the measurement was detected, 1 or 2;
- Name of the slab-column connections in which the sensors was placed (A1, A2, A3, B1, B2, B3, C1, C2, C3, D1, D2, D3);
- Cardinal point (N= north; S=south; E=east; W=west) for the sensors in the slabs and U=upper and B= bottom for the sensors in the columns.

An example of each sensor typology in the slab-column connection A1 and column A1 are here reported:

SR-1-A1-E

CR-1-A1-U

SC-1-A1-E

M-1-A1

V-1-A1

N-1-A1

4.3.1 ETHERNET-BASED SERVO-HYDRAULIC REAL-TIME CONTROLLER (ELSAREC)

In hybrid testing and in general mechanical testing of large-scale structures, the actuation of the specimen is typically performed using servo/hydraulic actuators connected to an electronic control system. The commercial controllers may present some relevant limitations mainly due to an inability to modify certain aspects of the setup or testing methodology. In the ELSA laboratory, a custom controller is used to overcome the limitations found in the commercial controllers.
In large scale mechanical/structural tests the system complexity grows exponentially because, in addition to the actuation system, a large number of sensors are often involved. These tests are very expensive and difficult to repeat, so the tendency is to use as many sensors as possible in order to collect all possible information. Consequently, this involves a great number of sensors and cables. The drawbacks of

the actuation system together with the high number of sensors and cables make the work very complex.
With an aim to improve this acquisition system, the team of the ELSA laboratory developed a new approach that was called ElsaREC. ElsaREC means Elsa Real-time EtherCAT Controller and data acquisition system, it is based on EtherCAT data transfer protocol and is the product of many years of research and work (since 2012). EtherCAT is a transfer protocol based on an Ethernet bus, that allows the creation of device networks of different topologies (i.e. lines, trees or stars). The devices connected are generally Input-Output modules, conditioning apparatus or CPUs that exchange information by means of the EtherCAT bus, with a clock sampling to the order of one millisecond or even less. The main advantage of this technology is that it makes possible to accurately synchronize devices spatially distributed with a simultaneity to the order of tens of microseconds [1].
ElsaREC controller and the data acquisition system is based on EtherCAT commercial modules and assembled in suitable boxes (Figure 4.14).

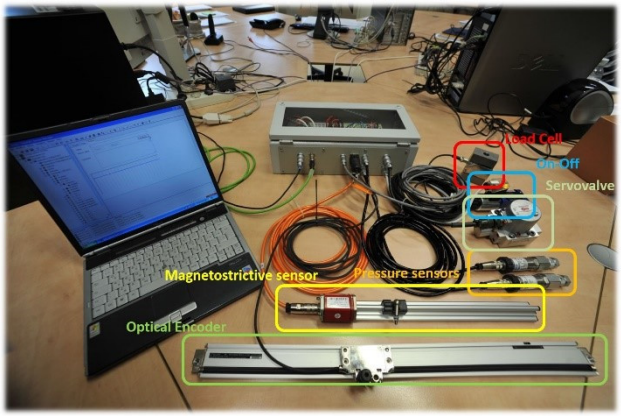

Figure 4.14 Slave module.

Figure 4.14 shows the control slave module of a servo-hydraulic actuator. The slave is connected to all sensors and valves that permit the functioning of the actuator.
The diagram of a typical control and acquisition system with the ElsaREC system is reported in Figure 4.15.

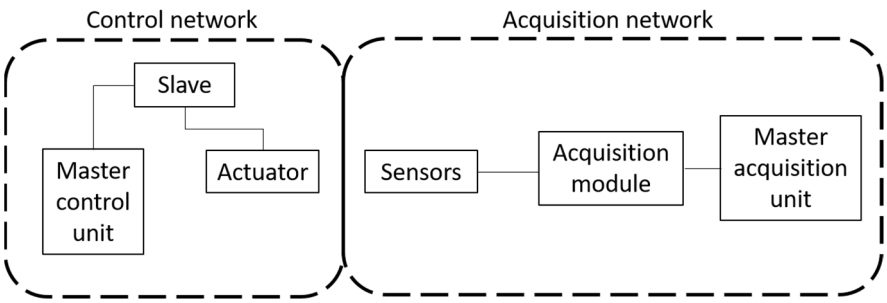

Figure 4.15 Architecture of the control/acquisition system.

With this new system, each actuator is provided with a slave control module that maintains the analogue part of the system close to the actuator. Each slave is then connected with just two cables, an EtherCAT and a power supply, creating the control network. The ElsaREC data acquisition system has been designed with the same philosophy of the control system, by creating a series of slave data acquisition boxes (Figure 4.16) that provide the conditioning and the digitalization of sensors routinely used during the ELSA experimentation; (linear encoders, linear potentiometers, magnetostrictive sensors, inclinometers, strain gages and load cells).

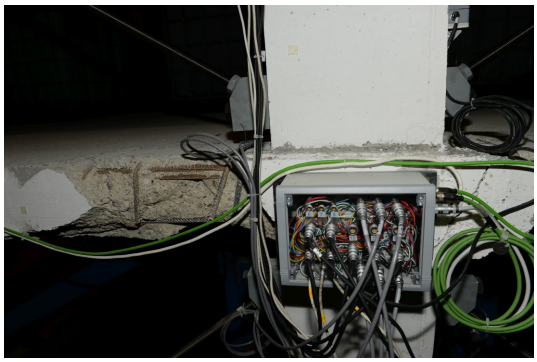

Figure 4.16 Data acquisition box.

In the case of large scale tests, sensors are grouped for spatial location and connected to a tailored slave box that conditions-digitalizes different type of sensors while keeping the analogue cabling lengths to a minimum. The boxes are simply connected with a robust data bus and a single power supply cable to a centralized Master Unit that has access at any time to all the available data.
The assembling of the boxes is relatively rapid, because the sensor plugs are already prepared, and it only requires the preparation of an ad-hoc plug plate.
Compared with the previous generation of ELSA servo-hydraulic controllers and data acquisition system the proposed architecture presents several advantages:

- The versatility of the utilisation of a modular structure of commercial EtherCAT in cases of particular test setups;
- The guarantee of the ISO 9001 standard requirements due to the utilization of commercial certified modules;
- The possibility to use modules under difficult environmental conditions;
- The reduction of the distance between analogue components and the AD converters thereby decreasing the noise of the signal;
- The improvement in the EtherCAT technologies allowed to increase the number of slaves that could be managed simultaneously by the master unit;
- The reduction of the number of cables that connect the control PC (Master Unit) to the EtherCAT modules to only two cables (power supply and EtherCAT bus) in a line topology network;

- Through the presence of a series of LEDs, the electrical connections of each module could be monitored.

The ElsaREC controller and data acquisition system was used for the first time on a full-scale building mock-up.
The actuation system is moderately complex, with four servo-hydraulic actuators having a capacity of 500 kN and a stroke of 1m each. On the other hand, the data acquisition system is of huge complexity in terms the number and typology of sensors. In detail a total of 200 data acquisition channels were used:

- 24 3-axial column load cells (72 independent Whetstone bridge channels) placed at the middle of each column to measure normal force and in-plane shear force and bending moment;
- 48 linear displacement transducers to measure the crack propagation in the two slabs;
- 32 inclinometers to measure the lower and upper rotation in columns;
- 48 inclinometers to measure the in-plane rotation of the slab in proximity to the columns.

The few network cables of the system can be easily fixed firmly to the structure, thereby reducing potential damage to the DAQ or control system cabling during the test execution.

4.3.2 MIXEDFEEDBACK CONTROL STRATEGY

Another innovation adopted during the SlabSTRESS test campaign consisted in the use of the MixedFeedback control strategy based on a user-defined control variable function of all the variables accessible to the Master Unit at a slave level for each time sampling. The classical force or displacement control modality for every controlled valve, was replaced with this more versatile control strategy. However, due to the high torsional stiffness of the specimen and the short distance between the actuators, a more effective and stable control strategy was needed.
This feature may improve the performance for the control of the tested structure as concerns spurious rotation and redundant forces in multi-degree of freedom structures [2].
The MixedFeedback strategy was used to control the displacement of each floor with null rotation. Previously, the same displacement was controlled by the comparison between the two actuators acting in the same direction on the floor, and its respective structural displacement transducer (a high resolution Heidenhain encoder) attached to the floor in a position aligned to the actuator axis.
For each floor two control mode were defined; one for the translation (measured by the average of the Heidenhain encoders) and the other for the rotation, indirectly measured by the transducer internal to each actuator.
The drawback of this innovation consisted in the approval of a negligible amount of

spurious rotation, but this was brought to a reliable stable control.
Finally, during the SlabSTRESS project, the adoption of ElsaREC system has guaranteed the correct execution of all the tests without any incident of data loss, and produced the high quality and reliability of the results.

4.3.3 INSTRUMENTATIONS

CRACK OPENING DISPLACEMENT TRANSDUCERS

The COD transducer is a potentiometer, a linear displacement transducer. The potentiometers are measuring devices that use an electrical circuit with a variable resistance, and in output give an analogical signal proportionate to the measured displacement.

Figure 4.17 a) COD transducer b) Schematize of a potentiometer.

The analogical signal is defined by the position of the handle (C) that specifies the electric resistance given from the terminal (A, B).
In the Slab STRESS project, COD transducers were used to measure the opening of punching shear cracks through the increase of slab thickness. A different number of displacement transducers were placed at each connection, according to the slab-column connections typology. Four for the interior, three for the edge and two for the corner (Figure 4.18). For these sensors too holes were made previously in the slab.

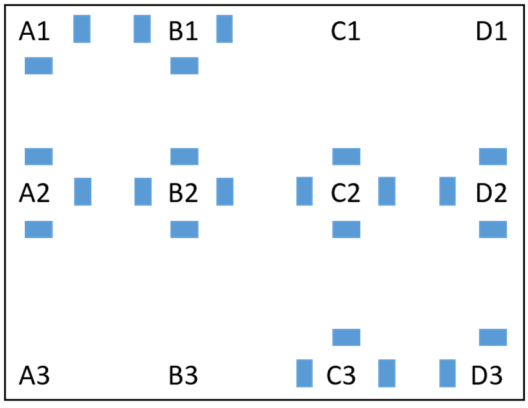

Figure 4.18 COD transducers layout.

INCLINOMETERS

The inclinometer is a sensor used to measure slope angles with respect to the direction of gravity. In the Slab STRESS project, sensors are placed on the slab to measure its rotation: flexural rotation to the front and back of the connection (SW and SE), in the loading direction, and torsional rotation to the sides (SN and SS). All measured rotation being along the loading direction (east-west).

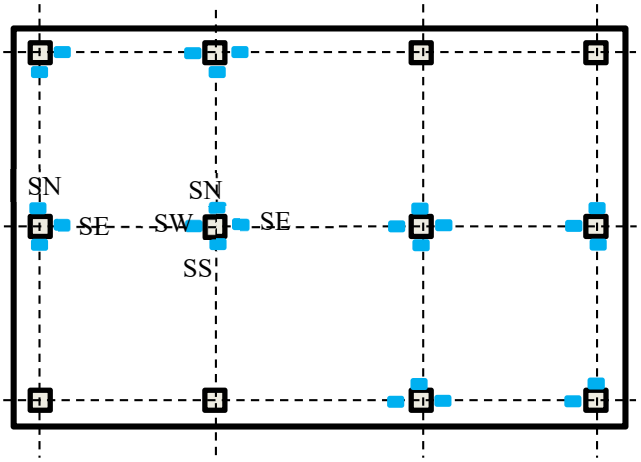

Figure 4.19 Inclinometers for slab deformations.

To check the presence of relative rotation, inclinometers are also placed at the base of the columns on the first and second floor. Hence the inclinometers in the columns are at both ends, all measuring rotation along the loading direction (east-west).

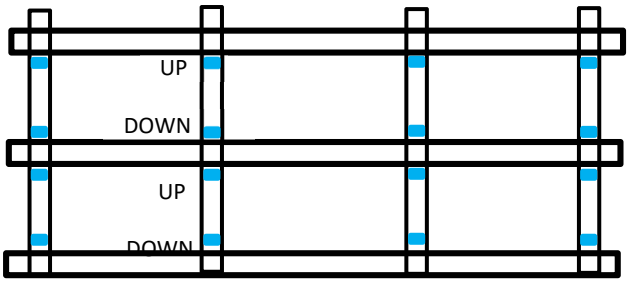

Figure 4.20 Inclinometers for columns.

The inclinometers used are the Seika SB1U (Figure 4.21), a sensor for measuring uniaxial acceleration or inclination.

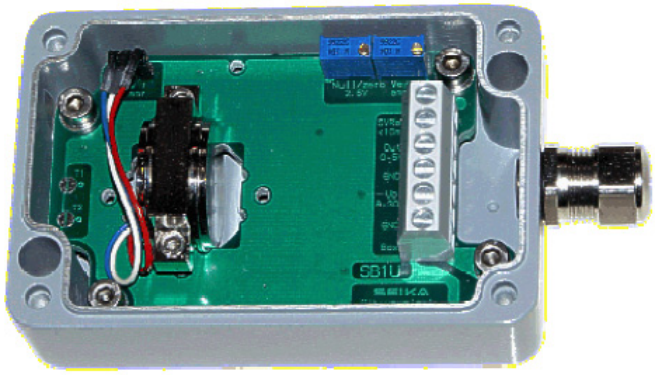

Figure 4.21 Seika SB1U inclinometer used for the Slab STRESS test.

The sensor has a signal conditioner with 0 ... 5V output and a separate, highly stable voltage supply that can be used externally as a reference point. Furthermore, the signal conditioner includes an active low pass filter, whose upper cut-off frequency / settling time which can be adjusted to suit the measurement task, and a noise voltage filter to guarantee the EMC. Interference signals caused by unwanted ground currents are eliminated by electrically isolating sensors and signal conditioners from the housing.

TRANSDUCERS FOR INTERNAL ACTIONS MEASUREMENTS (LOAD CELLS)

The internal force and moment of the columns (shear force, axial force and bending moment) were measured by using a novel device designed for the purpose, consisting of a steel stub located in the middle of each column. The JRC create this system appositely.

In the central part of each column are load cells consisting of a steel stub obtained from standard HEM profiles, creating a notch in the web. The cells are completed with square pinned plates at their extremities. The material is structural steel S335.

The end plates are connected to the central stub by bolts and to the RC column with threaded bars. The threads remain within the members due to the shape of the HEM profile. The stiffness of the plates approximates a rigid behaviour and improves the transmission of the normal stresses from steel stub to the concrete.

The load cells were of three types, small, medium and large in function of the column typology where positioned, respectively: corner, edge and internally.

Figure 4.22 Load Cell.

The measured quantities are strains in the flanges and along the sides of the hexagonal hole, and were derived successively to obtain the shear, moment and axial forces. The notch is motivated by the need to increase the strains in the web and provide more accurate measurements.
The design is carried out by analysing the effects of actions during the laboratory tests. Stresses were calculated by using large displacement analysis and were shown to remain below the yield of the material, without buckling effects.
The transducers for measuring the internal action were placed at the mid-height of the columns during the construction of the specimen, while strain gauges were installed afterwards.

4.4 Calibration of sensors

Before the testing phase could begin, some necessary preliminary procedures were carried out, among which the calibration and positioning of sensors, the positioning of load and the safety procedures.
The calibration procedure represents a crucial step in large-scale experimentation due to the intrinsic complexity of this kind of test. The SlabSTRESS project was the first test performed at ELSA with a systematic calibration procedure for all the sensors adopted in the experimentation.
All the sensors adopted in the SlabSTRESS test campaign were previously calibrated to ensure a correct quality level of the measurement system. The whole measurement chain was being calibrated (sensors, cables and acquisition boxes) using the calibration bench for displacement transducers. Potentiometric displacement transducers (Displacement transducer) were mounted directly on a dedicated bench using two certified linear encoders as reference, while angular rotation for inclinometers was obtained using a proper “swing” frame designed to

transform linear movement to an angular one.
The calibration of the load cells mounted at the middle of each column required the design of an ad-hoc bench able to produce representative loads for what concerning shear, axial forces and bending moments (see later).
The actuators with their internal instruments were also calibrated.
For each batch of sensors (all the sensors connected to the same acquisition box) two tests were performed. The first to determine the sensitivity of each sensor best fitted to the master measurements (high-precision certificated sensors). The second one being necessary to compute some statistics related to the accuracy, reversibility, repeatability and resolution of each sensor.
The calibration experiment consists of applying a number of load cycles on each sensor and then later for the measurements to be compared with a traceable measurement provided by an instrument previously calibrated (known as reference sensor).
Regarding all the main features of a measuring system, here the accuracy, the resolution, the repeatability and the reversibility will be analysed. The accuracy of the sensor measurements is the most important result of the test, since it identifies the maximum difference between the analysed sensor and the reference one. The other parameters; resolution, repeatability and reversibility, determine the quality of the sensor at the moment of the calibration test.
The description of each of these is reported in the following sections using a generic force $\boldsymbol{F}$ to present the equations adopted. Displacements and rotations are then used in following sections (4.4.1 and 4.4.2) instead of the force $\boldsymbol{F}$.

Accuracy

The accuracy error is understood as a systematic term in the error at the load cell and is acquired by the difference between the averaged value of the indicated force and the value of the true force. In general, the accuracy is a function of the true force and has different values at the loading

$$\boldsymbol{Q(F) = \bar{F}_l - F} \qquad \textbf{Eq. 4-1}$$

and unloading branches of the loop

$$\boldsymbol{Q'(F) = \bar{F}_l - F} \qquad \textbf{Eq. 4-2}$$

The associated values of relative accuracy are

$$\boldsymbol{q(F) = \frac{Q(F)}{F} * 100}\ (\%) \qquad \textbf{Eq. 4-3}$$

and unloading braches of the loop

$$\boldsymbol{q' = \frac{Q'(F)}{F} * 100}\ (\%) \qquad \textbf{Eq. 4-4}$$

Resolution

The force F_i is considered as the final value recorded after the analogue signal of the sensor is amplified, sampled at a known sampling frequency, converted into a digital value by the AD converter, averaged and recorded at the recording frequency.
The resolution of the AD converter depends on its number of bytes; in this case the converter has 16 bytes, which may guarantee a resolution to the order of twice the capacity of force divided by 2^{16}=65536. However, the force has an oscillation (noise) much greater than the resolution of the converter, so the resolution of the force for a constant true force F, is defined as half of the peak-to-peak oscillation amplitude of F_i

$$\boldsymbol{A(F) = \frac{F_i^{max} - F_i^{min}}{2}} \qquad \textbf{Eq.}\ 4\text{-}5$$

If during the test the signal was not kept constant at any moment, but was changing at a slow rate, a short lapse of the time history of the signal is taken during which the variation can be assumed to be linear with respect to the time, by applying a linear regression to the measured forces/time, and indicating "e" as the deviation of the measurement with respect to that linear regression straight line, it is possible to write Eq. 4-5 in the following

$$\boldsymbol{A(F) = \frac{e^{max} - e^{min}}{2}} \qquad \textbf{Eq.}\ 4\text{-}6$$

In reality, for non-zero physical force, the actuator needs to be under servo control in order to apply that force and the definition (2) implicitly considers the oscillation to be due to control errors on the testing bench as part of the resolution of the measurement.
If applied to non-zero physical forces, Eq. 4-5 assumes that the resolution of the true force F is much smaller than the resolution of the indicated force. The resolution of the true force The relative resolution is defined as

$$\boldsymbol{a(F) = \frac{A(F)}{|F|} * 100}\ (\%) \qquad \textbf{Eq.}\ 4\text{-}7$$

Repeatability

The repeatability error is the random variation of the indicated force among the different cycles and for the same true force. it is defined in the loading branch of the cycles as

$$\boldsymbol{B(F) = F_i^{max} - F_i^{min}} \qquad \textbf{Eq.}\ 4\text{-}8$$

and in the unloading branch of the cycles as

$$\boldsymbol{B'(F) = F_i'^{max} - F_i'^{min}} \qquad \textbf{Eq.}\ 4\text{-}9$$

The relative repeatability is defined as

$$\boldsymbol{b(F) = \frac{B(F)}{F} * 100\ (\%)} \qquad \textbf{Eq. 4-10}$$

Reversibility

The reversibility error is understood as the systematic difference between the values of the indicated force at the loading and unloading branches of the loop, for the same true force

$$\boldsymbol{V(F) = Q'(F) - Q(F)} \qquad \textbf{Eq. 4-11}$$

The relative reversibility error is given by

$$\boldsymbol{v(F) = \frac{V(F)}{F} * 100\ (\%)} \qquad \textbf{Eq. 4-12}$$

Sensor class for a given range

The standard ISO 7500-1 classifies the quality of the calibrated testing machine by defining the maximum admissible absolute value of the relative errors at every quality class 0.5, 1, 2 or 3, 3 is the worst (Table 4.1).

Table 4.1 Maximum permissible characteristic values of the force-measuring system.

Class of machine range	Relative accuracy $\|q\|$	Relative repeatability b	Relative reversibility $\|v\|$	Relative zero error $\|f_0\|$	Relative resolution a
0.5	0.5	0.5	0.75	0.05	0.25
1	1.0	1.0	1.5	0.1	0.5
2	2.0	2.0	3.0	0.2	1.0
3	3.0	3.0	4.5	0.3	1.5

The aim is to define the class of the sensor.
As previously reported (4.3.3) all sensors were grouped in ten boxes and successively fixed to the building. Each box was connected to the acquisition system with a single cable.
To represent the conclusion of the testing, only the results obtained with the box 1 are here reported. In this box, there were ten inclinometers and six displacement transducers.

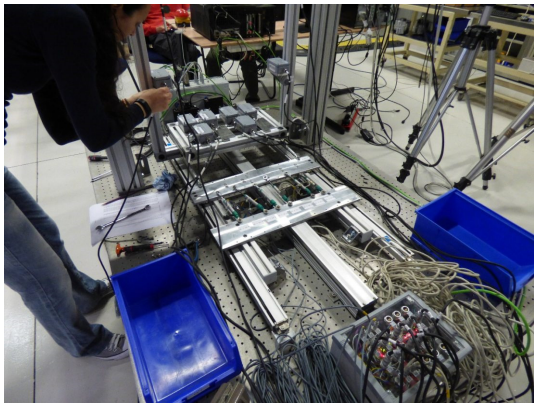

Figure 4.23 Sensors disposition for the calibration of box 1.

For each typology of sensors, the calibration campaign was divided into two phases; the first one with the aim to determine the sensors sensitivity (for the box 1, a9 for the inclinometer and a10 for the displacement transducer) the second one to finalise the calibration (for the box 1, a11 for the displacement transducer and a12 for the inclinometer).

Table 4.2 Tests description.

Name	Description	Tested amplitude	Room temperature (Celsius)	Recording period sec
a9	Inclinometer sensitivity determination	0.08 rad	20	200
a10	Displacement transducer sensitivity determination	0.01 mm	20	200
a11	Displacement transducer calibration	0.01 mm	20	200
a12	Inclinometer calibration	0.08 rad	20	200

4.4.1 Crack Opening Displacement transducer

For the COD transducer, a first experiment (nominally a10) regarded the sensitivity determination, the second one (identified as a11) the calibration.
The sensitivity determination is employed to find the corrections needed to bring the error average to zero. In this box, there are six displacement transducers (Figure 4.24).

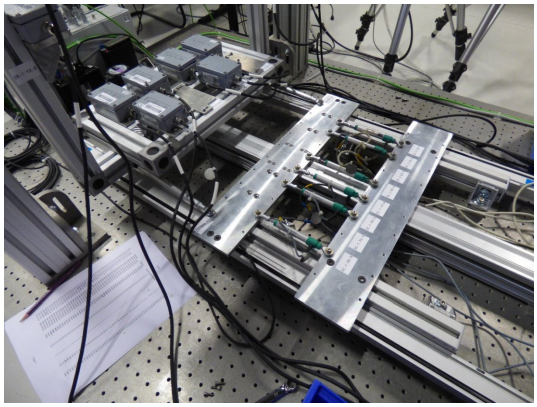

Figure 4.24 COD transducer disposition for the calibration.

The graphs below report the displacements of the two reference sensors (Figure 4.25 a), and the displacements measured with the six displacement transducers (Figure 4.25 b).

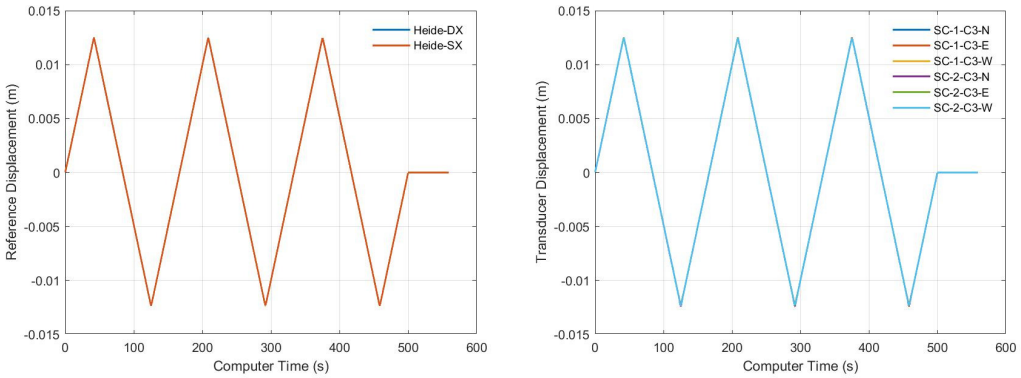

Figure 4.25 a) Displacements of the two reference sensors, and **b**) Displacements measured with the six COD transducers.

From the graph representing the errors revealed by the sensitivity campaign (Figure 4.26) it is possible to see that the values are very far from zero, this indicates that the measurements could be improved.

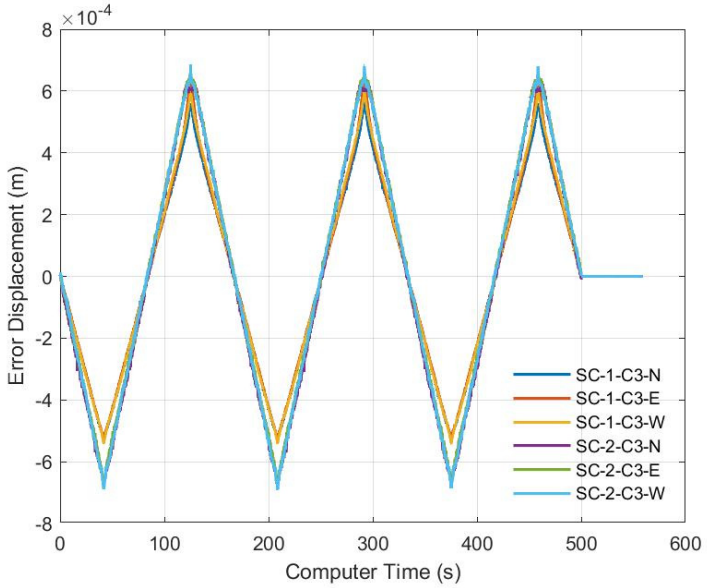

Figure 4.26 Error evaluation in the COD transducer sensitivity determination.

On the contrary, the error in the calibration experiments (Figure 4.27) is nearly equal to zero, the peaks that are present referring to values of displacements out of the displacement transducer ability.

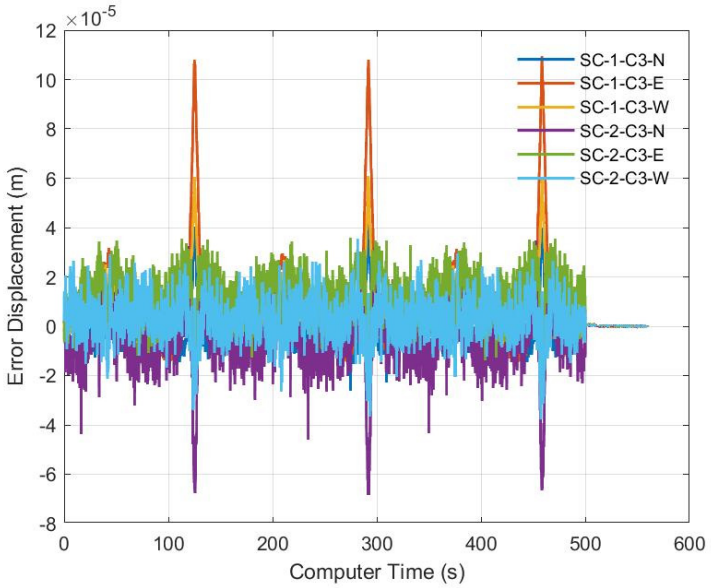

Figure 4.27 Error evaluation in the COD transducer calibration experiments.

These differences are more visible when analysing the graphs which represent the errors along paths of the instruments (Figure 4.28 and Figure 4.29).

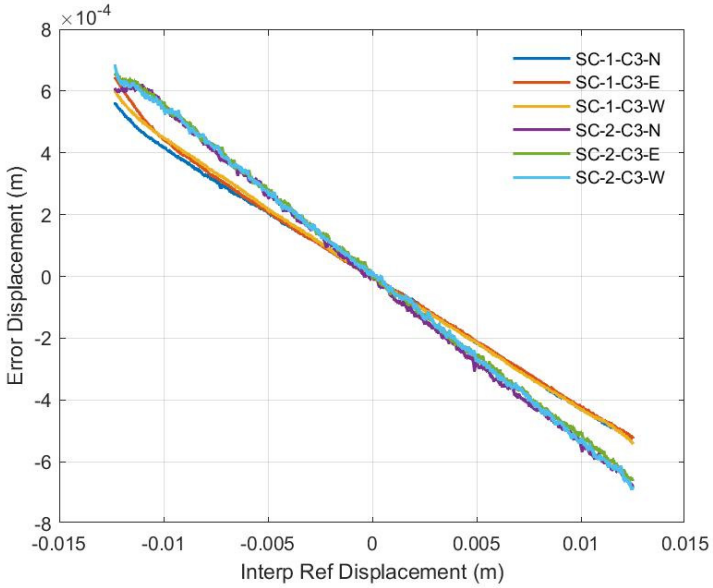

Figure 4.28 Errors along the paths of the instruments for the COD transducer sensitivity determination.

To evaluate the corrections needed to bring the error average to zero, during the calibration, the sensors errors (Figure 4.26) are multiplied by a factor proportional to the curve slope (Figure 4.28) obtained during the sensitivity test. On making the calculation previously described, the error average is near to zero (Figure 4.29).

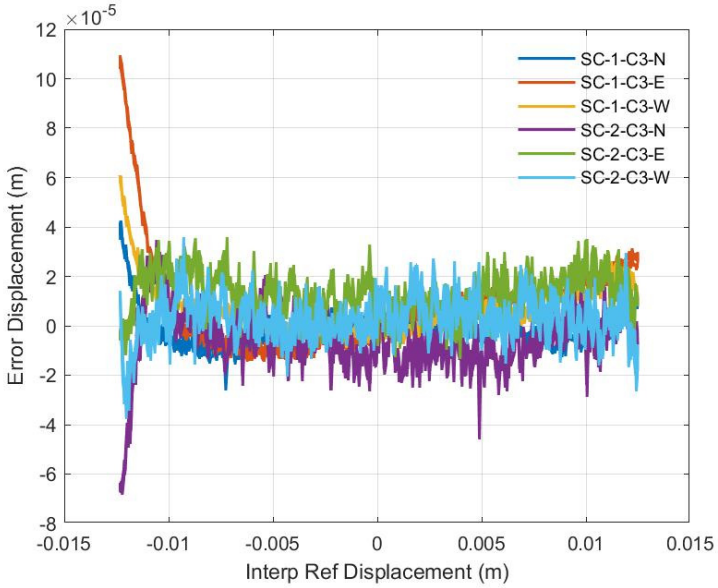

Figure 4.29 Error along the instruments paths of the instruments for the COD transducer calibration experiment.

All the parameters used to characterise the measurement (accuracy, resolution,

repeatability and reversibility) are here reported for a single sensor.
The procedure is the same for all the six displacement transducers.

Accuracy

Accuracy is the determination of error and is obtained by comparing the displacements measured by six displacement transducers with the displacements of the two reference sensors.
The difference is plotted at every point of loading and unloading branches in the positive and negative parts.
It is worth noting the difference between the accuracy of the sensitivity determination (Figure 4.30) and the calibration (Figure 4.31).

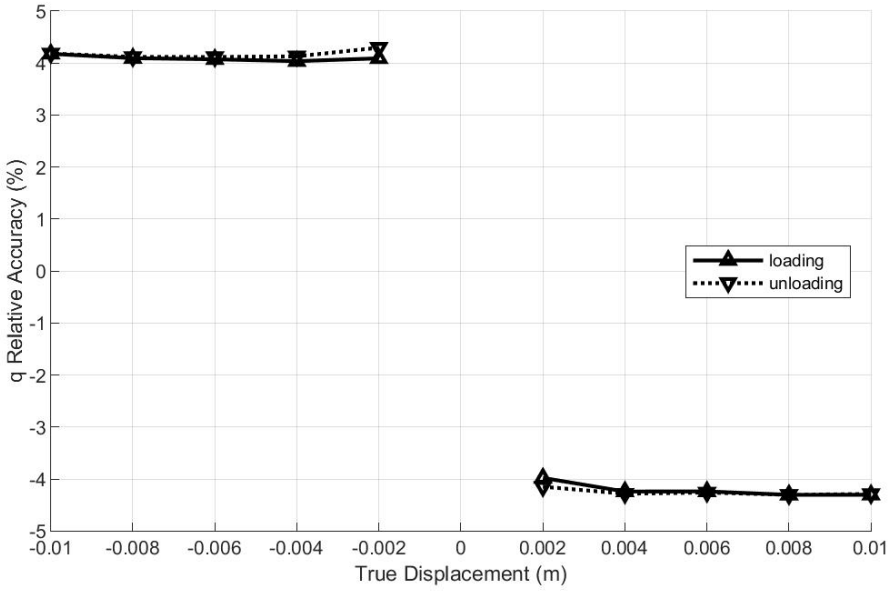

Figure 4.30 Accuracy for the COD transducer sensitivity determination.

Since the loading and unloading curves in the positive load are the same and also those for the negative load, it is possible to say that the analysed displacement transducer measures the same value of displacement in loading and unloading and is therefore accurate.

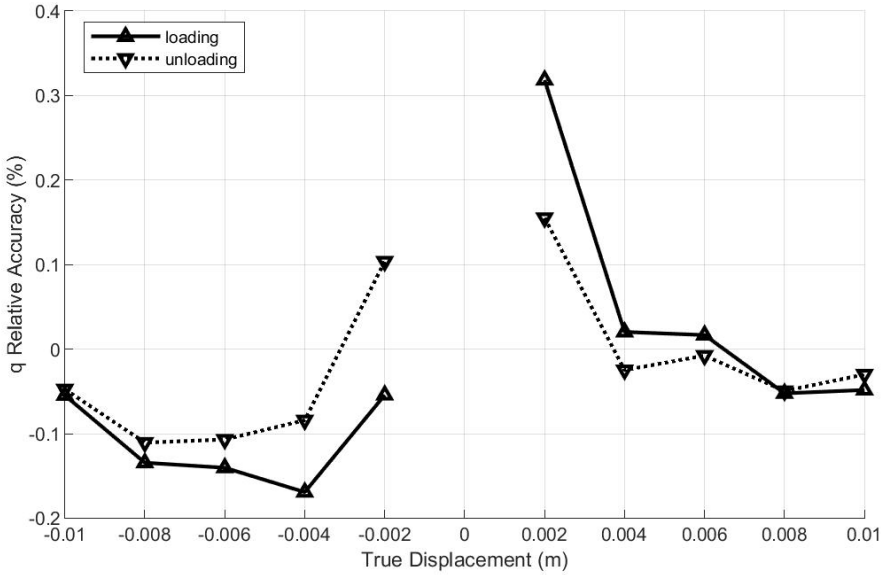

Figure 4.31 Accuracy for the COD transducer calibration experiment.

Reading the maximum value and comparing it with the values in Table 4.1 it is possible to note that, thanks to the sensitivity experiment the relative accuracy is modified, in fact it goes from 3 to 0.5.

Resolution

Successively, the resolution was analysed (Figure 4.33). It represents the minimum variation that it is possible to measure in the sensor. There are two line typologies; the continuous line represents the reading during the load from zero to positive values or from zero to negative values (loading), and the dotted line representing the opposite reading, during the load from positive value to zero or from negative values to zero (unloading) (Figure 4.32). As prescribed from the ISO 7500-1 three cycles were carried out.

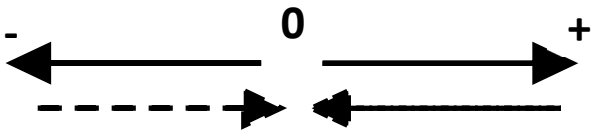

Figure 4.32 Loading and unloading cycle.

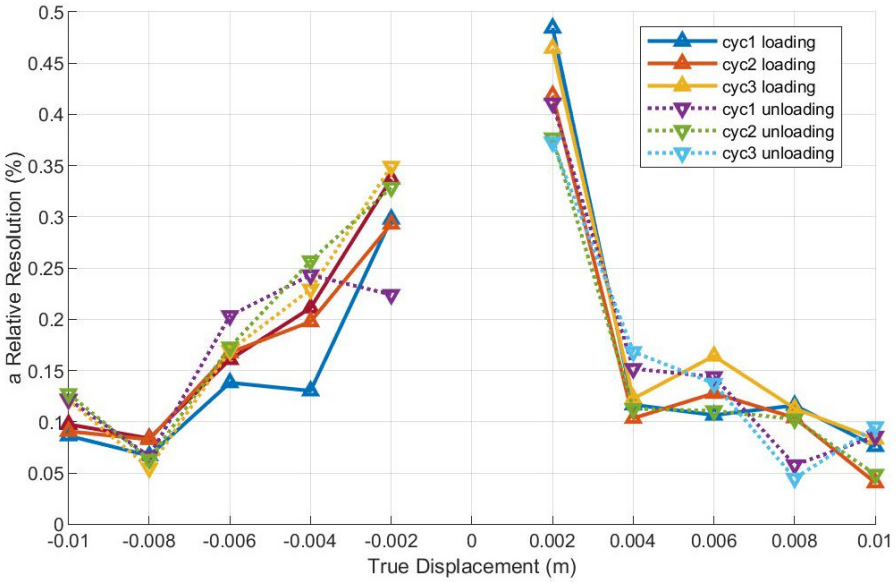

Figure 4.33 Relative resolution for the COD transducer calibration experiments (%).

Two experiments were made in this case also; the first one to determine the sensitivity, the second one for the calibration, but, since the results are similar, only the graphs regarding the calibration are reported.
From the graph in Figure 4.33, it is possible to note that in the analysed displacement transducer the loading and the unloading measures for the positive and negative branches are the same, so it is possible to affirm that the sensor has the same resolution.
Reading the maximum value and comparing it with the value in Table 4.1, a relative resolution of 0.5 is a good result.
The same observations could be made for the calibration graphs.

Repeatability

This is the representation of the variability of measurements obtained from the difference between the maximum and the minimum measures for the loading and for the unloading. If the sensor always passes at the same points it indicates that the measure is repeatable.

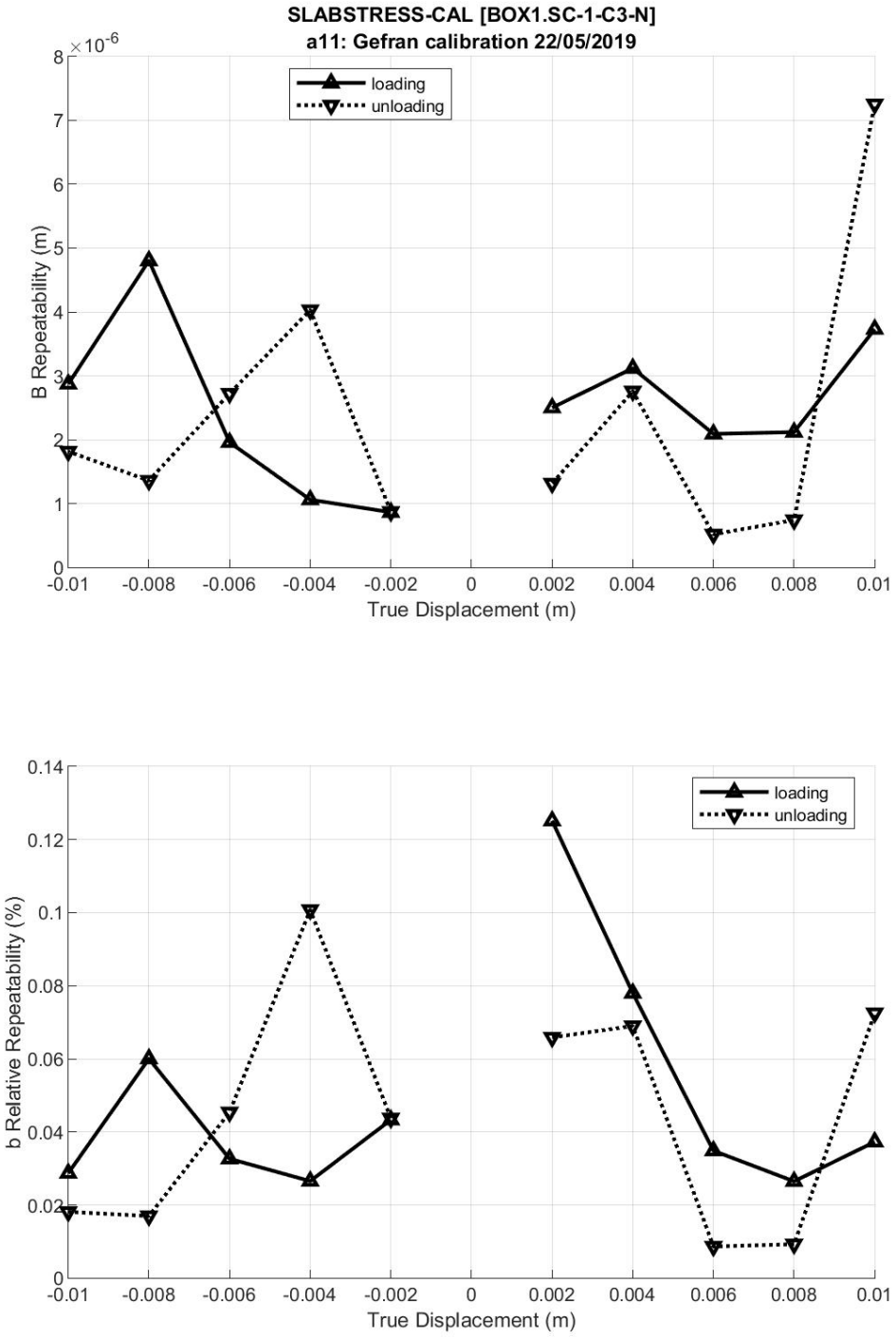

Figure 4.34 a) Repeatability and **b)** Relative repeatability (%) for the COD transducer calibration experiments.

In the analysed displacement transducer (Figure 4.34), it is possible to note that the loading measurements are different from those of unloading, but the scale is very small (micron) (Figure 4.34 a), the values are near to zero in any case so the measurements are repeatable.
Reading the maximum value of the relative repeatability (Figure 4.34 b) and comparing it with the value in Table 4.1, a relative repeatability of 0.13 is a good result.
The same observations could be made regarding the calibration graphs.

Reversibility

This represents the difference between the average of the loading measurements and the average of the unloading measurements for each analysed level.

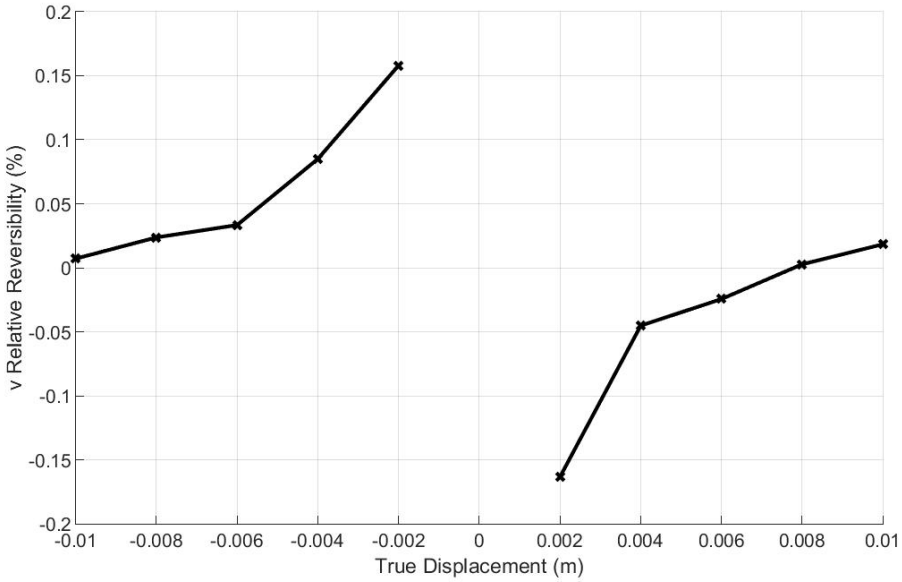

Figure 4.35 Relative reversibility for the COD transducer calibration experiments (%).

It is useful to know whether the sensor measures the same value for the loading and for the unloading cycle. Reading the maximum value of the relative reversibility (Figure 4.35) and comparing it with the value in Table 4.1, a relative reversibility of 0.15 is a quite good result.
Regarding the previous experiment, on the sensitivity, the relative reversibility was 0.2 and thanks to the sensitivity experiment it improves, in fact it goes 0.2 to 0.15.
As regards the analysed COD transducers, the maximum absolute value of all the parameters used to characterise the measurements (accuracy, resolution, repeatability and reversibility) is reported in Table 4.3. These values are expressed in percentage of the full scale.
In addition to these values, the 2*maximum standard error, is also present.

The last value (2*maximum standard error) represents the values on more than 90% of the specimens. It is used to assess the quality of the sensors.

Table 4.3 The channel calibration report for the analysed displacement transducer.

Channel	***Maximum absolute accuracy (%)***	***Maximum absolute repeatability (%)***	***Maximum absolute reversibility (%)***	***Maximum absolute resolution (%)***	***2 * Maximum standard error***
SC-1-C3-N	8.64E-02	5.80E-02	2.72E-02	1.02E-01	2.18E-05
SC-1-C3-E	1.48E-01	3.16E-02	2.77E-02	9.36E-02	3.9E-05
SC-1-C3-W	9.20E-02	2.81E-02	1.90E-02	9.20E-02	2.52E-05
SC-2-C3-N	1.06E-01	1.09E-01	2.82E-02	1.82E-01	2.93E-05
SC-2-C3-E	2.65E-01	7.84E-02	2.34E-02	1.52E-01	6.94E-05
SC-2-C3-W	1.26E-01	8.88E-02	1.61E-02	1.30E-01	3.29E-05

For this COD transducer, as can be seen from the last column (2*maximum standard error), the channel with the best quality is the SC-1-C3-N, whereas, the channel with the worst is the SC-2-C3-E.

4.4.2 INCLINOMETERS

As previously reported for the displacement transducer sensors, for the inclinometers also, a first experiment (called a9) regards the sensitivity determination while the second one (called a12) regards the calibration.
There are ten inclinometers Figure 4.36) and in this case as well, only the results regarding one of these as representative are here reported.

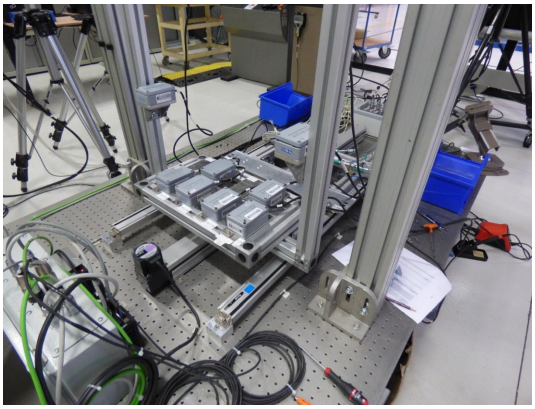

Figure 4.36 Inclinometers disposition for the calibration.

The description of each parameter used to characterise the measurement (accuracy, resolution, repeatability and reversibility) is here omitted, because it is the same of the displacement transducer previously described. In the following, only the graphs are reported with some conclusion.
The graphs below report the displacements of the two reference sensors (Figure 4.37 a), and the displacements measured with the ten inclinometers (Figure 4.37 b).

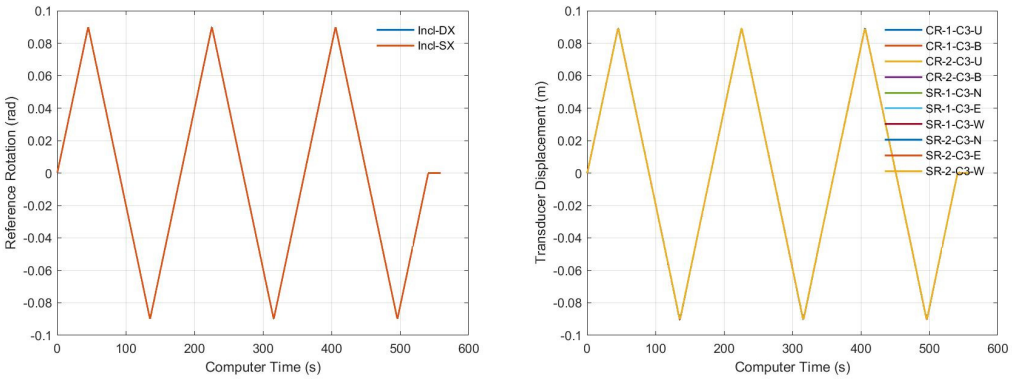

Figure 4.37 a) Displacements of the two reference sensors, and **b)** Displacements measured with the ten inclinometers.

As for the displacement transducer, for the inclinometer as well, the first analysis regards the sensitivity determination (Figure 4.38) and the calibration experiment (Figure 4.39).
Diversely from the displacement transducer, the sensitivity determination for the inclinometer is inessential as the manufacturing company already provides the correct measurements. Comparing Figure 4.26 and Figure 4.27 with Figure 4.37and Figure 4.38 it is possible to see that in the case of the displacement transducer case the sensitivity determination has led to an improved measurement, while in the inclinometer the improvement is small.

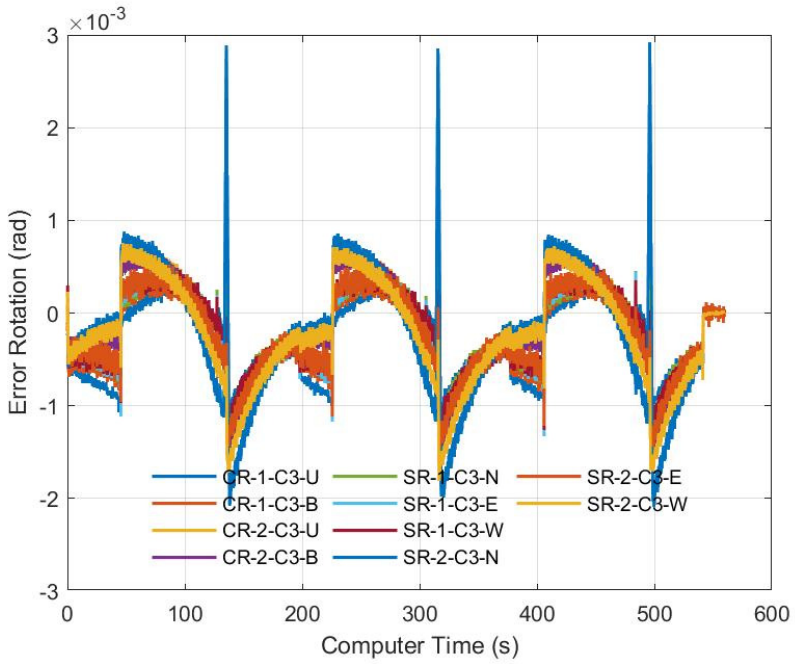

Figure 4.38 Error evaluation in the inclinometer sensitivity determination.

In Figure 4.38 the error values oscillate approximately -2 rad to approximately 0.9 rad, whereas in Figure 4.39, owing to the improvement resulting from the sensitivity experiments, the error values oscillate between approximately -1.5 rad and approximately 0.5 rad. The peaks that are present refer to values of rotation beyond the scope of the inclinometer.

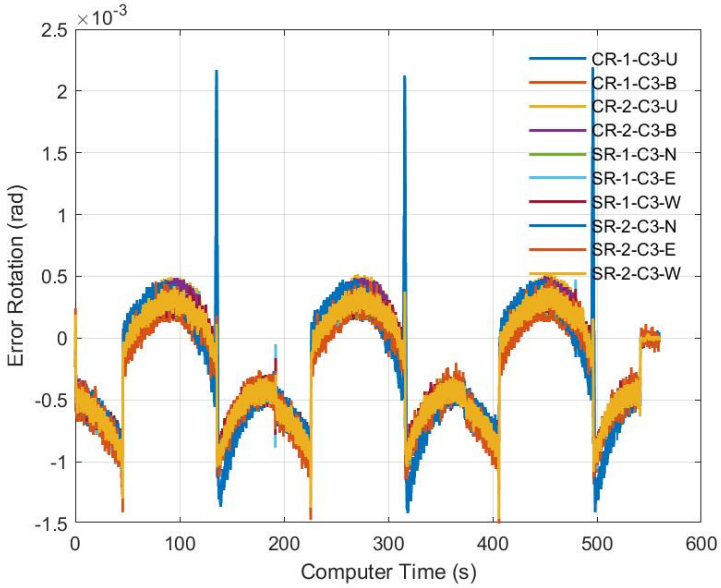

Figure 4.39 Error evaluation in the calibration experiments.

This improvement is more visible in Figure 4.40 and Figure 4.41 in which the error average is close to zero.

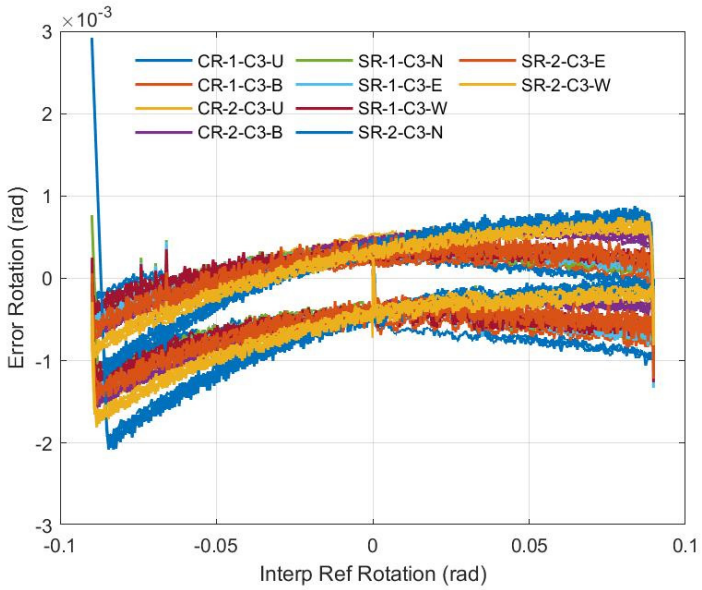

Figure 4.40 Errors along the instruments paths for the inclinometer sensitivity determination.

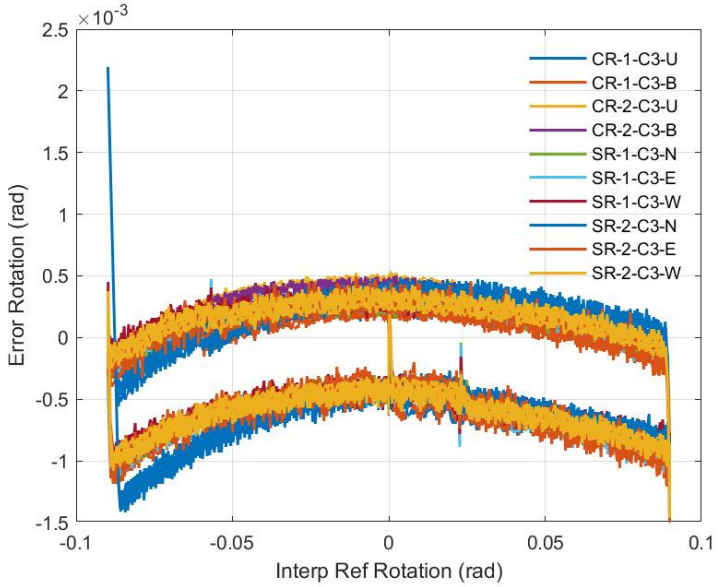

Figure 4.41 Error along the instruments paths for the inclinometer calibration experiment.

Here all the parameters used to characterise the measurements (accuracy, resolution, repeatability and reversibility) are here reported for one sensor only. The same procedure is followed for all the ten inclinometers.

Accuracy

As for the displacement transducer, also for the inclinometer, the difference between the displacements measured using the ten inclinometers and the displacements of the two reference sensors is plotted for every point at the loading and unloading branches in the posititve and negative parts.

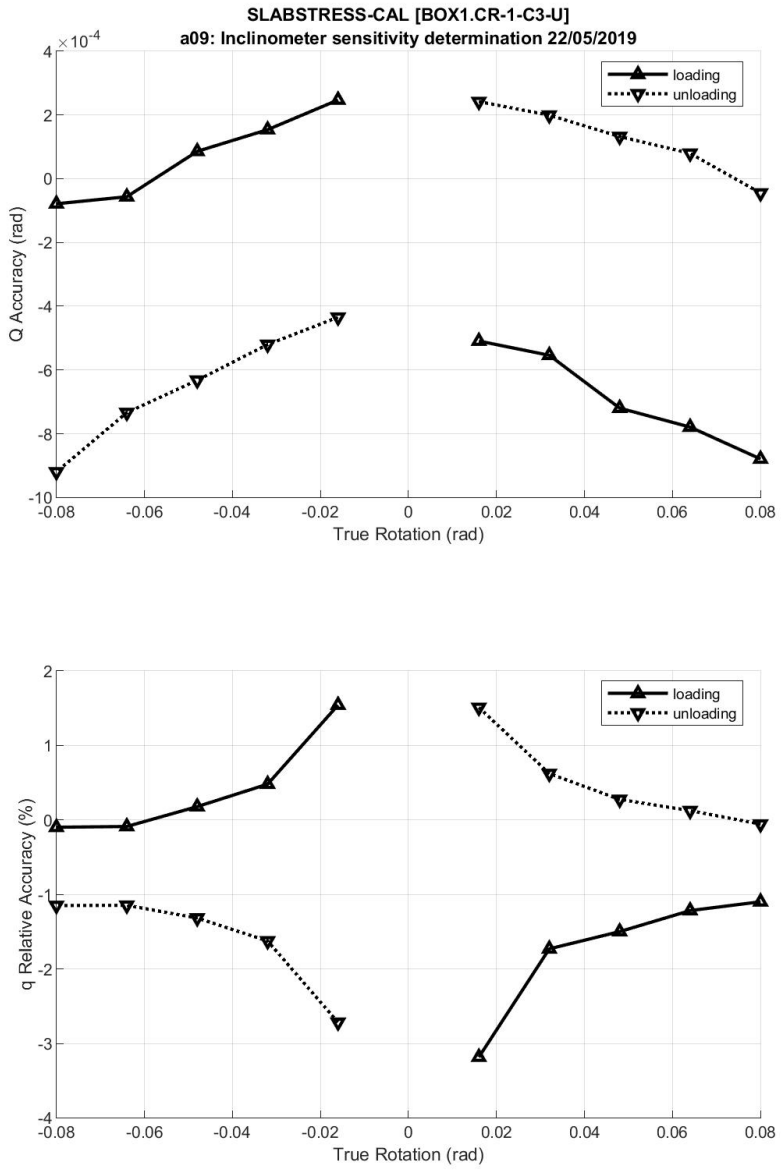

Figure 4.42 a) Accuracy (rad) and **b)** Relative Accuracy (%) for the inclinometer sensitivity determination.

From Figure 4.42 a it is possible to note that the loading measurements differ from the unloading, but the scale is very small, the values are near to zero so the measurements are accurate.

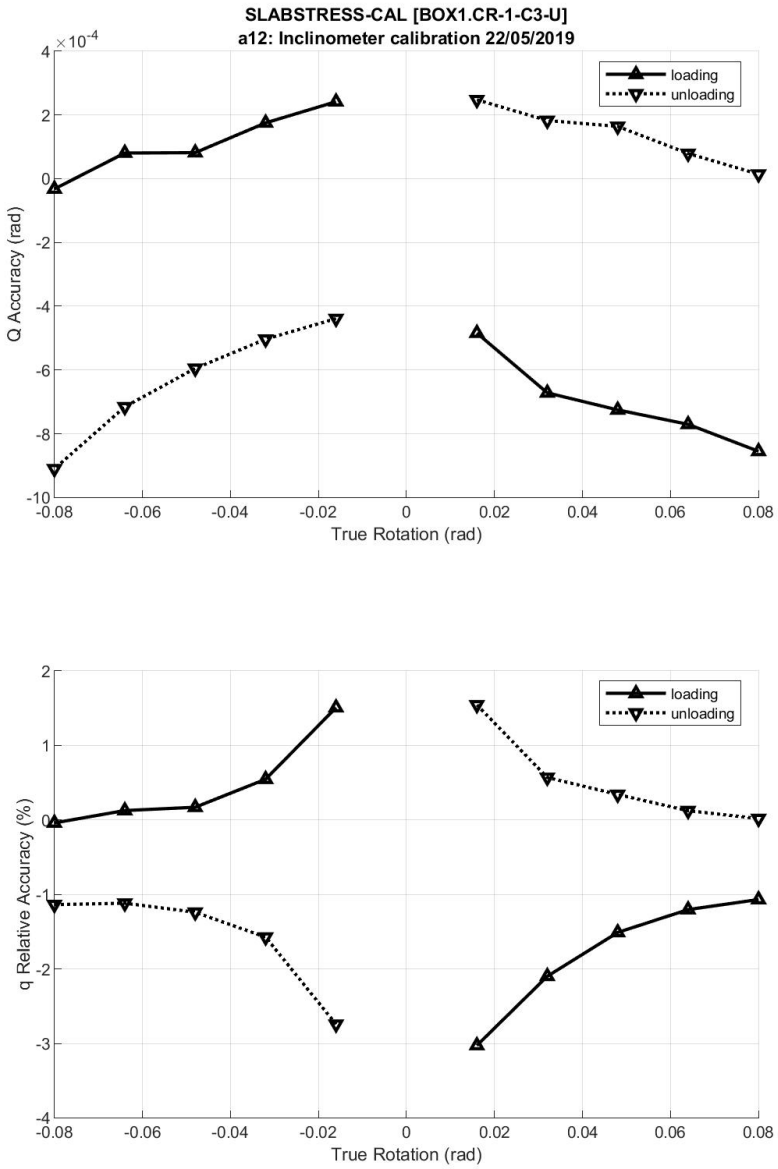

Figure 4.43 a) Accuracy (rad) and **b)** Relative Accuracy (%) for the inclinometer calibration experiment.

On comparing the maximum value of the relative accuracy (Figure 4.42b and Figure 4.43 b) with the values in Table 4.1 it is possible to note that diversely from the displacement transducer, in this case the sensitivity experiment did not affect the

accuracy, it was between 1.5 for the sensitivity determination and remained the same in the calibration.

Resolution

In this case, two experiments were carried out; the first one to determine the sensitivity, the second one for the calibration, but, since the results are similar, only the graphs regarding the calibration were reported.
From the graph in Figure 4.44, it is possible to note that in the analysed inclinometer the loading and the unloading measurements for the positive and negative branch are the same, so it is possible to affirm that the sensor has the same resolution.
Comparing the maximum value with the value in Table 4.1, a relative resolution of 0.55 is considered to be a good result.
The same observations could be made for the calibration graphs.

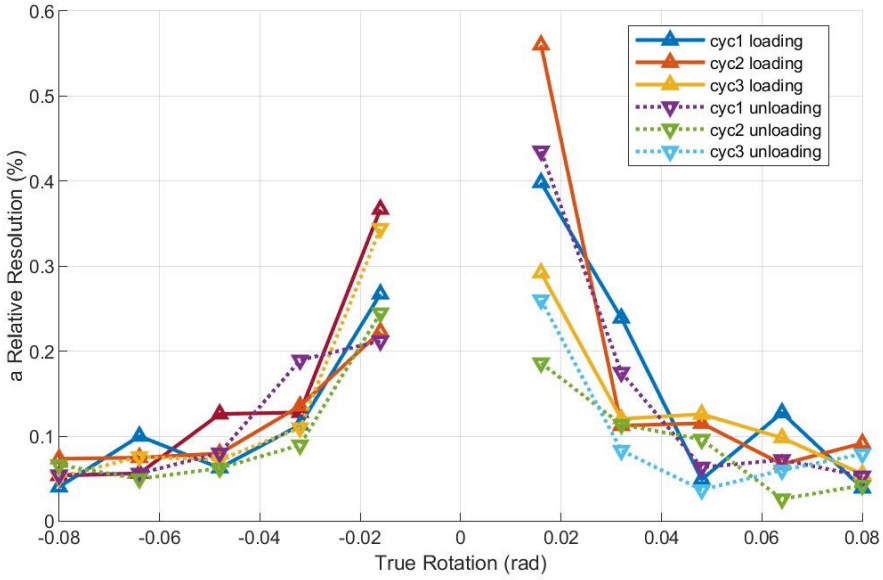

Figure 4.44 Relative resolution for the inclinometer calibration experiment (%).

Repeatability

In the analysed inclinometer (Figure 4.45), it is possible to note that the loading measurements are little different from those of unloading but the scale is very small (micron) (Figure 4.45 a), the values are however near to zero so the measurements can be replicated.
Reading the maximum value of the relative repeatability (Figure 4.45 b) and comparing that with the value in Table 4.1, a relative repeatability of 1.6 is not a satisfactory result, while effecting the sensitivity determination, this value remains unaltered.

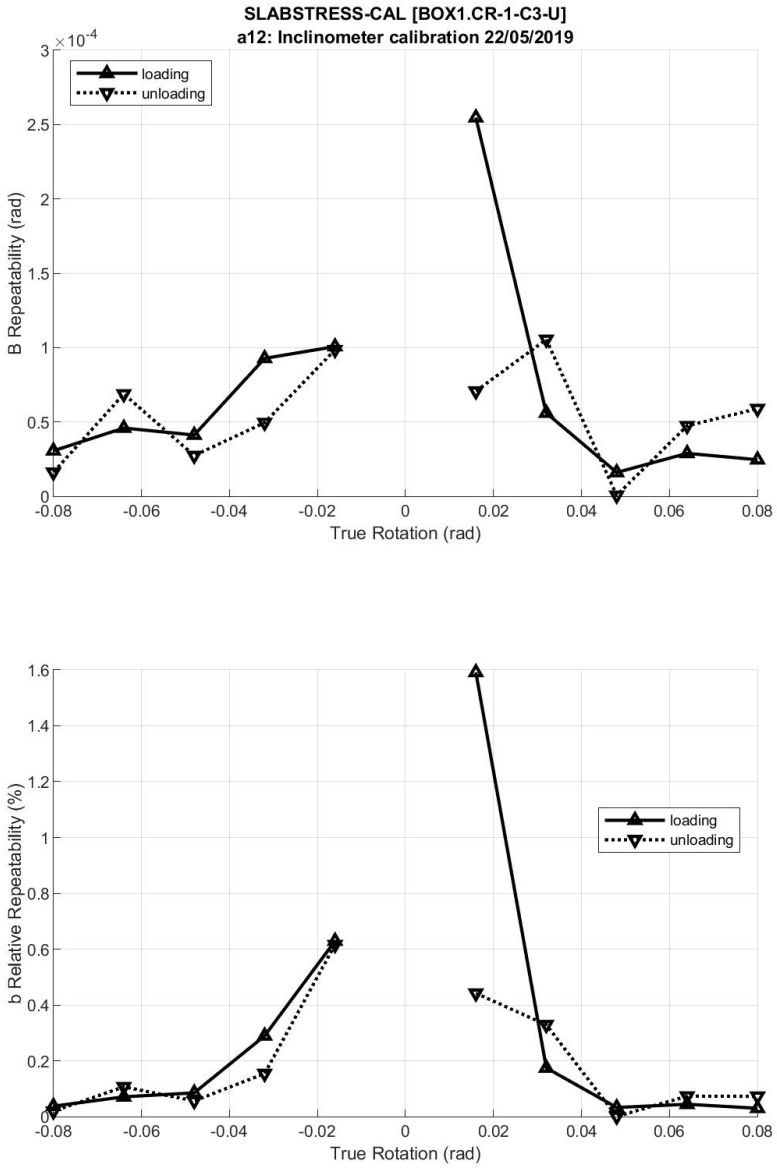

Figure 4.45 a) Repeatability and **b)** Relative repeatability for the inclinometer calibration experiment (%).

Reversibility

Reading the maximum value of the relative reversibility (Figure 4.46) and comparing it with the value in Table 4.1, a relative reversibility of 4.5 is not a good result but on doing the sensitivity determination the class of the sensor remains the same.

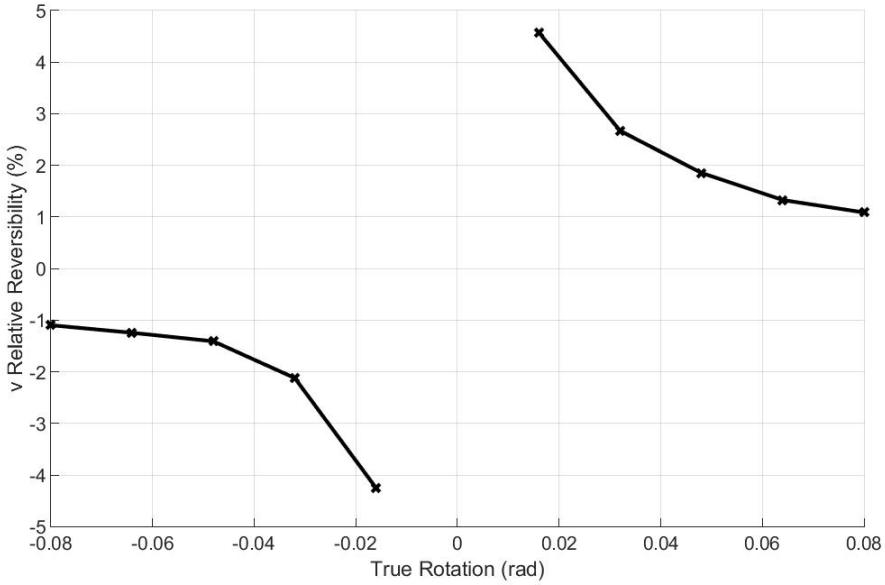

Figure 4.46 Reversibility for the inclinometer calibration experiment (%).

For the analysed inclinometers, the maximum absolute value of all the parameters adopted to characterise the measurement (accuracy, resolution, repeatability and reversibility) is reported in Table 4.4. These values are expressed in percentage of the full scale.
In addition to these values, the 2*maximum standard error, is also present.
The final value (2*maximum standard error) represents the values of more than 90% of the specimens. It is used to evaluate the quality of the sensor.

Table 4.4 The channel calibration report for the analysed inclinometer.

Channel	*Maximum absolute accuracy (%)*	*Maximum absolute repeatability (%)*	*Maximum absolute reversibility (%)*	*Maximum absolute resolution (%)*	*2 * Maximum standard error*
CR-1-A2-U	1.10	7.83E-02	1.00	5.37E-02	0.001557
CR-1-A2-B	0.92	7.83E-02	0.95	9.48E-02	0.001286
CR-2-A2-U	1.13	7.83E-02	1.08	5.04E-02	0.001587
CR-2-A2-B	0.97	7.83E-02	0.99	1.00E-01	0.001361
SR-1-A2-N	1.09	7.83E-02	1.00	1.05E-01	0.001552
SR-1-A2-S	1.01	7.83E-02	0.97	1.14E-01	0.001416
SR-1-A2-E	0.99	7.83E-02	1.01	1.59E-01	0.001393
SR-2-A2-N	1.05	7.83E-02	1.02	1.34E-01	0.001467
SR-2-A2-S	1.16	7.83E-02	1.03	1.68E-01	0.001627
SR-2-A2-E	1.10	7.83E-02	1.03	1.51E-01	0.001543

For the analysed inclinometers, the channel with the best quality result is the CR-1-A2-B, whereas, the channel with the worst is the SR-2-A2-S.

4.4.3 TRANSDUCERS FOR INTERNAL ACTIONS MEASUREMENTS (LOAD CELLS)

Due to the limited time constraints for mock-up construction, transducers to measure internal actions were placed inside the columns before being individually calibrated. Therefore, a calibration of two identical samples for each type of transducer (internal, edge and corner columns) was performed according to a special calibration

procedure. In this way it was possible to obtain the calibration data for the two same cells embedded in the structure. For this purpose, a dedicated setup with three degrees of freedom was designed and constructed, and all six load cells were tested, two identical ones for each dimension.
The calibration required a special setup designed appositely.
The design was executed in order to figure the best way to construct the setup, making it as compact as possible, self-equilibrated so that it could be placed in any position, accommodating all the three types of load cells (small, medium and large, of different dimensions), and using available short actuators.

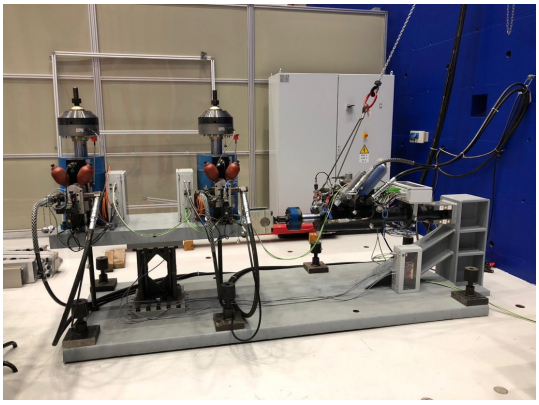

Figure 4.47 Load Cell calibration.

Two vertical actuators developing up to 800kN in compression and one horizontal actuator with a force stroke of +-200kN is used in order to apply a combination of vertical force, momentum and shear to the load cell (Figure 4.48), being the upper limit possible to be reached during the test.

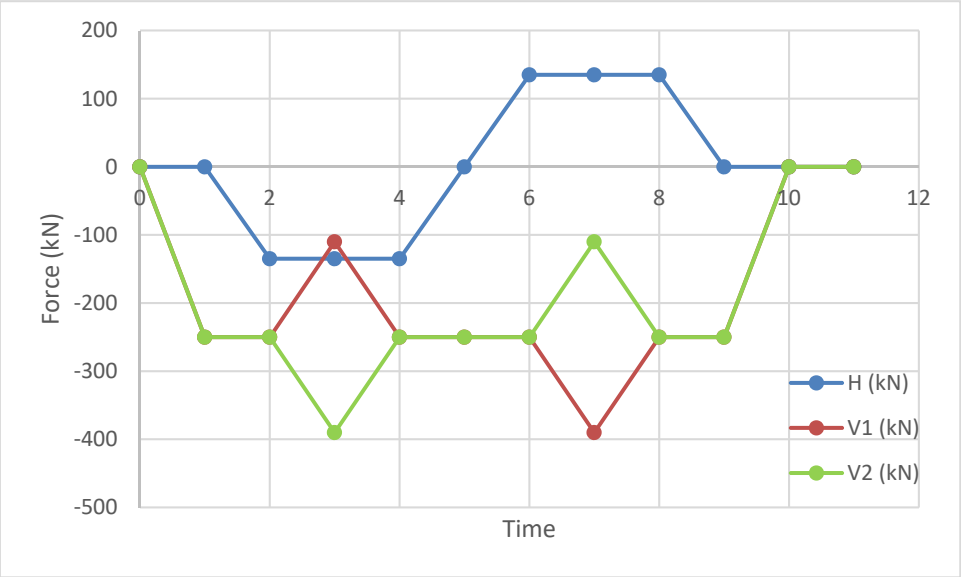

Figure 4.48 Applied forces for the load cells calibration.

The purpose of the calibration is not only to derive a multipliable factor that translates the voltage taken from the amplifiers to a physical quantity, but also to tune the range of the amplifier itself in order to avoid any saturation.
The calibration phase reached internal stress levels comparable to those reached during the tests. In Table 4.5 the values of the forces applied using the three actuators are reported; H indicates the horizontal one, V1 and V2 the two verticals. The last three columns of the table contain the axial force (N), the shear (V) and the bending moment (M) that were generated into the load cell.
The calibration began with the loading of the structure using the two vertical actuators in order to reach the target of vertical force that is kept constant. Then a shear force is imposed, which adds some additional moment. Successively, this moment is increased by using the two vertical actuators (by adding some force on one actuator and subtracting it from the other one) up to the target value. After which the additional moment is removed and then the shear force is reversed. A difference of vertical force is then applied to reach the maximum value of the moment in the other direction. Then again this additional moment is removed and the shear is next brought to zero as are the two vertical forces. This sequence is applied three times in order to perform the calibration.

Table 4.5 Loading values for the calibration of the load cells.

Time	H (kN)	V1 (kN)	V2 (kN)	h (m)	l (m)	N (kN)	V (kN)	M (kNm)
0	0	0	0	0.3285	0.5	0	0	0
1	0	-250	-250	0.3285	0.5	-500	0	0
2	-135	-250	-250	0.3285	0.5	-500	-135	44.3475
3	-135	-110	-390	0.3285	0.5	-500	-135	184.3475
4	-135	-250	-250	0.3285	0.5	-500	-135	44.3475
5	0	-250	-250	0.3285	0.5	-500	0	0
6	135	-250	-250	0.3285	0.5	-500	135	-44.3475
7	135	-390	-110	0.3285	0.5	-500	135	-184.348
8	135	-250	-250	0.3285	0.5	-500	135	-44.3475
9	0	-250	-250	0.3285	0.5	-500	0	0
10	0	0	0	0.3285	0.5	0	0	0
11	0	0	0	0.3285	0.5	0	0	0

The loading path reported in Figure 4.48 and in the 2nd, 3rd and 4th columns of Table 4.5 has generated into the load cell a specific loading shape for the shear (V), the axial force (N) and the bending moment (M), reported with the red lines in Figure 4.49 and in the last three column of Table 4.5.
The blue lines in Figure 4.49 are the forces read from the load cell.
The load cell calibration procedure achieved excellent results for the measurement of shear and the moment, but very poor results for the vertical load.
Various attempts for regluing or repairing the related strain-gauges, met without success, so it was decided not to consider the reading of the vertical load to be

reliable.

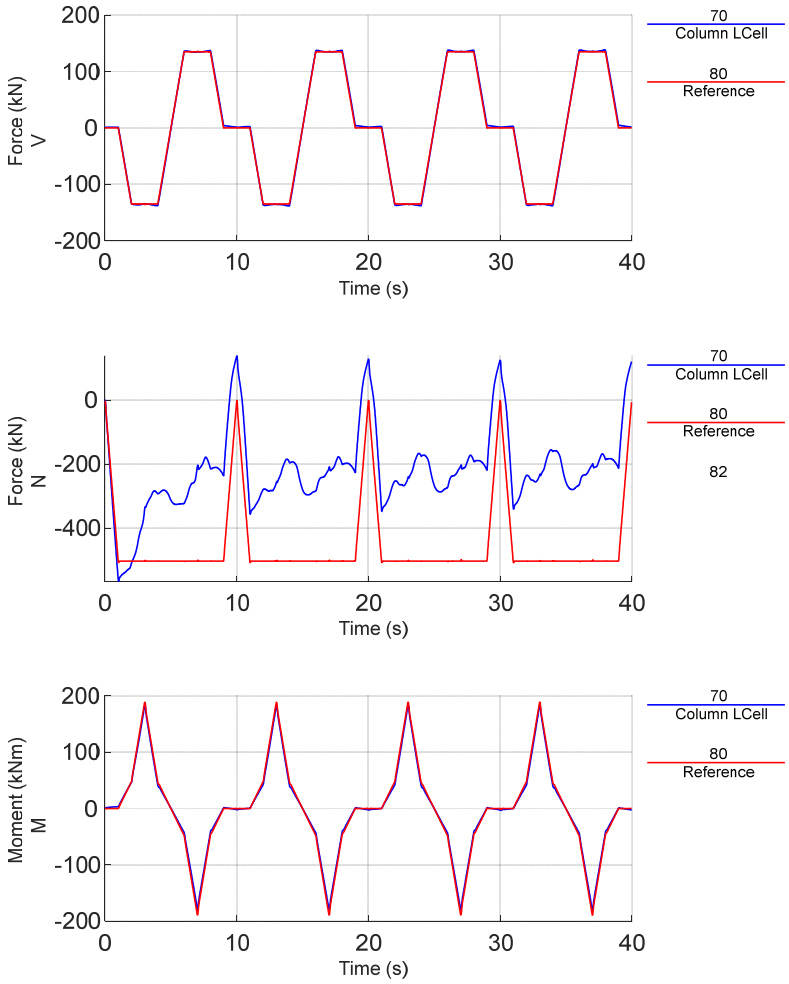

Figure 4.49 Applied loading shape and reading in the load cell.

Due to logistical and economic reasons, by using the described procedure, not all the devices used in the setup were calibrated and this fact may have induced small errors due to variability in the materials and geometry. Figure 4.50 shows an example of the extent of this error. The shear force for both floors is plotted against the inter storey drift ratio for the first seismic test. The blue lines indicate the 1st floor, whereas the red ones the 2nd floor, the continuous lines show the measurements of the actuator load cells, the dotted lines represent the measurements of the column load cells. The difference between the two is due to such variability.

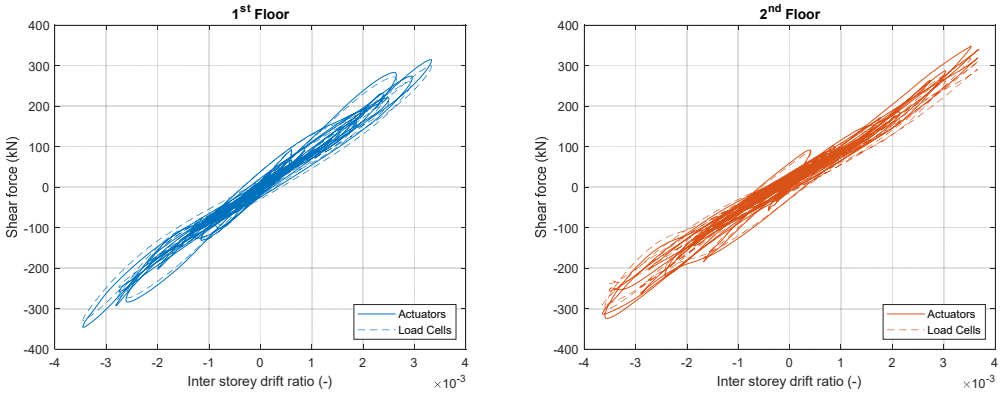

Figure 4.50 Error between actuators and load cells measurements.

4.5 Loading System

A pair of hydraulic actuators connected to the ELSA reaction wall and aligned along the North-South direction imposed the horizontal displacement to each floor of the building. Each jack had a stroke of ±500 mm and a working load of 500 kN for a total load capacity of 2000 kN. A load cell was arranged above the piston rod of each actuator to measure the force imposed on the structure.
Four high-resolution (2µm) displacement transducers placed along the East-West load line continuously measured the horizontal displacements at each floor level. These Heidenhain optical encoders were mounted on two references frames providing feedback to the PID controller of each actuator.

4.6 Positioning of Sensors Layout

The 48 crack opening displacement (COD) transducer sensors measured the crack opening in the slab during the punching. The sensors were placed at a distance of 90 mm from the column side with the pole passing through a hole (Figure 4.51).

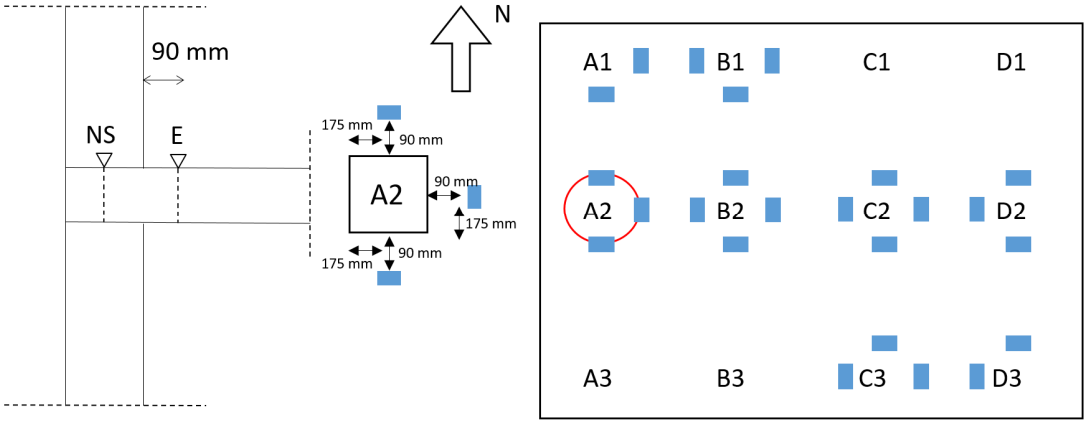

Figure 4.51 Crack opening displacement (COD) transducer layout.

The lower part of the sensor was connected to the slab (bottom side) using a plastic cap glued directly to the slab. The sensor was later mounted on the upper side of the slab by employing chemical anchors, and was then cabled to the related acquisition box (Figure 4.52).

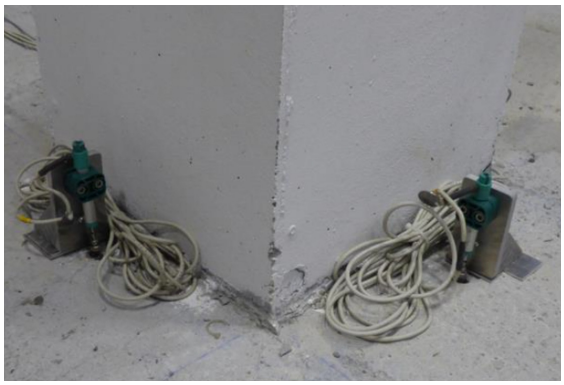

Figure 4.52 Crack opening displacement (COD) transducer.

The 80 inclinometer transducers were mounted to measure the rotation of the column and the slab in the proximity to the column (Figure 4.53).

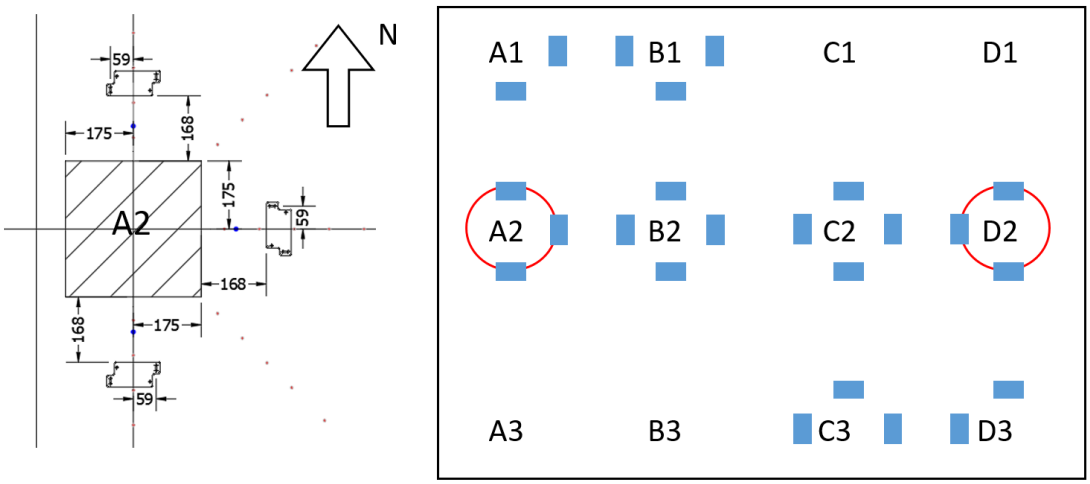

Figure 4.53 Inclinometer positioning.

A series of prepared extension cables and chemical anchors were collocated on which to mount the sensors on the structure (Figure 4.54). Lastly, sensors were cabled to the acquisition boxes.

Figure 4.54 Inclinometer positioning and safety system.

After the positioning of each sensor, the 10 boxes were then installed and each cable was connected.

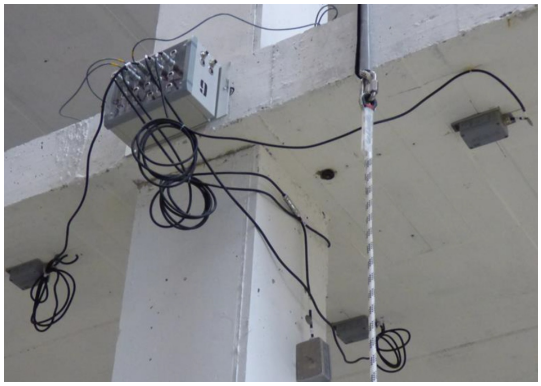

Figure 4.55 Box positioning.

The final phase consisted in tuning the control system by carrying out some tests that needed to be performed at very low amplitude to avoid damaging the structure. At the same time, for some of these tests it was necessary to bring the control almost to a level of instability, in order to calculate the safety margin.

4.7 Safety Procedure

The test control algorithms were provided to activate safety measures that during this experimental campaign were increased by passive safety measures designed to avoid catastrophic failure caused by unexpected events during the test.

4.7.1 PASSIVE SAFETY MEASURES

Three different passive safety measures were applied to the structure.
The first was an anti-torsion safety system (Figure 4.56), a safety bracing along the short West and East side of the structure (A and D). This system was to prevent the specimen from undergoing excessive torsion during the test (resulting from

unforeseen accidents in the control system or during the removal of the damaged specimen from the laboratory).

Figure 4.56 Anti-torsion safety system.

Algorithms that prevent the excessive drift difference of two actuators on each floor already controlled the torsion of the mock-up.
The other two fall protection systems that completed the passive safety measures regarded the possible collapse of the 2nd floor or of some connections to collapse. They consisted of props on the lower floor (Figure 4.57 b) and metal capitals on the upper floor (Figure 4.57 a).

Figure 4.57 Safety measures, a) capitals at 1st floor and b) props on ground floor.

In case of necessity, the benefits of these two safety measures would be realised during the transportation of the structure from the laboratory and when it was dismantled, for the protection of the workers.

4.7.2 ACTIVE SAFETY MEASURES

A second set of safety measures is related to the safety of the ELSA laboratory staff. It included safety lines and access to the floors using footbridges, and fixed ropes.

Figure 4.58 Safety measures related to the safety of the ELSA laboratory staff.

All these systems were designed to be activated only in case of emergency, while they did not alter the structural behaviour of the mock-up under normal conditions.

4.8 Test programme

The testing phase was characterised by different load typologies and intensity, and with different weights distributed on the flat slabs. These contributed to define different phases of the test.

The testing programme was divided in two phases: the first one was the pseudo-dynamic test run with numerically modelled walls and the second one is the cyclic quasi-static tests (Table 4.6).

Seismic loading was applied using the pseudo-dynamic technique with linear substructuring for two levels of seismic activity, the service limit state (SLS) and the ultimate limit state (ULS). During these two tests, the slabs were loaded for gravity loading by self-weight and supplementary weight from water tanks on the 1st floor and concrete blocks on the 2nd.

Successively, cyclic tests were made to test the floors for gravity and lateral cyclic loading of increasing amplitude up to near-failure conditions (punching of the slab at first floor). The first cyclic test was conducted up to a drift of 2.5%. After this first phase, some connections (two lateral on the long side and one internal) were strengthened and then the structure was submitted once more to a cyclic test up to 6% drift.

For the final phase, the water tanks were removed from the first floor and the

building was tested with constraints on the displacement on the first floor.
Two are the goals of the experimental campaign: the first to verify the seismic performance of a flat-slab structure, designed with ductile virtual walls as primary seismic members and frames as secondary seismic members. The second is the study of the performance of the flat slab frame beyond the design displacements.

Table 4.6 Test description.

Test typology	Test name	Internal ID	Test aim
Pseudo-dynamic	Seis - SLS	e03	Seismic performance at SLS
	Seis - ULS	e06	Seismic performance at ULS
Cyclic quasi-static	Cyc -1	e02	Cyclic response until punching shear failure in the 1st floor (2.5% drift)
	Cyc - 2	e04	Behaviour of repaired and strengthened connections (6% drift)
	Cyc -3	h03	Ultimate drift capacity of the structure (collapse)

The two pseudo-dynamic tests were performed on the whole building with the real structure and the two numerical simulated shear walls to study its seismic performance at the Serviceability (test Seis - SLS) and the Ultimate Limit State (test Seis - ULS). The test Seis - ULS also had the aim of verifying the requirement of Eurocode 8, whereby the flat slab frame maintains the capacity to bear gravity loads when subjected to the maximum deformation reached for the seismic design action. The cyclic quasi-static tests were performed on the specimen after the first pseudo-dynamic tests. During these tests the structure, without the numerical shear walls, was subjected to cyclic loading with increasing displacements. The sequence of the displacements was planned to achieve a progressive and controlled damage to the slab-column connections. Three are the tests of this phase, each of them with a different final scope. The first one, the Cyc-1 was run to study the cyclic response of the flat-slab frame until the punching shear failure appeared on the 1st floor. Subsequently some chosen connections on the 1st floor (B1, C2 and C3) were strengthened and the test Cyc-2 was executed. Finally, the test Cyc-3 with the aim to analyse the ultimate capacity of the structure. Since at the end of the tests Cyc-2 most of the slab-column connections on the 1st floor was heavily damaged, the main focus of the tests Cyc-3 was on the response on the 2nd floor.

4.8.1 THE PSEUDO-DYNAMIC TECHNIQUE

The pseudodynamic (PsD) testing method is a hybrid technique based on an equation of motion formulated for a discrete number of degrees of freedoms (DoFs), integrated in time, using appropriate numerical schemes [14]. The seismic response of large-size specimens can be obtained by combining the experimental restoring forces with the analytical inertia and seismic-equivalent forces. The method is based on an equation that combines a numerical model for the inertial and external forces

with an experimental model for the restoring forces.
PsD testing consists of a step-by-step integration of the discrete DoF equation of motion Eq. 4-13:

$$\boldsymbol{Ma} + \boldsymbol{r}(\boldsymbol{d}) = \boldsymbol{f}(\boldsymbol{t}) \qquad \textbf{Eq. } 4\text{-}13$$

Where:
M: is the theoretical mass matrix,
a: is the unknown vector of acceleration,
*r(d):*is the unknown restoring force, experimentally obtained at every time integration step by quasi statically imposing the computed displacements
d: is the unknown vector of displacement,
f(t): are the known external forces obtained by multiplying the specified ground acceleration by the theoretical masses.
For each PsD test, the prototype or accelerogram time *t* and the experimental time *T*, are defined. The prototype or accelerogram time, corresponds to the time of the original problem with an earthquake excitation that may last for a few tens of seconds. The experimental time corresponds to the real time and may extend to several hours until the end of the execution of experimentation in the laboratory. Every integration step takes one sampling period of the control system (δT).
The method is called PsD when the real (experimental) time is much longer than the prototype time used in the equation of motion Eq. 4-13. This means that the inertial forces that are on the right hand side of the equation need to be computed numerically since they cannot be measured in the (quasi-static) experiment.
This technique is a hybrid testing method that combines restoring forces measured on a physical substructure with restoring forces coming from a numerical substructure. Thus, the global restoring force vector is composed of the restoring force vectors in the numerical substructure (called A) and the experimental (physical) substructure (called B)

$$\boldsymbol{r}(\boldsymbol{t}) = \boldsymbol{r_A}(\boldsymbol{t}) + \boldsymbol{r_B}(\boldsymbol{t}) \qquad \textbf{Eq. } 4\text{-}14$$

As is the usual praxis in ELSA, the equivalent damping distortion introduced to the response from the control errors, was assessed and shown to be negligible, so that the quality of the results was un affected.

Advanced hardware and software configuration was set up to ensure a speed data communication between the servo-controllers and the main computer solving the equation of motion.

THE SEISMIC TESTS: SEIS - SLS AND SEIS – ULS

During these two tests, the slabs were loaded with self-weight gravity and supplementary weight, with additional water tanks on the first floor and concrete blocks on the second (see Chapter 3).

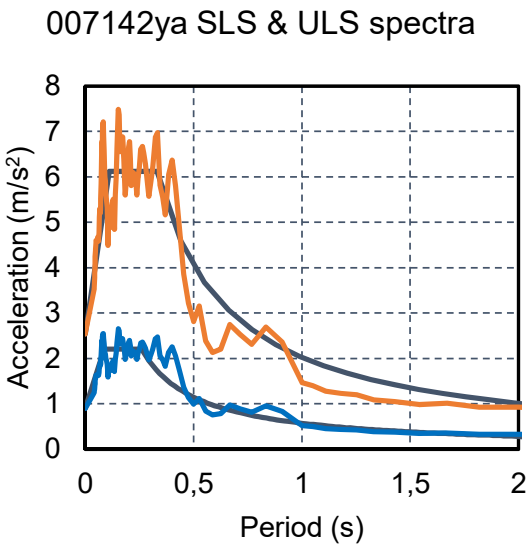

Figure 4.59 Pseudo-acceleration response spectra of the input accelerogram and design spectra at SLS (blue line) and ULS (orange line).

The ductile RC walls, the primary seismic elements of the structure, were not physically constructed but were numerically simulated during the test by the pseudo-dynamic procedure.

During the two seismic tests, the specimen was considered not as a single building but as part of a building having two numerical shear walls, in order to study its seismic performance at the Serviceability and Ultimate Limit States (SLS and ULS). The aim of the Seis - ULS seismic test is to verify whether the flat slab frame maintains its capacity to bear gravity loads when subjected to the maximum deformations reached for the seismic design action, a requirement of Eurocode 8 [3].

The Y component of signal 00712ya recorded during the 6.3 magnitude Bingöl earthquake which occurred on the 1st of May 2003, was used as the input ground motion for the seismic tests. In respect of Eurocode 8 [3] elastic spectra for the SLS and the ULS, the original peak ground acceleration of 2.92 m/s^2 was scaled at 31% for the test Seis - SLS and at 87% for the test Seis - ULS.

The response of the SlabSTRESS model to the chosen accelerogram $a_g(t)$) was obtained in the ELSA laboratory by solving the equation of motion:

$$\boldsymbol{M\ddot{d}(t) + r(t) = -MI_g a_g(t)} \qquad \textbf{Eq. 4-15}$$

Where:

$\ddot{d}(t)$: are the two degrees of freedom for the longitudinal displacements on the floor

$r(t)$: are the respective restoring forces present.

The right hand side of the equation represents the inertial forces, obtained by multiplying the ground acceleration a_g, by the theoretical mass matrix M and the incidence vector of the earthquake I_g. They need to be computed numerically,

through a theoretical lumped mass matrix M.
Eq. 4-15 in terms of relative displacements to the ground this was solved using the PsD method with substructuring.
Regarding the restoring forces $r(t)$, the numerical substructure $r_A(t)$ derived from the shear walls was simulated numerically, whereas the experimental (physical) substructure $r_B(t)$ was measured from the physical specimen when submitted to the solved displacements.
The mass of the walls was considered within the M matrix, together with the mass of the physical structure ($M = M_A + M_B$).

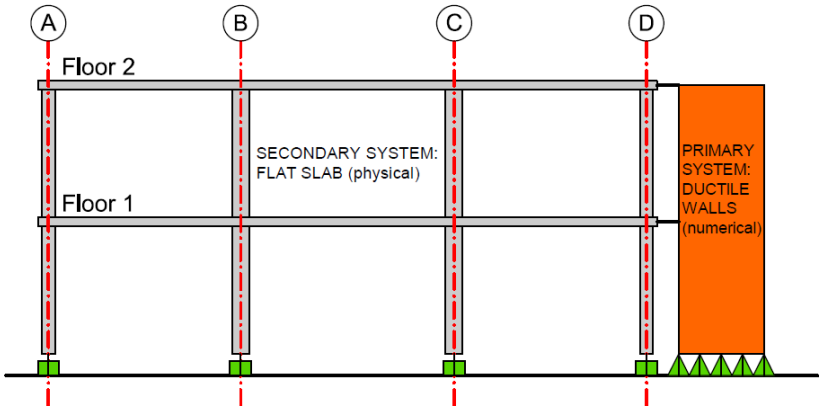

Figure 4.60 Building with virtual walls.

This experimental campaign used an evolved version of the continuous PsD method introduced at ELSA around twenty years ago [14].
This method is based on the subdivision of each original time increment of the accelerogram (0.005s in this case) into an elevated number of sub-steps (2000 in this case) and, at each sub-step, the physical forces are measured, whereas the numerical ones are computed, and the following displacements are solved and imposed on the specimen. Every sub-step is performed in one sampling period of the real-time controller (1ms currently). This is possible in the controller used whenever the numerical model consists of constant matrices of stiffness and viscous damping.
This algorithm strategy is called monolithic substructuring [15] since both substructures use the same time discretization in a common solving algorithm (Explicit Newmark). Considering that the prototype time increment of every sub-step of the accelerogram was $0.005/2000 = 2.5 \cdot 10^{-6} s$, being executed in 1ms of real time, it can be said that the experiment was performed with a time dilation of $1 \cdot 10^{-3}/2.5 \cdot 10^{-6} = 400$.
Each of the two levels of the structure was subjected to a different lateral displacement (Figure 4.61), for the 1st floor the design value of inter-story drift was 0.072% whereas for the 2nd floor, 0.12%. During the tests the maximum inter-story drift level recorded was 0.1% for the 1st floor and 0.13% for the 2nd, values close to that of the design and to the 0.5% value prescribed by the EC8 [3] at the DLS for

buildings with non-structural elements of brittle materials attached to the structure.

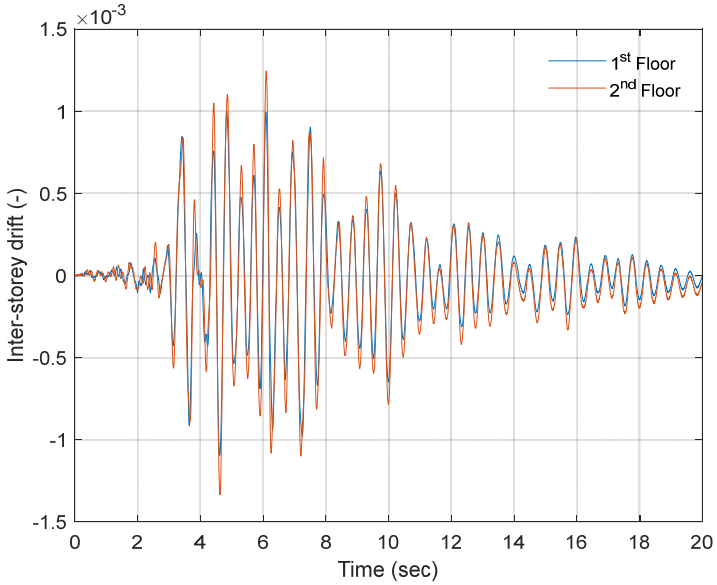

Figure 4.61 Inter-storey drift recorded during the Seis-SLS.

As in the previous Seis-SLS, in this test also, each of the two levels of the structure was subjected to a different lateral displacement (Figure 4.62) with two different design values of inter-story drift higher than the values of the Seis-SLS, 0.25% for the 1st floor and 0.42% for the 2nd. The inter-story drift values recorded during the test were 0.34% for the 1st floor and 0.36 for the 2nd one.

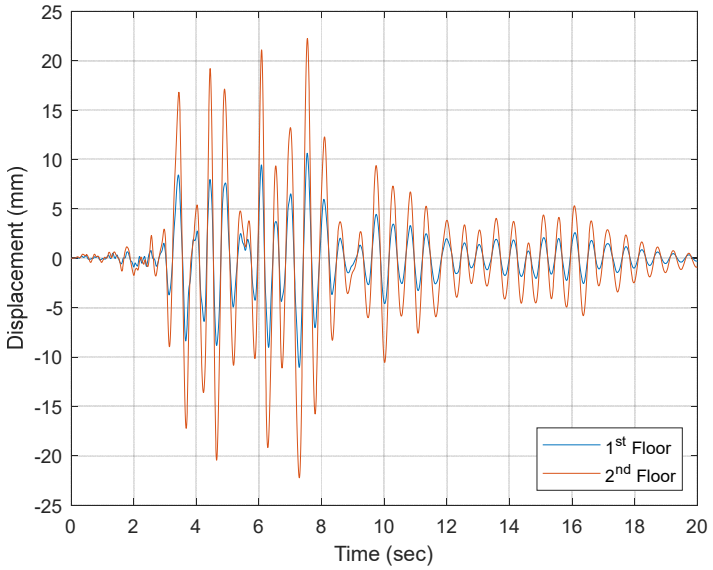

Figure 4.62 Lateral displacement used for the Seis-ULS.

4.8.2 CYCLIC TESTS

For tests Cyc-1 and Cyc-2 a displacement history was imposed on the 2nd floor whereas half of the measured horizontal force at the 2nd floor was imposed on the 1st one.

The displacement history on the 2nd floor for test Cyc-1, consisted of sets of three cycles with increasing global drift ratio: 0.25%, 0.50%, 1.0%, 1.5%, 2.0%, 2.25% and 2.5%.

Test Cyc-2 was performed for single cycles of global drift ratio 2.5%, 3.0%, 4.0%, 5.0% and 6.0%.

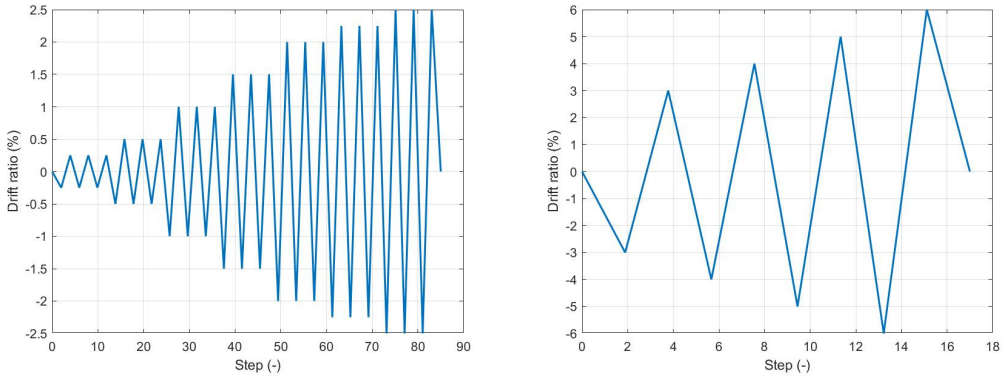

Figure 4.63 Displacement history at 2nd floor for test a) B1 and b) B1R.

For the last test, the Cyc-3, a different displacement history from the previous two tests was applied. This choice was made to the heavy damage incurred to the slab-column connections on 1st floor and to the fact that the displacements on 1st floor reached the maximum stroke of the actuators. The displacement history was imposed only to the 2nd floor whereas zero displacement was imposed to the 1st one.

The cyclic tests were conducted using the displacements control.

At both floors the rotation was controlled using the control system, the displacement of the top floor was controlled through the mean values of the two Heidenhain sensors installed on the reference frames, whereas on the bottom floor, the force was controlled through the sum of the forces measured at the actuators.

For the last test, the first floor was blocked (using the Temposonics only, the displacement transducers mounted on the pistons) whereas the motion of the 2nd floor was imposed (Temposonics only, here as well). The fact that the Heidenhain sensors were not further used was motivated by the high level of cracking of both slabs.

FIRST CYCLIC TEST CYC-1

For the test Cyc-1 (f02), the building was loaded vertically with concrete blocks on the 2nd floor and water tanks on the 1st (see chapter 3 for more detail), laterally with the cyclic path imposed by the actuators. As visible in Figure 4.64, the force imposed

on the 1st floor was half that of the force measured on the 2nd floor.

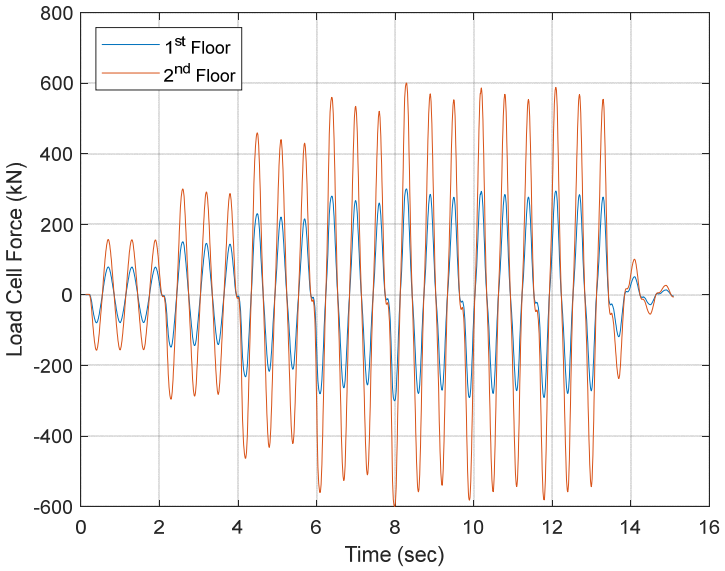

Figure 4.64 Floor forces imposed by the actuators for the Test Cyc-1.

TEST WITH REPAIRED CONNECTIONS

For the test Cyc-2 (g04), the building was loaded as in the test B1, vertically with concrete blocks on the 2nd floor and water tanks on the 1st, and laterally with the cyclic path imposed by the actuators (see chapter 3 for more detail). As it is possible to see from Figure 4.65, the force imposed on the 2nd floor (603 kN) was twice that of the force on the 1st (301.8 kN)

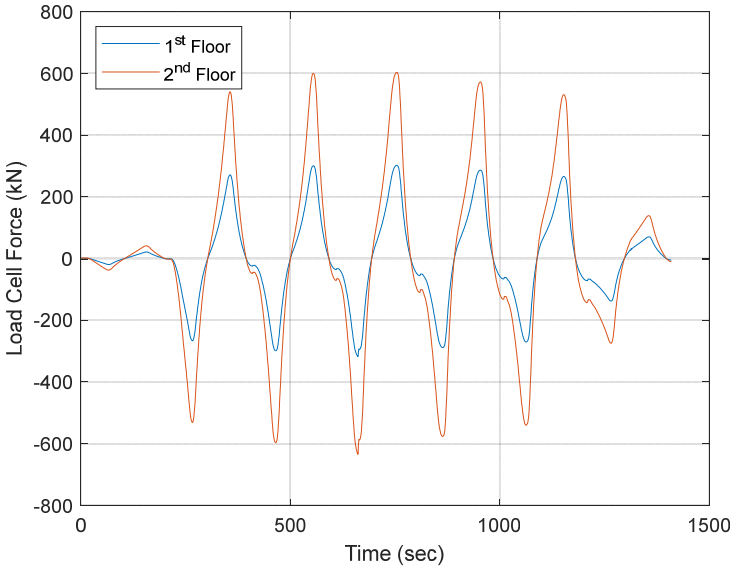

Figure 4.65 Floor forces imposed by the actuators for the test Cyc-2.

At the end of the first cyclic test, the most damaged connections were those on the two short edges, A and D but the damaged was such that no strengthening could be added. The decision was then taken to strength some connections in the central section of the specimen (line B and C).
One connection for each typology, with and some in the half with the longitudinal reinforcement smeared layout and some in the other half with the longitudinal reinforcement concentrated layout, were the criteria for choosing which connections to strengthen. Post-installed bolts were used in the joints B1, C2 and C3 located at the 1st floor this way (Figure 4.66). In this manner a direct comparison between the response of un-strengthened and strengthened connections could be made. This operation represents a realistic scenario in which repair and retrofitting are carried out after a major seismic event.

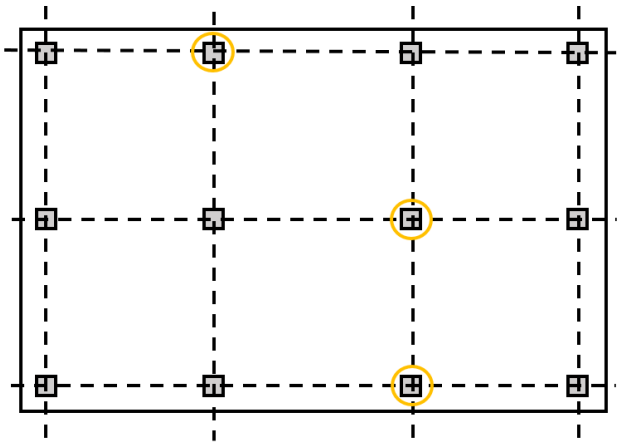

Figure 4.66 Strengthened connections.

Threaded bars (8.8 steel grade) with 10 mm diameter were installed, with rigid circular washers having an external diameter of 40 mm and 10 mm thickness. Nuts on both sides enabled the pre-loading of each bolt, ensuring the efficiency of the post-installed fastening (Figure 4.68).
The reinforcement was designed before the mock-up was manufactured, therefore small plastic tubes (4 mm diameter) were placed into concrete slab to ensure the positioning and verticality of drilled holes, avoiding any interference with longitudinal rebars and measuring devices (Figure 4.67). Nevertheless, the applicability of this technique to ordinary applications remains valid, it is only slower to carry out and less precise as for positioning.

Figure 4.67 Plastic tubes positioning in the slab-column connections that will be strengthened.

The tubes did not alter the cracking pattern: during the surveys performed after each test, the radial cracks of the plate resulted unaffected by the pre-holes.
Once test B1 was concluded, water tanks were removed from the first floor, both for practical reasons related to the installation, in order to reproduce the removal of non-structural loads, as would have been the praxis in an intervention on a real building.
The slabs were drilled, following the pre-holes, the lower surface was smoothed using an epoxy resin to allow the lower washer to sit on a plane, and the bolts were installed and tightened with a torque wrench to apply a preload of 10 kN.

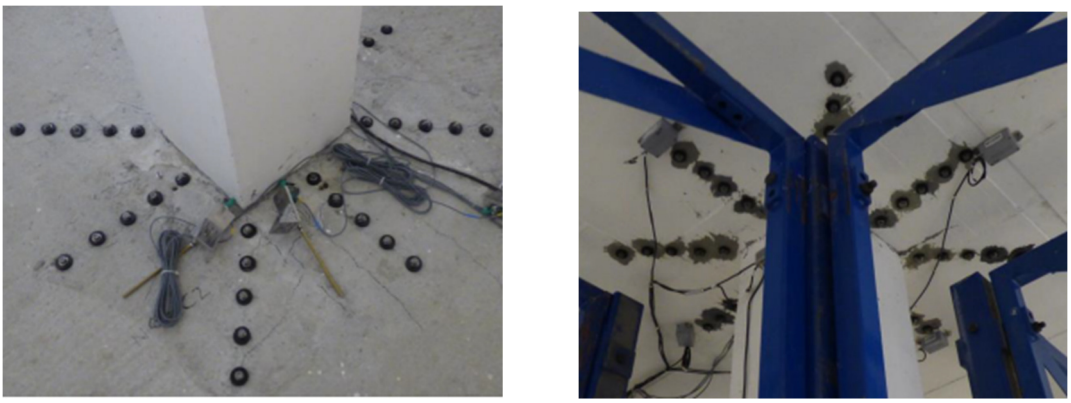

Figure 4.68 Repair of the central column on the 1st floor.

Finally, the water tanks and measuring instruments were then relocated before resuming the test Cyc-2.

FINAL TESTS

After testing with the reinforcements, heavy damage was also seen to be present at the base of the column, so the final test was first started by strictly blocking the displacement of the actuator on the first floor. The demand of force was such that the actuator on the 1st floor reached saturation (2x500 kN), so the blocking condition was relaxed to allow displacement on the 1st floor proportional to the one on the 2nd but much more contained (in order to keep the damage at the base of the columns unchanged). This last test was performed by increasing 4 times the proportionality factor between the displacements up to the saturation of the actuators in both directions.

4.9 Summary

In this chapter the experimental campaign was presented.
The first section of the chapter was dedicated to the describe of the hosting structure (the JRC's ELSA laboratory in Ispra, Italy.), the construction phases and the transfer of the real scale specimen into the laboratory.
The test setup and the instrumentation used to acquire the data were then described in detail. An entire section was dedicated to explain the calibration procedure for the measuring equipment used, with a reference to the quantities investigated and the obtained results. To give an entire overview of the instrumentation, the positioning of sensors and loading devices were also illustrated, together with the description of the loading system and the safety procedures.
The chapter ends with a description of each test that characterised the experimental campaign, i.e. the two seismic and the three cyclic tests. A special section was dedicated to the description of the pseudo-dynamic procedure.

References

[1] https://www.ethercat.org/en/technology.html#1.1

[2] SERA D27.1. Improvement of testing accuracy by introduction of mixed control (JRC) (2018)

[3] CEN (European Committee for Standardization). 2004. Design of structures for earthquake resistance, general rules, seismic actions and rules for buildings part 1. Eurocode 8, Brussels, Belgium: CEN.

[4] NTC2008 - Norme tecniche per le costruzioni 2008 (NTC 2008) - D.M. 14 Gennaio 2008 (D.M. 14/1/08) – in Italian.

[5] CEN (European Committee for Standardization). 2004. Design of concrete structures, general rules and rules for buildings part 1.1. Eurocode 2, Brussels, Belgium: CEN.

[6] M. N., Fardis. Seismic Design, Assessment and Retrofitting of Concrete Buildings: based on EN-Eurocode 8 (Geotechnical, Geological, and Earthquake Engineering). 2009.

[7] P. Bisch, E. Carvalho, H. Degee, P. Fajfar, M. Fardis, P. Franchin, M. Kreslin, A. Pecker, P. Pinto, A. Plumier, H. Somja, G. Tsionis. “Eurocode 8: Seismic Design of Buildings Worked examples”. EC 8: Seismic Design of Buildings”, Lisbon, 10-11 Feb. 2011.

[8] D. Coronelli, L. Martinelli, (2017) “La progettazione sismica dei sistemi a piastra in cemento armato” Pàtron Editore, 116 pp.

[9] NTC2018 - Norme tecniche per le costruzioni 2018 (NTC 2018) - D.M. 17 Gennaio 2018 (D.M. 17/1/18) – in Italian.

[10] Ramos António, Rui Marreiros, André Almeida, Brisid Isufi, Micael Inácio, Punching of Flat Slabs under Reversed Horizontal Cyclic Loading, ACI Fall Convention 2016, Philadelphia, October 2016.

[11] Hueste, M. B. D., Browining, J., Lepage, A., Wallace, J., W. (2007) “Seismic Design Criteria for Slab-column Connections”. ACI Structural Journal, V. 104, No. 4, pp. 448-458.

[12] F. J. Molina, P. Pegon, M. Peroni, B. Viaccoz and P. Petit. “Procedure for load cell calibration at ELSA Reaction Wall”.

[13] ISO 7500-1:2004, Metallic materials – Verification of static uniaxial testing machines – Part 1: tension/compression testing machines – Verification and calibration of the force-measuring system, CEN, Brussels, August 2004.

[14] F. J. Molina, G. Magonette, P. Pegon, B. Zapico (2011). “Monitoring damping in psudo-dynamic tests.” Journal of Earthquake Engineering, 15:6, 877-900.

[15] P. Pegon, F. J. Molina, G. Magonette. “Continuous pseudo-dynamic testing at ELSA” in “Hybrid Simulation; Theory, Implementation and Applications”, Eds. Saouma VE, Sivaselvan MV, Taylor & Francis/Balkema Publishers, 2008, .79-88.

5 Methodology for data analysis

5.1 Introduction

This chapter contains the description of the methodology that was applied to the SlabSTRESS experimental results.
The behaviour of the structure was analysed at two different levels, the global and the local, using static and kinematic parameters. On a global level, the behaviour of the structure was studied in its entirety, the 1st and the 2nd floor as 2 DOF. The behaviour of each slab-column connection was also studied at local level, enabling to observe and analyse the differences between the different typologies of slab-column connections.
All the global analyses were performed using the inter-storey drift ratio as main coordinates to represent the behaviour of the structure. At local level the inter-storey drift ratio was correlated to local measures, columns and slabs rotations allowing to comparison with the SlabSTRESS results of previous experiments.
The aim of this chapter is to present and explain the procedure as followed, for a detailed analysis of the obtained results, see the dedicated chapter; Chapter 6 for the two seismic tests, Seis-SLS and Seis-ULS, Chapter 7 for the first cyclic test, Cyc-1 and Chapter 8 for the second cyclic test, Cyc-2. All these chapters present the same work organization divided into global and local analysis.
Finally reported is the procedure followed to obtain the conversion factors that allow to convert the inter-storey drift ratio to the column-slab rotation, in function of the slab-column connections typology.

5.2 Method description

The SlabSTRESS specimen was designed to achieve as many results as possible from the experimental campaign conducted at the JRC ELSA laboratory. The full-scale mock-up has real boundary and building conditions, two floors, different slab-column connections typology (internal, edge and corner), different longitudinal reinforcement typology (smeared and concentrated), presence or absence of the punching shear reinforcement, and finally some connections that were strengthened.
Given the complexity of the analysed structure, a simplifying procedure was required to break it down into parts allowing an analysis to be more easily approached, each part allowing to make a comparison with the experimental results obtained formerly.
Previous research on this topic was mainly performed on single slab-column joint or sub assemblages and only few cases report results on an entire building.

Tests of this typology and dimension, with the simultaneous acquisition of extensive data regarding real scale structural elements on two different scales, were never made previously. As reported in detail in Chapter 2, Fick et al., 2017 [1] conducted a study on a real-scale specimen but without considering the local response. Moehle and Diebold, 1984 [2] studied the local behaviour but analysed a structure consisting of one floor only. Kang and Wallace, 2004 [3] used the reinforcement deformation to study the local behaviour without producing direct measurements of internal action.
The procedure here presented allowed for the calculation of a connection between the global behaviour, usually expressed with the inter-storey drift ratio and the local one analysed using the rotation of each slab-column connection. The purpose being that to obtain the relationship between the inter-storey drift ratio and the column-slab rotation.
The relationship so created showed that the behaviour changed on each floor, not all the slab-column connections had the same response.
Simplified models were set up to represent the structure, using the main statics and kinematics parameters.
Observing to the structure from a global point of view, there are the two floors displacements that it is possible to obtain from the displacements transducers (Heidenhain), from these, the displacement of each floor and the displacement of the global structure is obtained.
The analysis becomes more complex moving from the global to the local observation. There are several slab-column connections with much local deformation such as rotation, slabs cracks opening and different slabs rotation on both sides of the loading application (flexure or torsion).
Therefore, a combination of these measurements has been used to describe local quantities. (see Chapter 5.3.1 for the global behaviour and Chapter 5.4.1 for the local one).

Global actions are obtained by the forces in the actuators at the two floors (two for each floor). Static internal forces and moments are measured with the load cells, giving local static quantities.
Using the internal forces and moments described above two simplified models were adopted, to characterise the structure from a global and a local point of view.
The simplified model that represents the global behaviour of the structure consists of a two degree of freedom system (Figure 5.1).

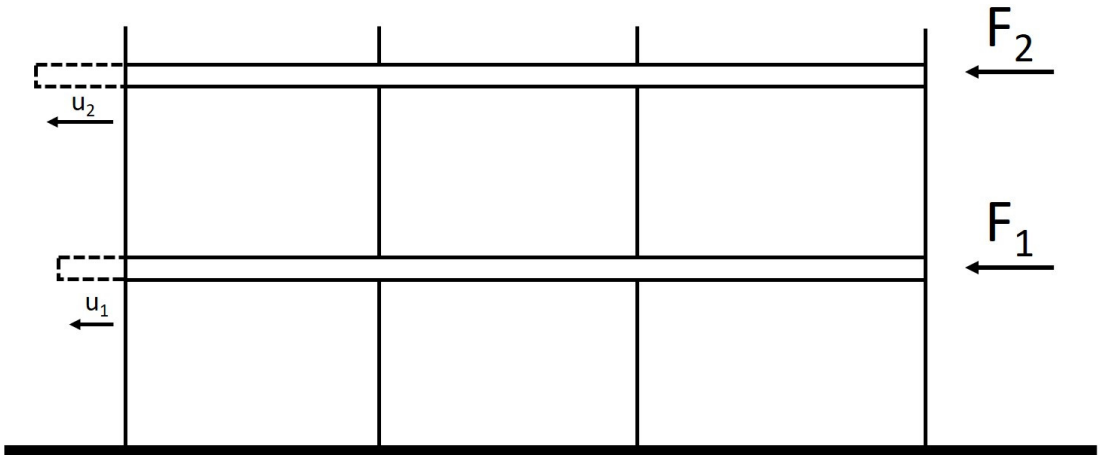

Figure 5.1 Simplify model of the global behaviour 2 DoF system.

Two static parameters, one force for each floor, and two kinematics parameters, one displacement for each floor describe this system. These parameters were acquired using load cells on the actuators and displacement transducers applied on two references frames near the structure for the displacements (see Chapter 4 for a more detailed description).

The loading system transmitted two forces, one for each floor, consequently the structure was subjected to two displacements whereas all the displacements out of the plan (torsion) have been avoided by the controller system.

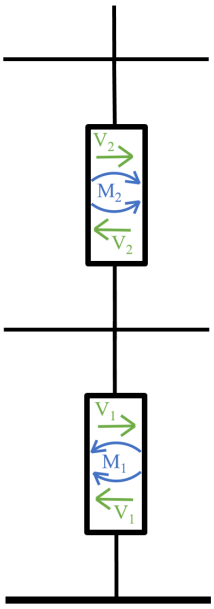

Figure 5.2 Static parameters of the local system.

The local system was more complex due to the presence of the slab-column connections. The static parameters are three for each slab-column connection: one shear, one bending moment and one axial force; so six for each column (Figure 5.2).

These parameters were acquired using the load cells steel member systems located at the centre of each column on each floor, appositely designed for this experimental campaign (see Chapter 4 for a more detailed description).
During the calibration procedure (see Chapter 4), it was noticed that the acquisition for the axial force was poor compared to the requested accuracy. Various attempts were made to solve the problem without success, so it was decided not to consider reliable the reading of the axial force at the centre of the column.
The slabs and the columns rotations are the local kinematics parameters that are recorded using the inclinometers, and the slabs cracks opening recorded by using the displacement transducers (see Chapter 4).
Using the acquired data for the rotation of the slab and the column in each slab-column connection, it was possible to derive the relative rotation of the slab with respect to the column.
The first phase of the analysis was executed in order to have a clearer idea of the behaviour of the mock-up in general, and in more detail that of each slab-column connection. The static and the kinematic parameters of the two scales of study (the global static ones with the local statics ones and the global kinematic ones with the local kinematic ones) were then presented.
Successively, for a deeper and more detailed study, some "composite indicators" were calculated combining the data obtained during the first phase of the analysis (the static parameters of the forces with the kinematic ones of the displacements)
In order to describe the local and the global damage of the structure the stiffness degradation was utilised, thereby making it possible to represent the post-elastic behaviour of the structure with a single variable as a function of the drift.
To calculate the ability of the entire structure and of each of the slab-column connections to deform plastically before failure, the global and the local ductility was analysed.
Finally, since the structure was dissipative, it was necessary to study the energy dissipation in both global and local systems, by always using the same static parameters for the forces and the kinematic ones for the displacements. The forces applied to the global system are dissipated into all the slabs-column joints and into the column bases, developing local rotation and deformation in both the columns and the slabs, also creating a relationship between the two structural elements.
The presented methodology is used for an in depth analysis of the relation between the global and the local structural analysis of flat slab buildings, following procedures from the literature that were studied and adapted to this work.

5.3 Global response

The global behaviour was studied, considering the two floors that constituted the specimen, the 1st one located at 3.2 m and the 2nd one at 6.4 m from the ground (for a detailed description of the structure see chapter 3).
Since the experimental campaign involved two different test typologies: seismic and

cyclic, with different output, the studied measurements and their analysis varied with the two test typologies.

5.3.1 STATIC AND KINEMATICS PARAMETERS

The static and the kinematics parameters were analysed, considering the measurements recorded during the two tests, seismic and cyclic.
The total shear force at the base was obtained by the sum of all the measurements of load cells mounted on pistons (two for each storey). The global drift ratio was calculated as the ratio between the displacement recorded from the displacements transducer on the 2nd floor (Heidenhain) and the height of the structure.
For the cyclic tests only, the backbone curve as the envelope of the maximum values of shear force and inter-storey drift was carried out (Figure 5.3). These values will be used in the next analyses.

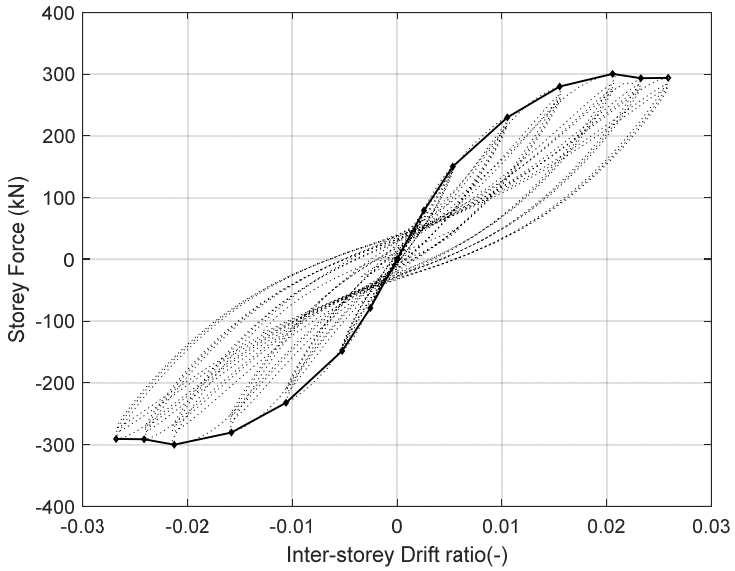

Figure 5.3 Example of the backbone curve for the cyclic tests.

5.3.2 COMPOSITES INDICATORS

STIFFNESS

The study of the stiffness was performed using different approaches for the seismic and the cyclic tests.
The initial stiffness of the structure was calculated for the seismic tests, whereas the stiffness deterioration (Le et al., 2020 [4]) was studied for the cyclic ones.

Seismic Tests

Two different procedures were followed to test the stiffness of the entire structure and the stiffness of each floor. The initial stiffness of the entire structure was

calculated using the base shear force versus top displacement relation. The base shear is equal to the sum of the four load cells forces (two for each storey), whereas the top displacement corresponds to the 2nd floor displacement.
Since the recorded behaviour is not monotonic, the initial stiffness has been calculated as the angular coefficient of the interpolation line obtained from the points cloud formed with the acquired base shear force and the top displacement (Figure 5.4).

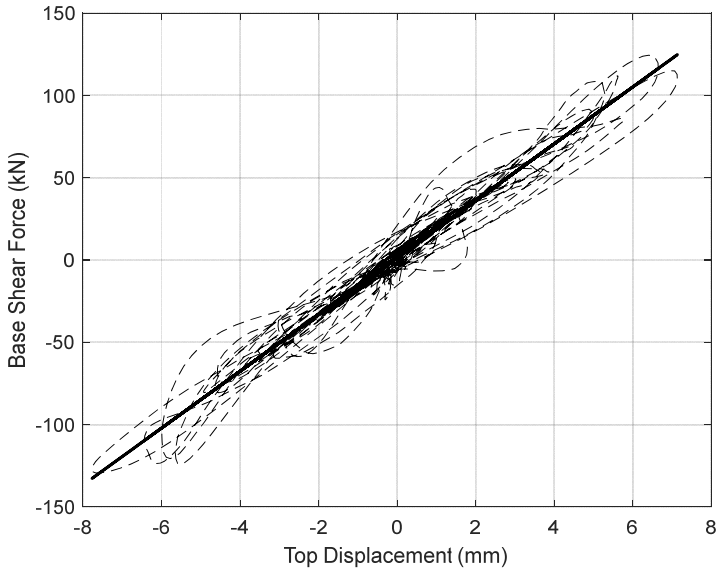

Figure 5.4 Example of the procedure followed to obtain the approximate stiffness of the structure for the cyclic tests.

Since the test was pseudo-dynamic, the followed procedure enabled to approximate the stiffness value directly.
A similar procedure was followed to obtain the stiffness of each of the two floors. Instead of using the base shear force and the top displacement, the shear forces and the displacements of each floor were used. The forces on the 1st floor are calculated as the sum of the four load cells forces (two for each storey), while for the 2nd floor the sum of the two load cells on that floor are used. The displacements are those of each floor. The shear force and the displacement of each floor give the interpolation the slopes of which indicate the stiffness of the two floors.

Cyclic Tests

Two floors had different characteristics of reinforcement and gravity loading and the experimental campaign aimed to study the influence of these differences. Therefore, differing from the seismic stiffness analysis, for the cyclic tests the stiffness analysis was only made for the two floors and not for the entire structure.
The stiffness deterioration of each floor, was determined by comparing the secant

stiffness of each hysteresis loop of each floor and the initial secant stiffness of each floor. The initial secant stiffness corresponds to that calculated in the seismic tests (previous section).
The secant stiffness has been calculated for each hysteresis loop as the ratio between the maximum shear force and the displacement (see Section 5.4.1). These have been evaluated separately for the positive and the negative drift values and for each of the two floors (Figure 5.5).

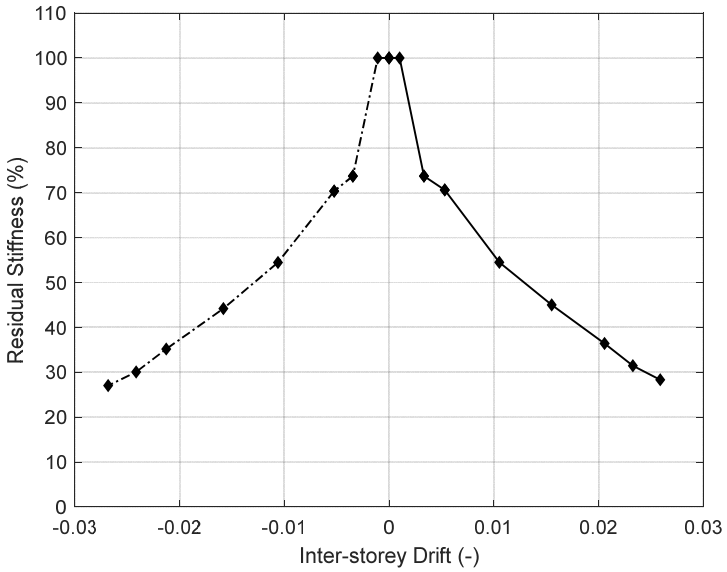

Figure 5.5 Example of the determination of the stiffness deterioration ratio for the positive and the negative drift's value, for one floor of the cyclic tests.

The drift was considered positive (push) when the displacement history was imposed from west to east (Eastward), whereas it was considered negative (pull) when the displacement history was imposed in the opposite sense from east to west (Westward).

DUCTILITY

Since the seismic tests had an almost elastic behaviour, the study of ductility was performed for cyclic tests only.
The "ductility" represents the ability of a structure to undergo wide cyclic deformation in the inelastic range. without a substantial reduction in strength. It is usual to calculate a ductility factor where this is defined as the ratio between the deformation at failure and the corresponding deformation when yielding occurs.
The use of a ductility factor allows to express the maximum deformation in non-dimensional terms as the index of inelastic deformation for seismic design and analysis (Park, 1988 [5]). In this work, the ductility factor is expressed in terms of the displacements (Li et al., 2013 [6]).
The displacement ductility factor, μ is defined as the ratio between the displacement

corresponding to the failure point, d_u, and the displacement at yielding d_y.

$$\mu = \frac{d_u}{d_y} \qquad \text{Eq. 5-1}$$

The displacement ductility factor may vary between 1 for an elastically responding structure to as high as 7 for ductile structure, but is typically in the range 3 to 6 (Park, 1988 [5]).
These displacements are determined by the envelope curve of the hysteresis loop (Le e al., 2020 [4]). The displacement corresponding to the failure point, d_u, is defined as the displacement corresponding to 5%, 10%, 15%, 20% drop in the loading resistance. The first two values 80% and 85% of the resistance are defined on Eurocode 8 [7], whereas the other two values, 90% and 95% of the resistance were chosen as explorative values to extend the range of observation.
The yield displacement determination is based on Eurocode 8 [7].
In Figure 5.6, an example of the followed procedure for the determination of the idealized elasto-perfectly plastic force-displacement relationship, is reported.

Based on Eurocode 8 [7]:

- The blue line represents the backbone of the storey force versus the I-S drift experimental data;
- The black line represents the elasto-plastic branch of an idealized SDOF system;
- The point *A* represents the formation of the plastic mechanism and it is determined with the maximum shear force F_{max} and the corresponding displacement d_m;
- The yield force F_y is equal to the base shear force at the formation of the plastic mechanism. It also represents the ultimate strength of the idealized system.

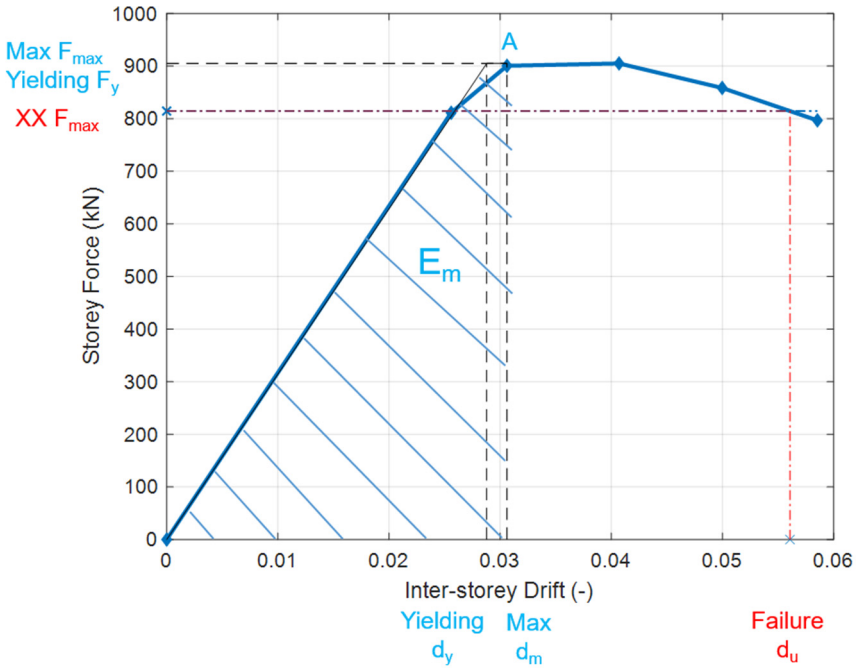

Figure 5.6 Determination of an idealized perfect elasto- plastic force-displacement relationship [1].

The idealized system was determined in such a way that the area under the experimental and the idealized force-deformation curves resulted to be equal.
Based on this assumption, the yield displacement of the idealized system d_y is given by:

$$d_y = 2 * \left(d_m - \frac{E_m}{F_y} \right) \qquad \text{Eq. 5-2}$$

With E_m the area under the curve of the experimental data.

Table 5.1 reports the corresponding values of force and drift of the three main points (limit, yielding and failure) obtained with the procedure described above.

Table 5.1 Example of shear force and drift ratio at different characteristic points.

Floor, Drift	Limit Point		Yielding Point		Failure Point		
1st, Positive	Shear Max (kN)	Drift (-)	Shear Yielding (kN)	Drift (-)	0.80 Shear Max (kN)	Drift (-)	μ (-)
	904.9	0.031	904.9	0.029	814.4	0.056	1.9

The values of limit, yielding and failure are reported for each floor and for both the drift, positive and negative.
This analysis was made for all the four analysed residual loads of 80%, 85%, 90% and 95%, to evaluate the differences between the four percentages.

For each of the four analysed residual loads, the graph with the representation of the procedure followed, to define the yielding and the failure points for each floor, is reported and if the conditions to reach failure are respected, a red line indicates the failure load and the corresponding displacement (Figure 5.7).

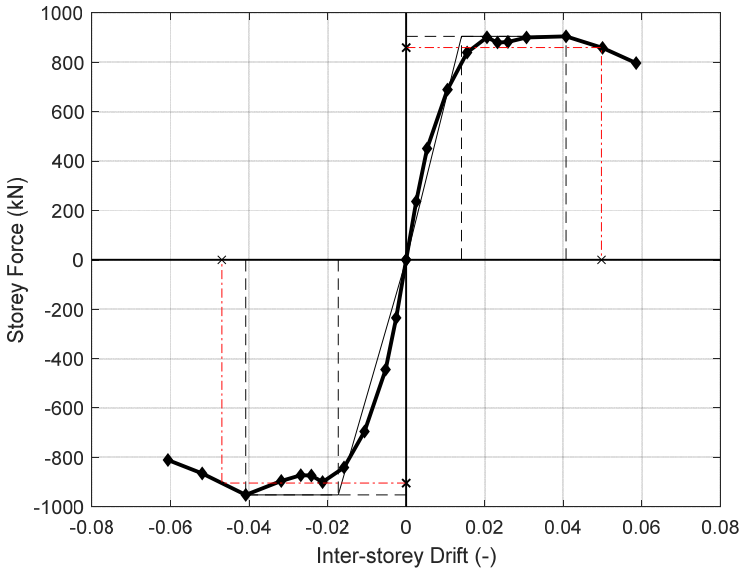

Figure 5.7 Example of the definition of the yielding and failure points for one floor of the cyclic tests.

Once the failure is recorded, the inter-storey drift corresponding to the shear force at failure should be included between the inter-storey drift corresponding to the maximum value of shear and the maximum inter-storey drift.
In Table 5.1 if the failure is verified, the cell corresponding to the drift value of the failure point failure is highlighted in yellow, if not, there is a sign '-'. In the last column of Table 5.1 the displacement ductility factor calculated as Eq.5-1 is reported, obviously, this field is filled in only if the failure is verified.

ENERGY

The energy dissipated from each floor was calculated as the cumulative integral using the cumulative trapezoidal numerical integration between the force applied with the actuators and the displacements of the structure. This was calculated for each floor and for each test.
For the 1st floor the shear force was obtained from the sum of the four load cells forces (two for each floor, Eq.5-3), whereas for the 2nd floor the shear force was reached by adding only the two load cells acting on that floor.

$$Shear_{\,1^{st}floor} = Actuator\ force_{\,1^{st}\,floor\,South} + Actuator\ force_{\,1^{st}\,floor\,North} + Actuator\ force_{\,2^{nd}floor\,South} + Actuator\ force_{\,2^{nd}floor\,North} \quad \text{Eq. 5-3}$$

$$Shear\ _{2^{nd}floor} = Actuator\ force._{2^{nd}\ floor\ South} + Actuator\ force._{2^{nd}\ floor\ North} \quad \text{Eq. 5-4}$$

Regarding the displacement, for the 1st floor the values recorded from the sensor were used (Eq. 5-5), for the 2nd floor the difference between the 2nd and the 1st floor values was used (Eq. 5-6).

$$Displacement\ _{1^{st}floor} = Heid.disp._{1^{st}\ floor} \quad \text{Eq. 5-5}$$

$$Displacement\ _{2^{nd}floor} = Heid.disp._{2^{nd}\ floor} - Heid.disp._{1^{st}\ floor} \quad \text{Eq. 5-6}$$

The procedure followed was the same for the seismic and the cyclic tests but the representation in the graphs is different. For the two seismic test the dissipated energy was reported in function of the accelerogram time, for the two cyclic test it was reported in function of the steps number, Figure 5.8 a and b respectively.

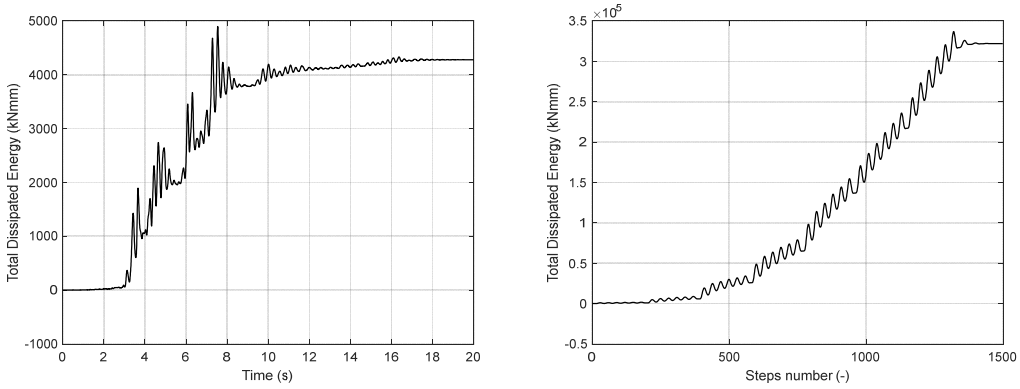

Figure 5.8 Example of the floor dissipated energy for the a) seismic and b) cyclic tests.

The energy dissipated from the entire structure is obtained considering all the four load cells forces (Eq.5-7) and the displacement at the top of the structure, the 2nd floor (Eq. 5-8).

$$Shear\ _{Tot} = Actuator\ force\ _{1^{st}\ floor\ South} + Actuator\ force\ _{1^{st}\ floor\ North} + Actuator\ force\ _{2^{nd}floor\ South} + Actuator\ force\ _{2^{nd}floor\ North} \quad \text{Eq. 5-7}$$

$$Displacement\ _{Tot} = Heid.disp._{2^{nd}\ floor} \quad \text{Eq. 5-8}$$

Also in this case, the dissipated energy was reported in function of the accelerogram time for the seismic tests and in function of the steps number for the cyclic ones.

5.4 Local response

The local behaviour was studied considering all the 24 slab-column connections of the specimen, 12 for each floor.
To study the behaviour of each structural component, slabs and columns, 48 linear transducers, 80 inclinometers and 24 steel stubs with load cells were used (see chapter 4). The main aim of the connections data evaluation is to know the different behaviour of the slab-column connections having different characteristics: three different typologies (edge, internal and corner), different gravity shear ratio, with or without the transversal reinforcement, different layout of the longitudinal reinforcement (concentrated and smeared). The final purpose aims to be the assessment of the seismic response for each typology.
As for the global behaviour, also in the local analysis, the studied measurements and their analysis vary with the test typology, seismic or cyclic.

5.4.1 STATIC AND KINEMATICS PARAMETERS

The analysis of the static and the kinematics parameters was carried out considering the unbalanced moment versus the inter-storey drift ratio as a starting point.
The unbalanced moments were calculated using the data collected from the load cells in the columns (Figure 5.9), continuously recorded during the seismic and cyclic tests.

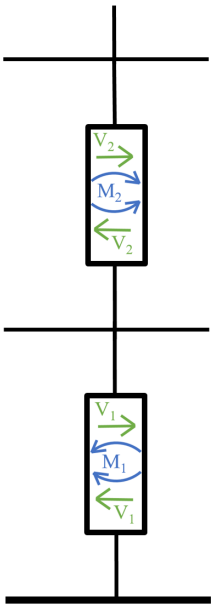

Figure 5.9 Diagram to calculate the unbalanced moment.

Where:

- V_1 is the shear force recorded from the load cells located in the columns below the slab;
- V_2 is the shear force recorded from the load cells located in the columns above

the slab;

- M_1 is the bending moment recorded from the load cells located in the columns below the slab;
- M_2 is the bending moment recorded from the load cells located in the columns above the slab.

The unbalanced moments for each connection on both floors were calculated as followed:
For the 1st floor the shear force and the bending moment recorded from the load cells located in the columns below the slab (subscript 1) added to the shear force and the bending moment recorded from the load cells located in the columns above the slab (subscript 2) Eq. 5-3.

$$UM_{1^{st}floor} = V_1 * \frac{h}{2} - M_1 + V_2 * \frac{h}{2} + M_2 \qquad \text{Eq. 5-9}$$

For the 2nd floor, since there were no load effects above the slab, the unbalanced moment was calculated only with the shear force and the bending moment of the columns below the slab (subscript 2) Eq. 5-4.

$$UM_{2^{nd}floor} = V_2 * \frac{h}{2} - M_2 \qquad \text{Eq. 5-10}$$

The bending moment was assumed to be positive when the fibres on the west side were in tension. The inter-storey drift was calculated using the data recorded by the linear optical encoders.
For the 1st floor, the inter-storey drift corresponded to the ratio between the absolute displacement of the first floor slab level and the column height (3200 mm) Eq. 5-5.

$$IS\ drift_{1^{st}floor} = \frac{Heidenhain\ displacement_{1^{st}\ floor}}{3200} \qquad \text{Eq. 5-11}$$

For the 2nd floor, the inter-storey drift was the ratio between the difference of the absolute displacement between the 2nd and the 1st floor and the column height (3200 mm) Eq. 5-6.

$$IS\ drift_{2^{nd}floor} = \frac{Heid.disp._{2^{nd}\ floor} - Heid.disp._{1^{st}\ floor}}{3200} \qquad \text{Eq. 5-12}$$

This procedure was followed for all the experimental campaign, for the two seismic tests and the two cyclic ones
For the cyclic tests only, the backbone curve as the envelope of the maximum values of the unbalanced moment and inter-storey drift was effected. These values will be used in the next analyses.

To obtain the backbone curve the same procedure adopted for the global analysis and described in 5.2 was followed. It was repeated for each slab-column connection on each floor and for both floors (Figure 5.10).

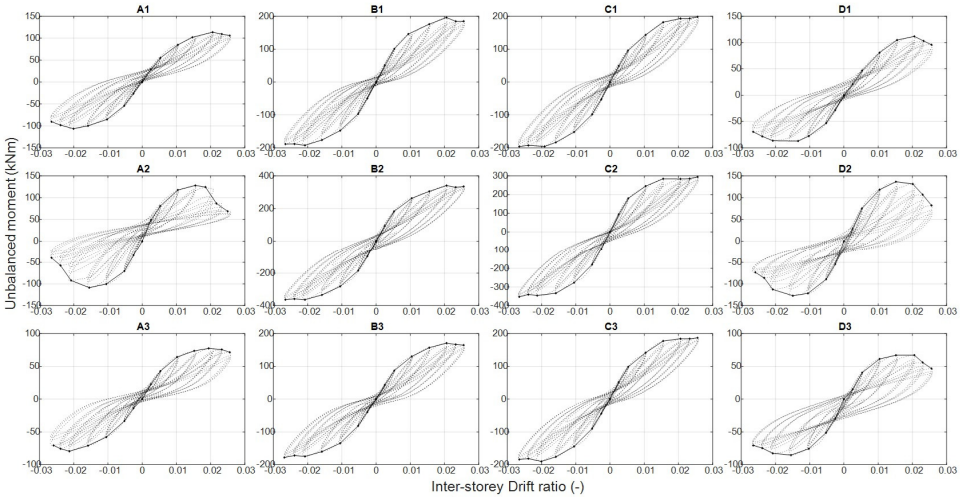

Figure 5.10 Example of the static and kinematic analysis with backbone curves for one floor of the cyclic tests. Unbalanced moment vs inter-storey drift for all connections in the floor.

For the two cyclic tests, the obtained unbalanced moment versus the inter-storey drift graphs were used to compare the slab-column connections with different characteristics and to ascertain how these differences influenced the final response of the structure.

Table 5.2 Summary of the connections comparison in test Cyc-1.

Long. reinf. / Typology	Smeared	Concentrated
Corner	A1	D1
	A3	D3
Lateral long side	B1	C1
	B3	C3
Lateral short side	A2	D2
Internal	B2	C2

For the first cyclic test, Cyc-1, the comparison is made between the connections of the same typology but located in one of the two halves of the slab with different longitudinal reinforcement (smeared in the west side and concentrated in the east

one) and gravity shear ratio.

For the corner connections the comparison was made between A1 with D1 and A3 with D3, for the lateral ones placed on the long side, B1 with C1 and B3 with C3, for the lateral ones placed along the short side, A2 with D2 and finally for the internal connections, B2 with C2. In Table 5.2 the summary of the comparison between the connections that was made for the cyclic test cyc-1, is reported and the position of the connections in the plan of the specimen is represented in Figure 5.11.

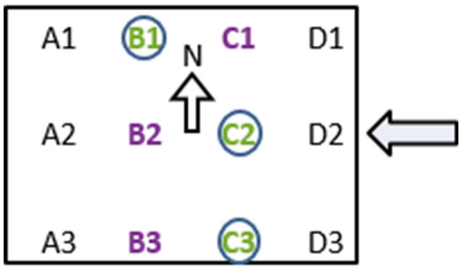

Figure 5.11 Strengthened connections position.

Similarly, for the second cyclic test, the Cyc-2, the comparison between the strengthened and the un-strengthened connections was made. The connections that were strengthened were B1, C3 and C2, each one was compared directly with the corresponding un-strengthened, respectively B3, C1 and B2 (see Table 5.3).
In Figure 5.11 the strengthened connections are written in green and encircled whereas the corresponding un-strengthened ones are written in purple. This convention will be used in chapter 8 for the comparison between the strengthened and the un-strengthened connections at the end of the test Cyc-2.

Table 5.3 Summary of the connections comparison in test Cyc-2.

Typology	Strengthened	Un-strengthened
Lateral long side	B1	B3
	C3	C1
Internal	C2	B2

5.4.2 Composite Indicators

Stiffness

In this analysis as in the similar global one, the procedure followed varied according to the test typology, whether seismic or cyclic.
For the seismic test the initial stiffness of each slab-column connections in each floor was calculated, whereas for the cyclic the stiffness deterioration of each slab-column connections on each floor (Le et al., 2020 [4]) was studied.

For both tests, the procedure followed was the same for the global analysis.

Seismic Tests

To calculate the stiffness of each slab-column connection on each floor, the shear force recorded in each load cell in the middle of the column and the inter-storey displacement of each floor were used. With these values, a point cloud for each slab-column connection was formed.
The interpolation among the point clouds gives the slope of each slab-column connection. The angular coefficient of these lines corresponds exactly to the searched stiffness (Figure 5.12). The procedure was repeated for all the slab-column connections and for both floors.

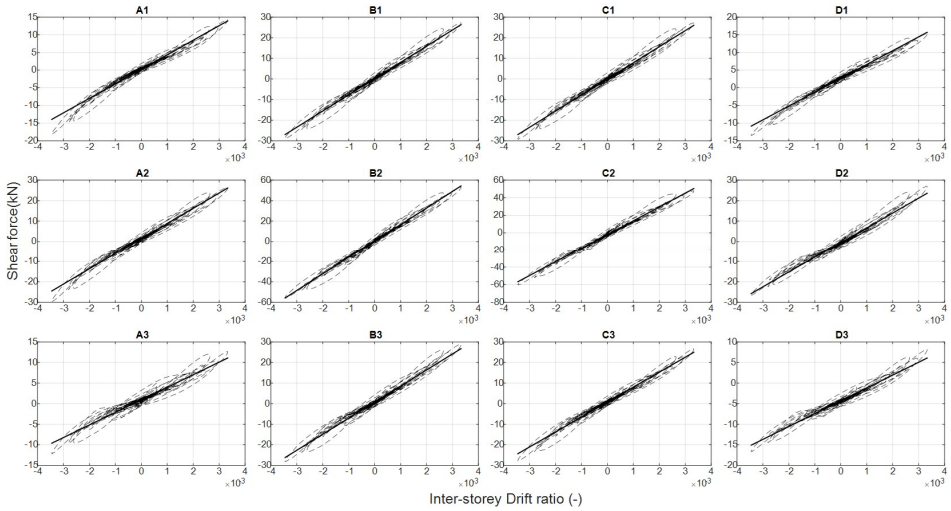

Figure 5.12 Example of the procedure followed to obtain the approximate stiffness of each connections in one floor for the seismic tests.

Cyclic Tests

As for the global analysis, also for the local one, the stiffness deterioration for each slab-column connection on each floor for both the cyclic test, Cyc-1 and Cyc- 2, was studied. The procedure followed was the same used to calculate the global stiffness deterioration (5.3.2).
This stiffness deterioration for each slab-column connection on each floor, was determined by the ratio between the secant stiffness of each hysteresis loop of each slab-column connection on each floor and the initial secant stiffness of each slab-column connection on each floor. The initial secant stiffness corresponds to that calculated in the seismic tests (paragraph above).
For each hysteresis loop, the secant stiffness was calculated by the ratio between the maximum shear force in the semi-loop and the displacement. The maximum values

of shear force correspond to those recorded in each load cell in the middle of the column and the displacement corresponds to that obtained with the static and kinematics parameters analysis (see chapter 5.4.1). This was calculated for each slab-column connections separately for the positive and the negative drift values and for each of the two floors (Figure 5.13). In each graph, the four different tests were represented by four different coloured diamonds.
The stiffness deterioration of both the cyclic test, Cyc-1 and Cyc-2, was calculated in relation to the initial stiffness of the structure, calculated using the results of the first seismic test, Seis-SLS.

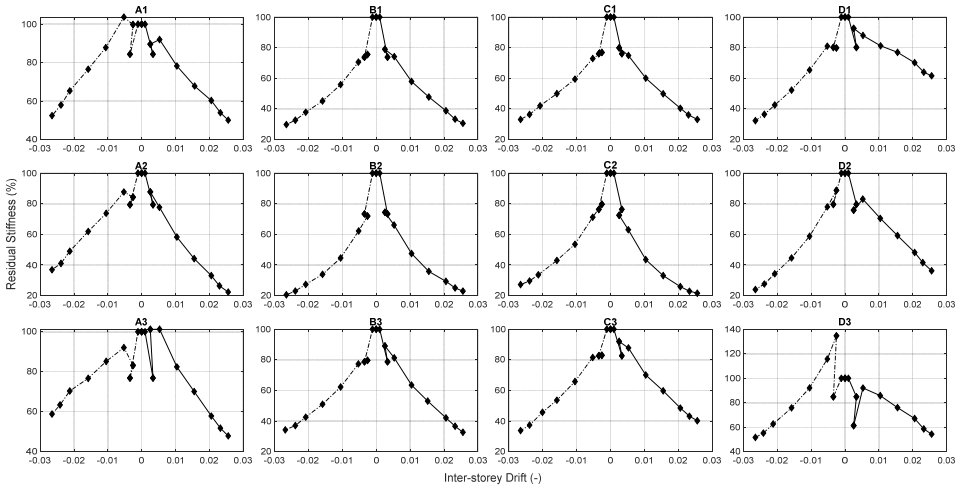

Figure 5.13 Example of the stiffness deterioration for one floor of the cyclic test.

DUCTILITY

The procedure followed was the same as that of the global analysis (for a detailed description see Chapter 5.3.2) but using the unbalanced moment instead of the shear force. The analysis it was repeated then for all the slab-column connections on both floors. Here too, the analysis was repeated for all the four residual loads of 80%, 85%, 90% and 95%.

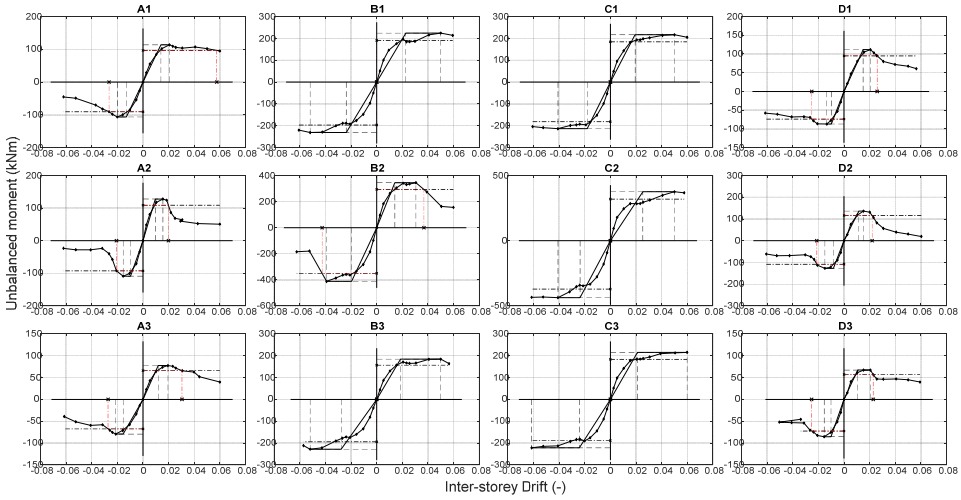

Figure 5.14 Example of the definition of the yielding and failure points for the slab-column connections in one floor of the cyclic tests.

The conditions from which the failure is verifiable are the same as those of the global analysis and also the conventions used in the graphs and in the tables are the same (see chapter 5.3.2).

ENERGY

The energy dissipated from each slab-column connection on each floor was calculated as the cumulative integral, the cumulative trapezoidal numerical integration between the shear force recorded with the load cells during the tests (see chapter 5.4.1) and the displacement of the floor in which the analysed connection is present.
This was done for each floor and for both seismic and cyclic tests.

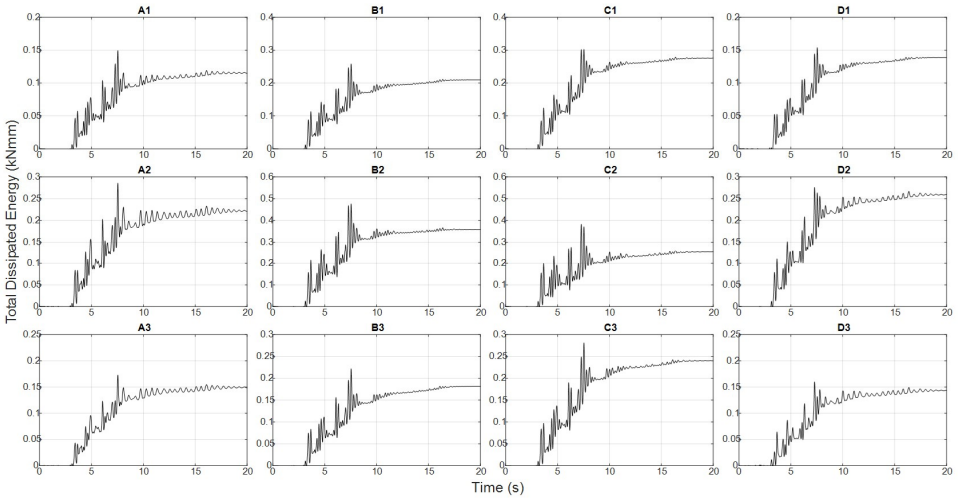

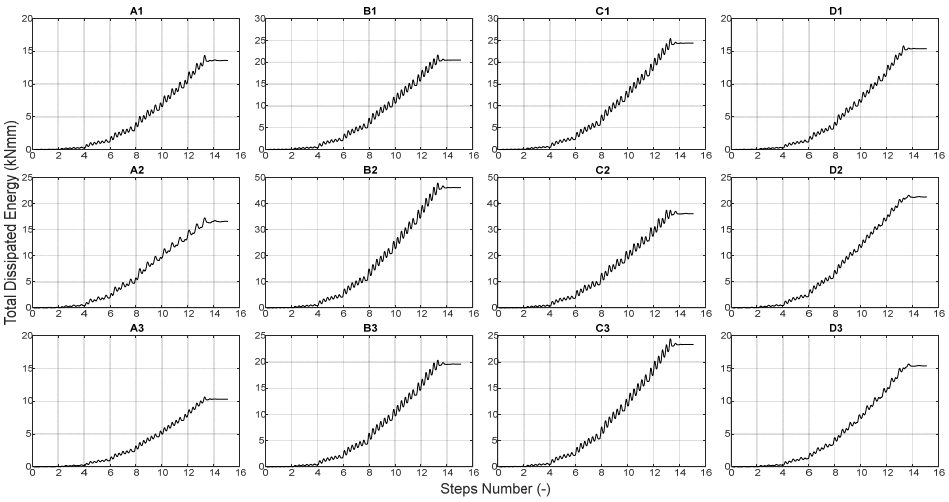

Figure 5.15 Example of the slab-column connections dissipated energy for one floor in a) seismic and b) cyclic tests.

The procedure followed for the local analysis was the same as for the seismic and the cyclic tests but is represented differently on the graph. For the two seismic test the dissipated energy was reported in function of the accelerogram time, for the two cyclic tests it was reported in function of the steps number, Figure **5.8** a and b respectively.

5.4.3 OBSERVED DAMAGE

For a thorough analysis of the damage, the inter-storey drift versus the slab crack opening for the seismic tests and the unbalanced moment versus the slab crack opening, recorded by the linear transducer, were also analysed.
Both the analyses were carried out on all the connections through slab displacement transducers (eight of the twelve, for a deepened description see chapter 4) for the 1st and the 2nd floor.
As described in chapter 4, the number of sensors inserted into each connection is in function of the connections typology (Table 5.4).

Table 5.4 Slab crack opening sensors position.

Connections		Sensors position			
Typology	Name	North	South	East	West
Corner	A1		x	x	
	D3	x			x
Edge	A2	x	x	x	
	B1		x	x	x
	C3	x		x	x
	D2	x	x		x
Internal	B2	x	x	x	x
	C2	x	x	x	x

The inter-storey drift and the unbalanced moment are calculated as previously reported (Chapter 5.4.1 Eq. 5-3, Eq. 5-4, Eq. 5-5, Eq. 5-6).
For the first cyclic test only, Cyc-1, the sketch of the cracking formation for the 1st and the 2nd floor was drawn.

5.5 Inter-storey drift and column-slab rotation

The inter-storey drift is the most used parameter to describe the seismic global response of a structure, but it does not describe the behaviour of each floor and of each slab-column connection to the floors in the best way.
The main difference between the two floors consists in the presence of the columns that for the 1st floor are above and below the slab whereas for the 2nd floor they are only below the slab. So using the inter-storey drift ratio the behaviour of the 1st floor is well described, but this is not the case for the 2nd floor, for which it was observed that the rotation gives a better representation of the behaviour of each slab-column connection in addition to permitting to compare the SlabSTRESS results to those of previous experiments. The column-slab rotation is defined as the relative rotation between the slab and the column. For this reason, all the analyses made previously, are repeated, using the column-slab rotation instead of the inter-storey drift ratio as x-axis in the reported graphs.
Different preliminary analyses were made taking the column-slab rotation as a valid parameter. First of all, the sensitivity analysis of the rotation parameters was developed, to understand if there was a relationship between the measured rotation and the inter-storey drift ratio. Successively, the parameters of the linear regression were determined to know if the evaluation was valid. These are the slope of the line, the coefficient of the linear determination (R^2) and the standard deviation. Finally, the two measurements, the inter-storey drift and the column-slab rotation of each slab-column connection on each floor, were plotted in the same graphs to evidence their relationship.
After the column-slab rotation was determined, all the local analysis done with the inter-storey drift ratio were repeated with the column-slab rotation, and the description of the followed procedure is reported here.
After the description of all the analyses, the procedure that was followed to obtain the conversion factors that allow to convert the inter-storey drift ratio to the column-slab rotation, in function of the slab-column connections typology (internal, edge with loading parallel or perpendicular and corner) is reported.
These values of conversion obtained enable a simplification of the numerical analyses where the inter-storey drift is known but the corresponding rotation is not known.

5.5.1 Sensitivity Analysis

A prelaminar sensitivity analysis of the slab and column rotation was made to evaluate the ratio between the drift ratio and the column-slab rotation. Since the sensors were not applied to all the slab-column connections, the graphs with the

rotation on both floors were designed only for the eight connections bearing the instrumentations.
Figure 5.16 a and b report position of the inclinometers on the slabs and in the columns respectively. The positions are the same for both floors.

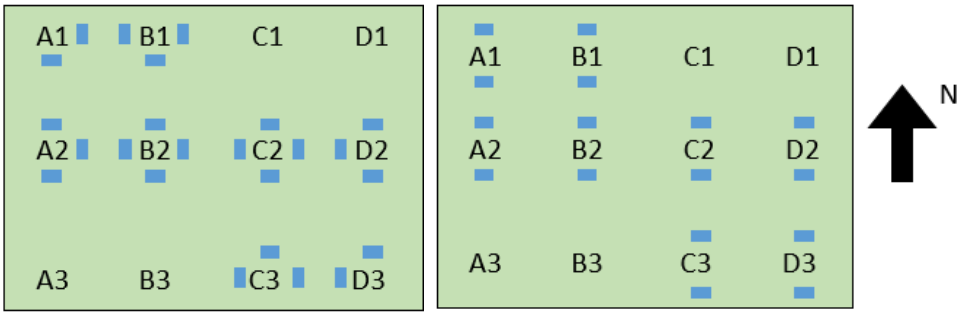

Figure 5.16 Inclinometers position a) on the slabs and b) on the columns.

Figure 5.17 and Figure 5.18 report the rotation versus the inter-storey drift ratio of each sensors in the slabs and Figure 5.19 and Figure 5.20 report the rotation versus the inter-storey drift ratio of each sensor on the columns.
All the graphs were drawn for each connection on each floor and for all the four tests (Seis-SLS, Seis-ULS, Cyc-1, Cyc-2). Blue lines are used for the 1st floor, red lines for the 2nd. Above each graph the name of the tests is reported.
The sensors around each column are outlined with a rectangle Each rectangle indicates the slab-column connection in the position that it has in the slab. Not all the slab-column connections have been instrumented, so the rectangle for the four lateral connections (A3, B3, C1 and D1) was omitted (see Figure 5.16 for the instrumented connections). Inside each rectangle, the graph of the detected measure is reported. Each graph indicates the position of the sensor that took the reading (see Figure 5.16 for the sensors position).
For sensors in the slabs the relationship between the inter-storey drift and the rotation (Figure 5.17 and Figure 5.18) appears non-linear, with some exceptions; whereas for the columns this relationship is linear in all the sensors (Figure 5.19 and Figure 5.20) indicating that the columns remained elastic during the tests. For the slab sensors in both floors (Figure 5.17 and Figure 5.18) it is possible to observe a difference in the measurements to one order of magnitude, between the ones located in the North-South directions and the ones in the West-East, this it was different from the sensors in the columns on both floors (Figure 5.19 and Figure 5.20) which all recorded values of similar magnitude. The same behaviour is observed in both the seismic and the cyclic test.

Figure 5.17 Slab rotation vs inter-storey drift ratio from each sensors in the 1st floor, test Cyc-2.

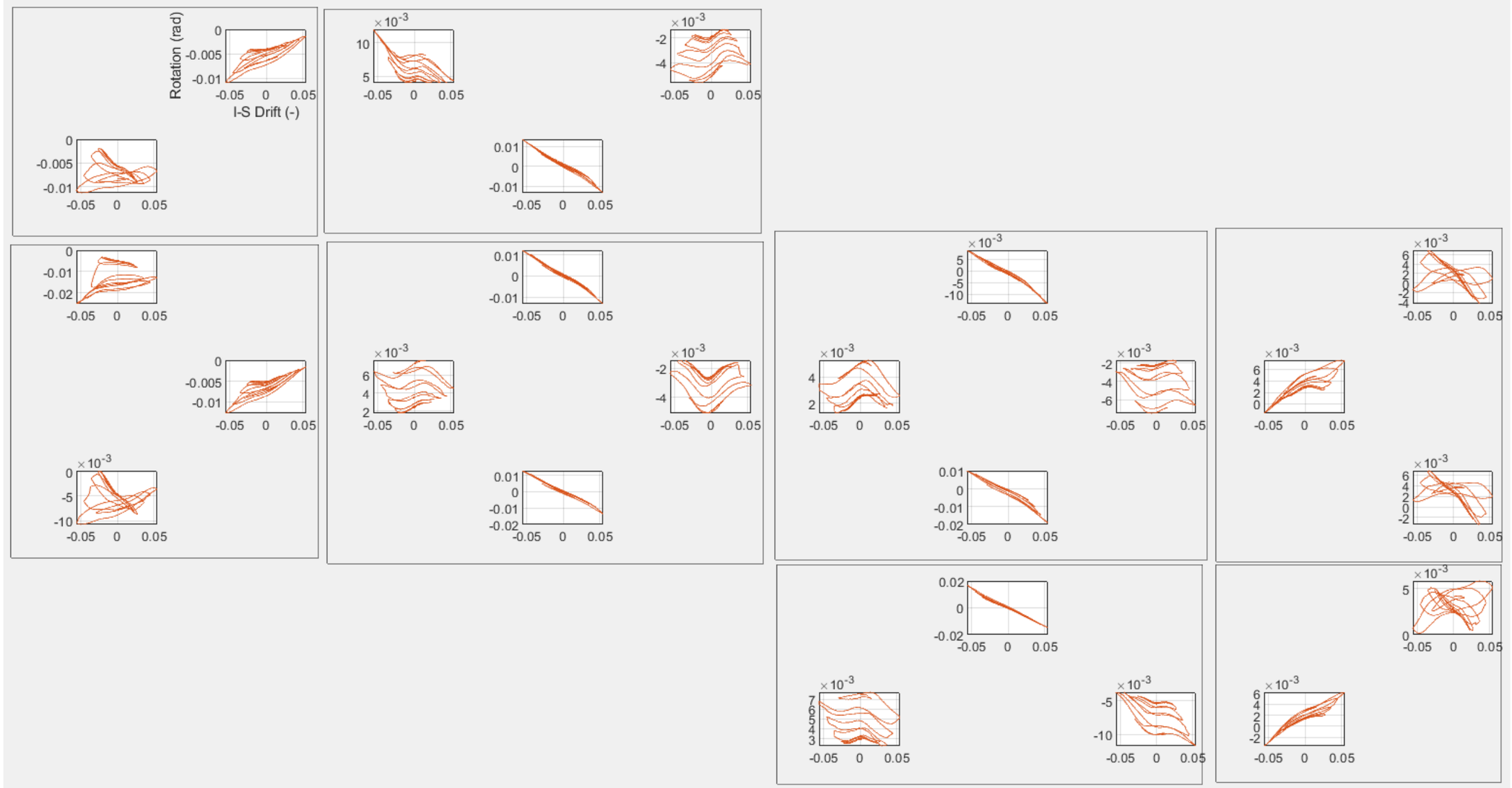

Figure 5.18 Slab rotation vs inter-storey drift ratio from each sensors in the 2nd floor, test Cyc-2.

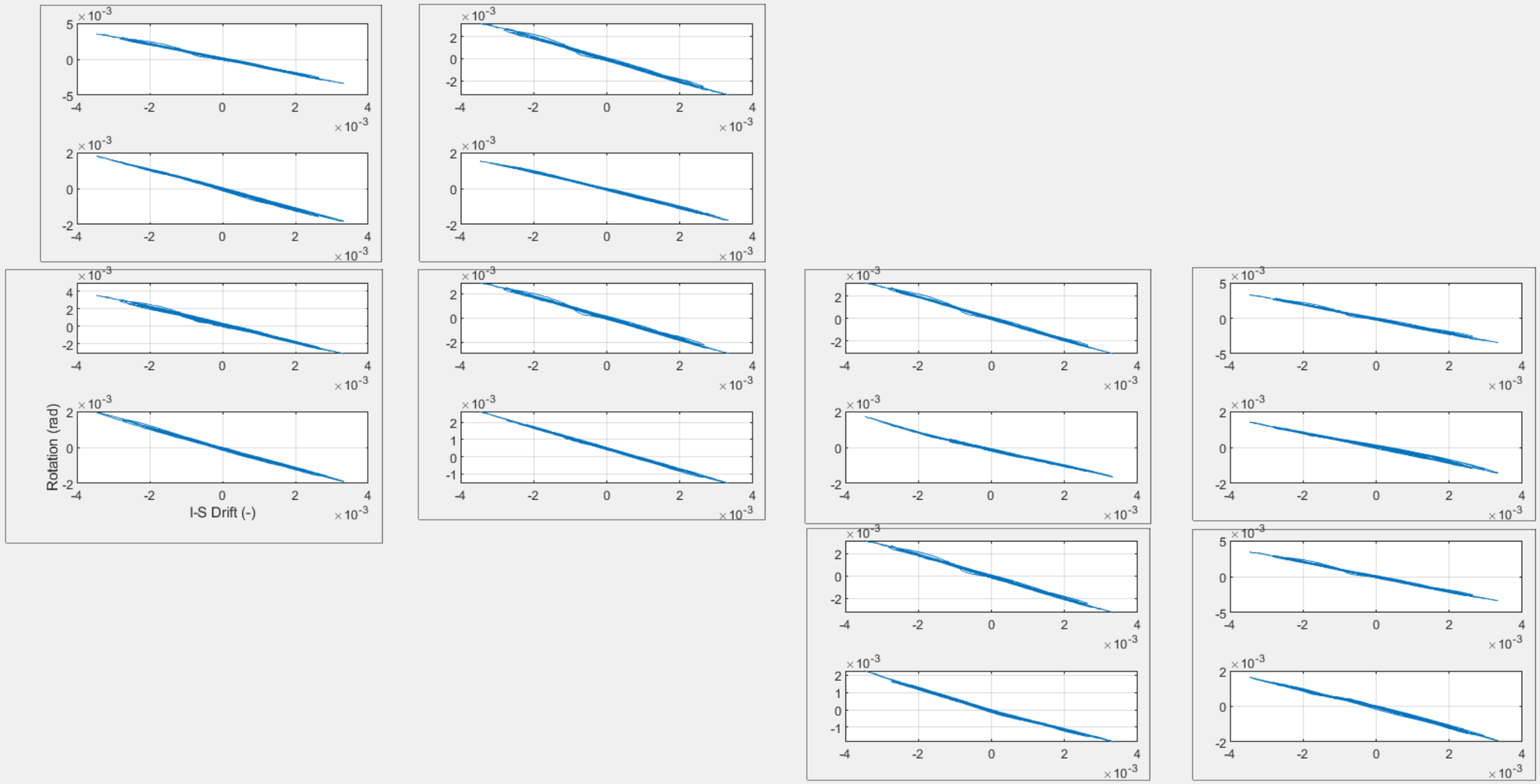

Figure 5.19 Column rotation vs inter-storey drift ratio from each sensors, 1st floor, test Cyc-2.

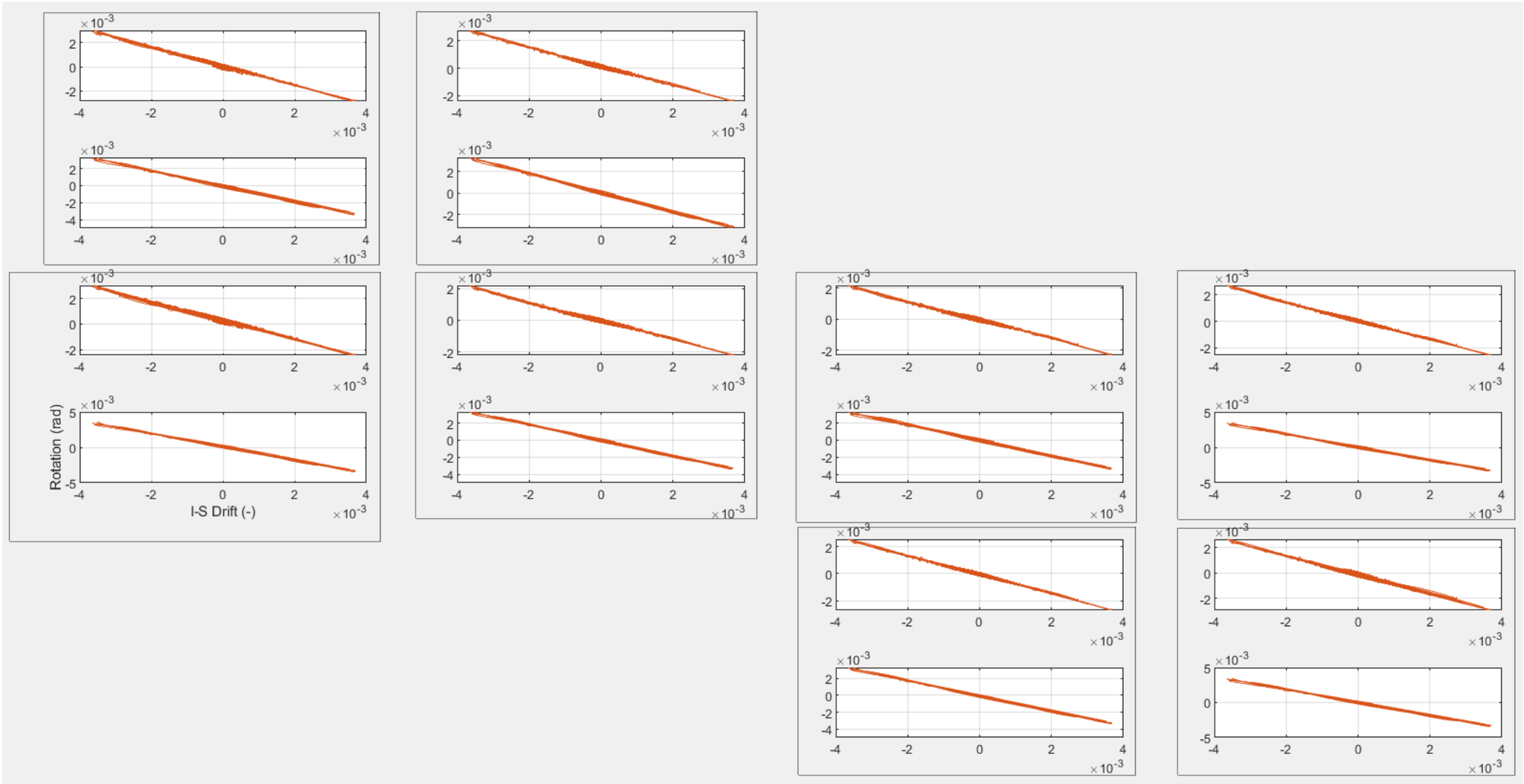

Figure 5.20 Column rotation vs inter-storey drift ratio from each sensors, 2nd floor, test Cyc-2.

5.5.2 CORRELATION BETWEEN COLUMN AND SLAB ROTATION

The parameters of the linear regression were determined to know if the evaluation was valid.

The slope of the line (Slope in Table 5.5), the coefficient of the linear determination (R^2 in Table 5.5) and the standard deviation (Std in Table 5.5) were obtained from the minimum square regression line.

These analyses were made for both slabs and all the columns equipped with the sensors.

Table 5.5 reports the obtained parameters for the slabs and columns sensors in all the connections in the B and C alignments.

Table 5.5 Linear regression parameters for the connections in the B and C alignments.

Floor	N-S Axis	E-W Axis	N/S-T/B	Slab/Column	Slope	R^2	Std
1	1	B	S	Slab	-0.278	0.984	0.003
			T	Column	-0.999	0.996	0.011
			B	Column	-0.646	0.983	0.007
	2	B	N	Slab	-0.269	0.988	0.003
			S	Slab	-0.335	0.943	0.004
			T	Column	-0.932	0.995	0.011
			B	Column	-0.801	0.988	0.009
	2	C	N	Slab	-0.338	0.956	0.004
			S	Slab	-0.345	0.982	0.004
			T	Column	-0.975	0.996	0.011
			B	Column	-0.637	0.986	0.007
	3	C	N	Slab	-0.344	0.983	0.004
			T	Column	-0.982	0.996	0.011
			B	Column	-0.755	0.992	0.009
2	1	B	S	Slab	-0.158	0.986	0.002
			T	Column	-0.744	0.997	0.007
			B	Column	-1.059	0.998	0.010
	2	B	N	Slab	-0.164	0.984	0.002
			S	Slab	-0.178	0.982	0.002
			T	Column	-0.683	0.996	0.007
			B	Column	-1.055	0.998	0.010
	2	C	N	Slab	-0.155	0.981	0.002
			S	Slab	-0.166	0.981	0.002
			T	Column	-0.660	0.997	0.007
			B	Column	-1.067	0.998	0.011
	3	C	N	Slab	-0.195	0.970	0.002
			T	Column	-0.747	0.997	0.007
			B	Column	-1.055	0.998	0.010

Since the slab on the lateral short sides (alignments A and D Figure 5.29) underwent great stress during the first cyclic test, the sensors located there were removed and all the analyses with the column-slab rotation for the test Cyc-2 were carried out for the connections in the alignments B and C (B1, B2, C2 and C3) alone.

5.5.3 COLUMN-SLAB ROTATION CALCULATION

The aim of this section is to study the relative rotation between the two elements that compose the structure, the columns and the slabs. This relationship is well reproduced by the column-slab rotation expressed as the difference of the rotation between the column and the slab.

$$Chord\ rotation\ = Column\ rotation - Slab\ rotation \qquad \text{Eq. 5-13}$$

For the columns on the 1st floor the rotation was obtained as the mean between the sensors above and below the slab, whereas for the columns on the 2nd floor the rotation corresponds to the measure recorded by the one sensor present.

$$Column\ rotation_{\ 1^{st}\ floor}\ = \frac{Above\ slab + Below\ slab}{2} \qquad \text{Eq. 5-14}$$

$$Column\ rotation_{\ 2^{nd}\ floor}\ = Below\ slab \qquad \text{Eq. 5-15}$$

The treatment for the sensors was more complex in the slabs due to the presence of sensors in all the four cardinal directions.
In function of the loading action, it is possible to identify two different sections in the area of slab around the column, one in which the rotation is caused by bending under the gravity and lateral loads (the one parallel to the loading application) and the other in which the rotation is due to torsional rotations (the one perpendicular to the loading application). The first one corresponds to the alignments A and D (East-West direction), the second one to the alignments 1 and 3 (North-South direction) (see Figure 5.21).

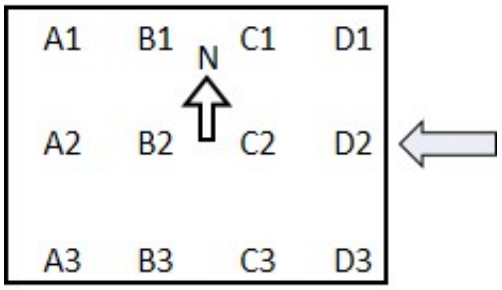

Figure 5.21 Alignments representations in the plan.

As reported in 5.5.1 a one order magnitude difference in the measurements in the both floors slabs was observed between the sensors located in the North-South directions and the ones in the opposite East-West one. This difference is due to the two different rotations causing bending and torsion.

For the sensors in the north-south direction, since the two sensors have the same sign, the mean was calculated:

$$Slab\ NS\ direction = \frac{North\ slab + South\ slab}{2} \qquad \text{Eq. 5-16}$$

The treatment for the sensors in the East-West direction was different it was recorded with opposite sign, so for this reason, the semi-difference was evaluated:

$$Slab\ EW\ direction = \frac{East\ slab + West\ slab}{2} \qquad \text{Eq. 5-17}$$

The mean between the two values (Eq. 5-16 and Eq. 5-17) was calculated:

$$Slab\ rotation = \frac{(Slab\ NS\ direction) + (Slab\ EW\ direction)}{2} \qquad \text{Eq. 5-18}$$

Figure 5.22, Figure 5.23, Figure 5.24, Figure 5.25, Figure 5.26, Figure 5.27 Figure 5.28 and Figure 5.29 report the calculated rotation versus the inter storey drift ratio for all the connections in the 1st (Figure 5.22, Figure 5.24, Figure 5.26, Figure 5.28) and the 2nd (Figure 5.23, Figure 5.25, Figure 5.27, Figure 5.29) floor, for the test Seis-SLS, Seis-ULS, Cyc-1 and Cyc-2 respectively.

The legends in the figure below have the following meaning:

- Column = column rotation (Eq. 5-14 or 5-15 depending on the floor),
- Slab S =sensor reading,
- Slab E = sensor reading,
- Slab W = sensor reading,
- Slab N = sensor reading,
- Slab NS =slab rotation in direction North-South (Eq. 5-16)
- Slab EW = slab rotation in direction East-West (Eq. 5-17)
- Column-Slab = slab column relative rotation, the difference between the column and the slab rotation (Eq. 5-13).

It is worth noting the steady decrease in the slab rotations in both directions (North-South and East-West) and on both floors between the seismic (Figure 5.22, Figure 5.23, Figure 5.24, Figure 5.25) and the cyclic tests (, Figure 5.26, Figure 5.27 Figure 5.28, Figure 5.29). The divergences between the slab rotation and the column rotation highlight that the torsion during the seismic tests has damaged the connections in the A and D alignments.
The damage to the 1st floor slab in the A and D alignments during the test Cyc-2 caused the sensors to be removed, actually the values of all the sensors in the slab

are zero Figure 5.28).
As for the columns rotation, their behaviour remains linear in all the sensors, on both floors and in all the tests (Figure 5.22, Figure 5.23, Figure 5.24, Figure 5.25, Figure 5.26, Figure 5.27 Figure 5.28 and Figure 5.29) indicating that all the columns near the slab were remained elastic throughout the experimental campaign.

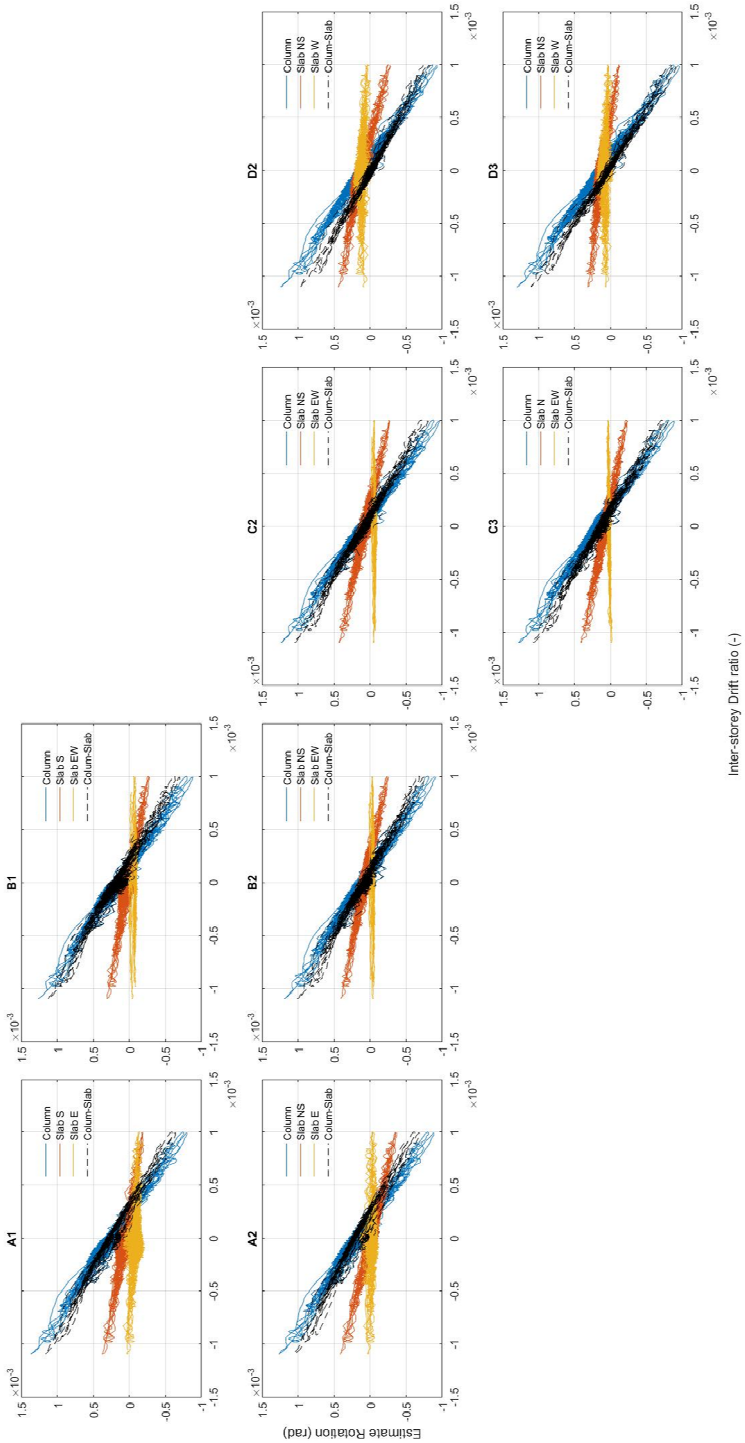

Figure 5.22 Inter-storey drift versus rotation for all the connections, 1st floor, test Seis-SLS.

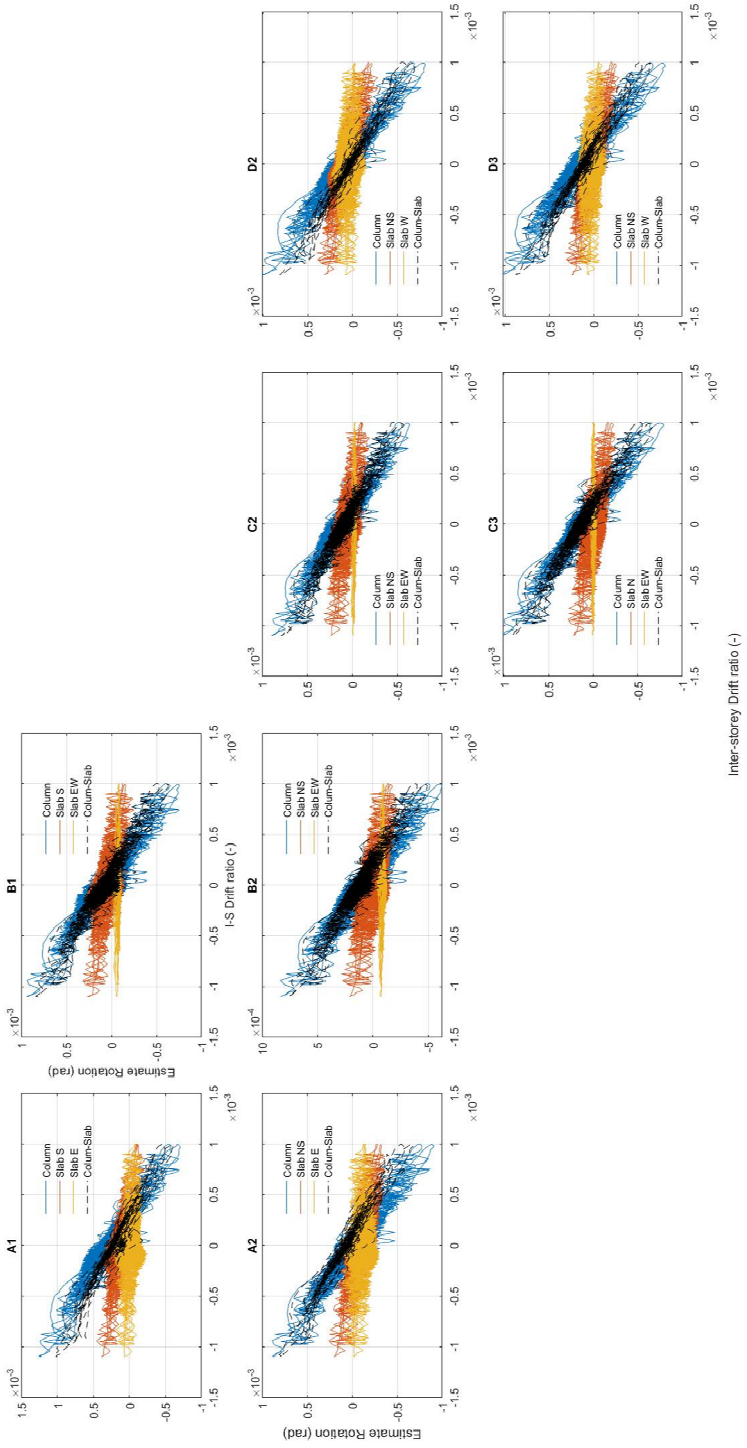

Figure 5.23 Inter-storey drift versus rotation for all the connections, 2nd floor, test Seis-SLS.

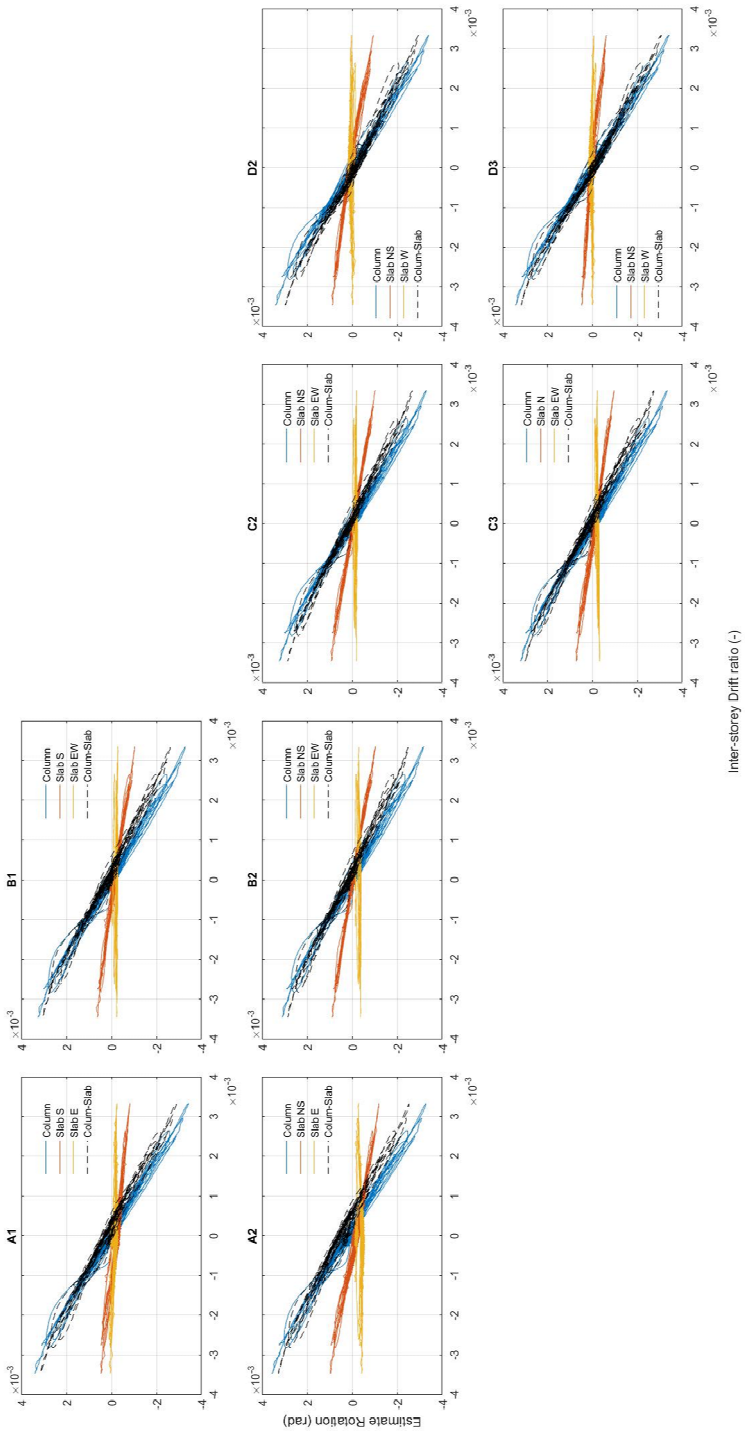

Figure 5.24 Inter-storey drift versus rotation for all the connections, 1st floor, test Seis-ULS.

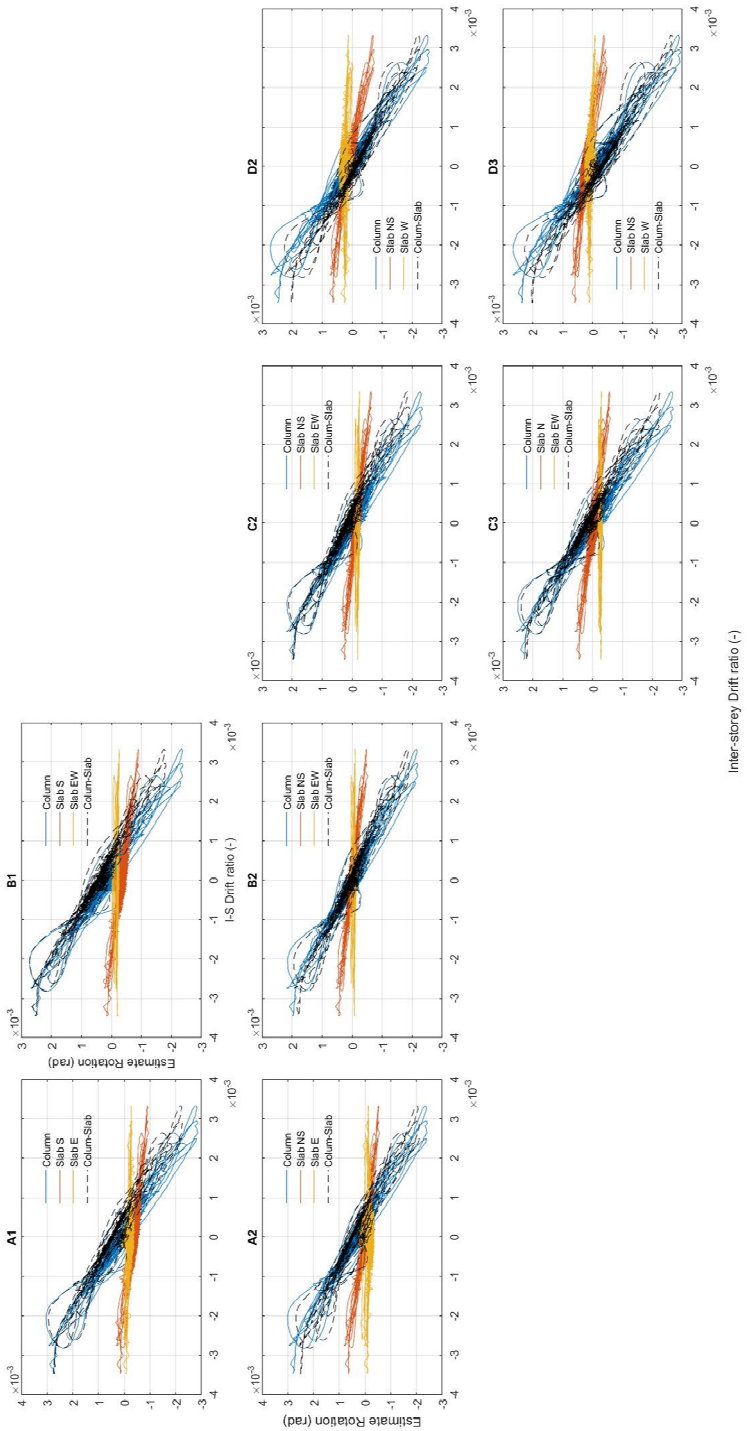

Figure 5.25 Inter-storey drift versus rotation for all the connections, 2nd floor, test Seis-ULS.

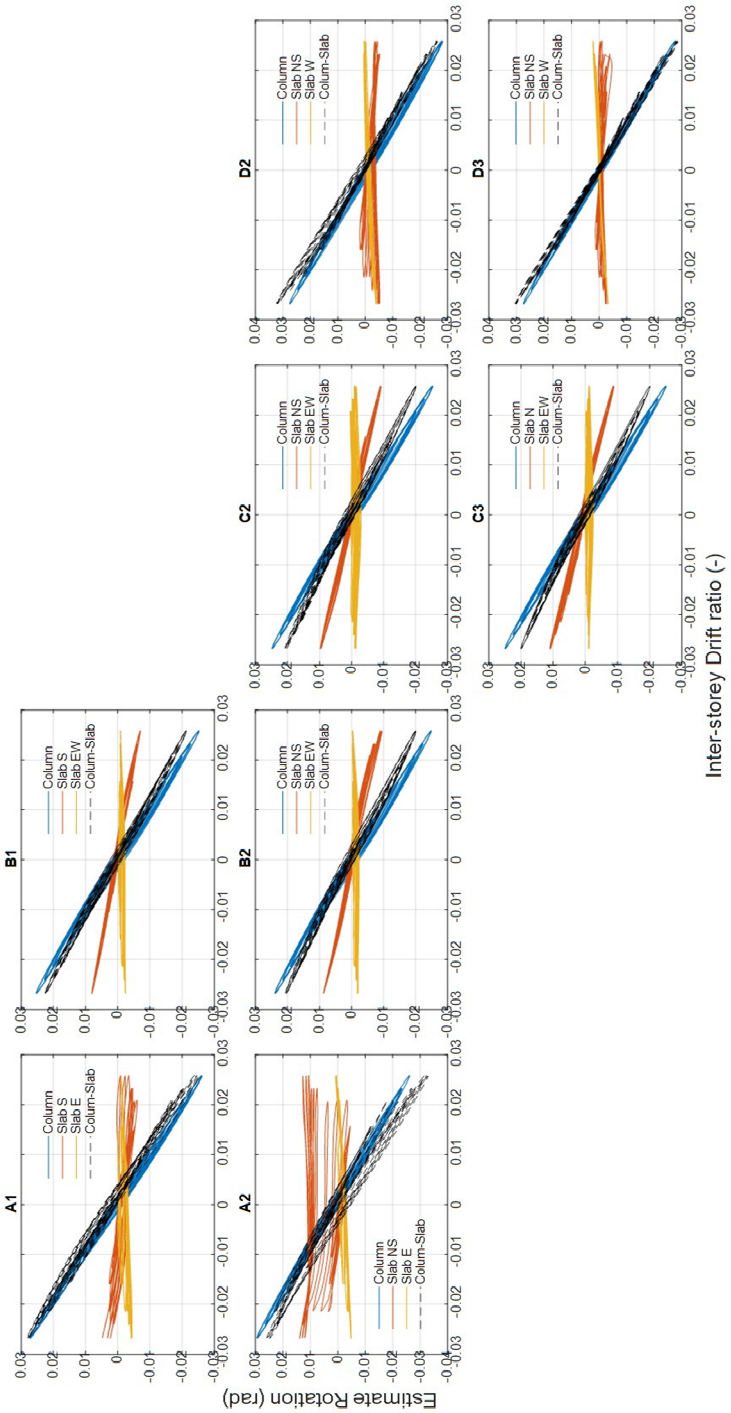

Figure 5.26 Inter-storey drift versus rotation for all the connections, 1st floor, test Cyc-1.

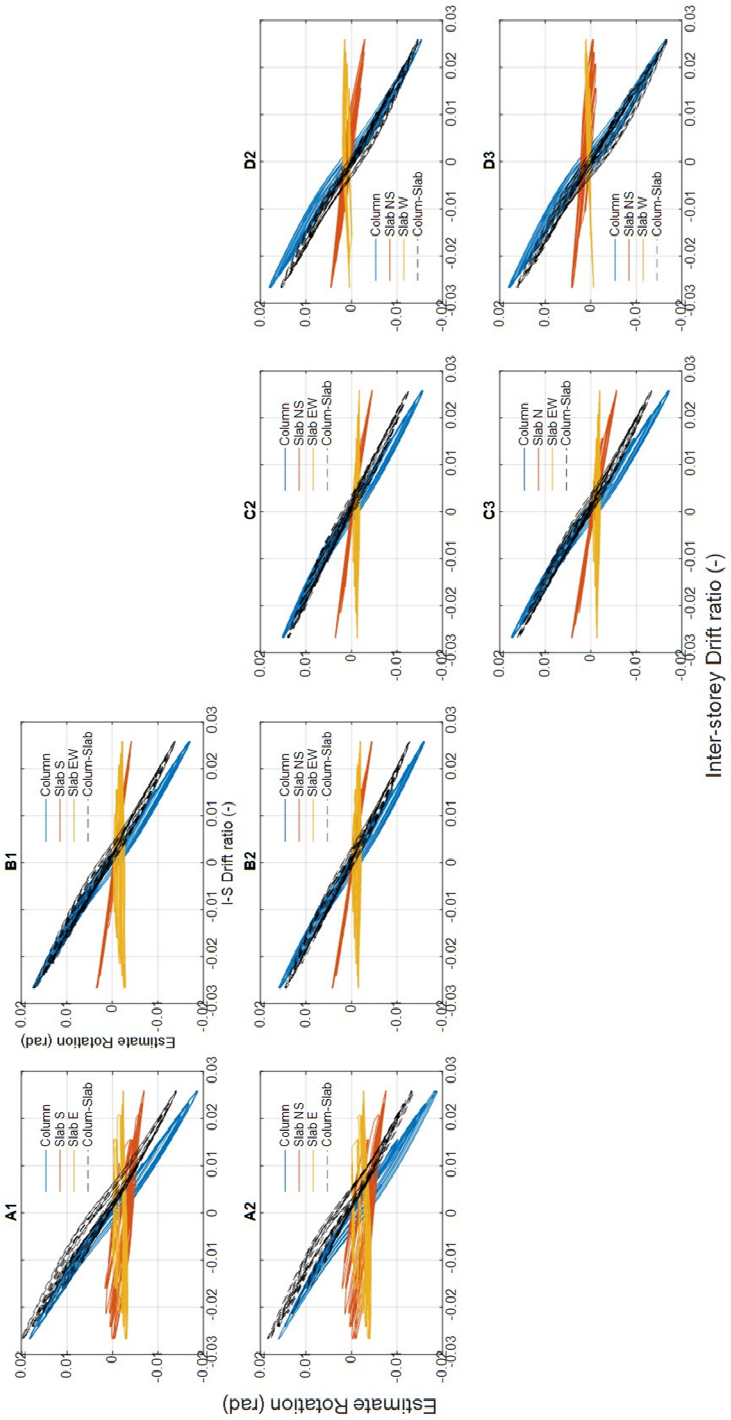

Figure 5.27 Inter-storey drift versus rotation for all the connections, 2nd floor, test Cyc-1.

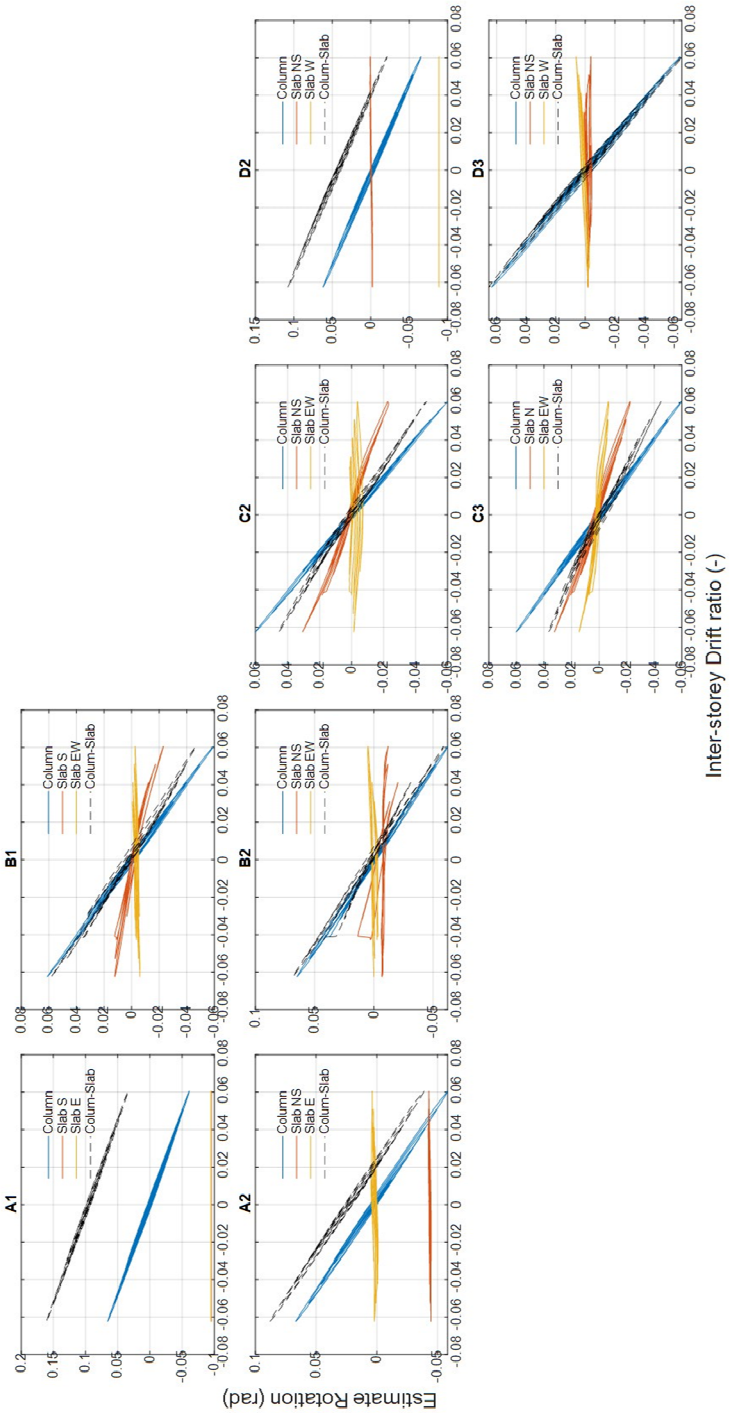

Figure 5.28 Inter-storey drift versus rotation for all the connections, 1st floor, test Cyc-2.

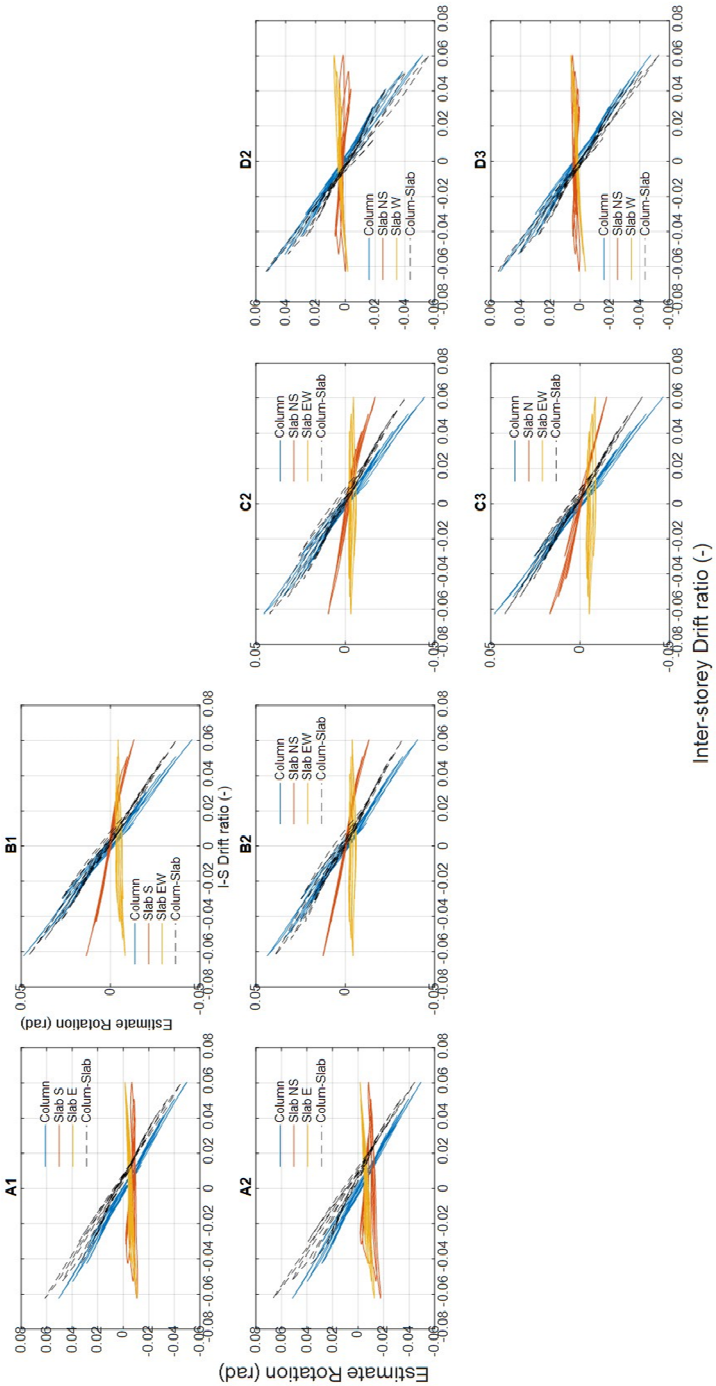

Figure 5.29 Inter-storey drift versus rotation for all the connections, 2nd floor, test Cyc-2.

5.5.4 STATIC AND KINEMATICS PARAMETERS

The local analysis of the static and the kinematics parameters, developed with the column-slab rotation, was carried out only considering the unbalanced moment only in the column where both static and kinematic measures are available.
Some sensors were removed due to the damage accumulated at the end of the first cyclic test (alignments A and D Figure 5.29). Graphs considering the two cyclic tests in sequence, are reported only for the slab-column connections with sensors in the alignments B and C (B1, B2, C2 and C3).
The unbalanced-moment was calculated as explained 5.3.1 using Eq. 5-3 and Eq. 5-4, whereas for the column-slab rotation Eq. 5-13 was used.

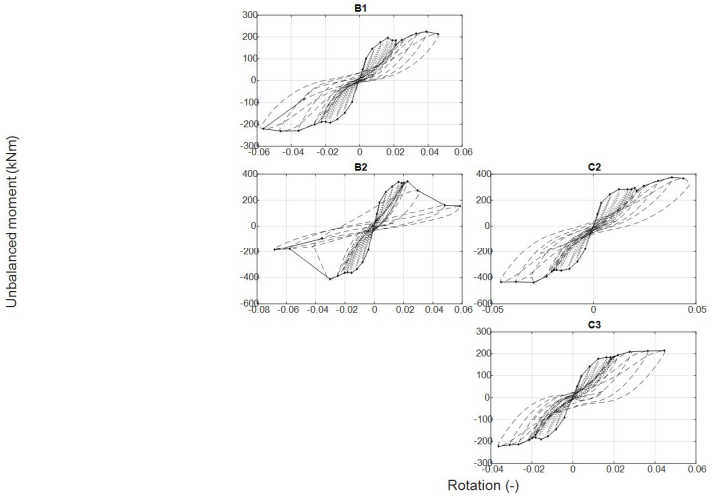

Figure 5.30 Example of the unbalanced moment versus rotation for one floor, test Cyc-1+Cyc-2.

5.5.5 COMPOSITES INDICATORS

STIFFNESS

The procedure followed is similar to the stiffness calculation with the inter-storey drift ratio. The seismic analysis differs from the cyclic one; for the seismic test the initial stiffness of each slab-column connection on each floor was calculated, whereas for the cyclic analysis the stiffness deterioration of each slab-column connections on each floor (Le et al., 2020 [1]) was studied.

Seismic Tests

To calculate the stiffness of each slab-column connection on each floor, the unbalanced moment calculated as described in 5.4.1 using Eq. 5-9 and Eq. 5-10 and the column-slab rotation obtained as Eq. 5-13 of each slab-column connection were used. With these values, a point cloud for each slab-column connection was formed.

The interpolation lines were obtained from the previously obtained point clouds and lastly the slope of these lines in each slab-column connection were calculated as the angular coefficient of these lines, corresponding exactly to the requested stiffness of the analysed connection (Figure 5.31). The procedure was repeated for all the slab-column connections and for both floors.

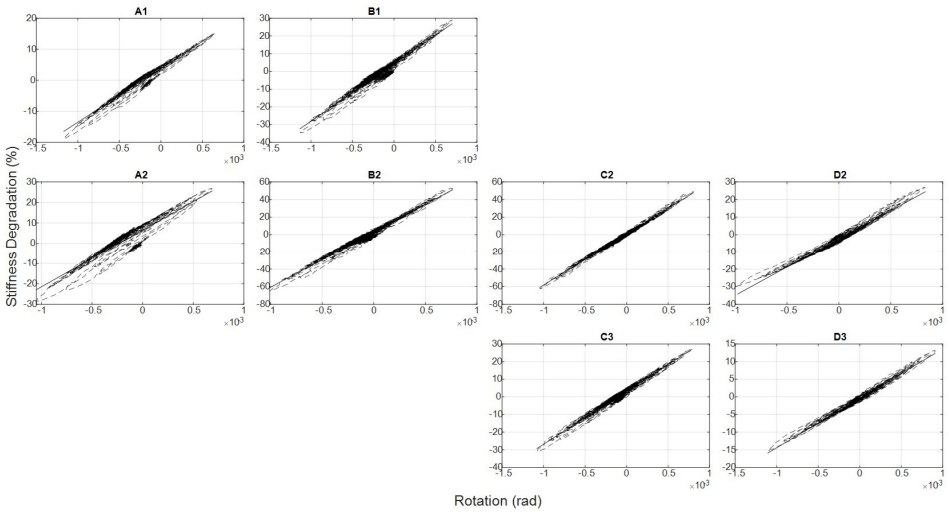

Figure 5.31 Example of the procedure followed to obtain the approximate stiffness with the rotations of each connections in one floor for the seismic tests..

Cyclic Tests

For both the cyclic tests the stiffness deterioration of each slab-column connection on each floor, was studied. To do so, the stiffness of each slab-column connection on each floor, the unbalanced moment calculated as described in 5.4.1 using Eq. 5-9 and Eq. 5-10 and the column-slab rotation obtained as Eq. 5-13 of each slab-column connection were used.

This stiffness deterioration for each slab-column connection on each floor, was determined by the ratio between the secant stiffness of each hysteresis loop of each slab-column connection on each floor and the initial secant stiffness of each slab-column connection on each floor. The initial secant stiffness corresponds to that calculated in the seismic tests (paragraph above).

For each hysteresis loop, the secant stiffness was calculated by the ratio between the maximum unbalanced moment in the loop and the corresponding rotation. The maximum values of unbalanced moment and rotation correspond to those obtained in the statics and kinematics parameters analysis (see chapter 5.3.1). This was calculated for each slab-column connection, separately for the positive and the negative drift values, and for each of the two floors (Figure 5.32).

The stiffness deterioration resulting from the cyclic tests, Cyc-1 and Cyc-2, was calculated in relation to the initial stiffness of the connection, which was calculated

from the results of the first seismic test, Seis-SLS.

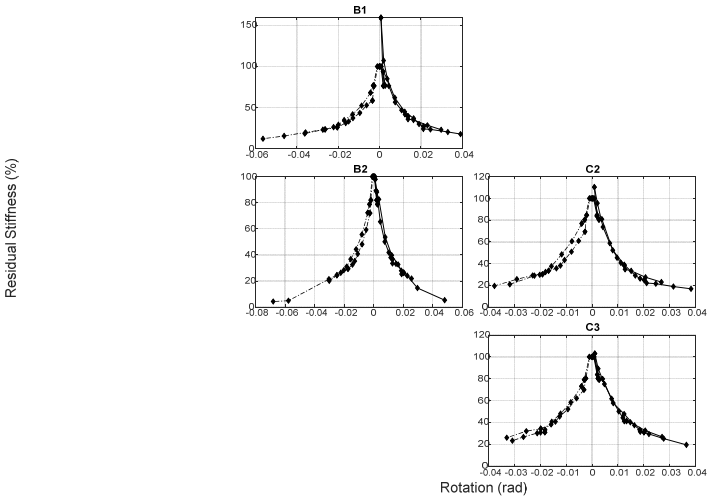

Figure 5.32 Example of the stiffness deterioration with the rotation for one floor of the cyclic test

DUCTILITY

This was calculated using the backbone curve and it was only developed for the cyclic tests.

The procedure followed was the same as that for local ductility calculated with the inter-storey drift (for the detailed description see Chapter 5.3.2) but in this analysis the rotation was used in the place of the inter-storey drift ratio. The local ductility was calculated only for the residual loads of 80%, 85% always for both floors and only for the second cyclic test Cyc-2 considering also the first one, Cyc-1.

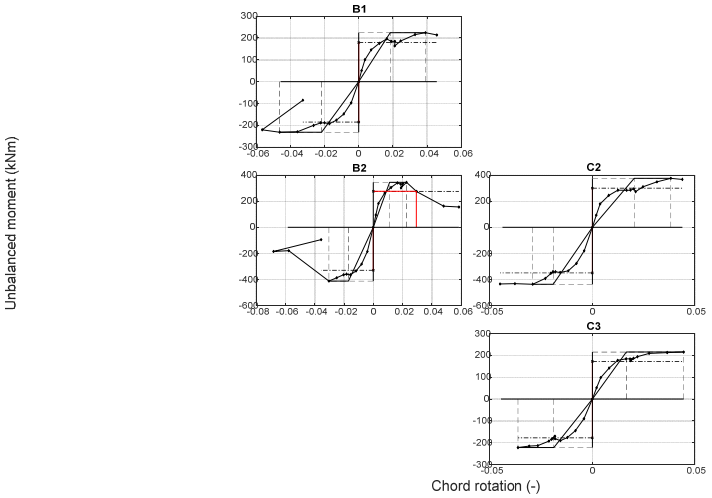

Figure 5.33 Example of the definition of the yielding and failure points with the rotation for the slab-column connections on one floor of the cyclic tests.

The condition by which the failure is verified is the same as that of the local analysis with the inter-storey drift ratio, and the signs used in the graphs and in the tables are also the same (see chapter 5.3.2).

ENERGY

The energy dissipated from each slab-column connection on each floor was calculated as the cumulative integral, using the cumulative trapezoidal numerical integration between the unbalanced moment recorded during the tests (see Chapter 5.3.2) and the rotation of each slab-column connection, calculated as reported in Figure 5.34. This was made for each floor and for both seismic and cyclic tests.

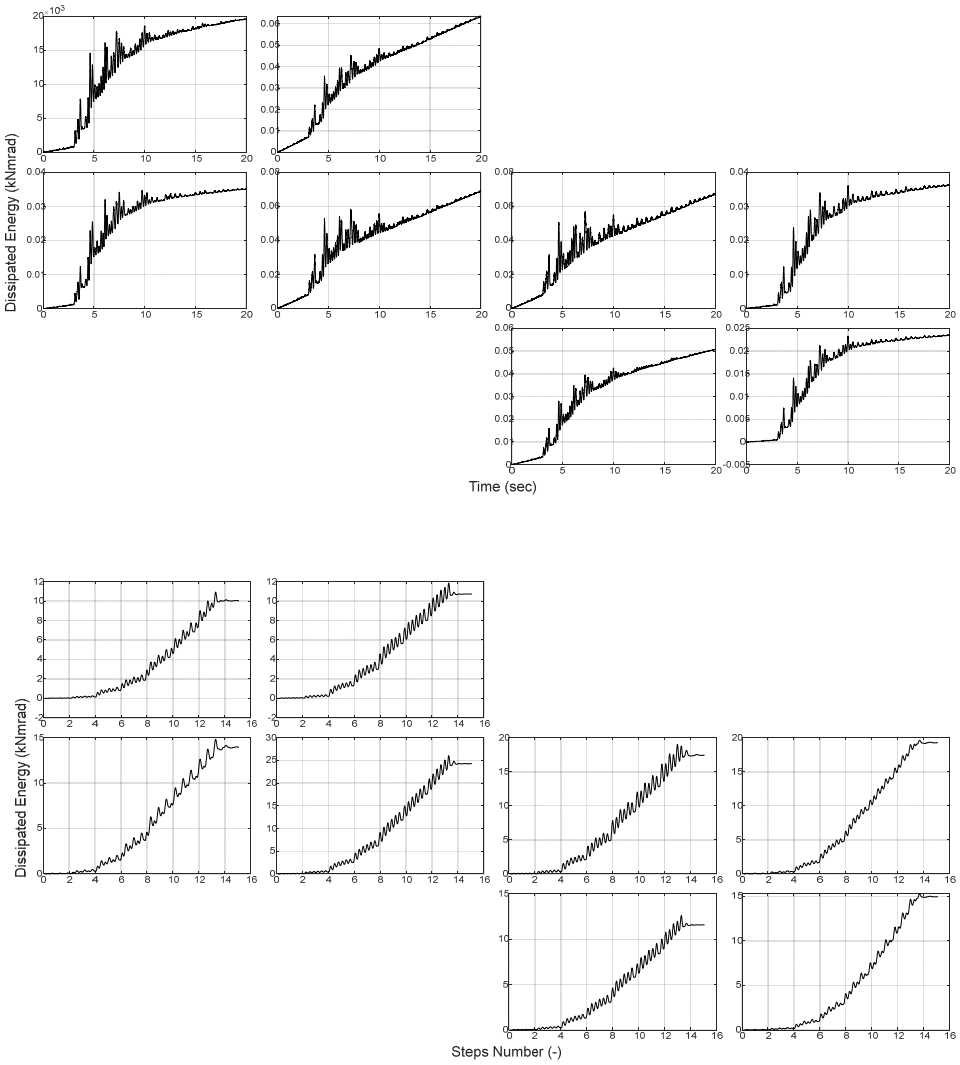

Figure 5.34 Example of the slab-column connections dissipated energy with the rotation for one floor in a) seismic and b) cyclic tests.

The procedure followed was the same for the seismic and the cyclic tests, as in the

previous local analysis with the inter-storey drift ratio, but the representation in the graphs is different. For the two seismic test the dissipated energy was reported in function of the accelerogram time, for the two cyclic test it was reported in function of the steps number, Figure **5.8** a and b respectively.

5.5.6 CORRELATION BETWEEN INTER-STOREY DRIFT AND COLUMN-SLAB IN THE STRUCTURE

The coefficients that enable to use the inter-storey drift instead of the rotation, were obtained from a statistical analysis. The values reported in Table 5.6, Table 5.7 and Table 5.8 are represented in the same location that the connections have in the structure.

The analysis was made separately for the two cyclic tests separately, Table 5.6 for the first cyclic test Cyc-1 and Table 5.7 for the second cyclic test Cyc-2 and then in Table 5.8 the differences between the second cyclic test and the first is reported to highlight the differences between the two tests. For the two cyclic tests separately, (Table 5.6 for test Cyc-1 and Table 5.7 for test Cyc-2) the obtained data confirm that the evaluation is good, in fact the R2 parameter are always high so the linearization is good, while the standard deviation is very low.

On analysing the linear regression line for the tests Cyc-1 (Table 5.6) it is possible to observe that the behaviour of the connections is almost always symmetrical on both floors excepting the B1 connections on the 1st floor.

B1 was one of the first connections to suffer and also the most damaged. It was strengthened and thanks to this, it did not fail. Diversely the connections C2 and C3 showed a better response after strengthening but they were un-damaged at the beginning of the test Cyc-2 so the strengthening was effective.

Table 5.6 Parameters of the statistical analysis, test Cyc-1.

Test Cyc-1												
Floor	Linear regression line				R^2				Std Deviation			
1	0.961	0.835			0.989	0.996			0.011	0.009		
	1.036	0.788	0.787	1.050	0.962	0.993	0.992	0.989	0.012	0.009	0.009	0.012
			0.784	1.066			0.995	0.995			0.009	0.012
2	0.738	0.669			0.969	0.992			0.007	0.007		
	0.683	0.593	0.574	0.666	0.971	0.993	0.994	0.995	0.007	0.006	0.006	0.007
			0.643	0.718			0.992	0.995			0.006	0.007

Table 5.7 Parameters of the statistical analysis, test Cyc-2.

Test Cyc-2												
Floor	Linear regression line				R^2				Std Deviation			
1	1.030	0.849			0.996	0.989			0.023	0.019		
	1.044	0.966	0.765	1.057	0.995	0.982	0.993	0.995	0.024	0.022	0.017	0.024
			0.684	1.072			0.984	0.996			0.016	0.024
2	0.894	0.742			0.987	0.996			0.018	0.015		
	0.920	0.641	0.664	0.869	0.971	0.989	0.986	0.973	0.019	0.013	0.014	0.018
			0.683	0.899			0.997	0.989			0.014	0.018

Table 5.8 Parameters of the statistical analysis, test Cyc-2. - Cyc-1.

Test Cyc-2 - Cyc-1												
Floor	Linear regression line				R^2				Std Deviation			
1	0.069	0.013			0.007	-0.007			0.013	0.010		
	0.008	0.178	-0.022	0.008	0.034	-0.011	0.001	0.006	0.012	0.013	0.009	0.012
			-0.100	0.006			-0.010	0.000			0.007	0.012
2	0.156	0.073			0.018	0.003			0.011	0.008		
	0.237	0.048	0.090	0.203	-0.001	-0.004	-0.008	-0.023	0.012	0.007	0.008	0.011
			0.040	0.181			0.005	-0.006			0.007	0.011

From the difference between the two cyclic tests, reported in Table 5.8, some values are negative, in more detail the linear regression line for the connections C2 and C3 on the 1st floor and the R^2 coefficient for the connections B1, B2, C3 on the 1st floor and A2, B2, C2, D2 and D3 on the 2nd floor. These results are due to the difference between the rotation and the drift. If the slab-column connection failed, the drift value was very similar to the rotation, if it did not fail this meant that it was more rigid. As revealed in Table 5.8 (R^2 very low), it is not possible to obtain the linearization by considering both the cyclic tests, due to the changes which occurred between the two tests.

5.6 Summary

In this chapter the methodology applied to the SlabSTRESS results for the study of the global and the local behaviour of the structure was presented.
The reported methodology is based on procedures present in literature that were studied and adapted to this work.
The analysis is based on two simple models for the mock-up in general and in more detail on each slab-column connection. Using static and kinematic parameters, a comparison between the two level of study was made, successively a deeper analysis was conducted with some “composites indicators”.
Two different parameters were used to perform the analysis, the inter-storey drift ratio, to represent the global behaviour of the structure, and the column and slab rotations at the local level.

A detailed description of the analysis is reported, that has permitted to consider the rotation as a valid parameter (see Chapter 5.5) and finally, the conversion factors that allowed to convert the inter-storey drift ratio to the column-slab rotation in function of the slab-column connection typology, is also reported.
With the results obtained, a comparison with the experimental results obtained in the past, mainly on single slab-column connections will be possible, together with a simplification of that numerical analysis in which the inter-storey drift is known but where corresponding rotation is unknown.

References

[1] Fick, D. R., Sozen, M. A., Kreger, M. E. (2017) “Response of Full-Scale Three-Story Flat-Plate Test Structure to Cycles of Increasing Lateral Load” ACI Structural Journal, V. 114, No. 6, pp. 1507-1518.

[2] Moehle J. P., Diebold J. W. (1984) “Experimental Study of the Seismic Response of a Two-Story of a Flat-Plate Structure”. University of California, Berkeley.

[3] Kang, T. H.-K., Wallace, J. W. “Shake Table Tests of Reinforced Concrete Flat Plate Frames and Post-Tensioned Flat Plate Frames” (2004). 13th World Conference on Earthquake Engineering, Vancouver, B.C., Canada. Paper No.1119.

[4] Le, D.D., Nguyen, X.-H., Nguyen, Q.-H. (2020) “Cyclic Testing of a Composite Joint between a Reinforced Concrete Column and a Steel Beam”. Applied sciences.

[5] Park, R. (1988) “Ductility evaluation from laboratory and analytical testing”. Proceedings of Ninth World Conference on Earthquake Engineering, August 2-9, Tokyo-Kyoto, Japan (Vol. VIII).

[6] Li, B., Lam, S-s., Wu, b., Wang, Y-y. (2013) “Experimental investigation on reinforced concrete interior beam-column joints rehabilitation by ferro cement jackets”. Engineering Structures 56, 897-909.

[7] CEN. EN 1998-1. Eurocode 8: Design of structures for earthquake resistance - Part 1: General rules, seismic actions and rules for buildings. 2004

6 Seismic tests

6.1 Introduction

The two seismic tests SEIS-SLS and SEIS-ULS were carried out with the PsD technique. The aim of the tests is the verification of the design of the structure with primary and a secondary flat slab frame.
Test SEIS-SLS adopted a ground motion compatible with the NTC2018 [1] response spectrum at the Damage Limit State (DLS), while test SEIS-ULS a ground motion compatible with the Life Safety Ultimate Limit State, which is the limit state equivalent to the Ultimate Limit State (ULS) in Eurocode 8 [2].
This section reports the description of the results of both two seismic tests, the Seis-SLS firstly and then the Seis-ULS. Both the tests were analysed following the same procedure, the global behaviour is reported here, followed by the local one.
The global analyses for the two tests Seis-SLS and Seis-ULS were made in terms of base shear versus global drift ratio, whereas the local study was developed using the unbalanced moment versus the inter-storey drift ratio and the slab crack opening versus the inter-storey drift ratio.
For a detailed description of the followed methodology see Chapter 5.

6.2 The Damage Limit State (Test Seis-SLS, e03)

Using the pseudo-dynamic technique, the flat slab of SlabSTRESS together with the two numerical walls, were subjected to a ground motion compatible with the NTC2018 [1] response spectrum at the Damage Limit State (SLS, a_{max}=0.884 m/s^2).
The global response, followed by the local one is reported here.

6.2.1 GLOBAL BEHAVIOUR

The followed procedure is reported in Section 5.2.1.
The global response of the structure is reported in Figure 6.1; the two lines represent the two parts of the response, the flat slab (blue line) and the virtual walls (red line), that include both an elastic and inelastic contribution. The response is almost linear for both elements.

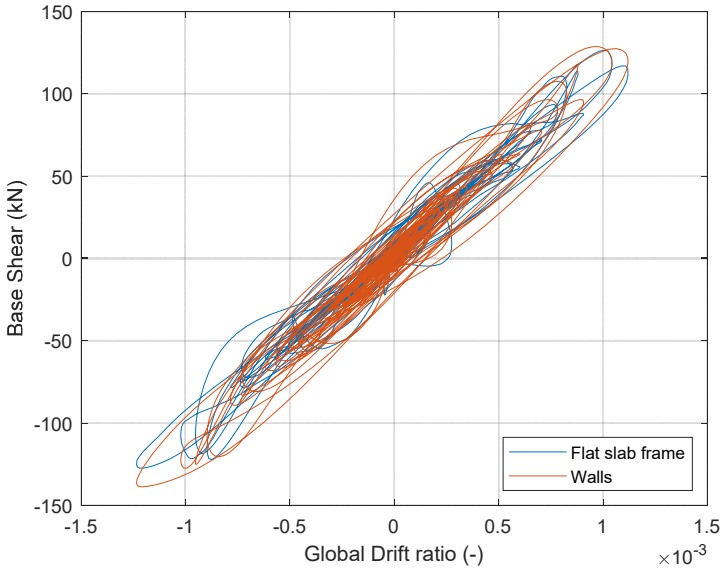

Figure 6.1 Base shear force vs global drift ratio, Seis-SLS.

The base shear reached a maximum value of 126.42 kN for the flat slab frame and 128.6 kN for the wall component with a maximum top displacement of 7.1 mm, corresponding to a maximum global relative drift of 0.11%.
The maximum recorded inter-storey drift was 0.1% for the 1st floor and 0.12% for the 2nd one.

Figure 6.2 a and b report the forces and the lateral storey displacements for the analysed seismic test. Due to the combination with the numerical shear walls, the 1st floor force is lower.

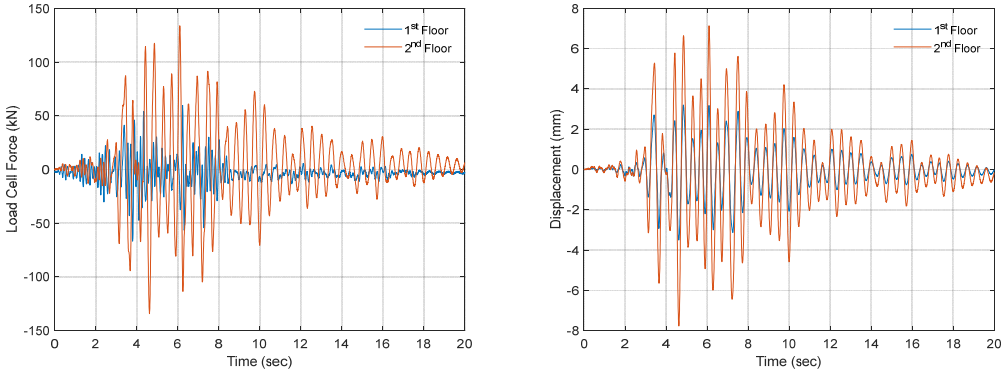

Figure 6.2 Load cells force and Lateral displacement used for the Seis-SLS.

STIFFNESS

The followed procedure, is reported in Chapter 5.2.2.
In Figure 6.3 the dashed line reports the measured values of the base shear force

versus the top displacement relation, the unbroken line the interpolation line.
The undamaged stiffness obtained is 17.3 kN/mm. This value will be used in the following analysis as reference value for undamaged behavior.
Since the test was pseudo-dynamic, the followed procedure permitted to calculate an approximate stiffness.

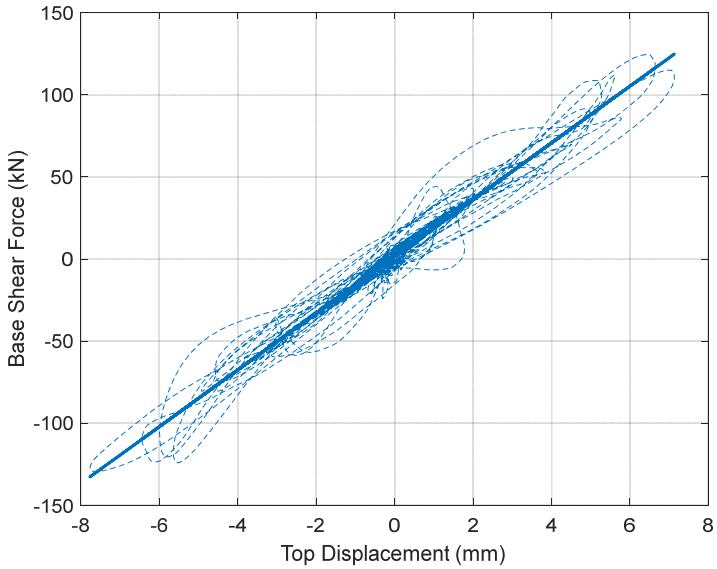

Figure 6.3 Stiffness of the structure, Test Seis-SLS.

A similar procedure (described in chapter 5.2.2) was followed to obtain the stiffness of each of the two floors (Figure 6.4).

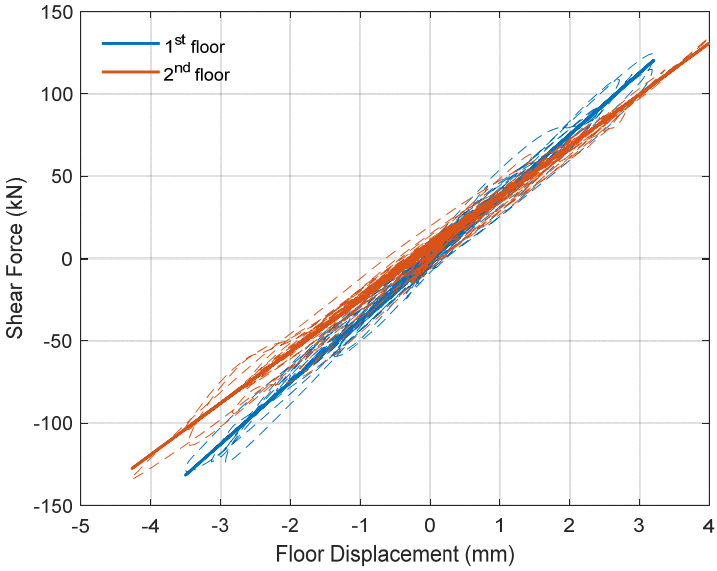

Figure 6.4 Stiffness of each floor, blue for the 1st, red for the 2nd, Test Seis-SLS.

The initial stiffness obtained for the two floors is 37.6 kN/mm for the 1st floor and 31.3 kN/mm for the 2nd.

ENERGY

The evolution of the total energy dissipated by the structure and the energy dissipated at the two-storey levels is shown in Figure 6.5 and Figure 6.6 respectively. The energy dissipated by the structure is obtained from the summation of the products of each displacement input by its associated response force (see Section 5.2.4 for a more detailed description).

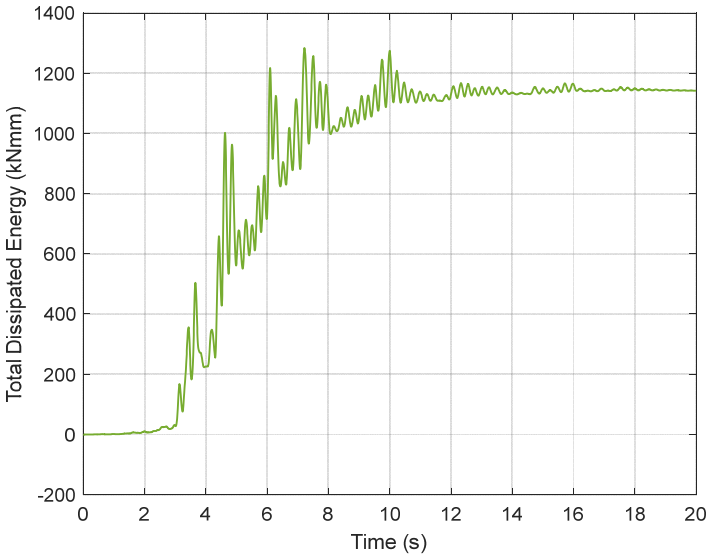

Figure 6.5 Structure energy dissipation. Test Seis-SLS (e03).

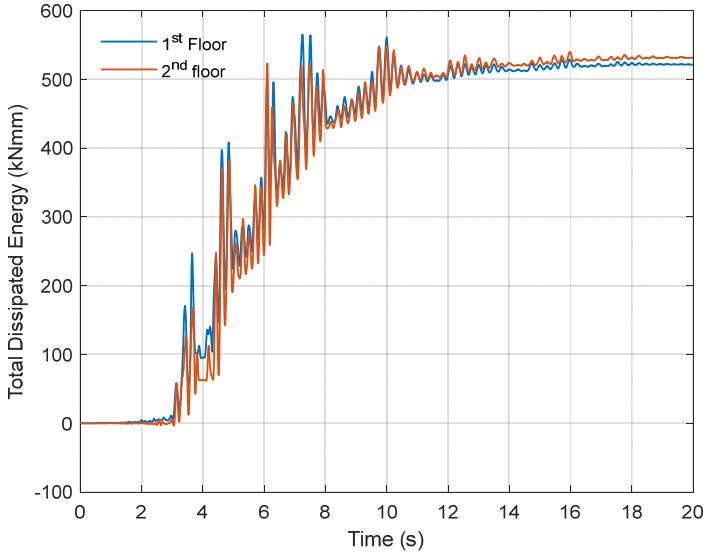

Figure 6.6 Floor energy dissipation, blue line 1st floor, red line 2nd floor. Test Seis-SLS (e03).

The two floors dissipated to nearly the same value. From 0 they reached gradually the maximum value of around 500 kNmm and then remained stable until the end of the test (Figure 6.6). The intensity of the accelerogram decreased after 10 seconds, consequently the dissipated energy rose slightly. On both floors it is possible to observe a mean parabolic trend with some peak that represents the kinematic component of the energy. These are also visible in the accelerogram in correspondence to the maximum displacements.
In Table 6.1 the maximum shear force and the maximum displacement of each floor are reported.

Table 6.1 Shear force and relative displacement for the seismic tests.

	1st floor	2nd floor
Shear force (kN)	59.67	133.79
Displacement (mm)	3.20	3.99
Global energy dissipated (kNmm-kJ)	521.4	531.6

6.2.2 LOCAL BEHAVIOUR

This paragraph presents the results obtained from the local behaviour analysis of each of the twenty-four slab-to-column connections (twelve per storey); the procedure followed to study the local behaviour, together with the equations used, are given in Section 5.3.1.

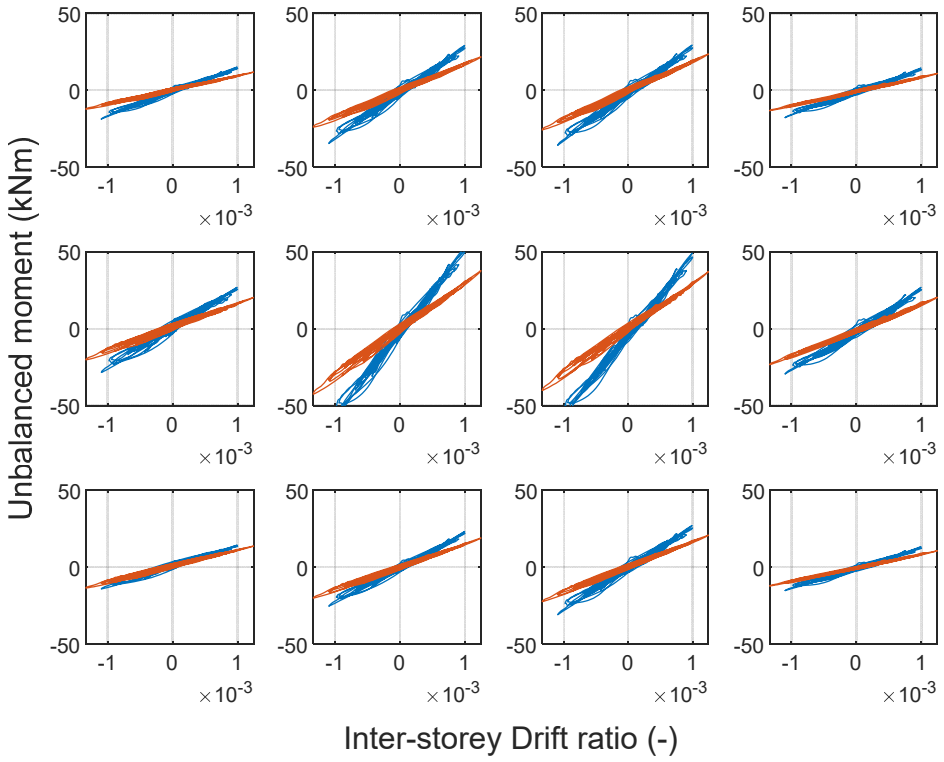

Figure 6.7 Unbalanced moment vs inter-storey drift test Seis-SLS. 1st floor blue line, 2nd floor red line.

Figure 6.7 reports the unbalanced moment versus the inter-storey drift ratio graphs for each slab-column connection.
Each graph is located in the position corresponding to that of the slab-column connection has in the structure (see chapter 3 for the detailed drawing).
The two floors are both reported in the same graph, the 1st floor with a blue line, the 2nd floor with a red line.
As expected, the two central connections B2 and C2 in Figure 6.7 reached the highest unbalanced moment values, whereas the corner A1, A3, D1 and D3 the lowest. Consequently, the main contribution to the stiffness of the building, in terms of drift, is provided by central columns. It is worth nothing that with elastic behaviour the lateral columns (A2-D2, B1-B3 and C1-C3) all provide equal response to the same displacement.
In all the connections, the 1st floor reached unbalanced moment values slightly higher than those of the 2nd even though the forces applied to the 1st were lower than the force applied to the 2nd (Figure 6.2 a).

STIFFNESS

The stiffness of each slab-column connection on each floor was calculated following the same procedure used for the global behaviour, and reported in detail in Section 5.3.2.
In Figure 6.8, the blue lines were used for the 1st floor, the red ones for the 2nd, the dashed lines indicate the measured values of the floor shear and the maximum displacement reached during the test, the continuous lines indicate the interpolation lines.
After the graphs of each slab-column connections, a table with the obtained values of local stiffness was reported (Table 6.2).

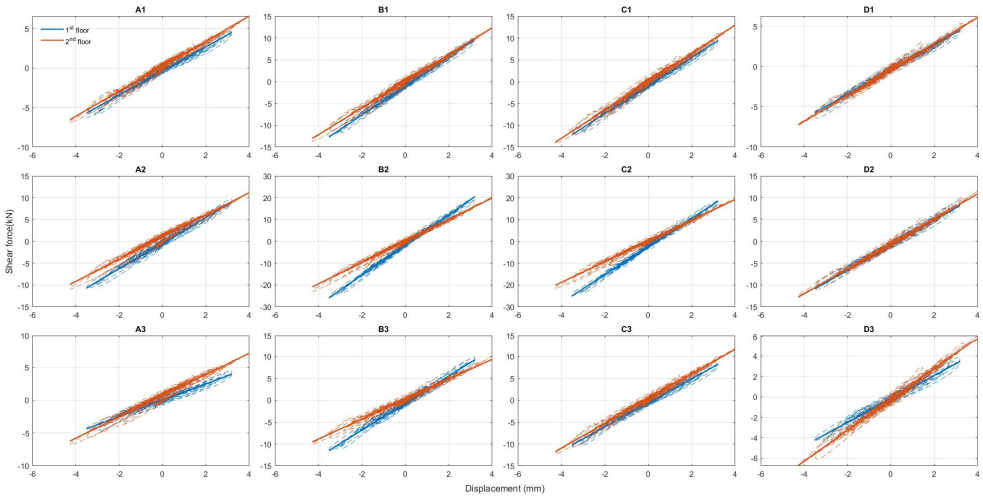

Figure 6.8 Shear force vs displacement, test Seis-SLS. 1st floor blue line, 2nd floor red line.

Table 6.2 Stiffness of connections (kN/mm), Test Seis-SLS.

1st Floor	A	B	C	D	2nd Floor	A	B	C	D
1	1.52	3.33	3.21	1.53	1	1.58	3.06	3.25	1.60
2	2.94	6.91	6.46	2.86	2	2.54	4.92	4.75	2.86
3	1.24	3.10	2.75	1.15	3	1.62	2.28	2.82	1.51

The two internal connections B2 and C2 on both floors reached the higher value of stiffness, whereas the corners A1, A3, D1 and D3 the lower.
The shear forces in the connections on the two floors are very close, due to the combination frame-wall.
The higher stiffness of the first floor connections is related to their configuration with two column stubs connected to the slab.

DISSIPATED ENERGY

To calculate the local energy dissipation, the same procedure adopted to analyse the global energy dissipation (Chapter 6.1.1) was followed but applied to each slab-column connections of each floor.
As reported in chapter 5, the energy dissipated was calculated by using the displacement firstly and then the rotation as component of the deformation, whereas shear is the force component.
For a more detailed explanation of the methodology, see chapter 5.3.4 for the analyses of the displacement and chapter 5.4.7 for analyses of the rotation.
In Table 6.3 and Table 6.4 the maximum values of the dissipated energy of each connection on each floor were reported, calculated with the displacement and the rotation respectively, were reported.

Table 6.3 Dissipated energy of each connections on each floor, test Seis-SLS. Energy calculated with the displacement (kNmm=kJ).

1st Floor	A	B	C	D	2nd Floor	A	B	C	D
1	29.24	53.47	55.7	26.24	1	28.64	62.09	65.18	34.51
2	54.3	87.93	86.08	54.77	2	49.62	77.03	68.78	57.96
3	27.15	58.26	50.98	25.08	3	37.28	47.71	60.25	33.35

Table 6.4 Dissipated energy of each connections on each floor, test Seis-SLS. Energy calculated with the rotation (kNm x rad).

1st Floor	A	B	C	D	2nd Floor	A	B	C	D
1	0.0196	0.0635			1	0.0126	0.0659		
2	0.0352	0.0690	0.0675	0.0364	2	0.0176	0.0707	0.0688	0.0172
3			0.0508	0.0235	3			0.0436	0.0188

Figure 6.9 and Figure 6.10 report the graphs of the dissipated energy of each connections on each floor calculated with the displacement and with the rotation respectively.

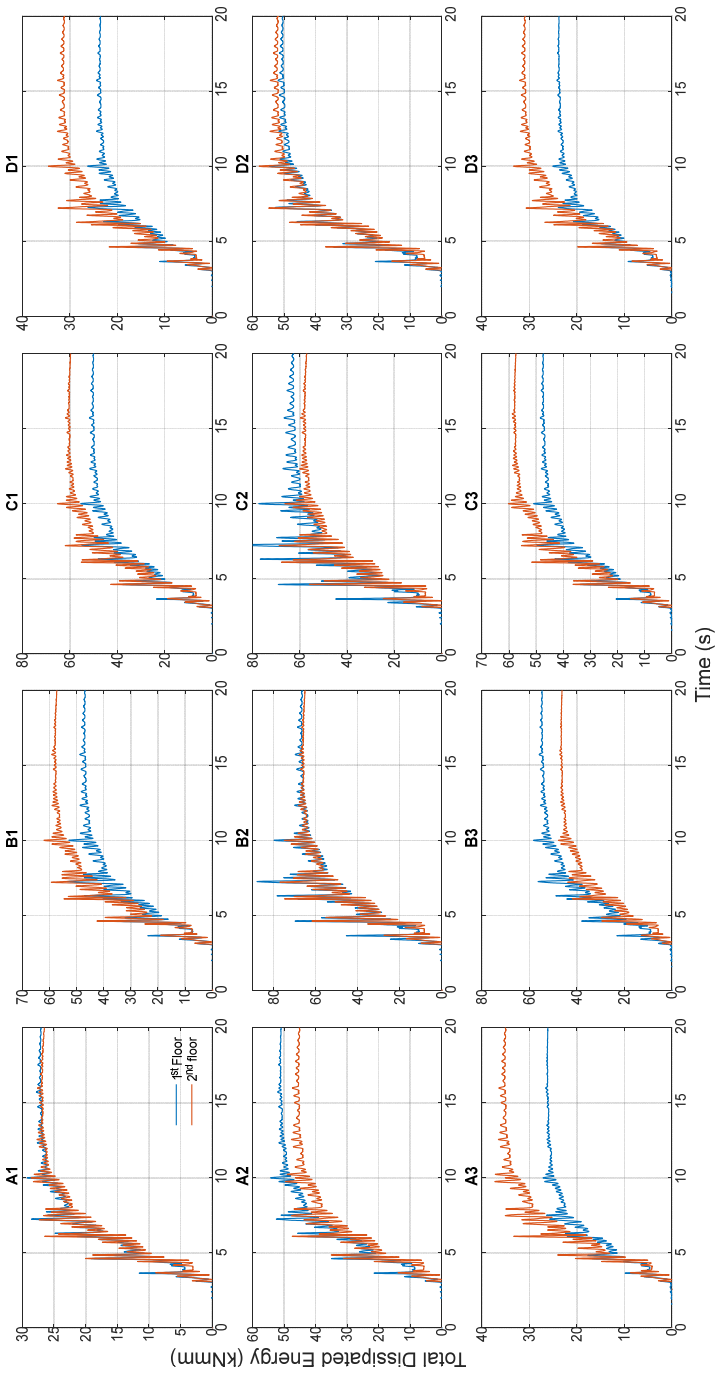

Figure 6.9 Dissipated energy for each connections, test Seis-SLS. 1st floor blue line, 2nd floor red line. Energy calculated with the displacement.

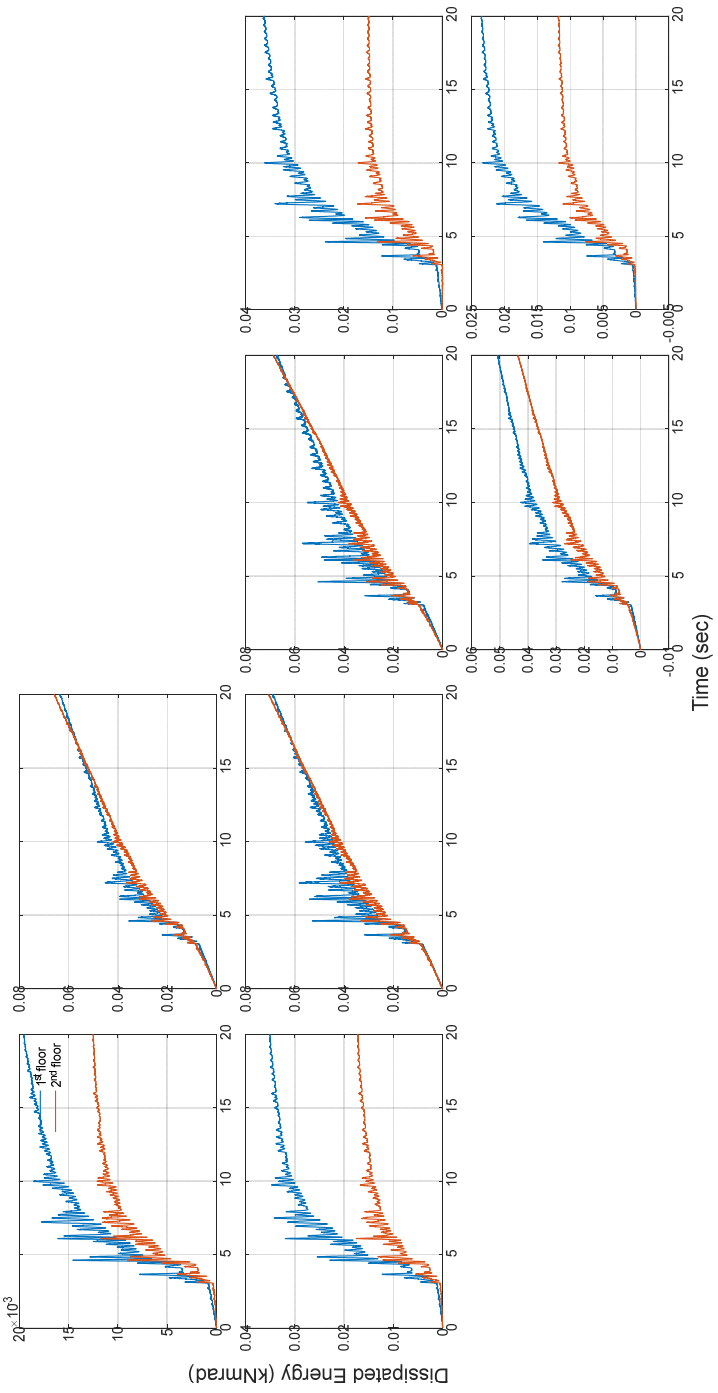

Figure 6.10 Dissipated energy for each connection, test Seis-SLS. 1st floor blue line, 2nd floor red line. Energy calculated with the rotation.

In both the representations the 1st floor (blue line) is more dissipative than the 2nd one (red line), whereas in the two internal connections the dissipation on the two floors is very close.
Using the rotation to calculate the energy, the four connections in the B and C alignments (B1, B2, C2, C3) change the shape of the graphs, as compared to those in Figure 6.9 in which the energy was calculated with the displacement. It seems that these connections continue to dissipate energy from the beginning of the test to the end. The rotation measurements had a higher noise level compared to that of the measured small rotation. Therefore, for such slight rotations, the energy calculated thereby is not considered to be meaningful.
The difference between the two calculated energies is not so significant, because the rotation measured during the first tests was so much reduced as to be overlooked, due to the level of noise.
For the lateral connections (A1, A2. D2, D3) after the time of 10 seconds, the rotation was constant with the energy, when the rotation lessened, the energy rose and vice-versa,
As in the global analysis so for the local one, the kinematic component of the energy is visible in all the connections, reported in both graphs.

CRACK OPENING DISPLACEMENT

The crack opening displacement analysis was not made on all the slab-column connections but only for the one with the displacement transducers mounted on the slab surface. Each graph is positioned to correspond to the slab-column connection in the structure. Four different colours were used to identify the four different sides of the sensors, yellow for the east, red for the south, green for the west and blue for the east.
During the Seis-SLS, there was no significant crack opening in the slabs, the maximum recorded values on the west and east sensors were close to $0.5*10^{-3}$ mm for both floors but only in some of the sensors (Figure 6.11 and Figure 6.12).

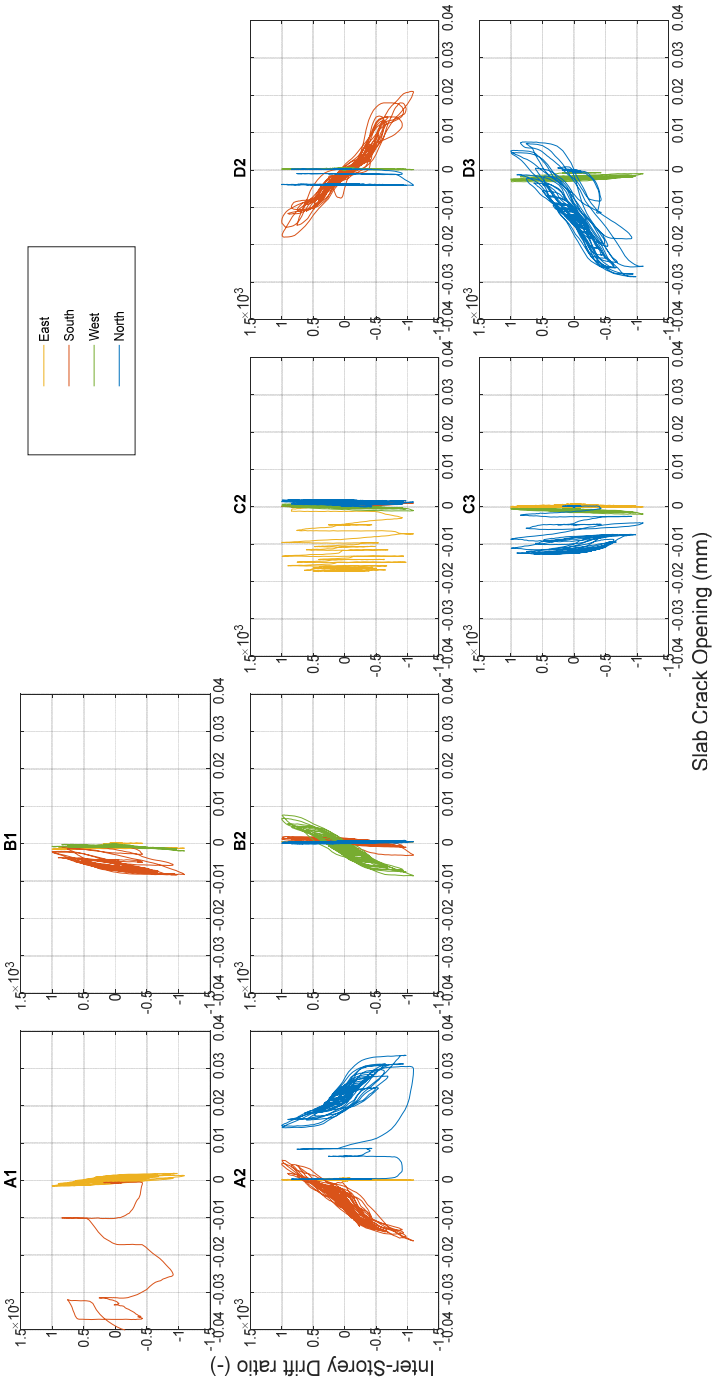

Figure 6.11 Slab Crack Opening vs Inter-story drift ratio for connections with sensors, 1st floor, Seis-SLS.

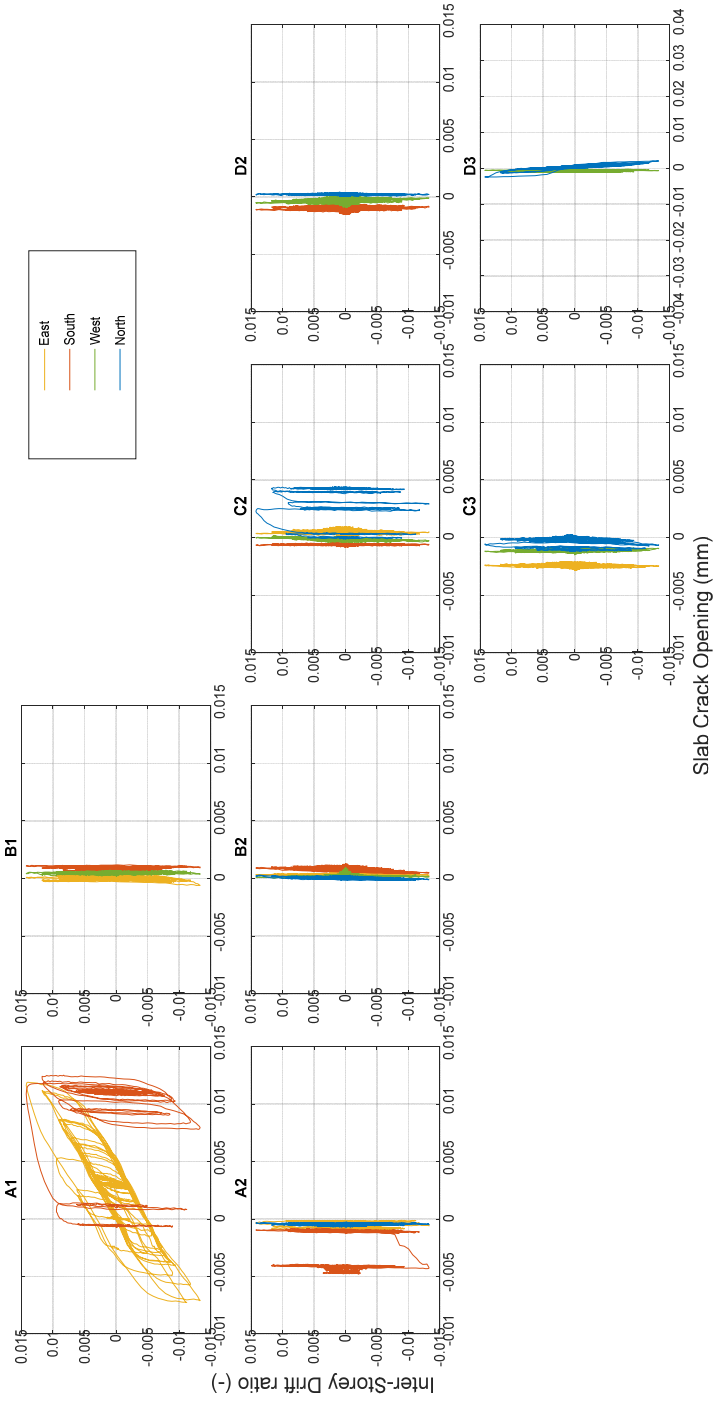

Figure 6.12 Slab Crack Opening vs Inter-story drift ratio for connections with sensors, 2nd floor, Seis-SLS.

The crack openings are very small, thus confirming the nearly elastic response recorded at the global level. The wider cracks were measured in the connections on the A and D lines, showing different trends from B and C lines interior and edge connections. On the 1st floor (Figure 6.11), only the sensor on the west in the B2 connection (green line) recorded regular symmetric cycles of increasing amplitude with similar maximum positive and minimum negative values of about 0.8×10^{-3} mm in absolute value. The same behaviour was recorded on the 2nd floor, the east one in the A1 connection with maximum amplitude in positive and negative of about 12×10^{-3} mm in absolute value.

6.3 The Ultimate Limit State (Test Seis-ULS, e06)

Testing continued with the pseudo-dynamic technique, the flat slab of SlabSTRESS together with the two numerical walls, were subjected to a ground motion compatible with the Life Safety Ultimate Limit State, which is the limit state equivalent to the Ultimate Limit State (ULS, a_{max}=2.498 m/s^2) in Eurocode 8 [2].
As for the previous seismic test, the global response, then the local one are analysed here.

6.3.1 GLOBAL BEHAVIOUR

The followed procedure is reported in Chapter 5.2.1.
The global response of the structure is reported in Figure 6.13; as for the previous seismic test, the two lines represent the two parts of the analysis, the flat slab (blue line) and the virtual walls (red line), that include both elastic and inelastic contribution.

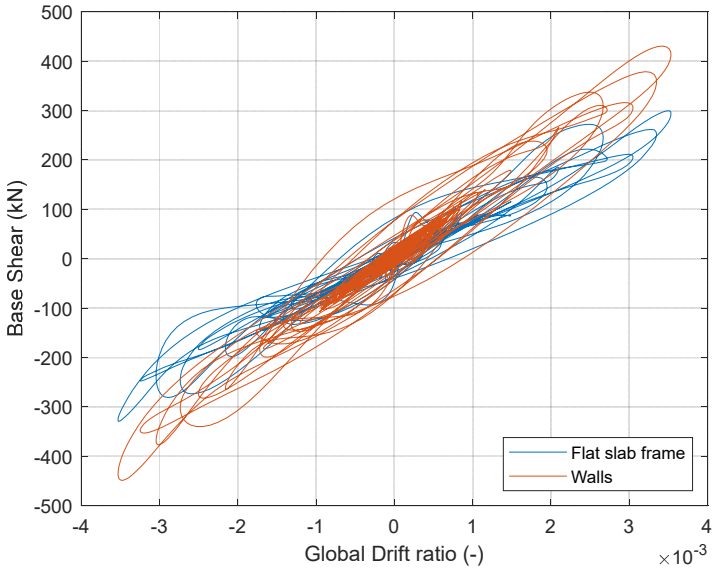

Figure 6.13 Base shear force vs drift, Seis-ULS.

Even if the effects of the seismic action were higher than in the previous seismic test Seis-SLS, the structure was not subject to much damage, both elements having an almost linear response.
The base shear reached maximum values higher than those in Seis-SLS, 299.45 kN for the flat slab frame and 430.46 kN for the wall component, with a maximum top displacement of 22.3 mm.
The recorded values of inter-story drift ratio from the test where 0.34% for the 1st floor and 0.36% for the 2nd. The almost equal inter-story drift ratio at the two levels reflect the frame-wall interaction.
Figure 6.14 a and b report the forces and the storey lateral displacement for the second seismic test Seis-ULS.

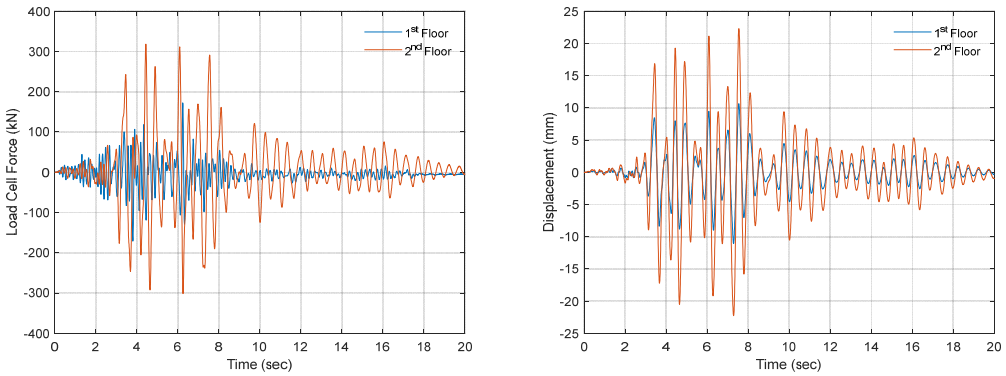

Figure 6.14 Load cells force and Lateral displacement used for the Seis-ULS.

STIFFNESS

The followed procedure is reported in Chapter 5.2.2.
In Figure 6.15 the dashed line reports the measured values of the base shear force versus the top displacement relation and the unbroken tract the interpolation line. The obtained stiffness is 12.5 kN/mm. Since this was a pseudo-dynamic test, the followed procedure permitted to calculate an approximate stiffness.
Compared to the previous seismic test, the stiffness of the test Seis-ULS, was 28% lower than the test Seis-SLS.

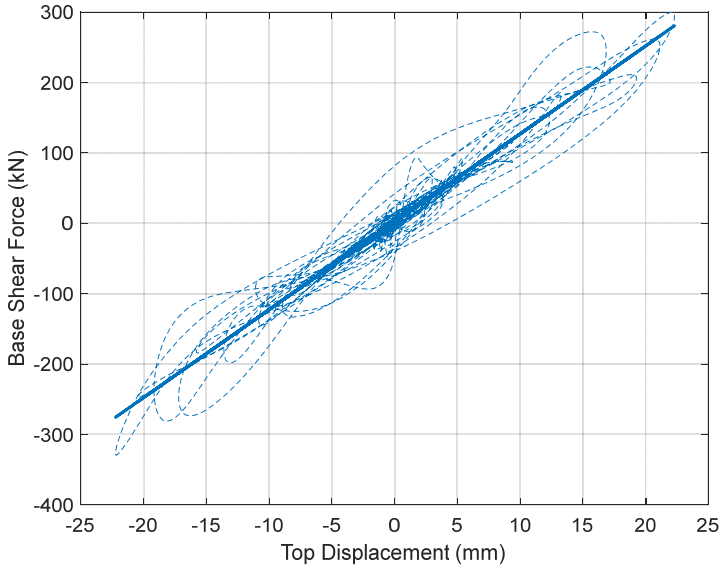

Figure 6.15 Stiffness of the structure, Test Seis-ULS.

A similar procedure (described in chapter 5.2.2) was followed to obtain the stiffness of each of the two floors (Figure 6.16). The obtained stiffness for the two floors is 27.7 kN/mm for the 1st floor and 23.75 kN/mm for the 2nd. Compared to the previous seismic test, the stiffness of the test Seis-ULS for the 1st floor was 26% lower than the test Seis-SLS, for the 2nd floor the stiffness of the test Seis-ULS was 24% lower than the test Seis-SLS.

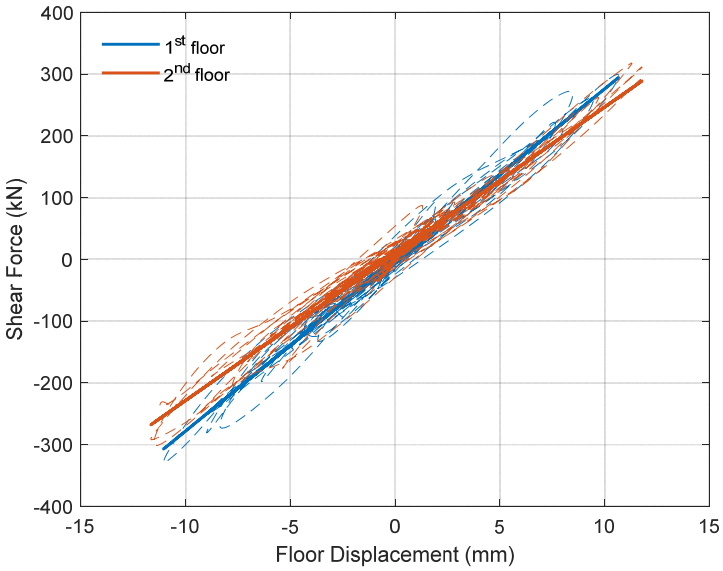

Figure 6.16 Stiffness of each floor, blue for the 1st, red for the 2nd, Test Seis-ULS.

ENERGY

The evolution of the total energy dissipated by the structure and the energy dissipated at the two-storey levels is shown in Figure 6.17 and Figure 6.18 respectively.

The energy dissipated by the structure is obtained as from the summation of the products of each displacement input by its associated response force, see Section 5.2.4 for a more detailed description.

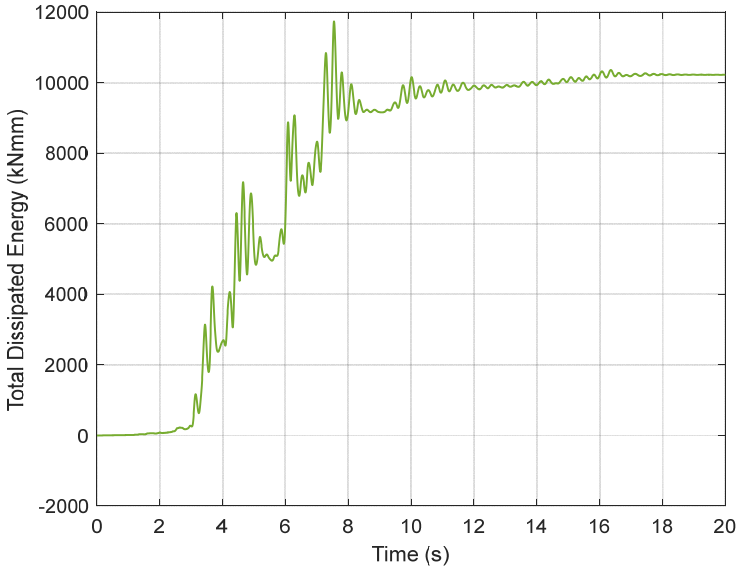

Figure 6.17 Structure energy dissipation. Test Seis-ULS (e06).

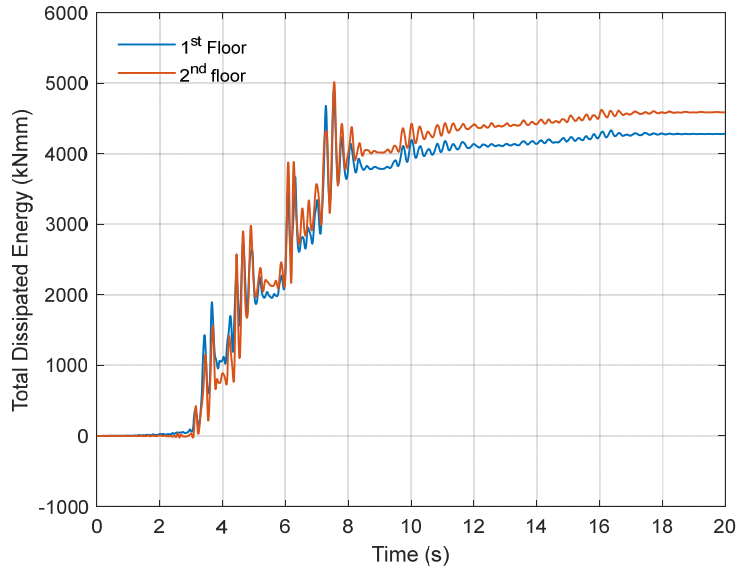

Figure 6.18 Floor energy dissipation, blue line 1st floor, red line 2nd floor. Tet Seis-ULS (e06).

As for the previous seismic test, Seis-SLS, the two floors dissipated in similar mode. Testing from 0 the two floors reached a maximum value of 4897 kNmm for the 1st floor (blue line in Figure 6.18) and around 7% higher for the 2nd one (red line in Figure 6.18), 5014 kNmm. The kinematic component of the energy is also present in this test.
Between the two seismic tests, Seis-SLS and Seis-ULS a difference of one order magnitude is visible in the dissipated energy, by way of the seismic action and the displacement reached by the structure (Table 6.1 for test Seis-SLS and Table 6.5 for test Seis-ULS).

Table 6.5 Shear force and displacement for the seismic tests.

	1st floor	2nd floor
Shear force (kN)	172.257	318.19
Displacement (mm)	10.66	11.78
Global energy dissipated (kNmm-kJ)	4279.7	4586.7

As for the global energy dissipation analysis, here too a difference of one order magnitude is observable respect the local energy dissipation of the previous seismic test (Seis-SLS, Chapter 6.1.1) to the effects of the seismic action and the displacement reached by the structure.

6.3.2 LOCAL BEHAVIOUR

The local analysis was carried out as reported in chapter 5.3.1 in which a detailed description of the procedure followed is reported.
Figure 6.19 reports the unbalanced moment versus the inter-storey drift ratio graphs for each slab-column connection. Each graph is represented in the corresponding position that the slab-column connection has in the structure (see chapter 3 for the detailed drawing). The two floors are both reported in the same graph, the 1st floor with a blue line, the 2nd floor with a red one.

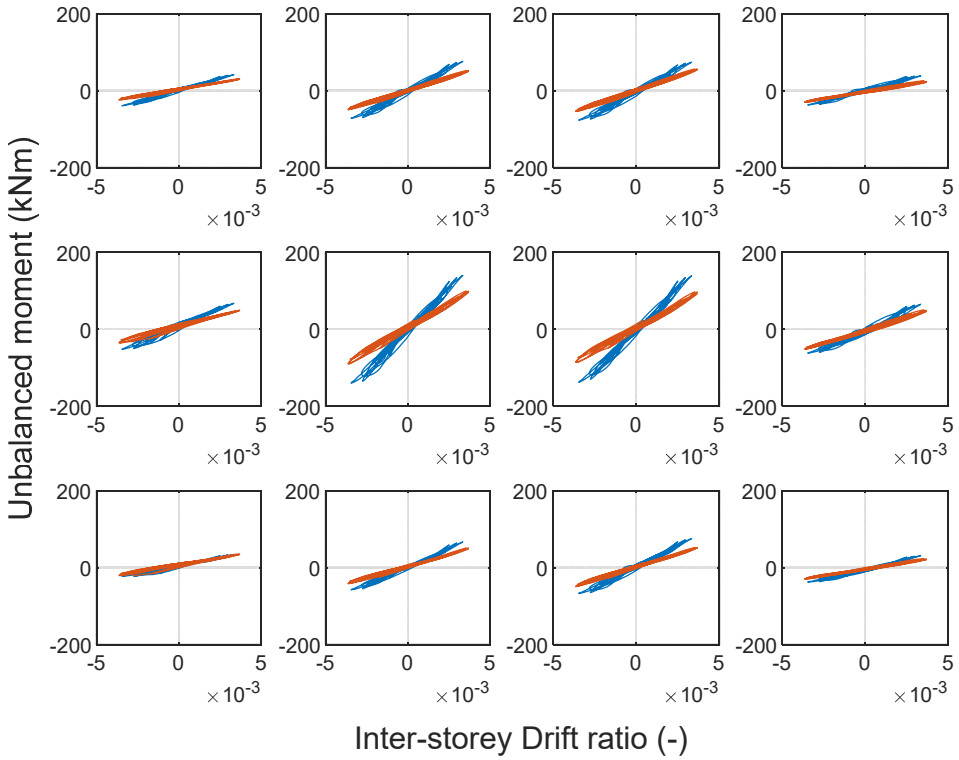

Figure 6.19 Unbalanced moment vs inter-storey drift test Seis-ULS. 1st floor blue line, 2nd floor red line.

The local response of the slab-column connections in terms of unbalanced moment versus the inter-story drift ratio (Figure 6.19) mirrors that of the first seismic test, Seis-SLS (chapter 6.1.2).
As expected, the two central connections B2 and C2 recorded the highest value of unbalanced moment, the corner A1, A3, D1 and D3 the lowest.

STIFFNESS

The stiffness of each slab-column connection on each floor was calculated following the same procedure used for the global behaviour, and reported in detail in Section 5.3.2.
In Figure 6.20, the blue lines indicated the 1st floor, the red ones the 2nd, the broken lines indicate the measured values of the base shear and the top displacement reached during the test, the continuous lines indicate the interpolation lines.
Following the graphs of each slab-column connection, a table with the obtained values of local stiffness was reproduced (Table 6.6).

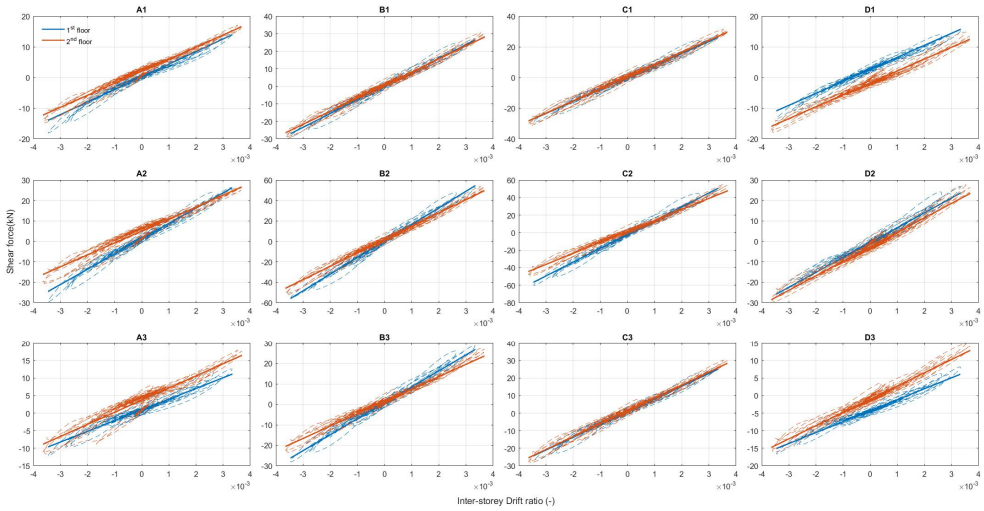

Figure 6.20 Shear force vs displacement, test Seis-SLS. 1st floor blue line, 2nd floor red line.

Table 6.6 Connections stiffness, Test Seis-SLS (kN/mm).

1st Floor	A	B	C	D	2nd Floor	A	B	C	D
1	1.28	2.46	2.44	1.22	1	1.23	2.33	2.47	1.21
2	2.33	5.07	4.93	2.27	2	1.83	4.07	3.92	2.21
3	0.95	2.44	2.27	0.97	3	1.08	1.89	2.30	1.18

The two internal connections B2 and C2 on both floors floor reached the higher value of stiffness, whereas the corners A1, A3, D1 and D3 the lower. As for the previous test, the shear forces in the connections on the two floors are very close due to the combination frame-wall.
Compared with the previous cyclic test Seis-SLS, the stiffness is lower in all the connections.

Dissipated Energy

To calculate the local energy dissipation, the same procedure was followed as for analysis of the global energy dissipation, (Chapter 6.1.1) but applied to each slab-column connections on each floor.
As reported in chapter 5, the dissipated energy was calculated firstly using the displacement values, and then the rotation as the displacement component, whereas the force component is the shear.
For a more detailed explanation of the methodology, equations and graphs were produced, see chapter 5.3.4 for the analyses concerning displacement, and chapter 5.4.7 for those done with the rotation.
In Table 6.7 and Table 6.8 the maximum values were reported for the dissipated energy of each connection on each floor, calculated with the displacement and with the rotation respectively.

Table 6.7 Dissipated energy of each connection on each floor, test Seis-ULS. Energy calculated with the displacement (kNmm=kJ).

1st Floor	A	B	C	D	2nd Floor	A	B	C	D
1	215.69	384.38	424.83	221.87	1	254.76	489.19	555.97	286.22
2	412.67	743.29	687.73	398.61	2	463.21	817.12	731.61	489.12
3	218.64	421.89	384.84	227.44	3	331.03	372.19	511.57	274.34

Table 6.8 Dissipated energy of each connection on each floor, test Seis-ULS. Energy calculated with the rotation (kNmxrad).

1st Floor	A	B	C	D	2nd Floor	A	B	C	D
1	0.164	0.264			1	0.119	0.200		
2	0.293	0.461	0.636	0.309	2	0.119	0.282	0.255	0.177
3			0.290	0.181	3			0.196	0.126

Figure 6.21 and Figure 6.22 report the graphs of the dissipated energy of each connection on each floor calculated with the displacement and with the rotation respectively.

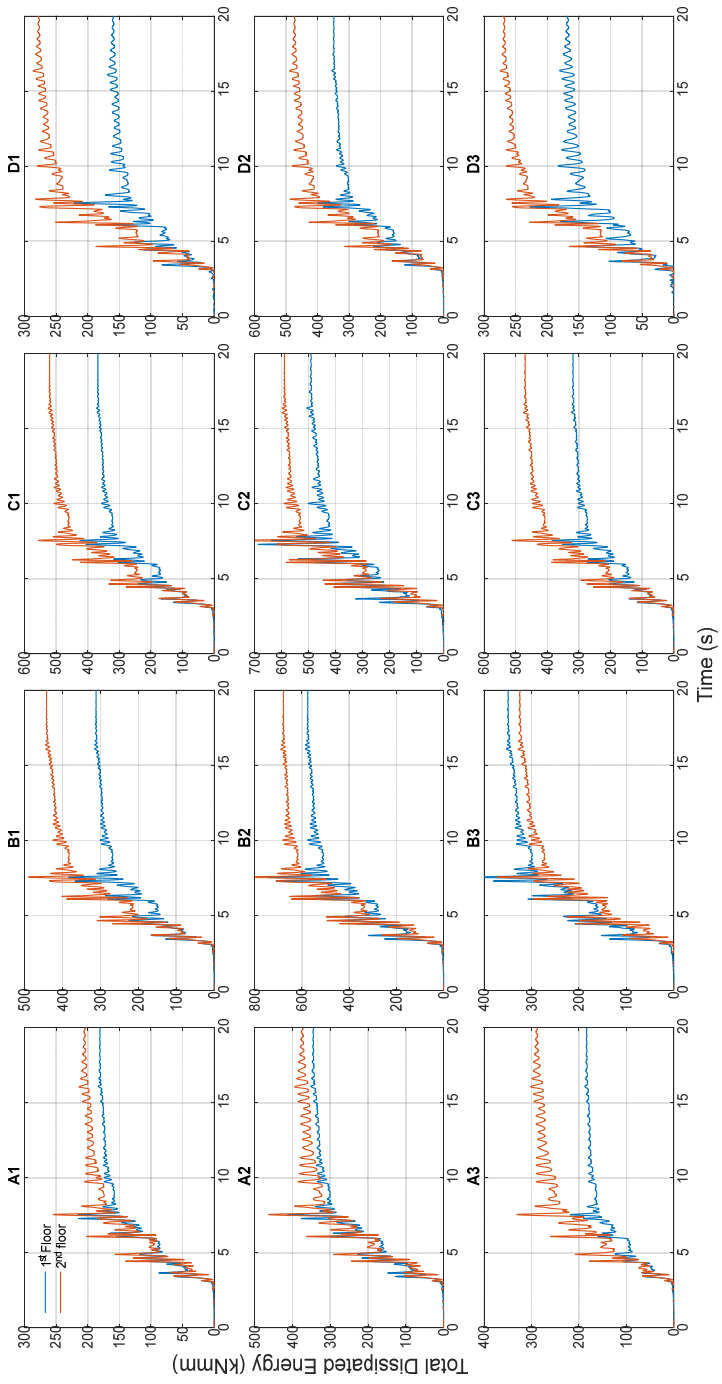

Figure 6.21 Dissipated energy for each connections, test Seis-ULS. 1st floor blue line, 2nd floor red line. Energy calculated with the displacement**.**

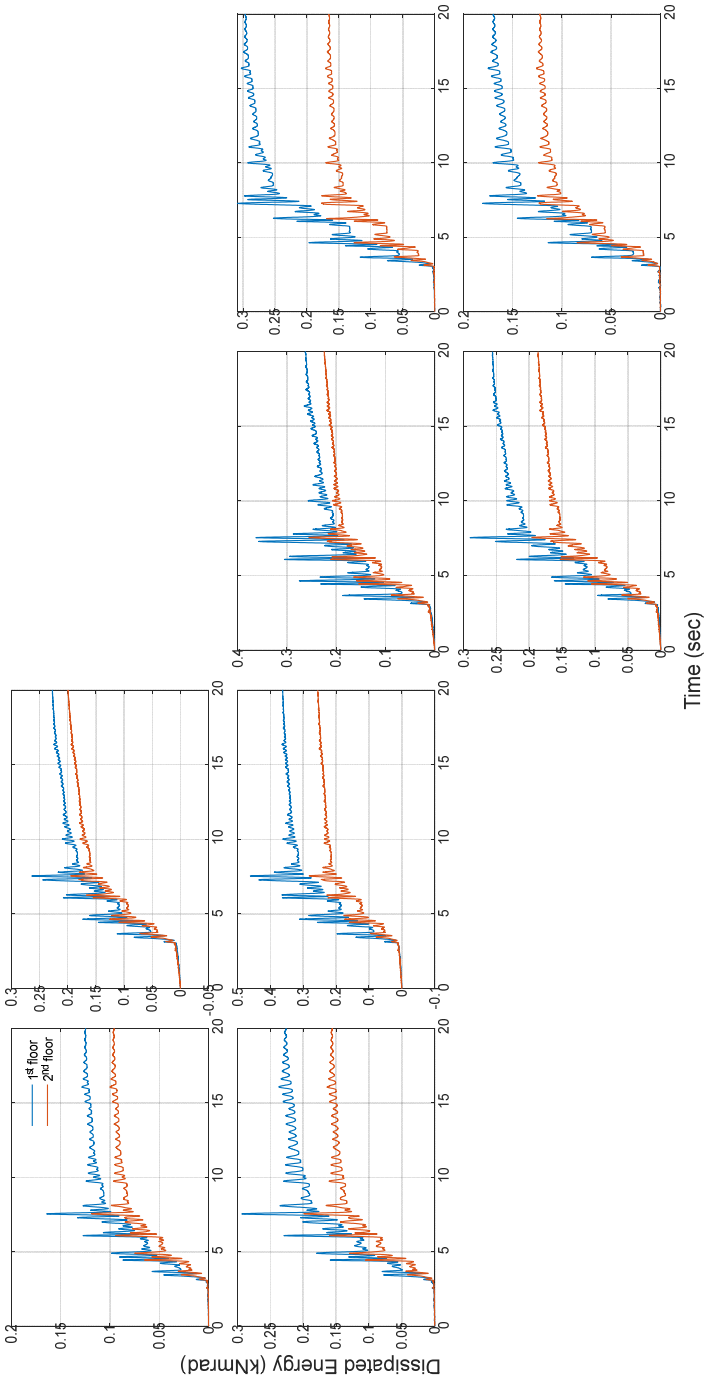

Figure 6.22 Dissipated energy for each connection, test Seis-SLS. 1st floor blue line, 2nd floor red line. Energy calculated with the rotation

Using the inter-storey drift to calculate the energy, the 2nd floor results to be more dissipative than the 1st one in all the connections, whereas using the rotation the 1st floor overtakes the 2nd one in all the connections.
This difference was probably due to the fact that as explained in Chapter 5, the slab-column rotation better depicts the real response of the slab-column connections on the two different floors. On the 1st floor the slab-column rotation considers both the sensors above and below the slab, whereas for the columns on the 2nd floor the rotation corresponds to the measure recorded only by the sensor present.
On observing the crack opening analysis in the followed section, it is possible to note that the energy calculated with the rotation gives a better explanation of what really happened. In fact, the higher cracks openings were recorded on the 1st floor.
In the representation with the local energy dissipation calculated using the displacement (Figure 6.21), the internal connection B2 was the most dissipative on both floors, together with the similar C2. The corners A1, A3, D1 and D3 were the less dissipative.
Differing from the previous seismic test, during this test the behaviour of the central connections in both the representations (Figure 6.21 and Figure 6.22) mirrored that of the lateral ones. During this test the rotation was greater than in the previous Seis-SLS, so that noise did not affect the measurements as much as in the test Seis-SLS.
After 10 seconds the resultant dissipation remained stable for both floors and all the connections.
Compared to the previous seismic test, all the connections were more dissipative.

CRACK OPENING DISPLACEMENT

Each graph is located in the position corresponding to that which the slab-column connection has in the structure. As for the previous analysis, the crack opening displacement analysis was not made with regard to all the slab-column connections but only for those with the displacement transducers mounted on the slab surface.
Four different colours were used to identify the four different sides of the sensors, yellow for the east, red for the south, green for the west and blue for the east.
During the test, sensors recorded crack openings larger than in the previous Seis-SLS with an always very small maximum value.

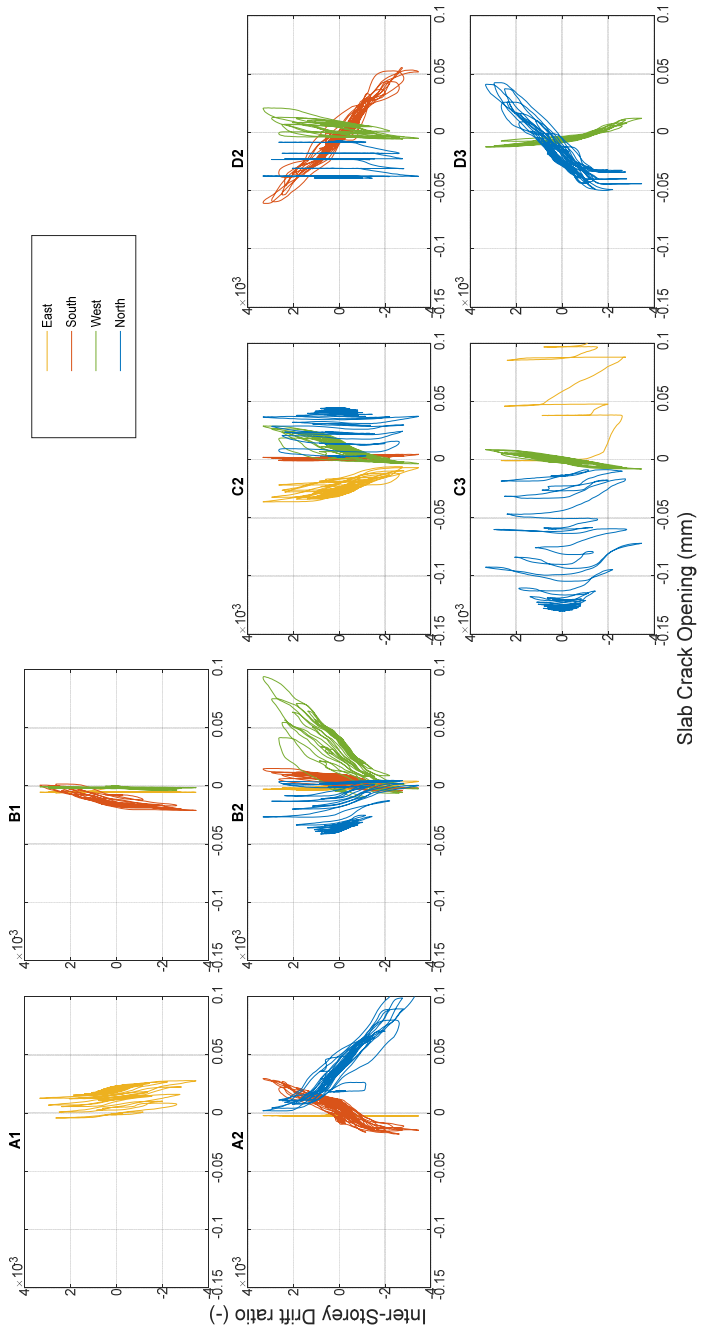

Figure 6.23 Slab Crack Opening vs Inter-story drift ratio for connections with sensors, 1st floor, Seis-ULS.

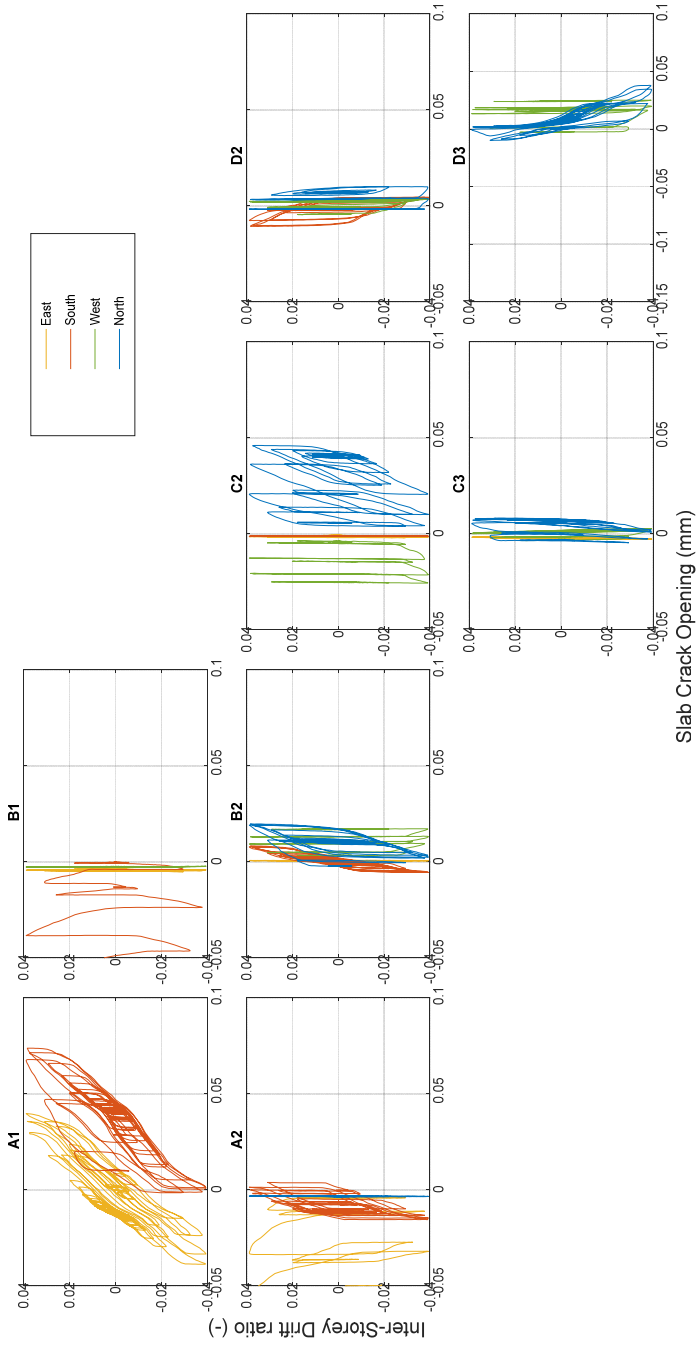

Figure 6.24 Slab Crack Opening vs Inter-story drift ratio for connections with sensors, 2nd floor, Seis-ULS.

On the 1st floor (Figure 6.23) the maximum value recorded from the east sensor was

close to 0.2 mm in the C3 connection, and also that from the opposite sensor, on the west, and 0.1 mm in the B2 connection.
For the 2nd floor (Figure 6.24) the maximum values recorded were 0.04 mm from the east sensor in the A1 connection and 0.02 mm from the west sensor in the D3 connection. The differences in the two floors are related to the use of shear reinforcement.

6.4 Summary

A summary of the main results obtained at the end of the two seismic tests and a comparison between the two are reported here.

- The stiffness of the test Seis-ULS, was lower than that of the test Seis-SLS;
- During the second seismic test, Seis-ULS, a global energy dissipation of one order magnitude higher than the first seismic test was recorded (Table 6.9). This difference being due to the applied forces and the displacement reached by the structure.

Table 6.9 Global energy dissipation for the two seismic tests.

Test	Global Energy dissipated (kNmm)
Seis- SLS	1287
Seis-ULS	11735

The same consideration is valid also for the energy dissipation on each floor. The energy dissipated from each floor during the two seismic tests, has a difference of one order magnitude between the two tests (Table 6.10). This difference derived from the observations made in the previous point;

Table 6.10 Shear force and displacement for the two seismic tests.

Test		1st floor	2nd floor
Seis- SLS	Shear force (kN)	59.67	133.79
	Displacement (mm)	3.20	3.99
	Global energy dissipated (kNmm-kJ)	521.4	531.6
Seis-ULS	Shear force (kN)	172.257	318.19
	Displacement (mm)	10.66	11.78
	Global energy dissipated (kNmm-kJ)	4279.7	4586.7

- The local response of the slab-column connections in terms of unbalanced moment versus the inter-story drift ratio of the two tests are similar from a phenomenological point of view (Figure 6.7 and Figure 6.19);
- The local stiffness decreased from the first seismic test, Seis-SLS, to the second one, Seis-ULS. At the end of the test Seis-ULS, all the connections reported lower values of stiffness, in relation to damage accumulation;
- Considering the local energy dissipation, different slab-column connection

behaviour in function of the typology, the method used to calculate the energy (inter-storey drift ratio or rotation) and in the dissipation values were followed. In the Seis-ULS test, the dissipation on each floor changed with the displacement typology used in the energy calculation. With the inter-storey drift ratio, the 2nd floor was more dissipative than the 1st one in all the connections, whereas with the rotation the 1st floor overcame the 2nd one in all the connections.
In the Seis-SLS test, in the energy calculated with the rotation, the connections in the B and C alignments (B1, B2, C2, C3) continued to dissipate energy from the start of the test to the end showing the joint behaviour. With the energy calculated with the inter-storey drift ratio, this behaviour is not evident as the local rotation is hidden. For the lateral connections (A1, A2. D2, D3) after a time of 10 seconds the energy dissipation remained almost constant.
Diversely from the previous seismic test, during Seis-SLS test the energy behaviour of the central connections in both the representations (Figure 6.21 and Figure 6.22) remained similar to that of the lateral ones.
Compared with the previous seismic test, in Seis-ULS test all the connections were more dissipative;

- Finally, during both the seismic tests, there was very limited crack opening in the slabs.

References

[1] NTC2018 - Norme tecniche per le costruzioni 2018 (NTC 2018) - D.M. 17 Gennaio 2018 (D.M. 17/1/18) – in Italian.

[2] CEN. EN 1998-1. Eurocode 8: Design of structures for earthquake resistance - Part 1: General rules, seismic actions and rules for buildings. 2004

[3] Le, D.D., Nguyen, X.-H., Nguyen, Q.-H. (2020) “Cyclic Testing of a Composite Joint between a Reinforced Concrete Column and a Steel Beam”. Applied sciences.

[4] Park, R. (1988) “Ductility evaluation from laboratory and analytical testing”. Proceedings of Ninth World Conference on Earthquake Engineering, August 2-9, Tokyo-Kyoto, Japan (Vol. VIII).

7 Cyclic test Cyc – 1

7.1 Introduction

The results obtained during the seismic experimental campaign showed a very limited damage in the secondary flat slab frame with primary walls. The cyclic tests aimed at exploring full response of the flat slab up to failure.
As defined in the test programme, the set-up of the first cyclic test was to reach a failure in some connection, with the possibility of strengthening it, and then continue the experimental campaign with a second cyclic test. For this purpose, a limited inter-storey drift of 2.5% was chosen for the former.
Firstly, the global response is reported and then the local one. The overall behaviour is analysed in terms of shear-displacement relationship, stiffness deterioration, ductility and energy dissipation.
Regarding the behaviour of the slab-column connection, a thorough description for each one is reported in terms of unbalanced moment, ductility, and energy dissipation. A more detailed analysis of the crack formation is also reported using the crack opening measurements recorded, the slab rotation, the photographic materials and the measurements derived from all this at test conclusion.
As described in chapter 3, the 2nd floor had the shear reinforcement that was not present on the 1st floor, both floors had a different longitudinal reinforcement layout, smeared in the west half of the structure (connections in the A and B lines) and concentrated in the east part (connections in the C and D lines). Thus detailed comparison to assess the behaviour of the concentrated and smeared reinforcement connections and the role of the shear reinforcement was performed, based on the analysis.
With the aim to explore the effects of different gravity shear ratio, two different added load values were used for the Eastern and Western halves of the first floor slab.
For a detailed description of the methodology followed, the equations used and the graphs set up, see chapter 5.

7.2 Preliminary aspects

The loading entity was changed between the seismic tests and this first cyclic one.
The experiment Cyc-1 was conducted with two different loads on the two halves of the slab on the 1st floor. The west side of the slab was loaded with tanks for a total weight of 240 kN, the east side of the slab was loaded with tanks for a minor total

weight of 108 kN. The load on the 2nd floor was kept the same as in the previous experiment (Table 7.1 and Figure 7.1).

Table 7.1 Added loads on the 1st and 2nd floor, Test B1 (f02).

Floor	Typology	Number	Weight (kN)	Load (kN)	Area (m2)	(kN/m^2)
1	West side					
	Tanks	24	10	240	68.9	3.48
	East side					
	Tanks	24	4.5	108	68.9	1.57
2	Blocks	9	66	594	137.8	4.31

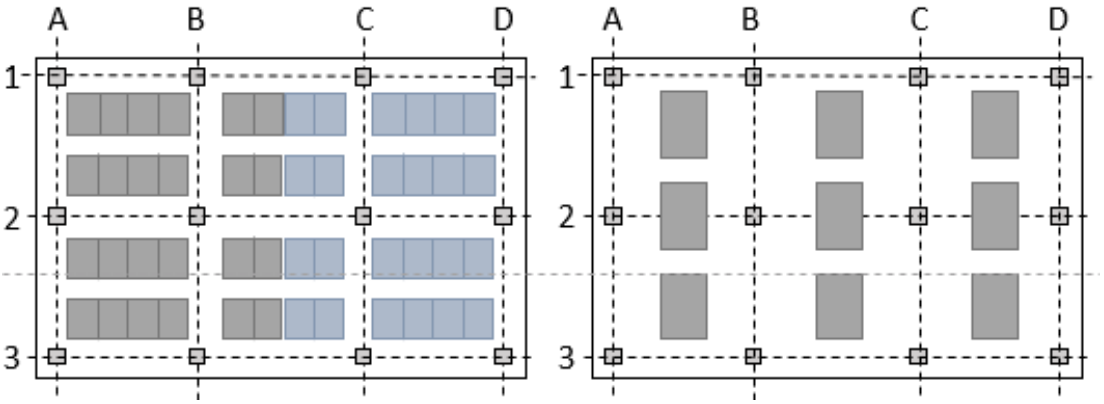

Figure 7.1 Added Loads distribution on the 1st and 2nd floor, Test B1 (f02).

The loading change results in a change to the gravity shear ratio. In Table 7.2 the gravity shear ratio values of each slab-column connection typologies in each floor are reported.

Table 7.2 Gravity shear ratio.

Floor		Internal	Edge	Corner
1st	West	0.29	0.20	0.18
	East	0.22	0.15	0.13
2nd	-	0.32	0.22	0.19

For a detailed description of the test programme, see Chapter 4.

7.3 Global behaviour

The response of the entire structure and then the response of each floor in terms of stiffness deterioration, ductility and energy dissipation is reported here. The stiffness degradation was analysed to describe the global damage of the structure, whereas the global ductility was studied to ascertain whether the entire structure would undergo a plastic deformation before failure. Finally, since the structure was

dissipative, the energy dissipation of each floor and of the entire structure was shown. For test Cyc-1 a displacement history was imposed on the 2nd floor whereas half of the measured horizontal force on the 2nd floor was imposed on the 1st one.
In Figure 7.2 the global base shear versus the roof displacement is shown.

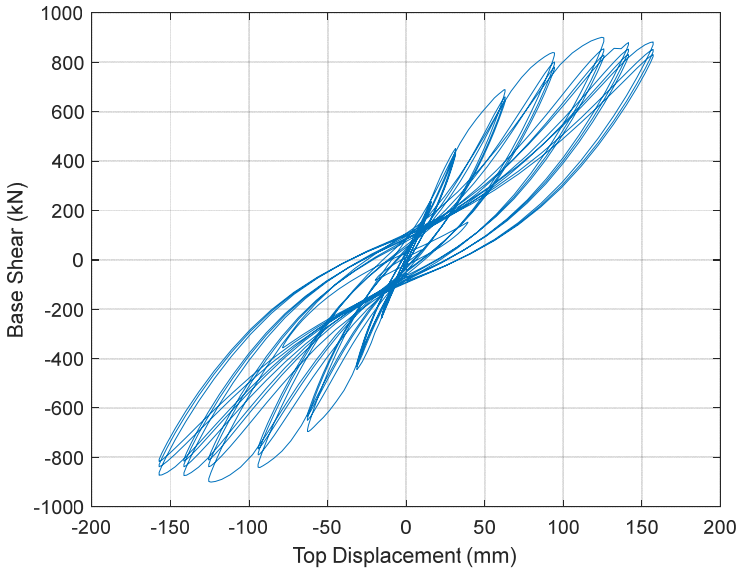

Figure 7.2 Base shear vs. top displacement for the Test Cyc-1.

The structure reached a global load at 1.8% drift that remained nearly constant in following cycles then a progressive stiffness loss and pinching of the cycles and an increase of the displacement was observed.
At peak drift value, the specimen reached a maximum displacement of 157 mm.
From a drift value of 1.8%, the base shear force remained almost constant (around 901 kN) until reaching the maximum drift value (2.5%) with a small loss of resistance for a drift of 1.9% and a displacement of 132 mm. After attaining the maximum base shear at 1.8% drift, a very limited strength reduction showed, until reaching a maximum drift value of 2.5%. For each drift level there was limited strength deterioration between the three cycles.
The horizontal plateau of the base shear force shows that the structure allowed for a phase of plastic deformation, with a stable global response up to the maximum value of the drift (2.5%).
At the end of the test, some cracking and compression damage was observed at the base of the columns on the 1st floor.

7.3.1 FLOOR BEHAVIOUR

As shown in Figure 7.3 and Figure 7.4, the force recorded on the 2nd floor (V_{max}=600.5 kN) was double that of the 1st floor (V_{max}=300.5 kN).
The blue line represents the time history of displacement imposed on the 1st floor to

a peak inter-story drift ratio of 2.5%, whereas the 2nd floor, red line, was subjected to a peak inter-story drift ratio of 2.3% (Figure 7.4).
The force on the 2nd floor reached a plateau (see Figure 7.3 a), although the displacements increases continue in the following cycles (see Figure 7.3 b). The force reached at the step number around 820, when the top drift ratio reached 1.8%, corresponds to the maximum load of the structure.
At this inter-story drift ratio value, different plastic events developed, the yielding of ground floor column bases, and yielding of the longitudinal reinforcement. From this inter-story drift value to the end of testing, the force stabilized.

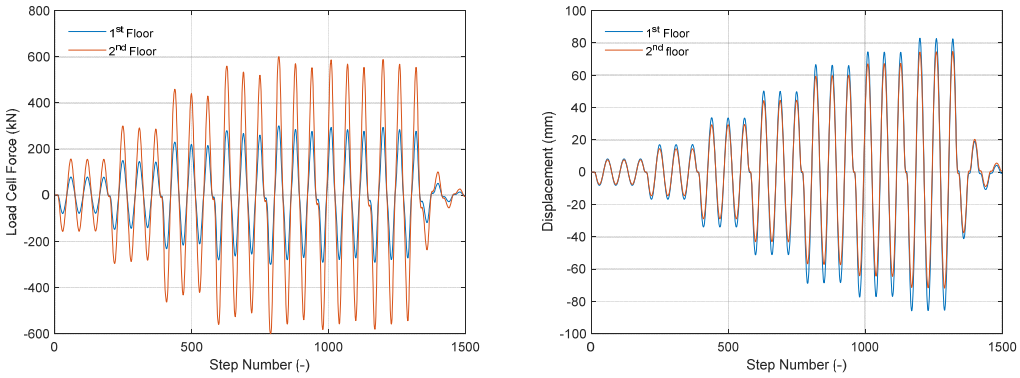

Figure 7.3 a) Floor load cell force and b) floor displacement imposed by the actuators for the Test Cyc-1.

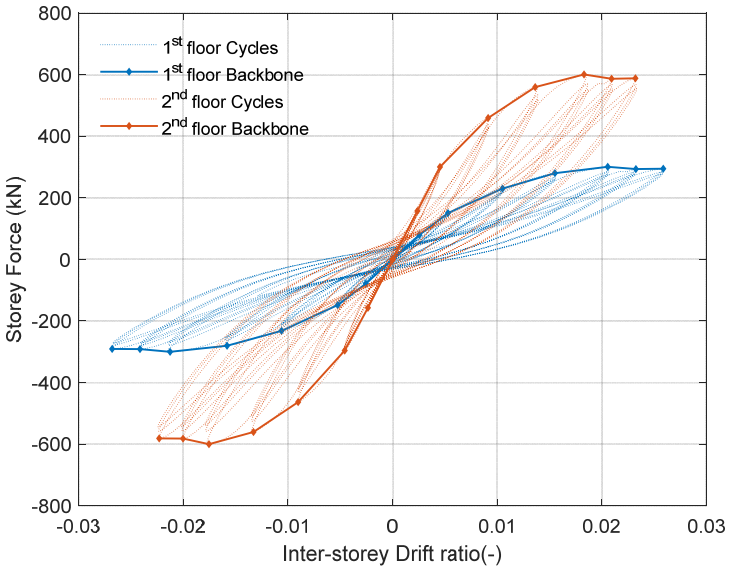

Figure 7.4 Storey forces for the Test Cyc-1.

The 1st floor reached an inter storey drift 10% higher than the 2nd one, the 1st one in fact was free to move being subjected to half the force registered on floor 2.

With a representation of the storey force versus the inter storey drift relations it seems that the 2nd floor was more dissipative than the 1st one. This representation of the forces applied on each floor should not be confused with the fact that, the 1st floor bearing of the force applied on both this and on the 2nd floor, would in fact be more dissipative and would suffer greater damage than that of the 2nd floor, as will be shown in the following sections.

7.3.2 STIFFNESS DETERIORATION

The stiffness degradation was calculated to describe the damage to each floor of the building. The followed procedure, the equations used and the graphs set up are reported in Chapter 5.2.2.
The stiffness deterioration was calculated with reference to the first value of the secant stiffness of the first test made, Seis-SLS. The stiffness deterioration ratio versus the inter-storey drift is reported in Figure 7.5 and Table 7.3, whereas in Figure 7.6 the negative branches were reported with the absolute value to display the symmetry.

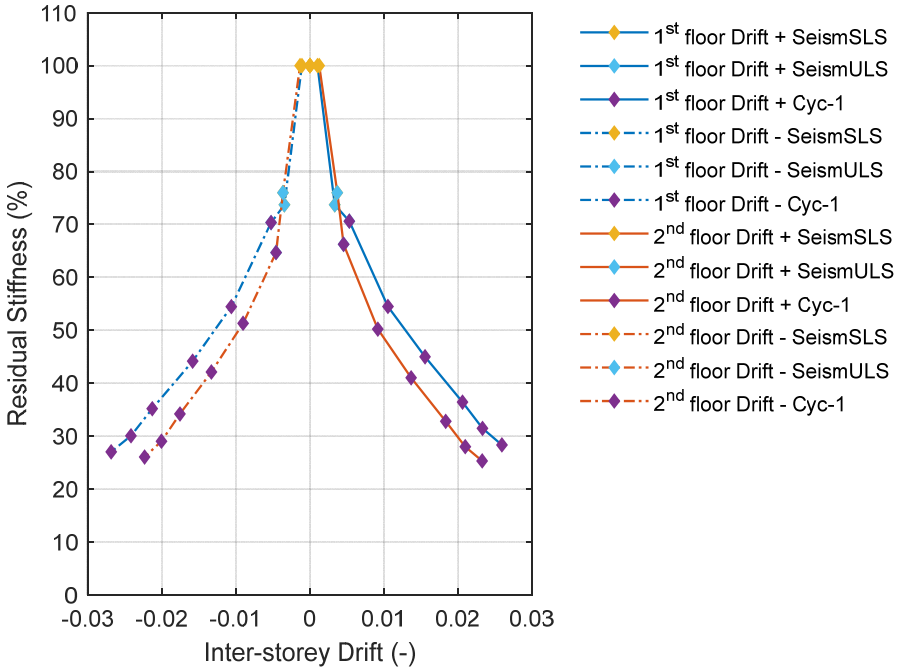

Figure 7.5 Stiffness deterioration ratio Test Seis-SLS (e03) +Seis-ULS (e06) +Cyc-1 (f02).

It is possible to observe a gradual loss of stiffness with a similar trend for both positive (from west to east) and negative (from east to west) loading directions (Figure 7.5 and Figure 7.6). From 100% it reached 27.03% and 28.33% for the 1st floor, for the negative and the positive drift respectively, whereas for the 2nd floor, from 100% it reached 26.04% and 25.31 for the negative and the positive drift respectively (Table 7.3).

Table 7.3 Stiffness deterioration values, Test Cyc-1 (f02).

	Pull (from east to west)		Push (from west to east)	
	Drift (%)	Stiffness Degradation (%)	Drift (mm/mm)	Stiffness Degradation (%)
1st Floor	-0.0011	100	0.0010	100
	-0.0035	73.7	0.0033	73.7
	-0.0053	70.34	0.0053	70.61
	-0.011	54.46	0.0105	54.49
	-0.016	44.17	0.0155	44.99
	-0.021	35.18	0.0206	36.42
	-0.024	30.06	0.0233	31.46
	-0.027	27.03	0.0259	28.33
2nd Floor	-0.0013	100	0.0012	100
	-0.0036	75.99	0.0037	75.99
	-0.0046	64.69	0.0045	66.24
	-0.0090	51.31	0.0091	50.21
	-0.0133	42.11	0.0136	41.03
	-0.0175	34.18	0.0183	32.79
	-0.0200	29.03	0.0209	28.00
	-0.0223	26.04	0.0232	25.31

Both the floors showed the same stiffness deterioration. During the two seismic tests (yellow and light blue diamonds in Figure 7.5) both the floors showed limited stiffness deterioration with the 2nd one slightly higher than the 1st one (76% for the 2nd one compared to 74% for the 1st one). This slight difference could be explained by the fact that the 2nd floor was provided with shear reinforcement.
The 1st floor without shear reinforcement cracked more than the 2nd one that was with shear reinforcement. At the end of test, the stiffness degradation of both floors is almost the same (Table 7.3).

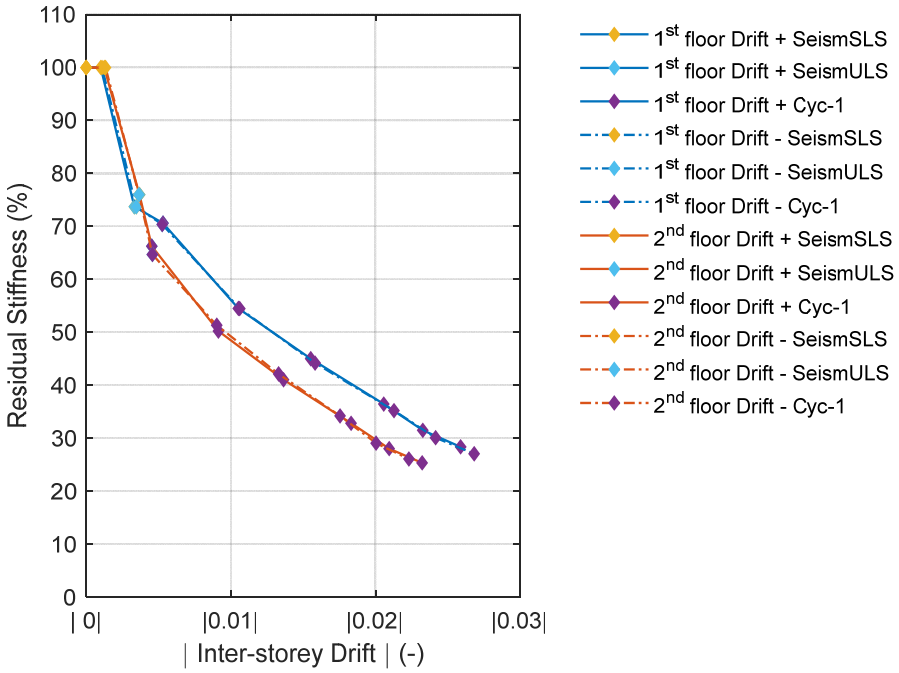

Figure 7.6 Stiffness deterioration absolute value Test Seis-SLS (e03) +Seis-ULS (e06) +Cyc-1 (f02).

Finally, as it is possible to observe from Figure 7.6, the two branches of the drift, positive and negative, are perfectly symmetrical for the 1st and the 2nd floor.

7.3.3 DUCTILITY

In order to assess the potential of the entire structure to deform plastically before failure, its global ductility was studied. The procedure, the equations used and the graphs set up are reported in Chapter 5.2.3.
The study of ductility considered the four analysed residual resistance 80%, 85%, 90% and 95% that are reported in the following Figure 7.7 a, b, c and d.
For each of them, the graph representing the load level corresponding to the percentage taken into consideration (point-dashed line, blue for the 1st floor and red for the 2nd), is reported, and if the conditions to reach failure were respected, a red continuous line indicated the failure force and the corresponding displacement.
The graphs are followed by a table (Table 7.4) that reports the shear force and the corresponding drift ratio of the three characteristic points (Limit, Yielding and Failure) and in the last column the displacement ductility factor.
Values for the 1st and the 2nd floor and for the positive and the negative drift are reported.

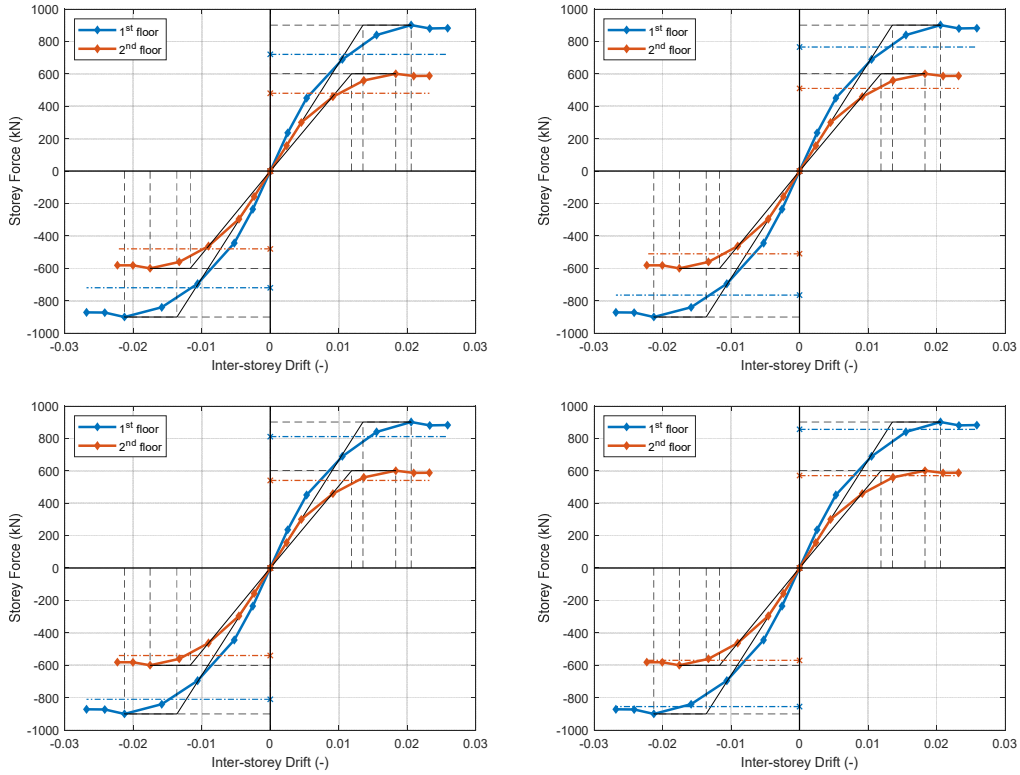

Figure 7.7 Definition of the yielding and failure at a) 80%, b) 85%, c) 90%, d) 95% points, Test Cyc-1 (f02). Line: blue for the 1st floor, red for the 2nd. Horizontal dashed line, force at failure.

As can be seen in Figure 7.7 and in Table 7.4, for the Test Cyc-1 (f02) neither the 1st floor nor the 2nd floor, reached failure point in any of the analysed percentages so this value was not reported in the table.

Table 7.4 Shear force and drift ratio at limit, yielding and failure at 80%, 85%, 90%, 95% points, Test Cyc-1 (f02).

	Limit Point		Yielding Point	
	Shear Max (kN)	Drift (-)	Shear Yielding (kN)	Drift (-)
1 st floor positive	901.1	0.021	901.1	0.014
1st floor negative	-900.2	-0.021	-900.2	-0.014
2nd floor positive	600.6	0.018	600.6	0.012
2nd floor negative	-600.0	-0.018	-600.0	-0.012
1 st floor positive	901.1	0.021	901.1	0.014
1st floor negative	-900.2	-0.021	-900.2	-0.014
2nd floor positive	600.6	0.018	600.6	0.012
2nd floor negative	-600.0	-0.018	-600.0	-0.012
1 st floor positive	901.1	0.021	901.1	0.014
1st floor negative	-900.2	-0.021	-900.2	-0.014
2nd floor positive	600.6	0.018	600.6	0.012
2nd floor negative	-600.0	-0.018	-600.0	-0.012
1 st floor positive	901.1	0.021	901.1	0.014
1st floor negative	-900.2	-0.021	-900.2	-0.014
2nd floor positive	600.6	0.018	600.6	0.012
2nd floor negative	-600.0	-0.018	-600.0	-0.012

7.3.4 Energy dissipation

Finally, since the structure was dissipative, the energy dissipation of each floor and of the entire structure was analysed. The procedure followed to obtain this data together with the equations used and the graphs set up are reported in Chapter 5.2.4. The evolution of energy dissipation in the building and at the two-storey levels is shown in Figure 7.8 and Figure 7.9 respectively.
The procedure followed to obtain this, together with the equations used and the graphs set up is reported in Chapter 5.2.4.

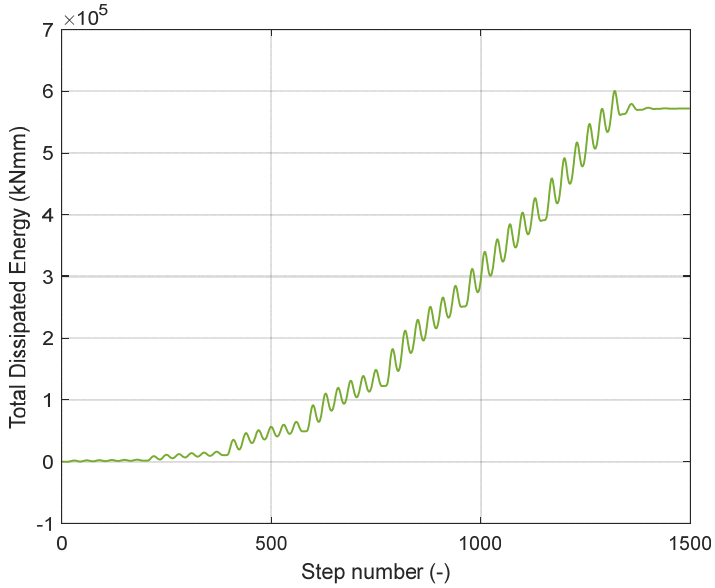

Figure 7.8 Structure energy dissipation. Test Cyc-1 (f02).

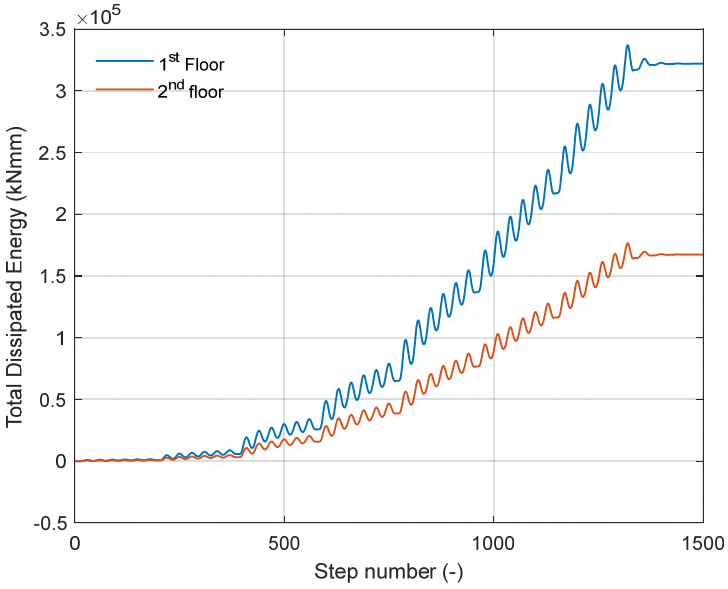

Figure 7.9 Floor energy dissipation, blue line 1st floor, red line 2nd floor. Test Cyc-1 (f02).

The 1st floor dissipated more than twice that of the 2nd one (Figure 7.9). This higher energy dissipation of the 1st floor is due to the force used, in fact to calculate the energy dissipation for the 1st floor, all the forces applied by the four load cells (two for each floor) were used.
At the end of the first cyclic test, the 1st floor was that which reported more damage even though only slight, confirming its greater energy dissipation.

7.4 Local behaviour

The response of each of the twenty-four slab-column connections (twelve for each floor) is analysed in detail in terms of stiffness degradation, local ductility and local dissipated energy. The procedure followed, the equations used and the graphs set up are reported in Chapter 5.3.1.

Figure 7.10 reports the unbalanced moment versus the inter-storey drift ratio graphs for each slab-column connection. Contrary to the previous seismic test, here it also was possible to obtain the backbone curve for each graph (see Chapter 5.3.1).

The two floors are both reported in the same graph. In each graph, the punctuated lines were used to represent the unbalanced-moment versus the inter-storey drift ratio values, whereas the continuous lines were used for the envelope of the maximum values, the backbone curves. The name of the slab-column connection is reported in the graph.

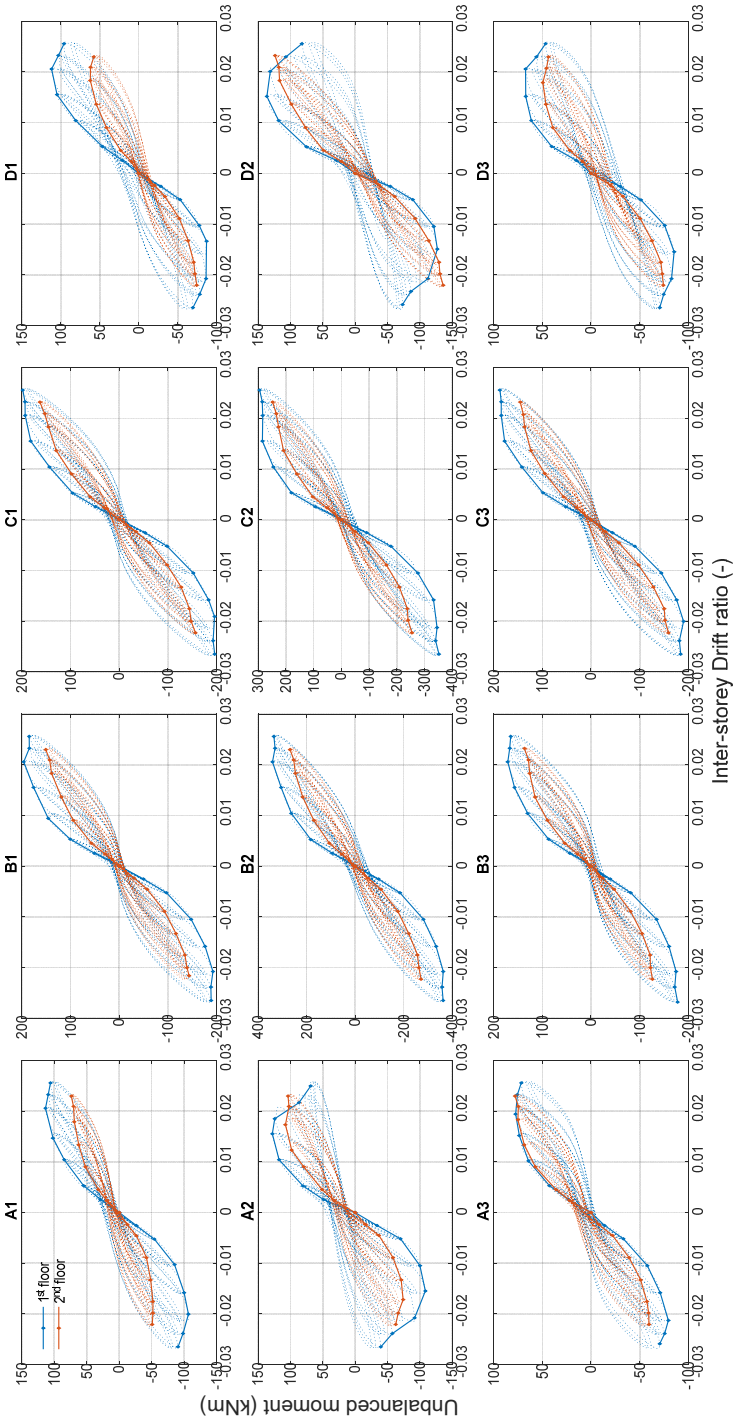

Figure 7.10 Unbalanced moment vs inter-storey drift Test Cyc-1. 1st floor blue line, 2nd floor red line.

The central connections (line B and C) are those which reached the highest values of unbalanced moment, in particular the internal B2 and C2.
From the representation of all connections, it is evident that the two edge line connections on the 1st floor, perpendicular to the loading application (A and D), were more stressed than the other two line connections (B and C). The connections in the lateral alignment A and D have showed a drop of the unbalanced moment with a redistribution of load in the central B and C. This indicates the reaching of failure in these connections, that will be further analysed in the following. The interior and edge connections along lines B and C on the 1st floor show the reaching of a plateau. The 2nd floor showed a stable response in most connections, with the exception of connection A2 on the edge and D1 and D3 in the corners. The interior and edge connections show a stable nonlinear response with a progressive loss of stiffness.
In Table 7.5, all the maximum and the minimum values for the unbalanced moment of all the connections and for both floors, are reported.

Table 7.5 Maximum and minimum unbalanced moment for each connection (kNm), Test Cyc-1.

Floor	**A1**		**B1**		**C1**		**D1**	
	Min	Max	Min	Max	Min	Max	Min	Max
1st	-106.46	113.6	-192.36	196.1	-195.88	198.16	-111.77	87.08
2nd	-51.91	73.8	-143.34	150.9	-156.41	162.89	-62.22	74.39
Floor	**A2**		**B2**		**C2**		**D2**	
	Min	Max	Min	Max	Min	Max	Min	Max
1st	-108.63	127.9	-363.46	340.7	-352.43	294.59	-136.52	127.18
2nd	-74.34	107.8	-271.87	268.3	-255.07	247.48	-123.81	136.17
Floor	**A3**		**B3**		**C3**		**D3**	
	Min	Max	Min	Max	Min	Max	Min	Max
1st	-79.52	77.4	-177.99	170.9	-190.12	187.08	-67.09	85.42
2nd	-59.62	78	-126.27	136.5	-159.19	145.31	-49.39	74.36

The internal B2 and C2 reached the highest values of unbalanced moment caused by the two bending moments, the two shears and the two torsions that acted on them. The edge slab-column connection typology lost one torsion and some width from the bending and shear.
Finally, in the corner slab-column connection typology the resistant sections were a quarter of the other ones, so the unbalanced moment reached there was the lowest.
Of the two floors, the 1st one reached the highest values of unbalanced moment for the positive drift value (loading from east to west) and the lowest values of unbalanced moment for the negative drift value (loading from west to east).

7.4.1 DIFFERENT LONGITUDINAL REINFORCEMENT

The following analysis focuses on the different behaviour of the two halves of the slab with two different longitudinal reinforcement layouts, the west side with smeared longitudinal reinforcement and the east side with concentrated longitudinal reinforcement (Figure 7.11). In addition, the added gravity load was higher in the west side than in the east side (see 7.2). the study aimed at understanding the effect of the two different reinforcement layouts on the response in general and the failure mode in particular.

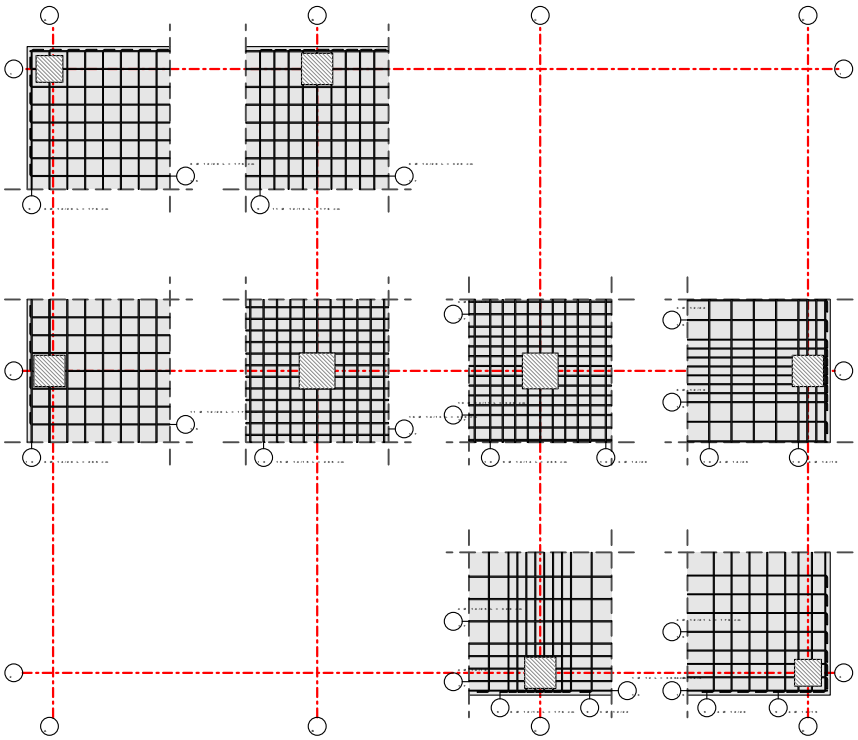

Figure 7.11 Longitudinal reinforcement, smeared in A and B and concentrated in C and D.

The comparison is made between the connections of the same typology, in the two halves of the slab having different longitudinal reinforcement. For each comparison, a plan of the specimen is presented, where the connections analysed in that paragraph are encircled.
The total reinforcement quantity was the same, but the distribution of reinforcement changed. The total reinforcement cross section was the same for the hogging reinforcement, the blue circles represent the connections in the west half of the slab bearing the smeared longitudinal reinforcement and the highest added gravity load, whereas the red circles represent the connections in the east part of the slab with the concentrated longitudinal reinforcement and the lowest additional gravity load.
The comparison graphs are reported, with the same colour scheme.

CORNER CONNECTIONS: A1, A3, D1, D3

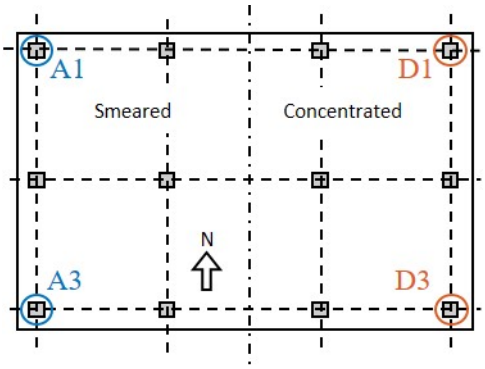

Figure 7.12 Corner connections in plan.

For the two connections located to the north (A1 and D1), the two opposite sides west and east showed a different trend on the 1st and the 2nd floors.
To draw a comparison between the connections located in the two halves of the slab, due to their asymmetry it was necessary to invert the drift sign of the connection D1.
For the 1st floor, for negative inter-storey drifts, the negative unbalanced moments were quite similar, whereas for the positive inter-storey drifts there resulted to be a nearly 30 kNm difference between the maximum value of A1 and D1.
On the 2nd floor this difference will be noted for negative inter-storey drift with 10 kNm between A1 and D1.

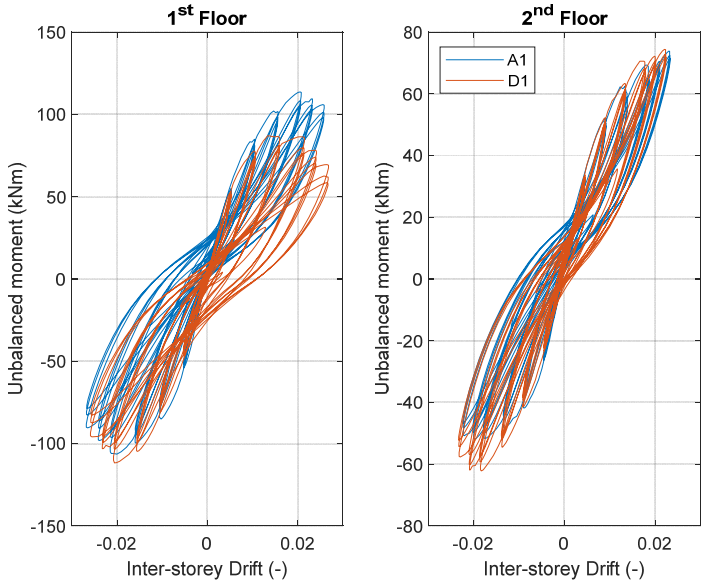

Figure 7.13 Unbalanced moment vs Inter-Storey drift, connections A1 D1.

A different pattern of behaviour was observed in the two connections located to the south (A3 and D3). To draw a comparison between the connections located in the two halves of the slab, due to their asymmetry it was necessary to invert the drift sign

of the connection D3. Both the connections located at the two opposite sides, west and east, showed the same trend on the 1st and the 2nd floor. The difference in the maximum value of unbalanced moment was seen in the negative inter-storey drift for both floors of around 10 kNm. For negative inter-storey drift, the unbalanced moment was higher in the connection A3 than in D3.

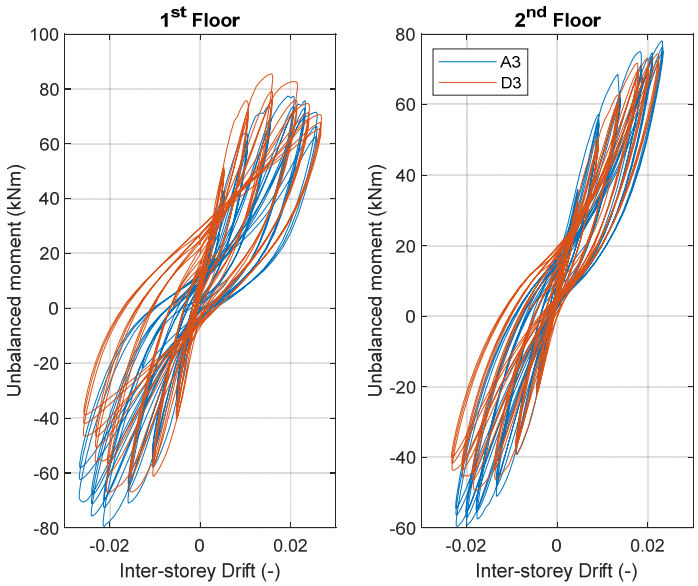

Figure 7.14 Unbalanced moment vs Inter-Storey drift, connections A3 D3.

LATERAL CONNECTIONS PLACED ON THE LONG SIDE: B1, B3, C1, C3

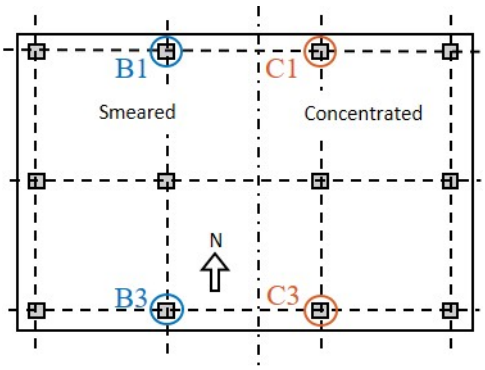

Figure 7.15 Lateral long side connections in plan.

Lateral connections on the long side located to the north (B1 and C1), showed a very similar trend for the 1st floor with maximum value of unbalanced moments to be rather similar for positive and negative inter-storey drift.
For the 2nd floor, slightly more than a 10 kNm difference was observed for both the positive and the negative values of the inter-storey drift.

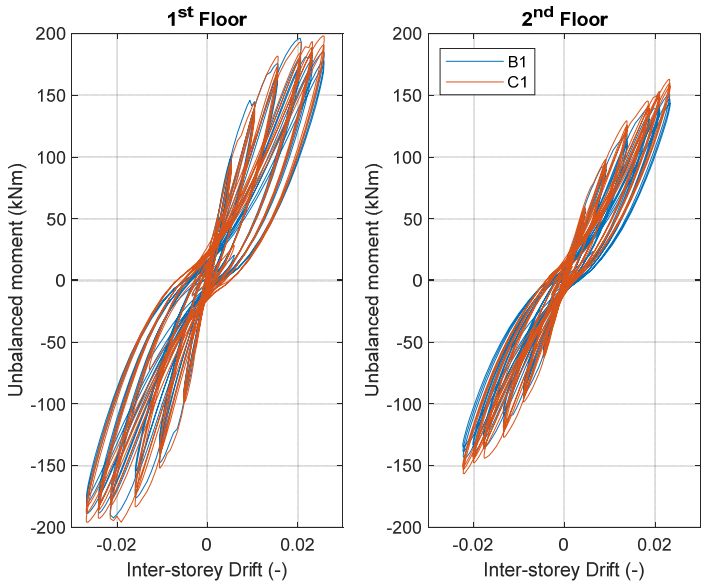

Figure 7.16 Unbalanced moment vs Inter-Storey drift, connections B1 C1.

For the 1st floor, regarding the south side, the connections B3 and C3 showed a 17 kNm difference in positive inter-storey drift and 13 kNm for the negative one; for the 2nd floor, 9 kNm as the positive value of the inter-storey drift and 33 kNm for the negative.

On both floors, the connection C3 reached the highest values of unbalanced moment for the positive inter-storey drift and the lowest for the negative inter-storey drift. This can be interpreted as the effect of the concentrated reinforcement.

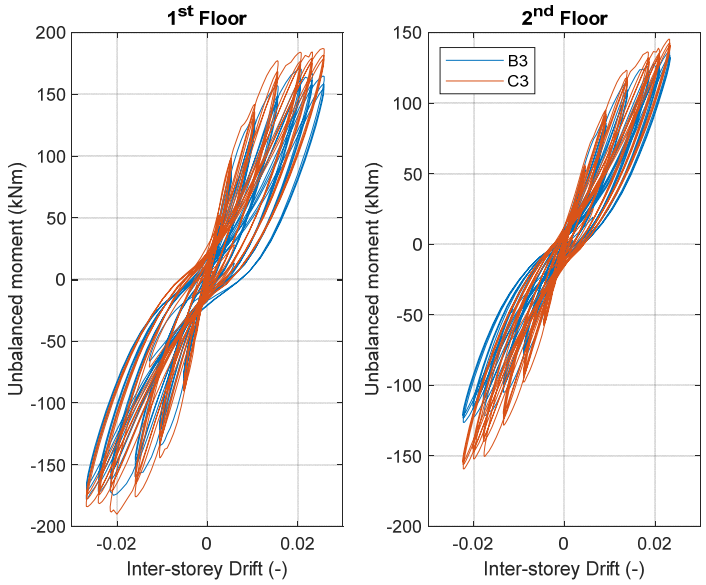

Figure 7.17 Unbalanced moment vs Inter-Storey drift, connections B3 C3.

LATERAL CONNECTIONS PLACED ALONG THE SHORT SIDE: A2 D2

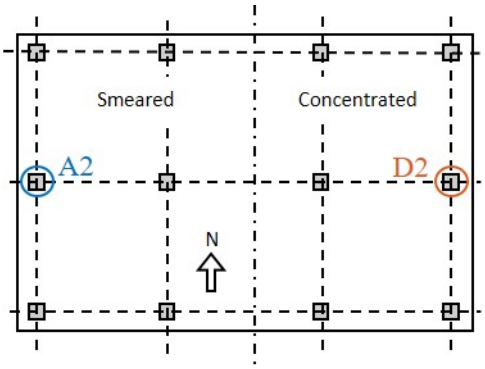

Figure 7.18 Lateral short side connections in plan.

As for the corner connections, the lateral A2 and D2 the drift sign was also inverted in order to make the comparison between the two asymmetric connections. To draw a comparison between the connections located in the two halves of the slab, due to their asymmetry it was necessary to invert the drift sign of the connection D2.
On the 1st floor there was a different unbalanced moment response only for negative drift, for positive drift, the values of unbalanced moment for both the connections were almost the same.
The D2 connection in the 1st floor was the first one to record a punching failure for an inter-storey drift ratio of 2%. The connection A2 at comparable drift reached a different failure that will be further analysed in the following.
For the 2nd floor the difference in unbalanced moment response is evident for both the drift signs, more emphatically in the negative values of drift than in the positive ones.
The greater differences, both in positive and in negative values of unbalanced moments, revealed by the comparisons made in this section, are visible for the 2nd floor with 30 kNm difference in positive and 50 kNm in negative.
The D2 connection showed the largest unbalanced moment on the 2nd floor, with higher values of both positive and negative simultaneously.

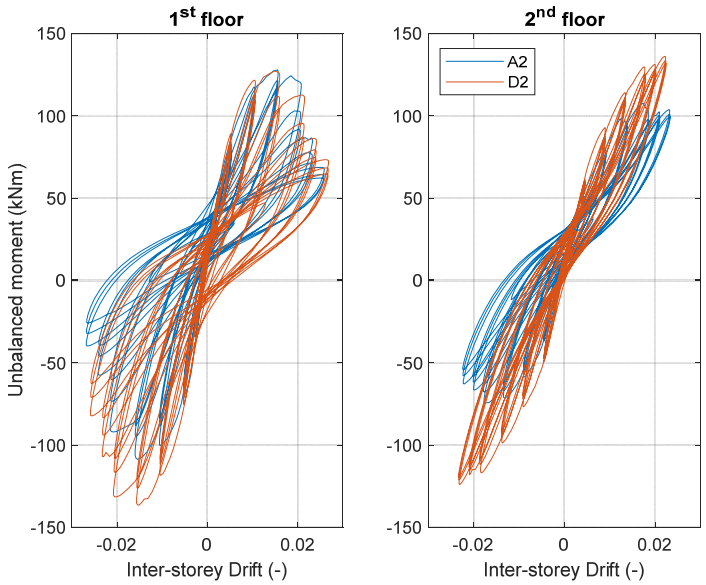

Figure 7.19 Unbalanced moment vs Inter-Storey drift, connections A2 D2.

INTERNAL CONNECTIONS: B2, C2

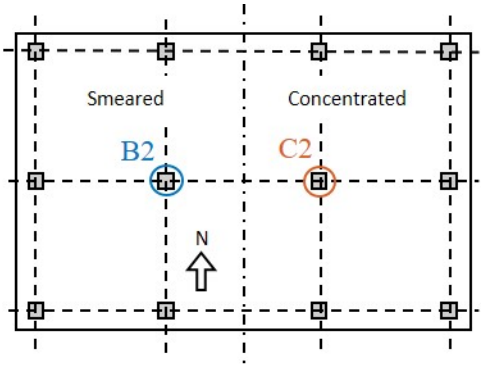

Figure 7.20 Internal connections in plan.

Lastly, the internal connections B2 and C2. The most significant difference was noted in the positive inter-storey drift of the 1st floor with 46 kNm differences between the two connections. For the 2nd floor the difference in unbalanced moment between the two connections was around 20 kNm.
The differences were fewer in the unbalanced moments for the negative value of the inter-storey drift, with 11 kNm for the 1st floor and 16 kNm for the 2nd.
Between the two connections, B2 outperformed C2 for both positive and negative values of unbalanced moment.

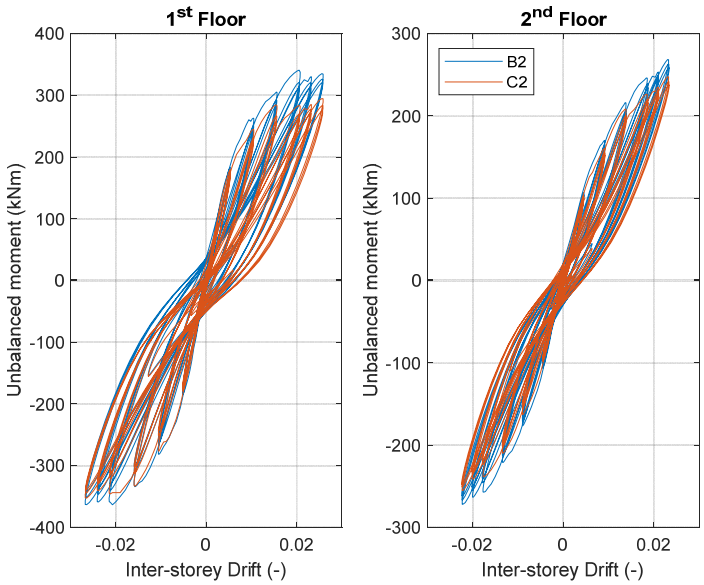

Figure 7.21 Unbalanced moment vs Inter-Storey drift, connections B2 C2.

In conclusion, in the eastward direction of the inter-storey drift, the connections with the highest and the lowest unbalanced moment were located in the west half of the slab on both floors, this was the part of the slab with the smeared longitudinal reinforcement and the highest additional gravity loading. These connections were the internal (B2) for the highest unbalanced moment for both floors, and the corner connections for the lowest, A3 in the south for the 1st floor and A1 in the north for the 2nd.

Regarding the westward values of the inter-storey drift, the behaviour was similar to that of the previous one, but the connection which reported the highest value of unbalanced moment was in the east half of the slab, with concentrated longitudinal reinforcement and less additional gravity loading, while the connection which had the lowest values was in the other side.

In Figure 7.22 a summary of the results is reported, the connections with the maximum and minimum values of unbalanced moment for each floor were hooped and near to the name of the connection the sign of the drift was written (+ = positive and – = negative) and the maximum or minimum value reached (> = maximum value, < = minimum value).

Blue was used for the half of the slab with less longitudinal reinforcement and red for the other half with the most longitudinal reinforcement. This was configured for the 1st (Figure 1.33 a) and the 2nd (Figure 1.33 b) floor separately.

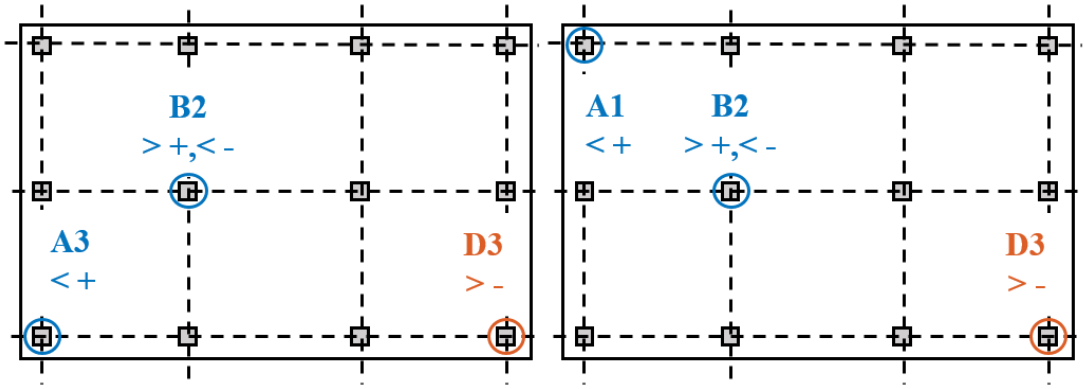

Figure 7.22 Summary of the maximum and minimum unbalanced moment in the connections for the a) 1st floor and b) 2nd floor, Test Cyc-1 (f02).

7.4.2 Stiffness Deterioration

The stiffness degradation was computed to describe the damage of each slab-column connection on each floor of the building. As done for the global analysis, the stiffness deterioration was calculated with reference to the first value of the secant stiffness of the first test carried out, Seis-SLS. The procedure followed, the equations used and the graphs set up are reported in Chapter 5.3.

The stiffness deterioration ratio versus the inter-storey drift is reported in Figure 7.23, whereas in Figure 7.24 the negative drift branches were reported with the absolute value to display the symmetry.

In all the connections located on the perimeter of the structure, edge (A2, B3, C3, D2, C1 and B1) and corner (A1, A3, D1 and D3) typology, the residual stiffness of the 1st floor was greater than that of the 2nd one.

For the lateral short side connections, edge (A2 and D2) and corner (A1, A3, D1 and D3) typology, this difference was greater than in the lateral connections in the long side (B1, C1, B3 and C3).

The internal connections B2 and C2 are the only two for which the 2nd floor had a stiffness deterioration greater than that on the 1st floor.

With the two internal connections the 2nd floor has higher stiffness deterioration than the 1st one from the start of the experimental campaign, whereas in all the other edge and corner connections the tendency differs. During the two seismic tests, the values for the two floors are the same, or sometimes the 2nd one is superior to the 1st one, then after an inter-storey drift ratio of 0.5%, the 1st floor overtakes the 2nd one.

From the stiffness analysis reported in Figure 7.25 it is possible to observe that the stiffness of the 1st floor was greater than that of the 2nd one, in all the connections. This difference was probably due to the local confinement and to the columns configuration effects. The loss of the local confinement was higher for the edge and corner slab-column connection typologies of the 2nd floor because they had one or two free edges and an entire column below, and a half column above. The internal slab-column connection typology on the 2nd floor, being well confined, was subject

to a minor effect by the presence of a half column above.
The two internal connections B2 and C2 in the 1st floor, recorded the highest initial stiffness value 7 kNmm and 6.5 kNmm respectively. These high values could have influenced the stiffness deterioration and have led to the behaviour observed in Figure 7.23 and Figure 7.24.
The differences between the response of the connections on the short or long side of the structure depended on the direction of the loading. This is more visible in Figure 7.24 in which in the connections located on the short side of the structure (alignment A and D) subjected to torsion, there is an evident asymmetry between the two directions of loading. On the contrary, there is a perfect symmetry in the connections located on the long side of the structure and subjected to bending.

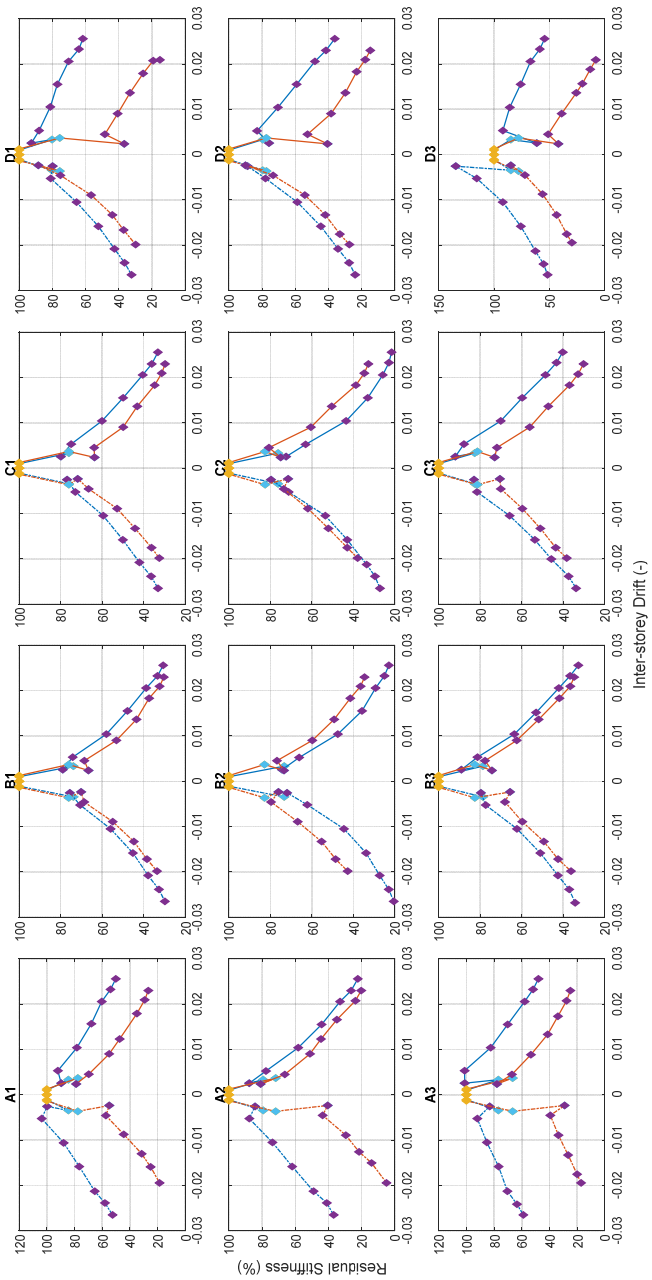

Figure 7.23 Residual stiffness vs I-S drift ratio. Stiffness deterioration ratio Test Seis-SLS (e03) +Seis-ULS (e06) +Cyc-1 (f02). Line: blue for the 1st floor, red for the 2nd, continuous, westward loading, dashed, eastward loading. Points: yellow, test Seis-SLS (e03), light blue, test Seis-ULS (e06), purple, test Cyc-1 (f02).

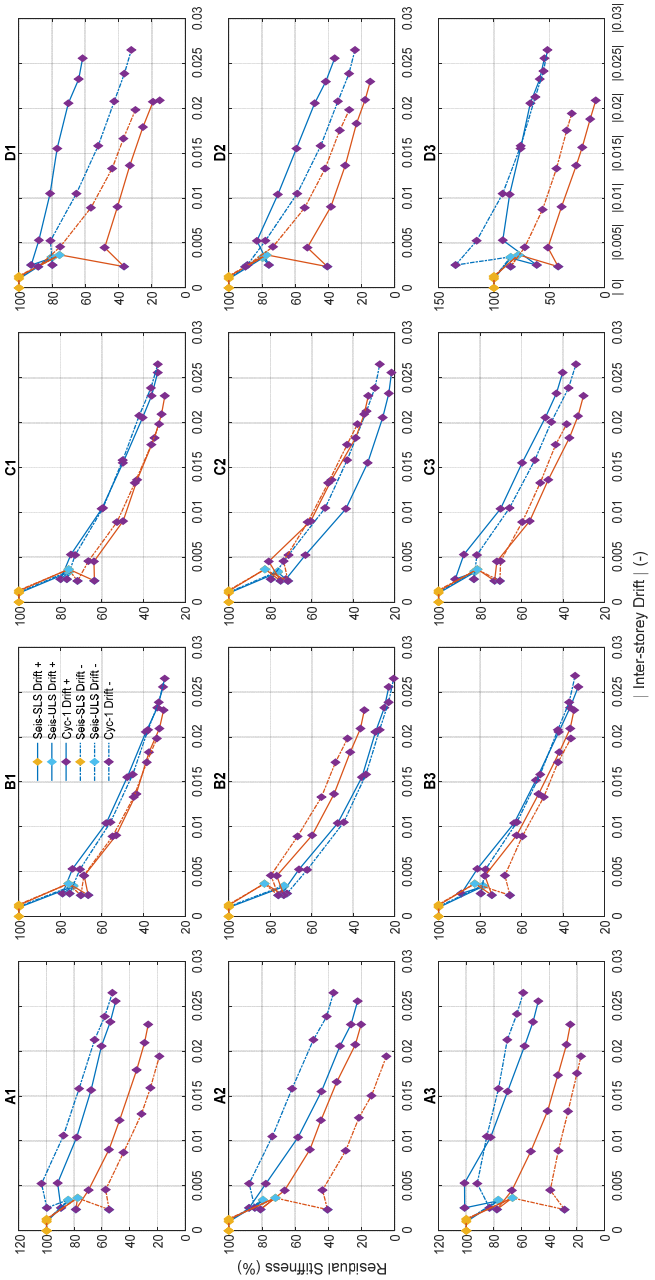

Figure 7.24 Residual stiffness vs I-S drift ratio. Stiffness deterioration ratio absolute value Test Seis-SLS (e03) +Seis-ULS (e06) +Cyc-1 (f02). Line: blue for the 1st floor, red for the 2nd, continuous, westward loading, dashed, eastward loading. Points: yellow, test Seis-SLS (e03), light blue, test Seis-ULS (e06), purple, test Cyc-1 (f02).

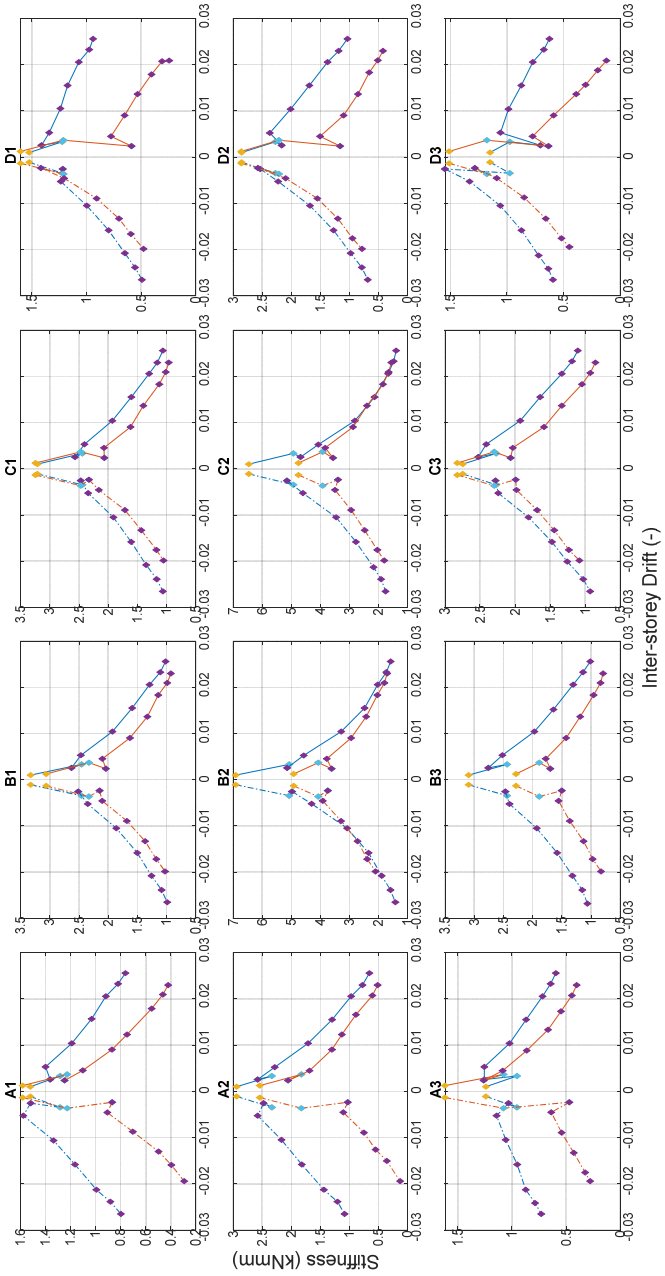

Figure 7.25 Stiffness vs I-S drift ratio, Test Seis-SLS (e03) +Seis-ULS (e06) +Cyc-1 (f02). Line: blue for the 1st floor, red for the 2nd, continuous, westward loading, dashed, eastward loading. Points: yellow, test Seis-SLS (e03), light blue, test Seis-ULS (e06), purple, test Cyc-1 (f02).

7.4.3 DUCTILITY AND ULTIMATE DRIFT CAPACITY

The ductility of each of the twenty-four slab-column connections (twelve for each floor) is reported following the methodology reported in Chapter 5.2.3 together with the equations used and the graphs set up.
As for the global analysis, also for the local one, all the four percentages of the residual resistance 80%, 85%, 90% and 95% are analysed and reported in the following Figure 7.26, Figure 7.27, Figure 7.28 and Figure 7.29.
For each of these, the graph representing the analysed percentage (point-dashed line, blue for the 1st floor and red for the 2nd) is reported and where conditions to reach failure are respected, a red continuous line indicates the failure force and the corresponding displacement.
After the graphs, a table with the shear and the corresponding drift of the three characteristic points (Limit, Yielding and Failure) is reported with all the column connections (Table 7.7, Table 7.9, Table 7.11 and Table 7.13).
The last line for each floor reports the displacement ductility factor, μ.
For each of the four percentage drops in loading resistance, a table with the displacement ductility factor for the failed connections only, is reported (Table 7.6, Table 7.8, Table 7.10 and Table 7.12).
Finally, a summary outlining of the connections failure is reported (Figure 7.30) together with a summary table for the maximum unbalanced moment and the corresponding inter-storey drift ratio for all the connections (Table 7.14) and a summary of all the displacement ductility factor for all the four percentage drops in loading resistance and all the failed connections (Table 7.15).

80% OF THE MAXIMUM UNBALANCED MOMENT

The first connections to fail were those on the 1st floor, on the short side (A and D), parallel to the reaction wall and orthogonal to the applied forces (Figure 7.26). The two central connections on the short side, A2 and D2 failed both in positive and in negative drifts, whereas the edge D1 only in negative and D3 only in positive (Table 7.7). No failures were recorded for the 2nd floor.
In the failed connections (A2, D1, D2 and D3), all the ductility factor μ factors for the negative drift value resulted higher than those of the positive drift (Table 7.6).

Table 7.6 Displacement ductility factor for the failed connections at 80%, Test Cyc-1 (f02).

	Floor	Drift	A2	D1	D2	D3
μ (-)	1st	Positive	2.14	-	1.97	2.21
		Negative	2.19	2.66	2.63	-

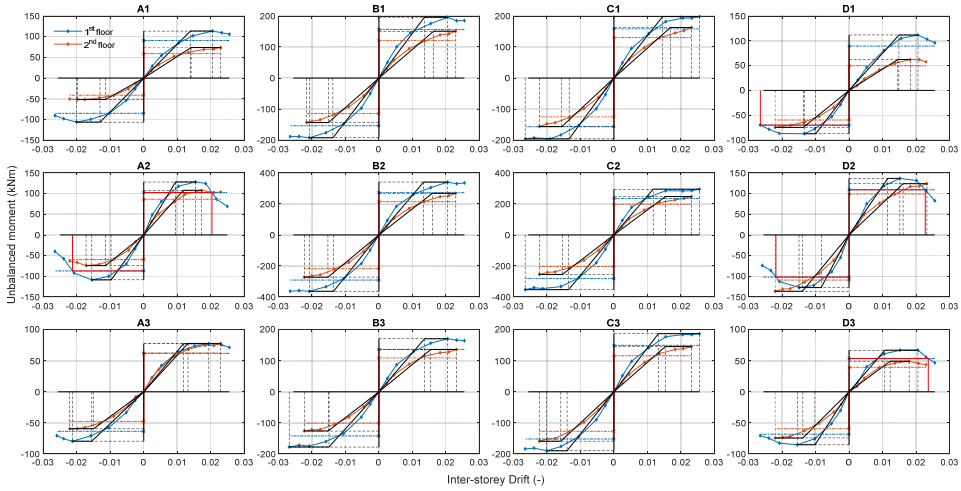

Figure 7.26 Unbalanced Moment vs Inter-story drift ratio. Definition of the yielding and failure at 80% points for all the connections, Test Cyc-1 (f02). Line: blue for the 1st floor, red for the 2nd. Horizontal dashed line, force at failure. Vertical red line, drift at failure.

Table 7.7 Unbalanced moment drift at limit, yielding and failure at 80% for all the connections, Test Cyc-1 (f02). Yellow highlighted cells, failed connections.

		Connections	A1	A2	A3	B1	B2	B3	C1	C2	C3	D1	D2	D3
			1	2	3	4	5	6	7	8	9	10	11	12
1 Floor positive	Limit point	UM Max (kNm)	113.64	127.96	77.41	196.16	340.74	170.96	198.16	294.59	187.08	111.77	136.52	67.09
		Drift (-)	0.021	0.016	0.019	0.021	0.021	0.021	0.026	0.026	0.026	0.021	0.015	0.021
	Yielding point	UM Yielding (kNm)	113.64	127.96	77.41	196.16	340.74	170.96	198.16	294.59	187.08	111.77	136.52	67.09
		Drift (-)	0.014	0.010	0.012	0.014	0.013	0.014	0.015	0.012	0.013	0.015	0.012	0.011
	Failure point	0.80 UM Max (kNm)	90.91	102.37	61.93	156.93	272.59	136.77	158.53	235.67	149.66	89.42	109.22	53.67
		Drift DRu (-)		**0.020**	-	-	-	-	-	-	-		**0.023**	**0.024**
		μ (-)	-	2.14	-	-	-	-	-	-	-	-	1.97	2.21
1 Floor negative	Limit point	UM Max (kNm)	-106.46	-108.63	-79.52	-192.37	-363.46	-178.00	-195.88	-352.43	-190.12	-87.08	-127.19	-85.42
		Drift (-)	-0.020	-0.015	-0.021	-0.021	-0.021	-0.027	-0.027	-0.027	-0.020	-0.013	-0.015	-0.015
	Yielding point	UM Yielding (kNm)	-106.46	-108.63	-79.52	-192.37	-363.46	-178.00	-195.88	-352.43	-190.12	-87.08	-127.19	-85.42
		Drift (-)	-0.013	-0.010	-0.015	-0.014	-0.014	-0.015	-0.013	-0.014	-0.014	-0.010	-0.008	-0.010
	Failure point	0.80 UM Max (kNm)	-85.17	-86.91	-63.62	-153.89	-290.77	-142.40	-156.71	-281.94	-152.10	-69.67	-101.75	-68.33
		Drift DRu (-)	-	**-0.021**	-	-	-	-	-	-	-	**-0.026**	**-0.022**	-
		μ (-)	-	2.19	-	-	-	-	-	-	-	2.66	2.63	-
2 Floor positive	Limit point	UM Max (kNm)	73.83	107.81	78.03	150.92	268.35	136.50	162.88	247.48	145.31	62.22	123.81	49.40
		Drift (-)	0.023	0.017	0.023	0.023	0.023	0.023	0.023	0.023	0.023	0.018	0.023	0.018
	Yielding point	UM Yielding (kNm)	73.83	107.81	78.03	150.92	268.35	136.50	162.88	247.48	145.31	62.22	123.81	49.40
		Drift (-)	0.014	0.012	0.013	0.016	0.016	0.015	0.017	0.015	0.015	0.015	0.016	0.012
	Failure point	0.80 UM Max (kNm)	59.07	86.25	62.42	120.74	214.68	109.20	130.31	197.99	116.25	49.77	99.05	39.52
		Drift DRu (-)	-	-	-	-	-	-	-	-	-	-	-	-
		μ (-)	-	-	-	-	-	-	-	-	-	-	-	-
2 Floor negative	Limit point	UM Max (kNm)	-51.92	-74.34	-59.62	-143.34	-271.87	-126.27	-156.41	-255.07	-159.20	-74.40	-136.17	-74.36
		Drift (-)	-0.020	-0.017	-0.022	-0.022	-0.022	-0.022	-0.022	-0.022	-0.022	-0.022	-0.022	-0.022
	Yielding point	UM Yielding (kNm)	-51.92	-74.34	-59.62	-143.34	-271.87	-126.27	-156.41	-255.07	-159.20	-74.40	-136.17	-74.36
		Drift (-)	-0.011	-0.011	-0.015	-0.015	-0.015	-0.015	-0.016	-0.015	-0.016	-0.014	-0.014	-0.014
	Failure point	0.80 UM Max (kNm)	-41.53	-59.48	-47.70	-114.67	-217.50	-101.02	-125.13	-204.05	-127.36	-59.52	-108.94	-59.49
		Drift DRu (-)	-	-	-	-	-	-	-	-	-	-	-	-
		μ (-)	-	-	-	-	-	-	-	-	-	-	-	-

85% OF THE MAXIMUM UNBALANCED MOMENT

For the 85% of the maximum unbalanced moment, the connections that failed were the same as those of the previous section (Figure 7.26) with the addition of one on the short edge on the north-west side, A1 and the central short west side, A2, on the 2nd floor (Figure 7.27). The drift at failure are shown in (Table 7.9).
The 2nd floor displacement ductility factor was lower than that of the 1st floor. For the 1st floor the values trend followed that of the previous analysed percentage, 80%. For the positive drift, all the connections had a similar μ, whereas for the negative one the connections on the east side had a higher ductility factor higher compared to those on the west side (Table 7.8).

Table 7.8 Displacement ductility factor for the failed connections at 85%, Test Cyc-1 (f02).

	Floor	Drift	A1	A2	D1	D2	D3
μ (-)	1st	Positive	-	2.08	-	1.90	2.13
		Negative	2.03	2.13	2.53	2.55	2.47
μ (-)	2nd	Positive	-	-	-	-	-
		Negative	-	1.92	-	-	-

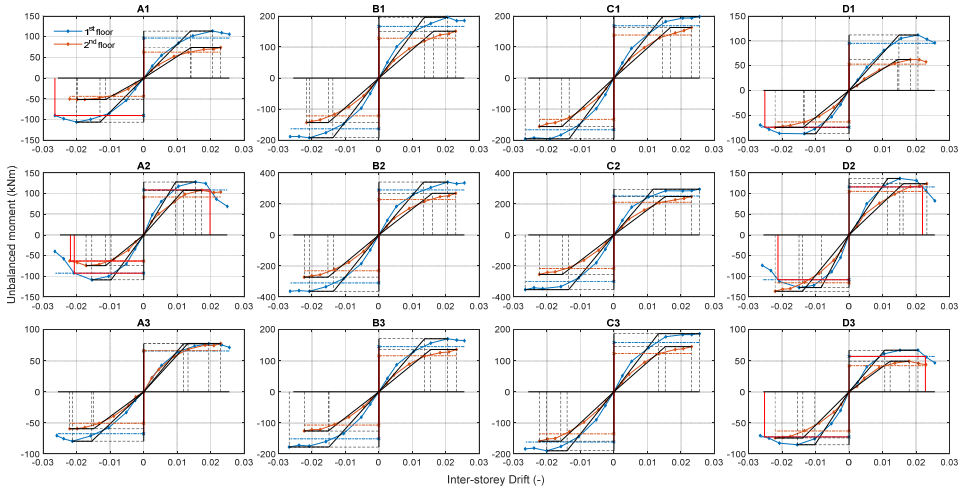

Figure 7.27 Unbalanced Moment vs Inter-story drift ratio. Definition of the yielding and failure at 85% points for all the connections, Test Cyc-1 (f02). Line: blue for the 1st floor, red for the 2nd. Horizontal dashed line, force at failure. Vertical red line, drift at failure.

Table 7.9 Unbalanced moment drift at limit, yielding and failure at 85% for all the connections, Test Cyc-1 (f02). Yellow highlighted cells, failed connections.

		Connections	A1	A2	A3	B1	B2	B3	C1	C2	C3	D1	D2	D3
			1	2	3	4	5	6	7	8	9	10	11	12
1 Floor positive	Limit point	UM Max (kNm)	113.64	127.96	77.41	196.16	340.74	170.96	198.16	294.59	187.08	111.77	136.52	67.09
		Drift (-)	0.021	0.016	0.019	0.021	0.021	0.021	0.026	0.026	0.026	0.021	0.015	0.021
	Yielding point	UM Yielding (kNm)	113.64	127.96	77.41	196.16	340.74	170.96	198.16	294.59	187.08	111.77	136.52	67.09
		Drift (-)	0.014	0.010	0.012	0.014	0.013	0.014	0.015	0.012	0.013	0.015	0.012	0.011
	Failure point	0.85 UM Max (kNm)	96.59	108.77	65.80	166.73	289.63	145.32	168.44	250.40	159.01	95.00	116.04	57.03
		Drift DRu (-)		**0.020**	-	-	-	-	-	-	-		**0.022**	**0.023**
		μ (-)	-	2.08	-	-	-	-	-	-	-	-	1.90	2.13
1 Floor negative	Limit point	UM Max (kNm)	-106.46	-108.63	-79.52	-192.37	-363.46	-178.00	-195.88	-352.43	-190.12	-87.08	-127.19	-85.42
		Drift (-)	-0.020	-0.015	-0.021	-0.021	-0.021	-0.027	-0.027	-0.027	-0.020	-0.013	-0.015	-0.015
	Yielding point	UM Yielding (kNm)	-106.46	-108.63	-79.52	-192.37	-363.46	-178.00	-195.88	-352.43	-190.12	-87.08	-127.19	-85.42
		Drift (-)	-0.013	-0.010	-0.015	-0.014	-0.014	-0.015	-0.013	-0.014	-0.014	-0.010	-0.008	-0.010
	Failure point	0.85 UM Max (kNm)	-90.49	-92.34	-67.59	-163.51	-308.94	-151.30	-166.50	-299.56	-161.60	-74.02	-108.11	-72.60
		Drift DRu (-)	**-0.026**	**-0.021**	-	-	-	-	-	-	-	**-0.025**	**-0.021**	**-0.025**
		μ (-)	2.03	2.13	-	-	-	-	-	-	-	2.53	2.55	2.47
2 Floor positive	Limit point	UM Max (kNm)	73.83	107.81	78.03	150.92	268.35	136.50	162.88	247.48	145.31	62.22	123.81	49.40
		Drift (-)	0.023	0.017	0.023	0.023	0.023	0.023	0.023	0.023	0.023	0.018	0.023	0.018
	Yielding point	UM Yielding (kNm)	73.83	107.81	78.03	150.92	268.35	136.50	162.88	247.48	145.31	62.22	123.81	49.40
		Drift (-)	0.014	0.012	0.013	0.016	0.016	0.015	0.017	0.015	0.015	0.015	0.016	0.012
	Failure point	0.85 UM Max (kNm)	62.76	91.64	66.32	128.28	228.09	116.03	138.45	210.36	123.52	52.89	105.24	41.99
		Drift DRu (-)	-	-	-	-	-	-	-	-	-	-	-	-
		μ (-)	-	-	-	-	-	-	-	-	-	-	-	-
2 Floor negative	Limit point	UM Max (kNm)	-51.92	-74.34	-59.62	-143.34	-271.87	-126.27	-156.41	-255.07	-159.20	-74.40	-136.17	-74.36
		Drift (-)	-0.020	-0.017	-0.022	-0.022	-0.022	-0.022	-0.022	-0.022	-0.022	-0.022	-0.022	-0.022
	Yielding point	UM Yielding (kNm)	-51.92	-74.34	-59.62	-143.34	-271.87	-126.27	-156.41	-255.07	-159.20	-74.40	-136.17	-74.36
		Drift (-)	-0.011	-0.011	-0.015	-0.015	-0.015	-0.015	-0.016	-0.015	-0.016	-0.014	-0.014	-0.014
	Failure point	Drift DRu (-)	-44.13	-63.19	-50.68	-121.84	-231.09	-107.33	-132.95	-216.81	-135.32	-63.24	-115.75	-63.21
		Drift (-)		**-0.022**	-	-	-	-	-	-	-	-	-	-
		μ (-)	-	1.92	-	-	-	-	-	-	-	-	-	-

90% OF THE MAXIMUM UNBALANCED MOMENT

For the 90% of the maximum unbalanced moment, the following connections are added to the previous failed connections: the southeast edge one, A3 for the negative drift and the edge south-west, D3 in the 2nd floor and the D1 in the 1st floor for the positive (Figure 7.28).
The drift values are of the same order of magnitude for the previous percentage drop, with slightly lower values (Table 7.11).
Here too, the 2nd floor displacement ductility factor is lower than those of the 1st floor. For the 1st floor the values trend follows that of the previous analysed percentages. For the positive drift, all the connections have a similar μ, whereas for the negative one the connections on the east side have a displacement ductility factor higher than those on the west side (Table 7.10).

Table 7.10 Displacement ductility factor for the failed connections at 90%, Test Cyc-1 (f02).

	Floor	Drift	A1	A2	A3	D1	D2	D3
μ (-)	1st	Positive	-	2.02	-	1.62	1.83	2.06
		Negative	1.89	1.95	1.65	2.39	2.41	2.26
μ (-)	2nd	Positive	-	-	-	-	-	-
		Negative	-	1.73		-	-	-

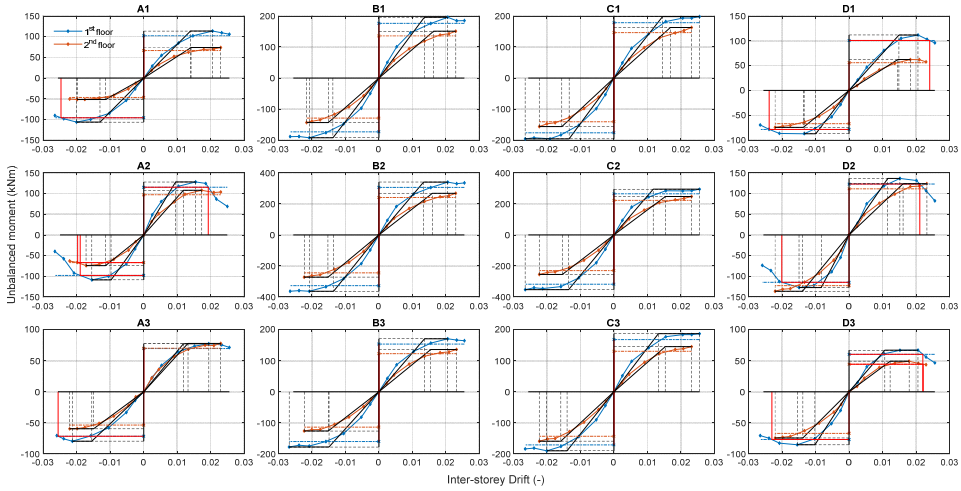

Figure 7.28 Unbalanced Moment vs Inter-story drift ratio. Definition of the yielding and failure at 90% points for all the connections, Test Cyc-1 (f02). Line: blue for the 1st floor, red for the 2nd. Horizontal dashed line, force at failure. Vertical red line, drift at failure.

Table 7.11 Unbalanced moment drift at limit, yielding and failure at 90% for all the connections, Test Cyc-1 (f02). Yellow highlighted cells, failed connections.

		Connections	A1	A2	A3	B1	B2	B3	C1	C2	C3	D1	D2	D3
			1	2	3	4	5	6	7	8	9	10	11	12
1 Floor positive	Limit point	UM Max (kNm)	113.64	127.96	77.41	196.16	340.74	170.96	198.16	294.59	187.08	111.77	136.52	67.09
		Drift (-)	0.021	0.016	0.019	0.021	0.021	0.021	0.026	0.026	0.026	0.021	0.015	0.021
	Yielding point	UM Yielding (kNm)	113.64	127.96	77.41	196.16	340.74	170.96	198.16	294.59	187.08	111.77	136.52	67.09
		Drift (-)	0.014	0.010	0.012	0.014	0.013	0.014	0.015	0.012	0.013	0.015	0.012	0.011
	Failure point	0.90 UM Max (kNm)	102.27	115.17	69.67	176.54	306.67	153.87	178.35	265.13	168.37	100.59	122.87	60.38
		Drift DRu (-)	-	**0.019**	-	-	-	-	-	-	-	**0.024**	**0.021**	**0.022**
		μ (-)	-	2.02	-	-	-	-	-	-	-	1.62	1.83	2.06
1 Floor negative	Limit point	UM Max (kNm)	-106.46	-108.63	-79.52	-192.37	-363.46	-178.00	-195.88	-352.43	-190.12	-87.08	-127.19	-85.42
		Drift (-)	-0.020	-0.015	-0.021	-0.021	-0.021	-0.027	-0.027	-0.027	-0.020	-0.013	-0.015	-0.015
	Yielding point	UM Yielding (kNm)	-106.46	-108.63	-79.52	-192.37	-363.46	-178.00	-195.88	-352.43	-190.12	-87.08	-127.19	-85.42
		Drift (-)	-0.013	-0.010	-0.015	-0.014	-0.014	-0.015	-0.013	-0.014	-0.014	-0.010	-0.008	-0.010
	Failure point	0.90 UM Max (kNm)	-95.81	-97.77	-71.57	-173.13	-327.12	-160.20	-176.30	-317.18	-171.11	-78.38	-114.47	-76.88
		Drift DRu (-)	**-0.025**	**-0.019**	**-0.026**	-	-	-	-	-	-	**-0.024**	**-0.020**	**-0.023**
		μ (-)	1.89	1.95	1.65	-	-	-	-	-	-	2.39	2.41	2.26
2 Floor positive	Limit point	UM Max (kNm)	73.83	107.81	78.03	150.92	268.35	136.50	162.88	247.48	145.31	62.22	123.81	49.40
		Drift (-)	0.023	0.017	0.023	0.023	0.023	0.023	0.023	0.023	0.023	0.018	0.023	0.018
	Yielding point	UM Yielding (kNm)	73.83	107.81	78.03	150.92	268.35	136.50	162.88	247.48	145.31	62.22	123.81	49.40
		Drift (-)	0.014	0.012	0.013	0.016	0.016	0.015	0.017	0.015	0.015	0.015	0.016	0.012
	Failure point	0.90 UM Max (kNm)	66.45	97.03	70.23	135.83	241.51	122.85	146.60	222.74	130.78	56.00	111.43	44.46
		Drift DRu (-)	-	-	-	-	-	-	-	-	-	-	-	**0.022**
		μ (-)	-	-	-	-	-	-	-	-	-	-	-	1.80
2 Floor negative	Limit point	UM Max (kNm)	-51.92	-74.34	-59.62	-143.34	-271.87	-126.27	-156.41	-255.07	-159.20	-74.40	-136.17	-74.36
		Drift (-)	-0.020	-0.017	-0.022	-0.022	-0.022	-0.022	-0.022	-0.022	-0.022	-0.022	-0.022	-0.022
	Yielding point	UM Yielding (kNm)	-51.92	-74.34	-59.62	-143.34	-271.87	-126.27	-156.41	-255.07	-159.20	-74.40	-136.17	-74.36
		Drift (-)	-0.011	-0.011	-0.015	-0.015	-0.015	-0.015	-0.016	-0.015	-0.016	-0.014	-0.014	-0.014
	Failure point	0.90 UM Max (kNm)	-46.72	-66.91	-53.66	-129.00	-244.68	-113.64	-140.77	-229.56	-143.28	-66.96	-122.56	-66.92
		Drift DRu (-)	-	**-0.020**	-	-	-	-	-	-	-	-	-	-
		μ (-)	-	1.73	-	-	-	-	-	-	-	-	-	-

95% OF THE MAXIMUM UNBALANCED MOMENT

Finally, the last percentage of the maximum unbalanced moment, 95%. The lateral North long side, B1, the edge of the short side A1 and A3 for the 1st floor and the edge North-west short side D1 and the central short west side A2 for the 2nd floor, all calculated for the positive drift, are added to the previous failed connections (Figure 7.29).

The drift values are of the same order of magnitude as those of the previous percentage drop, with slightly lower values when compared to those (Table 7.13).

Here too, the 2nd floor displacement ductility factor is lower than that of the 1st floor, except for the positive drift in the connection D1 in which the 2nd floor (μ=1.53) is slightly higher than the 1st floor drift (μ=1.50).

All the connections, for the 1st and the 2nd floor, for the positive and the negative drifts, have a similar μ, for the negative drift, the connections in the east side have displacement ductility factors higher than those in the west side (Table 7.12).

Table 7.12 Displacement ductility factor for the failed connections at 95%, Test Cyc-1 (f02).

	Floor	Drift	A1	A2	A3	B1	D1	D2	D3
μ (-)	1st	Positive	1.73	1.96	2.06	1.68	1.50	1.76	1.99
		Negative	1.73	1.77	1.54	-	2.23	2.11	2.10
μ (-)	2nd	Positive	-	1.77	-	-	1.53	-	1.61
		Negative	-	1.62	-	-	-	-	-

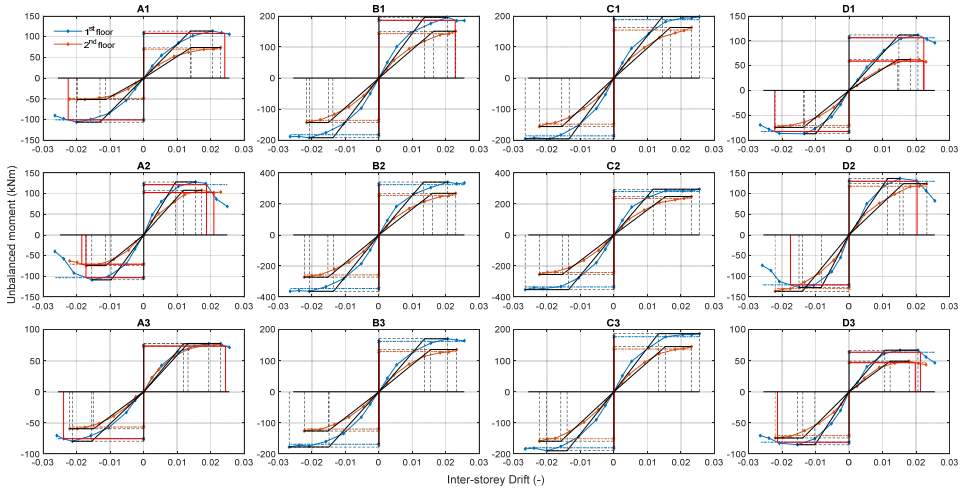

Figure 7.29 Unbalanced Moment vs Inter-story drift ratio. Definition of the yielding and failure at 95% points for all the connections, Test Cyc-1 (f02). Line: blue for the 1st floor, red for the 2nd. Horizontal dashed line, force at failure. Vertical red line, drift at failure.

Table 7.13 Unbalanced moment drift at limit, yielding and failure at 95% for all the connections, Test Cyc-1 (f02). Yellow highlighted cells, failed connections.

		Connections	A1	A2	A3	B1	B2	B3	C1	C2	C3	D1	D2	D3
			1	2	3	4	5	6	7	8	9	10	11	12
1 Floor positive	Limit point	UM Max (kNm)	113.64	127.96	77.41	196.16	340.74	170.96	198.16	294.59	187.08	111.77	136.52	67.09
		Drift (-)	0.021	0.016	0.019	0.021	0.021	0.021	0.026	0.026	0.026	0.021	0.015	0.021
	Yielding point	UM Yielding (kNm)	113.64	127.96	77.41	196.16	340.74	170.96	198.16	294.59	187.08	111.77	136.52	67.09
		Drift (-)	0.014	0.010	0.012	0.014	0.013	0.014	0.015	0.012	0.013	0.015	0.012	0.011
	Failure point	0.95 UM Max (kNm)	107.95	121.57	73.54	186.35	323.70	162.42	188.25	279.86	177.72	106.18	129.69	63.74
		Drift DRu (-)	**0.024**	**0.019**	**0.024**	**0.023**	-	-	-	-	-	**0.022**	**0.020**	**0.021**
		μ (-)	1.73	1.96	2.06	1.68	-	-	-	-	-	1.50	1.76	1.99
1 Floor negative	Limit point	UM Max (kNm)	-106.46	-108.63	-79.52	-192.37	-363.46	-178.00	-195.88	-352.43	-190.12	-87.08	-127.19	-85.42
		Drift (-)	-0.020	-0.015	-0.021	-0.021	-0.021	-0.027	-0.027	-0.027	-0.020	-0.013	-0.015	-0.015
	Yielding point	UM Yielding (kNm)	-106.46	-108.63	-79.52	-192.37	-363.46	-178.00	-195.88	-352.43	-190.12	-87.08	-127.19	-85.42
		Drift (-)	-0.013	-0.010	-0.015	-0.014	-0.014	-0.015	-0.013	-0.014	-0.014	-0.010	-0.008	-0.010
	Failure point	0.95 UM Max (kNm)	-101.13	-103.20	-75.55	-182.75	-345.29	-169.10	-186.09	-334.80	-180.62	-82.73	-120.83	-81.15
		Drift DRu (-)	**-0.023**	**-0.017**	**-0.024**	-	-	-	-	-	-	**-0.022**	**-0.018**	**-0.021**
		μ (-)	1.73	1.77	1.54	-	-	-	-	-	-	2.23	2.11	2.10
2 Floor positive	Limit point	UM Max (kNm)	73.83	107.81	78.03	150.92	268.35	136.50	162.88	247.48	145.31	62.22	123.81	49.40
		Drift (-)	0.023	0.017	0.023	0.023	0.023	0.023	0.023	0.023	0.023	0.018	0.023	0.018
	Yielding point	UM Yielding (kNm)	73.83	107.81	78.03	150.92	268.35	136.50	162.88	247.48	145.31	62.22	123.81	49.40
		Drift (-)	0.014	0.012	0.013	0.016	0.016	0.015	0.017	0.015	0.015	0.015	0.016	0.012
	Failure point	0.95 UM Max (kNm)	70.14	102.42	74.13	143.37	254.93	129.68	154.74	235.11	138.05	59.11	117.62	46.93
		Drift DRu (-)		**0.021**	-	-	-	-	-	-	-	**0.022**		**0.020**
		μ (-)	-	1.77	-	-	-	-	-	-	-	1.53	-	1.61
2 Floor negative	Limit point	UM Max (kNm)	-51.92	-74.34	-59.62	-143.34	-271.87	-126.27	-156.41	-255.07	-159.20	-74.40	-136.17	-74.36
		Drift (-)	-0.020	-0.017	-0.022	-0.022	-0.022	-0.022	-0.022	-0.022	-0.022	-0.022	-0.022	-0.022
	Yielding point	UM Yielding (kNm)	-51.92	-74.34	-59.62	-143.34	-271.87	-126.27	-156.41	-255.07	-159.20	-74.40	-136.17	-74.36
		Drift (-)	-0.011	-0.011	-0.015	-0.015	-0.015	-0.015	-0.016	-0.015	-0.016	-0.014	-0.014	-0.014
	Failure point	0.95 UM Max (kNm)	-49.32	-70.63	-56.64	-136.17	-258.28	-119.96	-148.59	-242.31	-151.24	-70.68	-129.37	-70.64
		Drift DRu (-)		**-0.018**	-	-	-	-	-	-	-	-	-	-
		μ (-)	-	1.62	-	-	-	-	-	-	-	-	-	-

SUMMARY OF THE CONNECTIONS FAILURES

The Figure 7.30 schematically resumes the failures of the connections for all four load resistance drop rates. Failed connections are circled. As the percentage load resistance drop decreases, the number of the failed connections increases.

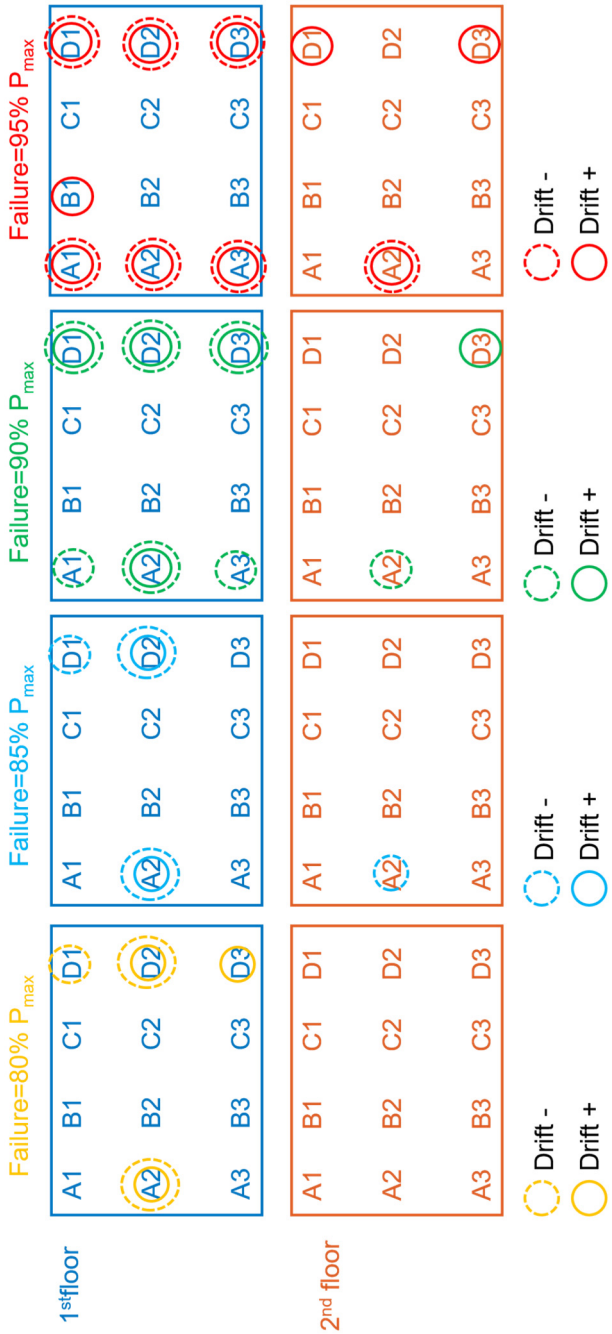

Figure 7.30 Connections failure for the analysed percentages of drop of the loading resistance, Test Cyc-1 (f02). Circled is the failed connection. Negative drift: westward loading, positive drift, eastward loading.

Table 7.14 reports the maximum unbalanced moment and the corresponding inter storey drift ratio for all connections, for both floors and both the loading directions, for each of the four percentages of the loading resistance drop.

Table 7.14 Maximum Unbalanced moment and corresponding inter story drift ratio for all the connections, Test Cyc-1.

	Connections	A1	A2	A3	B1	B2	B3	C1	C2	C3	D1	D2	D3
1 Floor positive	80%												
	UM Max (kNm)	113.64	127.96	77.41	196.16	340.74	170.96	198.16	294.59	187.08	111.77	136.52	67.09
	Drift (-)	0.021	0.016	0.019	0.021	0.021	0.021	0.026	0.026	0.026	0.021	0.015	0.021
	85%												
	UM Max (kNm)	113.64	127.96	77.41	196.16	340.74	170.96	198.16	294.59	187.08	111.77	136.52	67.09
	Drift (-)	0.021	0.016	0.019	0.021	0.021	0.021	0.026	0.026	0.026	0.021	0.015	0.021
	90%												
	UM Max (kNm)	113.64	127.96	77.41	196.16	340.74	170.96	198.16	294.59	187.08	111.77	136.52	67.09
	Drift (-)	0.021	0.016	0.019	0.021	0.021	0.021	0.026	0.026	0.026	0.021	0.015	0.021
	95%												
	UM Max (kNm)	113.64	127.96	77.41	196.16	340.74	170.96	198.16	294.59	187.08	111.77	136.52	67.09
	Drift (-)	0.021	0.016	0.019	0.021	0.021	0.021	0.026	0.026	0.026	0.021	0.015	0.021
1 Floor negative	80%												
	UM Max (kNm)	-106.46	-108.63	-79.52	-192.37	-363.46	-178.00	-195.88	-352.43	-190.12	-87.08	-127.19	-85.42
	Drift (-)	-0.020	-0.015	-0.021	-0.021	-0.021	-0.027	-0.027	-0.027	-0.020	-0.013	-0.015	-0.015
	85%												
	UM Max (kNm)	-106.46	-108.63	-79.52	-192.37	-363.46	-178.00	-195.88	-352.43	-190.12	-87.08	-127.19	-85.42
	Drift (-)	-0.020	-0.015	-0.021	-0.021	-0.021	-0.027	-0.027	-0.027	-0.020	-0.013	-0.015	-0.015
	90%												
	UM Max (kNm)	-106.46	-108.63	-79.52	-192.37	-363.46	-178.00	-195.88	-352.43	-190.12	-87.08	-127.19	-85.42
	Drift (-)	-0.020	-0.015	-0.021	-0.021	-0.021	-0.027	-0.027	-0.027	-0.020	-0.013	-0.015	-0.015
	95%												
	UM Max (kNm)	-106.46	-108.63	-79.52	-192.37	-363.46	-178.00	-195.88	-352.43	-190.12	-87.08	-127.19	-85.42
	Drift (-)	-0.020	-0.015	-0.021	-0.021	-0.021	-0.027	-0.027	-0.027	-0.020	-0.013	-0.015	-0.015
2 Floor positive	80%												
	UM Max (kNm)	73.83	107.81	78.03	150.92	268.35	136.50	162.88	247.48	145.31	62.22	123.81	49.40
	Drift (-)	0.023	0.017	0.023	0.023	0.023	0.023	0.023	0.023	0.023	0.018	0.023	0.018
	85%												
	UM Max (kNm)	73.83	107.81	78.03	150.92	268.35	136.50	162.88	247.48	145.31	62.22	123.81	49.40
	Drift (-)	0.023	0.017	0.023	0.023	0.023	0.023	0.023	0.023	0.023	0.018	0.023	0.018
	90%												
	UM Max (kNm)	73.83	107.81	78.03	150.92	268.35	136.50	162.88	247.48	145.31	62.22	123.81	49.40
	Drift (-)	0.023	0.017	0.023	0.023	0.023	0.023	0.023	0.023	0.023	0.018	0.023	0.018
	95%												
	UM Max (kNm)	73.83	107.81	78.03	150.92	268.35	136.50	162.88	247.48	145.31	62.22	123.81	49.40
	Drift (-)	0.023	0.017	0.023	0.023	0.023	0.023	0.023	0.023	0.023	0.018	0.023	0.018
2 Floor negative	80%												
	UM Max (kNm)	-51.92	-74.34	-59.62	-143.34	-271.87	-126.27	-156.41	-255.07	-159.20	-74.40	-136.17	-74.36
	Drift (-)	-0.020	-0.017	-0.022	-0.022	-0.022	-0.022	-0.022	-0.022	-0.022	-0.022	-0.022	-0.022
	85%												
	UM Max (kNm)	-51.92	-74.34	-59.62	-143.34	-271.87	-126.27	-156.41	-255.07	-159.20	-74.40	-136.17	-74.36
	Drift (-)	-0.020	-0.017	-0.022	-0.022	-0.022	-0.022	-0.022	-0.022	-0.022	-0.022	-0.022	-0.022
	90%												
	UM Max (kNm)	-51.92	-74.34	-59.62	-143.34	-271.87	-126.27	-156.41	-255.07	-159.20	-74.40	-136.17	-74.36
	Drift (-)	-0.020	-0.017	-0.022	-0.022	-0.022	-0.022	-0.022	-0.022	-0.022	-0.022	-0.022	-0.022
	95%												
	UM Max (kNm)	-51.92	-74.34	-59.62	-143.34	-271.87	-126.27	-156.41	-255.07	-159.20	-74.40	-136.17	-74.36
	Drift (-)	-0.020	-0.017	-0.022	-0.022	-0.022	-0.022	-0.022	-0.022	-0.022	-0.022	-0.022	-0.022

Regarding the displacement ductility factor, it can be observed that this increases as the considering percentage of load resistance decreases (Table 7.15).
The maximum value of the displacement ductility factor (μ=2.66), was recorded for the 20% drop of the loading resistance in the edge north-east connection D1 in the 1st floor, for the negative drift, whereas the minimum value (μ=1.50) was recorded in the same connection but for the positive drift and for 5% drop of the loading resistance.

Table 7.15 Displacement ductility factor at failure for the analysed percentages of drop of the loading resistance, Test Cyc-1 (f02).

	Floor	Drift	A1	A2	A3	B1	D1	D2	D3
80%									
μ (-)	1st	Positive	-	2.14	-	-	-	1.97	2.21
		Negative	-	2.19	-	-	2.66	2.63	-
85%									
μ (-)	1st	Positive	-	2.08	-	-	-	1.90	2.13
		Negative	2.03	2.13	-	-	2.53	2.55	2.47
μ (-)	2nd	Positive	-	-	-	-	-	-	-
		Negative	-	1.92	-	-	-	-	-
90%									
μ (-)	1st	Positive	-	2.02	-	-	1.62	1.83	2.06
		Negative	1.89	1.95	1.65	-	2.39	2.41	2.26
μ (-)	2nd	Positive	-	-	-	-	-	-	-
		Negative	-	1.73	-	-	-	-	-
95%									
μ (-)	1st	Positive	1.73	1.96	2.06	1.68	1.50	1.76	1.99
		Negative	1.73	1.77	1.54	-	2.23	2.11	2.10
μ (-)	2nd	Positive	-	1.77	-	-	1.53	-	1.61
		Negative	-	1.62	-	-	-	-	-

7.4.4 ENERGY DISSIPATION

The same procedure followed to analyse the global energy dissipation (Chapter 7.2.4) was followed to calculate the local energy dissipation, by applying it to each slab-column connection.

As reported in Chapter 5, the dissipated energy was calculated using the displacement firstly and then the slab-column rotation as the kinematic quantity (displacement component), whereas in both the analyses shear force was used as the static quantity (force component).

For a more detailed explanation of the methodology, the equations and the graphs set up, see chapter 5.3.4 for the analyses made with the inter-storey drift ratio and chapter 5.4.7 for the ones made with the rotation.

In Table 7.16 and Table 7.17 the maximum values of the dissipated energy of each connection on each floor were reported, calculated with the inter-storey drift ratio and with the rotation respectively, were reported.

Table 7.16 Maximum value of dissipated energy of each connections on each floor, test Cyc-1. Energy calculated with the displacement (kNmm=kJ).

1st Floor	A	B	C	D	2nd Floor	A	B	C	D
1	$2.30*10^4$	$3.59*10^4$	$3.78*10^4$	$2.20*10^4$	1	$1018*10^4$	$2.03*10^4$	$2.36*10^4$	$1.38*10^4$
2	$3.76*10^4$	$7.4*10^4$	$5.49*10^4$	$3.61*10^4$	2	$1.65*10^4$	$3.75*10^4$	$3.48*10^4$	$2.06*10^4$
3	$1.73*10^4$	$3.96*10^4$	$3.94*10^4$	$1.95*10^4$	3	$1.20*10^4$	$1.63*10^4$	$2.24*10^4$	$1.42*10^4$

Table 7.17 Maximum values of dissipated energy of each connections on each floor, test Cyc-1. Energy calculated with the rotation (kNm*rad=kJ).

1st Floor	A	B	C	D	2nd Floor	A	B	C	D
1	10.9	11.9	-	-	1	4.1	6.1	-	-
2	14.8	26.0	19.0	19.6	2	6.1	9.8	8.7	6.2
3	-	-	12.6	15.3	3	-	-	6.3	4.2

Figure 7.31 and Figure 7.32 report the graphs of the dissipated energy of each connection on each floor (blue line for the 1st floor, red line for the 2nd) calculated with the inter-storey drift ratio and with the rotation respectively.

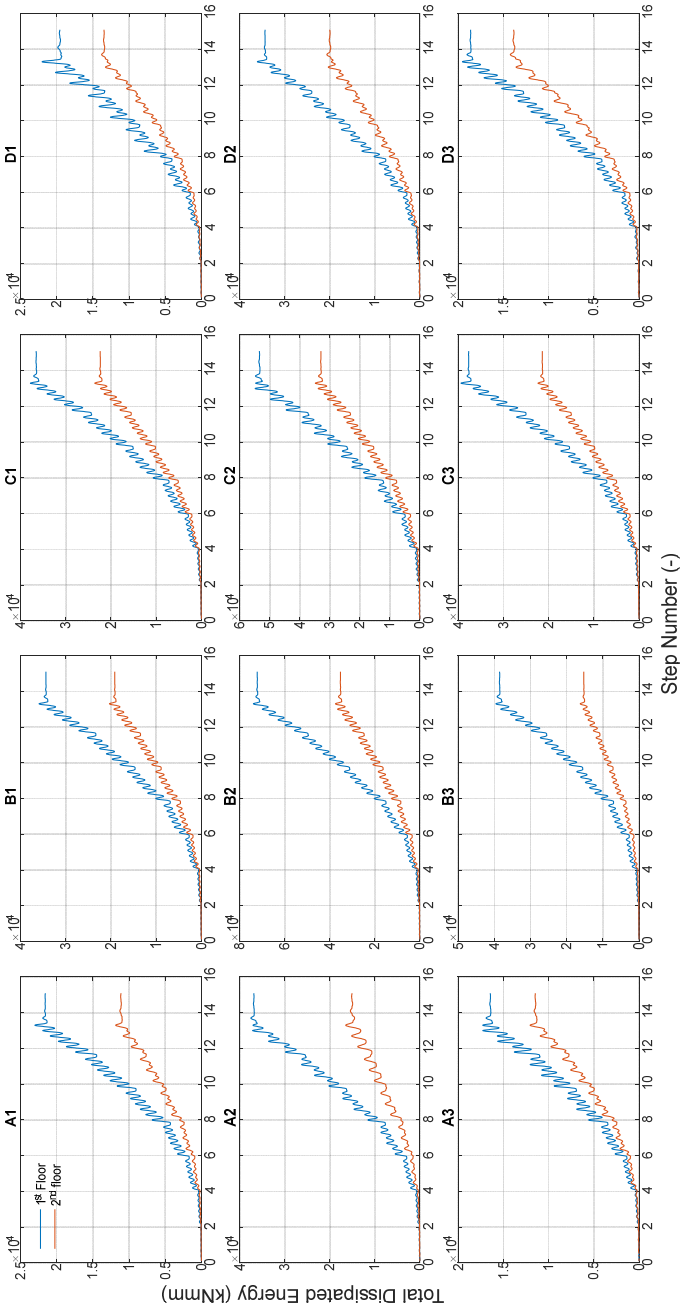

Figure 7.31 Dissipated energy for each connections, test Cyc-1. 1st floor blue line, 2nd floor red line. Energy calculated with the displacement.

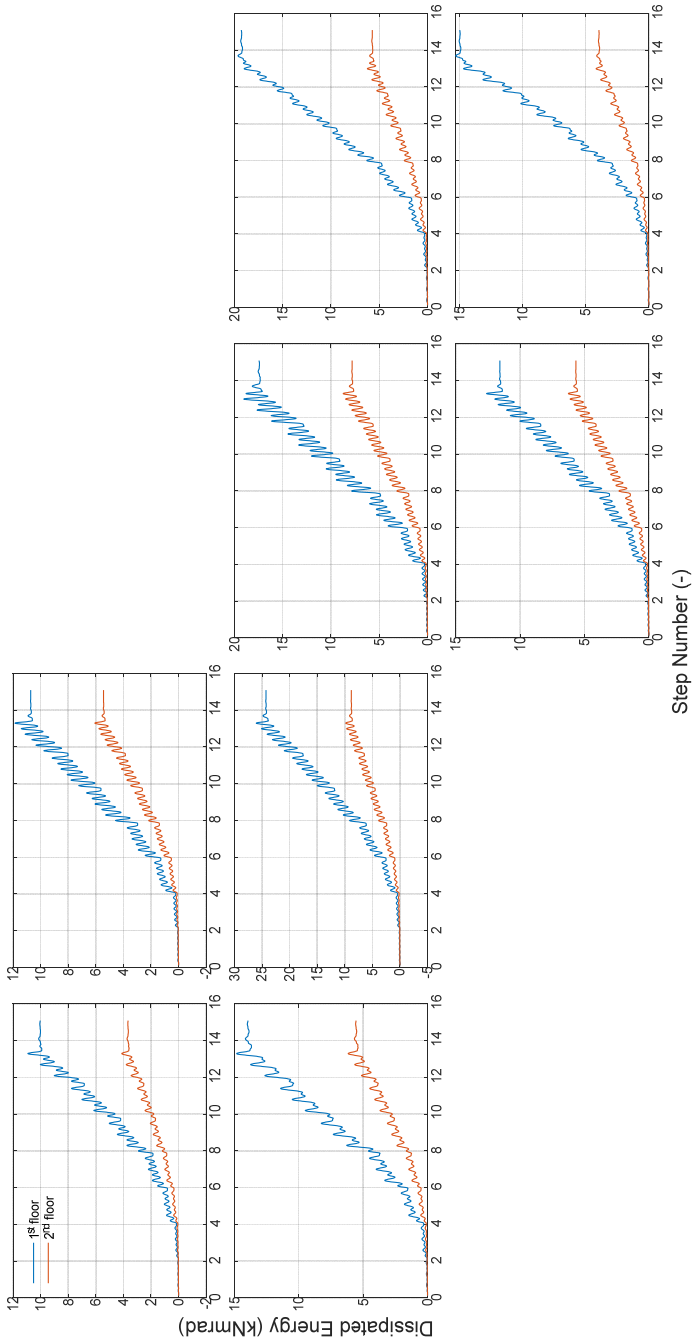

Figure 7.32 Dissipated energy for each connections, test Cyc-1. 1st floor blue line, 2nd floor red line. Energy calculated with the rotation.

In both the representations and in all the connections, the 1st floor (blue line) is more dissipative then the 2nd one (red line).
The internal connections B2 and C2 are the two that dissipated the highest values of energy on both floors and in both the energy calculations, using the inter-storey drift ratio and the rotation.
Using the displacement to calculate the energy, the alignments B and C are the most dissipative, this difference is not present when using the rotation in the energy calculation. This is probably due to the fact that the drift does not reflect precisely the real behaviour of the slab-column connections. The drift has the same value independently from the slab-column connections typology and position in the slab.

7.4.5 OBSERVED DAMAGE

On analysing the cracking formation at the end of the test in Figure 7.33 for the 1st floor and in Figure 7.35 for the 2nd floor, it is possible to observe that the greater damage occurred in the edge and corner slab-column connections, more on the 1st floor than on the 2nd. Observation on the deck during testing was not possible for safety reason.
The wider cracking was observed in the two external short sides perpendicular to the loading application A and D.

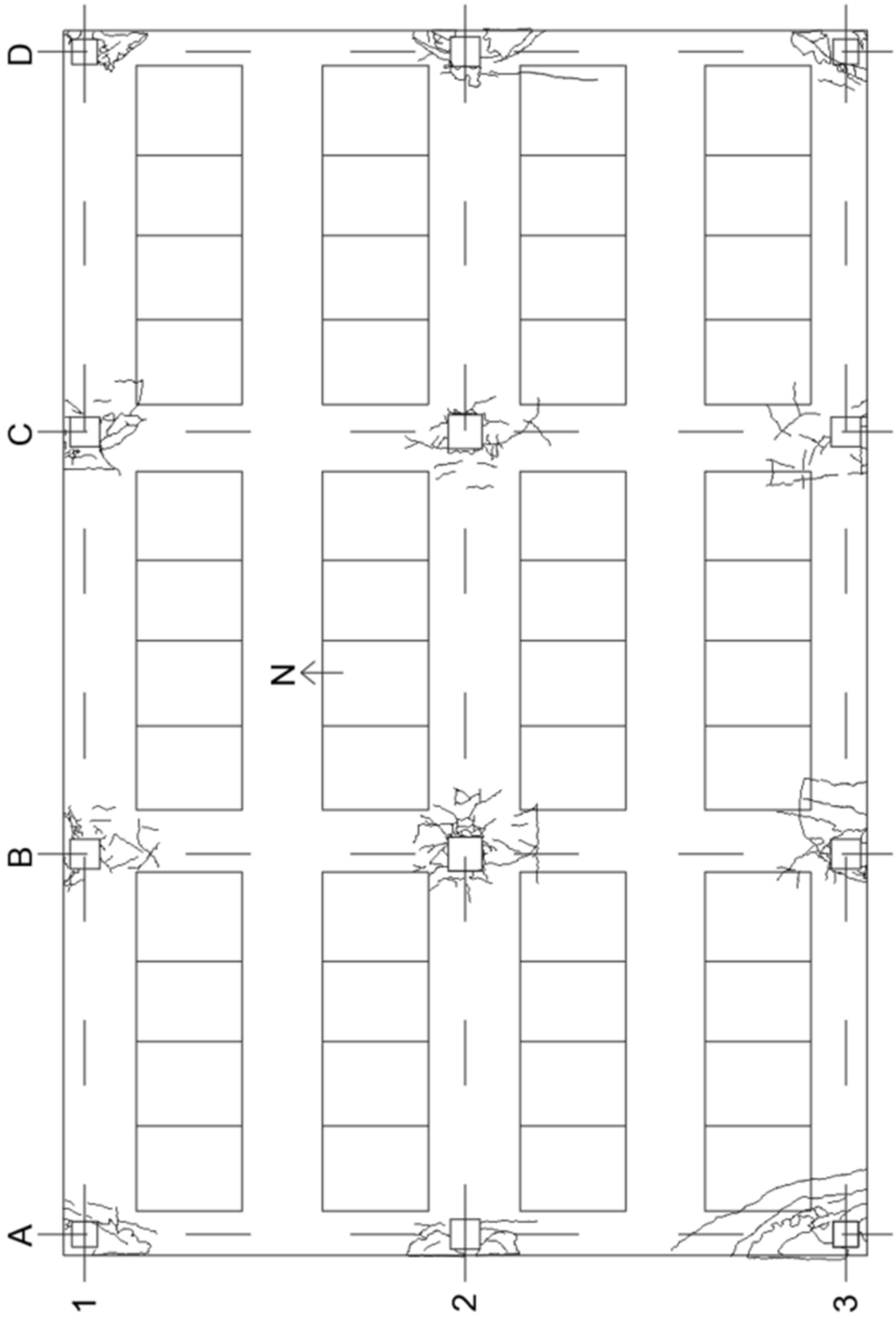

Figure 7.33 Crack pattern intrados 1st floor Test Cyc-1 (f02).

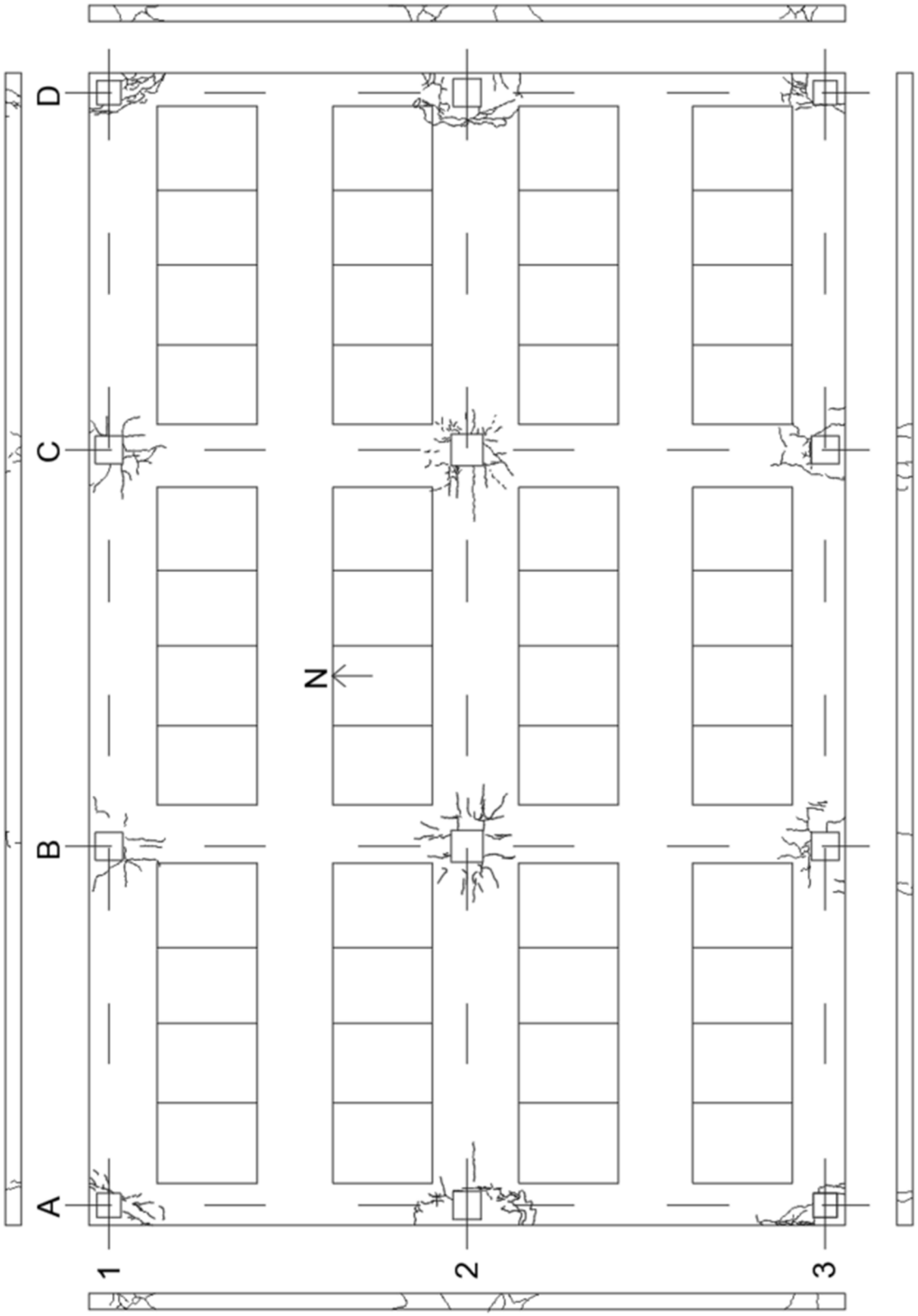

Figure 7.34 Crack pattern extrados 1st floor Test Cyc-1 (f02).

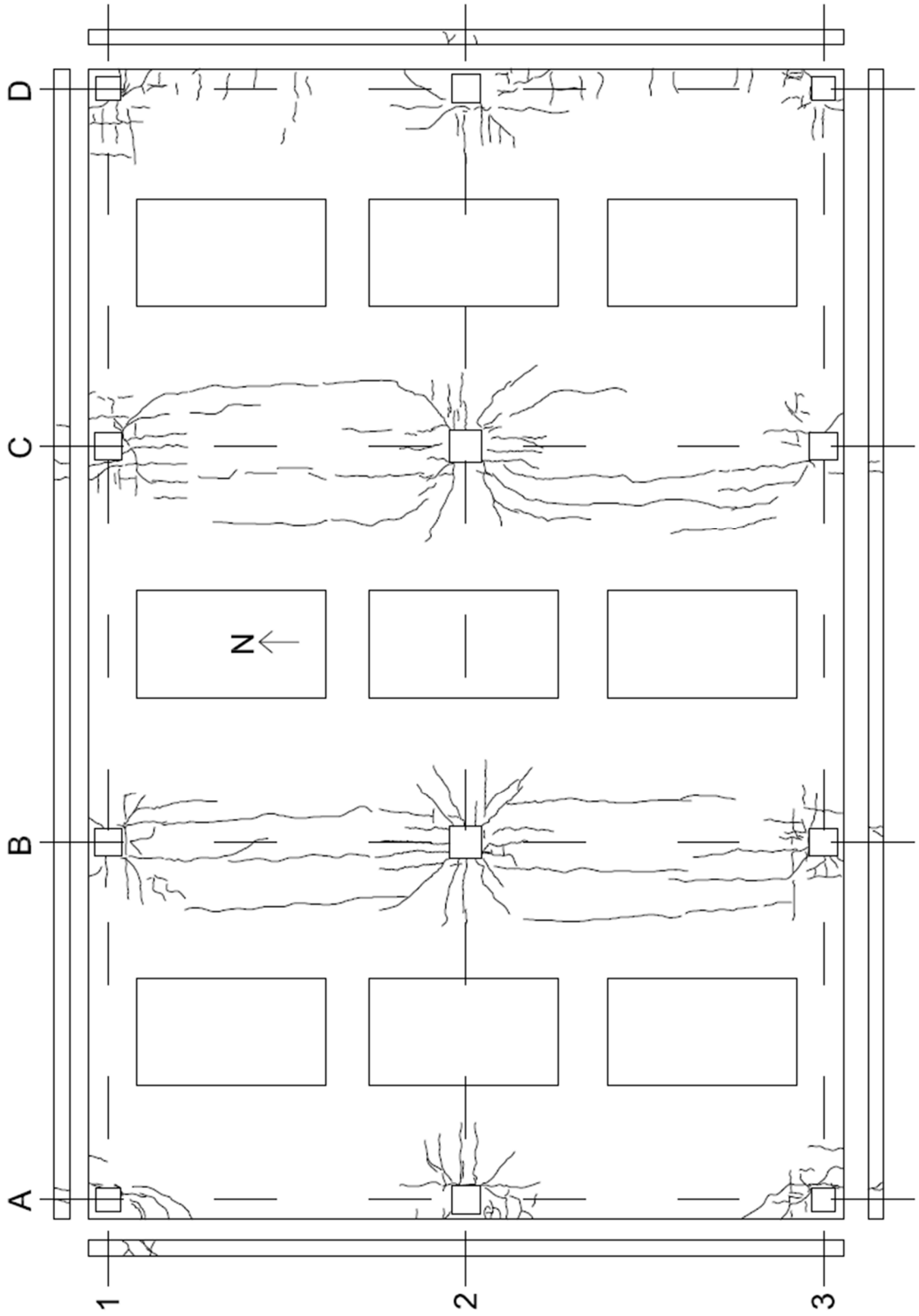

Figure 7.35 Crack pattern extrados 2nd floor Test Cyc-1 (f02).

From a visual analysis, it was possible to observe that the first cracking appeared around the drift of 1.5% obtained from the analysis of the previous section and summarised in Figure 7.30 and Table 7.15.
After the drift value of 1.5% the two lateral connection located at the centre of the short side A2 (east) and the D2 (west) on the 1st floor and along the vertical surface of the side of the slab (Figure 7.36) started to show significant damage. The cracks formed are of torsion and shear typologies.

Figure 7.36 a) A2 and b) D2 connections after the 1.5% drift, tests Cyc-1 (f02).

At a drift value of 2%, in the same connections, the cracks opened wider.

Figure 7.37 a) A2 and b) D2 connections after the 2% drift, tests Cyc-1 (f02).

At a higher drift level, 2.5%, the corner connections, always on the short side of the structure D1 (Figure 7.38 b) and D3 east (Figure 7.38 c) and A1 west (Figure 7.38 a) reported very significant damage with the detachment of part of the edge of the slab.

Figure 7.38 a) A1, b) D1 and c) D3 connections after the 2.5% drift, tests B1 (f02).

The previous two, A2 and D2 reported a greater level of damage (Figure 7.39). At 2.5% drift, the concrete was expelled reporting serious damage which evidenced the importance of the integrity reinforcement.

Figure 7.39 a) A2 and b) D2 connections after the 2.5% drift, tests B1 (f02).

By comparing the two most damaged connections at the end of the first cyclic test, it is possible to note that the failure mode present on the side of both is a combination of punching shear (Figure 7.40) and torsion(Figure 7.39).
Figure 7.40 a shows that a sliding crack opened in A2 on the East face, at the interface with column, without the formation of a punching cone. The typical punching cracks are observed in connection D2 on the opposite side of the slab. The difference can be interpreted with the different reinforcement layout. The following section will

deepen into the analysis of these phenomena on the basis of the slab thickness variation measurements, related to cracking.

Figure 7.40 a) A2 and b) D2 slab-column connections after the 2.5% drift, tests B1 (f02).

7.4.6 UNBALANCED MOMENT VERSUS SLAB CRACK OPENING

For a more thorough analysis of the damage, the unbalanced moment versus the slab crack opening, recorded by the linear transducer, was analysed. The analysis was carried out on all the connections with the displacement transducers (eight of the twelve) for the 1st and the 2nd floor.
As described in chapter 4, the number of sensors inserted in each connection is in function of the connection typology (Table 7.18).

Table 7.18 Slab crack opening sensors position.

Connections		Sensors position			
Typology	Name	North	South	East	West
Corner	A1		x	x	
	D3	x			x
Edge	A2	x	x	x	
	B1		x	x	x
	C3	x		x	x
	D2	x	x		x
Internal	B2	x	x	x	x
	C2	x	x	x	x

Initially the analysis is carried out for each floor, with the graph for unbalanced moment-slab crack opening of each connection followed by a table with the peak crack width of each, to discern the differences between connections typology. After that, the comparison between the 1st and the 2nd floor is reported. The unbalanced moment is calculated as previously reported (see cap. 7.4).

1ST FLOOR

On the 1st floor, a growing plastic deformation was observed in all connections, with different maximum values. The maximum values were recorded in connections A2 and D2, both located on the lateral short sides, west and east respectively (Figure 7.41).

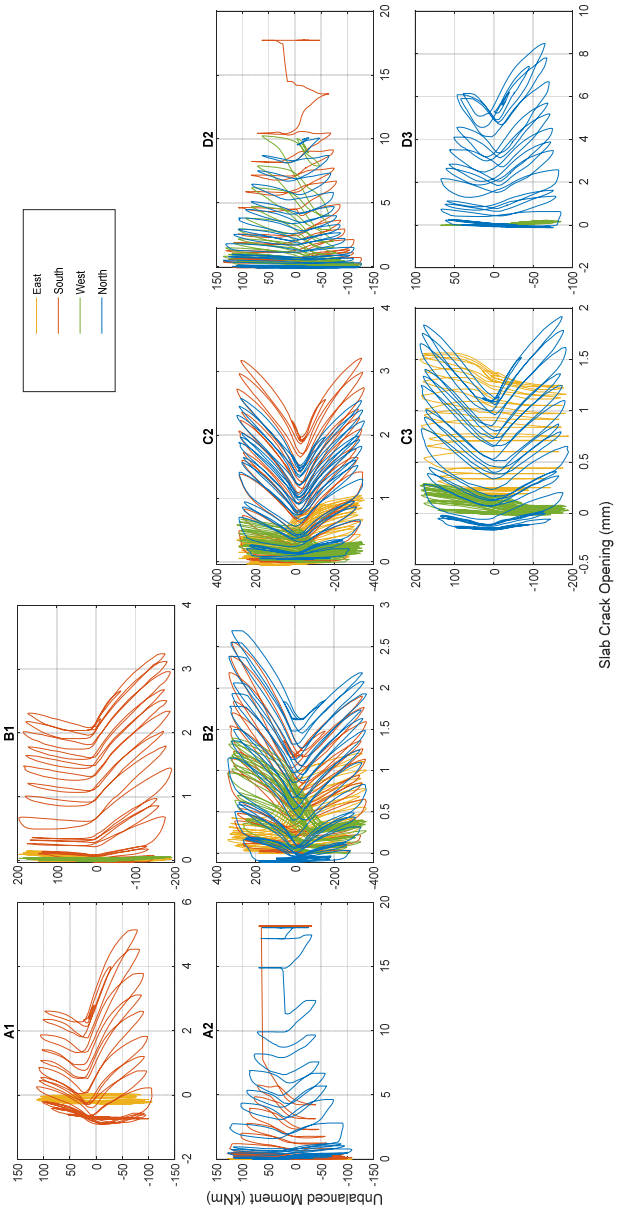

Figure 7.41 Unbalanced moment versus slab crack opening for the 1st floor, Test Cyc-1 (f04).

Table 7.19 Peak crack width for each sensor on the 1st floor, Test Cyc-1 (f02).

Floor	Connection	Typology	Side	Peak Crack Width (mm)
1	A1	Edge	East	0.04
			South	5.1
	A2	Lateral short	North	18.0
			East	0.04
			South	18.2
	B1	Lateral long	East	0.1
			South	3.2
			West	0.1
	B2	Internal	North	2.7
			East	1.2
			South	2.6
			West	1.4
	C2	Internal	North	2.6
			East	1.0
			South	3.2
			West	0.7
	C3	Lateral long	North	1.9
			East	1.6
			West	0.3
	D2	Lateral short	North	10.1
			South	17.7
			West	10.2
	D3	Edge	North	8.5
			West	0.2

In connection A2, the sensors on the north and south side recorded the widest openings in the slab, 18.2 mm for the south and 18 mm for the north (Table 7.19).
On the other side, in connection D2, the sensor on the south side also recorded the widest opening in the slab, 17.7 mm. other connections recorded sizeable values as well, particularly on the North and South side.
It is possible to observe three different shapes in the trend of the graph: the first one, the most widespread, regards the connections of the lateral short side, A2 and D2, the second one, with a lesser diffusion of the crack in the slab, for the edge connections, A1 and D3.
For the A1 connection the widest openings in the slab were recorded by the south sensor of 5.1 mm, for the D3, the north one recorded the higher value of 8.5 mm.

The last of the trend shapes regards the internal and the lateral long side connection typologies. These recorded the most concentrated crack openings, from 0 to around 3 mm.

2ND FLOOR

Here the situation differed from that on the 1st floor, because the measurements of the slab thickness increase show much smaller values than in the 1st floor. This is clearly the effect of the shear reinforcement in the 2nd floor slab. A comparison of the two floor is shown in the following section. The spreading of cracking and inelastic deformation was observed in the connection D3, on the south side edge and in the connections A2, lateral short west side (Figure 7.42), that was the one that reported the widest openings in the slab, 1.7 mm from the north sensor (Table 7.20).

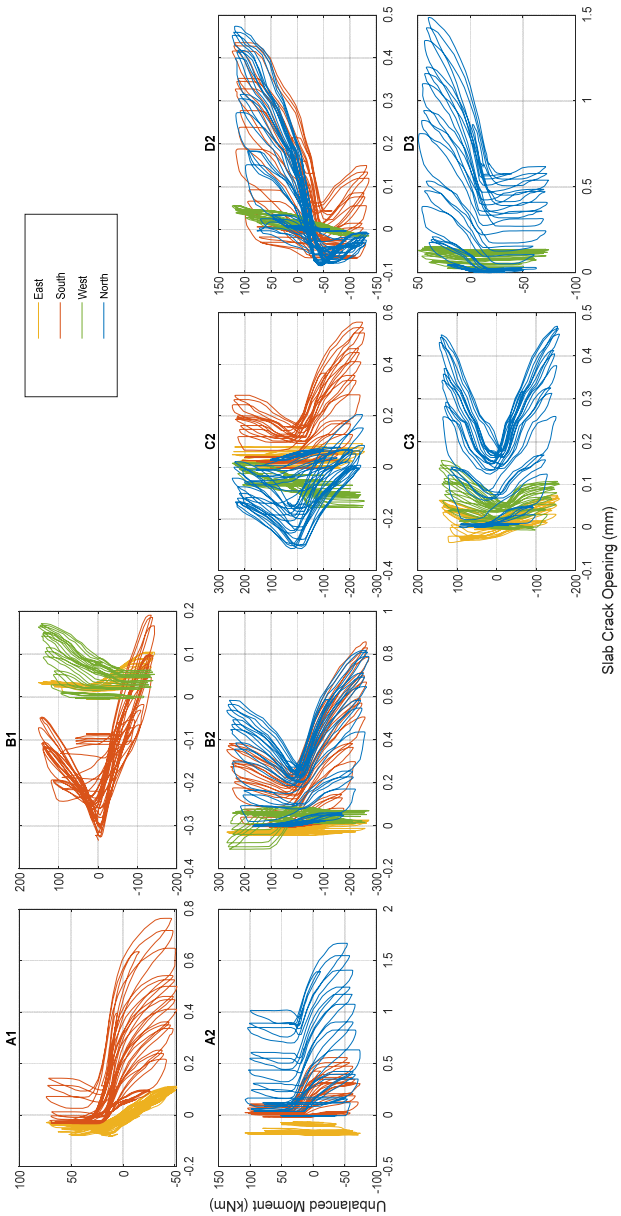

Figure 7.42 Unbalanced moment versus slab crack opening for the 2nd floor, Test Cyc-1 (f04).

Table 7.20 Maximum crack width for each sensor for the 2nd floor, Test Cyc-1 (f02).

Floor	Connection	Typology	Side	Peak Crack Width (mm)
2	A1	Edge	East	0.1
			South	0.8
	A2	Lateral short	North	1.7
			East	-0.1
			South	0.6
	B1	Lateral long	East	0.1
			South	0.2
			West	0.2
	B2	Internal	North	0.8
			East	0.03
			South	0.9
			West	0.1
	C2	Internal	North	0.2
			East	0.1
			South	0.6
			West	0.02
	C3	Lateral long	North	0.5
			East	0.1
			West	0.2
	D2	Lateral short	North	0.5
			South	0.4
			West	0.1
	D3	Edge	North	1.5
			West	0.2

In this case it is not easy, to individuate a common trend in the graphs' shape, but it

is evident that the edge connections A1 and D3 located on the opposite side, mirrored the trend of the north and south sensors.

COMPARISON BETWEEN 1ST AND 2ND FLOOR

Here the comparison made between the two floors, is here reported. Both the figures are scaled with the reference to the maximum values of slab crack opening, which were recorded on the 1st floor. In this way, the differences are more evident (Figure 7.43).

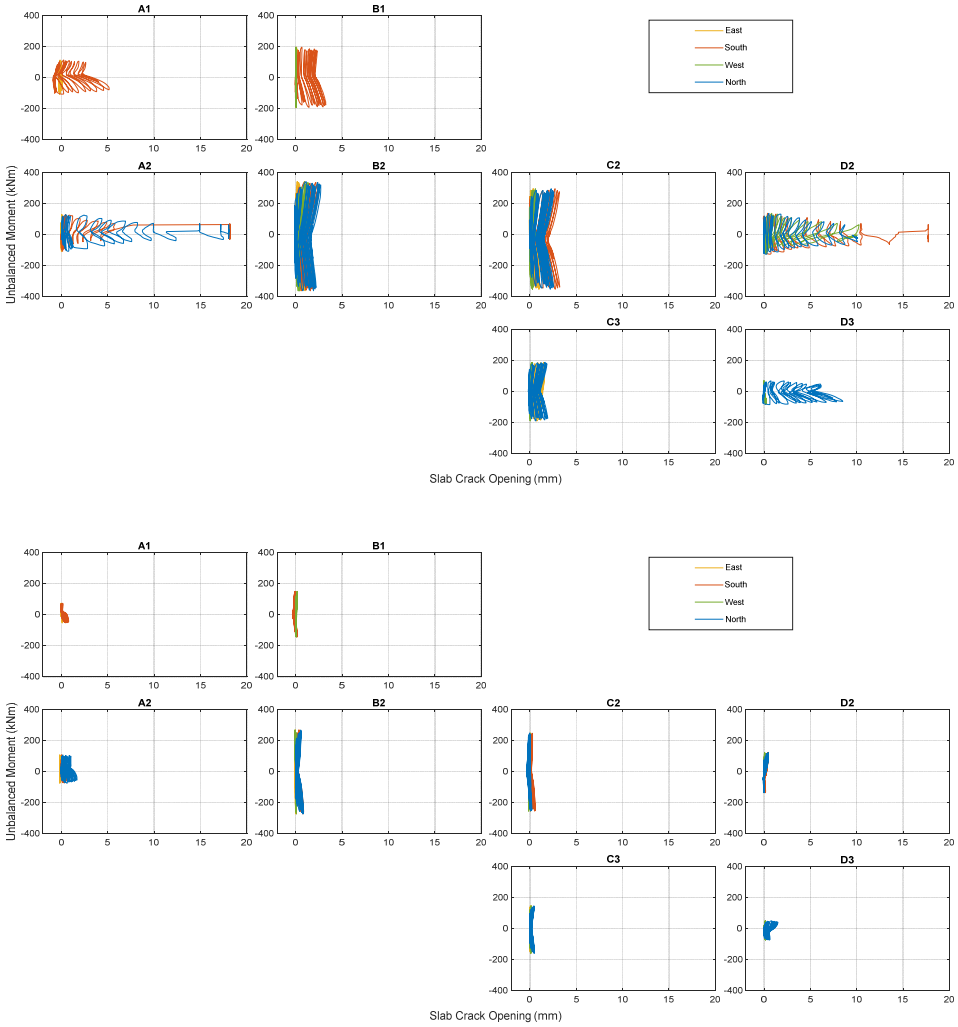

Figure 7.43 Comparison between unbalanced moment versus slab crack opening for the 1st (a) and the 2nd (b) floor, Test Cyc-1, (f02).

Table 7.21 Peak crack width, comparison between 1st and 2nd floor, tests B1 (f02).

Connection	Typology	Side	Peak Crack Width (mm)	
			1st floor	2nd floor
A2	Lateral short	North	18.0	1.7
		East	0.04	-0.1
		South	18.2	0.6
D2	Lateral short	North	10.1	0.5
		South	17.7	0.4
		West	10.2	0.1
A1	Edge	East	0.04	0.1
		South	5.1	0.8
D3	Edge	North	8.5	1.5
		West	0.2	0.2
B1	Lateral long	East	0.1	0.1
		South	3.2	0.2
		West	0.1	0.2
C3	Lateral long	North	1.9	0.5
		East	1.6	0.1
		West	0.3	0.2
B2	Internal	North	2.7	0.8
		East	1.2	0.03
		South	2.6	0.9
		West	1.4	0.1
C2	Internal	North	2.6	0.2
		East	1.0	0.1
		South	3.2	0.6
		West	0.7	0.02

The 1st floor recorded wider openings than those on the 2nd floor. For the 1st floor the cracks have a magnitude order from 0 mm to around 20 mm, whereas for the 2nd floor that is ten times less, with a maximum opening of around 2 mm.
On the 1st floor, connections of the same typology (lateral, internal and edge), recorded openings of the same dimension.
The connections located on the lateral short side (A2 and D2) recorded the widest openings, then the connections located at the edges (A1 and D3) and finally the two internal (B2 and C2) and the two lateral on the long side (B1 and C3) recorded the narrowest openings.

As regards the 2nd floor, the connection A2 located on the short side recorded the widest openings on that floor, although around ten times than those of the 1st floor. The edge connection D3 also recorded an opening of the same value, then all the other connections, disregarding their typology, recorded openings smaller than 1 mm with the two lateral connections on the long side, B1 and C3 that measured the lowest values.
It is possible to note that all the connections in the central part of the slab (B1, B2, C2, C3) on the 1st floor recorded openings lower than those of the connection located on the border (A1, A2, D2, D3).
In all the connections, the sensors recorded similar patterns except for the A2 and D2 where the three different sensors each recorded a different pattern. For the connections A2 and D2, some visual comparison is given in Figure 7.44 and Figure 7.45.
It is evident that the 2nd floor connections (Figure 7.45a and b) had a very similar crack layout, starting from the corner of the column and proceeding diagonally into the slab, and then from the corner of the column, orthogonally.
The crack diffusion on the two floors (Figure 7.44 and Figure 7.45) was very similar. Especially for the A2 connection (Figure 7.44 a and Figure 7.45 a), some cracks were evidenced in the same position on both floors with the addition of the diagonal one from the edge of the column, only clearly visible only on that of the 2nd floor.
Regarding the D2 connection (Figure 7.44 b and Figure 7.45 b), on the 1st floor the crack pattern appeared more irregular and widespread than on the 2nd one.

Figure 7.44 Damage in the slab-column connections, 1st floor a) A2, b) D2.

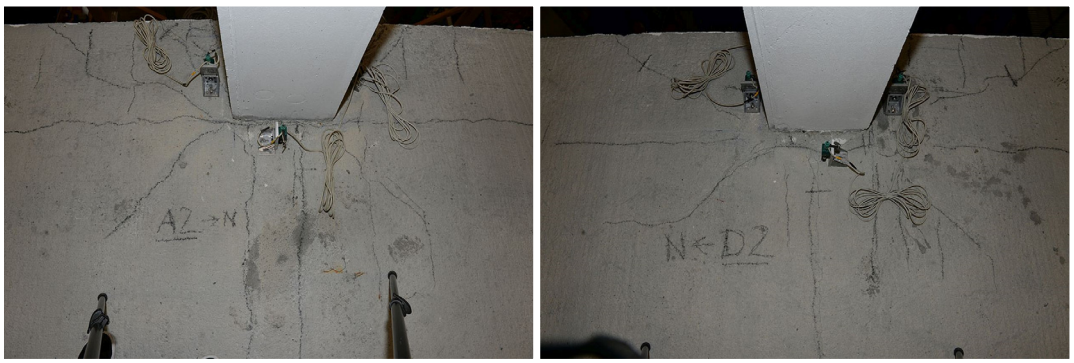

Figure 7.45 Damage in the slab-column connections, 2nd floor a) A2, b) D2.

In the north and south corners, the connection D2 at the 2nd floor, showed cracks smaller than those of the A2 connection (D2 ≃ 10 mm, A2 0.5-1.2 mm) it seems that the increased quantity of longitudinal reinforcement had improved the response on these sides.

7.4.7 UNBALANCED MOMENT VERSUS SLAB ROTATION

The same analysis undertaken for the slab crack opening, was also applied to the slab rotation, recorded by the inclinometers.
The analysis was carried out on all the connections with inclinometers (the same eight analysed in the slab crack opening, see Table 7.18) for the 1st and the 2nd floor. As described in chapter 4, the number and the location of the sensors, depends on the connection typology (internal, lateral and edge).
The unbalanced moment is calculated as previously reported (see cap. 7.4).

1ST FLOOR

For the 1st floor the connection with the highest slab rotation in the slab is the lateral A2 on the short west side (Figure 7.46); the north sensor recorded a slab rotation of 25.1/1000 rad (Table 7.22).

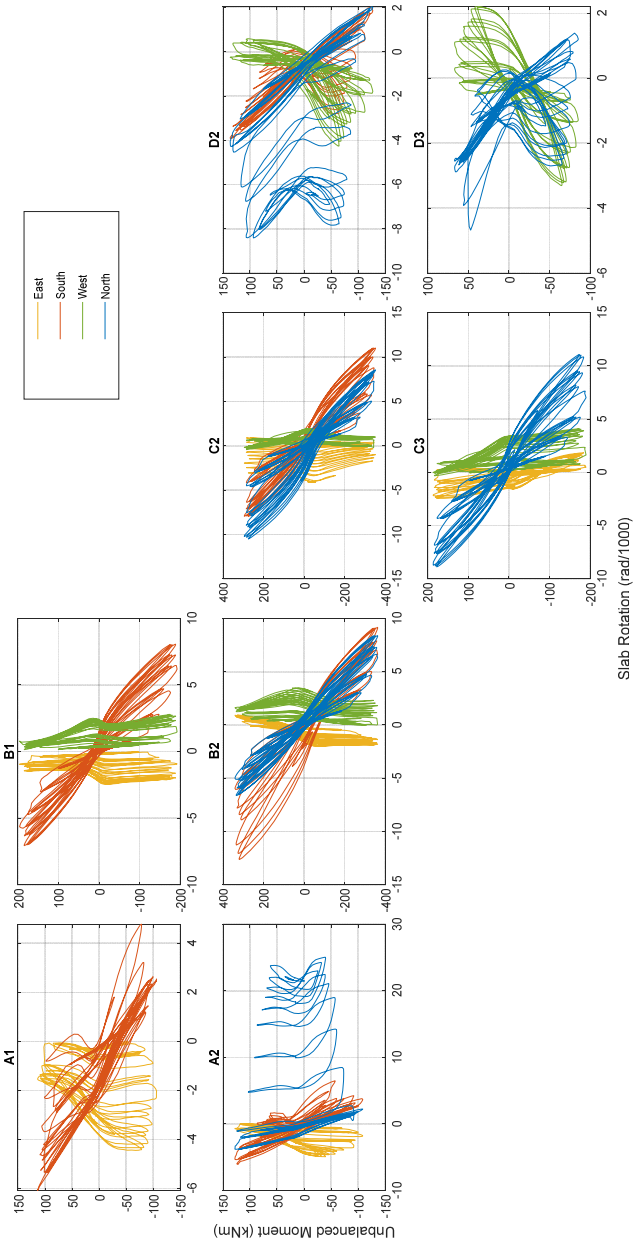

Figure 7.46 Unbalanced moment versus slab rotation for the 1st floor, Test Cyc-1 (f02).

In the A1, A2, D2 and D3 connections, it is clear that in the crack development, from nearly 1/1000 rad the slab rotation increases greatly and this is also evident in the crack opening (Figure 7.41) with a significant enlargement of the opening. This increase in the slab rotation recorded from the north sensor, represents the formation of torsional crack.
The internal connections (B2 and C2) and the connections in the lateral long south side C3, recorded slab rotations within the same range of values.
In these two connections (B2 and C2), the east and west sensors recorded an increase in the slab rotations which indicated the formation of shear-flexural cracking.
For the connection A2 on the lateral short, west, side, the slab rotation in the positive outnumbers the slab rotation in the negative, whereas for the connection on the opposite side, D2 the sensors detected an opposite behaviour, the slab rotations in negative outnumbered those in positive. This behaviour derived from the symmetrical geometry of the A2 and D2 connections. This trend is visible in the value recorded by the north sensor only.
In the connections in the central area of the slab (B1, B2, C2 and C3), all the four sensors followed the same path.
For the two corner connections, A1 and D3, the slab rotations are nearly equally distributed both in positive and in negative, with the north sensor that has recorded slab rotation mirrored by those of the south.

Table 7.22 Peak slab rotation for the 1st floor, Test Cyc-1 (f02).

Floor	Connection	Typology	Side	Peak Slab Rotation (rad/1000)
1	A1	Edge	East	0.002
			South	4.8
	A2	Lateral short	North	25.1
			East	0.8
			South	6.5
	B1	Lateral long	East	0.02
			South	8.1
			West	2.8
	B2	Internal	North	8.4
			East	0.9
			South	9.2
			West	3.5
	C2	Internal	North	8.5
			East	0.9
			South	11.0
			West	1.9
	C3	Lateral long	North	11.1
			East	1.8
			West	4.1
	D2	Lateral short	North	2.0
			South	2.0
			West	0.6
	D3	Edge	North	1.4
			West	2.2

2ND FLOOR

Regarding the 2nd floor, the connection with the highest slab rotation in the slab is D2 (Figure 7.47), the lateral in the short east side, the sensor in the north side recorded a maximum value of 4.6/1000 rad (even if with very small differences compared to some other connections).

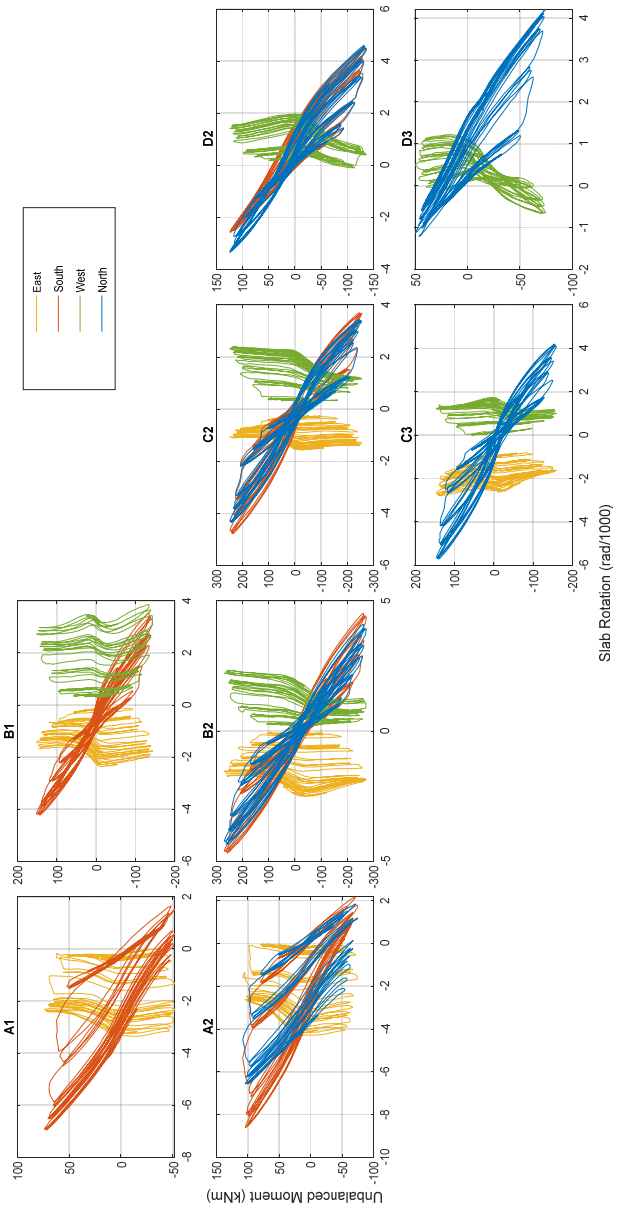

Figure 7.47 Unbalanced moment versus slab rotation for the 2nd floor, Test Cyc-1 (f02).

For the corner connections A1 and D3, the path representation was mirrored as a consequence of the symmetrical geometry of the corner and edge connections. In A2, all the slab rotations are mainly negative, in D3 are mainly positive.
The four connections in the central area of the slab (B1, B2, C2 and C3) measured slab rotation values both in positive and in negative practically within the same range of values (Figure 7.23). All the sensors located in the same position (north, south, west, east) recorded values that follow the same path.
In all the connections, the west sensor detected slab rotations all in positive, the east sensors detected slab rotations all in negative while the north and the south sensors recorded slab rotation values both in positive and in negative. This is due to the slab rotation induced by the gravitational load. The lateral actions had the effect of modifying the slab rotations around the initial values that were imposed on the gravitational load that have those signs.

Table 7.23 Peak slab rotation for the 2nd floor, Test Cyc-1 (f02).

Floor	Connection	Typology	Side	Peak Slab Rotation (rad/1000)
2	A1	Edge	East	0.004
			South	1.7
	A2	Lateral short	North	1.8
			East	-0.02
			South	2.2
	B1	Lateral long	East	-0.1
			South	3.5
			West	3.9
	B2	Internal	North	4.1
			East	-0.1
			South	4.5
			West	2.3
	C2	Internal	North	3.4
			East	-0.2
			South	3.7
			West	2.4
	C3	Lateral long	North	4.2
			East	-0.8
			West	1.7
	D2	Lateral short	North	4.6
			South	4.5
			West	2.0
	D3	Edge	North	4.2
			West	1.2

COMPARISON BETWEEN 1ST AND 2ND FLOOR

Both the figures are scaled referring to the maximum value of slab rotation, on the 1st floor (Figure 7.48). In this way, the differences are more evident.

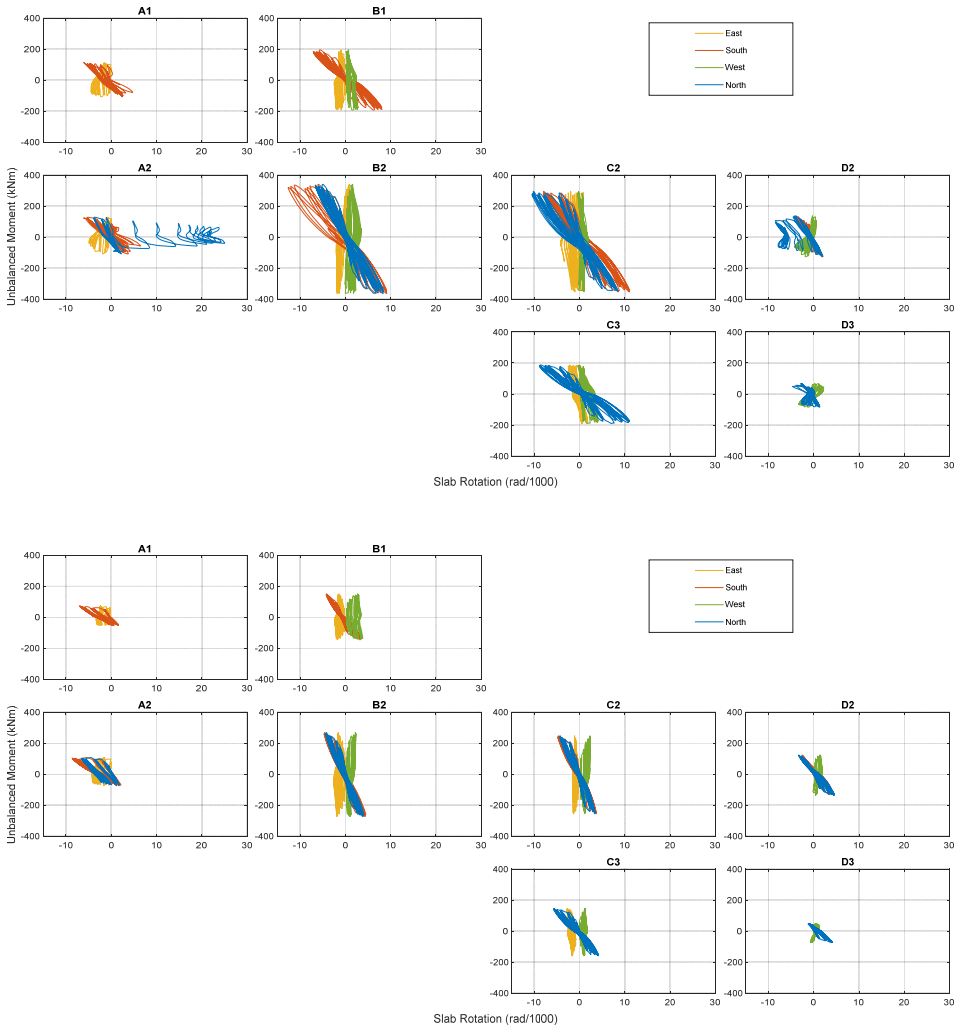

Figure 7.48 Comparison between unbalanced moment versus slab rotation for the 1st (a) and the 2nd (b) floor, Test Cyc-1, (f02).

Table 7.24 Peak slab rotation, comparison between 1st and 2nd floor, tests B1 (f02).

Connection	Typology	Side	Peak Slab Rotation (rad/1000)	
			1st Floor	2nd Floor
A1	Edge	East	0.002	0.004
		South	4.8	1.7
D3	Edge	North	1.4	4.2
		West	2.2	1.2
A2	Lateral short	North	25.1	1.8
		East	0.8	-0.02
		South	6.5	2.2
D2	Lateral short	North	2.0	4.6
		South	2.0	4.5
		West	0.6	2.0
B1	Lateral long	East	0.02	-0.1
		South	8.1	3.5
		West	2.8	3.9
C3	Lateral long	North	11.1	4.2
		East	1.8	-0.8
		West	4.1	1.7
B2	Internal	North	8.4	4.1
		East	0.9	-0.1
		South	9.2	4.5
		West	3.5	2.3
C2	Internal	North	8.5	3.4
		East	0.9	-0.2
		South	11.0	3.7
		West	1.9	2.4

As can be seen from the comparison made between the two floors, the slab rotations of the 1st floor are higher than those of the 2nd one. this can be explained by the different geometry of the connections at the two floors, with either two or one columns moment transfer respectively.

7.5 Summary

A summary of the main results obtained at the end of the first cyclic test is made;

- Regarding the global behaviour, it is possible to note a ductile response up to the maximum value of the drift (2.5%), although higher damage resulted in some connections. The structure reached a maximum load and then remained stable showing ductility and developing plastic deformation with an applied load redistribution (Figure 7.2). As is clearly evident in Figure 7.10, the

connections in the lateral alignment A and D showed a drop in the unbalanced moment, with a redistribution of load in the central B and C;

- A global ductility values is not calculated, because the test was stopped before reaching failure. The ductility analysis shows that the yield point is a rather high drift ratio value. This is related to the relative low stiffness of the flat slab frame. On the whole a good nonlinear deformation capacity is shown;
- From the four analysed percentage drops in loading resistance (80%, 85% 90% and 95%) it was possible to observe that the most reliable values are the those of the Eurocode 8 [1], the 80% and the 85%. The other two analysed percentages, 90% and 95% showed to be more sensitive. From a global analysis, the failure point was not reached in any of the analysed percentages, whereas in a local analysis some connections failed, but with load redistribution, no global effects have been seen. The 80% and the 85% are the effective criteria since they work well for both the global and the local analysis, registering the local failure and not the global;
- The 1st floor dissipated more energy than the 2nd one, also reporting more damage (Figure 7.9). This highlights the importance of the presence of the shear reinforcement (see Chapter 3). This behaviour was also observed in the local analysis and in both the representations with the inter-storey drift ratio and the slab-column rotations (Figure 7.31 and Figure 7.32, Table 7.16 and Table 7.17), all the connections on the 1st floor were more dissipative than those on the 2nd one. The most dissipative slab-column connections were obviously the internal B2 and C2 on both floors;
- The connections in the alignments A and D were those that showed the most damage (Figure 7.38 and Figure 7.39). The edge connection D2 in the 1st floor was the first to punch, for an inter-storey drift ratio of 1.5%. The design of the specimen was executed with the aim of reflecting as far as possible the common design mode for European structures as prescribed in EC8 [1]. For this reason, the reinforcement detailing on the edge of the slab was executed with a simple bending of the bars without hook. This caused damaged to the slab edge;
- From the connections in the short side (alignments A in Figure 7.38 and D in Figure 7.39) the efficiency of the integrity reinforcement is made clear. Two bottom bars in each direction were placed at each connection, following the EC2 [4]. This reinforcement was sufficient to avoid the collapse of the slab. From the edge connections in Figure 7.38 it is also possible to observe the catenary effect of the top reinforcement;
- From the local stiffness degradation analysis (Figure 7.23 and Figure 7.24) a different behaviour is perceived of the exterior connections in the direction orthogonal to the earthquake loading applications (lines A and D).

References

[1] CEN. EN 1998-1. Eurocode 8: Design of structures for earthquake resistance - Part 1: General rules, seismic actions and rules for buildings. 2004

[2] Le, D.D., Nguyen, X.-H., Nguyen, Q.-H. (2020) “Cyclic Testing of a Composite Joint between a Reinforced Concrete Column and a Steel Beam”. Applied sciences.

[3] Park, R. (1988) “Ductility evaluation from laboratory and analytical testing”. Proceedings of Ninth World Conference on Earthquake Engineering, August 2-9, Tokyo-Kyoto, Japan (Vol. VIII).

[4] CEN. EN 1992-1-1. Eurocode 2 — Design of concrete structures. Part 1-1: General rules and rules for buildings. 2004.

8 Cyclic test Cyc – 2

8.1 Introduction

The results of the second Cyclic test with gravity loading acting on each of the two floors and on a part of the connections on the 1st floor strengthened, are here presented.
The aim of the experimental program was to study the full response to failure for both connections with and without shear reinforcement. The 1st floor edge and corner connections reached failure during the first test Cyc-1, while the response of the 2nd floor showed that only one connection reached its resistance, followed by limited strength deterioration. In addition, the tests included the study of strengthening solutions for existing structures.
As for the previous cyclic test, the global response is reported first and then the local one. The global response is analysed by using the relationship between the base shear and the top displacement and successively in terms of stiffness deterioration ductility and energy dissipation.
Regarding the behaviour of the slab-column connections, a thorough description for each of them is here reported, in terms of unbalanced moment, ductility, and energy dissipation. A more detailed analysis of the crack formation is also reported using the photographic material.
A comparison between the strengthened and the un-strengthened connections of the 2nd floor is presented, to show their response in terms of unbalanced moment with respect to the inter-storey drift ratio.
The final section gives a summary of the results with some comparison to the previous cyclic test.
A detailed description of the methodology followed analysis of the response measurements can be found in chapter 5.

8.2 Preliminary aspects

This initial section reports some change in the mock-up before testing regarding; loading disposition and entity, and the removal of some instrumentation.
Due to the high level of damage reached during the previously cyclic tests and to some design decisions, the vertical load on the 1st floor was changed, whereas the vertical load on the 2nd floor remained the same. Because the slab-column connections along the two short sides (A and D) on the 1st floor were heavily damaged at the end of test Cyc-1, the two lines of tanks on the lateral short side were removed,

and thus the load was reduced on the outer halves of the span between the lines A and B and C and D. The 1st floor was loaded with 32 tanks of 10 kN each, whereas the vertical load on 2nd floor remained the same as in the previous tests, with 9 concrete blocks of 66 kN each (Table 8.1 and Figure 8.1).

Table 8.1 Added loads on the 1st and 2nd floor.

Floor	Typology	Number	Weight (kN)	Load (kN)	Area (m2)	(kN/m^2)
1	Tanks	32	10	320	137.8	2.32
2	Blocks	9	66	594	137.8	4.31

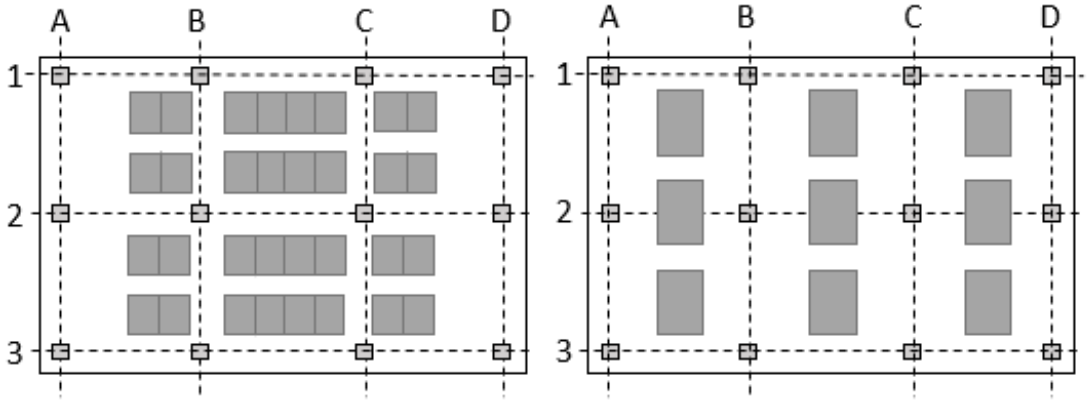

Figure 8.1 Added Loads distribution on the 1st and 2nd floor.

The different gravity loading distribution resulted in a change in the gravity shear ratio. In Table 7.2 the gravity shear ratio values of each slab-column connection typology of each floor are reported for both floors.

Table 8.2 Gravity shear ratio.

Floor	Internal	Edge	Corner
1st	0.29	0.20÷0.12	0.10
2nd	0.32	0.22	0.19

Because of the high damage level that resulted in the slab-column connections along the two short sides (A and D) on the 1st floor at the end of test Cyc-1, the instrumentation for the slab (inclinometers and through slab transducers) on the corresponding edge connections was removed. Consequently, a part of the measurements of the previous test is missing in Cyc-2.

8.3 Global behaviour

The response of the entire structure and then the response of each floor in terms of stiffness deterioration, ductility and energy dissipation is here reported. The stiffness degradation was analysed to describe the global damage of the structure, whereas the global ductility was studied to determine the ability of the entire structure to

deform plastically before failure. Finally, since the structure was dissipative, the energy dissipation of each floor and of the entire structure was shown. A detailed description of the methodology followed is reported in Chapter 5.
Unlike the previous cyclic test, only one cycle of global drift ratio was performed.

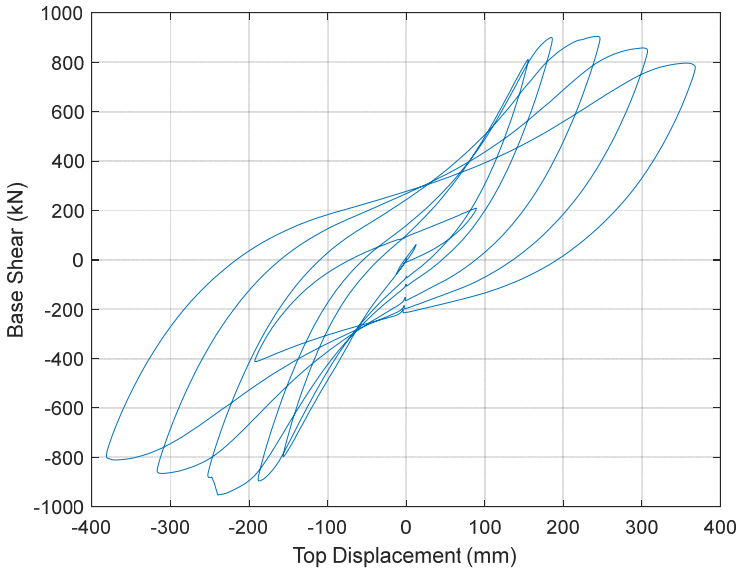

Figure 8.2 Base shear vs. top displacement for the test Cyc-2.

Figure 8.2 shows the global base shear versus the roof displacement. At the end of the previous test Cyc-1 the horizontal plateau of the base shear force at 901 kN indicated that the structure had entered a phase of plastic deformation. A slight increase of the base shear was observed during this test. During the third cycle at 4% drift ratio, the base shear reached -950 kN corresponding to a roof displacement of -240 mm (3.8% of the global top inter-storey drift). At this value of maximum base shear, the punching of an interior connection occurred.
This was followed by a global deterioration that continued steadily until the end of the test.
Once the maximum stroke of the actuators was reached, the test was terminated.
A post-test survey (see after) showed also the rupture of the longitudinal reinforcement at the base of the column B2.
The reduction in base shear, recorded from the beginning to the end of the test, was approximately 14%, this decrease being a consequence of three different factors: the punching of one of the interior connection, the increase of damage to the connections on the short side of the building and the second-order effects.

8.3.1 FLOOR BEHAVIOUR

As shown in Figure 4.65 and Figure 8.4, the force recorded at the 2nd floor (V_{max}=603 kN) was double the force imposed at the 1st floor (V_{max}=301.8 kN) according to the

loading scheme chosen.
In Figure 4.65 b, both floor displacements are reported. For the 1st floor the values recorded by the displacement transducer were used, for the 2nd floor the difference between the 2nd and the 1st floor values were used (Eq. 5-6).
The 1st floor, blue line, was subjected to peak inter-story drift ratio of 6.05%, whereas the 2nd floor, red line, was subjected to peak inter-story drift ratio of 5.4%.
The force on the 2nd floor reached the maximum value after t= 754.5 sec (see Figure 4.65), when the top drift ratio reached 3.6%. After that, the maximum load of the structure decreased slightly and the inter-storey drift increased up to the maximum value of 5.4%. At the same time of t=754.5 sec the force on the 1st floor also reached the maximum value and then decreased to the end of testing.

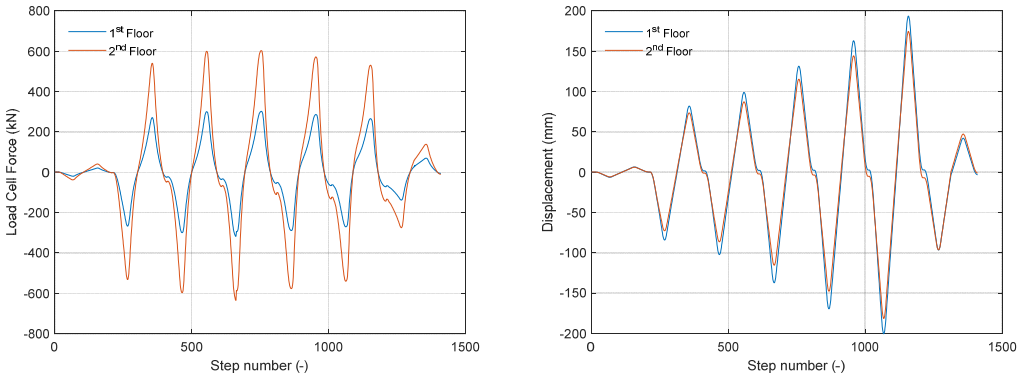

Figure 8.3 a) Floor load cell force and b) floor displacement imposed by the actuators for the Test Cyc-2.

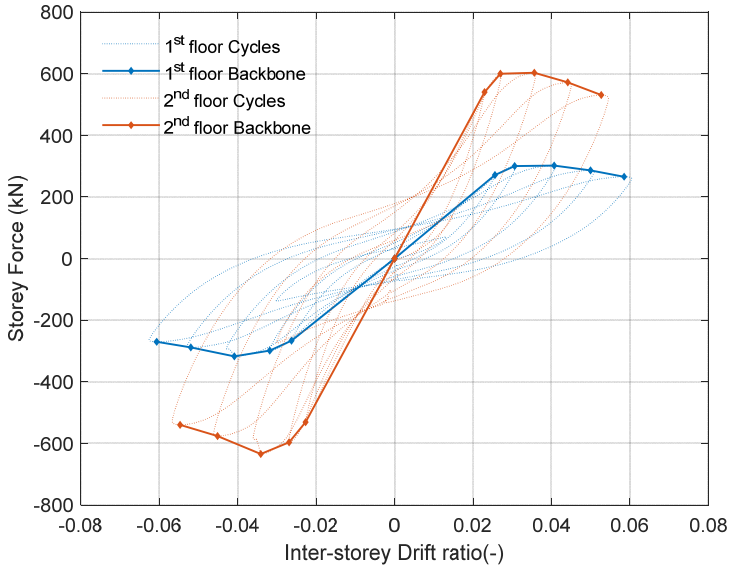

Figure 8.4 Storey forces for the test Cyc-2.

The 1st floor reached an inter storey drift 10% higher than the 2nd one. As will be shown in the next sections, the 1st floor bore the effects of the force applied on the 2nd floor as well, in fact it will be more dissipative and will suffer much more damage than the 2nd one.

8.3.2 STIFFNESS DETERIORATION

The stiffness degradation was analysed to describe the damage to each floor of the building. The followed procedure, the equations used and the graphs set up are reported in Chapter 5.2.2. the calculation was carried out considering all the previous tests, so the two seismic, Seis-SLS and Seis-ULS and the cyclic Cyc-1.
In the graphs below, each test is represented with a different coloured diamond, yellow for the first seismic, Seis-SLS, light blue for the second seismic, Seis-ULS, purple for the first cyclic, Cyc-1 and green for the second cyclic, Cyc-2.
The stiffness deterioration ratio versus the inter-storey drift is reported in Figure 8.5 and Table 8.3, whereas in Figure 8.6 the negative branches were reported with their absolute value to display the symmetry.

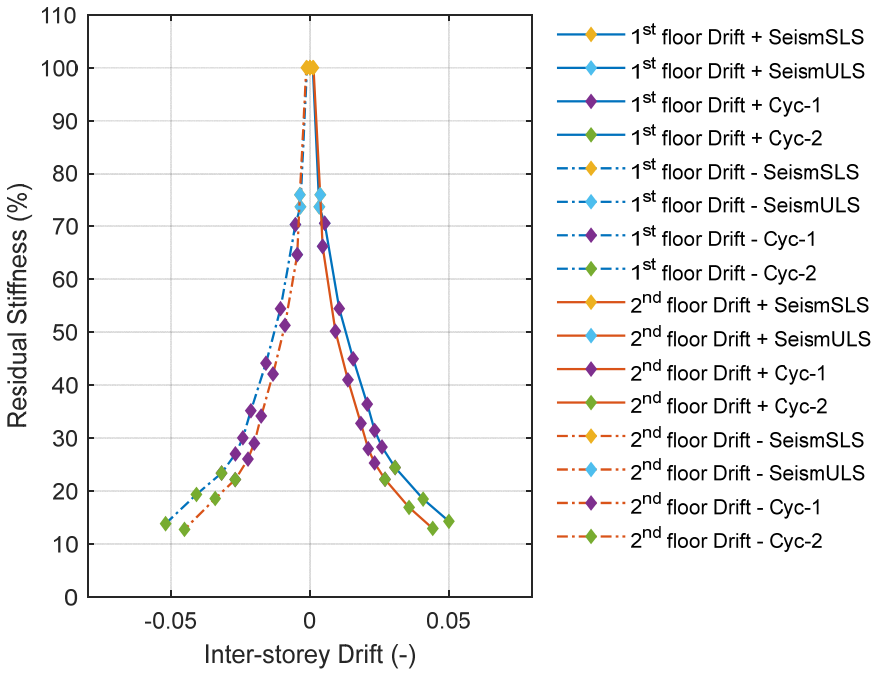

Figure 8.5 Stiffness deterioration ratio, test Cyc-2 (g04).

The decrease remains stable in both floors and in both positive and negative drift sign. From an initial value of 100% both floors and both drift signs have reached values between 13% and 14% (Figure 8.5).

Table 8.3 Stiffness deterioration values, test Cyc-2 (g04).

	Pull (from east to west)		Push (from west to east)	
	Drift (%)	Stiffness Degradation (%)	Drift (%)	Stiffness Degradation (%)
1st floor	-0.0011	100	0.0010	100
	-0.0035	73.70	0.0033	73.70
	-0.0053	70.34	0.0053	70.61
	-0.0106	54.46	0.0105	54.49
	-0.0158	44.17	0.0155	44.99
	-0.0213	35.18	0.0206	36.42
	-0.0242	30.06	0.0233	31.46
	-0.0268	27.03	0.0259	28.33
	-0.0318	23.40	0.0306	24.46
	-0.0409	19.36	0.0407	18.49
	-0.0519	13.84	0.0500	14.28
2nd Floor	-0.0013	100	0.0012	100
	-0.0036	75.99	0.0037	75.99
	-0.0046	64.69	0.0045	66.24
	-0.0090	51.31	0.0091	50.21
	-0.0133	42.11	0.0136	41.01
	-0.0175	34.18	0.0183	32.79
	-0.0200	29.03	0.0209	28.00
	-0.0223	26.04	0.0232	25.31
	-0.0269	22.18	0.0270	22.23
	-0.0341	18.60	0.0357	16.91
	-0.0452	12.76	0.0442	12.95

As observed during the previous cyclic test both floors were subjected to nearly the same stiffness deterioration. The 1st floor reached a final inter-storey drift ratio slightly higher than the 2nd one. The differences between the 1st and the 2nd floor are due to the shear reinforcement that was provided only in the 2nd one.

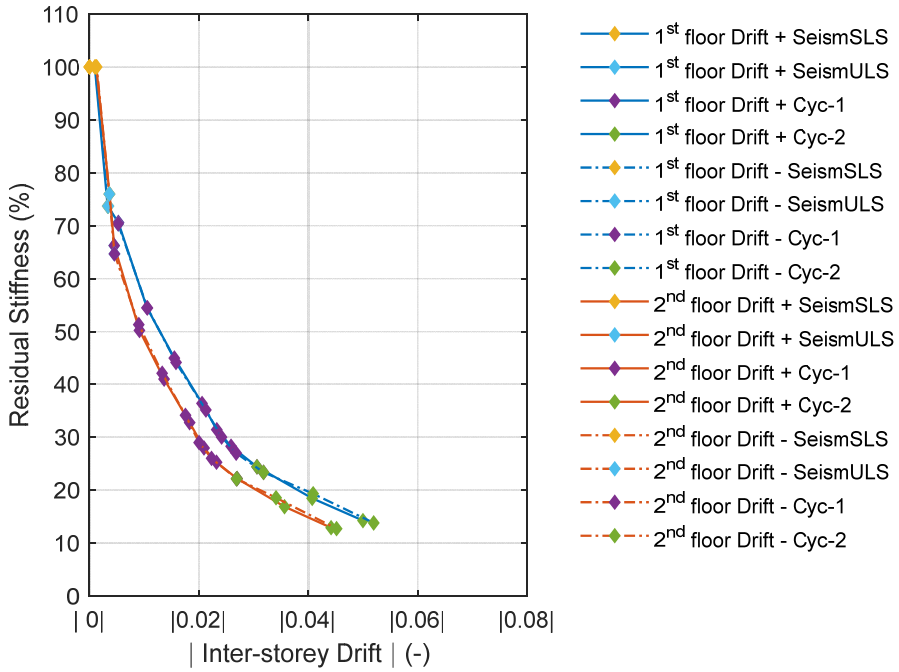

Figure 8.6 Stiffness deterioration absolute value, test Cyc-2 (g04).

Finally, as it is possible to observe from Figure 8.6, the two branches of the drift, positive and negative, are perfectly symmetrical for the 1st and the 2nd floor.

8.3.3 DUCTILITY

With the aim to ascertain the ability of the entire structure to deform plastically before failure, the global ductility was studied. The followed procedure, the equations used and the graphs set up are reported in Chapter 5.2.3.
The study of ductility considered the four analysed residual resistance 80%, 85%, 90% and 95% that are reported in the following Figure 8.7 a, b, c and d. For each of them, the graph with the representation of the analysed percentage (point-dashed line, blue for the 1st floor and red for the 2nd) is reported and if the conditions to reach failure are respected, a red continuous line indicates the failure force and the corresponding displacement.
The graphs are followed by a table (Table 8.4) that reports the shear force and the corresponding drift ratio of the three characteristic points (Limit, Yielding and Failure) and in the last column the displacement ductility factor.
Values for the 1st and the 2nd floor and for the positive and the negative drift are

reported. If there is failure, the column corresponding to the drift value at failure is highlighted in yellow, if not, there is a sign '-'.
As for the previous analysis, the ductility was analysed considering all the previous tests that were done (two seismic and one cyclic).

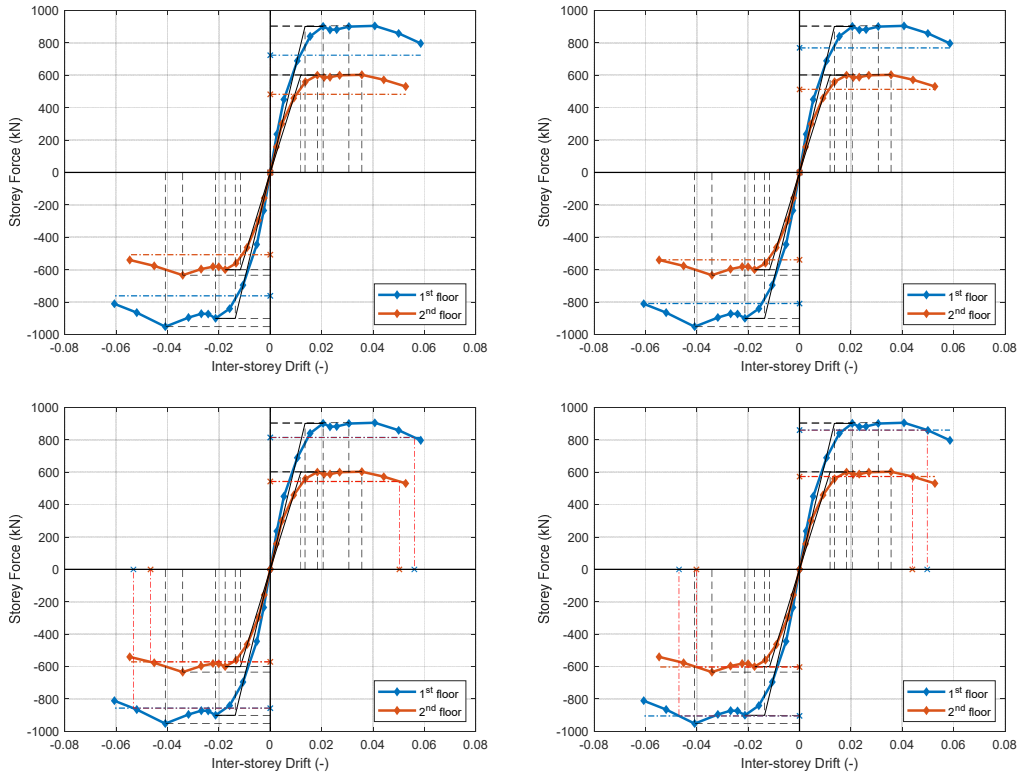

Figure 8.7 Definition of the yielding and failure at a) 80%, b) 85%, c) 90%, d) 95% points, test Cyc-1 (f02) + Cyc-2 (g04). Line: blue for the 1st floor, red for the 2nd. Horizontal dashed line, force at failure.

The failure criterion was not fulfilled for values of 80% and 85% of the maximum force (Figure 8.7 a and b), while failure is detected for the criteria 90% and 95% in both floors and both loading directions (Figure 8.7 c and d).
From Table 8.4, it is possible to observe that for both floors, for the positive drift, the displacement ductility factor is around 4 and for the negative drift it is around 3.
as it is possible to see from Table 8.4 the values of 90% and 95% of the residual resistance represent thresholds with of high sensibility. As reported in EC8, the 80% and the 85% of the residual resistance are the values that are more representative of structural collapse, the other two values of 90% and 95% were chosen as explorative values to widen the range of observation.

Table 8.4 Shear drift at limit, yielding and failure at 80%, 85%, 90%, 95% points, test B1 (f02). Yellow highlighted cells, failed.

	Limit Point		Yielding Point		Failure Point		
	Shear Max (kN)	Drift (-)	Shear Yielding (kN)	Drift (-)	XX Shear Max (kN)	Drift (-)	μ (-)
80%							
1st Floor positive	904.9	0.041	904.9	0.014	723.9	-	-
1st Floor negative	-951.6	-0.041	-951.6	-0.017	-761.3	-	-
2nd Floor positive	603.0	0.036	603.0	0.012	482.4	-	-
2nd Floor negative	-634.2	-0.034	-634.2	-0.015	-507.4	-	-
85%							
1st Floor positive	904.9	0.041	904.9	0.014	769.2	-	-
1st Floor negative	-951.6	-0.041	-951.6	-0.017	-808.9	-	-
2nd Floor positive	603.0	0.036	603.0	0.012	512.6	-	-
2nd Floor negative	-634.2	-0.034	-634.2	-0.015	-539.1	-	-
90%							
1st Floor positive	904.9	0.041	904.9	0.014	814.4	**0.056**	4.0
1st Floor negative	-951.6	-0.041	-951.6	-0.017	-856.5	**-0.053**	3.1
2nd Floor positive	603.0	0.036	603.0	0.012	542.7	**0.050**	4.1
2nd Floor negative	-634.2	-0.034	-634.2	-0.015	-570.8	**-0.047**	3.2
95%							
1st Floor positive	904.9	0.041	904.9	0.014	859.6	**0.050**	3.5
1st Floor negative	-951.6	-0.041	-951.6	-0.017	-904.0	**-0.047**	2.7
2nd Floor positive	603.0	0.036	603.0	0.012	572.9	**0.044**	3.6
2nd Floor negative	-634.2	-0.034	-634.2	-0.015	-602.5	**-0.040**	2.7

8.3.4 Energy Dissipation

Finally, the energy dissipation of each floor and of the entire structure was analysed. The procedure followed, together with the equations used and the graphs set up are reported in Chapter 5.2.4. The evolution of energy dissipation in the building and at the two-storey levels is shown in Figure 8.9 and Figure 8.8 respectively. In Figure 8.8 the energy dissipation for the whole structure is reported.

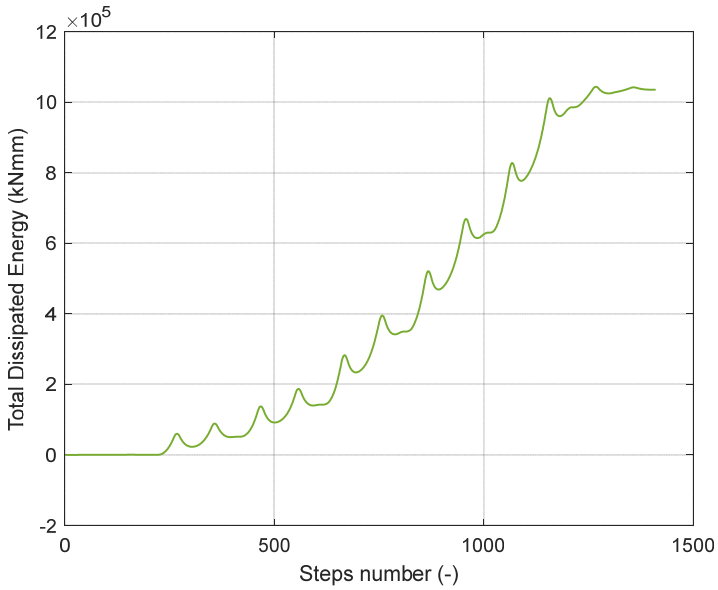

Figure 8.8 Structure energy dissipation. Tet cyc-2 (g04).

The energy dissipated from the structure during the cyclic test Cyc-2 was 1.3 times the energy dissipated during the previous Cyc-1 (Table 8.5).

Table 8.5 Energy dissipated from each floor, cyclic tests.

Test	Maximum dissipated energy (kJ)
Cyc-1	600690
Cyc-2	1043400

The energy dissipated from the 1st floor was about the twice as much compared to the 2nd one (Figure 8.9). This higher energy dissipation of the 1st floor is related to the force used to calculate it: in fact, to calculate the energy dissipation for the 1st floor, all the forces applied by the four load cells (two for each floor) were used. Moreover, as it will be possible to see from the local analysis and the deep observation of the cracking, the 1st floor reported the highest damage and of the two had not the shear reinforcement.

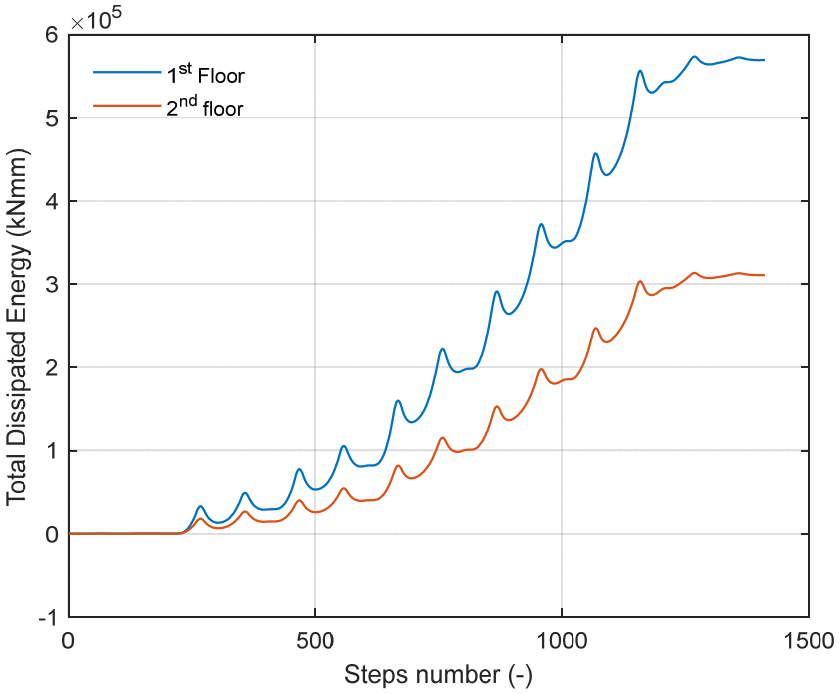

Figure 8.9 Floor energy dissipation, blue line 1st floor, red line 2nd floor. Tet Cyc-2 (g04).

Differing from the previous test typology, Seis-SLS and Seis-ULS, in which there was a one order magnitude difference between the two tests, for the cyclic typology this difference was not so large. The maximum acceleration of the seismic test Seis-ULS (2.498 m/s^2) was more than three times as much compared to that of the seismic test Seis-SLS (0.884 m/s^2). Regarding the cyclic tests, two different displacement histories were applied on the 2nd floor. A sets of three cycles with increasing global drift ratio (0.25%, 0.50%, 1.0%, 1.5%, 2.0%, 2.25% and 2.5%) was set up for the test Cyc-1. Differently, test Cyc-2 was performed for single cycles of global drift ratio (2.5%, 3.0%, 4.0%, 5.0% and 6.0%).
Each floor of the structure during the cyclic test Cyc-2 dissipated nearly twice as much the energy dissipated during the previous cyclic test, Cyc-1 (Table 8.6).

Table 8.6 Maximum energy dissipated from each floor, cyclic tests.

Floor / Test	1st	2nd
Cyc-1	3.3*10^5 kJ	1.7*10^5 kJ
Cyc-2	5.7*10^5 kJ	3*10^5 kJ

8.4 Local behaviour

The aims of this analysis are:

- The study of the response in the connections up to high drift ratios;
- Study of the failure modes, in particular punching failure in the internal slab-column connections;
- To compare the response of the strengthened connections to the un-strengthened;
- to study the different behaviour of the two halves of the slab with different longitudinal reinforcement layout (smeared and concentrated);
- to compare the response of slab-column connection with and without the shear reinforcement;
- to evaluate the load redistribution on the floor and to verify the efficiency of the integrity reinforcement with the occurrence of punching failure.

8.4.1 CONNECTION RESPONSE

The response of each of the twenty-four slab-column connections (twelve for each floor) is analysed in terms of stiffness loss, local ductility and local dissipated energy. The procedure followed, the equations used and the graphs set up are reported in Chapter 5.3.1.

Figure 8.10 reports the unbalanced moment versus the inter-storey drift ratio graphs for each slab-column connection. The reported results regard the whole cyclic experimental campaign so the test Cyc-1 followed by the test Cyc-2. The connections B1, C2 and C3 were strengthened after the test Cyc-1, see Chapter 3 and 4 for more details.

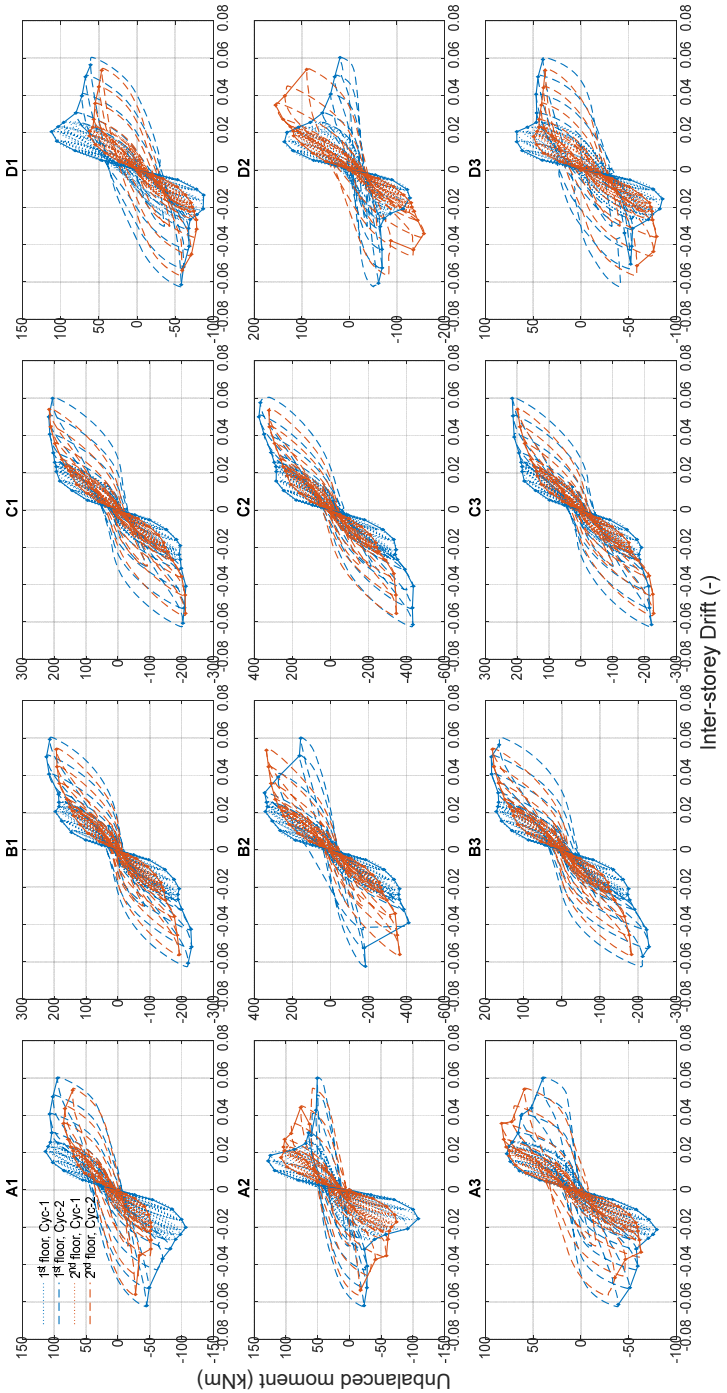

Figure 8.10 Unbalanced moment vs inter-storey drift , test Cyc1 + Cyc-2. Lines: dotted, test Cyc-1, dashed, test Cyc-2, blue ,1st floor, red, 2nd floor. Continuous = envelope.

In Table 8.7, all the maximum and the minimum values for the unbalanced moment for each connection and for both floors are reported.

Table 8.7 Maximum and minimum unbalanced moment for each connection (kNm), in both floors test Cyc-1+ Cyc-2.

1st Floor	A		B		C		D	
	Min	Max	Min	Max	Min	Max	Min	Max
1	-106.46	113.64	-231.20	224.37	-213.49	216.66	-87.08	111.77
2	-108.63	127.96	-411.68	345.03	-436.45	375.49	-56.73	136.52
3	-79.52	77.41	-228.35	184.15	-221.97	215.37	-46.73	67.09

2nd Floor	A		B		C		D	
	Min	Max	Min	Max	Min	Max	Min	Max
1	-51.93	85.37	-193.24	193.35	-212.11	215.49	-77.99	62.22
2	-74.34	107.81	-364.88	335.70	-347.03	322.29	-127.19	155.09
3	-63.00	82.94	-182.66	181.32	-228.32	198.95	-85.42	49.40

The load effects were redistributed from the edge slab-column connections typology in the alignments A and D to the internal slab-column connections typology in the alignments B and C (Figure 8.10). this can be observed at both floors. At the first floor the phenomenon started during test Cyc-1, whereas in test Cyc-2 for the 2nd floor. The strength deterioration of the 2nd floor nodes is less than at the 1st floor.

A sudden drop corresponding to an inter-story drift ratio value of 4.1% in negative (3.8% in the global top storey drift ratio) is visible in the interior connection B2 in the 1st floor (blue line in Figure 8.10). The unbalanced moment dropped sharply from 400 kNm to 180 kNm due to punching failure of the connection, ascertained by video recording and post-test visual inspection.

The interior strengthened connection C2 showed a better behaviour than the un-strengthened similar connection B2 with a stable response to the end of the test without noticeable failure. Only limited cracking damage was observed on the slab surface (see 8.5.3).

The effect of the strengthening is remarkable also in the other two connections B1 and C3. These are edge connections on the long side of the structure, parallel to the horizontal loading application, B1 on the North and C3 on the South. Neither connection failed, they reported some radial cracking around the columns and some damage in the slab cross section at the column face. The comparison with the corresponding un-strengthened connections (section 8.5) shows the efficiency of strengthening to limit damage.

After reaching the maximum value of unbalanced moment, a strength deterioration occurred in all the connections in the lines A and D. It is important to remember that before the tests started, the loading in the alignment A and D was removed.

The post critical response of the first floor connections along lines A and D showed the efficiency of the integrity reinforcement in avoiding the collapse of the floor, which consisting of two bottom reinforcement bars across the column in each direction.

Regarding the 2nd floor (red line in Figure 8.10), the maximum unbalanced moment was reached with a plateau in the response in some of the connections in the lines B and C for an inter-story drift ratio of approximately 0.05, whereas other connections showed a post-yield hardening response up to the end of the test; this can be seen for instance comparing B2 and C2, as well as other connections.
In the connections in the lines A and D the resistance was reached for an inter-story drift between 0.02 in A2, D1 and D3 and 0.04 in A1, A3 and D2 (section 8.4.5). the post critical response showed a more gradual reduction of moment, compared to the corresponding connections at the 1st floor. The analysis of the failure modes will be carried out in the following section (8.4.5).

8.4.2 Stiffness Deterioration

The stiffness degradation was analysed to describe the damage of each slab-column connection on each floor of the building. The followed procedure, the equations used and the graphs set up are reported in Chapter 5.3.
As in the global analysis, the stiffness deterioration was calculated considering all the previous tests, that is the two seismic, Seis-SLS and Seis-ULS and the cyclic Cyc-1.
As reported in Chapter 5, the stiffness deterioration was calculated using both the inter-storey drift ratio and the rotation.
The stiffness deterioration ratio versus the inter-storey drift is reported in Figure 8.11 whereas in Figure 8.13 the negative branches were reported with the absolute value to display the symmetry, in Figure 8.12 and Figure 8.14 instead the stiffness deterioration ratio versus the rotation and the corresponding absolute value are reported respectively.
After the graphs, a summary table with both floors and all the slab-column connections present in both the representations is reported with all the values of stiffness deterioration, inter-storey drift ratio and rotation (Table 8.8).

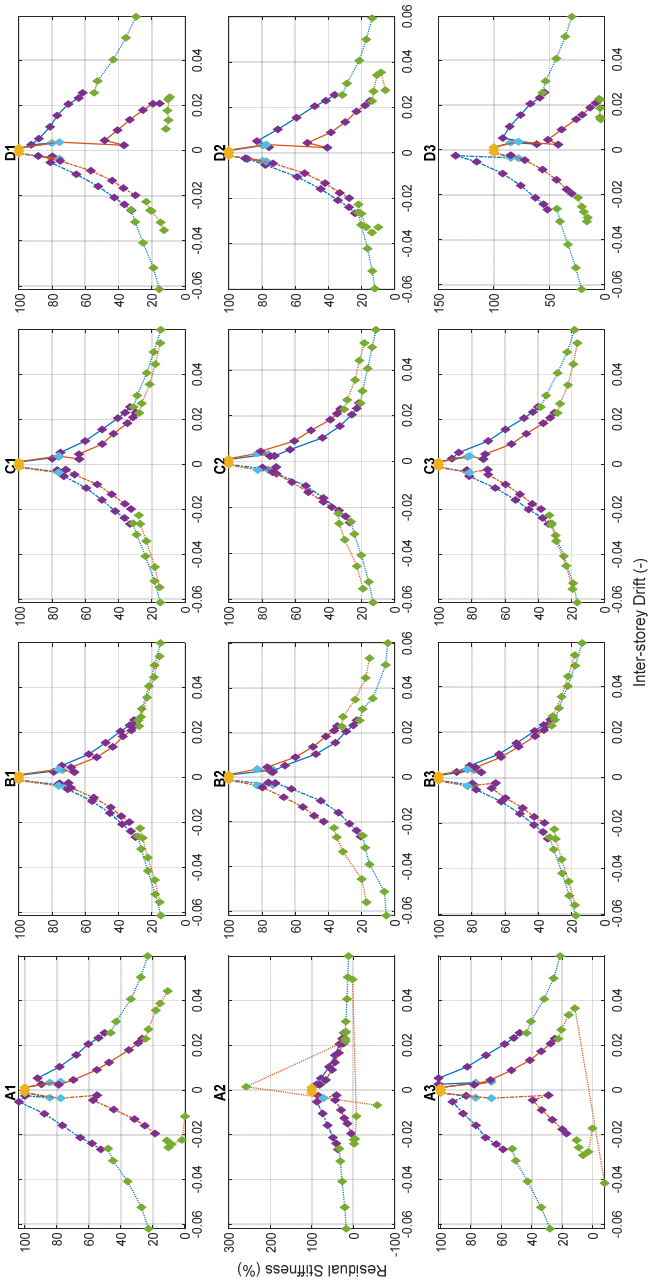

Figure 8.11 Residual stiffness vs I-S drift ratio. Stiffness deterioration ratio Test Seis-SLS (e03) +Seis-ULS (e06) +Cyc-1 (f02) +Cyc-2 (g04). Line: blue for the 1st floor, red for the 2nd, continuous, westward loading, dashed, eastward loading, dotted Test Cyc-2 (g04) with different gravity load. Points: yellow, test Seis-SLS (e03), light blue, test Seis-ULS (e06), purple, test Cyc-1 (f02), green, test Cyc-2 (g04).

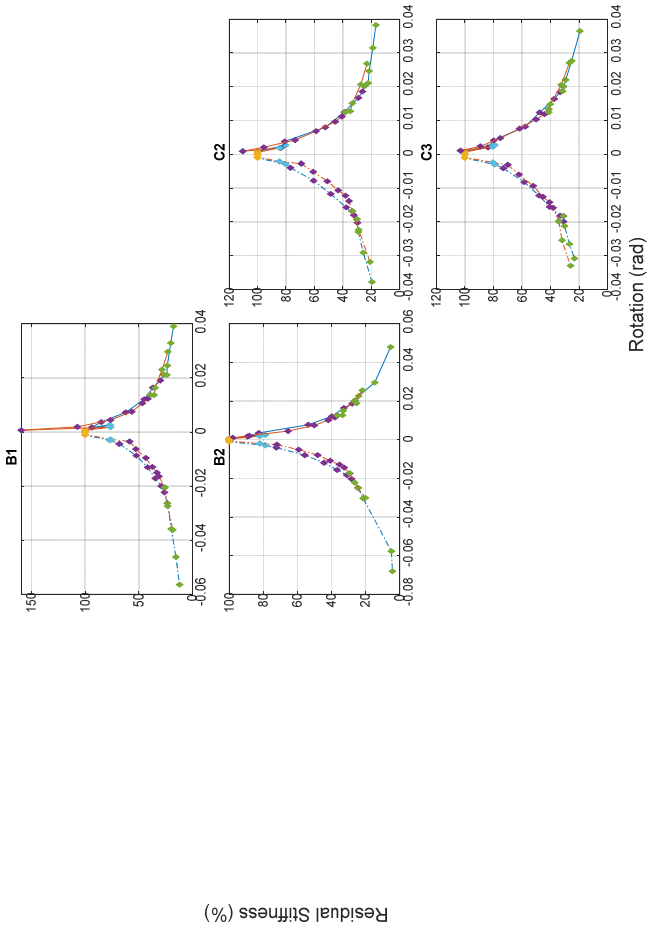

Figure 8.12 Residual stiffness vs Rotation. Stiffness deterioration ratio Test Seis-SLS (e03) +Seis-ULS (e06) +Cyc-1 (f02) +Cyc-2 (g04). Line: blue for the 1st floor, red for the 2nd, continuous, westward loading, dashed, eastward loading, dotted Test Cyc-2 (g04) with different gravity load. Points: yellow, test Seis-SLS (e03), light blue, test Seis-ULS (e06), purple, test Cyc-1 (f02), green, test Cyc-2 (g04).

On analysing the residual stiffness (Figure 8.11), it is possible to observe a drop of the residual stiffness comparable to that reached in the global behaviour (Figure 8.5).
During the second cyclic test Cyc-2, in the edge connections located on the long side of the structure (B1, C1, B3 and C3) the residual stiffness of the 1st and the 2nd floor became very similar (Figure 8.11).
In Figure 8.11 all the connections in the B and C alignment (internal and lateral long side) reached a residual stiffness lower than 10% whereas the connections in the A and D alignment (corner and lateral short side) higher than 10% (Table 8.8).
Using the column-slab rotation defined in Chapter 5 (Figure 8.12) the behaviour of the two floors becomes more similar, whereas the shape of the graphs and the values remain almost the same. Differently from the analysis with the inter-storey drift ratio, in Figure 8.11 the rotations of the 2nd floor are more similar to that of the 1st one.
The symmetry between the positive and the negative branches of the drift in the 1st and the 2nd floor (Figure 8.13) is well observable in the six central connections (B1, B2, B3, C1, C2, C3). Therefore, for these analyses they have not been taken into consideration. Similarly, in the previous chapter, the symmetry in the stiffness deterioration was verified in the global analysis whereas in the local one it was not observed in the alignments A and D.
Diversely, in the stiffness deterioration ratio absolute value with the rotation (Figure 8.14), there is a perfect symmetry between the two floor in all the analysed connections.
The strengthening did not affect the stiffness, in fact the strengthened and the un-strengthened similar connections (B1 vs B3, C3 vs C1 and C2 vs B2) have reported a very similar response. A detailed comparison is given in section 8.5.
The different longitudinal reinforcement layout (smeared and concentrated) seems not have influenced the stiffness degradation, since the slab-column connections in the two halves of the slab reported the same response.

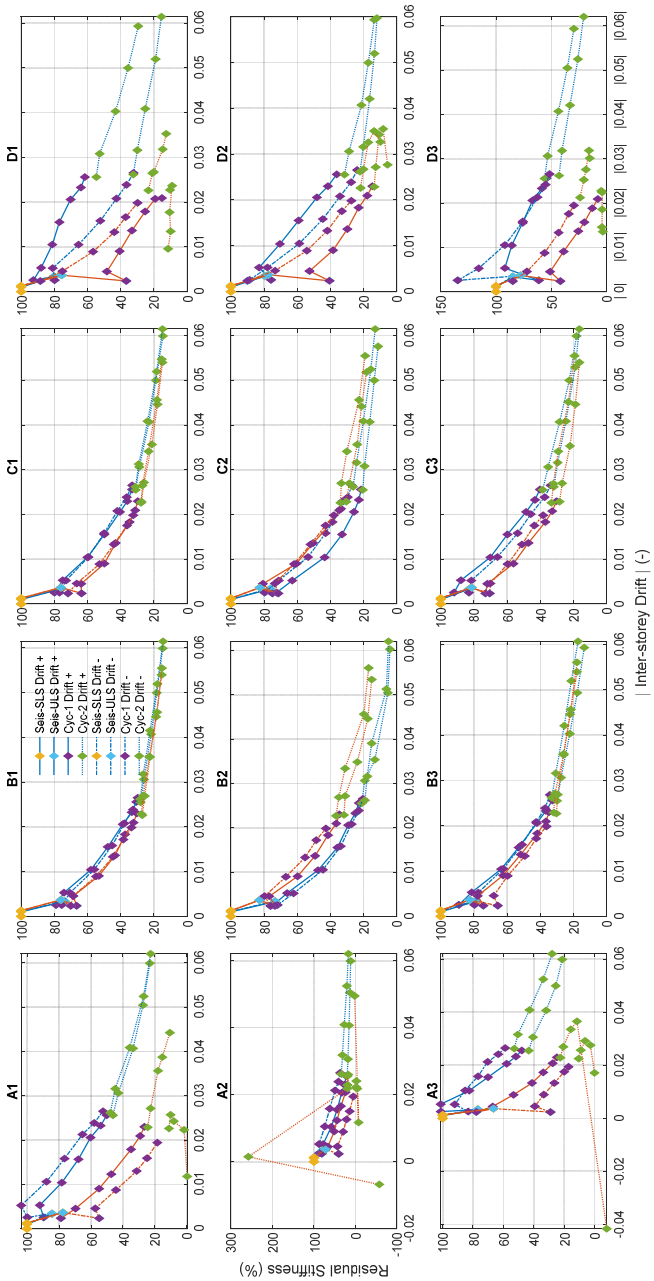

Figure 8.13 Residual stiffness vs I-S drift ratio. Stiffness deterioration ratio absolute value Test Seis-SLS (e03) +Seis-ULS (e06) +Cyc-1 (f02) +Cyc-2 (g04). Line: blue for the 1st floor, red for the 2nd, continuous, westward loading, dashed, eastward loading, dotted Test Cyc-2 (g04) with different gravity load. Points: yellow, test Seis-SLS (e03), light blue, test Seis-ULS (e06), purple, test Cyc-1 (f02), green, test Cyc-2 (g04).

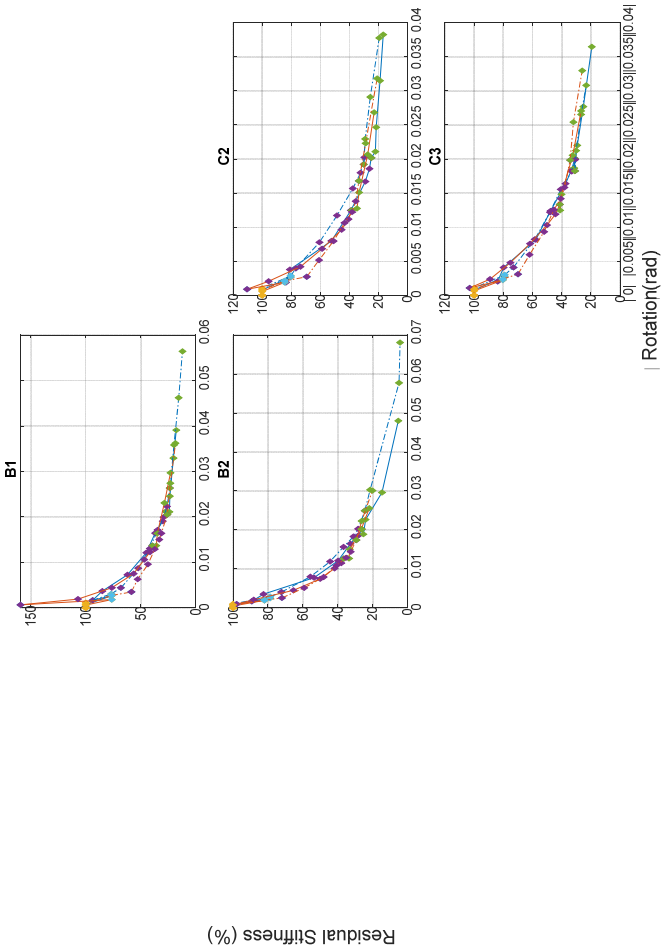

Figure 8.14 Residual stiffness vs Rotation. Stiffness deterioration ratio absolute value Test Seis-SLS (e03) +Seis-ULS (e06) +Cyc-1 (f02) +Cyc-2 (g04). Line: blue for the 1st floor, red for the 2nd, continuous, westward loading, dashed, eastward loading, dotted Test Cyc-2 (g04) with different gravity load. Points: yellow, test Seis-SLS (e03), light blue, test Seis-ULS (e06), purple, test Cyc-1 (f02), green, test Cyc-2 (g04).

As observed in the previous cyclic test, Cyc-1, the internal connections B2 and C2 are the only two in which the 2nd floor has a stiffness deterioration higher than that of the 1st.
In the two internal connections the 2nd floor overtakes the 1st one from the start of the experimental campaign. During the two seismic tests, the two floors report the same values or sometimes the 2nd one is above the 1st one, then after an inter-storey drift ratio of 0.5%, the 1st floor overcomes the 2nd one.
From the stiffness analysis reported in Figure 8.15 it is possible to observe that the stiffness of the 1st floor is higher than that of the 2nd one, in all the connections. This difference is probably related to the columns configuration effects.
The two internal connections B2 and C2 in the 1st floor, recorded the highest initial stiffness value 7 kN/mm and 6.5 kN/mm respectively.

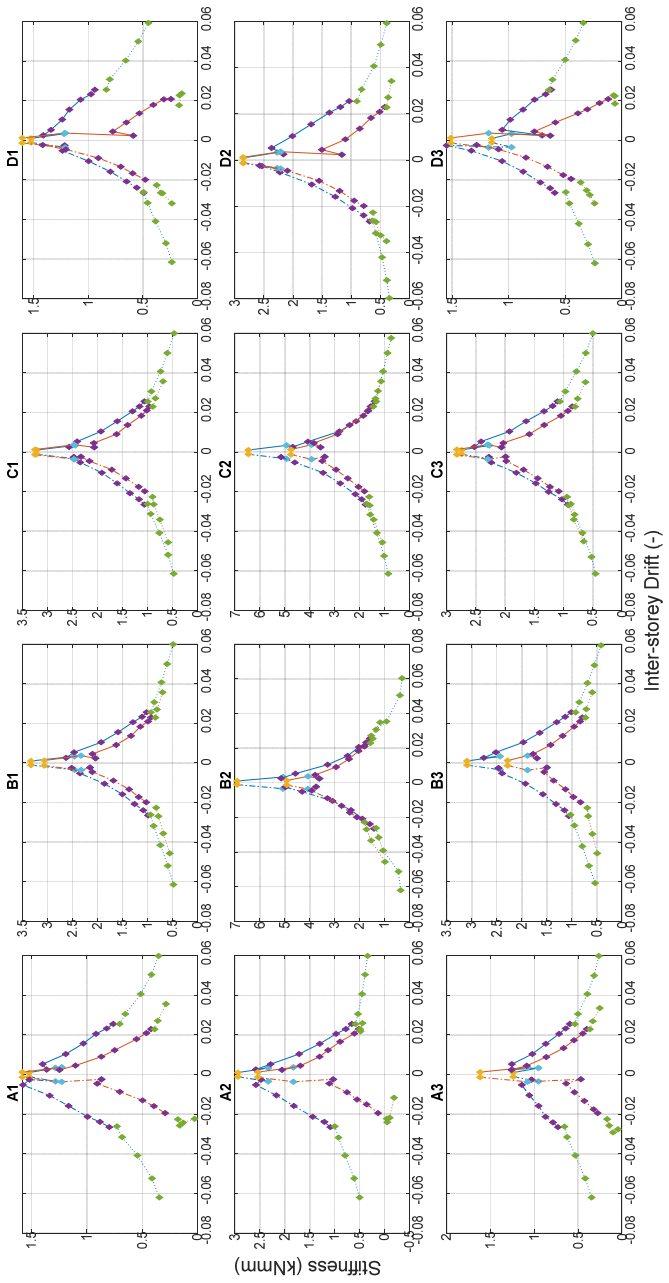

Figure 8.15 Stiffness vs I-S drift ratio, Test Seis-SLS (e03) +Seis-ULS (e06) +Cyc-1 (f02) +Cyc-2 (g04). Line: blue for the 1st floor, red for the 2nd, continuous, westward loading, dashed, eastward loading, dotted Test Cyc-2 (g04) with different gravity load. Points: yellow, test Seis-SLS (e03), light blue, test Seis-ULS (e06), purple, test Cyc-1 (f02), green, test Cyc-2 (g04).

Table 8.8 Residual Stiffness values of each connections, test Seis-SLS, Seis-ULS, Cyc-1, Cyc-2.

	Drift (-)	B1	B2	C2	C3	B1		B2		C2		C3	
						Rotation (rad)	Degradation (%)	Rotation (rad)	Degradation (%)	Rotation (rad)	Degradation (%)	Rotation (rad)	Degradation (%)
1st floor negative	0	100	100	100	100	0.0000	100.0	0.0000	100.0	0.0000	100.0	0.0000	100.0
	-0.00109	100	100	100	100	0.0007	100.0	0.0008	100.0	0.0008	100.0	0.0008	100.0
	-0.00346	73.8	73.4	76.3	82.7	0.0026	76.8	0.0025	78.8	0.0027	80.4	0.0027	79.1
	-0.00255	75.6	72.0	79.7	83.0	0.0017	93.7	0.0017	89.3	0.0019	83.6	0.0021	83.8
	-0.00525	70.6	62.2	71.2	81.6	0.0037	84.9	0.0035	82.6	0.0038	80.9	0.0041	79.8
	-0.01061	55.9	44.6	53.5	65.8	0.0073	62.1	0.0078	53.6	0.0080	52.3	0.0082	57.7
	-0.01583	45.2	33.9	43.0	53.7	0.0121	44.9	0.0121	39.8	0.0125	38.9	0.0124	47.7
	-0.02128	37.8	27.4	33.6	45.7	0.0164	37.0	0.0164	32.7	0.0167	29.0	0.0164	37.4
	-0.02387	32.6	23.0	29.6	37.4	0.0191	30.0	0.0187	27.9	0.0186	26.2	0.0184	33.3
	-0.02652	29.8	20.6	27.2	33.8	0.0212	27.0	0.0202	26.2	0.0202	24.9	0.0201	31.0
	-0.00195	24.6	23.8	58.1	20.6	0.0211	24.0	0.0189	25.3	0.0211	22.1	0.0187	31.5
	-0.02618	28.3	19.3	26.4	31.9	0.0246	23.5	0.0226	24.1	0.0247	21.5	0.0220	29.4
	-0.03159	26.4	17.9	24.3	29.5	0.0330	20.3	0.0296	14.6	0.0315	18.9	0.0277	25.2
	-0.04086	22.3	15.2	20.2	24.6	0.0391	17.8	0.0480	5.3	0.0383	16.8	0.0365	19.4
	-0.05244	17.9	6.3	15.7	19.0	0.0457	14.5	0.0584	4.2	0.0439	14.3	0.0445	16.1
	-0.06203	14.5	5.1	13.1	16.5								
	-0.02983	14.4	3.4	14.1	19.2								
1st floor positive	0	100	100	100	100	0.0000	100.0	0.0000	100.0	0.0000	100.0	0.0000	100.0
	0.001001	100	100	100	100	-0.0011	100.0	-0.0010	100.0	-0.0010	100.0	-0.0011	100.0
	0.003332	73.8	73.4	76.3	82.7	-0.0031	76.8	-0.0029	78.8	-0.0029	80.4	-0.0030	79.1
	0.002555	79.0	74.4	72.5	92.0	-0.0044	68.1	-0.0040	72.3	-0.0040	76.9	-0.0041	73.0
	0.005308	74.2	66.1	63.0	87.8	-0.0087	52.3	-0.0080	55.7	-0.0078	60.6	-0.0082	58.5
	0.010406	57.9	47.5	43.6	70.1	-0.0131	41.8	-0.0119	44.4	-0.0117	48.5	-0.0122	48.0
	0.015678	47.8	35.9	33.1	59.8	-0.0171	34.7	-0.0156	36.7	-0.0157	37.6	-0.0156	40.6
	0.020572	38.8	29.3	25.9	48.6	-0.0200	29.2	-0.0183	31.0	-0.0180	32.3	-0.0182	33.2
	0.023267	33.3	25.1	22.9	43.2	-0.0223	26.2	-0.0203	28.3	-0.0203	29.7	-0.0199	30.8
	0.025584	30.6	22.9	21.6	40.2	-0.0264	23.5	-0.0249	24.5	-0.0192	30.2	-0.0183	31.0
	0.002022	19.4	23.8	-7.5	40.5	-0.0358	19.8	-0.0303	21.5	-0.0229	29.2	-0.0212	30.2
	0.025591	28.0	21.2	20.6	38.6	-0.0462	15.5	-0.0577	4.9	-0.0291	25.6	-0.0266	26.7
	0.030613	26.0	19.3	19.5	35.3	-0.0564	12.1	-0.0681	4.3	-0.0378	19.5	-0.0308	23.2
	0.040695	21.7	13.3	16.3	28.4	-0.0326	8.0	-0.0356	4.2	-0.0450	16.5	-0.0363	20.4
	0.050454	18.3	5.5	13.6	22.5								
	0.059891	14.7	4.2	11.3	18.2								
	0.013096	17.8	5.4	7.0	22.1								
2nd floor negative	0	100	100	100	100	0.0000	100.0	0.0000	100.0	0.0000	100.0	0.0000	100.0
	-0.00133	100	100	100	100	0.0006	100.0	0.0005	100.0	0.0006	100.0	0.0007	100.0
	-0.00365	76.1	82.8	82.6	81.4	0.0018	76.4	0.0019	82.0	0.0019	84.6	0.0023	80.3
	-0.00236	70.1	76.1	71.5	70.5	0.0007	159.3	0.0010	98.0	0.0009	110.4	0.0011	103.0
	-0.00458	68.7	79.7	73.6	70.1	0.0019	107.1	0.0021	88.1	0.0021	95.5	0.0024	89.1
	-0.00873	54.9	66.9	61.9	59.7	0.0044	76.3	0.0045	65.4	0.0042	73.6	0.0048	75.1
	-0.01301	44.7	55.4	52.1	51.0	0.0075	56.5	0.0074	50.1	0.0068	58.8	0.0076	61.6
	-0.01592	38.4	48.6	43.0	43.6	0.0106	46.8	0.0101	41.8	0.0096	45.4	0.0103	50.1
	-0.01944	33.5	42.8	38.0	38.3	0.0123	41.6	0.0115	38.0	0.0112	40.6	0.0119	44.2
	-0.02095	21.1	53.9	50.7	44.6	0.0137	39.4	0.0126	36.6	0.0125	38.4	0.0133	41.3
	-0.00182	27.0	36.7	34.0	33.3	0.0137	35.9	0.0127	33.5	0.0128	34.8	0.0125	41.1
	-0.02262	25.5	35.0	33.5	32.1	0.0164	34.9	0.0150	33.2	0.0151	33.3	0.0148	40.1
	-0.02572	22.4	31.2	30.1	29.2	0.0231	28.4	0.0202	26.5	0.0207	27.4	0.0205	32.5
	-0.02425	18.1	19.9	22.8	23.1	0.0297	23.0	0.0256	21.9	0.0268	23.0	0.0271	26.7
	-0.02232	15.2	17.0	19.2	19.4	0.0366	18.9	0.0314	18.5	0.0331	18.8	0.0345	21.9
	-0.01182	12.3	16.9	17.8	17.6								
2nd floor positive	0	100	100	100	100	0.0000	100.0	0.0000	100.0	0.0000	100.0	0.0000	100.0
	0.001247	100	100	100	100	-0.0008	100.0	-0.0008	100.0	-0.0008	100.0	-0.0009	100.0
	0.003684	76.1	82.8	82.6	81.4	-0.0027	76.4	-0.0019	82.0	-0.0021	84.6	-0.0024	80.3
	0.002377	66.6	73.5	75.0	73.1	-0.0035	58.6	-0.0025	72.0	-0.0027	69.3	-0.0031	69.9
	0.004533	68.6	76.8	80.7	71.9	-0.0063	52.8	-0.0051	59.2	-0.0052	60.9	-0.0060	62.0
	0.009038	53.1	59.8	60.5	56.2	-0.0096	43.4	-0.0079	48.1	-0.0080	50.9	-0.0093	52.1
	0.012313	43.5	49.3	50.5	47.2	-0.0129	37.3	-0.0109	40.8	-0.0107	43.3	-0.0126	45.4
	0.017915	37.4	41.5	38.8	37.0	-0.0150	33.1	-0.0129	35.3	-0.0122	38.2	-0.0142	40.6
	0.020946	32.3	36.5	34.8	32.8	-0.0164	31.3	-0.0144	32.5	-0.0138	35.7	-0.0158	38.1
	0.022992	30.3	34.7	32.8	30.2	-0.0205	26.0	-0.0174	29.4	-0.0168	33.4	-0.0198	34.2
	0.001926	17.6	7.4	6.9	11.2	-0.0274	23.1	-0.0223	26.3	-0.0223	28.9	-0.0254	32.0
	0.022877	27.5	31.9	30.5	28.4	-0.0362	18.4	-0.0301	20.1	-0.0318	20.9	-0.0330	26.0
	0.027145	26.5	31.2	28.6	26.9	-0.0455	15.2	-0.0391	16.1	-0.0413	16.3	-0.0412	21.0
	0.035651	22.8	23.9	23.9	22.1								
	0.038722	18.7	17.6	21.4	18.9								
	0.044225	15.3	15.2	18.3	16.5								
	0.01461	9.5	9.9	10.6	11.6								

8.4.3 DUCTILITY AND ULTIMATE DRIFT CAPACITY

Following the methodology reported in Chapter 5.2.3 together with the equations

used and the graphs set up, the ductility of each of the twenty-four slab-column connections (twelve for each floor) is here reported.
As for the global analysis, also for the local one, all the four percentages of the residual resistance 80%, 85%, 90% and 95% are analysed and reported in the following Figure 8.16, Figure 8.17, Figure 8.18 and Figure 8.19.
For each of them, the graph with the representation of the analysed percentage is reported and if the conditions to reach failure are respected, a red continuous line indicates the failure force and the corresponding displacement.
After the graphs, a table with the shear and the corresponding drift of the three characteristic points (Limit, Yielding and Failure) is reported with in columns all the connections (Table 8.10, Table 8.12, Table 8.14 and Table 8.16).
The last line of each floor reports the displacement ductility factor, μ.
For each of the four percentage drop in loading resistance, a table with the displacement ductility factor for only the failed connections is reported (Table 8.9, Table 8.11, Table 8.13 and Table 8.15).
A summary sketch of the failed connections is reported (Figure 8.20) together with a summary table with the displacement ductility factor at failure for all the analysed percentages of drop in the loading resistance (Table 8.17) and a comparison with the previous cyclic test (Table 8.18).
Finally, in Table 8.19 the maximum and the minimum values of the displacement ductility factor for both the cyclic tests are reported.

80% OF THE MAXIMUM UNBALANCED MOMENT

For the 80% of the maximum unbalanced moment, the lateral short side connections in the 1st and the 2nd floor and the central B2 in the 1st floor failed (Figure 8.16). During this test and for this analysed percentage, the negative drift, corresponding to the first cycle for each displacement increase, accumulated more failures than the positive one (Table 8.10). Part of the edge connections at the 1st floor failed during test Cyc-1. All the 1st and 2nd floor connections on sides A and D failed.
All the connections on the 2nd floor reported a displacement ductility factor higher than that of to the 1st floor excepting for the two connections A3 and D2 positive drift in which the values in the 2nd floor were lower than the 1st (Table 8.9).

Table 8.9 Displacement ductility factor for the failed connections at 80%, test Cyc-1 (f02) + Cyc-2 (g04).

	Floor	Drift	A1	A2	A3	B2	D1	D2	D3
μ (-)	1st	Positive	-	2.14	3.38	2.74	1.86	1.97	2.21
		Negative	2.29	2.19	1.88	2.23	2.66	2.63	2.67
μ (-)	2nd	Positive	-	-	2.83	-	3.09	1.79	3.45
		Negative	2.91	2.74	2.13	-	3.36	-	2.96

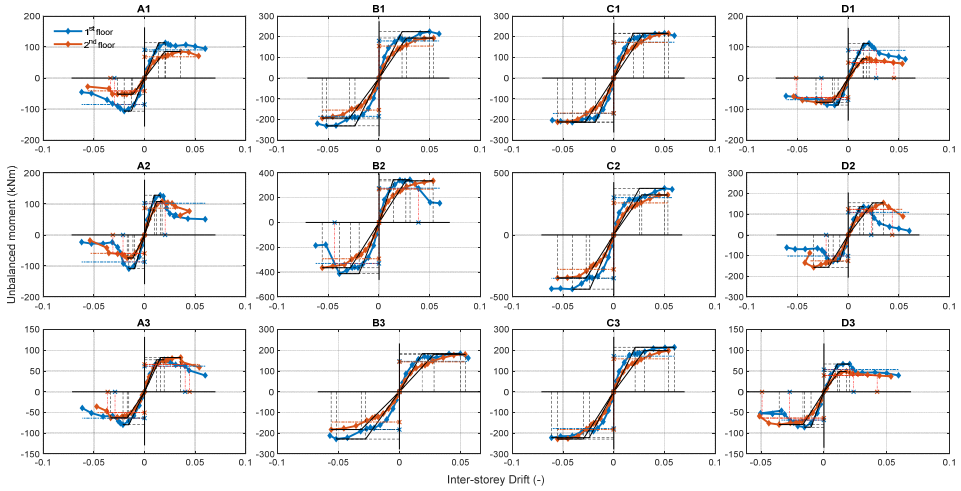

Figure 8.16 Unbalanced Moment vs Inter-story drift ratio. Definition of the yielding and failure at 80% points for all the connections, test Cyc-1 (f02) + Cyc-2 (g04). Line: blue for the 1st floor, red for the 2nd. Horizontal dashed line, force at failure. Vertical red line, drift at failure.

Table 8.10 Unbalanced moment drift at limit, yielding and failure at 80% for all the connections, test Cyc-1 (f02) + Cyc-2 (g04). Yellow highlighted cells, failed connections.

		Connections	A1	A2	A3	B1	B2	B3	C1	C2	C3	D1	D2	D3
			1	2	3	4	5	6	7	8	9	10	11	12
1 Floor positive	Limit point	UM Max (kNm)	113.64	127.96	77.41	224.37	345.03	184.15	216.66	375.49	215.37	111.77	136.52	67.09
		Drift (-)	0.021	0.016	0.019	0.050	0.031	0.050	0.050	0.050	0.060	0.021	0.015	0.021
	Yielding point	UM Yielding (kNm)	113.64	127.96	77.41	224.37	345.03	184.15	216.66	375.49	215.37	111.77	136.52	67.09
		Drift (-)	0.014	0.010	0.012	0.023	0.014	0.019	0.019	0.025	0.021	0.015	0.012	0.011
	Failure point	0.80 UM Max (kNm)	90.91	102.37	61.93	179.50	276.03	147.32	173.32	300.39	172.30	89.42	109.22	53.67
		Drift (-)	0.000	**0.020**	**0.040**	0.000	**0.039**	0.000	0.000	0.000	0.000	**0.028**	**0.023**	**0.024**
		μ (-)	0.00	2.14	3.38	0.00	2.74	0.00	0.00	0.00	0.00	1.86	1.97	2.21
1 Floor negative	Limit point	UM Max (kNm)	-106.46	-108.63	-79.52	-231.20	-411.68	-228.35	-213.49	-436.45	-221.97	-87.08	-127.19	-85.42
		Drift (-)	-0.020	-0.015	-0.021	-0.052	-0.039	-0.052	-0.041	-0.041	-0.061	-0.013	-0.015	-0.015
	Yielding point	UM Yielding (kNm)	-106.46	-108.63	-79.52	-231.20	-411.68	-228.35	-213.49	-436.45	-221.97	-87.08	-127.19	-85.42
		Drift (-)	-0.013	-0.010	-0.015	-0.024	-0.020	-0.028	-0.018	-0.024	-0.024	-0.010	-0.008	-0.010
	Failure point	0.80 UM Max (kNm)	-85.17	-86.91	-63.62	-184.96	-329.35	-182.68	-170.79	-349.16	-177.58	-69.67	-101.75	-68.33
		Drift (-)	**-0.030**	**-0.021**	**-0.029**	0.000	**-0.044**	0.000	0.000	0.000	0.000	**-0.026**	**-0.022**	**-0.027**
		μ (-)	2.29	2.19	1.88	0.00	2.23	0.00	0.00	0.00	0.00	2.66	2.63	2.67
2 Floor positive	Limit point	UM Max (kNm)	85.37	107.81	82.94	193.35	335.70	181.32	215.50	322.30	198.95	62.22	155.09	49.40
		Drift (-)	0.036	0.017	0.036	0.054	0.053	0.054	0.054	0.053	0.054	0.018	0.035	0.018
	Yielding point	UM Yielding (kNm)	85.37	107.81	82.94	193.35	335.70	181.32	215.50	322.30	198.95	62.22	155.09	49.40
		Drift (-)	0.020	0.012	0.016	0.027	0.026	0.028	0.029	0.028	0.030	0.015	0.024	0.012
	Failure point	0.80 UM Max (kNm)	68.30	86.25	66.36	154.68	268.56	145.05	172.40	257.84	159.16	49.77	124.07	39.52
		Drift (-)	0.000	0.000	**0.045**	0.000	0.000	0.000	0.000	0.000	0.000	**0.045**	**0.043**	**0.042**
		μ (-)	0.00	0.00	2.83	0.00	0.00	0.00	0.00	0.00	0.00	3.09	1.79	3.45
2 Floor negative	Limit point	UM Max (kNm)	-51.93	-74.34	-63.00	-193.24	-364.88	-182.66	-212.11	-347.03	-228.32	-77.99	-156.57	-79.24
		Drift (-)	-0.027	-0.017	-0.033	-0.056	-0.056	-0.056	-0.055	-0.055	-0.055	-0.032	-0.034	-0.036
	Yielding point	UM Yielding (kNm)	-51.93	-74.34	-63.00	-193.24	-364.88	-182.66	-212.11	-347.03	-228.32	-77.99	-156.57	-79.24
		Drift (-)	-0.012	-0.011	-0.017	-0.029	-0.028	-0.031	-0.028	-0.027	-0.030	-0.015	-0.020	-0.017
	Failure point	0.80 UM Max (kNm)	-41.54	-59.48	-50.40	-154.59	-291.91	-146.13	-169.69	-277.62	-182.66	-62.39	-125.26	-63.39
		Drift (-)	**-0.034**	**-0.031**	**-0.036**	0.000	0.000	0.000	0.000	0.000	0.000	**-0.051**	0.000	**-0.049**
		μ (-)	2.91	2.74	2.13	0.00	0.00	0.00	0.00	0.00	0.00	3.36	0.00	2.96

85% OF THE MAXIMUM UNBALANCED MOMENT

For 85% of the maximum unbalanced moment, the connections that have failed are the same as the 80% of the maximum unbalanced moment with two additional connections on the lateral short west side, A1 for positive drift on the 1st and 2nd floor and A2 for the positive drift on the 2nd floor (Figure 8.17 and Table 8.12)
As in the previous case, the displacement ductility factor on the 2nd floor was always higher compared with the 1st floor except for the two connections A3 and D2 in which the values on the 2nd floor were lower than the 1st (Table 8.11).

Table 8.11 Displacement ductility factor for the failed connections at 85%, test Cyc-1 (f02) + Cyc-2 (g04).

	Floor	Drift	A1	A2	A3	B2	D1	D2	D3
μ (-)	1st	Positive	4.11	2.08	2.57	2.60	1.74	1.90	2.13
		Negative	2.03	2.13	1.76	2.17	2.53	2.55	2.47
μ (-)	2nd	Positive	2.60	2.56	2.48	-	2.70	1.69	2.64
		Negative	2.87	1.92	2.09	-	3.18	-	2.85

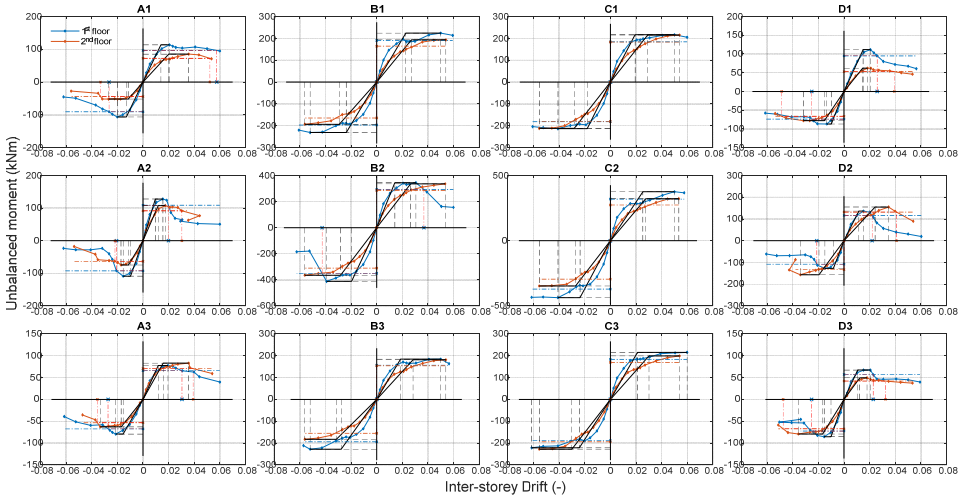

Figure 8.17 Unbalanced Moment vs Inter-story drift ratio. Definition of the yielding and failure at 85% points for all the connections, test Cyc-1 (f02) + Cyc-2 (g04). Line: blue for the 1st floor, red for the 2nd. Horizontal dashed line, force at failure. Vertical red line, drift at failure.

Table 8.12 Unbalanced moment drift at limit, yielding and failure at 85% for all the connections, test Cyc-1 (f02) + Cyc-2 (g04). Yellow highlighted cells, failed connections.

		Connections	A1	A2	A3	B1	B2	B3	C1	C2	C3	D1	D2	D3
			1	2	3	4	5	6	7	8	9	10	11	12
1 Floor positive	Limit point	UM Max (kNm)	113.64	127.96	77.41	224.37	345.03	184.15	216.66	375.49	215.37	111.77	136.52	67.09
		Drift (-)	0.021	0.016	0.019	0.050	0.031	0.050	0.050	0.050	0.060	0.021	0.015	0.021
	Yielding point	UM Yielding (kNm)	113.64	127.96	77.41	224.37	345.03	184.15	216.66	375.49	215.37	111.77	136.52	67.09
		Drift (-)	0.014	0.010	0.012	0.023	0.014	0.019	0.019	0.025	0.021	0.015	0.012	0.011
	Failure point	0.85 UM Max (kNm)	96.59	108.77	65.80	190.72	293.28	156.53	184.16	319.17	183.07	95.00	116.04	57.03
		Drift (-)	**0.058**	**0.020**	**0.030**	0.000	**0.037**	0.000	0.000	0.000	0.000	**0.026**	**0.022**	**0.023**
		μ (-)	4.11	2.08	2.57	0.00	2.60	0.00	0.00	0.00	0.00	1.74	1.90	2.13
1 Floor negative	Limit point	UM Max (kNm)	-106.46	-108.63	-79.52	-231.20	-411.68	-228.35	-213.49	-436.45	-221.97	-87.08	-127.19	-85.42
		Drift (-)	-0.020	-0.015	-0.021	-0.052	-0.039	-0.052	-0.041	-0.041	-0.061	-0.013	-0.015	-0.015
	Yielding point	UM Yielding (kNm)	-106.46	-108.63	-79.52	-231.20	-411.68	-228.35	-213.49	-436.45	-221.97	-87.08	-127.19	-85.42
		Drift (-)	-0.013	-0.010	-0.015	-0.024	-0.020	-0.028	-0.018	-0.024	-0.024	-0.010	-0.008	-0.010
	Failure point	0.85 UM Max (kNm)	-90.49	-92.34	-67.59	-196.52	-349.93	-194.10	-181.47	-370.98	-188.68	-74.02	-108.11	-72.60
		Drift (-)	**-0.026**	**-0.021**	**-0.027**	0.000	**-0.043**	0.000	0.000	0.000	0.000	**-0.025**	**-0.021**	**-0.025**
		μ (-)	2.03	2.13	1.76	0.00	2.17	0.00	0.00	0.00	0.00	2.53	2.55	2.47
2 Floor positive	Limit point	UM Max (kNm)	85.37	107.81	82.94	193.35	335.70	181.32	215.50	322.30	198.95	62.22	155.09	49.40
		Drift (-)	0.036	0.017	0.036	0.054	0.053	0.054	0.054	0.053	0.054	0.018	0.035	0.018
	Yielding point	UM Yielding (kNm)	85.37	107.81	82.94	193.35	335.70	181.32	215.50	322.30	198.95	62.22	155.09	49.40
		Drift (-)	0.020	0.012	0.016	0.027	0.026	0.028	0.029	0.028	0.030	0.015	0.024	0.012
	Failure point	0.85 UM Max (kNm)	72.57	91.64	70.50	164.34	285.35	154.12	183.17	273.95	169.10	52.89	131.82	41.99
		Drift (-)	**0.052**	**0.030**	**0.039**	0.000	0.000	0.000	0.000	0.000	0.000	**0.039**	**0.041**	**0.032**
		μ (-)	2.60	2.56	2.48	0.00	0.00	0.00	0.00	0.00	0.00	2.70	1.69	2.64
2 Floor negative	Limit point	UM Max (kNm)	-51.93	-74.34	-63.00	-193.24	-364.88	-182.66	-212.11	-347.03	-228.32	-77.99	-156.57	-79.24
		Drift (-)	-0.027	-0.017	-0.033	-0.056	-0.056	-0.056	-0.055	-0.055	-0.055	-0.032	-0.034	-0.036
	Yielding point	UM Yielding (kNm)	-51.93	-74.34	-63.00	-193.24	-364.88	-182.66	-212.11	-347.03	-228.32	-77.99	-156.57	-79.24
		Drift (-)	-0.012	-0.011	-0.017	-0.029	-0.028	-0.031	-0.028	-0.027	-0.030	-0.015	-0.020	-0.017
	Failure point	0.85 UM Max (kNm)	-44.14	-63.19	-53.55	-164.26	-310.15	-155.26	-180.29	-294.97	-194.07	-66.29	-133.09	-67.35
		Drift (-)	**-0.033**	**-0.022**	**-0.036**	0.000	0.000	0.000	0.000	0.000	0.000	**-0.049**	0.000	**-0.047**
		μ (-)	2.87	1.92	2.09	0.00	0.00	0.00	0.00	0.00	0.00	3.18	0.00	2.85

90% OF THE MAXIMUM UNBALANCED MOMENT

For 90% of the maximum unbalanced moment, only the connection on the long south side, B3 on the 1st floor and for the positive drift, was added to the connections failed during the previous analysed percentage (Figure 8.18and Table 8.14).
The displacement ductility factor on the 2nd floor was higher compared to that of the 1st floor except for the connections A1 positive drift, A2 negative drift and D2 positive drift in which the values of the 2nd floor were lower than those of the 1st (Table 8.13).

Table 8.13 Displacement ductility factor for the failed connections at 90%, test Cyc-1 (f02) + Cyc-2 (g04).

	Floor	Drift	A1	A2	A3	B2	B3	D1	D2	D3
μ (-)	1st	Positive	3.54	2.02	2.29	2.45	3.00	1.62	1.83	2.06
		Negative	1.89	1.95	1.65	2.11	-	2.39	2.41	2.26
μ (-)	2nd	Positive	2.42	2.42	2.31	-	-	2.06	1.60	1.80
		Negative	2.82	1.73	2.04	-	-	3.00	-	2.75

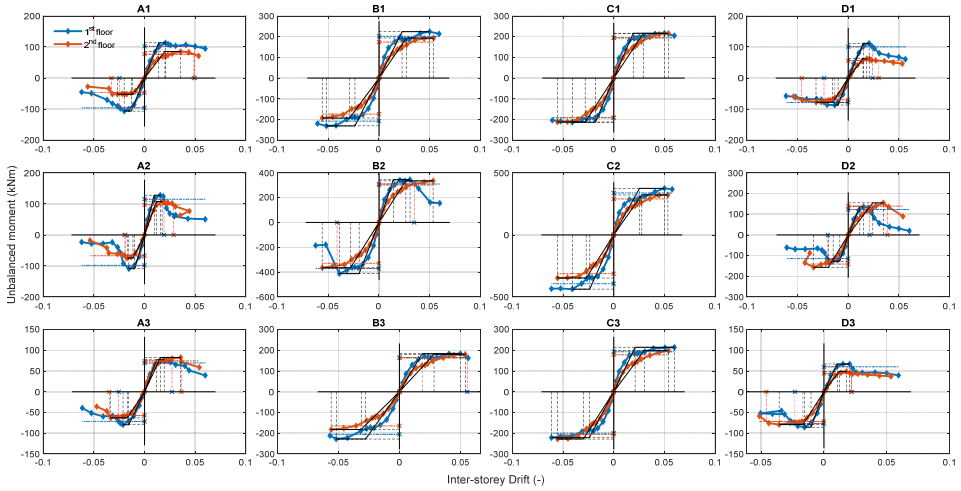

Figure 8.18 Unbalanced Moment vs Inter-story drift ratio. Definition of the yielding and failure at 90% points for all the connections, test Cyc-1 (f02) + Cyc-2 (g04). Line: blue for the 1st floor, red for the 2nd. Horizontal dashed line, force at failure. Vertical red line, drift at failure.

Table 8.14 Unbalanced moment drift at limit, yielding and failure at 90% for all the connections, test Cyc-1 (f02) + Cyc-2 (g04). Yellow highlighted cells, failed connections.

		Connections	A1	A2	A3	B1	B2	B3	C1	C2	C3	D1	D2	D3
			1	2	3	4	5	6	7	8	9	10	11	12
1 Floor positive	Limit point	UM Max (kNm)	113.64	127.96	77.41	224.37	345.03	184.15	216.66	375.49	215.37	111.77	136.52	67.09
		Drift (-)	0.021	0.016	0.019	0.050	0.031	0.050	0.050	0.050	0.060	0.021	0.015	0.021
	Yielding point	UM Yielding (kNm)	113.64	127.96	77.41	224.37	345.03	184.15	216.66	375.49	215.37	111.77	136.52	67.09
		Drift (-)	0.014	0.010	0.012	0.023	0.014	0.019	0.019	0.025	0.021	0.015	0.012	0.011
	Failure point	0.90 UM Max (kNm)	102.27	115.17	69.67	201.94	310.53	165.74	194.99	337.94	193.84	100.59	122.87	60.38
		Drift (-)	**0.050**	**0.019**	**0.027**	0.000	**0.035**	**0.056**	0.000	0.000	0.000	**0.024**	**0.021**	**0.022**
		μ (-)	3.54	2.02	2.29	0.00	2.45	3.00	0.00	0.00	0.00	1.62	1.83	2.06
1 Floor negative	Limit point	UM Max (kNm)	-106.46	-108.63	-79.52	-231.20	-411.68	-228.35	-213.49	-436.45	-221.97	-87.08	-127.19	-85.42
		Drift (-)	-0.020	-0.015	-0.021	-0.052	-0.039	-0.052	-0.041	-0.041	-0.061	-0.013	-0.015	-0.015
	Yielding point	UM Yielding (kNm)	-106.46	-108.63	-79.52	-231.20	-411.68	-228.35	-213.49	-436.45	-221.97	-87.08	-127.19	-85.42
		Drift (-)	-0.013	-0.010	-0.015	-0.024	-0.020	-0.028	-0.018	-0.024	-0.024	-0.010	-0.008	-0.010
	Failure point	0.90 UM Max (kNm)	-95.81	-97.77	-71.57	-208.08	-370.51	-205.52	-192.14	-392.81	-199.78	-78.38	-114.47	-76.88
		Drift (-)	**-0.025**	**-0.019**	**-0.026**	0.000	**-0.041**	0.000	0.000	0.000	0.000	**-0.024**	**-0.020**	**-0.023**
		μ (-)	1.89	1.95	1.65	0.00	2.11	0.00	0.00	0.00	0.00	2.39	2.41	2.26
2 Floor positive	Limit point	UM Max (kNm)	85.37	107.81	82.94	193.35	335.70	181.32	215.50	322.30	198.95	62.22	155.09	49.40
		Drift (-)	0.036	0.017	0.036	0.054	0.053	0.054	0.054	0.053	0.054	0.018	0.035	0.018
	Yielding point	UM Yielding (kNm)	85.37	107.81	82.94	193.35	335.70	181.32	215.50	322.30	198.95	62.22	155.09	49.40
		Drift (-)	0.020	0.012	0.016	0.027	0.026	0.028	0.029	0.028	0.030	0.015	0.024	0.012
	Failure point	0.90 UM Max (kNm)	76.84	97.03	74.65	174.01	302.13	163.18	193.95	290.07	179.05	56.00	139.58	44.46
		Drift (-)	**0.049**	**0.029**	**0.036**	0.000	0.000	0.000	0.000	0.000	0.000	**0.030**	**0.039**	**0.022**
		μ (-)	2.42	2.42	2.31	0.00	0.00	0.00	0.00	0.00	0.00	2.06	1.60	1.80
2 Floor negative	Limit point	UM Max (kNm)	-51.93	-74.34	-63.00	-193.24	-364.88	-182.66	-212.11	-347.03	-228.32	-77.99	-156.57	-79.24
		Drift (-)	-0.027	-0.017	-0.033	-0.056	-0.056	-0.056	-0.055	-0.055	-0.055	-0.032	-0.034	-0.036
	Yielding point	UM Yielding (kNm)	-51.93	-74.34	-63.00	-193.24	-364.88	-182.66	-212.11	-347.03	-228.32	-77.99	-156.57	-79.24
		Drift (-)	-0.012	-0.011	-0.017	-0.029	-0.028	-0.031	-0.028	-0.027	-0.030	-0.015	-0.020	-0.017
	Failure point	0.90 UM Max (kNm)	-46.74	-66.91	-56.70	-173.92	-328.39	-164.40	-190.90	-312.32	-205.49	-70.19	-140.92	-71.31
		Drift (-)	**-0.033**	**-0.020**	**-0.035**	0.000	0.000	0.000	0.000	0.000	0.000	**-0.046**	0.0000	**-0.046**
		μ (-)	2.82	1.73	2.04	0.00	0.00	0.00	0.00	0.00	0.00	3.00	0.00	2.75

95% OF THE MAXIMUM UNBALANCED MOMENT

This analysis shows all the connections which reached the maximum unbalanced moment, suffering a very limited strength deterioration.

For this last percentage of the maximum unbalanced moment, 95%, the connections on the 1st floor on the long South side, B3 for the negative drift, in the North side C1 for the positive drift and in the 2nd floor short east side D2 for the negative drift, were added to the previous ones (Figure 8.19).

The drift values are of the same order of magnitude as the previous percentage drop with values slightly lower compared to those (Table 8.16).

The displacement ductility factors on the 2nd floor were higher compared to the 1st floor except for the connections A2 negative drift, D2 positive and negative drift and D3 positive drift in which the values on the 2nd floor were lower than those on the 1st (Table 8.15).

Table 8.15 Displacement ductility factor for the failed connections at 95%, test Cyc-1 (f02) + Cyc-2 (g04).

	Floor	Drift	A1	A2	A3	B2	B3	C1	D1	D2	D3
μ (-)	1st	Positive	1.73	1.96	2.06	2.30	2.84	3.06	1.50	1.76	1.99
		Negative	1.73	1.77	1.54	2.05	2.00	-	2.23	2.11	2.10
μ (-)	2nd	Positive	2.25	2.19	2.29	-	-	-	1.53	1.52	1.61
		Negative	2.78	1.62	2.00	-	-	-	2.58	1.91	2.64

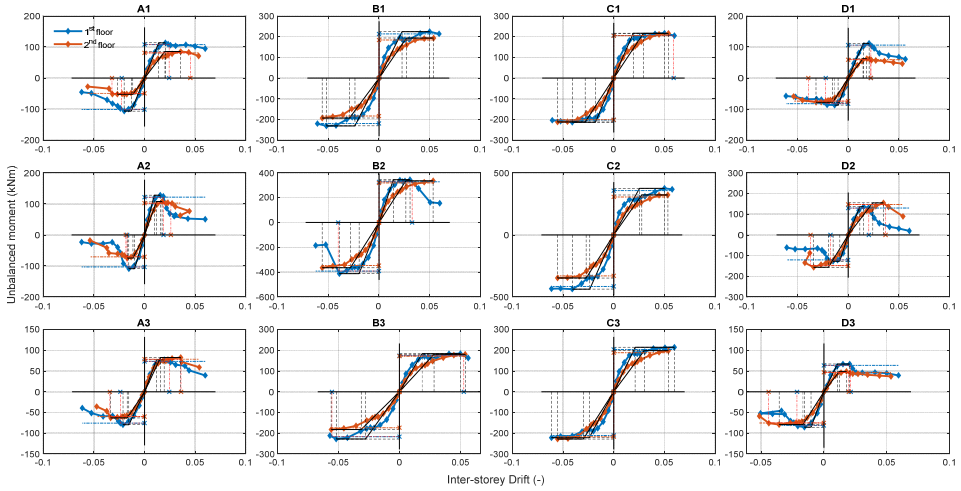

Figure 8.19 Unbalanced Moment vs Inter-story drift ratio. Definition of the yielding and failure at 95% points for all the connections, test Cyc-1 (f02) + Cyc-2 (g04). Line: blue for the 1st floor, red for the 2nd. Horizontal dashed line, force at failure. Vertical red line, drift at failure.

Table 8.16 Unbalanced moment drift at limit, yielding and failure at 95% for all the connections, test Cyc-1 (f02) + Cyc-2 (g04). Yellow highlighted cells, failed connections.

		Connections	A1	A2	A3	B1	B2	B3	C1	C2	C3	D1	D2	D3
			1	2	3	4	5	6	7	8	9	10	11	12
1 Floor positive	Limit point	UM Max (kNm)	113.64	127.96	77.41	224.37	345.03	184.15	216.66	375.49	215.37	111.77	136.52	67.09
		Drift (-)	0.021	0.016	0.019	0.050	0.031	0.050	0.050	0.050	0.060	0.021	0.015	0.021
	Yielding point	UM Yielding (kNm)	113.64	127.96	77.41	224.37	345.03	184.15	216.66	375.49	215.37	111.77	136.52	67.09
		Drift (-)	0.014	0.010	0.012	0.023	0.014	0.019	0.019	0.025	0.021	0.015	0.012	0.011
	Failure point	0.95 UM Max (kNm)	107.95	121.57	73.54	213.16	327.78	174.94	205.82	356.71	204.61	106.18	129.69	63.74
		Drift (-)	**0.024**	**0.019**	**0.024**	0.000	**0.033**	**0.053**	**0.059**	0.000	0.000	**0.022**	**0.020**	**0.021**
		μ (-)	1.73	1.96	2.06	0.00	2.30	2.84	3.06	0.00	0.00	1.50	1.76	1.99
1 Floor negative	Limit point	UM Max (kNm)	-106.46	-108.63	-79.52	-231.20	-411.68	-228.35	-213.49	-436.45	-221.97	-87.08	-127.19	-85.42
		Drift (-)	-0.020	-0.015	-0.021	-0.052	-0.039	-0.052	-0.041	-0.041	-0.061	-0.013	-0.015	-0.015
	Yielding point	UM Yielding (kNm)	-106.46	-108.63	-79.52	-231.20	-411.68	-228.35	-213.49	-436.45	-221.97	-87.08	-127.19	-85.42
		Drift (-)	-0.013	-0.010	-0.015	-0.024	-0.020	-0.028	-0.018	-0.024	-0.024	-0.010	-0.008	-0.010
	Failure point	0.95 UM Max (kNm)	-101.13	-103.20	-75.55	-219.64	-391.10	-216.93	-202.82	-414.63	-210.87	-82.73	-120.83	-81.15
		Drift (-)	**-0.023**	**-0.017**	**-0.024**	0.000	**-0.040**	**-0.055**	0.000	0.000	0.000	**-0.022**	**-0.018**	**-0.021**
		μ (-)	1.73	1.77	1.54	0.00	2.05	2.00	0.00	0.00	0.00	2.23	2.11	2.10
2 Floor positive	Limit point	UM Max (kNm)	85.37	107.81	82.94	193.35	335.70	181.32	215.50	322.30	198.95	62.22	155.09	49.40
		Drift (-)	0.036	0.017	0.036	0.054	0.053	0.054	0.054	0.053	0.054	0.018	0.035	0.018
	Yielding point	UM Yielding (kNm)	85.37	107.81	82.94	193.35	335.70	181.32	215.50	322.30	198.95	62.22	155.09	49.40
		Drift (-)	0.020	0.012	0.016	0.027	0.026	0.028	0.029	0.028	0.030	0.015	0.024	0.012
	Failure point	0.95 UM Max (kNm)	81.11	102.42	78.80	183.68	318.92	172.25	204.72	306.18	189.00	59.11	147.33	46.93
		Drift (-)	**0.045**	**0.026**	**0.036**	0.000	0.000	0.000	0.000	0.000	0.000	**0.022**	**0.037**	**0.020**
		μ (-)	2.25	2.19	2.29	0.00	0.00	0.00	0.00	0.00	0.00	1.53	1.52	1.61
2 Floor negative	Limit point	UM Max (kNm)	-51.93	-74.34	-63.00	-193.24	-364.88	-182.66	-212.11	-347.03	-228.32	-77.99	-156.57	-79.24
		Drift (-)	-0.027	-0.017	-0.033	-0.056	-0.056	-0.056	-0.055	-0.055	-0.055	-0.032	-0.034	-0.036
	Yielding point	UM Yielding (kNm)	-51.93	-74.34	-63.00	-193.24	-364.88	-182.66	-212.11	-347.03	-228.32	-77.99	-156.57	-79.24
		Drift (-)	-0.012	-0.011	-0.017	-0.029	-0.028	-0.031	-0.028	-0.027	-0.030	-0.015	-0.020	-0.017
	Failure point	0.95 UM Max (kNm)	-49.33	-70.63	-59.85	-183.58	-346.64	-173.53	-201.51	-329.67	-216.90	-74.09	-148.74	-75.28
		Drift (-)	**-0.032**	**-0.018**	**-0.034**	0.000	0.000	0.000	0.000	0.000	0.000	**-0.039**	**-0.037**	**-0.044**
		μ (-)	2.78	1.62	2.00	0.00	0.00	0.00	0.00	0.00	0.00	2.58	1.91	2.64

SUMMARY OF THE CONNECTION FAILURES

As previously presented, a schematic summary of the connection failures for all the four analysed percentages of drop of the loading resistance (yellow for 80%, light blue for 85%, green for 90% and red for 95%) and for both tests (Cyc-1 and Cyc-1+Cyc-2) is reported in Figure 8.20.
The circles represent the test Cyc-1, the squares, the test Cyc-1+Cyc-2, the continuous line, the positive drift, the dashed line, the negative drift.
All the connections which failed during the test Cyc-1, are considered failed also during the test Cyc-1+Cyc-2. It is possible to observe that also in this test, the number of failed connections increases as the considered residual resistance decreases.
During the test Cyc-2 it was possible to observe the torsional damage in the corner slab-column connection typology on the 1st floor, flexural and punching at the short side edge and torsional damage in the corner on the 2nd floor and the punching in the internal B2. The details of the cracking at failure are reported in the next section 8.4.5.
It must be remarked that some of the 1st floor connections reached a nearly constant maximum unbalanced moment, corresponding to the flexural limit resistance.

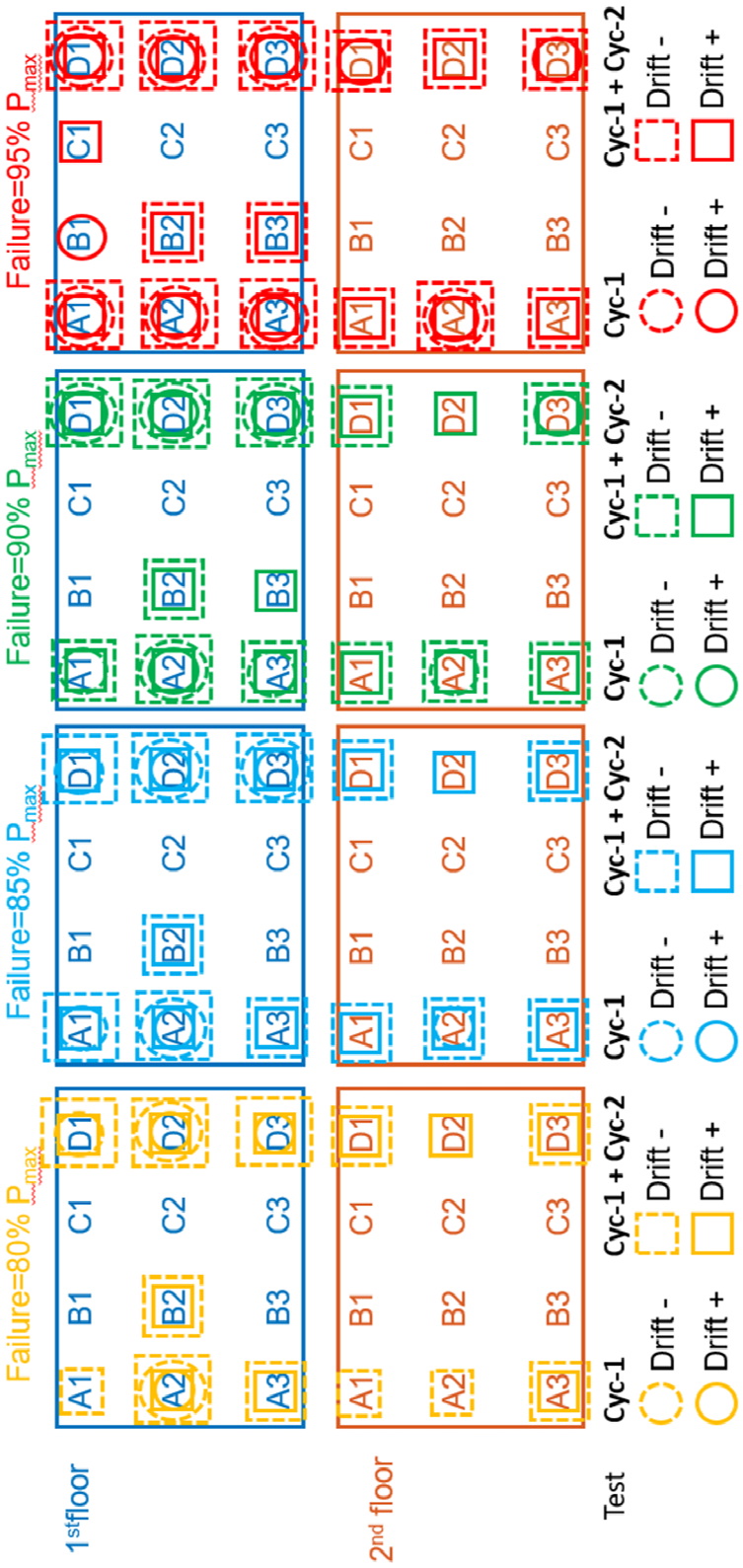

Figure 8.20 Connections failure for the analysed percentages of drop of the loading resistance, test Cyc-2 (g04). Circled and squared are the failed connections.

Regarding the displacement ductility factor, we observed that it decreases as the considered percentage of the residual strength decreases (Table 8.17).

Table 8.17 Displacement ductility factor at failure for the analysed percentages of drop of the loading resistance, test Cyc-2 (g04).

	Floor	Drift	A1	A2	A3	B2	B3	C1	D1	D2	D3
80%											
μ (-)	1st	Positive	-	2.14	3.38	2.74	-	-	1.86	1.97	2.21
		Negative	2.29	2.19	1.88	2.23	-	-	2.66	2.63	2.67
μ (-)	2nd	Positive	-	-	2.83	-	-	-	3.09	1.79	3.45
		Negative	2.91	2.74	2.13	-	-	-	3.36	-	2.96
85%											
μ (-)	1st	Positive	4.11	2.08	2.57	2.60	-	-	1.74	1.90	2.13
		Negative	2.03	2.13	1.76	2.17	-	-	2.53	2.55	2.47
μ (-)	2nd	Positive	2.60	2.56	2.48	-	-	-	2.70	1.69	2.64
		Negative	2.87	1.92	2.09	-	-	-	3.18	-	2.85
90%											
μ (-)	1st	Positive	3.54	2.02	2.29	2.45	3.00	-	1.62	1.83	2.06
		Negative	1.89	1.95	1.65	2.11	-	-	2.39	2.41	2.26
μ (-)	2nd	Positive	2.42	2.42	2.31	-	-	-	2.06	1.60	1.80
		Negative	2.82	1.73	2.04	-	-	-	3.00	-	2.75
95%											
μ (-)	1st	Positive	1.73	1.96	2.06	2.30	2.84	3.06	1.50	1.76	1.99
		Negative	1.73	1.77	1.54	2.05	2.00	-	2.23	2.11	2.10
μ (-)	2nd	Positive	2.25	2.19	2.29	-	-	-	1.53	1.52	1.61
		Negative	2.78	1.62	2.00	-	-	-	2.58	1.91	2.64

The maximum value of the displacement ductility factor (μ=4.11), was recorded for 85% of the residual resistance of the maximum load on the short edge north-west side connection A1 in the 1st floor, for the positive drift. The minimum value (μ=1.50) was recorded on the opposite connection on the north-east side, D1 on the same floor, for the positive drift and for 95% of the residual resistance of the maximum load.

The table below (Table 8.18) reports the comparison made between all the connections that failed during the test Cyc-1 and Cyc-1+Cyc-2.

Table 8.18 Displacement ductility factor at failure for the analysed percentages of drop of the loading resistance, test Cyc-1 (f02) and Cyc-2 (g04).

Test	Drift		1st floor				2nd floor			
			A	B	C	D	A	B	C	D
80% Cyc-1	Positivo	1	-	-	-	-	-	-	-	-
	Negativo		-	-	-	2.66	-	-	-	-
	Positivo	2	2.14	-	-	1.97	-	-	-	-
	Negativo		2.19	-	-	2.63	-	-	-	-
	Positivo	3	-	-	-	2.21	-	-	-	-
	Negativo		-	-	-	-	-	-	-	-
80% Cyc-2	Positivo	1	-	-	-	1.86	-	-	-	3.09
	Negativo		2.29	-	-	2.66	2.91	-	-	3.36
	Positivo	2	2.14	2.74	-	1.97	-	-	-	1.79
	Negativo		2.19	2.23	-	2.63	2.74	-	-	-
	Positivo	3	3.38	-	-	2.24	-2.83	-	-	3.45
	Negativo		1.88	-	-	2.67	2.13	-	-	2.96
85% Cyc-1	Positivo	1	-	-	-	-	-	-	-	-
	Negativo		2.03	-	-	2.53	-	-	-	-
	Positivo	2	2.08	-	-	1.9	-	-	-	-
	Negativo		2.13	-	-	2.55	1.92	-	-	-
	Positivo	3	-	-	-	2.13	-	-	-	-
	Negativo		-	-	-	2.47	-	-	-	-
85% Cyc-2	Positivo	1	4.11	-	-	1.74	2.6	-	-	2.7
	Negativo		2.03	-	-	2.53	2.87	-	-	3.18
	Positivo	2	2.08	2.6	-	1.9	2.56	-	-	1.69
	Negativo		2.13	2.17	-	2.55	1.92	-	-	-
	Positivo	3	2.57	-	-	2.13	2.48	-	-	2.64
	Negativo		1.76	-	-	2.47	2.09	-	-	2.85
90% Cyc-1	Positivo	1	-	-	-	1.62	-	-	-	-
	Negativo		1.89	-	-	2.39	-	-	-	-
	Positivo	2	2.02	-	-	1.83	-	-	-	-
	Negativo		1.95	-	-	2.41	1.73	-	-	-
	Positivo	3	-	-	-	2.06	-	-	-	-
	Negativo		1.65	-	-	2.26	-	-	-	-
90% Cyc-2	Positivo	1	3.54	-	-	1.62	2.42	-	-	2.06
	Negativo		1.89	-	-	2.39	1.73	-	-	3
	Positivo	2	2.02	2.45	-	1.83	2.31	-	-	1.6
	Negativo		1.95	2.11	-	2.41	2.04	-	-	-
	Positivo	3	2.29	3	-	2.06	-	-	-	1.8
	Negativo		1.65	-	-	2.26	-	-	-	2.75
95% Cyc-1	Positivo	1	1.73	1.68	-	1.5	-	-	-	1.53
	Negativo		1.73	-	-	2.23	-	-	-	-
	Positivo	2	1.96	1.68	-	1.76	1.77	-	-	-
	Negativo		1.77	-	-	2.11	1.62	-	-	-
	Positivo	3	2.06	-	-	1.99	-	-	-	1.61
	Negativo		1.54	-	-	2.1	-	-	-	-
95% Cyc-2	Positivo	1	1.73	-	-	1.5	2.25	-	-	1.53
	Negativo		1.73	-	3.06	2.23	2.78	-	-	2.58
	Positivo	2	1.96	2.3	-	1.76	2.19	-	-	1.52
	Negativo		1.77	2.05	-	2.11	1.62	-	-	1.91
	Positivo	3	2.06	2.48	-	1.99	2.29	-	-	1.61
	Negativo		1.54	2	-	2.1	2	-	-	2.64

The north short side edge connections A1 and D1 on the 1st floor are those in which the displacement ductility factor is of the greatest amplitude, with both the maximum and the minimum values (Table 8.19). The connection D1 for the 85% of the residual resistance of the maximum load and for the positive drift, reached the same value of μ for the two tests, equal to 1.50 and corresponding to the minimum value. The maximum value of 2.66 was reached by the connection D1, negative drift and a drop of the loading resistance equal to the 80% of the residual resistance of the maximum load for the test Cyc-1 and 4.11 for the connection A1, positive drift and a drop of the loading resistance equal to the 95% of the residual resistance of the maximum load for the Cyc-1+Cyc-2 test.

Table 8.19 Maximum and minimum values of the displacement ductility factor for the test Cyc-1 and Cyc-2 (g04).

Test	μ max/min	Connection	Floor	Drift	Residual resistance of the maximum load
Cyc-1	2.66	D1	1st	Negative	80%
	1.50	D1	1st	Positive	95%
Cyc-1+Cyc-2	4.11	A1	1st	Positive	85%
	1.50	D1	1st	Positive	95%

From the obtained results it is possible to choose the 85% of the residual resistance of the maximum load as the most reliable criteria to identify the collapse.

8.4.4 Energy Dissipation

To calculate the connection energy dissipation, the same procedure followed to analysed the global energy dissipation (Chapter 7.2.4) was followed but applied to each slab-column connection on each floor.

As reported in Chapter 5, the dissipated energy was calculated using the displacement firstly and then the slab-column rotation as the kinematic quantity (displacement component), whereas in both the analyses the shear force was used as the static parameter (force component).

For a detailed explanation of the methodology, the equations and the graphs set up, see chapter 5.3.4 for the analyses made with the inter-storey drift ratio and chapter 5.4.7 for those done with the rotation.

In Table 6.3 and Figure 8.22 the maximum values of the dissipated energy of each connection on each floor calculated with the inter-storey drift ratio and with the rotation respectively, were reported.

Table 8.20 Dissipated energy of each connections on each floor, test Cyc-2. Energy calculated with the displacement (kNmm=kJ).

1st Floor	A	B	C	D	2nd Floor	A	B	C	D
1	$4.12*10^4$	$5.49*10^4$	$6.09*10^4$	$4.09*10^4$	1	$1.64*10^4$	$2.98*10^4$	$3.56*10^4$	$2.06*10^4$
2	$5.41*10^4$	$5.66*10^4$	$7.56*10^4$	$4.45*10^4$	2	$1.78*10^4$	$5.18*10^4$	$5.47*10^4$	$2.68*10^4$
3	$3.24*10^4$	$6.65*10^4$	$6.17*10^4$	$3.47*10^4$	3	$1.62*10^4$	$2.62*10^4$	$3.51*10^4$	$1.89*10^4$

Table 8.21 Dissipated energy of each connections on each floor, test Cyc-2. Energy calculated with the rotation (kNm*rad=kJ).

1st Floor	A	B	C	D	2nd Floor	A	B	C	D
1	16.63	21.96	-	-	1	10.97	13.55		-
2	12.28	36.33	32.64	12.00	2	13.29	21.18	23.11	19.99
3	-	-	19.07	16.78	3	-	-	14.61	11.37

Figure 8.21 and Figure 8.22 report the graphs of the dissipated energy of each connection on each floor (blue line for the 1st floor, red line for the 2nd) calculated with the displacement and with the rotation respectively.

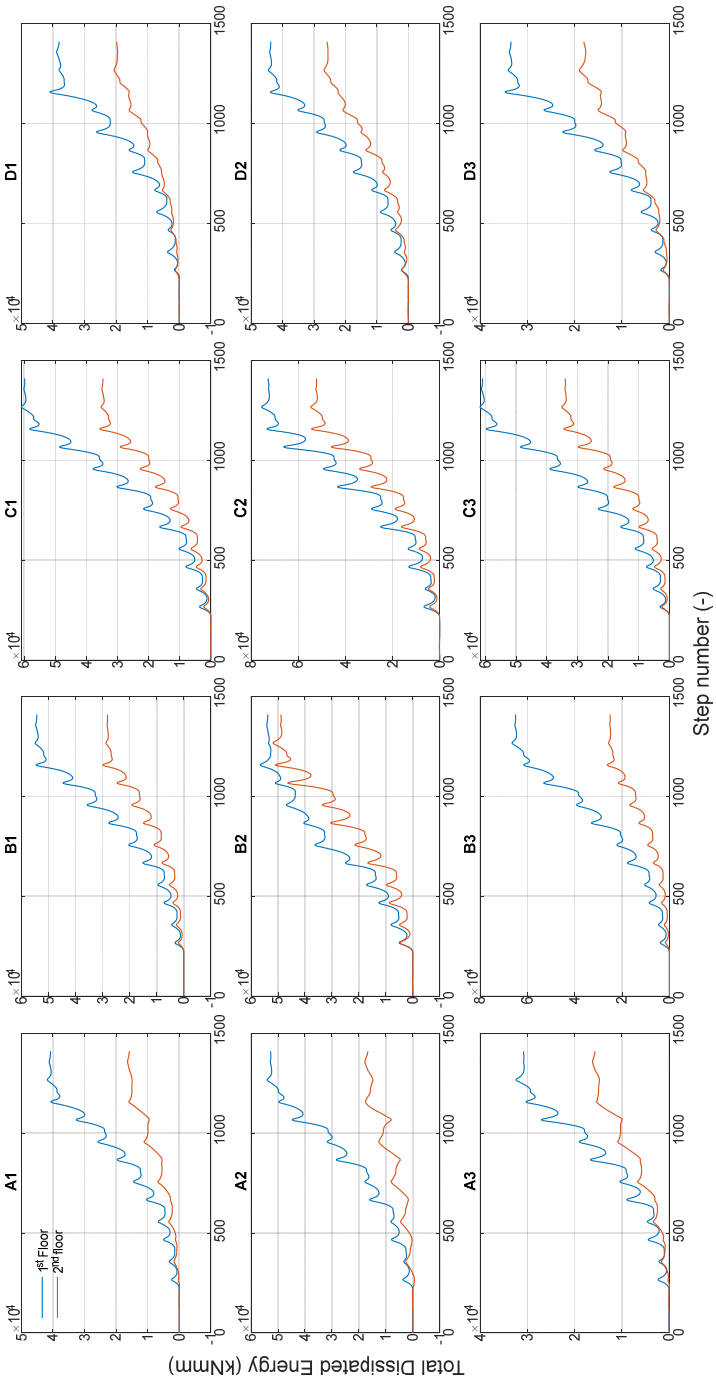

Figure 8.21 Dissipated energy for each connections, test Cyc-2. 1st floor blue line, 2nd floor red line. Energy calculated with the displacement.

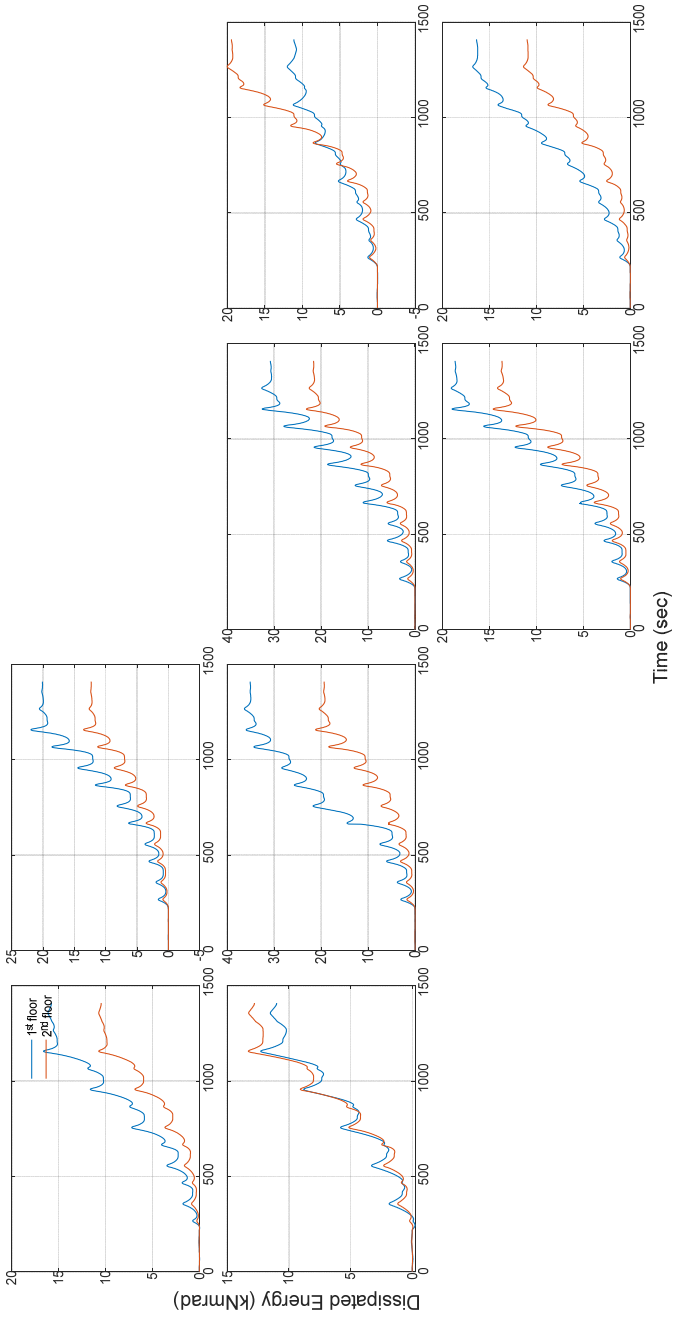

Figure 8.22 Dissipated energy for each connections, test Cyc-2. 1st floor blue line, 2nd floor red line. Energy calculated with the rotation.

As in the previous cyclic test, the energy dissipated from the 1st floor is higher than that of the 2nd floor in all the connections excepting in the D2 (only in the analysis with the rotation).
The internal connections B2 and C2 are obviously the two that in both the analyses dissipated more energy. The alignments B and C are the two that dissipated more energy in both floor using the inter-storey drift ratio to calculate the energy, whereas using the rotation they are the more dissipative on the 1st floor only.

8.4.5 OBSERVED DAMAGE

The noticeable cracking pattern that was evident during the Cyc-1 test worsened in the next test, in particular the crack pattern on the two external short sides, perpendicular to the loading application (A and D).
The most damaged connections on the 1st floor were on the short west side, the two corners A1 (Figure 8.23) and A3 (Figure 8.24) and the edge A2 (Figure 8.25). On the opposite (east) side, the corner D1 (Figure 8.26) and the lateral D2 (Figure 8.27) resulted to be most damaged.
From a deeper analysis of the cracks that opened in the connections and on the side of the slab, it was possible to note that all the connections in the alignments A and D reported a mixed failure mode with flexural and punching cracks. The formation of a the punching cone in the slab around the column was observed in most of the corner and edge connections (from Figure 8.23 to Figure 8.27). A summary of the failure mode observed in each of the failed connections is reported in Table 8.22. all these connections were on the 1st floor, without shear reinforcement.

Table 8.22 Failure analysis in the connections.

Connection	Typology	Cardinal position	Reinforcement layout	Punching	Torsion	Flexion	Bar buckling
A1	Corner	West	Smeared	-	X	X	-
D3	Corner	East	Concentrated	-	X	X	-
A3	Corner	West	Smeared	-	X	X	-
D1	Corner	East	Concentrated	X	X	X	-
A2	Edge	West	Smeared	X	X	-	-
D2	Edge	East	Concentrated	X	X	X	-
B2	Internal	West	Smeared	X	X	X	X
C2	Internal	East	Concentrated	-	-	X	-

The internal B2 connection was the only one punched with brittle failure (Figure

8.28).

Figure 8.23 A1 connection after test Cyc-2 (g04), a) slab-column connection, b) slab east side.

Figure 8.24 A3 connection after test Cyc-2 (g04), a) slab-column connection, b) slab west side.

Figure 8.25 A2 connection after test Cyc-2 (g04), a) slab-column connection, b) slab west side.

Figure 8.26 D1 connection after test Cyc-2 (g04), a) slab west side, b) slab-column connection.

Figure 8.27 D2 connection after test Cyc-2 (g04), a) slab east side, b) slab-column connection.

From Figure 8.26 a, it is possible to see the longitudinal reinforcement detail of the slab.
As it is possible to see in Figure 8.28, during the test the B2 connection punched and this was one of the causes of the onset of a the global load reduction.

Figure 8.28 B2 connection after test Cyc-2 (g04) a) north-south direction before the removal of the damaged concrete pieces and b) east-west direction after the removal of the damaged concrete pieces.

As described in chapter 3, the slab longitudinal reinforcement consisted of two bottom bars passing through the column as prescribed in the EC2 detailing rule [7]. On examining at the overall response of the structure after the test, it is possible to claim that this reinforcement was effective in avoiding a chain collapse. What is more the top reinforcement layer also gave an important contribution, as well evidenced by the deformation of the rebars and the consequent expulsion of the concrete covers. The top reinforcement remained stable given the slope of the extrados surface. This behaviour is observable around the punched connection B2 (Figure 8.28) in which all the reinforcement developed a catenary effect. In the B2 connection, for the cycle at 4% drift during the loading application from east to west, the unbalanced moment dropped significantly by 58%, from -412 kN to -171 kN (Figure 8.29). A considerable strength deterioration is noticeable for the same cycle also during the loading application in the opposite direction from west to east. The

two least cycles at a drift of 5% and 6% showed a very low stiffness.

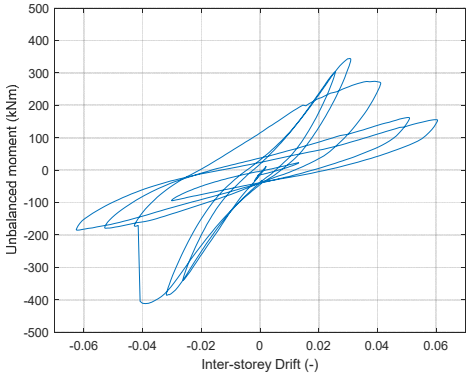

Figure 8.29 Unbalanced moment vs inter-story drift ration for the punched connection B2, 1st floor, test Cyc-2 (g04).

At the end of the test, after compression buckling, the breaking of the longitudinal reinforcement at the base of the column in the B2 connection (Figure 8.30) was observed. The reinforcement of the columns limited the cracking of these members, that would have increased the ultimate drift.

Figure 8.30 Base column connection B2 a) east and b) west, test Cyc-2 (g04).

The following section 8.5 is dedicated to a comparison of the 1st floor edge connections with or without strengthening on lines 1 and 2, and of connection C2 with strengthening, with respect to B2.
As regards the 2nd floor, the A and D alignment on the 2nd floor showed severe damage (Figure 8.31 and Figure 8.32) to the edge and corner connections, qualitatively similar to that observed on the 1st floor after test Cyc-1.

Figure 8.31 Damage in the A alignment in the 2nd floor, a) A1, b) A2, c) A3.

Figure 8.32 Damage in the D alignment in the 2nd floor, a) D1, b) D2, c) D3.

On the upper surface, radial cracking together with torsion cracking with some cover spalling were observed also on the east and west sides of the slab (Figure 8.33).

Figure 8.33 Cracking in 2nd floor, connections a) A2 west side and, b) D2 east side.

The slab-column connections on the North and South side (lines 1 and 3, intersections with B and C) reported damage due to torsion with some cover spalling on the upper surface, while flexural cracks showed on the vertical face of the slab edge.
In the internal and in the connections located on the side of the structure parallel to the loading application, radial cracking was observed (Figure 8.34).

Figure 8.34 Radial cracking in the internal connections on the 2nd floor a) B2, b) C2.

On the whole, very severe damage showed on the A and D edges of the 2nd floor; the images shown above are all relative to conditions after a drift of 6% was reached.

8.5 Comparison Between Strengthened and Un-Strengthened Connections

The comparison between connections of the same typology (lateral and central), with the same reinforcement details, with the same loads but with and without strengthening will be analysed in the sections 8.5.1, 8.5.2 and 8.5.3.
The comparison will be made between connections B1 and B3 that are lateral for the long side in the west half of the slab (section 8.5.1), the same in the east half of the slab, C1 and C3 (section 8.5.2)and the two internal B2 and C2 (section 8.5.3). The longitudinal reinforcement between these two last connections will be different.
For each comparison a plan of the specimen is firstly reported with the connections analysed in that paragraph encircled, and the strengthened connection coloured yellow. In these comparisons, violet indicates the unstrengthened connection and the green the strengthened. After the plan, the comparison graphs in terms of unbalanced moment versus the inter-storey drift ratio and the ductility analysis for a 15% drop of the loading resistance are reported, together with a photographic comparison between the two analysed slab-column connections at the end of the cyclic test Cyc-2. In all the graphs, the same colour scheme was used.

8.5.1 LATERAL CONNECTIONS, WEST HALF OF THE SLAB: B1, B3

The first comparison was made between the connections B1 and B3 located on the long side and on the west half of the slab. Here the reinforcement disposition was smeared. The connection B1 in the North (coloured in yellow) was strengthened whereas the connection B3 in the South was not.

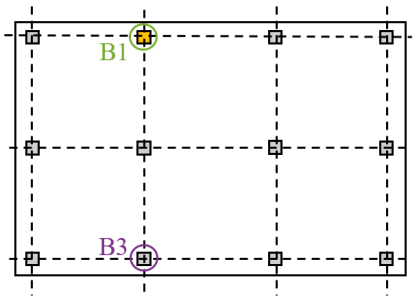

Figure 8.35 Lateral long side connections west half, with and without reparation.

The strengthened connection B1 always reached the higher and the lower values of unbalanced moment; -231.20 kNm for the negative branch of the drift and 224.37 kNm for the positive. The unstrengthened connection B3 recorded the higher differences in unbalanced moment in the positive drift with respect to the other connection with 40 kNm lower, 184.15 kNm, whereas for the negative one the unbalanced moment was close to that measured in B1, -228.35 kNm.

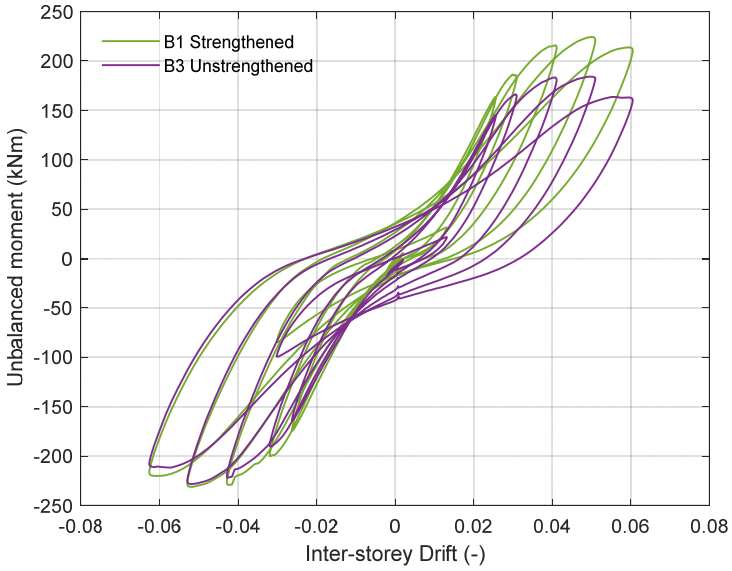

Figure 8.36 Unbalanced moment vs Inter-Storey drift, connections B1 B3, test CYC-2 (g04).

In Figure 8.37 the ductility analysis for the 85% of the residual resistance of the maximum load for the two analysed slab-column connections considering the two cyclic experiments is reported.

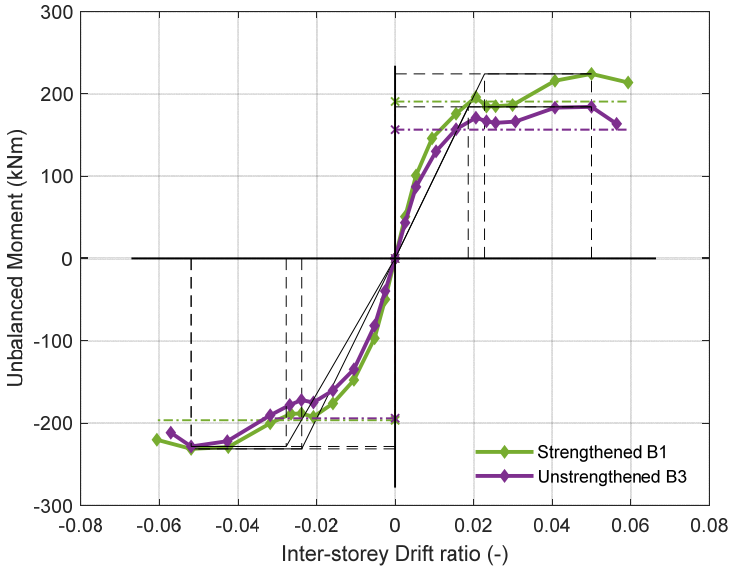

Figure 8.37 Ductility analysis for a 15% drop of the loading resistance, connections B1 and B3.

From Figure 8.37 it is possible to note that the two connections show a similar trend in the ductility analysis with nearly the same values of maximum unbalanced moment independently from the presence of the strengthening.
Failure was not observed in either of the two analysed connections (Figure 8.37 and Figure 8.38 a and b).

Figure 8.38 Connections a) B3 unstrengthen and b) B1 strengthened.

8.5.2 LATERAL LONG SIDE CONNECTIONS, EAST HALF OF THE SLAB: C1, C3

The same connections typology but on the east half of the slab and with a concentrated reinforcement disposition, that is displayed on the long side connections C1 and C3.

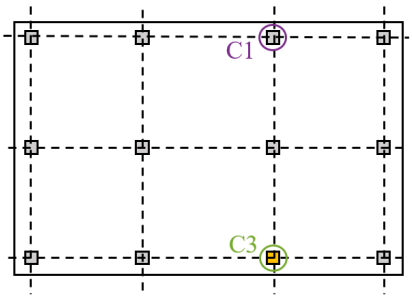

Figure 8.39 Lateral long side connections east half, with and without repair.

Between the two, C3 is the one that was strengthened (coloured in yellow). As for the negative value of the drift, the strengthened connections C3 reached the lowest values of unbalanced moment; -221.97 kNm against the values of -213.49 for the unstrengthen connection C1. As for the other branch of the drift, the positive one, the unstrengthen connection C1 reached the highest values of unbalanced moment; 216.66 kNm compared with the values reached by the strengthened connection C3, 215.37 kNm.

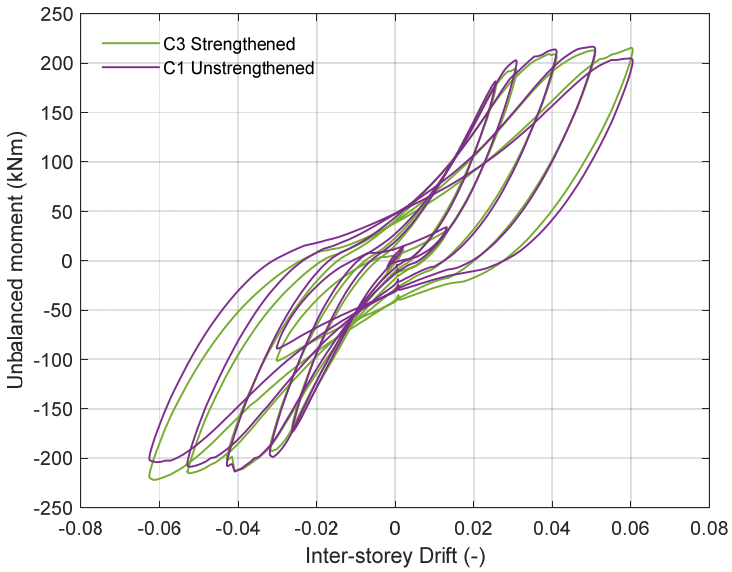

Figure 8.40 Unbalanced moment vs Inter-Storey drift, connections C1 C3, test CYC-2 (g04).

In Figure 8.41 the ductility analysis for the 85% of the residual resistance of the maximum load for the two analysed slab-column connections considering all the cyclic experiment is reported.

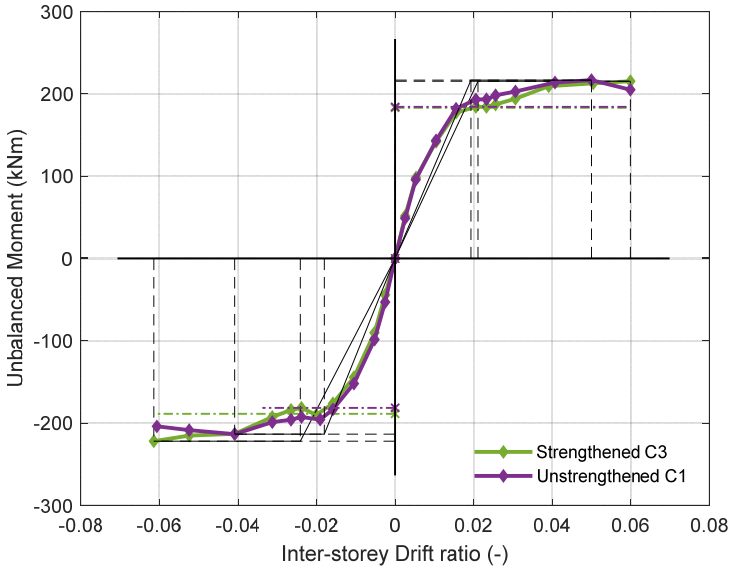

Figure 8.41 Ductility analysis for a 15% drop of the loading resistance, connections C1 and C3.

In this comparison, the two analysed connections show a similar trend in the ductility analysis with maximum values of unbalanced moment closer than the comparison between B3 and B1. Failure was not observed in either of the two analysed connections independently from the presence of the strengthening (Figure 8.41 and Figure 8.42 a and b). The effect of the strengthening can be seen only for the absence of any strength deterioration in C3, whereas C1 showed a slight reduction of the unbalanced moment after the peak.

Figure 8.42 Connections a) C1 unstrengthened and b) C3 strengthened.

8.5.3 INTERNAL CONNECTIONS: B2, C2

The last comparison was made between the internal connections B2 unstrengthened and C2 strengthened (coloured in yellow). In this case, the two connections had different longitudinal reinforcement layout, in B2 it was smeared, in C2 it was concentrated.

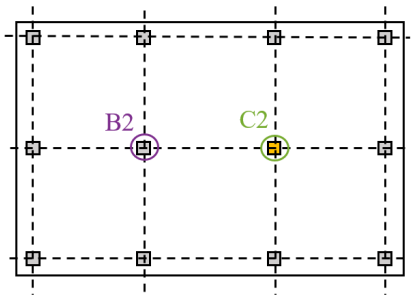

Figure 8.43 Internal connections, with and without reparation.

The strengthened connection C2 reached the highest unbalanced moment for the positive drift and the lowest for the negative.

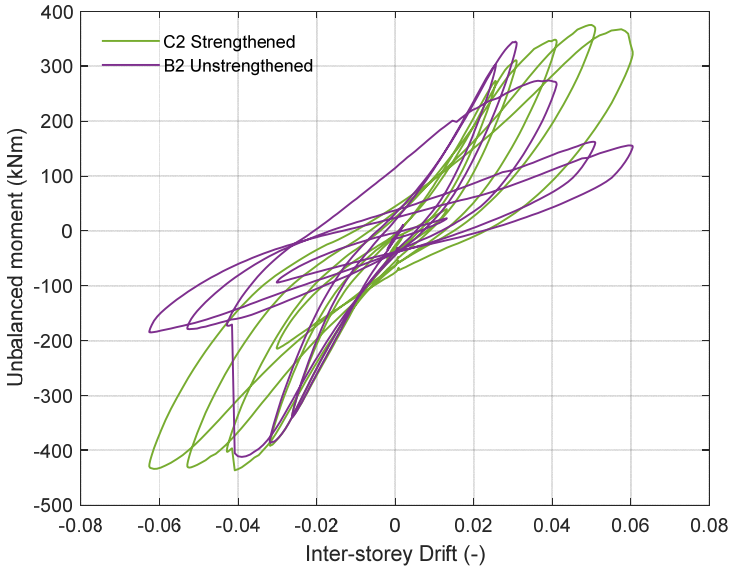

Figure 8.44 Unbalanced moment vs Inter-Storey drift, connections B2 C2, test CYC-2 (g04).

It is interesting to note that the internal unstrengthened connection B2, is the only one that reached the punching at -4.1% drift, then a sharp drop from an unbalanced moment of -405.1 kNm to -170.6 kNm.
In this case the behaviour of the strengthened connection C2 showed significant improvement compared to the similar but un-strengthened B2 (Figure 8.45), with no sign of failure showing.

Figure 8.45 B2 a) before and b) after the removal of the damaged concrete pieces and c) C2 connections at the end of the test CYC-2 (g04).

In Figure 8.46 the ductility analysis is reported for 85% of the residual resistance of the maximum load for the two analysed slab-column connections, considering the entire cyclic experiment.

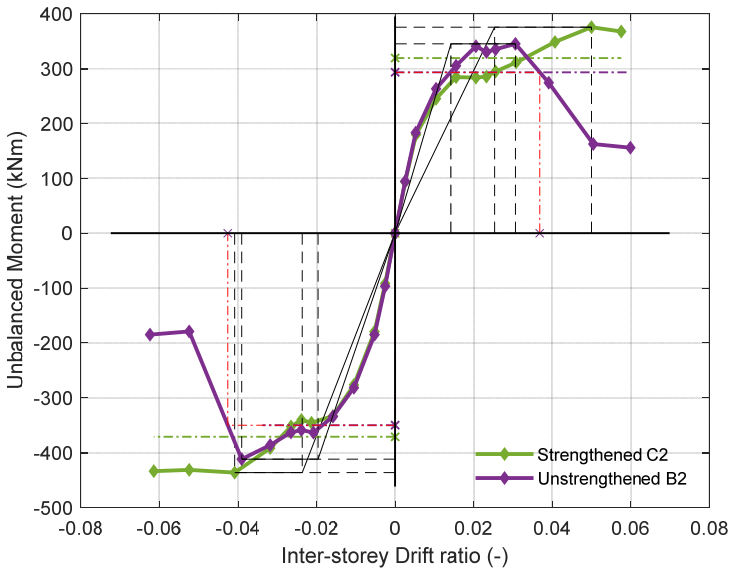

Figure 8.46 Ductility analysis for a 15% drop of the loading resistance, connections B2 and C2.

B2 was the only connection on lines B and C without unstrengthening that reached punching. Until the punching value of drift ratio (around 4%) the trend of the two analysed connections was almost the same with also the same unbalanced moment values.

8.5.4 SUMMARY OF THE STRENGTHENED AND UN-STRENGTHENED CONNECTIONS BEHAVIOUR

The response with maximum values of unbalanced moment was very similar for all the connections. The connections on the west side with a smeared reinforcement disposition, reached maximum unbalanced moment little higher than those in the east half of the slab with concentrated reinforcement layout. The strengthened B1 reached the highest unbalanced moment amongst of all the edge connections.
The un-strengthened B2 reached a brittle punching failure whereas the strengthened C2 showed only limited damage on the slab surface
The trend of the ductility analysis for the edge and the internal connections did not show differences between the strengthened and the un-strengthened connections. The only observed difference was in the internal typology after the punching in B2.
No relevant differences were observed in the energy dissipation (Table 8.23) between the two halves of the slab with smeared and concentrated reinforcement layout. All the edge connections dissipated at around the same values independently of strengthening. The strengthened internal C2 was the most dissipative but also reported the less damage.

Table 8.23 Dissipated energy in the B and C alignments (kNm=kJ).

1st Floor	A	B	C	D
1	-	$5.49*10^4$	$6.09*10^4$	-
2	-	$5.66*10^4$	$7.56*10^4$	-
3	-	$6.65*10^4$	$6.17*10^4$	-

8.6 Summary

This is a summary of the main results obtained at the end of the second cyclic test and a comparison with the first one are here reported.

- At the end of the test Cyc-1 (see Chapter 7) the structure had reached a plastic deformation stage, as also had all the connections. Test Cyc-2 started with a slight increase of the base shear and experienced the punching of an interior connection (B2 at the 1st floor) in the third cycle to 4% global drift ratio;
- A base shear reduction was observed as the consequence of the punching of the interior connection (B2);
- The connections in the short side of the structure continued to accumulate damage throughout test Cyc-2 (Figure 8.2);
- The 2nd floor reached a final relative residual stiffness higher than the 1st one (Figure 8.6) but this difference was lower compared to that of the previous

cyclic test.
At the end of the test Cyc-1, the difference in the relative residual stiffness between the two floors was higher;

- Amongst all the four percentages of the residual resistance used to calculated ductility it is possible to choose the residual stiffness equal to 85% of the maximum load as the most reliable criteria to identify the failure (Figure 8.7 and Table 8.4);
- Both the 1st and the 2nd floor, for both the loading direction reached the failure points for two of the analysed percentage drops in loading resistance (5% and 10%);
- The 1st floor dissipated twice as much compared to the 2nd one (Figure 8.9) and in general the dissipation during the test Cyc-2 was nearly twice as much compared to the energy dissipated during the previous Cyc-1 (Table 8.5);
- A brittle punching occurred in the internal connection B2 (Figure 8.10) while the strengthened interior connection C2, resisted to the end of the test without failure. The strengthening was also efficient in the edge connections B1 and C3 avoiding the failure.
- The connections that failed in test Cyc-1 (see chapter 7) continued to bear the gravity loads during the test Cyc-2 without the fall of the slab.
- The drop of the residual stiffness in all the connections is higher than the values reached in the global behaviour (Figure 8.11). the behaviour of the edge connections located on the long side of the structure (B1, C1, B3 and C3) was very similar on both floors.
- The description of the behaviour of the connections using the column-slab rotation as a kinematic parameter, instead of the drift ratio, seems to better capture the stiffness degradation. In this way, the curves of the two floors become more similar and perfectly symmetrical (Figure 8.12 and Figure 8.13);
- In Figure 8.47 and Figure 8.48 the time history of the displacement with the failure of the slab-column connections of each floor and the global history with the failure of the slab-column connections of each floor are reported.
  The blue line represents the 1st floor, the red line, the 2nd, the diamonds are used for the first cyclic test, the asterisk for the second cyclic test and the cross for the punching.
  Throughout the two tests the slab-column connections failed between 2% and 3.8% of inter-storey drift ratio.

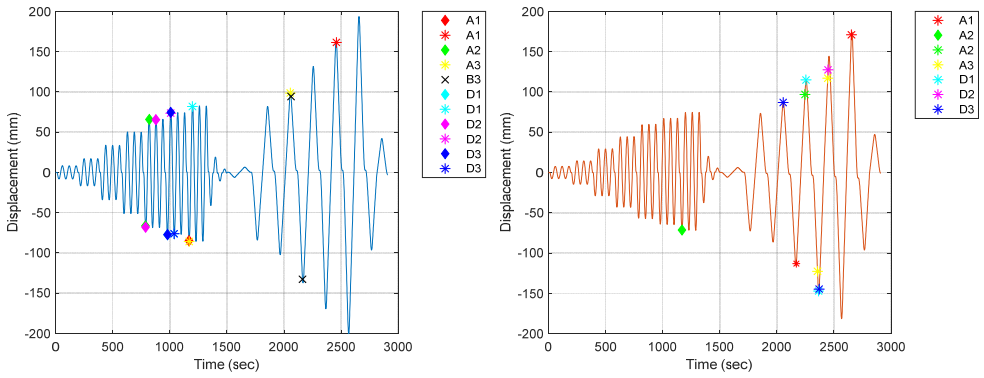

Figure 8.47 Time history of the displacements with local failure, diamond for the test Cyc-1, asterisk for the test Cyc-2, cross for the punching, a) 1st floor, b) 2nd floor.

On the 1st floor (Figure 8.47 a), the first connections that reach failure are the central edge due to torsion (A2 and D2), then the corner (A1, A3, D1, D3) then there is the punching in the central B2 for an inter-storey drift ratio of 3.8%. On the 2nd floor (Figure 8.47 b),the connections that reach failure are the ones on the short side (A and D).

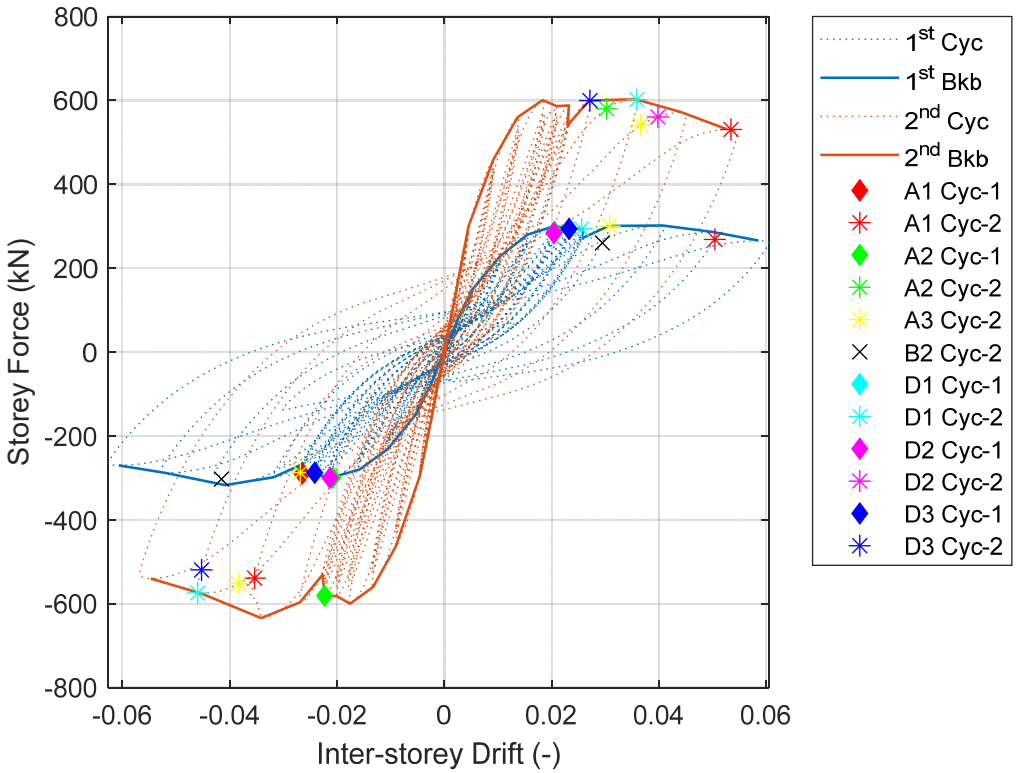

Figure 8.48 Global behaviour with local failure, blue line, 1st floor, red line, 2nd floor diamond for the test Cyc-1, asterisk for the test Cyc-2, cross for the punching.

- As in the previous cyclic test, the energy dissipated from the 1st floor is higher than the 2nd floor in all the connections (Figure 8.21 and Figure 8.22). The most dissipative slab-column connections remain obviously the internal B2 and C2 (Table 6.3 and Table 8.21);
- The 1st floor continued to showed damage in the edge and corner slab-column connections greater than that in the corresponding positions at the 2nd floor;
- The interior and edge connections (lines B and C) of the 2nd floor showed lower damage that the 1st floor;
- Using the ductility analysis and the dissipated energy to compare the 1st floor connections of the same typology with and without the strengthening (Chapter 8.5.1, 8.5.2 and 8.5.3) it was possible to observe that independently of the strengthening and from the longitudinal reinforcement layout, the trend of the curves and the maximum values of unbalanced moments are nearly the same and that the only one connection to fail with a brittle punching, was the un-strengthened internal B2 (Figure 8.45 and Figure 8.46);
- The strengthening was efficient since in the internal C2 connection did not reach failure, and showed limited damage.

References

[1] CEN. EN 1998-1. Eurocode 8: Design of structures for earthquake resistance - Part 1: General rules, seismic actions and rules for buildings. 2004

[2] Le, D.D., Nguyen, X.-H., Nguyen, Q.-H. (2020) “Cyclic Testing of a Composite Joint between a Reinforced Concrete Column and a Steel Beam”. Applied sciences.

[3] Park, R. (1988) “Ductility evaluation from laboratory and analytical testing”. Proceedings of Ninth World Conference on Earthquake Engineering, August 2-9, Tokyo-Kyoto, Japan (Vol. VIII).

[4] CEN (European Committee for Standardization). 2004. Design of concrete structures, general rules and rules for buildings part 1.1. Eurocode 2, Brussels, Belgium: CEN.

9 Comparison of results with Literature studies

9.1 Introduction

The outcomes of the SlabSTRESS experimental campaign are compared with the results found in the literature concerning similar tests on flat slab floor and flat slab multi-storey frames.
The SlabSTRESS project has introduced innovative aspects in the setup of the experiments. The mock-up is the first in the literature designed and tested as a secondary system with primary numerical ductile walls to be subjected to two different test typologies: the pseudo-dynamic and the cyclic. The structure corresponds to a multi-floor, flat-slab building in full scale with realistic slab thickness and boundary and construction process. Three different slab-column connections were investigated (interior, edge and corner) using a device designed for the purpose to measure the internal actions (shear force, axial force and bending moment) in the columns of both floors.
The comparison between the SlabSTRESS experimental results and the literature data was made firstly considering similar experiments on an entire building or on single flat-slab floors and then considering experiments on single slab-column connection.
Lastly, a summary of the goals reached is reported.

9.2 Design

The SlabSTRESS experimental campaign is the first to use the same real-scale specimen to perform seismic and cyclic tests, during the same experimental campaign.
Previous experiments on single flat-slab floors and on flat-slab buildings (Table 2.1) considered only one loading type: cyclic tests, Hwang and Moehle, 1993 [1], Rha et al., 2014 [2], Fick et al., 2017 [3](Table 9.2) or seismic (shaking table): Moehle and Diebold, 1984 [4] and Kang and Wallace, 2004 [5] (Table 9.2).
Moreover, in the SlabSTRESS seismic tests the presence of numerical walls as primary seismic elements resulted in experimentally exploring the interaction between flat slabs and a primary seismic system for the first time (albeit only in hybrid mode).

Table 9.1 Design description.

Author	Test typology	Design	Type of frame
Hwang and Moehle, 1993 [1]	Cyclic quasi-static (biaxial)	ACI 318-83, Prototype Structure high rise-building with secondary slabs, wind and seismic load effects calculated	Secondary
Rha et al., 2014 [2]	Cyclic/Monotonic quasi-static	Not specified	-
Fick et all., 2017 [3]	Cyclic quasi-static	Gravity Design – Direct Method ACI 318 (2002)	Gravity load design, without lateral load resisting elements
Moehle and Diebold, 1984 [4][14]	Shake table (biaxial)	Prototype Structure Primary slab frame for Zone 2 UBC 1982 and ACI 318-03	Primary
Kang and Wallace, 2004 [5]	Shake table	Secondary slab frames for buildings with primary walls or frames, ACI 318-02, Zone 4 (high) seismic region	Non-participating for high seismic risk regions / intermediate frames in moderate seismic regions
SlabSTRESS	Pseudo-dynamic/Cyclic	Primary numerical ductile walls (EN 1998-1) and secondary flat slab frames. Eurocode 2 and 8	Secondary

9.3 Flat slab floors and multi storey frames

9.3.1 GEOMETRY

A summary of the main geometric characteristics of the literature works compared with SlabSTRESS is reported in Table 9.2, together with some relationships between these parameters; among them, the slenderness i.e. ratio between the span of the specimen, in both directions, and the slab thickness and the ratio between the span of the specimen and the side of the column.

These parameters can be used to understand different aspects of the response of the entire structure or of the slab-column connection and to perform a comparison between the analysed tests.

In fact, Muttoni, 2008 [6] has demonstrated that the ultimate inter-storey drift ratio capacity depends not only on the gravity shear ratio but also other geometric parameters play a significant role. Among these parameters there are the effective depth of the slab, the column size and the slab slenderness L/d. The following sections analyse some of these characteristics.

Table 9.2 Description of the test specimen and geometry.

Author	Lateral loading type	Span L (m)	Span L' (m)	Span nr	Overhang (mm)	Slab thickness t (mm)	L/t	L'/t	Internal column c (m)	Lateral column c' (m)	L/c	Scale (%)	Floors nr	Transv. Reinf.
Hwang & Moehle, 1993 [1]	Cyclic quasi-static biaxial	2.74	1.83	3x3	-	81	34	23	0.24	0.16	11.4	40	1	-
Rha et al., 2014 [2]	Cyclic/Monotonic quasi-static	2.75	1.65	2x2	-	90	31	18	0.25	0.25	11.0	50	1	-
Fick et al., 2017 [3]	Cyclic quasi-static	6.1	6.1	2x1	1.5, 1.5	180	34	34	0.46	0.46	13.3	100	3	-
Moehele and Diebold, 1984 [4]	Shake table	1.83	1.83	3x1	0.9	61	30	30	0.14	0.14	13.1	30	2	-
Kang and Wallace, 2004 [5]	Shake table	2.06	2.06	2x1	0.9	89	23	23	0.2	0.2	10.3	30	2	Welded studs
SlabSTRESS	Pseudodynamic/Cyclic	5	4.5	3x2	-	200	25	23	0.4	0.3, 0.35	12.5	100	2	Headed studs

BOUNDARY CONDITIONS

In SlabSTRESS it was possible to observe how the damage spread into the real slab thickness considering also the cracking on the edge with the possibility of spalling in the areas with the most damaged connections. The damage observed in the edges of the slab on the 1st and the 2nd floor are reported in Figure 9.2 and Figure 9.1 respectively.

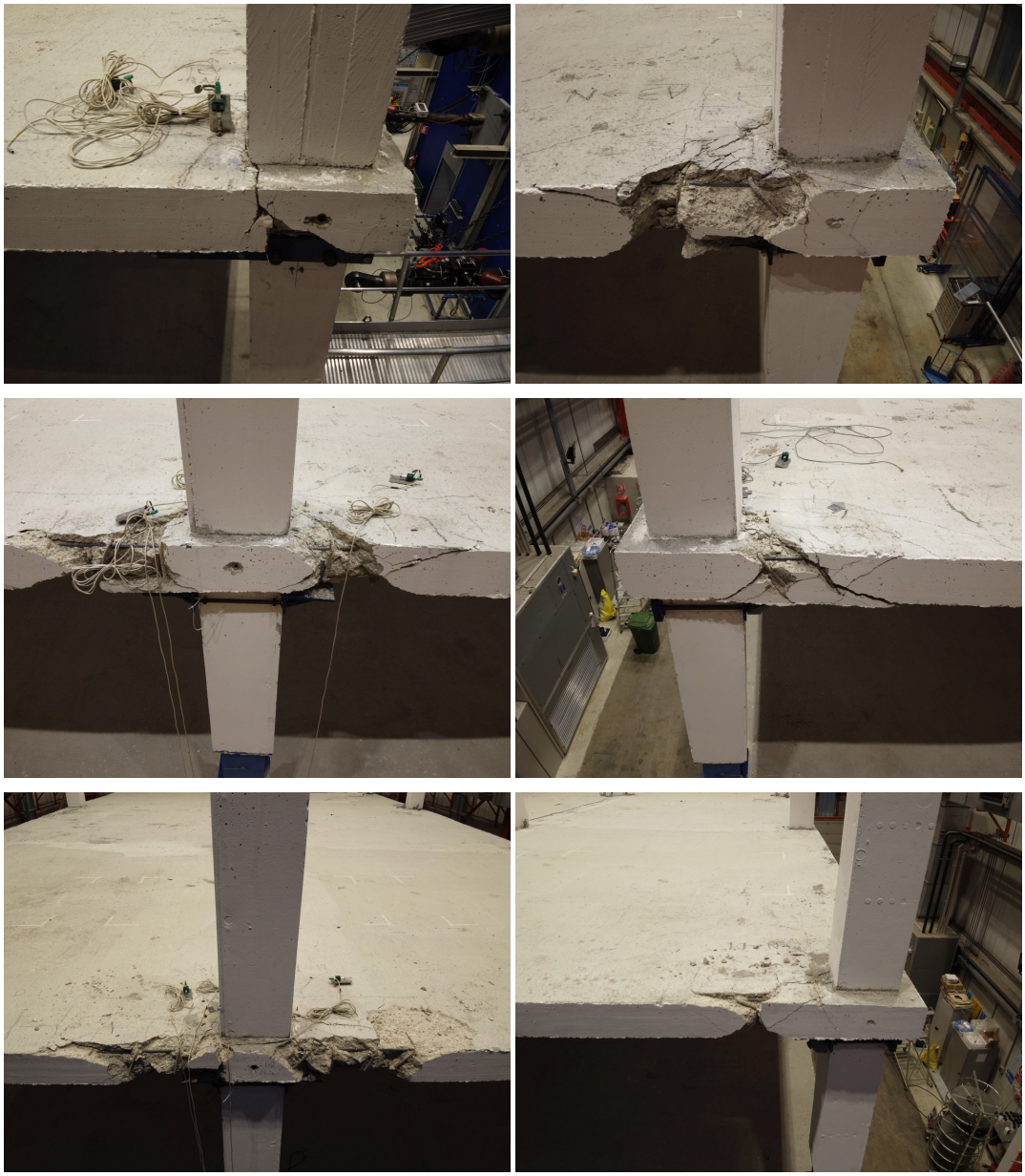

Figure 9.1 2nd floor slab edge damage, connections, clockwise direction a) D3 south, b) A3 west, c) A2, d) A1 west, e) D2, f) D1 east at the end of the experimental campaign for a 6%, drift, load applied in one direction.

Figure 9.2 1st floor slab edge damage, connections, clockwise direction a) A1, b) A2, c) A3, d) B1, e) D1 east, f) D1 north, g) D2 at the end of the experimental campaign.

The SlabSTRESS results were compared with the single floor specimen of Hwang and Moehle, 1993 [1]. Figure 9.3 shows the photographs of the damage in the corner (A1

and A4) and lateral connections (B1 and B4). These authors tested a single floor with the lateral loading applied in both directions and reported the photographs for only the long side of the specimen. The damage in the corner connections A1 and A4 was lower than that in the lateral B1 and B4. In both the lateral connections punching was reached with some spalling in the connection B4.

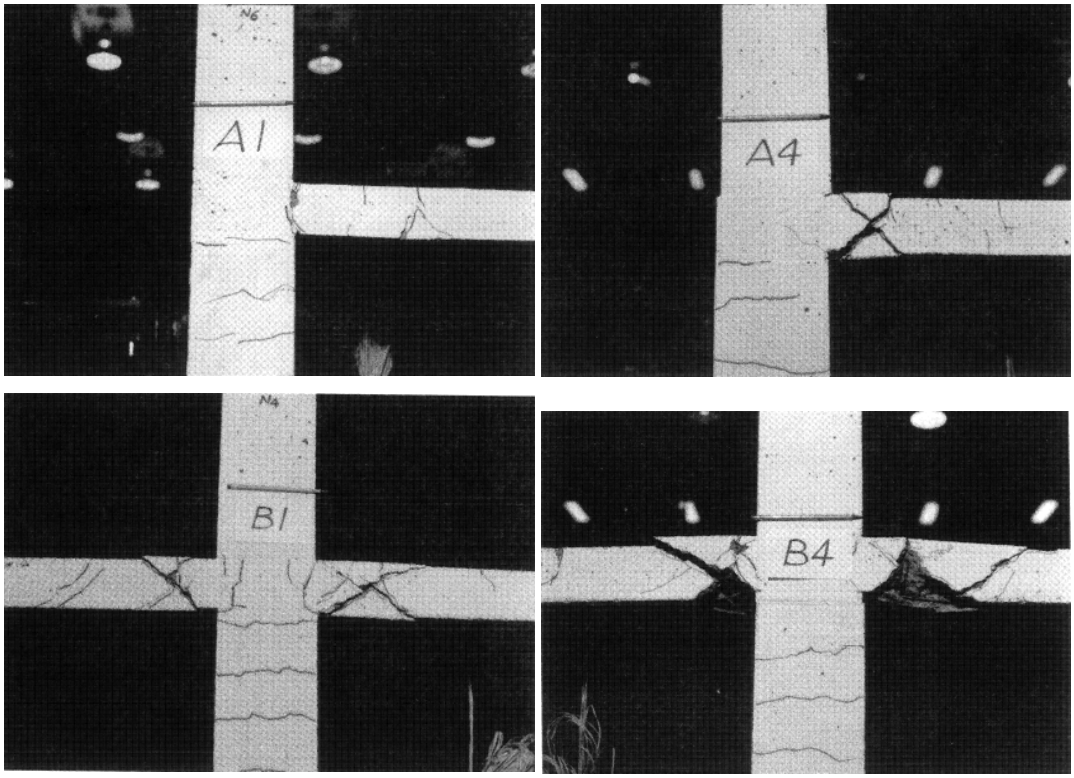

Figure 9.3 Hwang and Moehle, 1993 [1] photographs of damage of connections after 4% drift ratio, load applied biaxial.

Hwang and Moehle, 1993 [1] used the 180-degree hooks as end detail for the slab edge reinforcement, whereas SlabSTRESS used simple bending of the rebars.
Even if the differences in the geometry, in the boundary conditions and in the test set-up, in both the experiments it is possible to note the formation of cracks with double inclination together with the punching cone in the edge slab-column connections (connections B1 and B4 in Figure 9.3 and connections A2 and D2 in Figure 9.2 and Figure 9.1). this was more evident in SlabSTRESS than in Hwang and Moehle, 1993 [1]. Further developments with experimental tests are needed regarding the building details.

SLAB SLENDERNESS

As demonstrated by Muttoni, 2008 [6] slab slenderness is one of the geometric parameter keys in the definition of the ultimate inter-storey drift ratio capacity. It was shown that, the ultimate inter-storey drift ratio capacity increases for slender

slab.

In the analysis of slab slenderness in relation to the drift ratio capacity for all the reported literature works, Table 9.3, it is possible to note that Kang and Wallace, 2004 [5] was the experiment with the least slenderness that reached the lowest drift ratio capacity. SlabSTRESS reported a slab slenderness similar to that of Kang and Wallace, 2004 [5], 25 in comparison to 23, with a lower bound of the global drift ratio capacity of 2.5% for the first cyclic test and drift ratio capacity of approximately 6% for the second one.

Table 9.3 Slab slender and global drift ratio capacity.

Authors	Drift ratio capacity (%)		L/t	L'/t
Hwang & Moehle, 1993 [1]	4		34	23
Rha et al., 2014 [2]	6		31	18
Fick et al., 2017 [3]	2.9		34	34
Moehle and Diebold, 1984 [4]	5		30	30
Kang and Wallace, 2004 [5]	2.5-3		23	23
SlabSTRESS	Cyc-1	2.5(^)	25	23
	Cyc-2	6		

(^) lower bound of global drift ratio capacity

9.3.2 GLOBAL BEHAVIOUR

In the SlabSTRESS cyclic tests a displacement history was imposed on the 2nd floor (Figure 9.4) whereas half of the measured horizontal force on the 2nd floor was imposed on the 1st one. Before the second cyclic test, the gravity loading disposition and entity was changed (see chapter 3 for more details).

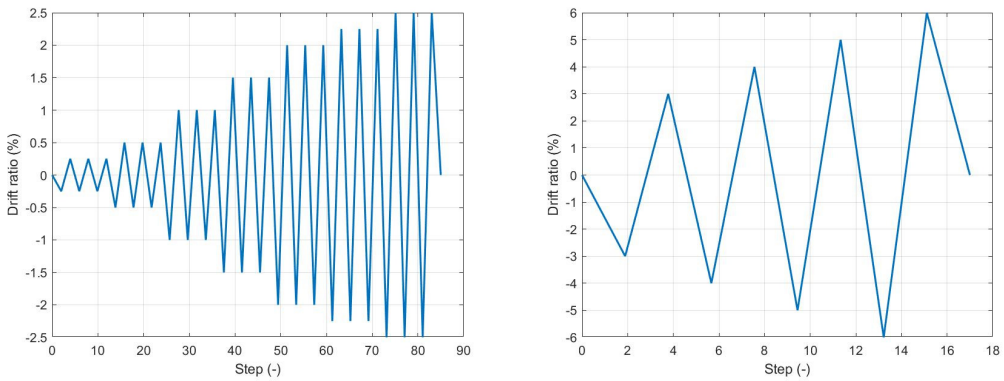

Figure 9.4 SlabSTRESS displacement history at 2nd floor for the a) 1st and b) 2nd cyclic test.

Due to the gravity loading changes and the application of strengthening after the first cyclic test, it may be considered that two partly different structural configurations were tested.
In Fick et al., 2017 [3] the structure was tested to failure under cycles of increasing quasi-static lateral displacement imposed on the 3rd top floor (Figure 9.5), with forces acting on the other floors controlled to vary linearly with height.

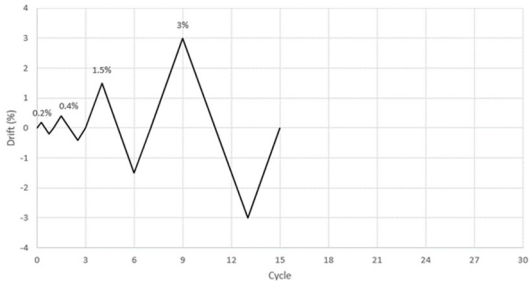

Figure 9.5 Fick et al., 2017 [3] lateral loading cycles.

In Hwang & Moehle, 1993 [1] a biaxial cyclic displacement history with increasing amplitude was imposed, with lateral drifts from 0.25% to 4%. The load protocol imposed two cycles in one direction, followed by two in the orthogonal direction (Figure 9.6).

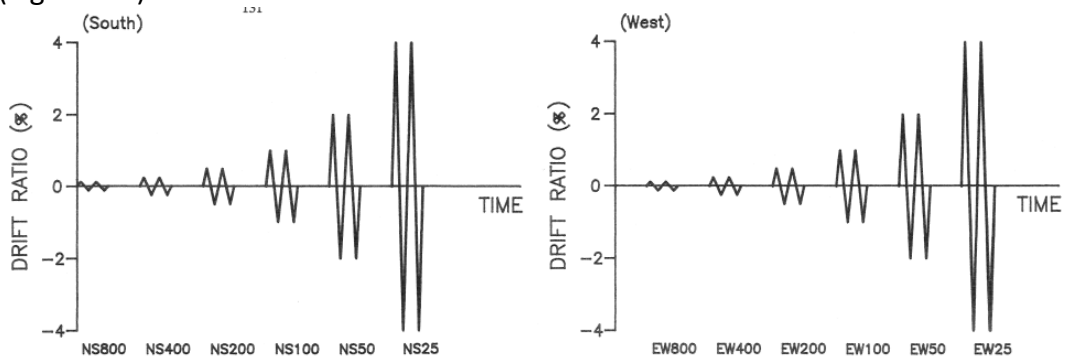

Figure 9.6 Hwang and Moehle, 1993 [1] lateral displacement history.

Rha et al., 2014 [2] imposed two different loading typologies and histories, lateral monotonic (LM) and lateral cyclic (LC). In Figure 9.7 the loading history for the LC specimen is reported.

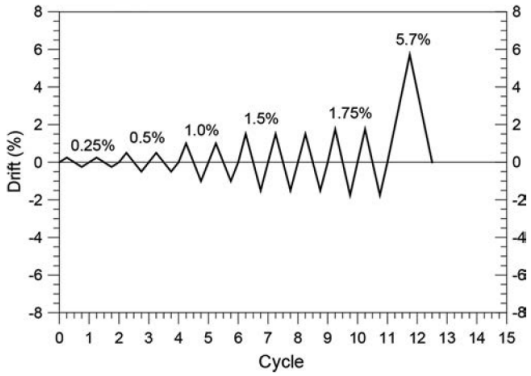

Figure 9.7 Rha et al., 2014 [2] lateral loading cycles.

The global behaviour of SlabSTRESS (Figure 9.8) can be compared with the global response of a similar complete building, the full scale cyclic test by Fick et al., 2017 [3] (Figure 9.10) and the complete scaled size floor tested for cyclic loading by Hwang and Moehle, 1993 [1] and Rha et al., 2014 [2] (Figure 9.10). It was also compared to Kang and Wallace, 2004 [5] (Figure 9.10) and Moehle and Diebold, 1984 [4] (Figure 9.9) shaketable test to have the comparison with a seismic test.

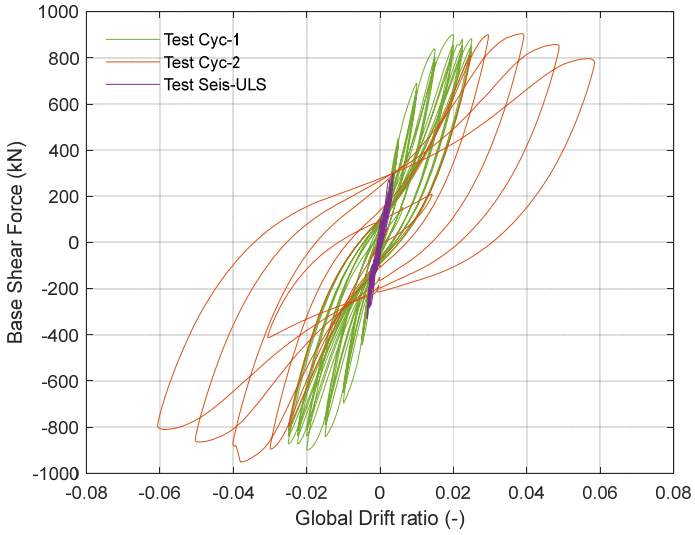

Figure 9.8 SlabSTRESS global behaviour, purple line, test Seis-ULS, green line, test Cyc-1, orange line, test Cyc-2.

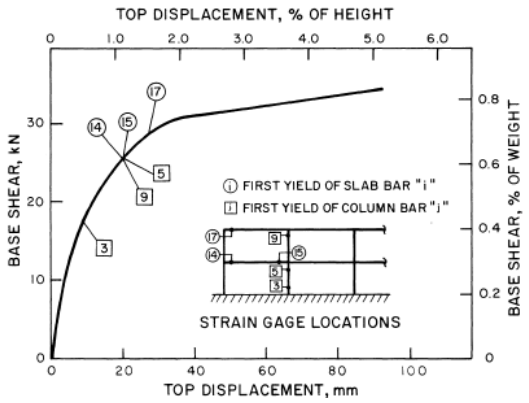

Figure 9.9 Moehle and Diebold, 1984 [4] envelope relation between base shear and second-floor, shaketable test.

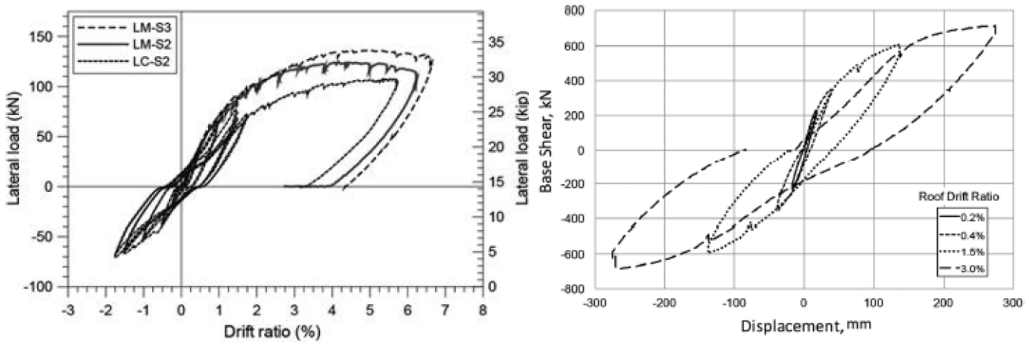

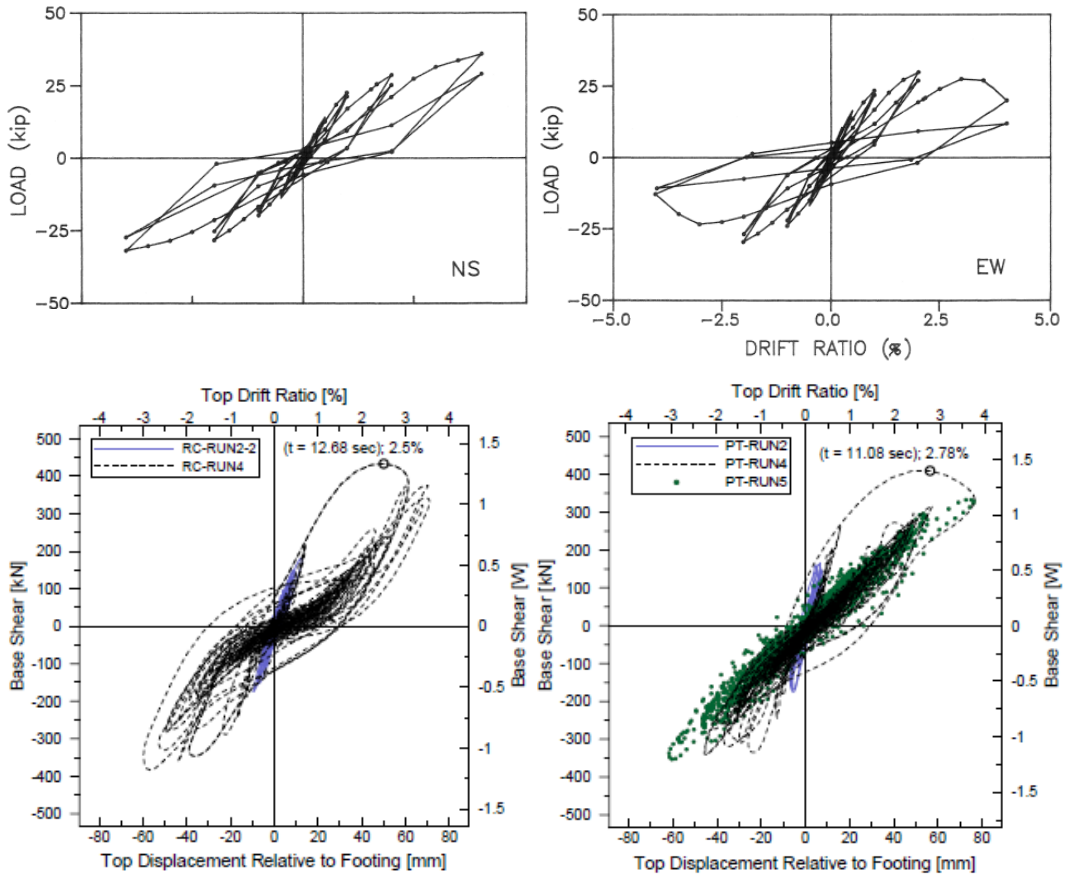

Figure 9.10 Global behaviour Rha et al., 2014 [2] (top left), Fick et al., 2017 [3] (top right), Hwang and Moehle, 1993 [1] (centre), Kang and Wallace, 2004 [5] (bottom).

The compared tests gravity shear ratio and ultimate drift ratios are given in Table 9.4.

Table 9.4 Punching failure comparison.

Authors	Test typology	Maximum drift ratio (%)	GSR	Drift ratio at punching (%)
Hwang & Moehle, 1993 [1]	Cyclic quasi-static biaxial	4	0.3	3.1÷3.7
Rha et al., 2014 [2]	Cyclic/monotonic quasi-static	6	0.28÷0.44	Cyclic:1.5
Fick et al., 2017 [3]	Cyclic quasi-static	2.9	0.21	Roof drift ratio:2.9 Storey drift ratio:3.3
Moehle and Diebold, 1984 [4]	Shaking table	5	0.25	(4.4)
Kang and Wallace, 2004 [5]	Shaking table	2.5-3	0.20÷0.25	3.12
SlabSTRESS	Cyclic and seismic	2.5	0.13÷0.32	Roof drift ratio:3.8 Storey drift ratio:4.1
		6	0.10÷0.32	

Regarding the loss of the lateral load bearing capacity, it is possible to distinguish two different typologies. Rha et al., 2014 [2] and SlabSTRESS recorded a limited loss of the lateral load resistance after reaching the maximum load. Fick et al., 2017 [3], Hwang and Moehle, 1993 [1] and Kang and Wallace, 2004 [5] recorded higher loss.
In SlabSTRESS the maximum load was reached for a global inter-storey drift ratio of 2%. After this value, there was a slight decrease until the drift ratio value of 2.5% (green line in Figure 9.8). After one connection was strengthened and the loading changes, the second phase of the test detected a punching failure in one 1st floor interior connection for a global inter-storey drift ratio of 3.8%. After this, the maximum value of load was reached for a global inter-storey drift ratio of 4%. The structure reached a final inter-storey drift ratio of 6% with a loss of the loading capacity of around 16%.
Rha et al., 2014 [2] is the only work that reached the same maximum inter-storey drift ratio as SlabSTRESS (6%) even if they tested a half scale flat plate floor. The specimen had only two spans for each direction and all the connection typologies, (corner, internal and lateral) with a gravity shear ratio higher than SlabSTRESS (Table 9.4). Rha et al., 2014 [2] recorded the same first punching even if for a drift ratio significantly lower, of 1.5% compared to SlabSTRESS roof drift ratio of 3.8%.
Fick et al., 2017 [3] was the only full scale test on a complete building with different

characteristics compared to SlabSTRESS. The structure had three stories, only two connection typology, internal and lateral, all having a 1.5m of overhang. In this specimen the first punching was recorded in an edge connection on the 2nd floor, for a storey drift ratio of 2.9% lower than those of SlabSTRESS. The test was stopped the test after punching, differently from SlabSTRESS in which the test was stopped because the maximum stroke of the actuators was reached.

Hwang and Moehle, 1993 [1] carried out a biaxial test on a single floor with a gravity shear ratio similar to that of SlabSTRESS (Table 9.4). The specimen included different types of column (internal, edge and corner) and also different shapes (rectangular and square). Differently from SlabSTRESS the first connection that punched was on the edge for a drift ratio very similar to that recorded in the roof of SlabSTRESS.

The lowest value of maximum drift ratio was reached by Kang and Wallace, 2004 [5] who carried out a shaking table test with shear reinforcement in the slab. The results showed a nonlinear response for greater intensity shaking. At a point for positive curvatures and higher slab curvature the column curvature dropped. A degradation of the moment transfer capacity in an internal slab-column connection of the reinforced concrete specimen was observed, indicating the occurrence of punching.

Moehle and Diebold, 1984 [4] recorded an apparent punch of an interior slab-column connection for a lateral drift of 4.4% of the specimen height. The failure was sudden with a severe sound indicating a brittle shear failure. Apparently, the failure cone was visible only on the top side of the slab. The spandrel beam showed a torsional failure for a lateral drift of 5.5% of specimen height so the exterior slab-column-spandrel assembly failed under negative unbalanced moment. The cover in the edge beam showed some spalling exposing the reinforcement. Despite the sudden brittle failure in the interior connection, the exterior connections continued to support load at increasing drifts.

Summing up, the compared tests used gravity shear ratio between 0.2 and 0.4, reaching ultimate drift ratios in a range between 2.9% and 6% (Table 9.4). The SlabSTRESS specimen reached 2.5% drift ratio in the first cyclic test without indications of a global failure; a 4% global drift ratio capacity (at peak lateral load) was reached in test Cyc-2. Using an alternative definition, approximately 6% global drift ratio capacity was reached for 15% reduction in the envelope of lateral load cycles. The test specimens and loading had numerous differences documented in the State of the Art chapter. Nevertheless, it can be concluded that the SlabSTRESS confirms the global nonlinear lateral deformation capacity of flat slabs, provided that the gravity shear ratio is controlled.

9.3.3 REINFORCEMENT DETAILING OF EDGE CONNECTIONS

SlabSTRESS the reinforcement detailing in the edge of the slab was done with a simple bending of the rebars without closed hook. This design detailing is quite common in the real slab buildings in Europe

Observing the D1 east connection at the end of the first cyclic test in Figure 9.11 it can be seen that this caused the damage of the edge (Figure 9.11 a). In literature to date, it was the first time that it was possible to observe this detail

This design detailing is quite common in the real slab buildings in Europe.

Figure 9.11 SlabSTRESS D1 east after test a) Cyc-1 and b) Cyc-2.

All the connections in the two short sides of the slab were too damaged to be repaired. Due to this and safety reasons, added vertical loading (water tanks) in these connections was removed and also some of the sensors.

The edge connections showed the higher levels of strength and stiffness deterioration in the two cyclic tests (see Chapters 7 and 8). The 180-degree hooks used by other authors (see chapter 2, Moehle and Diebold, 1984 [4], Rha et al., 2014 [2] and Kang and Wallace, 2004 [5]) corresponded to similar but less severe damage on the slab edges.

9.3.4 DISTRIBUTION OF FLEXURAL CRACKS IN THE COLUMNS

Moehle and Diebold, 1984[4], Fick et al., 2017 [3] and Kang and Wallace, 2004 [5] report a detailed observation of the distribution of flexural cracks in the columns. These are experiments that differ for the test typology, the scale and the inter-storey drift ratio, shaking table, 30% and 5.5% for the first one, cyclic quasi-static, 100% and 3.3% for the second one and shaking table, 30%, 3% for the last one (Table 2.1).

In Moehle and Diebold, 1984 [4] the longitudinal reinforcement in the columns consisted in eight 6.4mm deformed bars, continuous through the footing and welded with a steel plate at the base (Figure 9.12). To favour the development of inelastic deformations in the slab rather than the column, the design of the column was developed in such a way that in each column the flexural strength exceeded the unbalanced moment. Since the aim of the experiment was to study the inelastic behaviour of the slab as opposed to the column, they used the capacity design

method.

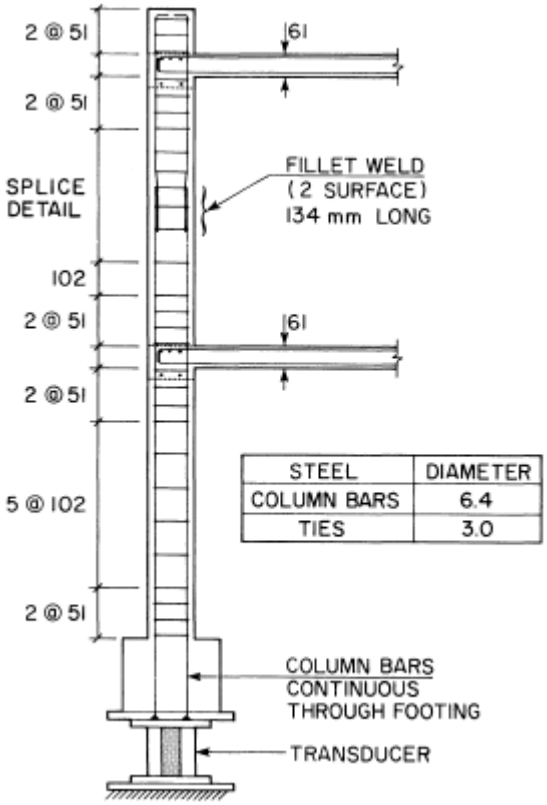

Figure 9.12 Moehle and Diebold, 1984 [4] column reinforcement detail.

At the end of the test programme they observed extensive spalling in both the columns typology, internal and external, at slab-column and footing-column interface, but no bar buckling was observed during any of the tests (Figure 9.13).

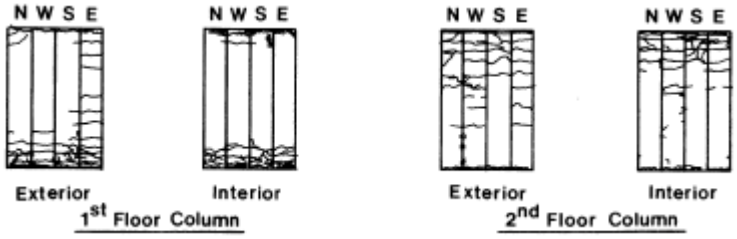

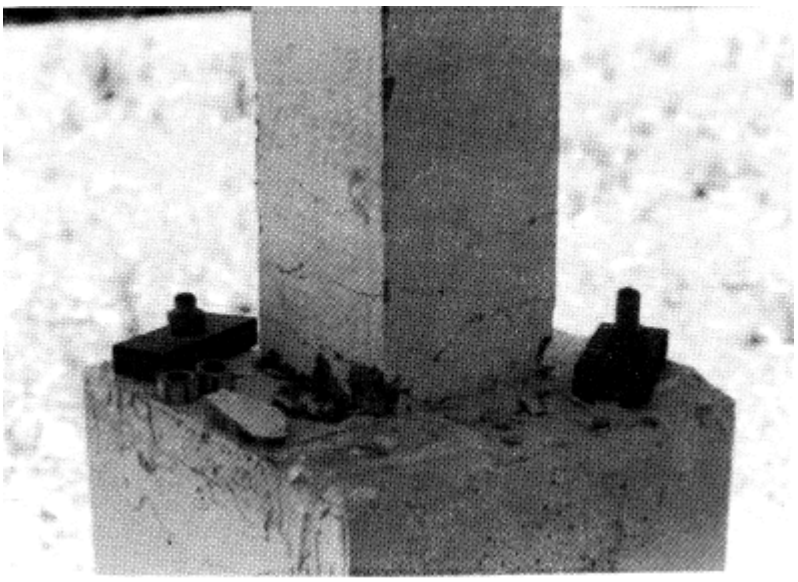

Figure 9.13 a) Crack pattern in the columns, b) footing of the exterior column, Moehle and Diebold, 1984 [4].

The column reinforcement of Fick et al., 2017 [3] is reported in Figure 9.14. They reported a gradual increase of the flexural cracking with the roof drift ratio (Figure 9.15).

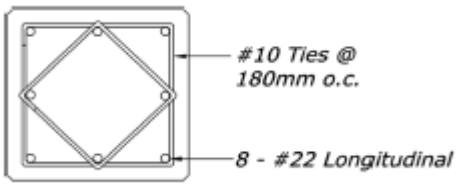

Figure 9.14 Fick et al., 2017 [3] column reinforcement.

The flexural cracks start for a roof drift ratio of 4% from the 1st and the 2nd storey column bottom, then grow progressively in extension to a roof drift ratio of 3%. For this last value, cracks were observed in almost all the column heights except the 1st floor column top and the 3rd floor column bottom.

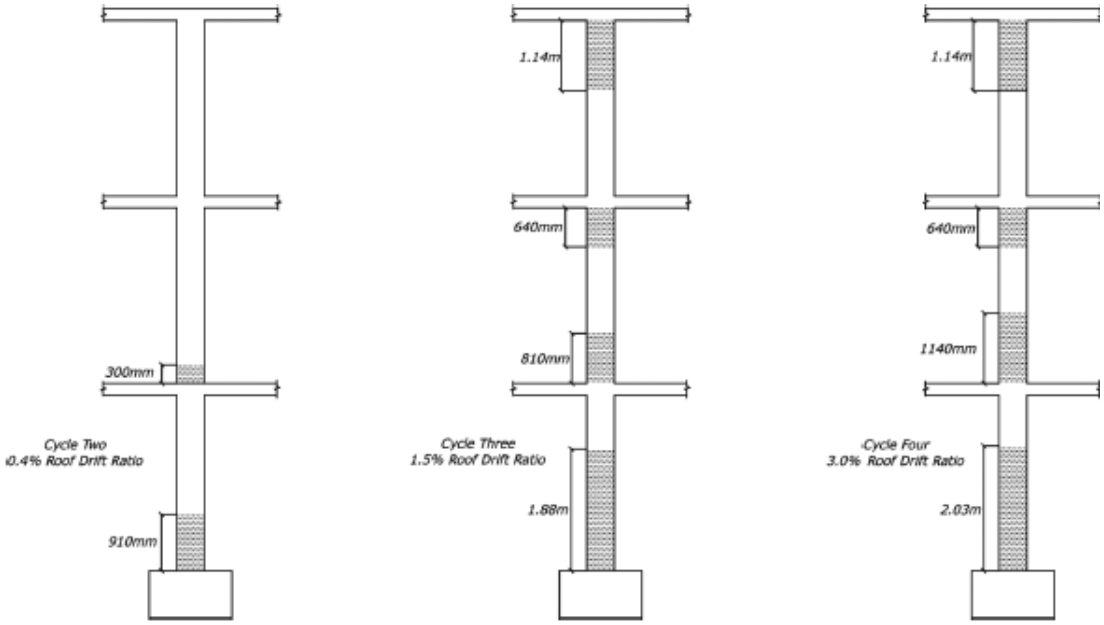

Figure 9.15 Cracking in the column, Fick et al., 2017 [3].

Kang and Wallace, 2004 [5] chose the column flexural strengths so that yielding and damage were concentrated in the slab-column connection instead of the column. For this reason, columns were reinforced with eight 12.7mm longitudinal bars with a nominal yield stress of 414 MPa (Figure 9.16).

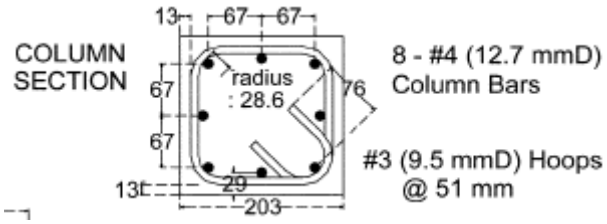

Figure 9.16 Kang and Wallace, 2004 [5], column reinforcement.

They observed a nonlinear response with yielding of slab reinforcement, yielding at column bases, and punching at slab-column connections for both specimens, reinforced-concrete slab-column frame (RC) and post-tensioned slab-column frame (PT) (Figure 9.10). They also reported the formation of hinge in some connections with loss of moment transfer strength.

Figure 9.17 Kang and Wallace, 2004 [5] damage at the column base of the RC specimen.

In SlabSTRESS the column design was developed to facilitate the formation of a plastic hinge at the base avoiding the formation of premature buckling of the compressed bars. The design was carried out considering the maximum slab moment at the floors.

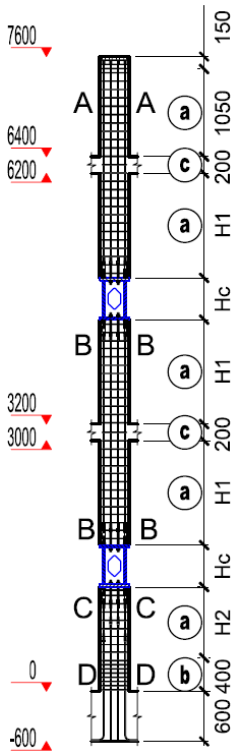

Figure 9.18 SlabSTRESS column reinforcement.

No cracks appeared in the column heights but the internal columns B2 and C2 reported a significant failure at the base. These damages are reported in Figure 8.30.

Figure 9.19 SlabSTRESS base column connection a) B2 west and b) C2 east.

The B2 was the same column that punched in the slab-column connections on the 1st floor during the cyclic test Cyc-1 for an inter-storey drift of 4% in negative. At the end of the test, after compression buckling, breaking of the longitudinal reinforcement at the base of the column in the B2 connection (Figure 8.30 a) was observed. The reinforcement of the columns limited the cracking of these members that would have increased the ultimate drift.
The column reinforcement in SlabSTRESS was chosen to avoid cracking and damage in the columns. As observed in Moehle and Diebold, 1984 [4] and Fick et al., 2017 [3] a lower percentage of reinforcement could have brought to a structure with higher deformability in non-linear field.

9.3.5 Crack pattern and Redistribution of the internal forces

The full-scale test with local measurements allowed to consider the structural response with redistribution of loads effects in the different types of connections with realistic boundary conditions.
Hwang and Moehle, 1993 [1] observed cracking and spalling during the experiments. The cracking started on the slab top near the columns (Figure 9.20). Successively top transverse cracks ran across the internal connections c2 and c3 and in the meantime bottom transverse cracks across centres of the spans. They also reported the presence of damage to the slab top and edges after the punching failure occurred in the connections and the shear cracks on the edge connections in the north side of the slab. From the lateral connections the load was redistributed in all the other connections.
Moehle and Diebold, 1984 [4] report drawing of the cracks pattern for the seismic tests (Table 2.1 for tests and specimen description). They observed the start of cracking around columns and along edge beams, with a few cracks extending across the full slab width (Figure 9.21). At the end of the experimental campaign a slight vertical displacement of the first floor slab surrounding one interior column indicated that if the test had been continued, a punching failure would have occurred. The slab damage on the 1st floor was more pronounced than the 2nd one. Although there were differences in test typology and specimen geometry, the load was redistributed from

the edge alignment to the internal ones also in this test.
In SlabSTRESS (Figure 9.22) the same crack pattern reported by Hwang and Moehle, 1993 [1] and Moehle and Diebold, 1984 [4] was observed. The radial cracking around the columns is present on both floors, whereas the formation of the cracks that run across the slab between the columns was only detected on the 2nd floor. This last crack typology was only in the direction perpendicular to the loading applications.
Finally, in Fick et al., 2017 [3] it was not possible to study the redistribution since they stopped the test after the first punching.

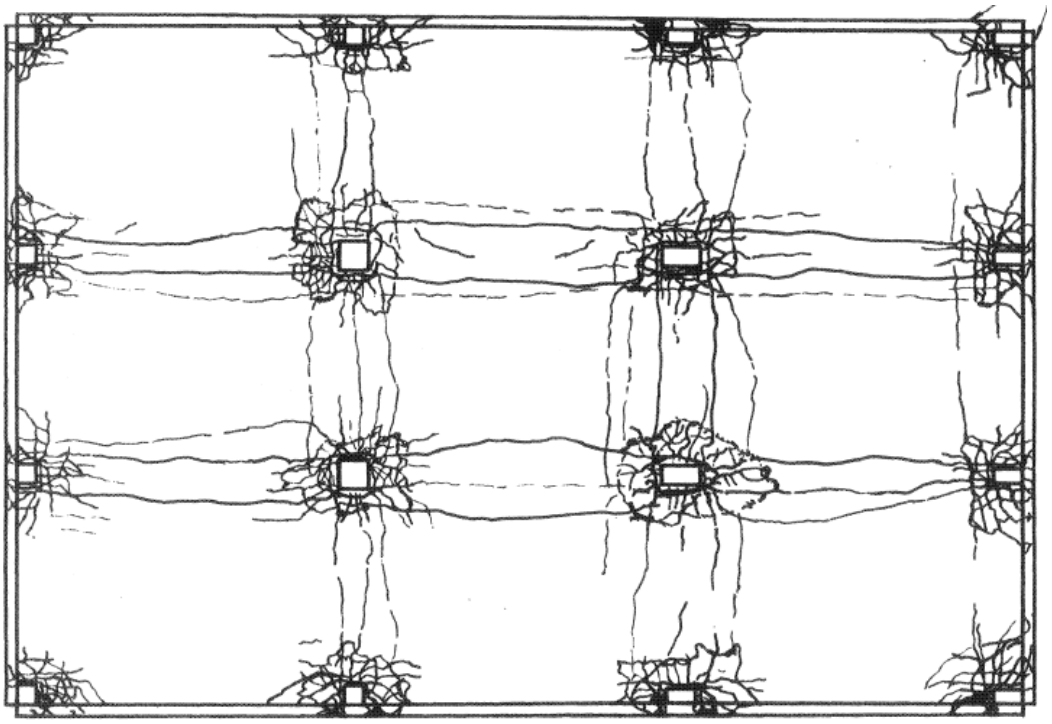

Figure 9.20 Hwang and Moehle, 1993 [1] cracks pattern of top and edge slab.

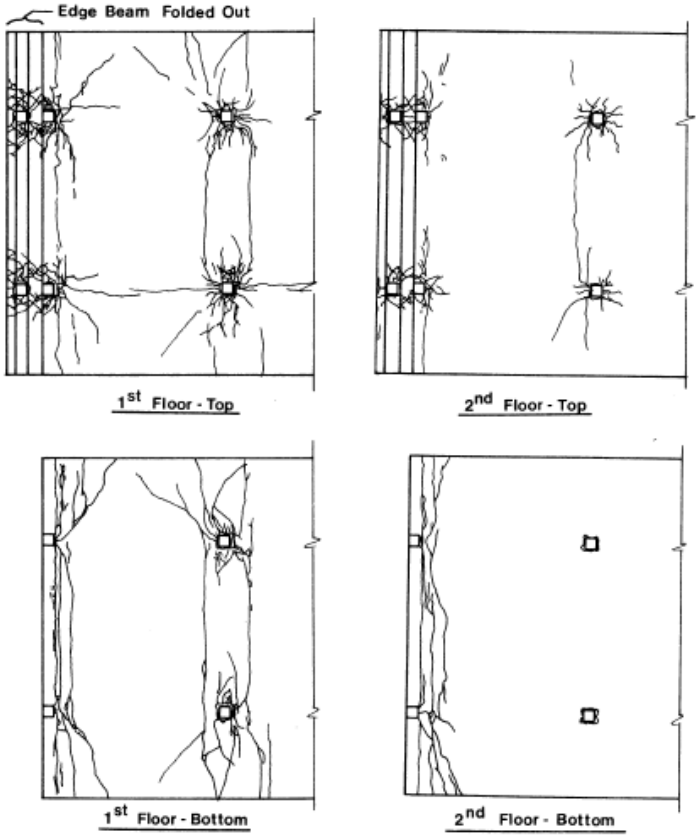

Figure 9.21 Moehle and Diebold, 1984 [4] slabs cracks observation.

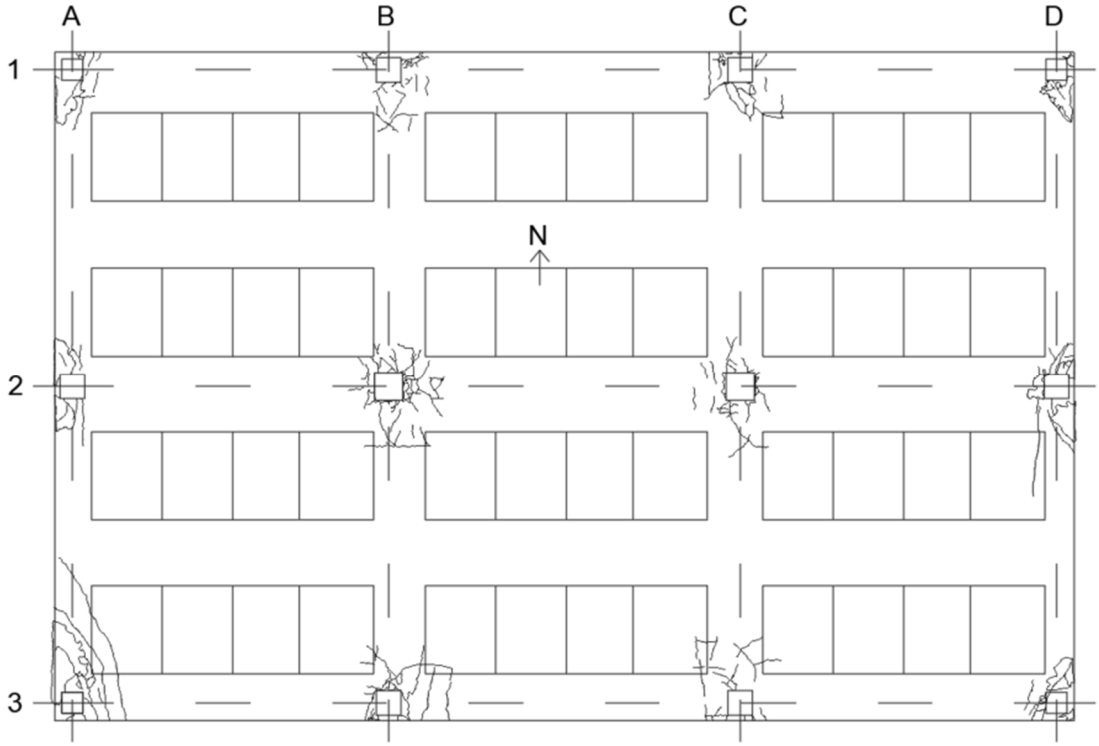

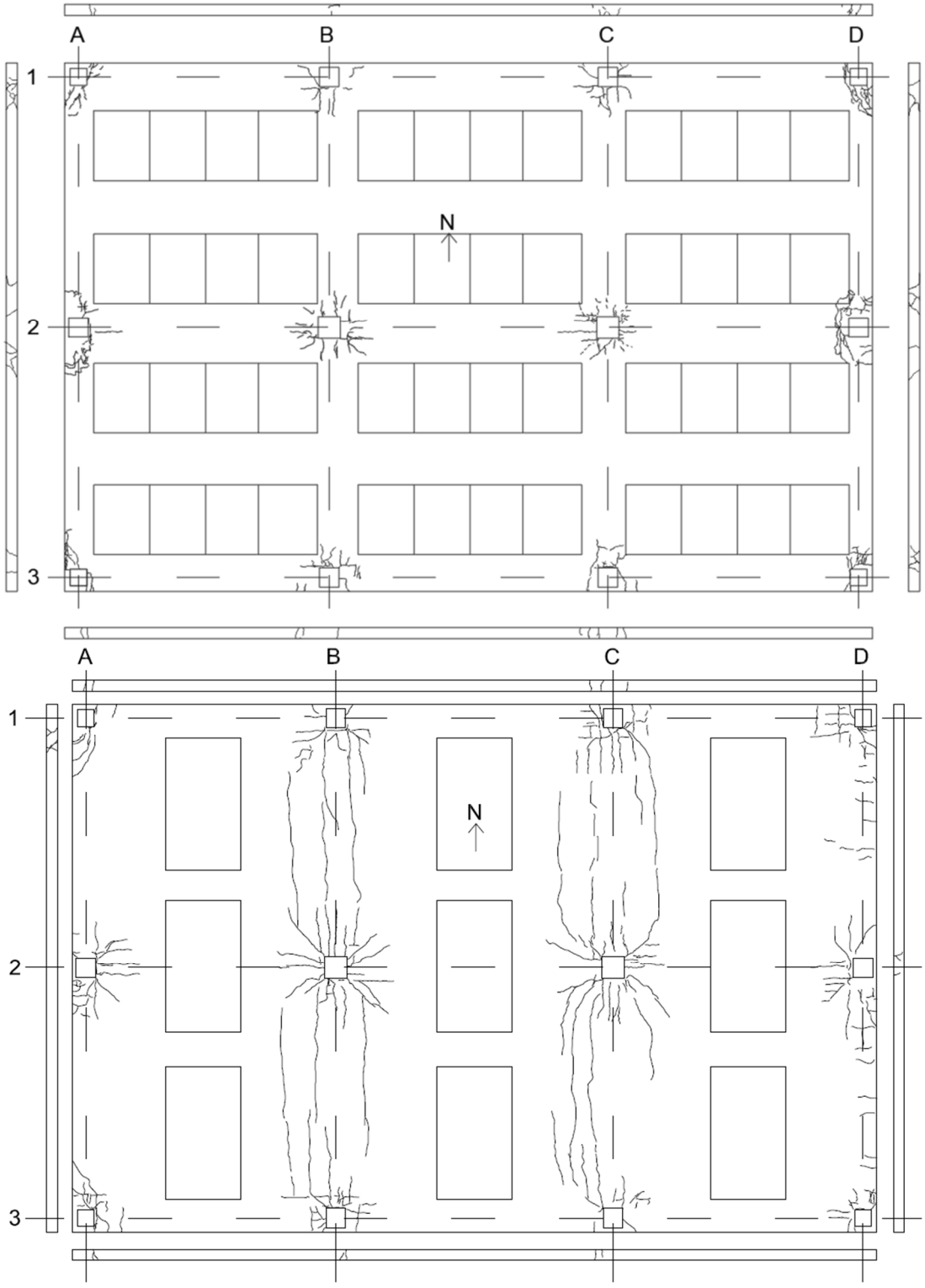

Figure 9.22 SlabSTRESS crack pattern a) intrados 1st floor, b) extrados 1st floor, c) extrados 2nd floor.

In SlabSTRESS the most damaged connections were those located on the side

perpendicular to the loading application (A2 and D2 in Figure 9.22). Similarly, in Hwang and Moehle, 1993 [1] the lateral connections on both sides (Figure 9.20) reported most damages due to the biaxial loading application.
In Figure 9.23 by Hwang and Moehle, 1993 [1] the small circle marks the occurrence of the punching shear failure. In Hwang and Moehle, 1993 [1] all the internal (b2, c2, b3, c3) and lateral connections with bending perpendicular (d2, d3) and parallel (c1, b4, c4) to the edge punched when the slab displaced to both the East and West directions. The connections a2, b1 and d1 failed only in the West directions. The corners a1, a4 and d4 and the lateral a3 survived.
A similar behaviour was observed in SlabSTRESS. The failure of the edge connections on lined A and D was followed by redistribution of load effects to the interior connections of lines B and C. From the analysis conducted in chapter 8 it is possible to observe that after the punching of the internal slab-column connection on the 1st floor, the bending moment and the shear force have redistributed following different patterns (Figure 9.24).

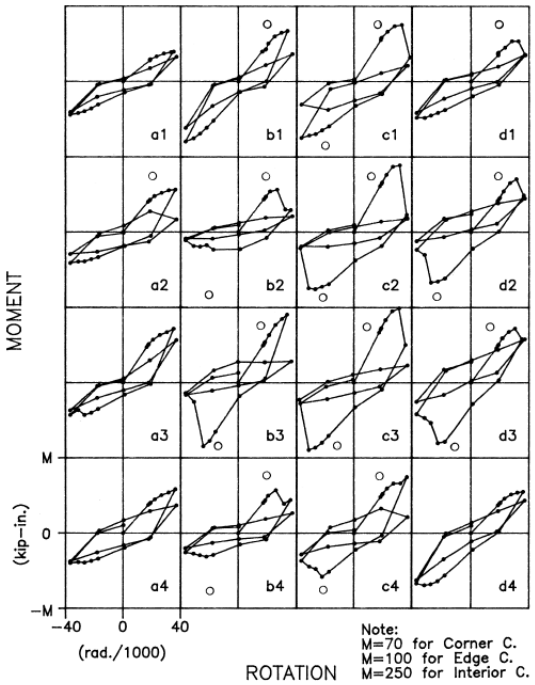

Figure 9.23 Hwang and Moehle, 1993 [1] moment-rotation in the East-West direction, drift 4% (last test).

This redistribution did not affected the global capacity of the building during test Cyc-1 (Figure 9.8).

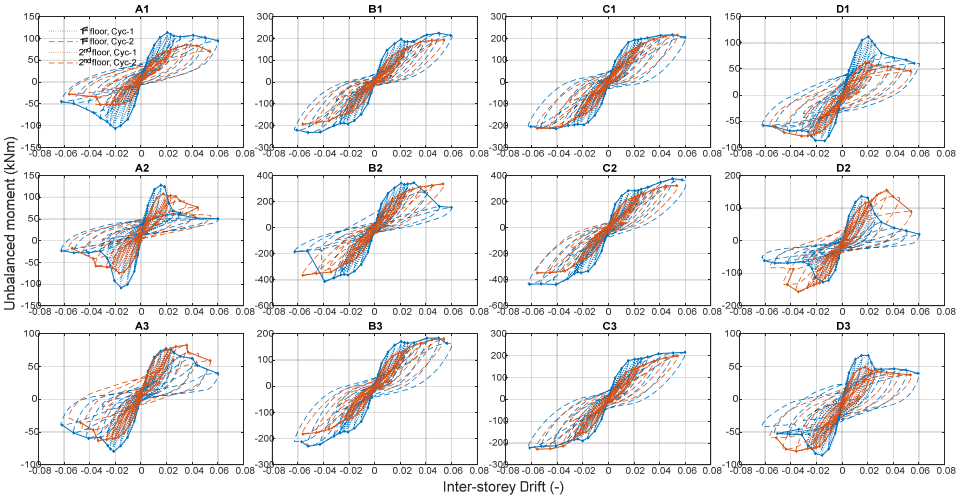

Figure 9.24 SlabSTRESS unbalanced moment vs rotation.

It is possible to observe in the analysed works that the load is redistributed from the edge alignment to the internal ones with a high vulnerability of the edge connections, that will be further discussed in the following section.

9.4 Connections response

9.4.1 COMPARISON WITH ISOLATED CONNECTIONS

Hueste et al., 2007 [22] collected a database of connection tests, and reported the peak drift and the gravity shear ratio for each specimen. The authors defined the peak drift as the drift corresponding to the peak lateral load.

Differently, Ramos et al., 2017 [8] used the drift at failure defined considering the failure of the specimen when the unbalanced moment drops to 80% of its peak value. To make the comparison with SlabSTRESS the values of the drift ratio were taken from the data collected in the ductility analysis (see Chapter 8). For the comparison with the Hueste et al., 2007 [22] data, the drift values corresponding to the "peak moment point" were used, whereas for the comparison with the Ramos et al., 2017 [8] the drifts of the "Failure point" corresponding to the drop of 80% of the unbalanced moment from its peak value were taken.

In Hueste et al., 2007 [22] the gravity shear ratio Vg/Vo represents the un-factored vertical gravity shear Vg divided by the theoretical punching shear strength without moment transfer defined according to ACI318-14 as $Vo=v_c b_o d$ with v_c nominal shear strength carried by the concrete, b_o the length of the perimeter of the critical section and d is the distance from the extreme compression fibre to the centroid of the longitudinal tension reinforcement.

The gravity shear ratio in Ramos et al., 2017 [8] was calculated as Vg/Vo where Vg is the slab shear force due to loading in the gravity direction and $Vo=v_c b_o d$ with v_c

nominal shear strength obtained in accordance with the ACI 318-14.
The data collected during the SlabSTRESS experiments regards both the positive and the negative drift. To make this comparison it was chosen to take into consideration the absolute value of the smallest drift. This choice was due to the fact that the smallest drift corresponds to the first failure.
The local comparison was make using the database collected by Hueste et al., 2007 [22] (Figure 9.25, Figure 9.26, Table 9.5, Table 9.6) and Ramos et al., 2017 (Figure 9.27, Table 9.7) with the results of experimental works on slab-column connections.
Both the databases regard only internal connections; Ramos et al., 2017 [8] considered tests without the shear reinforcement, whereas Hueste et al., 2007 [22] considered tests with (Figure 9.26 and Table 9.6) and without (Figure 9.25 and Table 9.5) the shear reinforcement.
Only the internal connections B2 and C2 of both floors of the SlabSTRESS results were considered for these comparisons. For Figure 9.25 and Table 9.5 without shear reinforcement, the internal connections B2 on the 1st floor at the end of the tests Cyc-2. For Figure 9.26 and Table 9.6 with shear reinforcement, no connections were considered since no one of the internal connections the 2nd floor and strengthened on the 1st floor failed. For Figure 9.27 and Table 9.7 without shear reinforcement, the internal connections B2 on the 1st floor at the end of the tests Cyc-2.

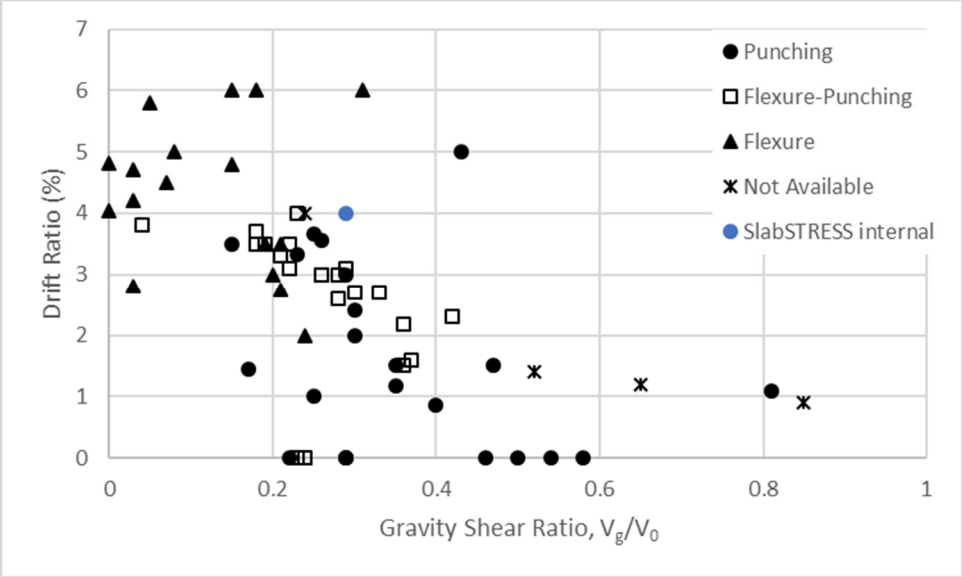

Figure 9.25 Database for interior slab-column connection specimen without shear reinforcement, Hueste et al., 2007 [22].

Table 9.5 Hueste et al., 2007 [22], Test data for interior slab-column connections without shear

reinforcement.

Author	Label	V_g/V_0	Peak drift, %	Failure Mode	Author	Label	V_g/V_0	Peak drift, %	Failure Mode
Dilger and Cao, 1991	CD1	0.85	0.9	NA	Hawkins and Moehle, 1990	Int. Join	0.24	4	NA
	CD2	0.65	1.2	NA	Megally and Ghali, 2000	MG-2A	0.58	1.17	P
	CD8	0.52	1.4	NA		MG-7	0.29	3.1	F-P
Durrani et al., 1995	DNY 1	0.2	3	F		MG-8	0.42	2.3	F-P
	DNY 2	0.3	2	P		MG-9	0.36	2.17	F-P
	DNY 3	0.24	2	F	Morrison and Sozen, 1983	S1	0.03	4.7	F
	DNY 4	0.28	2.6	F-P		S2	0.03	2.8	F
Elgabry and Ghali, 1987	1	0.46	NA	P		S3	0.03	4.2	F
Farhey et al., 1993	1	0	4.81	F		S4	0.07	4.5	F
	2	0	4.04	F		S5	0.15	4.8	F
	3	0.26	3.56	P	Pan and Moehle, 1989	AP 1	0.37	1.6	F-P
	4	0.3	2.4	P		AP 2	0.36	1.5	F-P
Ghali et al., 1976	SM 0.5	0.31	6	F		AP 3	0.18	3.7	F-P
	SM 1	0.33	2.7	F-P		AP 4	0.19	3.5	F-P
	SM 1.5	0.3	2.7	F-P	Pan and Moehe, 1992	1	0.35	1.5	P
Hanson and Hanson, 1968	A12	0.29	NA	P		2	0.35	1.5EW/0.79NS	P
	A13L	0.29	NA	P		3	0.22	3.1	F-P
	B16	0.29	NA	P		4	0.22	3.2EW/1.75NS	P
	B7	0.04	3.8	F-P	Robertson and Durrani, 1990	1	0.21	2.75	F
	C17	0.24	NA	F-P		2C	0.22	3.5	F-P
	C8	0.05	5.8	F		3SE	0.19	3.5	F
Islam and Park, 1976	1	0.25	3.67	P		5SO	0.21	3.5	F
	2	0.23	3.33	P		6LL	0.54	0.85	P
	3C	0.23	4	F-P		7L	0.4	1.45	P
Robertson and Johnson, 2006	ND1C	0.23	3 to 5	F-P		8I	0.18	3.5	F-P
	ND4LL	0.28	3	F-P	Robertson et al., 2002	1C	0.17	3.5	P
	ND5XL	0.47	1.5	P	Wey and Durrani, 1992	SC 0	0.25	3.5	P
	ND6HR	0.29	3	P		SC 2	0.18	6	F
	NC7LR	0.26	3	F-P		SC 4	0.15	6	F
	ND8BU	0.26	3	F-P		SC 6	0.15	5	P
Luo and Durrani, 1995	I.I	0.08	5	F	Zee abd Moehle, 1984	INT	0.21	3.3	F-P
	INT1	0.43	NA	P	SlabSTRESS Cyc-2	B2	0.29	4	P
	INT2	0.5	NA	P					
Symonds et al., 1976	S6	0.86	1.1	P					
	S7	0.81	1	P					

In Figure 9.25, Figure 9.26, Figure 9.27 and Table 9.5, Table 9.6 Table 9.7, flexural failure is denoted with “F”, punching shear failure is denoted with “P” and intermediate failure modes are reported as flexure-punching “FP”. NA indicates not available data.

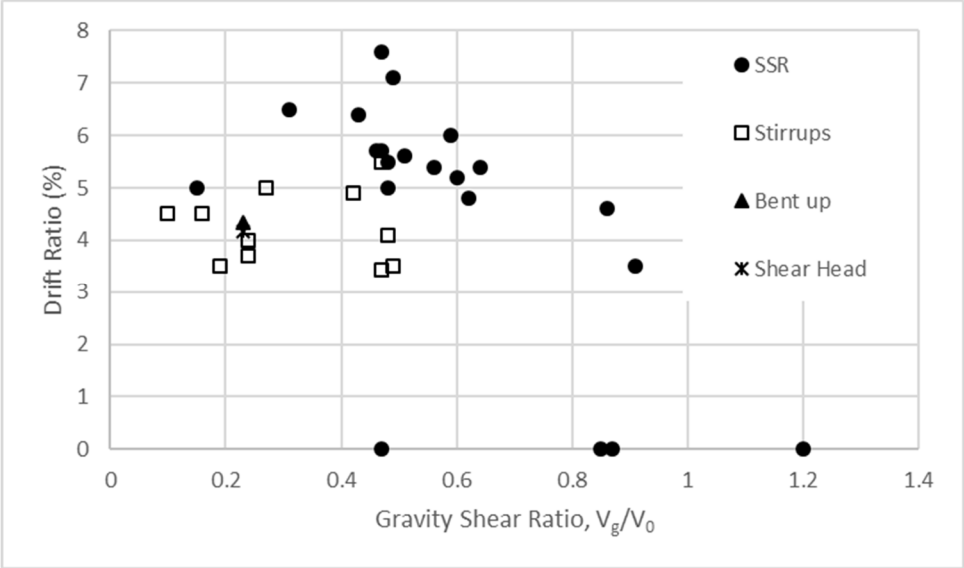

Figure 9.26 Database for interior slab-column connection specimen with shear reinforcement, Hueste et al., 2007 [22].

Table 9.6 Hueste et al., 2007 [22], Test data for interior slab-column connections with shear reinforcement.

Author	Label	V_g/V_0	Peak drift %	Shear reinforcement	Failure Mode	Author	Label	V_g/V_0	Peak drift %	Shear reinforcement	Failure Mode
Dilger and Brown, 1995	SJB-1	0.48	5.5	SSR	S[1]	Islam and Park, 1976	4S	0.23	4.33	Bent up	P
	SJB-2	0.47	5.7	SSR	S[1]		5S	0.23	4.17	Shear head	P
	SJB-3	0.48	5	SSR	S[2]		6CS	0.24	4	Stirrups	P
	SJB-4	0.43	6.4	SSR	S[2]		7CS	0.24	3.7	Stirrups	P
	SJB-5	0.47	7.6	SSR	S[1]		8CS	0.27	5	Stirrups	P
	SJB-8	0.46	5.7	SSR	S[2]	Robertson et al., 2002	2CS	0.16	4.5	Closed hoop	F
	SJB-9	0.49	7.1	SSR	S[2]		4HS	0.15	5	Headed stud	F
Dilger and Cao, 1991	CD3	0.91	3.5	SSR	NA		3SL	0.1	4.5	Single leg	F
	CD4	0.62	4.8	SSR	NA	Megally and Ghali, 2000	MG-10	0.6	5.2	SSR	NA
	CD6	0.64	5.4	SSR	NA		MG-3	0.56	5.4	SSR	NA
	CD7	0.51	5.6	SSR	NA		MG-4	0.86	4.6	SSR	F-P
Elgabry and Ghali, 1987	2	0.47	NA	SSR	P		MG-5	0.31	6.5	SSR	F-P
	3	0.87	NA	SSR	P		MG-6	0.59	6	SSR	F-P
	4	0.85	NA	SSR	P	Robertson and Durrani, 1990	4s	0.19	3.5	Closed hoop	F
	5	1.2	NA	SSR	P						
Hawkins et all., 1975	SS1	0.49	3.5	Stirrups	C[3]						
	SS2	0.47	3.43	Stirrups	P						
	SS3	0.48	4.1	Stirrups	F						
	SS4	0.47	5.5	Stirrups	NA						
	SS5	0.42	4.9	Stirrups	F						

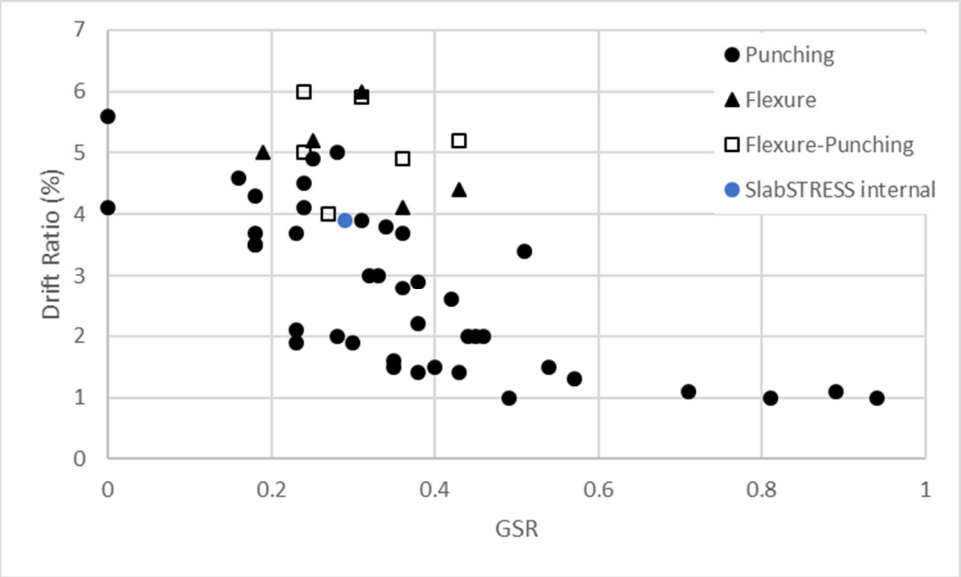

Figure 9.27 Database for interior connections specimen no shear reinforcement, Ramos et al., 2017 [8].

Table 9.7 Ramos et al., 2017 [8] test data for interior connection without shear reinforcement.

Author	ID	GSR (ACI 318)	$d_{r,u}$ (%)	Failure Mode	Author	ID	GSR (ACI 318)	$d_{r,u}$ (%)	Failure Mode
Hawkins et al., 1974	S-1	0.34	3.8	P	Emam et al., 1997	HHHC0.5	0.25	5.2	F
	S-2	0.45	2	P		HHHC1.0	0.25	4.9	P
	S-3	0.44	2	P		NHHC0.5	0.36	3.7	P
	S-4	0.42	2.6	P		NHHC1.0	0.36	2.8	P
Islam and Park, 1976	3C	0.24	4.1	P	Marzouk et al., 2001	HSLW0.5C	0.31	6	F
Symonds et al., 1976	S-6	0.89	1.1	P		HSLW1.0C	0.31	5.9	FP
	S-7	0.81	1	P		NSLW0.5C	0.43	4.4	F
Zee and Moehle, 1984	INT	0.31	3.9	P		NSLW1.0C	0.43	5.2	FP
Pan and Moehle, 1989, 1992	AP1	0.35	1.6	P		NSNW0.5C	0.36	4.1	F
	AP2	0.35	1.5	P		NSNW1.0C	0.36	4.9	FP
	AP3	0.18	3.7	P	Brown and Dilger, 2003	SJB-7	0.51	3.4	P
	AP4	0.18	3.5	P	Stark et al., 2005	C-02	0.38	2.9	P
Robertson, 1990	8I	0.18	4.3	P		C-63	0.38	2.2	P
	2C	0.19	5	F	Robertson and Jonson, 2006	ND1C	0.24	6	FP
	3SE	0.16	4.6	P		ND4LL	0.27	4	FP
	5SO	0.18	3.5	P		ND5XL	0.46	2	P
	6LL	0.54	1.5	P		ND6HR	0.28	5	P
	7L	0.38	1.4	P		ND7LR	0.24	5	FP
Wey and Durrani, 1992	SC0	0.24	4.5	P	Kang and Wallace, 2008	C0	0.3	1.9	P
Cao and Dilger, 1993	CD-1	0.94	1	P	Tian et al., 2008	L0.5	0.23	2.1	P
	CD-5	0.71	1.1	P	Song et al., 2012	RC1	0.43	1.4	P
	CD-8	0.57	1.3	P	Inacio et al., 2015	CHSC2	0.32	3	P
Farhey et al., 1993	1	0	5.6	P		CHSC3	0.33	3	P
	2	0	4.1	P	Almeida et al., 2016	C-50	0.49	1	P
	3	0.23	3.7	P		C-40	0.4	1.5	P
	4	0.23	1.9	P		C-30	0.28	2	P
Robertson et al., 2002	1C	0.15	3.5	P	SlabSTRESS Cyc-2	B2	0.29	3.9	P

The analysis of Figure 9.25 and Figure 9.27 and Table 9.5 and Table 9.7 shows that the values of gravity shear ratio in relation to the ultimate drift capacity of SlabSTRESS fall well into the literature data. The failure mode also reflects the database works well. It is important to note that the data collected during the SlabSTRESS experimental campaign were obtained by testing an entire, full-scale flat-slab building, whereas all the others in the literature were acquired by testing an isolated internal slab-column connection.

9.4.2 Failure in function of the Connections typology

First Punching

The comparison between the specimen plans is shown in Figure 9.28 and the summary of the main geometrical characteristics is reported in Table 9.2. Three tests have overhangs on two side of the slab.

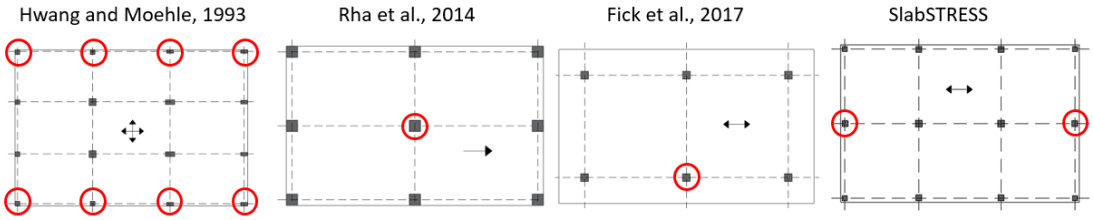

Figure 9.28 First connection to reach failure.

Despite the differences in scale and in the boundary conditions, the gravity shear ratio of the internal connections of all the analysed experiments are around the same value between 0.25 and 0.44.
Amongst all the analysed works on cyclic tests, the first connection to fail in two of them (Hwang and Moehle, 1993 [1] and SlabSTRESS was on the edge of the floor; in the other two (Rha et al., 204 [2] and Fick et al., 2017 [3]) it was the internal typology. The edges are the first to punch for common floor configurations.

Table 9.8 First connection punched.

Authors	Connection typology	GSR (authors)		GSR (calculated)	Maximum drift ratio (%)	Drift ratio at punching (%)	Connection punched
Hwang & Moehle, 1993 [1]	Internal	0.30		0.32	4	3.1÷3.7	Lateral
	Lateral	-		0.27			
	Corner	-		0.20			
Rha et al., 2014 [2]	Internal	0.44		0.41	6	Cyclic:1.5	Internal
	Lateral	0.28		0.24			
Fick et al., 2017 [3]	Internal	0.21		0.25	2.9	Roof drift ratio:2.9 Storey drift ratio:3.3	2nd floor, Internal
	Lateral	-		0.16			
Moehle and Diebold, 1984 [4]	Internal	-		0.25	5	-	(Internal)
Kang and Wallace, 2004 [5]	Internal	0.25		0.28	2.5-3	3.12	Internal
	Lateral	0.20		0.19			
SlabSTRESS	Internal	1st floor	2nd floor	-	6	Roof drift ratio:1.4 Storey drift ratio:1.5	1st floor, Lateral
		0.29	0.32				
	Lateral	0.20, 0.12	0.22				
	Corner	0.10	0.19				

SlabSTRESS is in agreement with Hwang and Moehle, 1993 [1] in the sequence of failures starting from the edges connections and moving through the interior of the slab. The results of Rha et al., 2014 [2] and Fick et al., 2017 [3] are considered to be related to the test configurations. Only one internal connection in Rha et al., 2014 [2] with higher gravity shear ratio, connections without edges in Fick et al., 2017 [3].

EDGE CONNECTIONS DAMAGE

The typical damage of edge connections is compared as follows. Hwang and Moehle, 1993 [1] (Figure 9.29), Rha et al., 2014 [2] (Figure 9.30) and SlabSTRESS (Figure 9.31) have reported the same edge and corner damage.

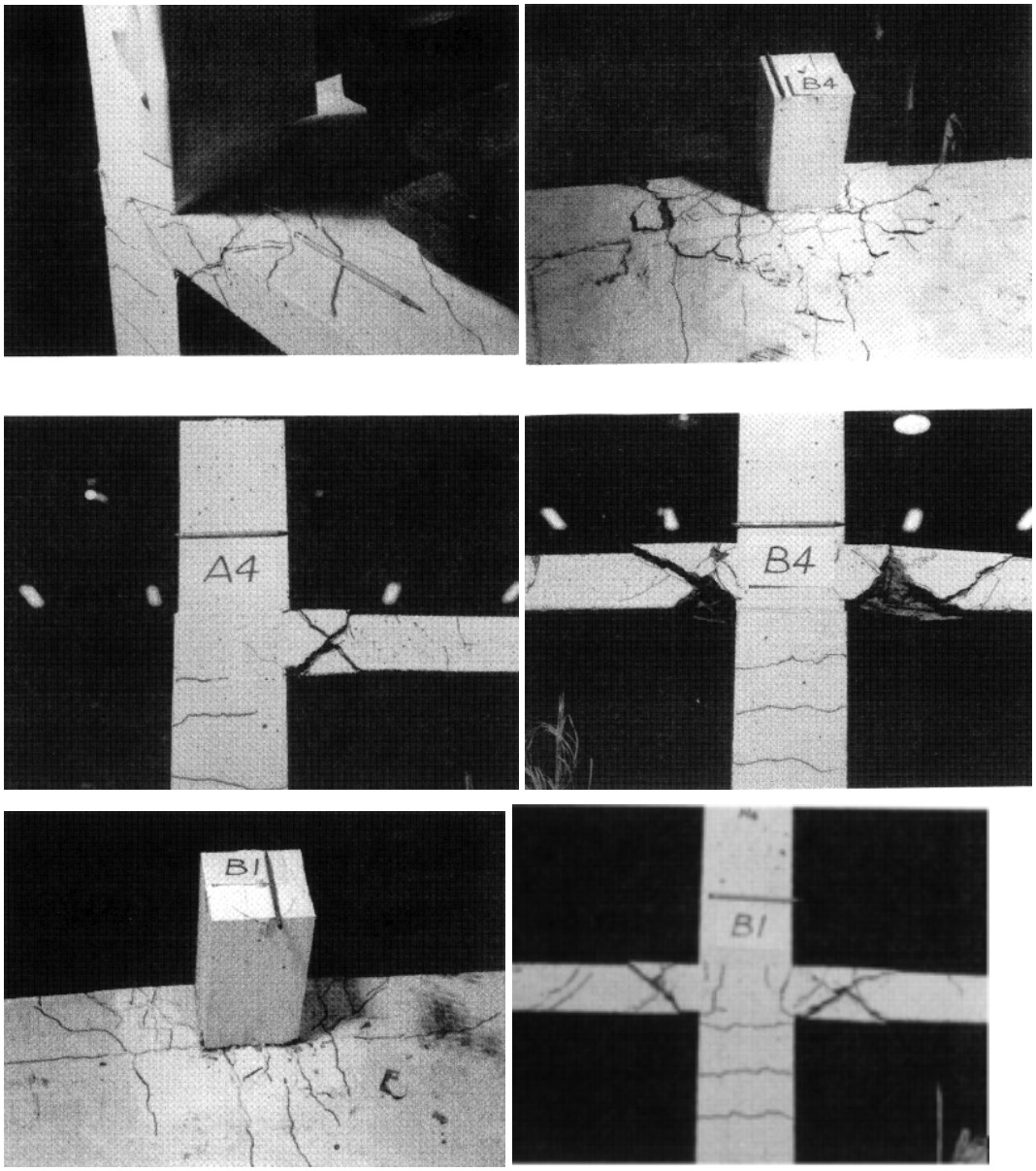

Figure 9.29 Hwang and Moehle, 1993 [1] connections damage.

Figure 9.30 Lateral crack in Rha et al., 2014[2].

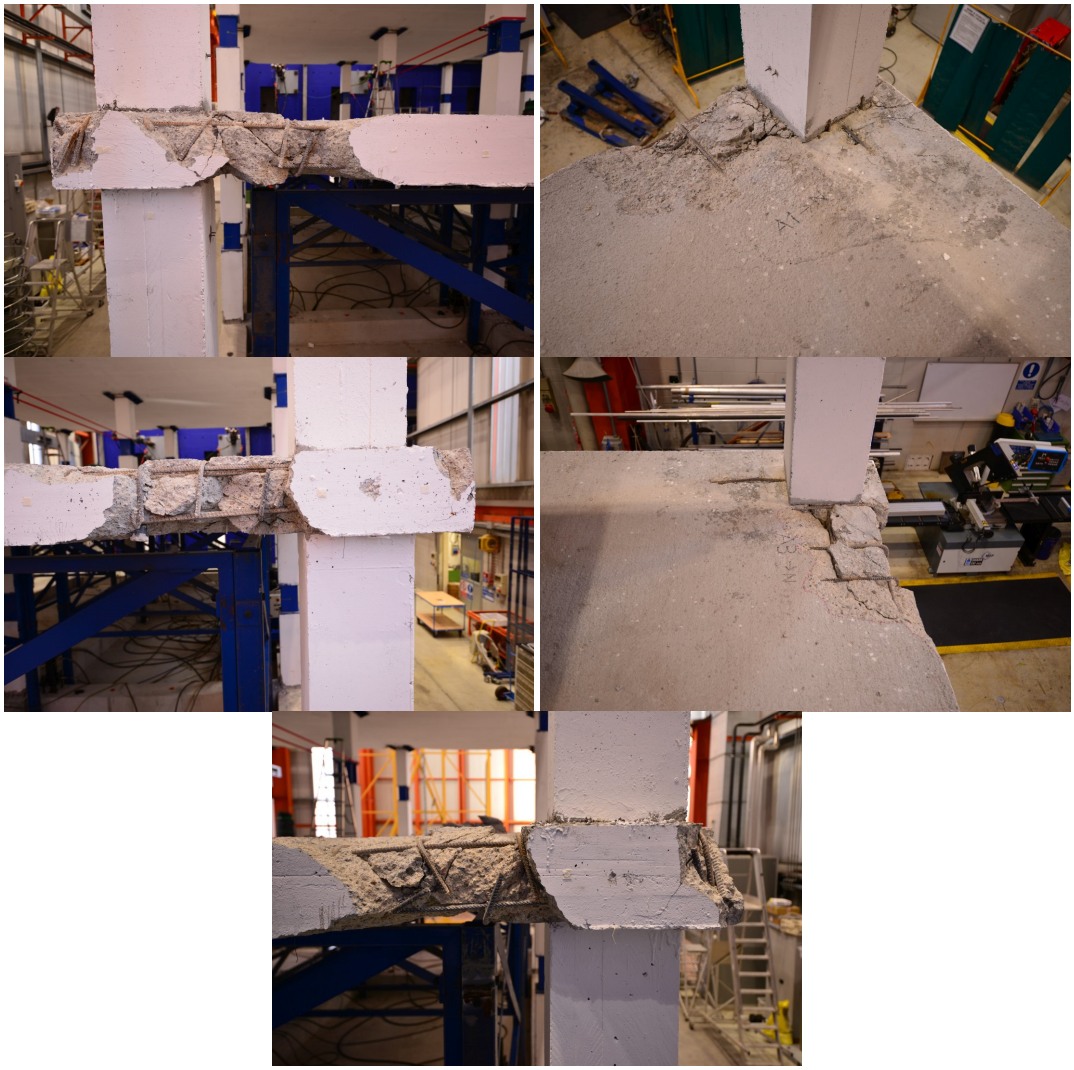

Figure 9.31 SlabSTRESS 1st floor slab damage, corner connection (clockwise) a) and b) A1 west, c) and d) A3 west, e) D1 east.

Different behaviours were observed depending on the loading typology, biaxial (Hwang and Moehle, 1993 [1]) or uniaxial (SlabSTRESS). In the latter the level of damage in the edge and corner connections differed if they were on the side of structure perpendicular or parallel to the loading application. Comparing Figure 9.31

with Figure 9.33 and from Table 8.11, it is possible to see that the lateral connections in the side parallel to the loading applications reported flexural cracks of limited entity.
All the connections on the short side of the structure, on both floors, reached failure with a mid-low displacement ductility factor (Table 8.11) for a residual load of 85% of the maximum unbalanced moment. For the 1st floor, in the alignment A, west side, the maximum value was reached from the corner connection A1, whereas in the east side from the edge connection D2. On the 2nd floor the maximum values were reached from the corner A1 in west side and the corner D1 in the east side.

Table 9.9 Displacement ductility factor (adim.) for the failed connections, SlabSTRESS.

1st Floor	A	B	C	D	2nd Floor	A	B	C	D
1	4.11	-	-	2.53	1	2.87	-	-	3.18
2	2.13	2.60	-	2.55	2	2.56	-	-	1.69
3	2.57	-	-	2.47-	3	2.48	-	-	2.85

LEGEND: (-) connections that do not reach failure

In Hwang and Moehle, 1993 [1] it is possible to observe the same response as for SlabSTRESS. Even if the loading was applied in a bidirectional manner, the same behaviour would have been expected on both sides of the structure. On the contrary, one of the two long side, the North one, of Hwang and Moehle, 1993 [1]reported a lower level of damage. This was probably due to the percentage of the reinforcement (see section 9.4.5).

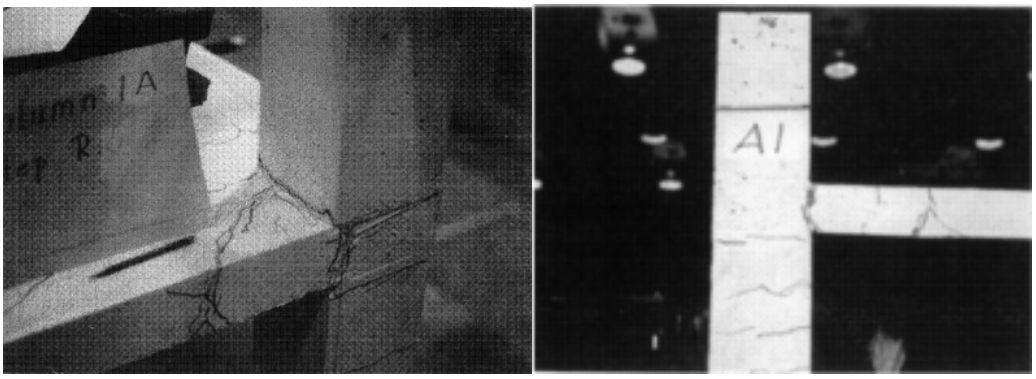

Figure 9.32 Hwang and Moehle, 1993 [1] connections damage.

Figure 9.33 SlabSTRESS 1st floor slab damage, edge parallel to lateral load direction, connection a) B1 north, b) B3 and c) C3.

It can be concluded that SlabSTRESS shared the same type of damage on edge connections, though with more severe cracking influenced by the detail of the reinforcement. This type of damage shows both with uniaxial loading perpendicular to the edge and biaxial loading. If the loading is parallel to the edge, the damage is much lower. The SlabSTRESS result is confirmed by ductility calculations as well.

PUNCHING OF INTERIOR CONNECTIONS

Amongst all the tests in which the punching was verified in the internal connection typology (Table 9.8), the two that tested a real-scale, multi-floor, flat-slab building, Fick et al., 2017 [3] and SlabSTRESS, recorded the punching for a similar value of inter-storey drift ratio, 3.3% and 4.1% respectively, even with different geometric characteristics (Table 9.2).

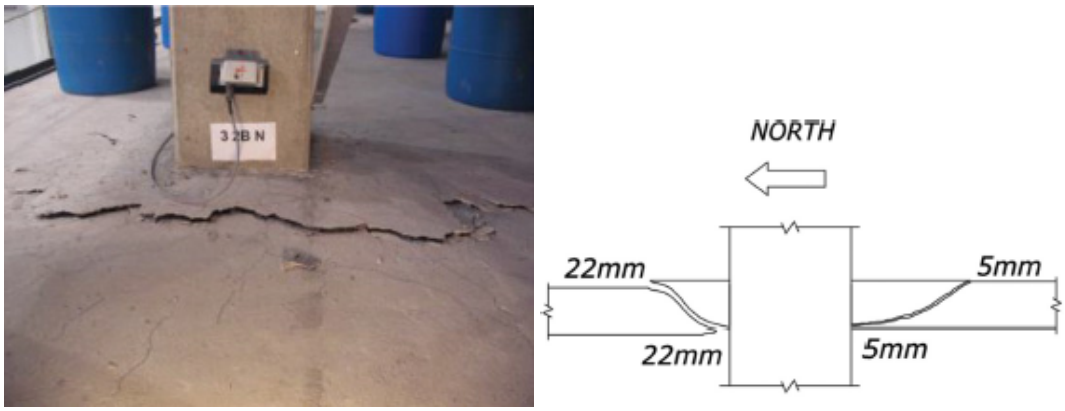

Figure 9.34 Punching in the central connection, Fick et al., 2017 .

In Fick et al., 2017 [3] the larger moment was verified in the 2nd floor connection and the punching occurred here. The test was stopped after this punching so the response of the structure after with the ensuring redistribution of load effects was not investigates.
Rha et al., 2014 [2] and SlabSTRESS reached the same maximum value of inter-storey

drift ratio of 6%. These are two different types of experiments, the first one on a single flat-slab floor, the second one on a multi-floor flat-slab building with shear reinforcement on the 2nd floor and one internal strengthened connection.

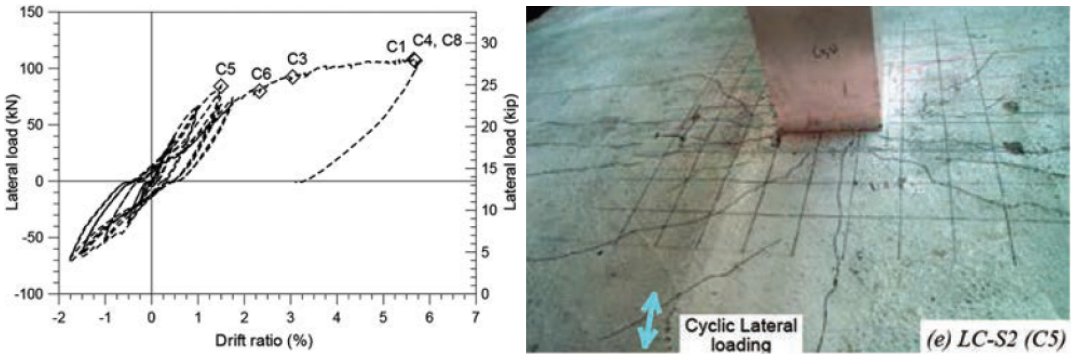

Figure 9.35 Punching in Rha et al., 2014 .

After the first punching in the internal connection, C5 (Figure 9.35) for an inter-storey drift ratio of 1.5% the failure propagated in the connections on the two sides perpendicular to the loading application (C6, C3, C1, C4) and finally in the connection on the side parallel to the loading application (C8) (Figure 9.35). The interior connection punched first, probably due to the different value of the gravity shear ratio (see chapter 2).

A different test typology and specimen geometry (see Table 2.1) was developed by Moehle and Diebold, 1984 [4], with a primary system design. At the end of the test the authors observed a small drop of the slab around an interior column, indicating the possibility of incipient punching failure for a gravity shear ratio and a maximum inter-storey drift ratio of 0.25 and 5%. The drift capacity is comparable to though higher than those of Fick et al., 2017 [3] and SlabSTRESS, the design as a primary slab frame can be the cause of the difference.

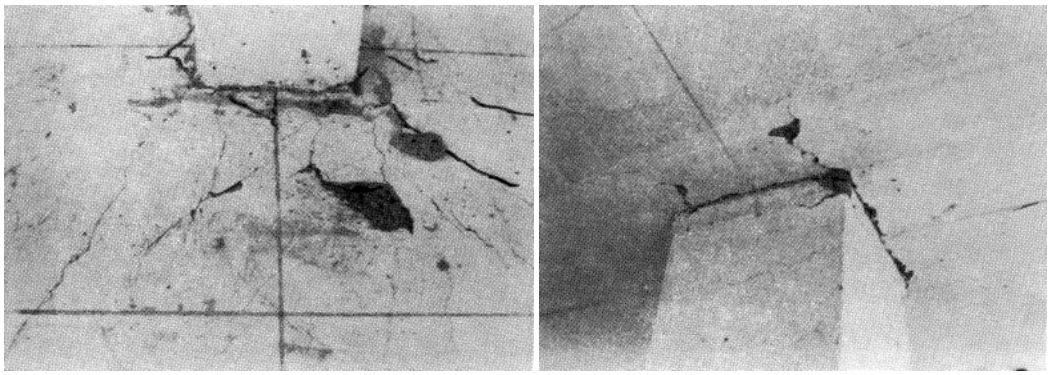

Figure 9.36 Moehle and Diebold, 1984 [4] punching failure in the 1st floor slab-column connection, view from a) top and b) bottom.

The SlabSTRESS internal punching occurred in the internal connections for an inter-storey drift ratio of 4.1%. In addition, the buckling of the longitudinal compressed

reinforcement was observed on the east side of the punched connection B2 near the column (Figure 9.37).

Figure 9.37 SlabSTRESS B2 connection east-west direction after the removal of damaged concrete pieces.

Summing up, all tests show that interior connection punching is a decisive phenomenon leading to severe consequences for the local and global response. The drift ratios where these phenomena occur are scattered in a range 3-6%, for the typical gravity shear ratios 0.25-0.3. Thus the global response can reach these rather high nonlinear deformation levels. The best performance is obtained in a primary system design.

SYNTHESIS OF SLABSTRESS CONNECTIONS FAILURE SEQUENCE

In SlabSTRESS (Figure 9.38) the connections on the side perpendicular to the loading application (alignments A and D) failed first for a lower inter-storey drift value and a progressive manner. The internal connection punching failure occurred for higher (nearly double) drift. This sequence of failures is confirmed by tests with similar configuration and biaxial loading as well. The level of drift of internal connection punching is comparable to those obtained in other floor and frame tests with similar gravity shear ratios.

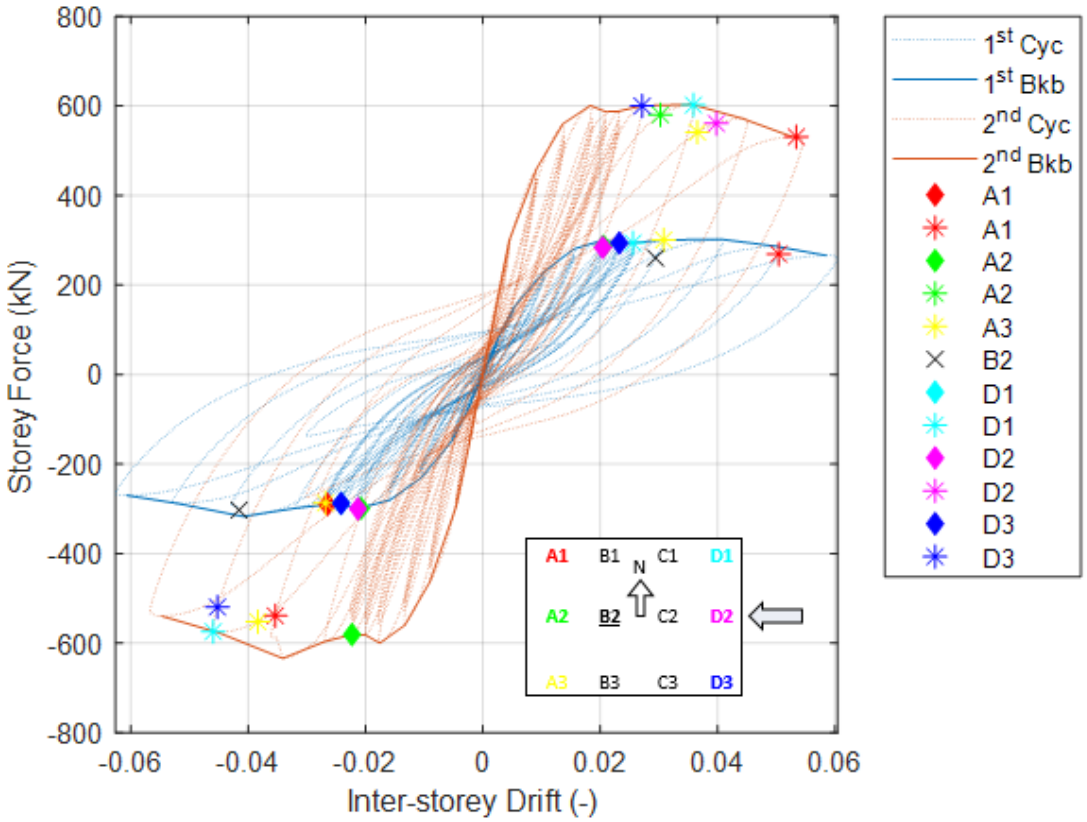

Figure 9.38 Global behaviour with local failure, blue line, 1st floor, red line, 2nd floor diamond for the test Cyc-1, asterisk for the test Cyc-2, cross for the punching.

9.4.3 INTEGRITY REINFORCEMENT

In Fick et al., 2017 [3] the bottom reinforcement was placed in correspondence to the columns and the support line. In Hwang and Moehle, 1993 [1] the bottom reinforcement was continuous in correspondence to the columns. In addition, integrity reinforcement bars were added at some points. Kang and Wallace, 2004 [5] considered two bars in each direction.
In SlabSTRESS two bottom longitudinal bars were placed, passing through the column in each direction at each connection, following the EC2 [9]. The specimen reached punching of one edge (D2) and one internal connection (B2), with severe damage on all connections on lines A and D on the 1st floor without any sudden and tragic collapse. This behaviour shows the efficiency of the integrity reinforcement.
In SlabSTRESS and in all the tests reported, the slab did not collapse. From the experimental point of view these results suggest that the collapse of the slab can be avoided provided that adequate integrity reinforcement.

9.4.4 SHEAR REINFORCEMENT

In SlabSTRESS the punching shear reinforcement with headed studs was only placed

the 2nd floor. This choice was made to test the performance of slab-column connections of different configurations (internal, edge and corner) when punching shear reinforcement is used in a flat-slab with realistic thickness.

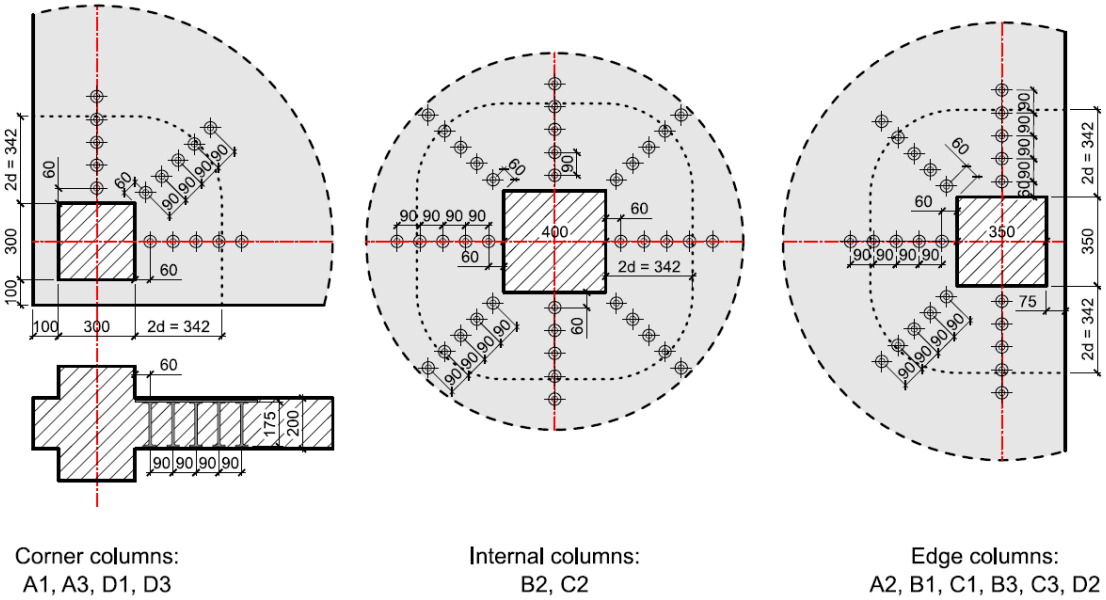

Figure 9.39 SlabSTRESS layout of shear reinforcement at slab-column connections at the 2nd floor.

Among all the analysed tests on single flat-slab floor and multi-floor flat-slab buildings, Kang and Wallace, 2004 [5] is the only one study using shear reinforcement. A shake table test was performed on a 30% scaled mock-up with shear reinforcement consisting of stud-rails. This shear reinforcement was placed in cross layout spaced at 0.5d = 35mm, extending 4d from the column face to prevent failure outside the shear reinforced zone.

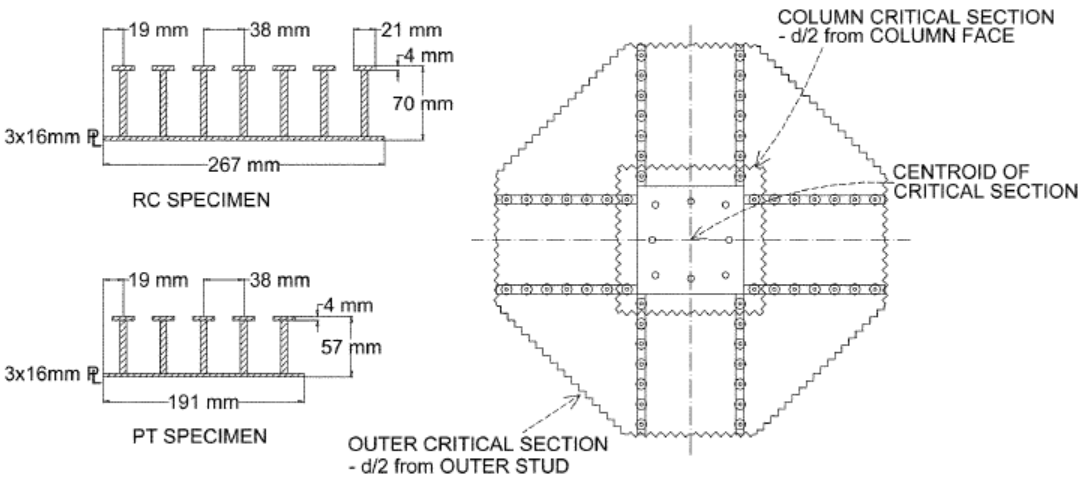

Figure 9.40 Kang and Wallace., 2004 [5] stud-rails disposition into the connection.

After the tests it was concluded that the use of shear reinforcement reduced the extent of damage, preventing the slab "dropping" (Figure 9.41 b) observed in specimens where shear reinforcement was not provided (Figure 9.41 c).

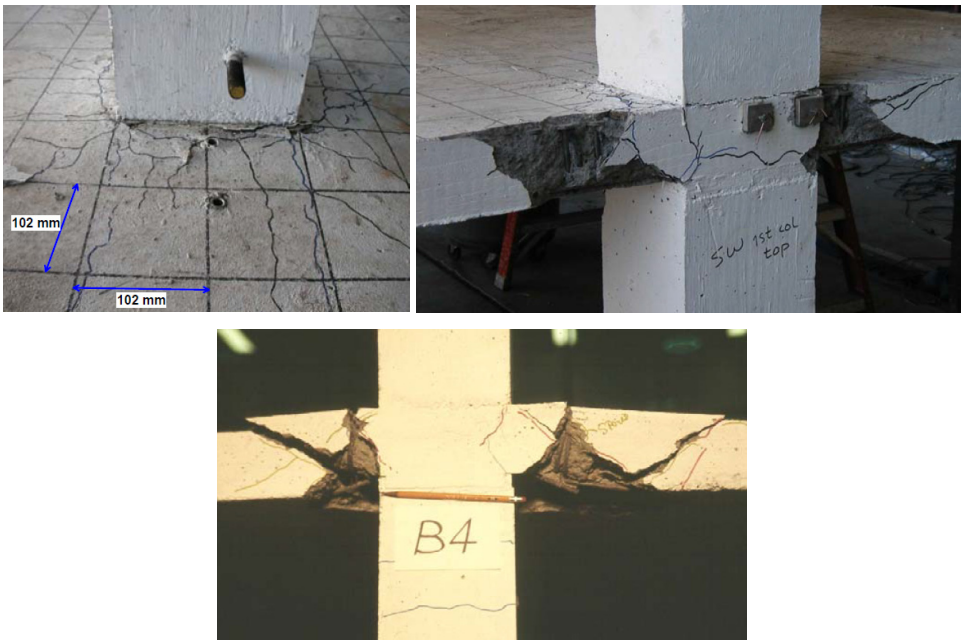

Figure 9.41 Slab damage a) and b) with shear reinforcement, Kang and Wallace, 2004 [5] c) without shear reinforcement, Hwang and Moehle, 1993 [1].

A similar response was observed when analysing cracking in the SlabSTRESS specimen. The failures of edge connections on lines A and D occurred earlier in test Cyc-1 in the slab-column connections on the 1st floor than in the 2nd floor (Figure 9.42 a and b respectively), and the interior connection punching occurred on the 1st floor.

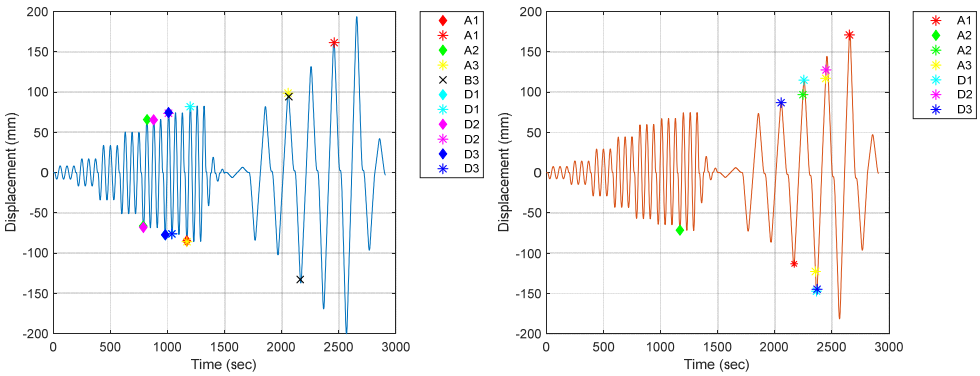

Figure 9.42 Time history of the displacements with local failure, diamond for the test Cyc-1, asterisk for the test Cyc-2, cross for the punching, a) 1st floor, b) 2nd floor.

The use of shear reinforcement reduced the intensity of damage, preventing the slab punching (Figure 9.43) and dropping (Figure 9.44 a) observed in specimens without shear reinforcement.

Figure 9.43 B2 connection a) 1st floor, b) 2nd floor.

Figure 9.44 A2 connection a) 1st floor, b) 2nd floor.

Although there were differences between the two tests (see Table 9.2), the recorded damage was similar. The internal connections of both test with shear reinforcement (Figure 9.41 a for Kang and Wallace, 2004 [5] and Figure 9.43 b for SlabSTRESS) showed cracking that extended from the column section without any punching. Similarly, in the edge connections, the presence of shear reinforcement contributed to decreasing the spread of cracking and prevented the slab from partly dropping. Only some cover spalling was reported (Figure 9.41 b for Kang and Wallace, 2004 [5] and Figure 9.44 b for SlabSTRESS).

9.4.5 DIFFERENT LONGITUDINAL REINFORCEMENT LAYOUT

In SlabSTRESS two different longitudinal reinforcement layouts, smeared and concentrated, were arranged on the east and west sides of both floors (Figure 7.11 and Chapter 3 for more details). This choice was dictated with the aim to achieve results varying this parameter from the experimental campaign conducted at the JRC ELSA laboratory.

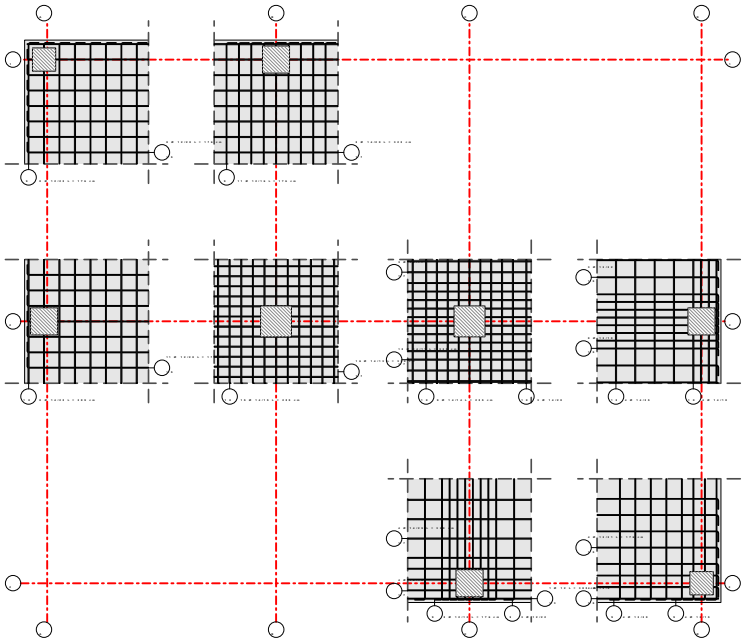

Figure 9.45 Longitudinal reinforcement, smeared in A and B and concentrated in C and D, SlabSTRESS.

From the analysis of literature works regarding flat-slab floors and frames, only Hwang and Moehle, 1993 [1] and Rha et al., 2014 [2] analysed different reinforcement ratios in their experiments. Differently from SlabSTRESS they did not consider a different layout of the reinforcement (concentrated and smeared) but rather a different amount of slab reinforcement.
Rha et al., 2014 [2] used three specimens and varied the bottom slab reinforcement, but the cyclic test was performed with only one reinforcement layout (Table 9.10).
Hwang and Moehle, 1993 [1] divided the floor slab into two halves symmetrically about a centreline in the long direction. In the south of the centreline the reinforcement satisfied the design requirement of ACI 318-83, whereas in the north the reinforcement was controlled by requirements for maximum spacing.

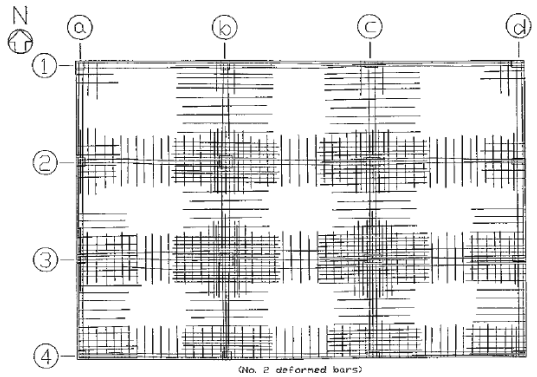

Figure 9.46 Tops steel layout, Hwang and Moehle, 1993 [1].

From the analysis of the photographs (Figure 9.29 and section "Edge connections damage"), it can be seen that the higher top reinforcement on the South side of the structure, causes a high level of damage.

Table 9.10 Rha et al., 2014 [2] test variables.

Name	Top (column strip)		Bottom	Load type
	Longitudinal, mm	Transverse, mm	Each way, mm	
G-S1	D10 at 150	D10 at 300	D10 at 300	Gravity
G-S2	D10 at 100	D10 at 150	D10 at 300	Gravity
LM-S2	D10 at 100	D10 at 150	D10 at 300	Monotonic
LM-S3	D10 at 100	D10 at 150	D10 at 300+3D 10	Monotonic
LC-S2	D10 at 100	D10 at 150	D10 at 300	Cyclic (+)
				Cyclic (-)

SlabSTRESS is the only experiment on a flat slab multi-storey frame that considered two different longitudinal reinforcement layouts, smeared and concentrated, for the same total quantity of top reinforcement. The most significant difference between the two halves of the slabs was in the failure typology. In A2, located in the half of the slab with the smeared layout, the failure occurred on the edge; the East side cracking was a crack at the column face (Chapter 7). With the concentrated layout, a punching failure occurred in D2, with the typical cone around the column (Chapter 7). In the other connections typologies, the failure (Figure 9.47) occurred independently from the reinforcement distribution, first on the central edges (A2, D2) and then in the corners (A1, A3, D1, D3). This confirmed Hwang and Moehle, 1993 [1] observation that a higher top reinforcement causes a high level of damage in the edge slab-column connection typologies.

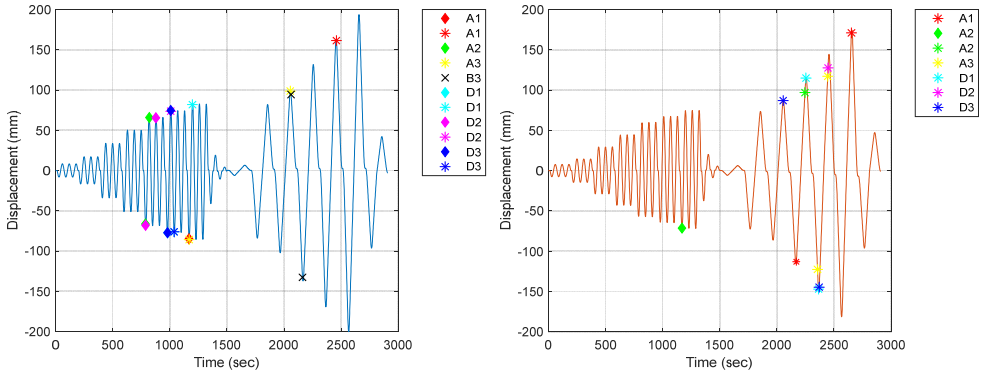

Figure 9.47 SlabSTRESS time history of the displacements with local failure, diamond for the test Cyc-1, asterisk for the test Cyc-2, cross for the punching, a) 1st floor, b) 2nd floor.

Similarly, it was not possible to observe a general behaviour of the connections in the two halves of the floor slab regarding the maximum value of unbalanced moment bear, the dissipated energy and the ductility factor (Chapter 8 for more details).

9.4.6 STRENGTHENING

SlabSTRESS was the first experiment in which some slab-column connections in a real scale flat slab frames were strengthened after a previous cyclic test had reached a global drift ratio of around 40% of the final value.

Among all the different flat slab strengthening techniques (Lapi et al., 2019 [10]) post-installed bolts were chosen to strengthen three slab-column connections. Also in the study of strengthening, all the literature works mainly regard isolated slab column connections strengthening; no experiments have previously been made on a full-scale multi-storey specimen with also the possibility to strengthen connections of different typologies.

During the test Cyc-1 slab-column connections were severely damaged on the A and D alignments on the 1st floor without transversal reinforcement, and could not be repaired. So, before the cyclic test Cyc-2, some of the slab-column connections along lines B and C were strengthened improving the punching-shear resistance. The strengthening was composed of post-installed bolts. It is important to note that the added load was changed before beginning the Cyc-2 test (see Chapters 3 and 8 for more details).

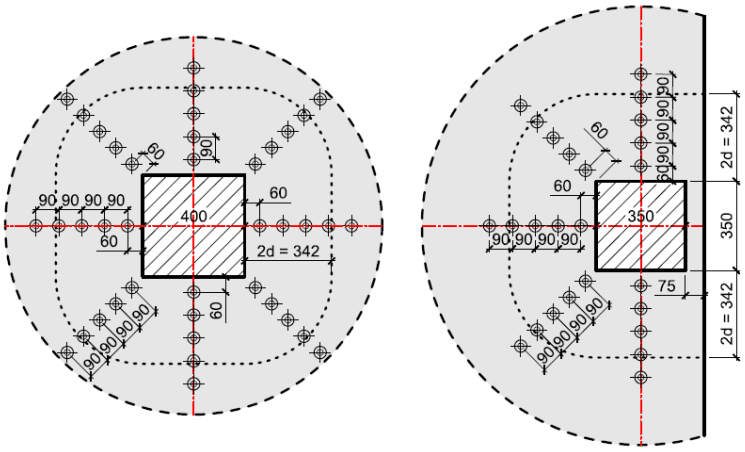

Figure 9.48 SlabSTRESS layout of strengthened connections at the 1st floor, a) C2, b) B1 and C3.

This operation represents a realistic scenario, in which retrofitting is carried out in earthquake damaged connections of a real-scale multi-floor building after a major seismic event.

A testing campaign with the same strengthening system in connections tested for concentric punching is reported for comparison. Almeida et al., 2019 [11] carried out experimental work on reinforced concrete flat-slab specimens with post-installed bolts as punching shear reinforcement. They tested two specimens with different steel bolt radial and cross placement geometries (Figure 9.49). The shear reinforcement was done with post-installed 8.8 class M10 steel bolts, inserted in 12 mm drilled vertical holes.

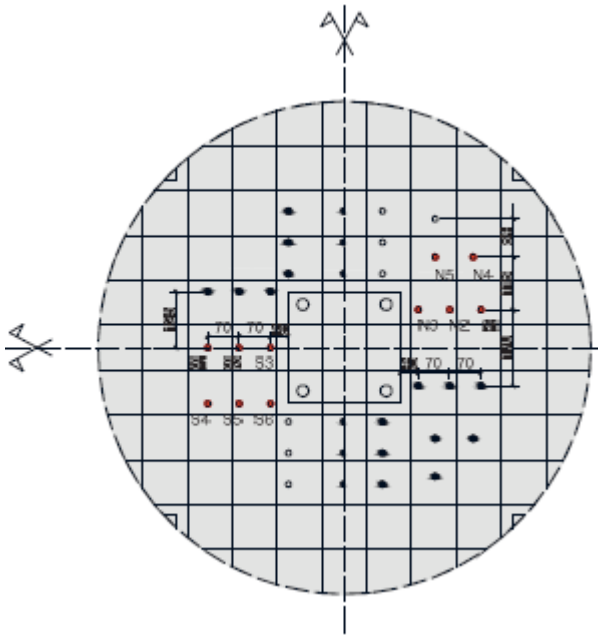

Figure 9.49 Post-installed shear reinforcement, Almeida et al., 2019 [11].

They observed that the post-installed steel bolts demonstrated to be an efficient solution for strengthening existing structures, improving the structural behaviour and the punching resistance.
Figure 9.50 reports the saw cuts of specimen a) without the shear reinforcement and with the shear reinforcement with b) radial and C) cross disposition. The typical punching failure formed in absence of the shear reinforcement.

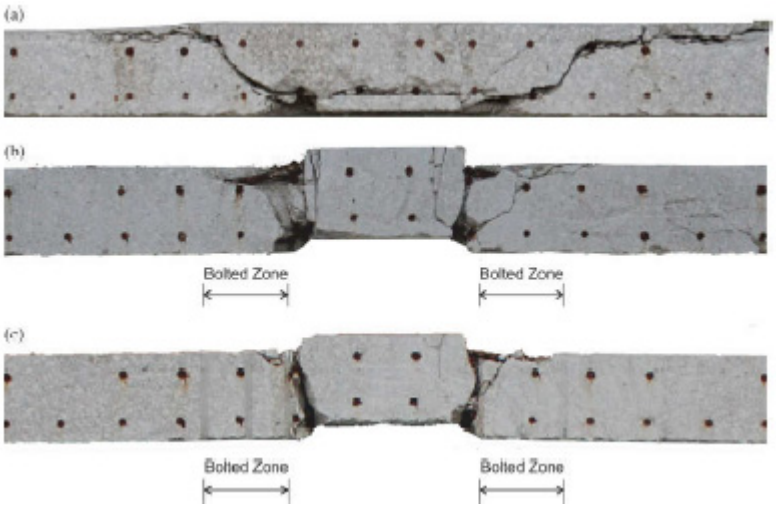

Figure 9.50 Saw cuts of the specimens a) without shear reinforcement, b) with radial and c) cross disposition of the post-installed steel bolts, Almeida et al., 2019 [11].

Similarly to observations by Almeida et al., 2019 [11], also in SlabSTRESS the connections without shear reinforcement (**Error! Reference source not found.** a)

reported greater damage compared to the connections with shear reinforcement. Similarly, in SlabSTRESS the strengthening avoided punching failure for combined gravity and lateral loading. As it is possible to see from Figure 9.51 a brittle punching occurred in the internal connection B2 (Figure 9.51 a) while the similar connection C2 was strengthened (Figure 9.51 b) and resisted to the end of the test without failure.

Figure 9.51 SlabSTRESS internal connections a) B2 un-strengthened and b) C2 strengthened.

Almeida et al., 2019 [11] also observed that the use of steel bolts as shear reinforcement provided higher drift capacity, higher maximum horizontal load, higher ductility and higher energy dissipation capacity.

Table 9.11 SlabSTRESS unbalanced moment and energy dissipation comparison.

	Connection	Drift (-)	Unbalanced moment (kNmm)	Dissipated energy (kJ)
Strengthened	B1	0.05	224.37	27.79
	C2	0.041	375.49	51.16
	C3	0.06	215.37	33.49
Un-strengthened	B3	0.05	184.15	31.10
	B2	0.031	345.03	45.58
	C1	0.041	216.66	34.24

In the analysis of drift capacity, the maximum unbalanced moment and the dissipated energy for the strengthened and un-strengthened connections in SlabSTRESS, it can be seen that the strengthened connections (B1, C2 and C3 in Table 9.11) reached higher values than the corresponding un-strengthened connections (B3, C1 and B2 in Table 9.11).

9.4.7 Measurement of Local Kinematic and Static Parameters

The measurement of the local forces in literature works on flat-slab floors or buildings has not always allowed the static and the kinematic behaviour of each slab-column connection to be obtained. As reported in Table 9.12, measurement of the local rotation is not widespread.

Table 9.12 Instrumentation.

Author	Measurements global	Local forces	Local deformations
Hwang & Moehle, 1993 [1]	Force-displacement	Column base forces (3 components). Slab moment transfer slab vertical deflections. Slab column rotations	Slab reinforcement (slab moment transfer)
Rha et al., 2014 [2]	Force-displacement	Column base vertical reaction and top lateral force	-
Fick et al., 2017 [3]	Force-displacement at three levels	-	-
Moehle and Diebold, 1984 [4]	Floor displacements, horizontal and vertical accelerations	Shear and moment below footings	Column and slab average deformations (near to connections) reinforcement strain.
Kang and Wallace, 2004 [5]	Floor and footing displacements and accelerations	Column and slab moment-curvature	Column and slab average deformations. Transverse reinforcement strains.
SlabSTRESS	Force-displacement at two levels	Shear force, axial force, bending moment in each column. Column and slab rotation.	Slab crack opening

SlabSTRESS together with Hwang and Moehle, 1993 [1]are the only two experimental studies on flat-plate frames in which both the global and the local measurements were acquired during the tests. The SlabSTRESS experimental campaign was the first in which the response of each slab-column connection was presented using both the inter-storey drift ratio and the column-slab rotation purposely calculated (see Chapter 5 for a more detailed explanation of the procedure followed).
Drakatos et al., 2016 [12] proposed a formula (Eq. 9-1) to calculate the slab-column connection rotation in which the rotation readings at the middle of the top surface of the slab (ψ_{col}) were subtracted from the mean of the measured slab rotation (ψ_{max} , ψ_{min}).

$$\psi_{SCC} = \frac{\psi_{max} - \psi_{min}}{2} - \psi_{col} \qquad \text{Eq. 9-1}$$

In the SlabSTRESS methodology, the slab rotation was considered as the mean of the inclinometer reading in only one direction (east-west) and the column rotation is exactly the reading of the sensor. In the SlabSTRESS test set -up the inclinometers were located in the slab all around the column and those on the column were both

on the top and bottom ends (Eq. 9-2).

$$Column - Slab\ Rotation\ = \frac{Above\ slab + Below\ slab}{2} - \frac{(NS) + (EW)}{2} \quad \text{Eq. 9-2}$$

This methodology allows studies into stiffness deterioration, ductility and energy dissipation as a function of the rotation, a parameter that exactly describe the local behaviour of each slab-column connection (for a more details, see Chapter 8). When the methodology presented here was used for the data analysis, it was also possible to put in relation the inter-storey drift ratio with the rotation, showing that this value depends on the slab-column connection typology and if the storey is a halfway floor or a top one. The main difference between the two floors consists in the presence of the columns that are above and below the slab on the 1st floor, but they are whole only below the slab on the 2nd floor. So using the inter-storey drift ratio the behaviour of the 1st floor is well described but it is not verified for the 2nd floor, for which it was observed that the rotation gives a better representation of the behaviour of each slab-column connection.

Hwang and Moehle, 1993 [1] used dial gages and clip gages to measure the deflections and rotations of the test slab. The instruments were attached to an over slab grid, which was made of steel angle sections supported by threaded rods anchored at the top of the column stubs.

The slab-column rotations were calculated as the measured vertical displacements, which were caused by the rigid rotation of column top stubs, divided by the associated level arms. They also calculated the ratio between the rotation and the inter-storey drift for each slab-column connection and each experiment.

Lastly, also Moehle and Diebold, 1984 [14] treated the rotation. They used direct current differential transformers to measure deformations of the footings and of columns and slabs near slab-column and column-footing connections and they derived the moment-rotation of the columns from the calculated moment-curvature relations with an analytical model.

Neither of the researches included an analysis on the relations between the local rotation and the inter-storey drift ratio.

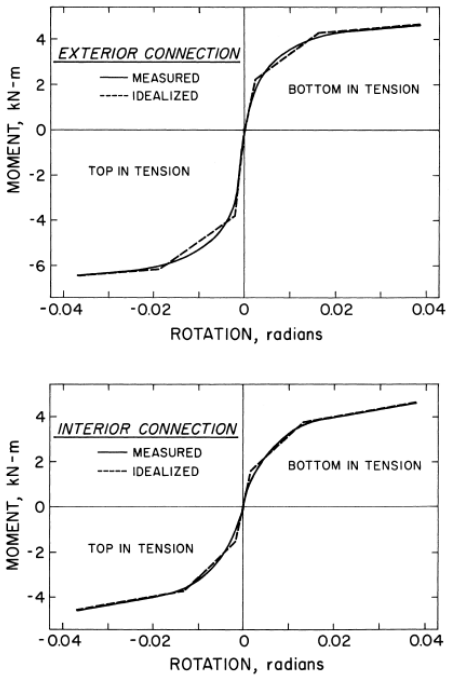

Figure 9.52 Moehle and Diebold, 1984 [4] derived moment-rotation.

Neither of the researches included an analysis on the relations between the local rotation and the inter-storey drift ratio.

ACQUISITION OF INTERNAL FORCES

SlabSTRESS was the first experiment on a two storey flat-plate frame in which the columns' internal forces (shear force, axial force and bending moment) were measured, on both floors, with a system designed *ad hoc* (Figure 9.53). The collected data was acquired with very accurate sensors that guarantee the validity of the results.

Figure 9.53 Load cell in SlabSTRESS.

Hwang and Moehle, 1993 [1] acquired the column shears and the axial loads in three orthogonal directions but only at the base of the columns using reaction transducers. The reaction transducer is a tripod consisting of a spherical bearing connector supported atop three inclined legs (Figure 9.54).

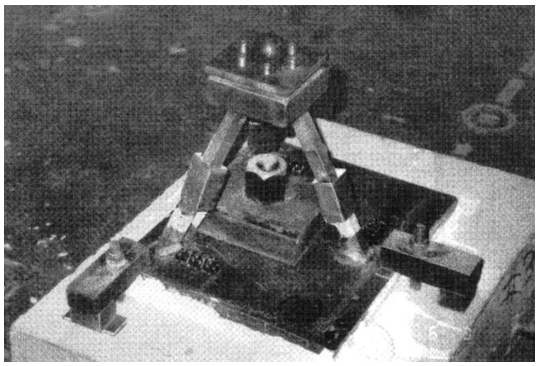

Figure 9.54 Photograph of reaction transducer, Hwang and Moehle, 1993 [1].

They put the tripod at the base of the column as a hinge, so for the setup setting the bending moment at the base is equal to zero. This is correct while the frame has an elastic behaviour but when plasticity starts at the base of the column, it become less accurate, since the plastic hinge changes the restrain condition, changing the bending moments at the column mid-height.
Figure 9.55 reports the bending moment recorded by the load cell in the internal B2 connection on the ground floor in the SlabSTRESS Cyc-2 test. This is the connection that punched and it is visible in the graph. At the time of 660, a significant drop of the bending moment is visible: this is the moment in which the connection punched. Before this point, a gradual increase of the moment brought to the formation of the plastic hinge at the base of the column.

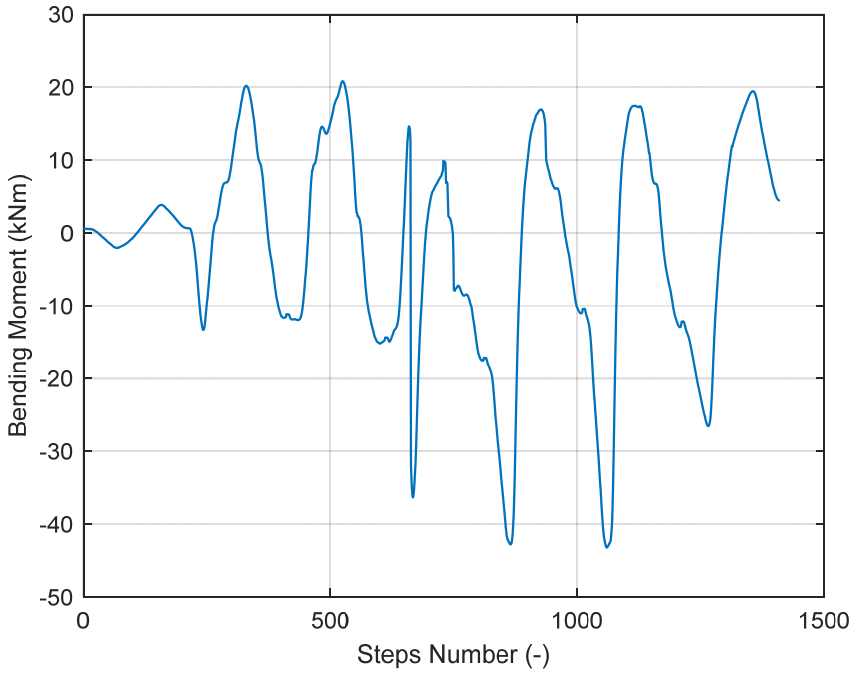

Figure 9.55 Bending moment in the B2 connection at ground floor, SlabSTRESS Cyc-2 test.

This demonstrates that the assumption of Hwang and Moehle, 1993 [1] for the setup of the tripod is not accurate in this condition.
In Table 9.13 the mean measuring error of Hwang and Moehle, 1993 [1] is reported whereas in Table 9.14 the standard deviation of errors for the SlabSTRESS measurements is reported.

Table 9.13 Mean error of measuring in Hwang and Moehle, 1993 [1]

Column typology	Column size (m)	V (kN)	N (kN)
Exterior	0.163*0.163	0.3	0.8
	0.244*0.122		
Interior	0.244*0.244	0.5	0.6
	0.325*0.163		

In the comparison between Hwang and Moehle, 1993 [1] results and SlabSTRESS, there is a one order of magnitude difference, which can also be seen in the two reported tables (Table 9.13 and Table 9.14).

Table 9.14 Standard deviation errors of SlabSTRESS measurements.

Column typology	Column size (cm)	V (kN)	N (kN)	M (kNm)
Edge	35*35	1.8	76	1
Internal	40*40	3.7	132	3.2
Corner	30*30	2	7	0.2

As widely explained in Chapter 4, the load cells calibration procedure achieved excellent results for the measurement of the shear and the moment, but very poor results for the vertical load. After various attempts to correct the measurement without success, it was decided to not consider as reliable the record of the vertical load. Similarly, Hwang and Moehle, 1993 [1] declared that some of the readings from the reaction transducers appeared to be in error probably due to loose electrical wires.

9.4.8 COMPARISON OF MODEL AND EXPERIMENTAL RESULTS

A part of the experimental results obtained during the SlabSTRESS campaign are here compared with the results of the models reviewed in Chapter 2 for punching resistance and deformation capacity:

- The North American ACI 318 [8] code model
- The model proposed by Setiawan et al., 2019 [44]

The former is formulated for the verification of punching resistance of interior, edge ad corner connections, both without or with shear reinforcement, under the effects of gravity and lateral actions. The deformation capacity is determined as a function of the gravity shear ratio using an empirically derived relation.
The latter represents a new proposal for the design and verifications of punching resistance and deformation capacity, within the framework of the CSCT and Model Code 2010 [39], [40].

ACI 318

The codified design approaches of the ACI 318 [8] was applied to both the edge and the interior slab-column connection typologies in both floors of the SlabSTRESS tests. All the results of the slab-column connections in the alignments B and C were used, with the nominal gravity shear forces of the connections. It was decided not to use the slab-column connections in the alignments A and D because the load cells in the columns did not measure accurately the axial forces, and thus the shear due to the seismic actions was unknown.
Considering only the connections in the alignments B and C in both floors and the two cyclic tests (Cyc-1 and Cyc-2), only one punching failure occurred in the 1st floor connection B2, during the Cyc-2 test.
Table 9.15 summarises the material properties and geometry of the slab-column connections used. In Table 9.16 and Table 9.17 the experimental maximum unbalanced moment results, are reported together with the model results. Given the nominal gravity shear force in the connections, the unbalanced moment reaching the shear strength in the connection is calculated; mean values of the material strength properties were used.

Table 9.15 Summary of properties of SlabSTRESS specimen for the ACI 318 [8] design approach.

Test	Floor	Connection	Typology	GSR	f'_c (MPa)	f_y (Mpa)	A_v (mm^2)	b_0 (mm)	d (mm)	V_u (kN)
Cyc-1	1	B1	Edge	0.20	33	500	-	1548	166	83
		B2	Internal	0.29	33	500	-	2264	166	202
		B3	Edge	0.20	33	500	-	1548	166	83
		C1	Edge	0.15	33	500	-	1548	166	63
		C2	Internal	0.22	33	500	-	2264	166	155
		C3	Edge	0.15	33	500	-	1548	166	63
	2	B1	Edge	0.22	33	500	393	1548	166	226
		B2	Internal	0.32	33	500	628	2264	166	226
		B3	Edge	0.22	33	500	393	1548	166	226
		C1	Edge	0.22	33	500	393	1548	166	226
		C2	Internal	0.32	33	500	628	2264	166	226
		C3	Edge	0.22	33	500	393	1548	166	226
Cyc-2	1	B1	Edge	0.20÷0.12	33	500	393	1548	166	202
		B2	Internal	0.29	33	500	-	2264	166	202
		B3	Edge	0.20÷0.12	33	500	-	1548	166	83
		C1	Edge	0.20÷0.12	33	500	-	1548	166	83
		C2	Internal	0.29	33	500	628	2264	166	202
		C3	Edge	0.20÷0.12	33	500	393	1548	166	202
	2	B1	Edge	0.22	33	500	393	1548	166	226
		B2	Internal	0.32	33	500	628	2264	166	226
		B3	Edge	0.22	33	500	393	1548	166	226
		C1	Edge	0.22	33	500	393	1548	166	226
		C2	Internal	0.32	33	500	628	2264	166	226
		C3	Edge	0.22	33	500	393	1548	166	226

Notes:
A_v is the cross-sectional area of shear reinforcement on one peripheral line.
b_0 is the length of perimeter of shear-critical section.
V_u is the gravity shear force transferred between the slab and the column.

During the first cyclic test, Cyc-1, reported in Table 9.16, none of the slab-column connections reached punching failure. The comparison of the unbalanced moments calculated with the ACI 318 [15] design approach and the SlabSTRESS experimental results shows that the calculated unbalanced moments are higher than the SlabSTRESS experimental results in all the connections in both floors.

Table 9.16 SlabSTRESS test Cyc-1 and ACI 318 [15]Unbalanced Moment (KNm) results.

	SlabSTRESS Cyc-1			ACI 318		
1st Floor		B	C		B	C
	1	196	198	1	209	221
	2	341	352	2	381	415
	3	178	190	3	209	221
2nd Floor		B	C		B	C
	1	151	163	1	270	270
	2	272	255	2	441	441
	3	137	159	3	270	270

LEGEND: black = connections without shear reinforcement; orange = connections with shear reinforcement

During the second cyclic test, Cyc-2, reported in Table 9.17, the internal slab-column connection, B2, in the 1st floor, punched. The comparison of the unbalanced moments calculated with the ACI 318 [15] design approach and the SlabSTRESS experimental results shows:

- 1st floor: the model results predict the punching in connection B2. The model resistance is higher than the experimental in all the strengthened connections, B1, C2 and C3. The model results are lower than the experimental for the two unstrenghtened connections C1 and B3;
- 2nd floor: model results higher than the experimental in all connections.

Table 9.17 SlabSTRESS test Cyc-2 and ACI 318 [15]Unbalanced Moment (KNm) at punching results.

	SlabSTRESS Cyc-2			ACI 318		
1st Floor		B	C		B	C
	1	231	217	1	282	209
	2	412	436	2	381	464
	3	228	222	3	209	282
2nd Floor		B	C		B	C
	1	193	215	1	270	270
	2	365	347	2	441	441
	3	183	228	3	270	270

LEGEND: black = connections without shear reinforcement; orange = connections with shear reinforcement

The ratios between the ACI 318 [15] design approach values and the SlabSTRESS experimental results, are reported in Table 9.18 and Table 9.19.
For the first cyclic test, Cyc-1, the ACI 318 [15] model considers the possibility that punching will happen for unbalanced moment higher than those measured. In fact, no punching failure was observed during this test. The model to test results ratios range 1.06-1.18.

Table 9.18 Ratio between ACI 318 [15] values and SlabSTRESS experimental results of test Cyc-1.

ACI 318/SlabSTRESS Cyc-1 (%)			
1st Floor		B	C
	1	106	111
	2	112	118
	3	117	116
2nd Floor		B	C
	1	179	166
	2	162	173
	3	198	170

LEGEND: black = connections without shear reinforcement; orange = connections with shear reinforcement

The unbalanced moment to drift relations in Chapter 7 show the development of plastic deformations for approximately constant moments in the final phase of the test. The ratios predicted for the 2nd floor are higher (1.62-1.98); this agrees with the connections response showing increasing moments with plastic deformations up to maximum 2.5% drift ratio.
A partly different scenario is shown by the comparison with test Cyc-2 results. All the model to test ratios higher than 100% are in connections that did not reached punching failure. The only connection with punching is the internal B2 in the 1st floor. For this connection, in fact, the model to test ratio is 93%. The ratio is lower than 100% for two other connections, the unstrengthened C1 and B3 on the 1st floor. No punching was observed in these connections during the experimental campaign, through sections 8.5.1 and 8.5.2 show sign of shear-flexural cracking on the top surface of the slab. The ratios for the 2nd floor are higher than 1, (1.18-1.48). the response of these connections showed the reaching of a nearly constant moment plateau.

Table 9.19 Ratio between ACI 318 [15] values and SlabSTRESS experimental results of test Cyc-2.

ACI 318/SlabSTRESS Cyc-2 (%)			
1st Floor		B	C
	1	122	96
	2	93	106
	3	91	127
2nd Floor		B	C
	1	140	125
	2	121	127
	3	148	118

LEGEND: black = connections without shear reinforcement; orange = connections with shear reinforcement

Finally, the comparison between the deformation capacity calculated with ACI 318 [15] and the values obtained during the SlabSTRESS experimental campaign. Is reported (Table 9.20). The empirical model is based on tests on interior connections, and provides a lower bound of the test results. This allows the calculation of the deformation capacity only for the internal slab-column connection without shear reinforcement. Hence the comparison with the SlabSTRESS results is done with only the internal B2 and C2 in the 1st floor for the first cyclic test and only the B2 for the test Cyc-2.
The value of f'_c for the concrete, used in the calculation of the GSR for the model, is that measured before the test and it is equal to 35MPa. To calculate the deformation capacity, it was chosen not to use the capacity reduction factor ϕ=0.75, since all the mean values were used.
The deformation capacity of the C2 connection, test Cyc-1 represents the maximum drift reached without failure, this connection was then strengthened.
The experimental values are higher than the model predictions, confirming the

conservativity of the model.

Table 9.20 Deformation capacity (Dr_u) SlabSTRESS connections.

	SlabSTRESS Cyc-1			
	Test		Model	
	B2	C2	B2	C2
Gravity shear ratio	-	-	-	0.2
Ultimate drift ratio	-	0.026(^)	-	0.025
	SlabSTRESS Cyc-2			
	Test		Model	
	B2	C2	B2	C2
Gravity shear ratio	-	-	0.3	-
Ultimate drift ratio	0.039	-	0.021	-

LEGEND: (^) lower bound value.

SETIAWAN ET AL., 2019

The Setiawan et al., 2019 [44] method was applied for assessing punching resistance and drift capacity of internal flat slab-column connections without shear reinforcement. The model is compared to the 1st floor connection B2 that reached punching during test Cyc-2.

Table 9.21 summarises the material properties and geometry of the slab-column connections used.

Table 9.21 Summary of properties of SlabSTRESS specimen for the Setiawan et al., 2019 [44] model.

GSR	Column side (mm)	Slab thickness (mm)	d (mm)	r_s (mm)	f'_c (MPa)	d_g (mm)	f_y (Mpa)	ρ_{hog} (%)	ρ_{sag} (%)	e_u (mm)	k_{emod} (-)	k_{elim} (-)
0.29	400	200	168	1045	35	12	500	0.0070	0.0034	850	0.36	0.29

Notes:

d_g is the maximum aggregate size.

f_y is the average yield strength of the flexural reinforcement bars.

ρ_{hog} is the ratio of flexural reinforcement at slab tension side (hogging).

ρ_{sag} is the ratio of flexural reinforcement at slab compression side (sagging).

The rotation calculated in Setiawan et al., 2019 [44] model, is the slab rotation due to deformation inside a radius r_s=0.22L of the column centreline, in which L is the slab span. The value of r_s in SlabSTRESS is 1045mm. The slab-column rotation measured in SlabSTRESS, refers to a distance of 168mm from the column, so it is not possible to carry out the comparison directly. Hence, the comparison should be done using the inter-storey drift ratio.

The internal connection B2 on the 1st floor reached punching during test Cyc-2 for an inter-storey drift value of 0.039. The inter-storey drift ratio for the Setiawan et al., 2019 [44] model is obtained dividing the slab-column rotation ψ_{SCC} by the factor 0.85 [19]. The obtained value of inter-storey drift ratio is 0.015/0.85=0.018. this is 54%

lower of the experimental result.
Table 9.22 reports the comparison between the results of the unbalanced moment obtained with the Setiawan et al., 2019 [44] method and the SlabSTRESS internal flat slab-column connection, B2 without shear reinforcement. The model predictions are nearly 56.5% lower than the experimental results.

Table 9.22 SlabSTRESS tests and Setiawan et al., 2019 [18] results.

Setiawan et al., 2019					SlabSTRESS	
Ψ_{min} (rad)	Ψ_{max} (rad)	Ψ_{scc} (rad)	I-S drift ratio	M (kNm)	I-S drift ratio	M (kNm)
-0.012	0.019	0.015	0.018	179	0.039	412

The model of Setiawan et al., 2019 [44] was applied also to three different experiments taken from the literature; Drakatos et al, 2016 [12], Tian et al., 2008 [20] and Robertson and Johnson, 2006 [21]. This was done as a verification, as the same tests have been predicted with success by Setiawan et al., 2019 [44]. Table 9.23 reports the geometrical characteristics of these tests.

Table 9.23 Geometrical characteristics of the analysed tests.

Tests	GSR	Column side (mm)	Slab thickness (mm)	d (mm)	r_s (mm)	f'_c (MPa)	d_g (mm)	f_y (Mpa)	ρ_{hog} (%)	ρ_{sag} (%)
Drakatos et al, 2016 [12]	0.424	390	250	198	1500	32.7	16	575	1.1200	0.3000
Tian et al., 2008 [20]	0.23	406	152	127	1828.5	25.6	10	469	0.5	0.3
Robertson and Johnson, 2006 [21]	0.247	250	115	96	603.5	35.4	10	450	0.7	0.42

The experimental results and the values obtained with the model for the three tests, are reported in Table 9.24. It is possible to observe that the model confirms all the results in terms of slab-column rotation, ψ_{SCC} and unbalanced moment, M, obtained during the tests, differently from what happened with the SlabSTRESS results.

Table 9.24 Experimental and model results of the analysed tests.

	Experimental							Model	
Tests	Ψ_{min} (rad)	Ψ_{max} (rad)	Ψ_{scc} (rad)	e_u (mm)	k_{emod} (-)	k_{elim} (-)	M (kNm)	M (kNm)	Ψ_{scc} (rad)
Drakatos et al, 2016 [12]	-0.002	0.011	0.078	812	0.46	0.23	384	333	0.070
Tian et al., 2008 [20]	-0.015	0.038	0.026	1210	0.406	0.35	128	104.9	0.025
Robertson and Johnson, 2006 [21]	-0.025	0.027	0.026	760	0.267	0.3	58	47.4	0.0297

Analyse the results obtained with the Setiawan et al., 2019 [44] model and the experimental tests, some questions remain open on the application of the model to the frame results. A possible modification consists of an increase of the portion of the slab (r_s) considered in the model, representing the distance from the column to the zero moment line. The authors propose the value of 22% of the span. Higher values lead to better though still conservative predictions of ultimate rotation and moment for the slab stress test. Undoubtedly the comparison discussed above considers only

one connection of a frame. The topic remains open to further investigation.

9.5 Summary

A summary of all the comparisons between the SlabSTRESS results and the literature works is reported here.

- The SlabSTRESS seismic tests explored for the first time (albeit only in hybrid mode) the interaction between flat slabs and a primary seismic system;
- The tests showed global deformation capacity of the structure up to 2.5% global drift ratio with the first floor without shear reinforcement and 6% with some strengthening. This confirms global tests of scaled floor and frame specimens reaching deformation capacities in the range 3-6%;
- The connection response confirms the deformation capacity results of the data bases collected in the literature, for specimens without and with shear reinforcement. Failure modes similar to those shown in the literature were observed. This result was achieved using realistic geometric dimensions and boundary conditions;
- The tests confirmed the redistribution of the internal forces and moments from the edge connections to the interior ones; common floor configurations confirmed the sequence of failure starting from the edge connections and moving through the interior of the slab;
- The damage on the edge slab-column connections was similar to that obtained in other tests on floors with either uniaxial or biaxial loading; high damage levels for these connections in SlabSTRESS for drift ratios between 2 and 6% can be related to the detail with a simple bend used for the longitudinal bars at the edge. Further developments with experimental tests are needed regarding the reinforcement detailing of edge connections;
- High column reinforcement ratio in SlabSTRESS was chosen to limit damage in these members. As observed in the literature, a lower percentage of reinforcement could have brought to a structure with higher deformability in non-linear field;
- All tests have shown that interior connection punching is a decisive phenomenon with severe consequences for the local and global response. Nevertheless, the global deformation levels reached were rather high;
- The integrity reinforcement as prescribed by the EC2 [9], was efficient design detail preventing the fall of the slab, other tests for scaled specimens obtained similar results;
- The shear reinforcement in the 2nd floor slab reduced the intensity of damage, confirming previous observations for isolated connections and one frame test

with stud shear reinforcement. Edge connections on line A and D reached failure for higher drifts than the 1st floor connections, and the interior and edge connections on lines B and C did not failed;

- SlabSTRESS considered two different longitudinal reinforcement layouts (smeared and concentrated) for the same total quantity of top reinforcement. It confirmed that a higher top reinforcement provokes a higher level of damage;
- The post-installed bolts chosen for strengthening demonstrated to be an effective solution. The strengthening contributed in the performance of the structure to reach high drift ratios. Further investigations are needed on the strengthening of other slab-column connections typologies (edge and corner);
- A methodology to put in relation the inter-storey drift ratio with the rotation was presented. In the local analysis the rotation gives a better representation of the behaviour of each slab-column connection;
- The proposed system to measure the internal forces achieved excellent results for the measurement of the shear force and the bending moment but not reliable results for the axial force. Further research is needed;
- A part of the experimental results obtained during the SlabSTRESS campaign were compared with the results of the North American ACI 318 [8] model and the model proposed by Setiawan et al., 2019 [44] in terms of punching resistance and deformation capacity. The model ACI 318 [15] shows a good agreement with the test results, predicting unbalanced moments that correspond to the failure modes and response observed. For the drift capacity, the analytical predictions are conservative;
- The comparison with the more advanced model proposed by Setiawan et al., 2019 [44] shows the need to investigate further the application of the model.

References

[1] Hwang, S.-J., Moehle, J. P. (1993) "An Experimental Study of Flat-Plate Structures under Vertical and Lateral Loads". Report N. UCB/EERC-93/03, Earthquake Engineering Research Centre, University of California, Barkeley, Feb. 1993, 278pp.

[2] Rha, C., Kang, T. H.-K., Shin, M., Yoon, J. B. (2014). "Gravity and Lateral Load-Carrying Capacities of Reinforced Concrete Flat Plate Systems". ACI Structural Journal, V. 111, No 4, 2014, pp. 753-764.

[3] Fick, D. R., Sozen, M. A., Kreger, M. E. (2017) "Response of Full-Scale Three-Story Flat-Plate Test Structure to Cycles of Increasing Lateral Load" ACI Structural Journal, V. 114, No. 6, pp. 1507-1518.

[4] Moehle J. P., Diebold J. W. (1984) "Experimental Study of the Seismic Response of a Two-Story of a Flat-Plate Structure". University of California, Berkeley.

[5] Kang, T. H.-K., Wallace, J. W. "Shake Table Tests of Reinforced Concrete Flat Plate Frames and Post-Tensioned Flat Plate Frames" (2004). 13th World Conference on Earthquake Engineering, Vancouver, B.C., Canada. Paper No.1119.

[6] Muttoni A (2008) Punching Shear Strength of Reinforced Concrete Slabs. ACI structural J 105:440–450. https://doi.org/10.14359/19858.

[7] Hueste, M. B. D., Browing, J., Lepage, A., Wallace, J., W. (2007) "Seismic Design Criteria for Slab-column Connections". ACI Structural Journal, V. 104, No. 4, pp. 448-458.

[8] Ramos, A. P., Marreiros, R., Almeida, A., Isufi, b., Inacio, M. (2017) "Punching of flat slabs under reversed horizontal cyclic loading", ACI-fib International Symposium Punching shear of structural concrete slabs.

[9] CEN. EN 1992-1-1. Eurocode 2 — Design of concrete structures. Part 1-1: General rules and rules for buildings. 2004.

[10] Lapi, M., Ramos, A. P., Orlando, M. (2019) "Flat slab strengthening techniques against punching-shear", Engineering Structures, Volume 180, Pages 160-180. https://doi.org/10.1016/j.engstruct.2018.11.033.

[11] Almeida, A., Ramos, A. P., Lucio, V., Marreiros, R. (2019). "Behaviour of RC flat slabs with shear bolts uncerd reversed horizontal cyclic loading". Structural Concrete. 2019; 1-16. https://doi.org/10.1002/suco.201900128.

[12] Drakatos I.-S, Muttoni, A., Beyer, K.,(2016) "Internal slab-column connections under monotonic and cyclic imposed rotations", Engineering Structures, Volume 123, 15 September 2016, Pages 501-516, ISSN 0141-0296, (https://doi.org/10.1016/j.engstruct.2016.05.038).

[13] ACI-ACSE Committee 421.1R, “Guide for shear Reinforcement for Slabs”

[14] ACI-ACSE Committee 421.2R, “Guide to Seismic Design of Punching Shear Reinforcement in Flat Plates”.

[15] ACI 318-14. Building Code Requirements for Structural Concrete. ACI; 2014.

[16] Fib (2010) “CEB-FIP Model Code 2010 – Frost complete draft.” Bulletin 55, Vol. 1, Federation International du Beton, Lausanne.

[17] Fib (2010) “CEB-FIP Model Code 2010 – Frost complete draft.” Bulletin 55, Vol. 2, Federation International du Beton, Lausanne.

[18] Setiawan, a., Vollum., R. L., Macorini, L., (2019) “Numerical and analytical investigation of internal slab-column connections subject to cyclic loading”. Engineering structures 184 (2019) 535-554.

[19] Drakatos I.-S, Muttoni, A., Beyer, K., (2018) “Mechanical model for drift-induced punching of slab-column connections without transverse reinforcement. ACI structural Journal 2018; 115 (2).

[20] Tian Y, Jirsa JO, Bayrak O, Widianto, Argudo JF. Behavior of slab-column connections of existing flat-plate structures. ACI Struct J 2008;105(5).

[21] Robertson IN, Johnson G. Cyclic lateral loading of non-ductile slab-column connections. ACI Struct J 2006;103(3):356–64. Farmington Hills, U.S.A.

10 Conclusions and Further Research

10.1 Introduction

The summary of results and conclusions are reported with the main topics treated in the dissertation: the test configurations, the design, global behaviour, redistribution of the internal forces, local behaviour, reinforcement layout and details, shear reinforcement, strengthening, the relation of the local phenomena and the global response and the measurement system.
Some results confirm findings obtained from individual connection and scaled frame tests. Other aspects are innovative Lastly, possible future developments in research are presented.
The information collected in this study represents the basis for a deeper understanding of flat slab response to combined gravity and lateral loading, the calibration of a model having the advantage of the measurements carried out on a complete real scale structure. This experimental work and its developments pave the way to new and more advantageous design rules, in particular for the European Codes.

10.2 Summary of the results and conclusions

Extensive experimental work has been carried out in the past with the aim to clarify flat slab design rules. Many tests investigated isolated slab column connections, fewer the single flat slab floor, and even fewer, complete frames. The SlabSTRESS project was developed to fill this gap.
This dissertation focuses mainly on the behaviour of a real scale flat-slab building with the aim to correlate the global behaviour of the response of single connections, considering their location within the floor, the longitudinal reinforcement layout and the presence of shear reinforcement.
The SlabSTRESS experimental campaign was performed at the ELSA Reaction Wall at the European Commission's Joint Research Centre (JRC) in Ispra (VA) during the transnational access activities of the SERA project.
The real-scale mock-up consisted of a reinforced concrete frame with two slab floors, supported by twelve columns. One floor was provided with transverse reinforcement.
The building was designed to consider the flat slabs as secondary members, with seismic resistant walls as primary ductile elements. The structure was designed to bear gravity loads and to be capable reaching a lateral relative inter storey drift

compatible with moderately-high seismic lateral actions. This design procedure was inspired by the method set out in the North American codes for the seismic design of flat slabs.
The primary seismic walls were not actually built in the structure but were virtual elements, simulated by the sub-structuring allowed for the pseudo-dynamic method used in the host lab.
In the first phase of the test programme two levels of seismic activity were simulated: that is the service limit state (SLS) and the ultimate limit state (ULS). The seismic loading was applied using the pseudo-dynamic technique with linear sub-structuring. Successively, during the second phase two cyclic tests were carried out to test the floors for a combination of gravity and lateral cyclic loading of increasing amplitude, up to near-failure conditions. Some of the damaged connections were strengthened before the second cyclic test.
Both the global and the local measurements were acquired. Each column on both floors was provided with an *ad hoc* designed system that allowed the internal forces and bending moment to be measured. A large number of sensors were used in this experimental campaign; 80 inclinometers, 48 extensometers and 192 strain-gauges, thus collecting a series of data. All the sensors had been previously calibrated to ensure the precision of the measurement system. A new controller and data acquisition system, called ElsaREC, was developed by the ELSA laboratory team and used for the first time, allowing a systematic calibration procedure for all the sensors adopted in the experiment at ELSA.
Using the main statics and kinematics parameters, two models were chosen to represent the structure both from a global and a local point of view. Two kinematics parameters, one displacement for each floor and two static parameters, one force for each floor, described the global system. These parameters were acquired by the load cells applied to the actuators, while displacement transducers applied on two reference frames near the structure recorded the corresponding displacements.
The local system to capture the behaviour of each slab-column connection was more complex. The slab and the column rotations represented the local kinematic parameters that were recorded using the inclinometers, and the slab cracks opening was recorded using the displacement transducers.
Local kinematic measurements were acquired in the surrounding area of the slab on eight out of the twelve columns. The three typologies of connection (internal, edge and corner) were analysed with four, three and two instrumented sides, respectively. Each side of slab-column connection was equipped with an inclinometer to measure slab rotation along the East-West direction and a set of displacement transducers to measure crack opening through an increase in the slab thickness.
Using the acquired slab rotation data and the column of each slab-column connection, it was possible to derive the relative rotation of the slab with respect to the column.
The static parameters are two for each slab-column connection: shear and bending

moment. The column and shear moment were acquired using load cells located at the centre of each column on each floor, specially designed for this experimental campaign.
The main conclusions for the global and the local response are summarised below.

10.2.1 Test Configuration

The interaction between flat slabs and a primary seismic system was experimentally explored for the first time (albeit only in hybrid mode) with the presence of numerical walls as primary seismic elements in the SlabSTRESS seismic tests. The pseudodynamic testing furnished results for the response of a building structure with shear walls and flat slabs, tested for the design level of seismic actions.

Previous studies left open some questions on the real scale flat-slab behaviour up to near failure conditions, as the only such test was interrupted on reaching the first punching failure in the structure, and the floor geometry did not include edge and corner columns on the perimeter of the slab. The test presented in this thesis centres on a very common building configuration (multi floor, real scale, three by two spans with several slab-column connections, presence of edge connections, etc.).

Testing a real-scale, flat-slab building resulted in an understanding of the behaviour of the connections, which connection typology fails first, how the system redistributes internal forces and damage and whether or not the flat slab floor collapse occurs or not.

10.2.2 Design

The efficiency of the design for a secondary structure was confirmed by the seismic tests. As a starting point the ACI 318-14 formulation based on the existing database of connection tests was used to determine the ultimate drift limit for the connections. Aspects of the design related to slab reinforcement layout, detailing and the use of shear reinforcement are commented on relation to the local behaviour.

10.2.3 Global behaviour

The seismic design was efficient. The global seismic response showed very limited damage up to an excitation, compatible with the ultimate limit state spectrum.

The global cyclic response confirmed the capacity of flat slab frames to develop inelastic deformation, reaching ultimate deformation capacity comparable with that observed in the state of the art.

The flat slab frame was designed as a secondary structure; the global drift ratio reached in the first cyclic test corresponds to that of other systems with such design – both scaled tests and one full scale test. The response highlighted what can be defined a plastic behaviour, with the structure reaching a maximum load that remained nearly constant in the non-linear response up to the occurrence of

punching of the interior connections.

It is remarkable that the severe damage shown on the edges of the structure had limited impact on the global response, particularly in the first cyclic test.

The high deformation levels reached in the second cyclic test are undoubtedly a consequence of the strengthening of connections on the first floor and the use of shear reinforcement on the second floor.

The floors did not collapse, and proved able to support the gravity loading at the end of the testing program.

10.2.4 Redistribution of the internal forces

The sequence of failures and the redistribution of internal forces and moments were started from the edges to the interior of the floors. Fick et al., 2017 [2] interrupted the test after the first punching, leaving the redistribution on a multi-storey, real scale building unexplored. The SlabSTRESS results summarized above confirm similar results of tests carried out on a scaled flat slab floor.

Although the structure was severely damaged by lateral action, no global collapse took place. This confirms the effectiveness of redistribution for structural strength.

10.2.5 Local Behaviour

The tests showed the severity of the damage and failure on edge and corner connections, even though the nonlinear response system in the first cyclic test showed the plastic behaviour highlighted previously. The connection failure sequence started from the edge connections and advanced internally through the slab.

It was confirmed that the punching of an interior connection is a decisive phenomenon with severe consequences on the local and global response.

Previous research provided numerous results for interior connections. The testing of the whole structure shows that the first failures occur at the perimeter.

The lateral drift capacity of the interior connections without shear reinforcement was 3.8% for one (gravity shear ratio 0.3) and higher than 2.5% for the other (gravity shear ratio 0.22); these values agree with the existing database of connections tests (Hueste et al., 2007 [4], Ramos et al., 2017 [5]) and the floor test with biaxial loading by Hwang and Moehle, 1993 [1].

The lateral drift capacity of the edge and corner connections without shear reinforcement was approximately 2% (gravity shear ratio ranging 0.13-0.2). A database comparable to those previously referenced was not found, showing the need for further research on these types of connections.

The energy dissipation of the column bases was also considered in the response given

by the real configuration of the structure. The column cracking influenced the ultimate deformability. Due to the relevance of columns in the configuration and response, they need suitable detailing.

10.2.6 Reinforcement layout and details

The integrity reinforcement as prescribed by the EC2 confirmed its effectiveness by preventing of slab fall after punching.

Two different reinforcement layouts were considered simultaneously in the same mock-up and for the first time, showing that the edge of the slab with concentrated reinforcement layout recorded a higher level of damage than the edge with smeared layout.

The anchorage detail with a simple bend of the longitudinal reinforcement on the free edges caused the damage to the edge by torsion from the end of the first cyclic test.

10.2.7 Shear reinforcement

The shear reinforcement with headed studs reduced the intensity of damage preventing punching, reaching higher ultimate drift for edge and internal connections, confirming previous results in the literature on connections.

The 2nd floor reported less damage than the 1st one. The edge connections on two sides reached failure at drift ratios approximately 3-4%. The internal connections reached a maximum drift ratio of 6% without much damage. The edges parallel to the loading were more damaged although no failures occurred there.

10.2.8 Strengthening

The strengthening technique with post-installed bolts showed to be an effective solution, avoiding punching in one internal connection and limiting damage on the edges.

10.2.9 Relation of the local phenomena and the global response

The inter-storey drift describes the seismic global response of the structure and of each storey, but this may be inaccurate when describing the behaviour of each floor and of each slab-column connection on the floor. This would be mainly due to the different arrangements of the columns on the two floors which must be considered: those for the 1st floor were above and below the slab whereas for the 2nd floor they were only whole below the slab (roof slab). It was observed that the slab-column rotation gave a better representation of the behaviour of each slab-column connection. The study of local behaviour as a function of different details can profit from the use of slab column rotations.

The conversion factors that allowed to convert the inter-storey drift ratio to the

column-slab relative rotation depending on the slab-column connection typology (internal, edge with loading parallel or perpendicular and corner) were obtained. These facilitate the simplification of the numerical analyses where the inter-storey drift is known but the corresponding rotation is not known.

10.2.10 MEASUREMENT SYSTEM

SlabSTRESS is the first test to measure global and local static and kinematics quantities for a multi storey full scale flat slab structure. A better understanding of the response was possible thanks to the relation between these two measurement levels.

A new system that was proposed to measure the internal forces achieved excellent results for the measurement of the shear force and the bending moment but did not give reliable results for the axial force.

10.2.11 MODEL AND EXPERIMENTAL RESULTS

SlabSTRESS experimental results were compared with the results of the North American ACI 318 [6] model and the model proposed by Setiawan et al., 2019 [9] in terms of punching resistance and deformation capacity.
The model ACI 318 [6] shows a good agreement with the test results, predicting unbalanced moments that correspond to the failure modes and response observed. For the drift capacity, the analytical predictions are conservative.
The comparison with the more advanced model proposed by Setiawan et al., 2019 [9][44] shows the need to investigate further the application of the model.

10.3 Further research

The experimental campaign suggests several points for future research.

In this thesis the gravity shear ratio was calculated using the ACI318 [6] definition of punching resistance. As a development of the SlabSTRESS research program, models (Drakatos et al., 2018 [7]; Muttoni et al., 2018 [8]) are being studied to be proposed for the new European codes.

A more realistic representation of the seismic scenario could be obtained with the biaxial loading tests, overcoming the difficulties of such tests. For the local behaviour, the effects of the combinations of different internal load effects on all the connections on the perimeter could be studied. The impact of these phenomena on the global response could be assessed.

The shear reinforcement improved the response of all connections, in particular the interior connections and those parallel to the loading application; the performance in the connections perpendicular to the loading application needs further investigation, because they were affected by damage similar to that on the 1st floor, but for higher drift ratios.

The anchorage detail on the free edges needs to be further studied; a detail that is common in European practice was studied; heavy local damage was observed in the tests; other tests in the literature used different details, but similar damage showed nevertheless.

The post-installation of bolts was effective for the internal slab-column connection typology but it was not possible to affirm the same for the lateral connections. The lateral connections on the side parallel to the loading application did not record any punching. The lateral connections to the edge of the slab perpendicular to the load application reached a level of damage of such entity that to consider repair and strengthening was impossible. Further studies would be required for the strengthening of the lateral connections.

The local system for recording the internal force needs further research to improve the measurements of the axial force.

The test results provide a basis for the calibration and development of models needed for an efficient design of flat slabs for seismic loading.

References

[1] Hwang, S.-J., Moehle, J. P. (1993) “An Experimental Study of Flat-Plate Structures under Vertical and Lateral Loads”. Report N. UCB/EERC-93/03, Earthquake Engineering Research Centre, University of California, Berkeley, Feb. 1993, 278pp.

[2] Fick, D. R., Sozen, M. A., Kreger, M. E. (2017) “Response of Full-Scale Three-Story Flat-Plate Test Structure to Cycles of Increasing Lateral Load” ACI Structural Journal, V. 114, No. 6, pp. 1507-1518.

[3] Rha, C., Kang, T. H.-K., Shin, M., Yoon, J. B. (2014). “Gravity and Lateral Load-Carrying Capacities of Reinforced Concrete Flat Plate Systems”. ACI Structural Journal, V. 111, No 4, 2014, pp. 753-764.

[4] Hueste, M. B. D., Browining, J., Lepage, A., Wallace, J., W. (2007) “Seismic Design Criteria for Slab-column Connections”. ACI Structural Journal, V. 104, No. 4, pp. 448-458.

[5] Ramos, A. P., Marreiros, R., Almeida, A., Isufi, b., Inacio, M. (2017) “Punching of flat slabs under reversed horizontal cyclic loading”, ACI-fib International Symposium Punching shear of structural concrete slabs.

[6] ACI. ACI 318-14. Building Code Requirements for Structural Concrete. ACI; 2014.

[7] Drakatos I.-S, Muttoni, A., Beyer, K., (2018) “Mechanical Model for Drift-Induced Punching of Slab-Column Connections without Transverse Reinforcement”. ACI Structural Journal, V. 115, No. 2, March 2018.

[8] Muttoni, A., Ruiz, M. F., Simoes, J. T., (2018) “The theoretical principles of the critical shear crack theory for punching shear failures and derivations of consistent close-form design expressions”. Structural Concrete. 2018; 19:174–190. https://doi.org/10.1002/suco.201700088

[9] Setiawan, a., Vollum., R. L., Macorini, L., (2019) “Numerical and analytical investigation of internal slab-column connections subject to cyclic loading”. Engineering structures 184 (2019) 535-554.

11 Appendices

11.1 Slab Gravity Design

Figure 11.1 reports the bending moment in the slab for the two directions.

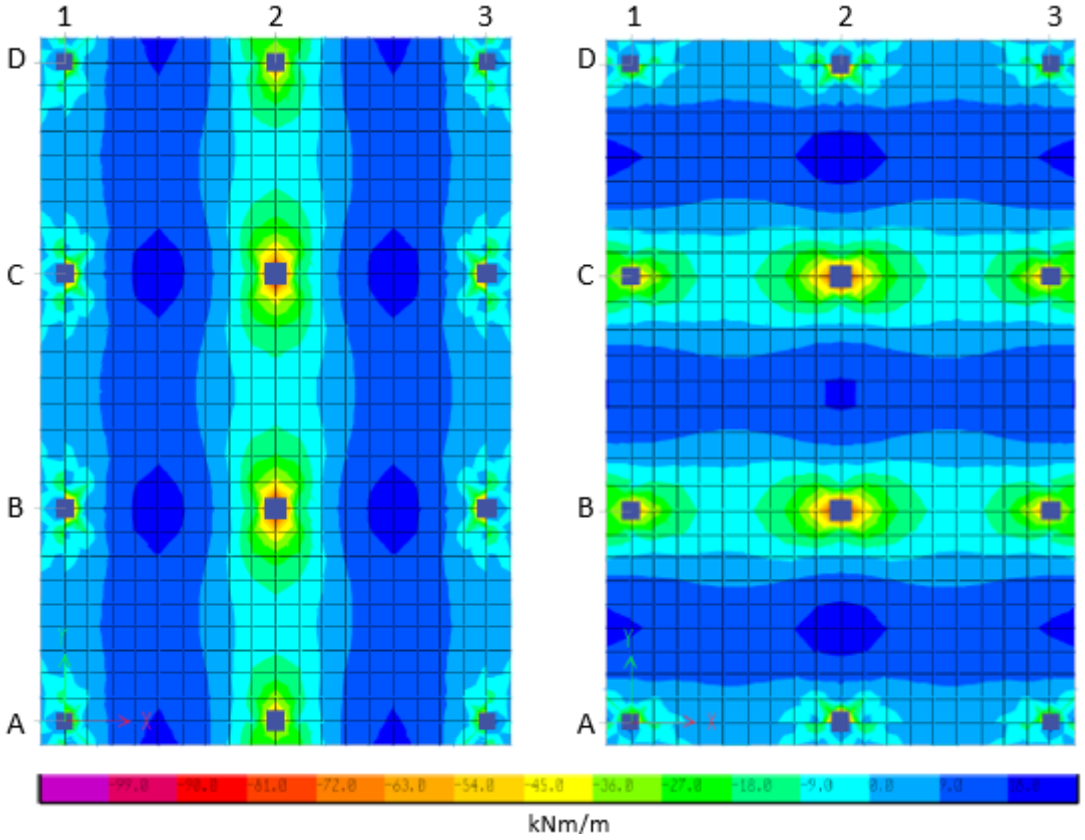

Figure 11.1 Bending moments in the slab (kNm/m).

The design of the longitudinal reinforcement is done with the strip method illustrated in Figure 11.2 whereas in Figure 11.3 the required reinforcement is reported.

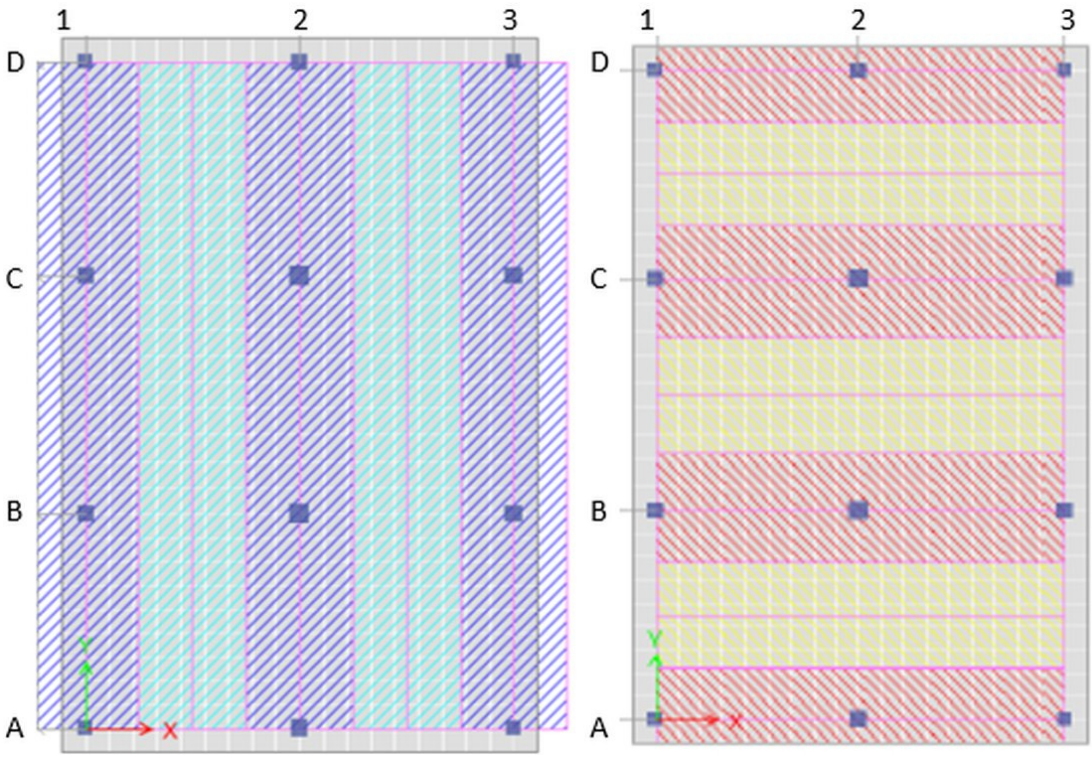

Figure 11.2 Design strip.

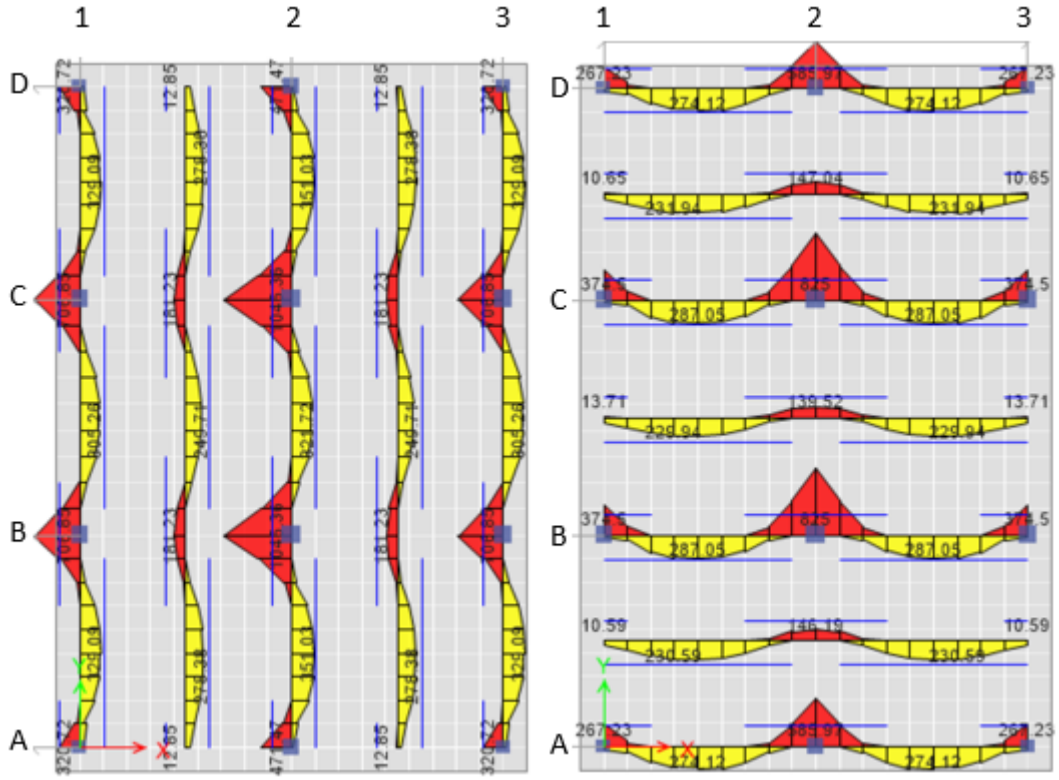

Figure 11.3 Required reinforcement (mm^2/m).

11.1.1 PUNCHING SHEAR DESIGN

The punching verifications were done for each connections typology in each floor.

Table 11.1 reports the obtained values for the shear (V_{ED}), the unbalanced moment giving around x axis (M_x), the unbalanced moment giving around y axis (M_y), the longitudinal reinforcement ratio in the slab in the short side of the specimen (ρx) and the longitudinal reinforcement ratio in the slab in the long side of the specimen (ρy).

Table 11.1 Results for gravitational load.

Connection	V_{ED} (kN)	ρx (%)	ρy (%)
Corner column 2nd floor	-45	0.32	0.30
Edge column long side 2nd floor	-95	0.31	0.42
Edge column short side 2nd floor	-101	0.45	0.29
Interior column 2nd floor	-226	0.59	0.64
Corner column 1st floor	-46	0.32	0.30
Edge column long side 1st floor	-96	0.31	0.42
Edge column short side 1st floor	-102	0.45	0.29
Interior column 1st floor	-221	0.59	0.64

The diameter of the top longitudinal reinforcement changes with the connections typology. In the interior columns have a diameter of 14 mm, in the corner columns 12 mm, in the edge columns located in the sort side, 12 mm in the long direction and 14 mm in the short direction and in the edge columns located in the long side, 14 mm in the long direction and 12 mm in the short direction.

The punching shear verification of four different connections typologies is here reported. The connections chosen are representative of the entire flat slab due to the symmetry of the model.

The punching shear verification is in accordance with Eurocode 2 [7] and regarding:

- The interior connection B2;
- The edge connection in the short side of the specimen, A2;
- The edge connections in the long side of the specimen, B3;
- The corner connection, A3.

The verifications are presented for both floors and also for the connections with concentrated reinforcement over the columns (east half of the specimen) since they have the same or higher longitudinal reinforcement ratio.

The factor β is calculated in accordance with Eurocode 2 [7], using the acting

unbalanced moments. However, a minimum value of 1.15, 1.40 and 1.50 for interior, edge and corner columns respectively is adopted.

The Combination of actions for non-seismic design situation = 1.3G + 1.5Q

The design can be reformulated with steel B450C, leading to a 10% increase in the amount of reinforcement, and a 5% increase of the punching strength without transverse reinforcement.

Table 11.2 Materials

Concrete	C30/37	$f_{cd} = \alpha_{cc}\frac{f_{ck}}{\gamma_c} = 20\ N/mm^2$	EN206-1
Bending reinforcement	B500C	$f_{yd} = \frac{f_{yk}}{\gamma_s} = 434.8\ N/mm^2$	EN 10080

INTERIOR CONNECTION B2

Table 11.3 Geometry for the interior connection B2

Geometry	
Slab Thickness	h_d=200 mm
Effective depth of slab	d_x=164 mm d_y=178 mm
Cover of reinforcement	c_u=15 mm c_o=15 mm
Reinforcement area	A_{sx}=1.026 mm^2 A_{sy}=880 mm^2
Reinforcement bars	ϕ_X=14/150 mm ϕ_Y=14/175 mm
Reinforcement ratio	ρ_x=0.63% ρ_y=0.49%
Square column	a=400 mm
Location	Middle

Table 11.4 Non seismic design for the interior connection B2

Loads	
Punching load	V_{Ed}=341.4 kN
Dynamic force	V_{dyn}=0.0 kN $V_{ed}*\beta$=392.6 kN
Basic control perimeter	
Basic length	U_1=3.749 mm
Design value of punching stress	$v_{Ed} = \frac{V_{Ed} * \beta}{u_1 * d} = 612.4\ kN/m^2$
Resistance without punching reinforcement	
	$v_{Rd,c} = \left[C_{Rd,c} * k_d * (\rho_1 * f_{ck})^{\frac{1}{3}}\right] * 1000 * f = 613.2\ kN/m^2 > v_{Ed} = 612.4\ kN/m^2$
	$C_{Rd,c} = \frac{C_{Rk,c}}{\gamma C} = 0.12$
	$v_{min} = \left(\frac{0.0525}{\gamma C}\right) * k_d^{\frac{3}{2}} * f_{ck}^{\frac{1}{2}} = 0.5422\ kN/m^2$
	$C_{Rd,c,max} = \frac{C_{Rk,c,max}}{\gamma C} * \left(0.1 * \frac{u_0}{d} + 0.6\right) = 0.12$
	k_{Max}=1.96

From the obtained results, no punching reinforcement is needed.

EDGE CONNECTION IN THE SHORT SIDE OF THE SPECIMEN A2

Table 11.5 Geometry for the edge connection A2

Geometry	
Slab Thickness	h_d=200 mm
Effective depth of slab	d_x=165 mm d_y=178 mm
Cover of reinforcement	c_u=15 mm c_o=15 mm
Reinforcement area	A_{sx}=452 mm^2 A_{sy}=669 mm^2
Reinforcement bars	ϕ_X=12/250 mm ϕ_Y=14/230 mm
Reinforcement ratio	ρ_x=0.27% ρ_y=0.38%
Square column	a=350 mm
Location	Left edge middle
Edge distance	r_a=75 mm

Table 11.6 Non seismic design for the edge connection A2

Loads	
Punching load	V_{Ed}=146.2 kN
Dynamic force	V_{dyn}=0.0 kN $V_{ed}*\beta$=204.7 kN
Basic control perimeter	
Basic length	U_1=2.278 mm
Design value of punching stress	$v_{Ed} = \frac{V_{Ed} * \beta}{u_1 * d} = 524\ kN/m^2$
Resistance without punching reinforcement	
	$v_{min} * 1000 * f = 542.2\ kN/m^2 > v_{Ed} = 524\ kN/m^2$
	$C_{Rd,c} = \frac{C_{Rk,c}}{\gamma C} = 0.12$
	$v_{min} = \left(\frac{0.0525}{\gamma C}\right) * k_d^{\frac{3}{2}} * f_{ck}^{\frac{1}{2}} = 0.5422\ kN/m^2$
	$C_{Rd,c,max} = \frac{C_{Rk,c,max}}{\gamma C} * \left(0.1 * \frac{u_0}{d} + 0.6\right) = 0.12$
	k_{Max}=1.96

From the obtained results, no punching reinforcement is needed.

EDGE CONNECTIONS IN THE LONG SIDE OF THE SPECIMEN, B3

Table 11.7 Geometry for the edge connection B3

Geometry	
Slab Thickness	h_d=200 mm
Effective depth of slab	d_x=164 mm d_y=178 mm
Cover of reinforcement	c_u=15 mm c_o=15 mm
Reinforcement area	A_{sx}=669 mm^2 A_{sy}=880 mm^2
Reinforcement bars	ϕ_X=14/230 mm ϕ_Y=14/175 mm
Reinforcement ratio	ρ_x=0.41% ρ_y=0.49%
Square column	a=350 mm
Location	Bottom edge middle
Edge distance	R_b=75 mm

Table 11.8 Non seismic design for the interior connection B3

Loads	
Punching load	V_{Ed}=148.3 kN
Dynamic force	V_{dyn}=0.0 kN $V_{ed}*\beta$=207.6 kN
Basic control perimeter	
Basic length	U_1=2.274 mm
Design value of punching stress	$v_{Ed} = \frac{V_{Ed} * \beta}{u_1 * d} = 533.8\ kN/m^2$
Resistance without punching reinforcement	
	$v_{Rd,c} = \left[C_{Rd,c} * k_d * (\rho_1 * f_{ck})^{\frac{1}{3}}\right] * 1000 * f = 571.1\ kN/m^2 > v_{Ed} = 533.8\ kN/m^2$
	$C_{Rd,c} = \frac{C_{Rk,c}}{\gamma C} = 0.12$
	$v_{min} = \left(\frac{0.0525}{\gamma C}\right) * k_d^{\frac{3}{2}} * f_{ck}^{\frac{1}{2}} = 0.5422\ kN/m^2$
	$C_{Rd,c,max} = \frac{C_{Rk,c,max}}{\gamma C} * \left(0.1 * \frac{u_0}{d} + 0.6\right) = 0.12$
	k_{Max}=1.96

From the obtained results, no punching reinforcement is needed.

CORNER CONNECTION, A3

Table 11.9 Geometry for the edge connection A3

Geometry	
Slab Thickness	h_d=200 mm
Effective depth of slab	d_x=167 mm d_y=179 mm
Cover of reinforcement	c_u=15 mm c_o=15 mm
Reinforcement area	A_{sx}=492 mm^2 A_{sy}=492 mm^2
Reinforcement bars	ϕ_X=12/230 mm ϕ_Y=12/230 mm
Reinforcement ratio	ρ_x=0.294% ρ_y=0.275%
Square column	a=300 mm
Location	Bottom Left corner
Edge distance	r_a=100 mm r_b=100 mm

Table 11.10 Non seismic design for the edge connection A3

Loads	
Punching load	V_{Ed}=69.4 kN
Dynamic force	V_{dyn}=0.0 kN $V_{ed}*\beta$=104.1 kN
Basic control perimeter	
Basic length	U_1=1.343 mm
Design value of punching stress	$v_{Ed} = \frac{V_{Ed} * \beta}{u_1 * d} = 447.9\ kN/m^2$
Resistance without punching reinforcement	
	$v_{min} * 1000 * f = 542.2\ kN/m^2 > v_{Ed} = 447.9\ kN/m^2$
	$C_{Rd,c} = \frac{C_{Rk,c}}{\gamma C} = 0.12$
	$v_{min} = \left(\frac{0.0525}{\gamma C}\right) * k_d^{\frac{3}{2}} * f_{ck}^{\frac{1}{2}} = 0.5422\ kN/m^2$

From the obtained results, no punching reinforcement is needed.

INTERIOR CONNECTION, B2

$V_{ED} * \beta = 348.4 * 1.15 = 400.7\ kN > V_{Rd,c} = 393.1\ kN$

Shear reinforcement is required but the action effects are only slightly larger than the corresponding design resistances.

OTHER CONNECTION, A2, B3, A3

For these three connections typologies, the action effects are smaller in the 2nd floor, so no shear reinforcement is required.

11.2 Column Design

11.2.1 INTERNAL FORCES

The results for internal forces and moments in the four different column typologies (internal, lateral long side, lateral short side and corner) are shown in the following Figure 11.4, Figure 11.5, Figure 11.6, and Figure 11.7

These are moment distributions based on equilibrium and the estimate of the maximum moments in the slab and at the base of the columns. The values of the maximum unbalanced moments are based on the ACI 421-07 recommendations [10], rounded with an approximate 20% increase to consider the effect that transverse reinforcement could yield higher values.

The internal forces consider the formation of a plastic hinge at the base of the columns.

The use of the plastic hinge simulates the yielding of the base, that will be caused by a more limited reinforcement ratio at this section. The corresponding moment distribution in the columns is that typical of a frame with lateral loads.

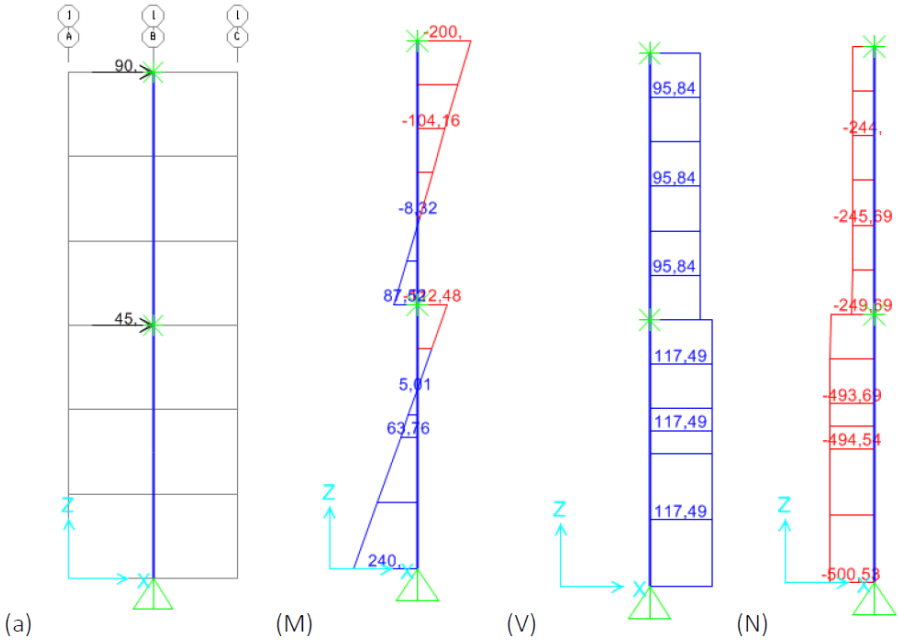

Figure 11.4 Internal column, laboratory test load effects: (a) Moments transferred form slab (kNm), (M) Bending moment (kNm), (V) Shear force (kN), (N) Axial force (kN).

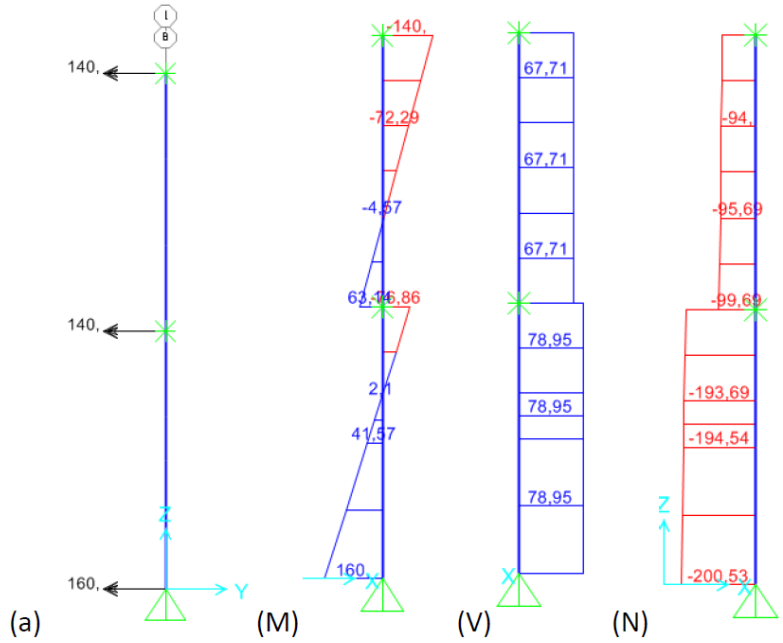

Figure 11.5 Lateral column long side, laboratory test load effects: (a) Moments transferred form slab (kNm), (M) Bending moment (kNm), (V) Shear force (kN), (N) Axial force (kN).

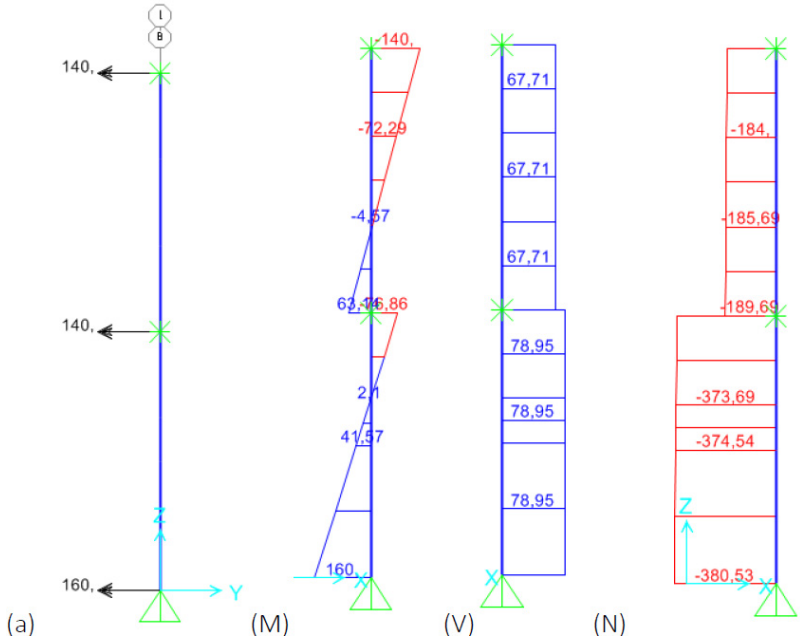

Figure 11.6 Lateral column short side, laboratory test load effects: (a) Moments transferred form slab (kNm), (M) Bending moment (kNm), (V) Shear force (kN), (N) Axial force (kN).

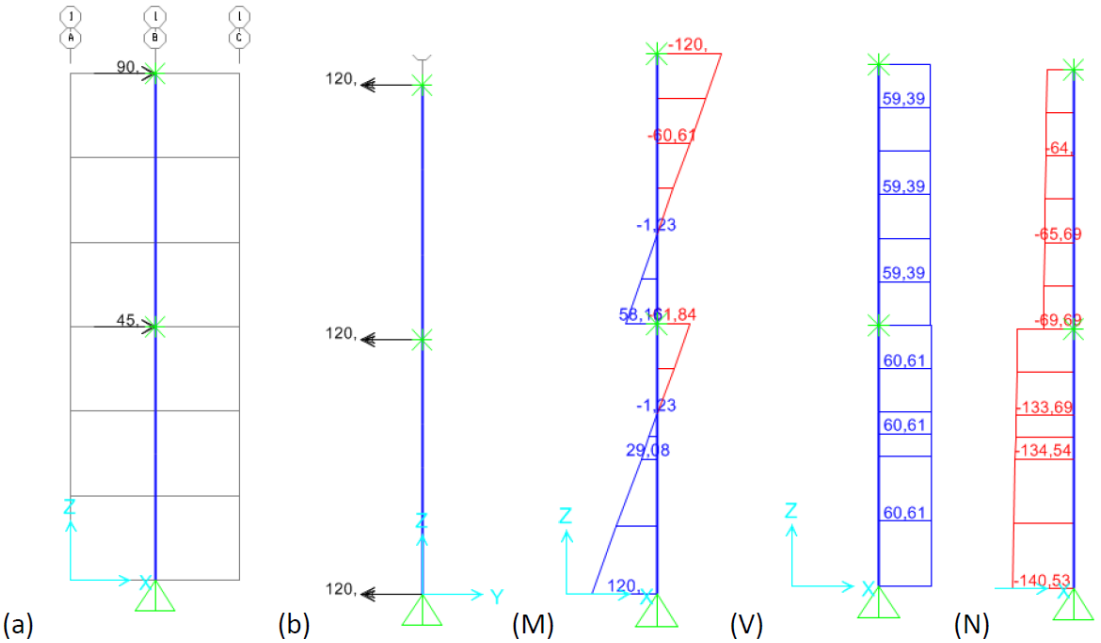

Figure 11.7 Corner column, laboratory test load effects: (a), (b) Moments transferred form slab (kNm), (M) Bending moment (kNm), (V) Shear force (kN), (N) Axial force (kN).

RESISTANCE VERIFICATIONS

Resistance values for mean material strength are calculated and compared to the internal forces and moments of the chapter 3.

The Moment-Axial Resistance diagrams are calculated following the Italian code NTC2008 [8].

The longitudinal reinforcement of the column is steel with a yield strength (f_{yk}) of 500 MPa above the base and 450 MPa at the base.

The estimates of the maximum moment and axial force are compared to the strength domain calculated with mean material strength, 550 MPa for the steel and 38 MPa (C30/37) for the concrete.

The moment-axial force diagrams for all the columns typologies in both floor are reported in the following. The diagrams are subdivided for column typology.

INTERNAL COLUMNS

In Table 11.11 the laboratory test load effects for the internal columns in each floor are collected together with the number and the diameter of the used bars.

The bending moment (M), the axial force (N) and the shear force (V) are reported for the base section with plastic hinge, the critical cross-section located at 0.5m from the column base and the top section at the connection with 1st floor (for the 1st floor column) and the top cross section at the connection with 2nd floor (for the 2nd floor column) (Table 11.11 and Figure 11.8).

Table 11.11 Laboratory test load effects for each column typology in each floor.

Floor	Section	M (kNm)	N (kN)	V (kN)	Bars (mm)
1st	Base	240	470	145	12Φ14
	Critical	170	470	145	12Φ16
	Top	113	490	117	12Φ20
2nd	Top	200	240	95	12Φ20

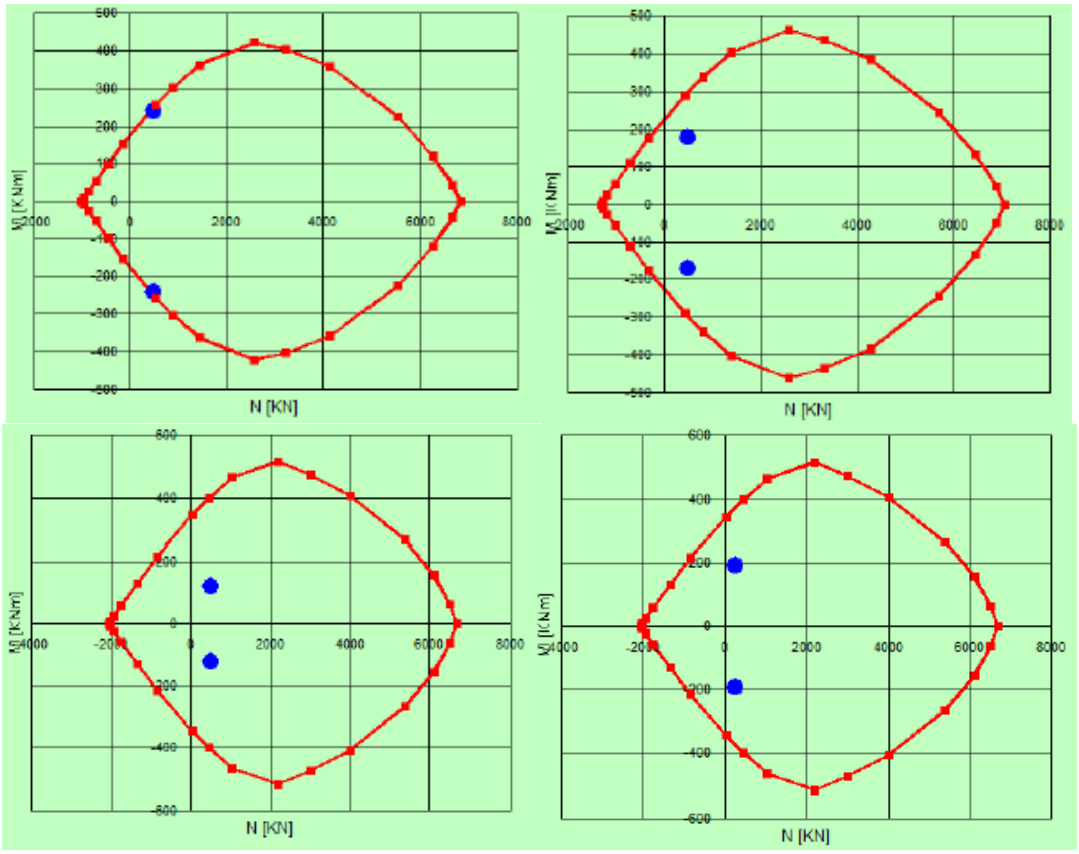

Figure 11.8 Moment-axial force diagrams a) base section 1st floor, b) critical cross-section 1st floor, c) top section 1st floor, d) top cross section 2nd floor.

The reinforcement ratio is increased with respect to the base of the column by using 12 bars with 20 mm diameter, while the bending moment is lower than the value at the base sections, both during the test with both floors loaded and with only the first floor loaded.

LATERAL COLUMN LONG SIDE

Using the same reinforcement in the lateral and corner columns brings the reinforcement ratios for the parts above the base plastic hinge zone respectively to 0.03 and 0.04, while the ratios in the plastic hinges are 0.015 and 0.02 respectively.

In Table 11.12 the laboratory test load effects for the lateral columns in the long side

of the structure, in each floor are collected together with the number and the diameter of the used bars.

The bending moment (M), the biaxial flexure (M_x, M_y), the axial force (N) and the shear force (V) are reported for the base section with plastic hinge in the 1st floor and the 2nd floor columns (Table 11.12 and Figure 11.9).

Table 11.12 Laboratory test load effects for each column typology in each floor.

Floor	Section	M (kNm)	N (kN)	V (kN)	Bars (mm)
1st	Base	160	200	79	12Φ14
		M_x=160	200		
		M_y=5	200		
2nd	Top	140	94		12Φ20

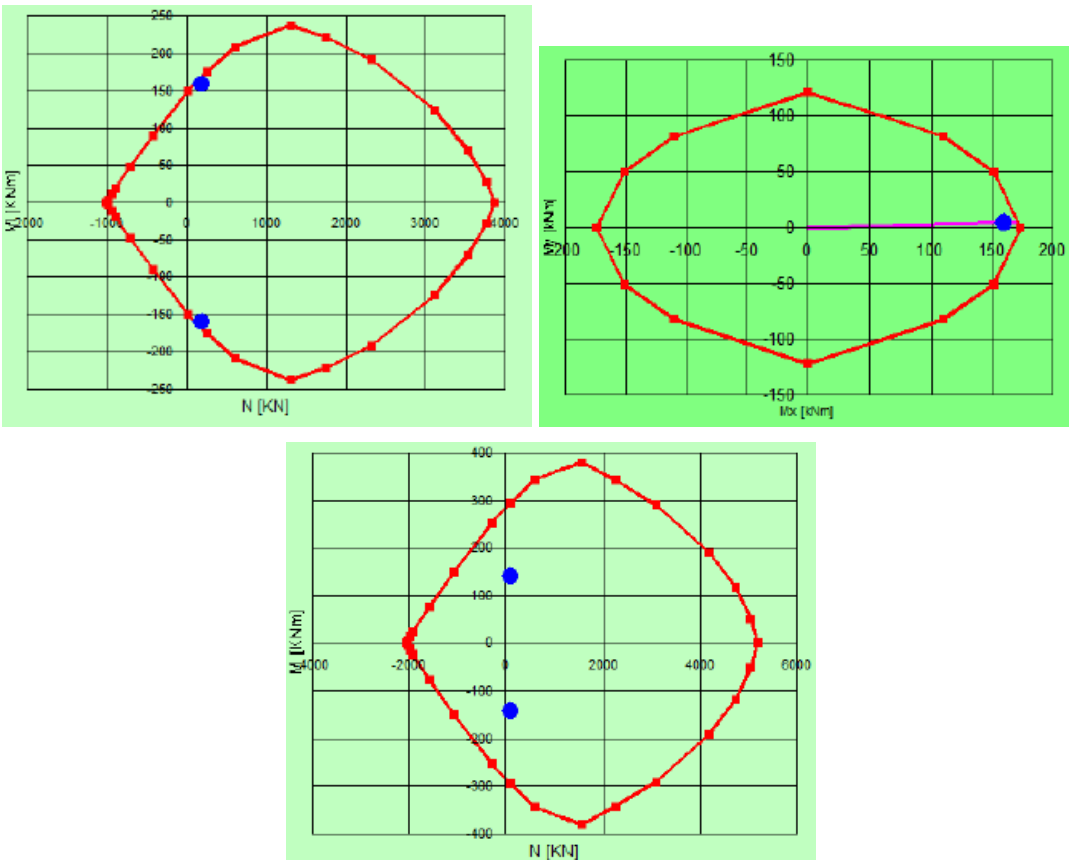

Figure 11.9 Moment-axial force diagrams a) base section 1st floor, b) biaxial flexure base section 1st floor, c) 2nd floor column.

For the top section at the connection with first floor, the reinforcement ratio is increased with respect to the base of the column by using 12 bars with 20mm diameter, while the bending moment is lower than the value at the base sections.

For the 2nd floor (Figure 11.9 c), the reinforcement ratio is increased with respect to

the first floor column by using 12 bars with 20mm diameter, while the bending moment is lower than the value in the first floor column. The moment due to gravity loads in the transverse direction is low.

LATERAL COLUMN SHORT SIDE

Using the same reinforcement in the lateral and corner columns brings the reinforcement ratios respectively to 0.03 and 0.04.

In Table 11.13 the laboratory test load effects for the lateral columns in the short side of the structure, in each floor are collected together with the number and the diameter of the used bars.

The bending moment (M) and the axial force (N) are reported for the base section with plastic hinge in the 1st floor and the 2nd floor column (Table 11.13 and Figure 11.10).

Table 11.13 Laboratory test load effects for each column typology in each floor.

Floor	M (kNm)	N(kN)	Bars (mm)
1st	160	380	12Φ14
2nd	140	184	12Φ20

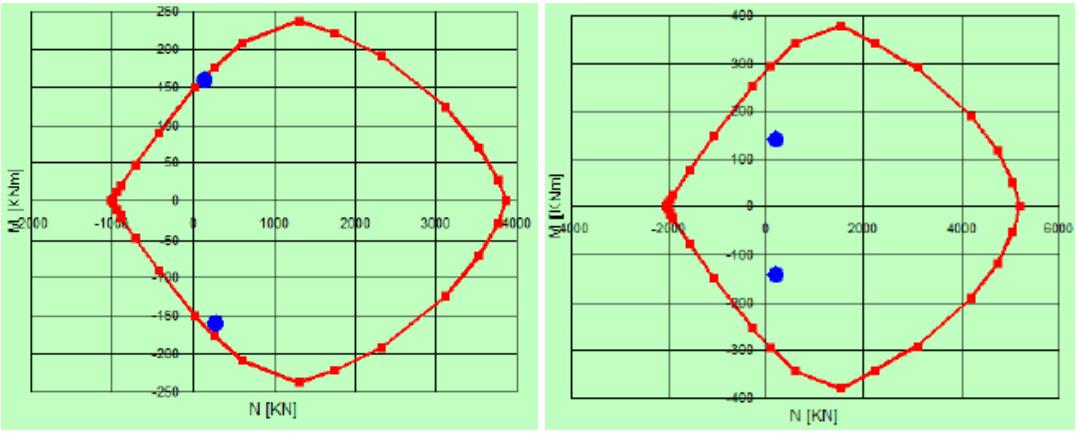

Figure 11.10 Moment-axial force diagrams a) base section 1st floor, b) 2nd floor column.

The reinforcement ratio for the 1st floor column in the top section at the connection with 1st floor is increased with respect to the base of the column by using 12 bars with 20mm diameter, while the bending moment is lower than the value at the base sections, both during the test with both floors loaded and with only the first floor loaded.

In the 2nd floor (Figure 11.10 b), the reinforcement ratio is increased with respect to the first floor column by using 12 bars with 20mm diameter, while the bending moment is lower than the value in the first floor column. The moment due to gravity loads in the transverse direction is low.

CORNER COLUMNS

Using the same reinforcement in the lateral and corner columns brings the reinforcement ratios respectively to 0.03 and 0.04.

In Table 11.14 the laboratory test load effects for the corner columns in each floor are collected together with the number and the diameter of the used bars.

The bending moment (M), the biaxial bending (M_x, M_y) and the axial force (N) are reported for the base section with plastic hinge in the 1st floor and the 2nd floor columns (Table 11.14 and Figure 11.11).

Table 11.14 Laboratory test load effects for each column typology in each floor.

Floor	Section	M (kNm)	N(kN)	Bars (mm)
1st	Base	120	140	12Φ14
		M_x=90		
		M_y=3		
2nd	Top	120	64	12Φ20

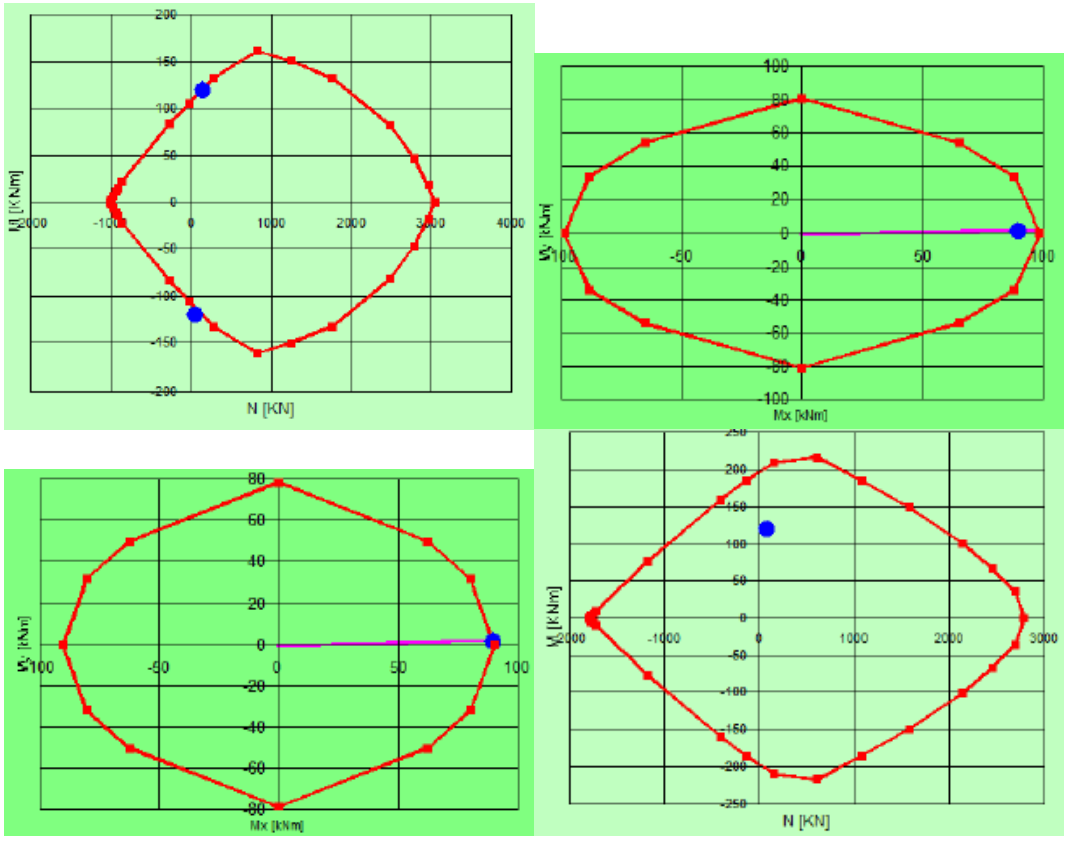

Figure 11.11 Moment-axial force diagrams a) base section 1st floor, b) biaxial bending base section 1st floor, N=130 kN, c) biaxial bending base section 1st floor, N=40 kN, d) 2nd floor column.

The reinforcement ratio for the 1st floor column in the top section is increased with respect to the base of the column by using 12 bars with 20mm diameter, while the

bending moment is lower than the value at the base sections, both during the test with both floors loaded and with only the first floor loaded.

In the 2nd floor (Figure 11.11 d), the reinforcement ratio is increased with respect to the first floor column by using 12 bars with 20mm diameter, while the bending moment is lower than the value in the first floor column. The moment due to gravity loads in the transverse direction is low.

11.2.2 DETAILING OF PLASTIC HINGE ZONES

The ductility demand during the laboratory test in the base columns is high, reaching 6% drift.

The axial compression is low, which is favourable for ductility.

An approximate calculation of the curvature demand is carried out following the Baker's equation for plastic hinge length with transverse steel.

$$l_p = 0.8 * k_1 * k_3 * \left(\frac{z}{d}\right) * x = 0.8 * 0.9 * 0.6 * \left(\frac{1500}{350}\right) * 77.1 = 142\ mm$$

Where *x* is the neutral axis depth at ultimate, *z* is the distance of contra flexure point from critical section and *d* is the effective depth.

For the plastic hinge length, the Corley's equation was used.

$$l_p = 0.5 * d + 0.2 * \sqrt{d} * \left(\frac{z}{d}\right) = 0.5 * 350 + 0.2 * \sqrt{350} * \left(\frac{1500}{350}\right) = 191\ mm$$

An average value of l_p equal to 0.175m was chosen.

To reach a drift of 0.06 requires a plastic rotation around 0.06 (the contribution of the elastic curvature is small at high inelastic drift).

The curvature demand is:

$$\frac{\vartheta_p}{l_p} = \frac{0.06}{0.175} = 0.3 \div 0.4\ m^{-1}$$

Figure 11.12 reports the inelastic moment-curvature diagram for the base of an internal column.

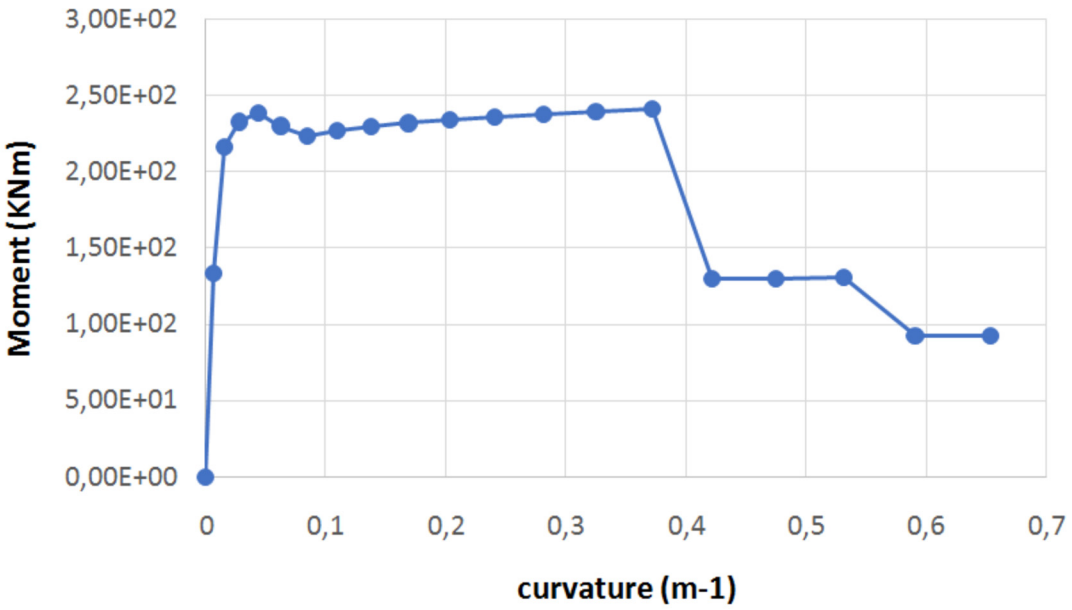

Figure 11.12 Moment-curvature of the base column section of an interior column (N=480 KN).

The curvature demand is very close to the capacity. To avoid failure of the column bases the test on the first floor was conducted up to 5% drift.

To determine the formation of plastic hinges, the reinforcement at the base of the columns has diameter 14mm. This reinforcement extends along a part of the member beneath the first steel stub, for a length of 70 cm. To ensure limited damage of the column, the remaining part of the member beneath the stub has 16mm bars. Couplers were used to change the bar diameter.

To guarantee ductility the buckling of the longitudinal reinforcement must be avoided.

Finally, four longitudinal bars per side have been placed, to provide core confinement. The very close spacing of stirrups to avoid buckling will provide concrete confinement.

11.2.3 Shear verifications

Plastic hinge zones

The shear verifications are carried out using the Italian Code NTC 2018 [6] for the bases of the columns in the plastic hinge zones, with respect to the load effects reached in the laboratory test.

Table 11.15 Shear verification in the critical zones at the base for internal and corner columns.

	Internal column	Corner column
B (mm)	400	300
H(mm)	400	300
F_{cd} (N/mm^2)	17	17
z (mm)	330.3	240.3
N_{Ed} (kN)	232	60
α_c (-)	1.09	1.04
Cot (-)	1.00	1.00
S (mm)	50	50
A_{st} (mm^2)	200	200
n_{st} (-)	6.61	4.81
F_{yd} (N/mm^2)	391	391
$V_{R,cd}$ (kN)	243.8	127.4
$V_{R,sd}$ (kN)	516.6	375.8
$V_{R,d}$ (kN)	243.8	127.4
$V_{E,d}$ (kN) (2nd floor)	75	60
$V_{E,d}$ (kN) (1st floor)	114	61
$M_{E,d}$ (kNm)	240	120
α_s	5.3	6.6
N_{Ed} (kN)	480	140
V_{dd} (kN)	175.95	175.95
	190.78	190.78
	175.95	175.95
V_{df}(kN)	143.6	80.8
	578	400.9

	144	81
V_{rds} sliding	319.6	256.7

SHEAR REINFORCEMENT

In the following the verification of the shear in the part of the column different from the critical zones at the base for the internal, lateral and corner columns are reported, with the most conservative assumption of truss angle 45°.

Internal column

$$V_r = A_{st} * \frac{z}{s} * f_{yst} = (4 * 50) * \frac{315}{200} * 500 = 150\ kN\ > V = 117\ kN$$

Lateral column

$$V_r = A_{st} * \frac{z}{s} * f_{yst} = (4 * 50) * \frac{279}{200} * 500 = 140\ kN\ > V = 79\ kN$$

Corner column

$$V_r = A_{st} * \frac{z}{s} * f_{yst} = (4 * 50) * \frac{234}{200} * 500 = 120\ kN\ > V = 60\ kN$$

11.2.4 FOUNDATIONS

The structure has a reinforced concrete foundation slab and beam grid connecting the columns.

This configuration provides a stiff base for the structure, modelled with fixed ends at the column bases

11.2.5 COLUMN STEEL STUB

The central parts of the column are load cells consisting of steel stubs (Figure 11.13), obtained from standard HEM profiles with an hexagonal void in the web.

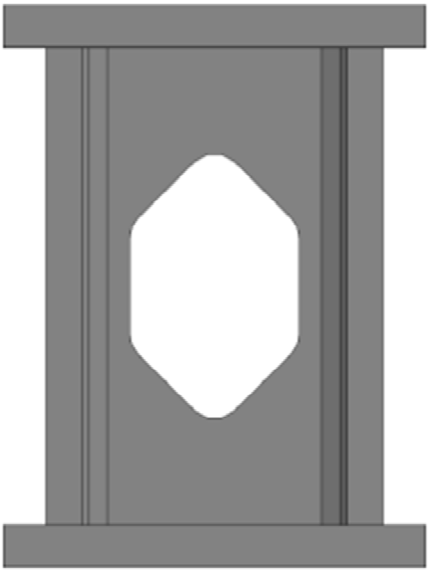

Figure 11.13 Steel stub in the column.

The material is structural steel S355. The cells will be completed with square plates at the ends.

The design is carried out numerically, analysing the effects of actions during the laboratory tests. Stresses are calculated using large displacement analysis, and shown to remain below the yield of the material without buckling effects.

The load cell system will be calibrated at JRC in order to establish the relations between internal forces and strains measured in the flanges and web. The calibration phase (see chapter 4) will reach internal stress levels comparable to those reached in the tests. This experimental test coupled with the analyses carried out here provide the safety of the system.

Three different steel stub dimension were used depending on the column dimensions.

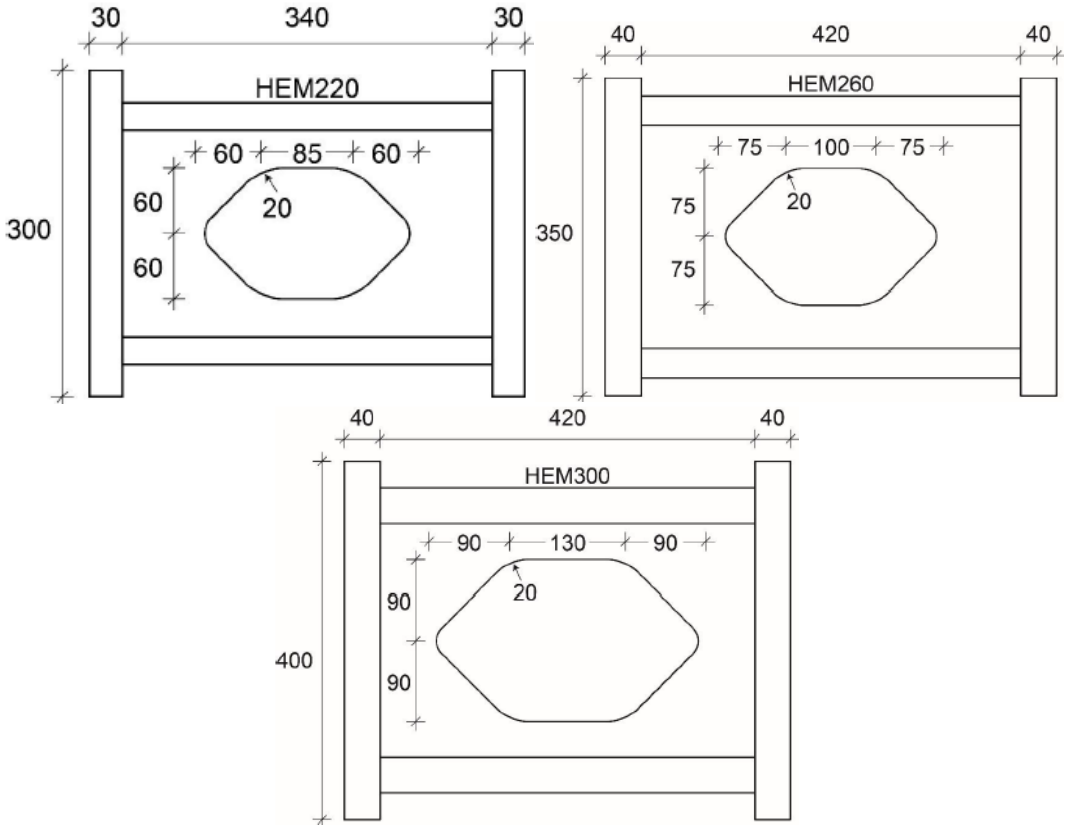

Figure 11.14 Side view of the steel stub for the a) corner 30*30 cm^2 columns, b) edge 35*35 cm^2 columns and c) interior 40*40 cm^2 columns (drawing rotated 90◦, units in mm).

The design kept in consideration the following aspects:

- The column member should approximate the stiffness of a RC column with limited cracking;
- Satisfaction of the strength verifications of the system with respect to plastic collapse and buckling phenomena;
- Avoidance of the plastic strains in the member as far as possible, in particular in correspondence of the measurement points;
- The connection of the steel stub to the reinforced concrete parts of the column above and beneath the cell should avoid the opening of interface contact cracks between the steel plates and the concrete.

CONNECTION

The end plates are connected to the central stub by bolts, and to the RC column with threaded bars. The threads remain within the members, due to the shape of the HEM profile.

The plates' stiffness approximates rigid behaviour and improves the transmission of the normal stresses from the steel stub to the concrete.

STIFFNESS

The stiffness of the composite columns was studied by means of a finite element model consisting of beam and solid elements. The beam elements were used at the extremities of the column, in the portions that are expected to exhibit a regular distribution of the normal and tangential stresses. The central portion of the column, with the steel stub and the adjacent diffusive zones, was modelled by means of solid tetrahedral elements.

The stiffness was evaluated by calculating the rotation of the column in simply supported conditions, with a rocker and roller, corresponding to a unit bending moment at one end (A in Figure 11.15). The calculations were carried out without/with the simultaneous application of an axial force, in order to ascertain the role played by second order effects on the bending stiffness.

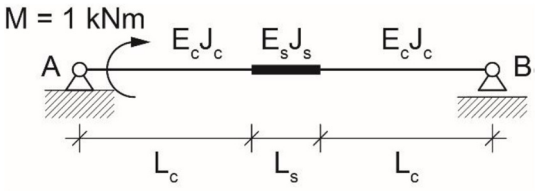

Figure 11.15 Reference structural scheme for the evaluation of the bending stiffness of the composite columns (Ls = 40 cm for the 30*30 cm^2 column; Ls = 50 cm otherwise).

The models used are similar for all the column typologies. Figure 11.16 reports an example of the model used for the 30*30 cm^2 column typology.

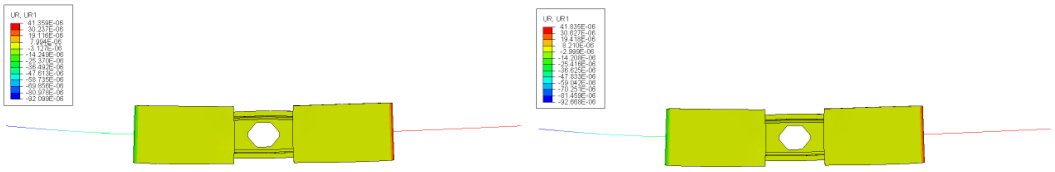

Figure 11.16 Composite beam-solid finite element model for evaluating the stiffness of the 30*30 cm^2 columns. a) geometric non linearity NOT included, b) geometric non linearity included, magnification factor = 1000.

The results of the models of the columns for the three different dimensions are collected in Table 11.16.

For each typology are reported:

The axial force that was applied together with the bending moment, in order to assess the role played by second order effects; the values for each column type were taken from the analyses on the laboratory test load effects (N_{max});

The rotation at the loaded end (A) without taking into account geometric non linearity (φ_{FO});

The rotation at the loaded end (A) taking into account geometric non linearity (φ_{SO});

The ratio between the "apparent" bending stiffness of the composite column EJ, and the stiffness E_cJ_c of an identical homogeneous concrete column (without the steel stub at mid-height) (α).

Table 11.16 Results of the models of the columns with steel stub.

Column (cm^2)	Profile	N_{max} (kN)	φ_{FO} (rad)	φ_{SO} (rad)	$\alpha=EJ/E_CJ_C$
30*30	HEM220	131	9.210E-0.5	9.267E-0.5	0.94
35*35	HEM260	335	4.876E-0.5	4.914E-0.5	0.92
40*40	HEM300	480	2.866E-0.5	2.888E-0.5	0.92

The results reported in Table 11.16 (obtained assuming E_c = 15000 MPa and E_s = 200000 MPa) clearly show that the insertion of the steel stub leads to a minor reduction of the stiffness with respect to a reinforced concrete column of same height and cross section. The values of coefficient α are between 0.92 and 0.94, which indicates that the aforementioned stiffness reduction is below 10% for all column types. Moreover, the stiffness reduction is approximately the same for all columns: this indicates that no major redistributions of the internal forces are to be expected because of the presence of the steel stubs. As a consequence, in the following the strength verifications will be performed using the values of internal forces as previously worked out.

STRENGTH VERIFICATION

Aiming to reach an elastic response of the system and avoid buckling of the composite columns, the same 3D finite elements models described in the previous section were used to study the response under imposed external loads (Figure 11.17).

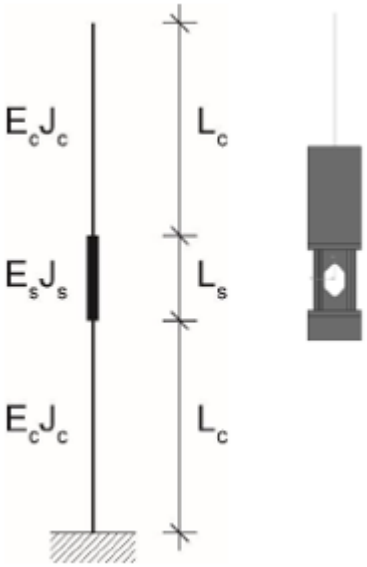

Figure 11.17 Structural scheme used for the strength verifications of the composite columns and corresponding finite element model.

The characteristics of the model are:

- The stiffness of the reinforced concrete portions (beam elements and solid tetrahedral elements) is governed by a reduced modulus of elasticity (E_c = 15000 MPa) to account for cracking;
- The composite columns are modelled as cantilevers, with a fixed end at the bottom, in order to increase the free length with respect to the actual situation where the columns are constrained by the slabs at the top, and the corresponding rotation is, at least in part, limited;
- The composite columns are subjected to forces at the top in order to reproduce the internal forces distribution worked out from the column model (see Table 11.17); conservative values with consideration of the possible unbalanced moment increase due to studs reinforcement were considered. These verifications are carried out for the ground floor columns;
- The geometric non linearity was taken into account in all the analysis.

Table 11.17 Forces at column top.

Column (cm^2)	M (kN)	N (kN)	V (kN)
30*30	70	131	38
35*35	230	335	90
40*40	255	480	145

All the analyses converged to a solution corresponding to the imposed external forces. Figure 11.18 a, b, c depict the Von Mises stress on the steel stub at the maximum forces for the three different column typologies (30*30 cm^2, 35*35 cm^2, 40*40 cm^2).

In all cases the applied stress is well below the elastic limit

$$f_{yd} = \frac{f_{yk}}{\gamma_s} = \frac{355}{1.15} = 310\ MPa$$

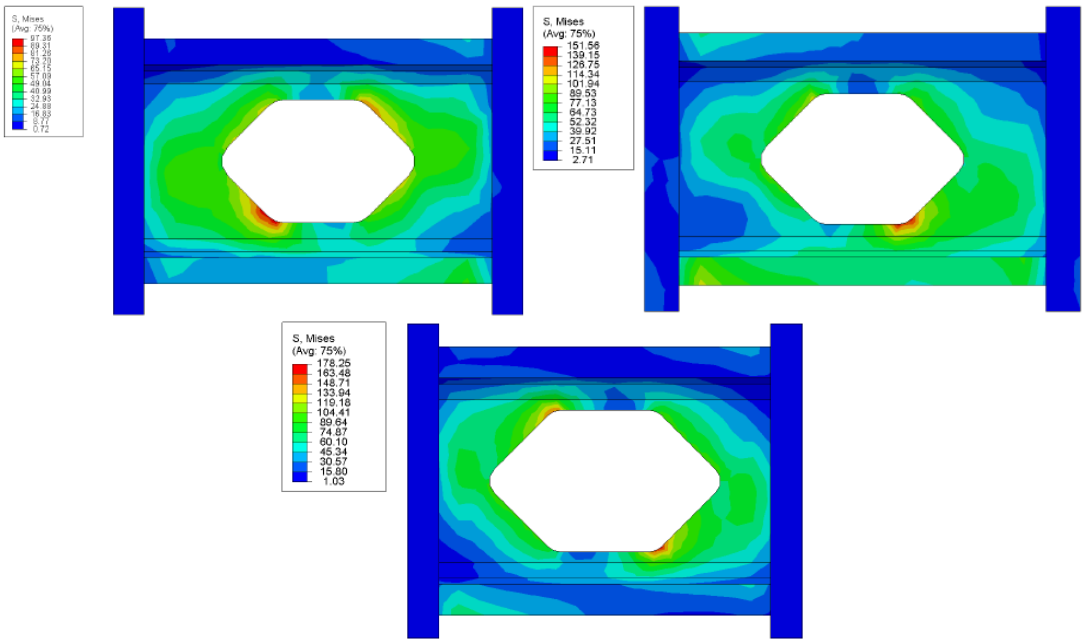

Figure 11.18 Von Mises stress in the steel stub of the a) 30*30 cm^2 columns (σ_{max}/f_{yd}=0.22), b) 35*35 cm^2 columns (σ_{max}/f_{yd}=0.49), c) 40*40 cm^2 columns (σ_{max}/f_{yd}=0.57).

11.3 Additional loads for the tests

Additional gravity loads were placed on the 1st and 2nd floor with different load entity and typology depending on the testing.

Water tanks (full or half-full) and concrete blocks were placed on the structure to impose vertical loads in addition to the self-weight of the flat-slab frame.

The choice to use these two different loading typologies was made for a practical reason. The concrete block can be easily put in position from the top using the rolling crane, whereas at the 1st floor it is needed to use water tanks that are brought in position empty, and then filled and emptied on the spot.

The loads differ in each experiments for disposition, size and typology.

The loads typology consists of water tanks on the 1st floor and concrete blocks on the 2nd floor.

Figure 11.19 Loads different typologies**.**

For the pseudo-dynamic test (Seis-SLS and Seis-ULS), the 1st floor was loaded with 48 tanks of 10 kN each, whereas the 2nd floor with 9 concrete blocks of 66 kN each (Table 11.18 and Figure 11.20).

Table 11.18 Added loads on the 1st and 2nd floor, Test Seis-SLS (e03) Seis-ULS (e06).

Floor	Typology	Number	Weight (kN)	Load (kN)	Area (m2)	(kN/m^2)
1	Tanks	48	10	480	137.8	3.48
2	Blocks	9	66	594	137.8	4.31

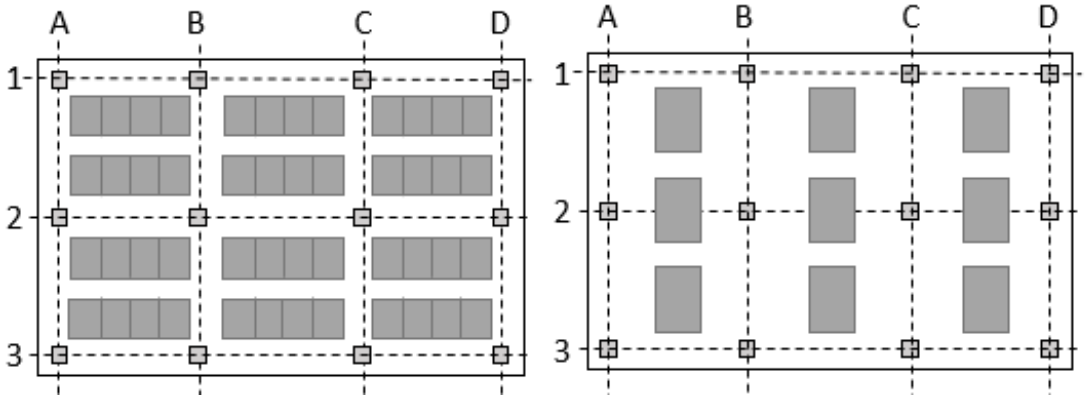

Figure 11.20 Added Loads distribution on the 1st and 2nd floor, Test Seis-SLS (e03) Seis-ULS (e06).

The experiment Cyc-1 (f02) was conducted with two different loads in the two halves of the slab on the 1st floor. The west side of the slab was loaded with tanks for a total weight of 240 kN, the east side of the slab was loaded with tanks for a minor total weight of 108 kN. The load on the 2nd floor was maintained the same as in the previous experiment (Table 7.1 and Figure 7.1).

Table 11.19 Added loads on the 1st and 2nd floor, Test Cyc-1 (f02)**.**

Floor	Typology	Number	Weight (kN)	Load (kN)	Area (m2)	(kN/m^2)
1	West side					
	Tanks	24	10	240	68.9	3.48
	East side					
	Tanks	24	4.5	108	68.9	1.57
2	Blocks	9	66	594	137.8	4.31

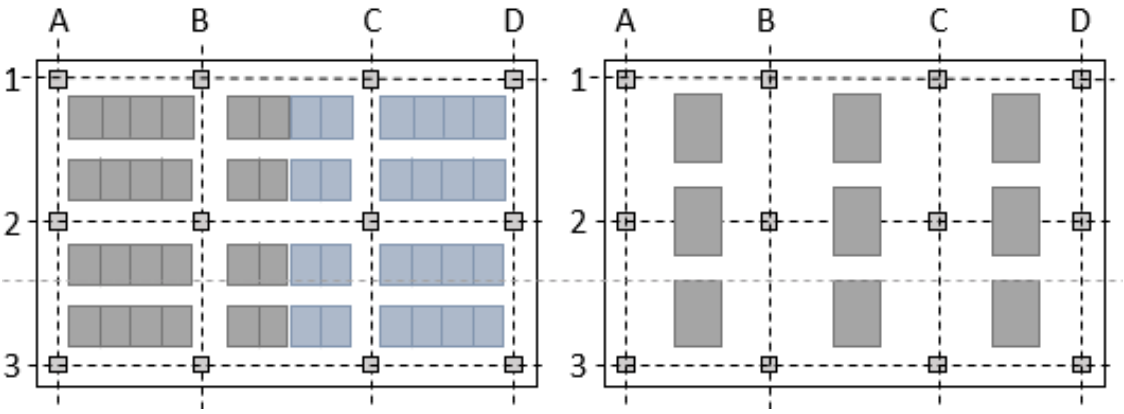

Figure 11.21 Added Loads distribution on the 1st and 2nd floor, Test Cyc-1 (f02).

For the experiment with the repaired connections, Cyc-2 (g04) and the final experiment, the vertical load on the 2nd floor remained the same whereas the vertical load on the 1st floor was changed.

Because the slab-column connections along the two short sides (A and D) on the 1st floor were heavily damaged at the end of test B1, the two lines of tanks on the lateral short side were removed, and the load was reduced on the outer halves of the span between the lines A and B and C and D.

The 1st floor was loaded with 32 tanks with 10 kN each, whereas the vertical load on 2nd floor remains the same as in the previous tests, 9 concrete blocks of 66 kN each (Table 8.1 and Figure 11.22).

Table 11.20 Added loads on the 1st and 2nd floor, Test Cyc-2 (g04).

Floor	Typology	Number	Weight (kN)	Load (kN)	Area (m2)	(kN/m^2)
1	Tanks	32	10	320	137.8	2.32
2	Blocks	9	66	594	137.8	4.31

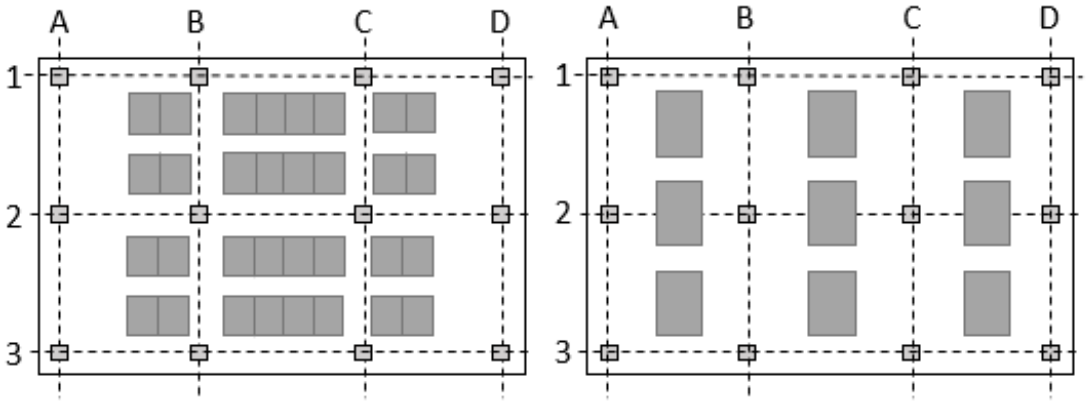

Figure 11.22 Added Loads distribution on the 1st and 2nd floor, Test Cyc-2 (g04).